UNIVERSITÉ DE STRASBOURG

ÉCOLE DOCTORALE DES SCIENCES DE LA VIE ET DE LA SANTÉ

Institut de Biologie Moléculaire des Plantes – CNRS – UPR2357

THÈSE présentée par :

Quentin SIMONNOT

soutenue le : **05 avril 2024**

pour obtenir le grade de : **Docteur de l'Université de Strasbourg**
Discipline/ Spécialité : Aspects Moléculaires et Cellulaires de la Biologie

Deciphering the roles of CCR4a and CCR4b deadenylases in the modulation of mRNA deadenylation and its interplay with uridylation in *Arabidopsis thaliana*

Thèse dirigée par :

Dr. Dominique GAGLIARDI **IBMP, université de Strasbourg**

Rapporteurs :

Pr. Stefan L. AMERES **Max Perutz Labs, université de Vienne**
Pr. Jean-Marc DERAGON **LGDP, université de Perpignan**

Autre membre du jury :

Pr. Carine MEIGNIN **IBMC, université de Strasbourg**

Acknowledgments

First, I would like to thank Pr. Carine Meignin, Pr. Jean-Marc Deragon and Pr. Stefan Ameres for having accepted to evaluate my work. I also would like to apologise for the postponment of my *Ph*D defense. I am sure that the discussion we will have will make up for it!

I would also like to express my gratitude to both Bertrand Séraphin and Todd Blevins for their assistance during the committee meetings and for their valuable input over the past three years. In particular, I want to thank Todd for the countless discussions we had about nanopore sequencing. I learned so much, and you made me fall in love with the technology.

Ces remerciements vont être assez longs, puisque cela fait quand même presque 6 ans que je suis à l'institut, en tant que stagiaire de master d'abord, puis en thèse. J'ai beaucoup appris en votre compagnie, et il me paraît normal d'avoir un mot pour chacun d'entre vous.

Je voudrais remercier en premier mon directeur de thèse, Dominique « Gag » Gagliardi, pour m'avoir accompagné pendant toutes ces années. Cela fait maintenant plus de 5 ans depuis notre première réunion du projet Végélab, où tu me présentais les données, et où j'étais obligé de t'enregistrer pour être sûr de tout comprendre plus tard (et je ne comprenais pas tout). Ta passion scientifique est vraiment communicative, tu auras su rendre le moindre graph, le moindre phasing de PABP super intéressant tout au long de ma thèse ! Tu pourrais presque me faire faire des trucs sur le pollen… oh… En tout cas, je n'oublie pas qu'on doit toujours aller skier un de ces 4, depuis le temps que tu me nargues avec tes photos ! Outre ça, tu as toujours été d'un grand support, tu savais me rassurer quand les manips ne marchaient pas, me remotiver quand j'étais au plus bas. Et ce qu'on peut dire, c'est que ça n'était pas facile. Tu t'es toujours montré patient envers moi, et surtout en cette fin de rédaction. C'est tout ça qui fait que je suis sincèrement heureux d'avoir fait ma thèse sous ta supervision, et je te souhaite d'encadrer encore de nombreux doctorants pour qu'ils aient la chance de travailler avec toi.

Heike, I cannot thank you enough for all the endless talks we've had in the 457, with you on my back and your marker, infamously stolen, on my bench! Jokes aside, I loved discussing with you about everything from food, to politics, to east Germany, to food again, and yes, science sometimes. It was always a pleasure to enter the lab and find a selection of fruits and vegetables fresh from your garden in front of my computer. Most importantly, you were so comprehensive and supportive especially when I needed it the most, and this, I will never forget. Be sure that when I come by Strasbourg, you will be the first to know so we can arrange a risotto!

Un grand merci à Hélène pour ton aide sur tous les aspects de la bioinfo qu'on a pu aborder pendant ces 3 dernières années (et il y en a eu). Tu t'es montrée patiente pour m'expliquer des concepts parfois un peu obscurs (la GLM par exemple) et grâce à ça j'ai beaucoup appris et pris goût (un peu) à la bioinfo. L'équipe a de la chance de t'avoir, tu apportes énormément à tout le monde et tu te rends très (trop ?) disponible pour aider dès qu'on le demande. On a beaucoup ri ensemble, parfois à tes dépens, parfois aux miens, mais toujours avec bienveillance. En tout cas maintenant avec Pietro, on a réussi à te faire parler en franglais, c'est une vraie victoire !

Merci à Damien d'avoir été là pour tes conseils et pour m'avoir fait rire (à mes dépens d'ailleurs). On peut dire que le running gag (pour blague, et non pas Gag qui fait un footing) sur le guacamole aura duré longtemps ! Je reste persuadé qu'il était bon mais juste (légèrement) oxydé…

Merci à tous ceux avec qui j'ai partagé le bureau. J'ai passé des années super à vos côtés, à rigoler et à râler sur tout ce qui n'allait pas. Merci à Pietro pour tous ces petits moments de complicité (toi qui me fais un doigt d'honneur en gros), pour ces discussions et ces moments passés au labo et en dehors. Pas merci pour tes blagues nulles par contre, je les ai toutes détesté. Merci à Aude, AKA l'infatigable, c'était toujours sympa de te croiser de manière inopinée à 23h un dimanche, avec la musique à fond dans le labo. Je te souhaite bonne chance pour la suite au Canada ! Merci à Hanzhang, pour ta bonne humeur et ton sourire perpétuel. Fais attention à ne pas trop rire aux blagues nulles de Pietro, il risque de prendre la confiance et de continuer sur des blagues encore pires. Merci à Jackson Peter (ou bien Peter Jackson ?) pour tous les conseils et tips sur R. Merci aussi beaucoup pour tes p'tits tops de musique le vendredi, j'ai découvert quelques pépites d'eurodance colombienne ! Merci à Élodie pour tout ce que tu as fait depuis que tu es arrivée, pour m'avoir aidée et tenue compagnie lors de nos heures passées à récolter des fleurs ou repiquer des plantes. Je suis très content que tu aies trouvé ta place dans le labo et je te souhaite de t'y plaire encore très longtemps. Merci beaucoup à Anne-Caroline avec qui j'ai partagé 2 ans de thèse. C'était génial de passer tout ce temps avec toi au labo et en dehors. Tu es devenue une véritable amie au fur et à mesure de ces années (amitié qui a commencé par une rencontre inopinée à la Laiterie avec Dali, je n'oublie pas) et j'ai beaucoup appris grâce à toi.

Merci beaucoup à tous les anciens membres du labo, Caroline, Marlène, Hélène, Jeanne, Thanin pour votre bonne humeur et vos conseils scientifiques, particulièrement Caroline qui m'a encadré pendant mon stage. Merci également aux stagiaires qui sont passés dans l'équipe et que j'ai pu encadrer, Nolwenn, Léon et Paul.

Merci à toute l'équipe de Pascal Genschik, et plus globalement, à tous ceux du 4ème. Je ne suis resté que 2 mois en stage de M1, mais je me suis tout de suite senti à ma place grâce à vous. Je n'oublierai pas ce stage sur FBW2 !

Merci à tous les doctorants avec qui j'ai partagé des moments tout au long de ma thèse. Juliette et Émilie, on se connaît depuis le master, et on peut dire qu'on aura fait un bon bout de chemin ensemble. J'aurais toujours comme bon souvenir nos lundi à « chez mon ex », et tous les litres de bière que Juliette aura renversée. Merci beaucoup à Léna et Jérémy pour les quelques discussions (douteuses) qu'on aura eues en dehors du labo. Merci à Luisa pour ta bonne humeur et tous les repas qu'on aura partagés au coréen ! Merci beaucoup à Anita, Amélie et Christopher pour le bureau qu'on a partagé quelques mois, c'était vraiment super de parler avec vous et de faire semblant de travailler (je rigole Gag). Merci à Solène pour tout, et surtout les magnifiques aquarelles !

Merci beaucoup à Anthony Gobert pour le début de la génération des CRISPR (ça m'a été un peu utile !). Merci à Jean Molinier pour ton input sur les expériences avec les UV et pour toutes les discussions autres qu'on a pu avoir. Thanks Ana Sede for showing me the pollen germination assay! Merci à la plateforme de bioinfo et particulièrement à Stéfanie et à David pour leurs conseils sur mes différents projets. Merci à Jérôme de la plateforme de microscopie, à Malek et Sandrine pour votre aide et vos conseils, merci aux membres de la plateforme de production de plantes, à Laurence du magasin, à Laurence de l'accueil et à Michèle de la laverie. Merci à vous tous, et plus globalement, merci à tout le personnel de l'IBMP pour ces années en votre compagnie.

Un grand merci à Philippe, Johana, Julie et Lauriane de la plateforme de spectrométrie de masse de l'IBMC. Vos conseils ont été précieux et nos collaborations ont mené à la réalisation de beaucoup d'interactomes ! Et c'était toujours un plaisir de passer 10 minutes en chambre froide en t-shirt pour broyer des fleurs (non).

Merci à Rémy Merret pour m'avoir encadré lors des purifs de polysomes. Je veux aussi remercier toute l'équipe, et tous ceux du LGDP avec qui j'ai pu discuter (et boire).

Bien évidemment, un énorme merci ira à tous mes amis qui ont été là pour me changer les idées, et sans qui ces dernières années auraient été fades : mes confrères de la FFIP Jean, Alex, Léo, Pierre, Nini et le Guigz (vous avez reçu le mail ? Y'a réunion le 5) ; Margaux, Dodo, Maiso, Greg, Martin, Fannie, Pauline, Laura, Paul, Etienne, Alain, Mike, Arthur, Victor, Olivier, Yasmine, Lisa, Katya, Annabelle, Lucie, Jeanne, Aurel, Hugo, Florian, William, Lucas. De par votre présence vous avez été un soutien énorme. Merci d'avoir été là pour cet épisode de ma vie, et je serais heureux de vous avoir à mes côtés pour ceux à venir.

Je voudrais aussi remercier Joffrey Mejias et Camille Syska, deux doctorants qui m'ont encadré lors de mon passage à l'INRA de Nice. Chacun a réussi à me transmettre son amour pour la science à sa manière. Particulièrement Joffrey, je n'ai jamais rencontré quelqu'un d'aussi passionné et passionnant que toi. Tu as su me transmettre toutes les valeurs de curiosité et de persévérance dont un chercheur à besoin. Tu as été un véritable mentor, et un acteur essentiel dans mon développement en tant que scientifique et en tant que personne.

Mes derniers remerciements, et non des moindres, seront pour Amandine et ma famille, qui ont été ma principale source de réussite et de motivation. Amandine merci d'avoir été à mes côtés pour tous les moments difficiles de cette fin de thèse. Tu as su te rendre disponible pour être à mes côtés et me réconforter, et tu t'es montrée patiente et compréhensive quand je ne le méritais pas forcément. Sois sûre que je serais là pour toi comme tu l'as été.

Merci à ma famille et particulièrement mes parents et mon frère pour m'avoir soutenu et encouragé à chaque instant. Vous m'avez accompagné tout du long de ma scolarité, et vous m'avez poussé à donner le meilleur de moi-même. Si j'en suis là, c'est grâce à vous. C'est difficile d'exprimer par écrit à quel point je vous suis reconnaissant pour tout, mais croyez-moi je le suis.

Cette thèse est signée de mon nom, mais c'est à vous tous que je la dois.

Table of contents

List of figures and tables

Introduction

Results

Discussion & perspectives

Supplementary material

Introduction

	Arabidopsis thaliana	***Homo sapiens***	***Drosophila melanogaster***	***Caenorhabditis elegans***	***Schizosaccharomyces pombe***	***Saccharomyces cerevisiae***
Decapping complex, decapping activators/ translation inhibitors	DCP1	DCP1	Dcp1	DCAP-1	Dcp1	Dcp1
	DCP2/TDT	DCP2	Dcp2	DCAP-2	Dcp2	Dcp2
	-	-	-	-	Edc1	Edc1
	-	-	-	-	-	Edc2
	-	EDC3	Edc3	EDC-3	Edc3	Edc3
	VCS	EDC4/Ge-1/HEDLS	Ge-1	EDC-4	Pdc1	-
	PAT1, PATH1, PATH2	PAT1L, PAT2L	Hpat/Patr-1	PATR-1	Pat1/Pdc2	Pat1
	DCP5, DCP5-L	LSM14A/Rap55	Tral	CAR-1	Dhh1/Ste13	Dhh1
	RH6, RH8, RH12	DDX6	Me31B	CGH-1	Scd6	Scd6
	LSM1-7	LSM1-7	Lsm1-7	LSM1-7	Lsm1-7	Lsm1-7
	nCBP	4EHP/eIF4E2	4EHP	IFE-4	-	-
	EXA1	GIGYF1, GIGYF2	GIGYF	GYF-1	Mpd2	Smy2, Syh1
Deadenylation	CCR4a, CCR4b	CCR4a/CNOT6, CCR4b/CNOT6L	Ccr4/Twin	CCR-4	Ccr4	Ccr4
	Caf1a to Caf1k (11 paralogs)	Caf1a/CNOT7, Caf1b/CNOT8	Pop2	CCF-1	Pop2	Pop2
	NOT1	CNOT1	Not1	NTL-1/LET-711	Not1	Not1
	NOT2a, NOT2b/VIP2, NOT3	CNOT2, CNOT3	Not2/Rga, Not3	NTL-2, NTL-3, TAG-153	Not2, Not3	Not2, Not3, Not5
	NOT4a, NOT4b, NOT4c	CNOT4	Not4	NTL-4	Not4/Mot2	Not4/Mot2
	NOT9a, NOT9b, NOT9c	CNOT9/CAF40	Caf40	NTL-9	Caf40	Caf40
	-	-	-	-	-	Caf130
	NOT10	CNOT10	Not10	-	-	-
	NOT11	CNOT11	Not11	NTL-11	-	-
	-	PAN2	Pan2	PANL-2	Pan2	Pan2
	-	PAN3	Pan3	PANL-3	Pan3	Pan3
	PARN/AHG2, RRD1	PARN	-	PARN-1, PARN-2	PARN	-
5' → 3' exoribonuclease	XRN4	XRN1	Pacman	XRN-1	Exo2	Xrn1

Table 1. Selection of factors involved in mRNA decay in eukaryotes.

1. The ^{m7}G-cap and poly(A) tail are important determinants of RNA fate

mRNA stability plays a pivotal role in gene expression and cellular function. The integrity of mRNA is constantly under assault by exonucleases, endonucleases, and other decay-promoting factors that are highly conserved throughout evolution (**Table 1** presents a selection of decay factors, and their orthologs in various eukaryotes, that will be of importance all along this manuscript). This susceptibility to degradation is mitigated by the tight regulation of decay processes, which, together with transcription, are essential to maintain appropriate mRNA levels. The stability of an mRNA is influenced by several factors, including its secondary structure, nucleotide composition, post-transcriptional modifications, and incorporation into ribonucleoprotein complexes, all of which collectively determine its half-life within the cell.

mRNA stability is primarily regulated by two essential co-transcriptional events: the addition of a 5' methyl-guanosine cap and the synthesis of a poly(A) tail at the 3' end. These modifications profoundly impact mRNA metabolism, not solely due to their biochemical properties, but mostly because they act as docking platforms for various protein factors essential for mRNA fate—specifically, maturation, export, translation, and stability. In the following section, I will explore the processes through which these modifications are appended to mRNAs and briefly discuss their importance in modulating mRNA metabolism.

1.1. The ^{m7}G-cap is a scaffold for RNP assembly

Capping is a specific feature of RNA Polymerase II (Pol II) transcripts. The enzyme complex responsible for the capping is recruited to Pol II mainly, but not exclusively, by binding its phosphorylated C-terminal domain (CTD) (McCracken *et al.*, 1997a; McCracken *et al.,* 1997b; Cho *et al.*, 1997; Gonzalez *et al.*, 2018). RNA Pol II transcripts are not only mRNAs but also include pre-miRNAs (microRNAs), lncRNAs (long non-coding RNAs), as well as a subset of snoRNAs (small nucleolar RNAs), and snRNAs (small nuclear RNAs) precursors, all of which are capped co-transcriptionally (Skuzeski *et al.*, 1984; Maxwell & Fournier, 1995, Lee *et al.*, 2004; Struhl, 2007; Marchese *et al.*, 2017).

The capping process begins as soon as the first 25–30 nucleotides are incorporated into the nascent transcript (Ramanathan *et al.*, 2016). First, the 5' end of the emerging mRNA molecule is modified by an enzyme known as RNA triphosphatase (TPase), which removes the γ phosphate

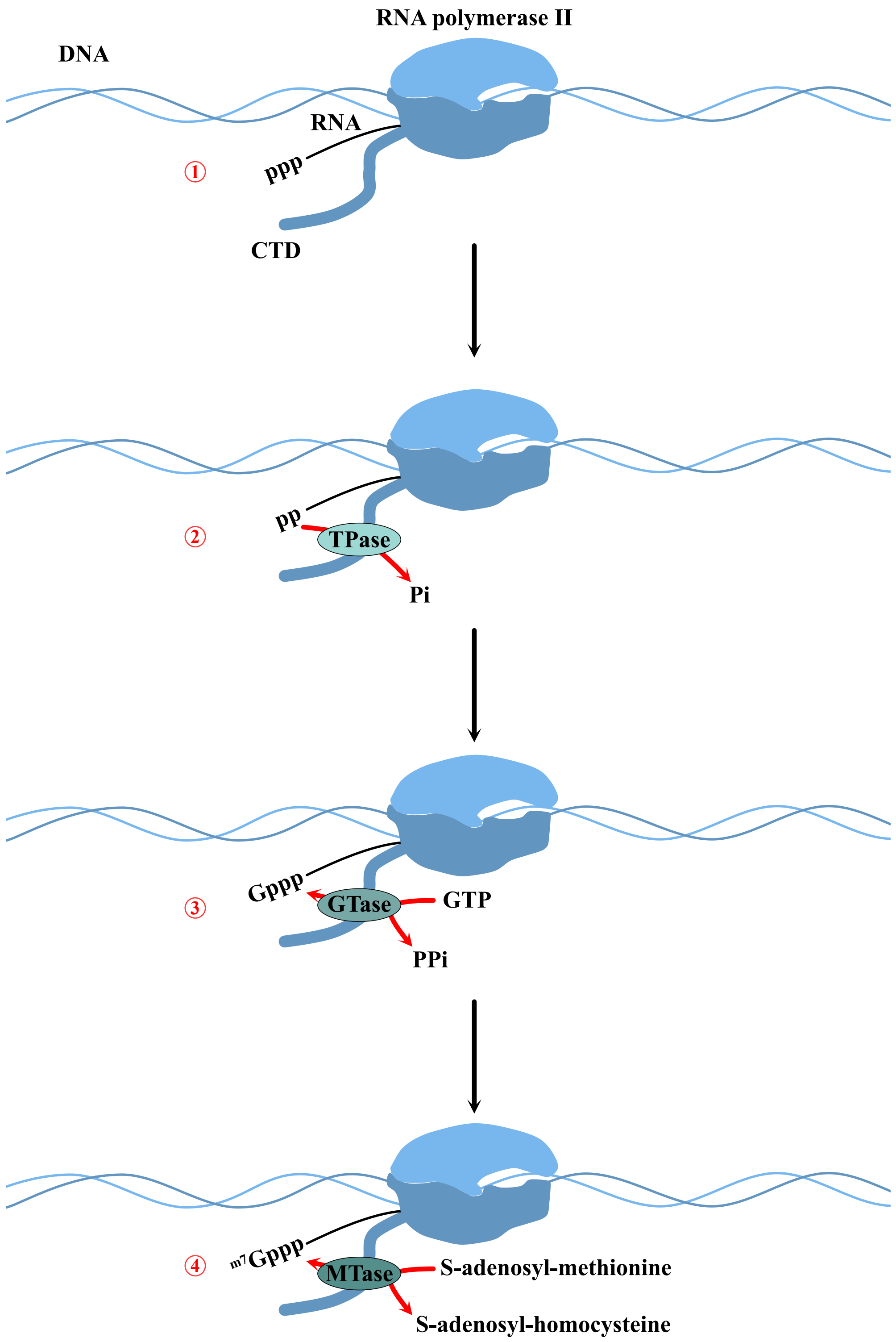

Figure 1. Synthesis of the canonical cap0 structure.
(1) The 5' end of the nascent transcript consists of a triphosphate extremity, vulnerable to 5’→3’ decay. Capping enzymes are recruited co-transitionally to the nascent RNA by interacting with the phopshorylated C-terminal domain (CTD) of the Pol II. **(2)** By the action of a triphosphatase (TPase), the 5' triphosphate of the RNA is dephosphorylated to a 5' diphosphate. **(3)** A guanosyl-transferase (GTase) uses GTP to link a GMP to the 5' end of the mRNA by an unconventionnal 5'-5' bound. **(4)** Finally, the methyltransferase (MTase) methylates the N7 of the guanosine to produce the canonical ^{m7}Gppp cap termed cap0.

from the 5' triphosphate end, leaving a diphosphate (**Figure 1**). Subsequently, a guanylyltransferase (GTase), adds a GMP in a reverse linkage (5' to 5' triphosphate bridge) to the 5' end of the mRNA. In mammals, a single enzyme, RNGTT, possesses both triphosphatase and guanylyltransferase activities (Tsukamoto *et al.*, 1998; Yamada-Okabe *et al.*, 1998), while in yeast, the activity is separated into two enzymes, Cet1 and Ceg1 (Ho *et al.*, 1998). Once the guanine nucleotide is added, it is further modified by the addition of a methyl group to the nitrogen at position 7 of the guanine base (^{m7}Gppp-RNA). This methylation is performed by the enzyme guanine-N7 methyltransferase (MTase) (Mao *et al.*, 1995; Saha *et al.*, 1999). This 5' cap configuration is known as cap0. In metazoans and eukaryotic viruses, this structure can be further modified by additional methylation at the sugar moiety of the first one or two nucleotides of the mRNA. These reactions are catalysed by 2'-O-methyltransferase enzymes CMTR1 and CMTR2, producing the cap1 (^{m7}GpppN$_m$p-RNA) and cap2 (^{m7}GpppN$_m$pN$_m$p-RNA) structures, respectively (Bélanger*et al.*, 2010; Werner *et al.*, 2011). These modifications facilitate mRNA translation and help differentiate self from non-self mRNAs (Daffis *et al.*, 2010; Devarkar *et al.*, 2016). If the first encoded nucleotide is a 2′-O-methyladenosine (A$_m$), it can be further methylated at the nitrogen at position 6 of the adenine base by PCIF1, forming the ^{m7}Gppp^{m6}A$_m$ cap (Wei *et al.*, 1975; Keith *et al.*, 1978, Akichika *et al.*, 2019, Boulias *et al.*, 2019). This modification is widespread and enhances mRNA stability (Mauer *et al.*, 2017; Sun *et al.*, 2021). Interestingly, species within the *Trypanosoma* order have an unusual hypermethylated cap termed cap4 (^{m7}Gppp^{m2-6}A$_m$pA$_m$pC$_m$p^{m3}U$_m$), which was shown to enhance translation (Perry *et al.*, 1987; Zamudio *et al.*, 2006; Zamudio *et al.*, 2009).

While the vast majority of mRNAs are ^{m7}G-capped, studies have shown that non-canonical capping, particularly with NAD$^+$, is widespread and conserved in eukaryotes, with evidence in mammals, yeast, and plants (Jiao *et al.*, 2017; Walters *et al.*, 2017; Wang *et al.*, 2019). Contrary to the intricate ^{m7}G-capping described previously, NAD$^+$ capping occurs as an *ab initio* capping, as Pol II can use NAD$^+$ as an initiating nucleotide (Bird *et al.*, 2016). While ^{m7}G-capping promotes mRNA stability, NAD$^+$-capped mRNAs are unstable, and their decay is initiated by the deNADding activity of the non-canonical decapping enzyme DXO (Jiao *et al.*, 2017). Interestingly, in Arabidopsis, DXO-family protein DXO1 is an essential component for ^{m7}G capping, as it interacts and activates RNMT1, the enzyme responsible for the MTase activity (Xiao et al., 2023). This finding raises the possibility of a potential interconnection between NAD+-RNA decapping and m7G capping in plants.

The ^{m7}G-cap protects Pol II transcripts from 5'→3' decay and provides a platform for the assembly of factors that mediate export, translation and decay. As soon as the transcripts exits the Pol II complex, the nuclear cap-binding complex (nCBC) binds the ^{m7}G moiety.

The nCBC consists of two proteins, the actual ^{m7}G-binding protein CBP20 and its cofactor CBP80. Although CBP20 is the protein that directly binds to the cap structure, it requires interaction with CBP80 to adopt the proper conformation necessary to bind the ^{m7}G cap (Izaurralde *et al.*, 1994; Kataoka *et al.*, 1995). It is noteworthy that NCBP3, a human cap-binding protein, associates with CBP80 to form an alternative nCBC. This alternative complex has distinct yet overlapping substrates compared to the canonical nCBC and is of critical importance during stress response (Rambout & Maquat, 2021).

The nCBC is a versatile complex that plays critical functions for mRNA's fate (reviewed in Gonatopoulos-Pournatzis & Cowling, 2014). Because it binds and covers the ^{m7}G moiety, it protects the 5'cap from decapping and subsequent 5' → 3' exonucleolytic decay, thereby participating in the stability of the pre-mRNA. Apart from protecting the cap, nCBC serves as a scaffold for the formation of mRNP involved in the regulation of essential processes in mRNA cycle such as pre-mRNA maturation and splicing (Izaurralde *et al.*, 1994; Colot *et al.*, 1996; Kühn *et al.*, 2007). Together with its binding partner ARS2 (SERRATE in plants), nCBC facilitates cap-proximal transcription termination (Flaherty *et al.*, 1997; Narita *et al.*, 2007), 3' end processing of Promoter Upstream Transcripts (PROMPTs) and short mRNAs (Gruber *et al.*, 2012; Hallais *et al.*, 2013; Iasillo *et al.*, 2017), miRNA processing (Laubinger *et al.*, 2008; Gruber *et al.*, 2009) and RNA export to the cytosol (Chi *et al.*, 2013). Mutually exclusive with those RNPs, nCBC-ARS interacts with the Nuclear Exosome Targeting (NEXT) and Poly(A) Tail Exosome Targeting (PAXT) complexes—cofactors of the nuclear RNA exosome. This interaction facilitates the targeting of RNAs that either fail to assemble or assemble slowly in processing- or export-RNPs, leading to their prompt degradation by the nuclear RNA exosome (Andersen *et al.*, 2013; Meola *et al.*, 2016; Bajczyk *et al.*, 2020, Melko *et al.*, 2020). Though the precise composition of nCBC-associated RNPs may vary in specific organisms, nCBC's crucial function in all these processes from processing to decay is conserved in all eukaryotes.

1.2. mRNA 3' ends are tagged by polyadenylation

Transcription termination of Pol II transcripts is initiated by the cleavage and polyadenylation of the nascent RNA (reviewed in Neve *et al.*, 2017). This process starts with the recognition of the polyadenylation signal (PAS), a sequence within pre-mRNA characterised by the AAUAAA

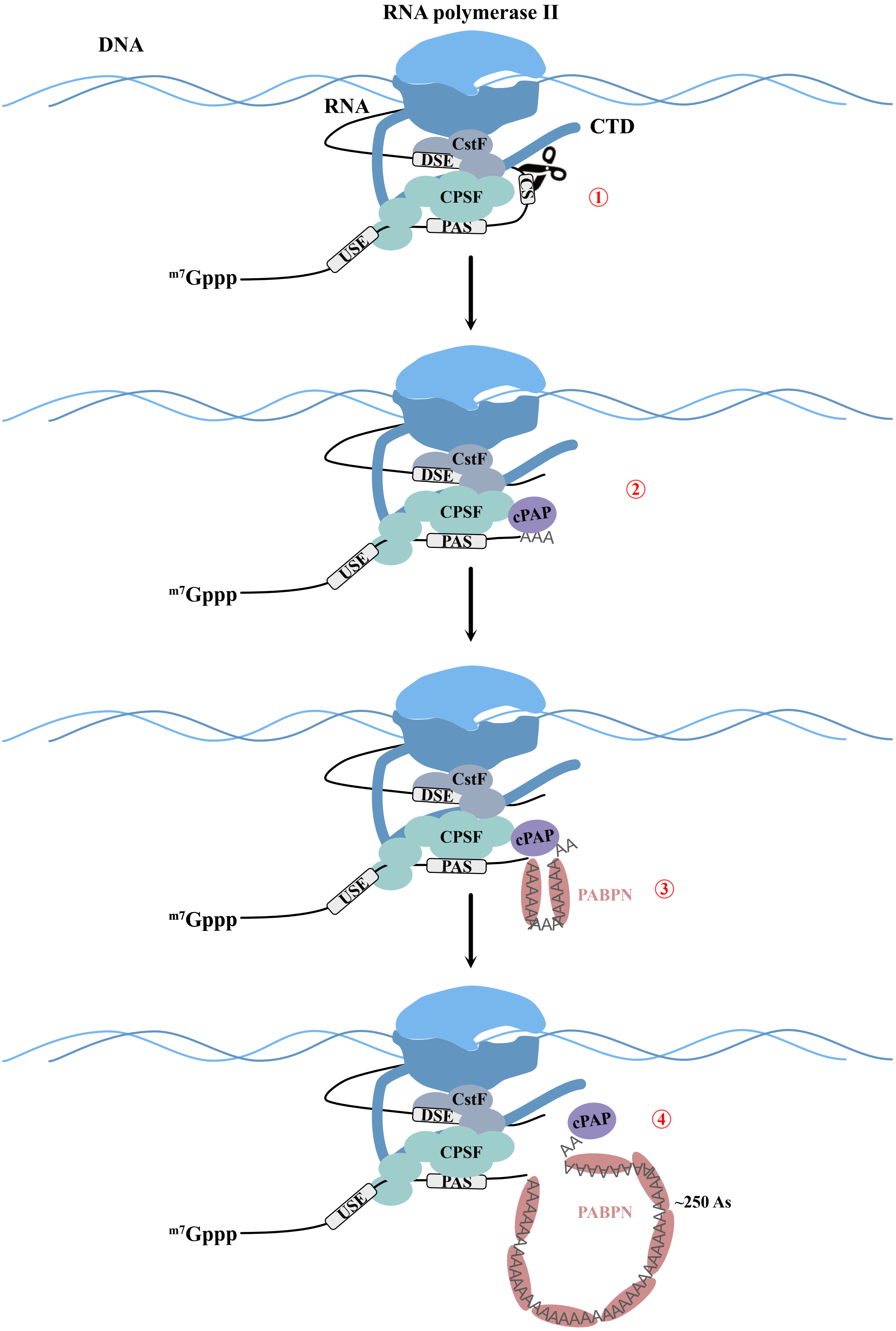

Figure 2. mRNA polyadenylation.
In humans, the polyadenylation site (PAS) contains the core AAUAAA hexamer sequence. Upstream (USE) and downstream (DSE) sequence elements are additional sequences that help to recruit and position the cleavage and polyadenylation specificity factor (CPSF) and associated proteins. **(1)** Upon recognition of the appropriate sequences, the CPSF cleaves the pre-mRNA at the cleavage site (CS). **(2)** The canonical poly(A) polymerase (cPAP) is recruited to the cleavage site and catalyses the distributive polyadenylation at the 3' end of the 5' cleaved fragment. **(3)** The binding of PABPNs to the nascent poly(A) tail increases the affinity of the cPAP to the mRNA, enhancing its processivity. Bound PABPNs adopt a spherical shape that is required to maintain the interaction between CPSF and cPAP, favouring its processivity **(4)** When the poly(A) tail reaches 250 As, PABPN can no longer be incorporated in the spherical particle. The contact between CPSF and cPAP is disrupted, leading to a decrease in the poly(A) polymerase activity followed by the dissociation of the cPAP. Adapted from Kühn *et al*., 2009, Moraes *et al*., 2010 and Nourse *et al*., 2020.

sequence (**Figure 2**). While highly conserved in mammals, only ~10% of mRNAs in plants contain the canonical PAS, highlighting species-specific regulation of polyadenylation events (reviewed in Yang *et al.*, 2021). The cleavage and polyadenylation specificity factor (CPSF) complex, upon recognising the PAS, assembles at this site. This is followed by the recruitment of additional factors, including the cleavage stimulation factor (CstF). CstF, which binds to a downstream GU-rich sequence, is crucial for correctly positioning the entire complex on the pre-mRNA. Subsequently, the CPSF-73 subunit catalyses cleavage 10-30 nucleotides downstream of the PAS (Ryan *et al.*, 2004; Dominski *et al.*, 2005; Mandel *et al.*, 2006). The stability of the CPSF-CstF complex is dependent of the presence of nCBC. As a consequence, depletion of CBC80 strongly reduce PAS cleavage (Flaherty *et al.*, 1997).

Because multiple polyadenylation sites exist within the pre-mRNA sequence, the choice of a proximal (closer to the 5' end), or a more distal (farther from the 5' end) PAS dictates the site of the cleavage, hence the length of the 3′ UTR. These 3'UTR isoforms allow for inclusion or exclusion of *cis*-regulatory elements, essential to regulate the metabolism of the matured transcript (reviewed in Tian & Manley, 2017).

Following cleavage, the canonical poly(A) polymerase (cPAP) is recruited to the cleavage site and catalyses the untemplated addition of adenosines to the 3' end of the cleaved mRNA. Once 11–14 adenosines have been added, nuclear poly(A) binding protein (PABPN) is able to bind the nascent poly(A) tail (Meyer *et al.*, 2002). This binding stimulates the activity of the cPAP by increasing its affinity for the RNA, switching the cPAP from a processive to a distributive activity (Kerwitz *et al.*, 2003). Additionally, the binding of PABPN to the nascent poly(A) tail restricts the binding of the CPSF to the PAS sequence, further increasing the specificity of the CPSF to PAS (Kühn*et al.*, 2009). In humans and plants, the elongation of the poly(A) tail is stopped when it reaches a length of ~250 nucleotides (Kühn*et al.*, 2009; Kühn*et al.*, 2017; Jia *et al.*, 2022; Alles *et al.*, 2023). By binding to the nascent poly(A) tail, PABPN serves as a molecular ruler for poly(A) synthesis. In fact, the size limitation of the poly(A) tail is thought to be a consequence of the spherical conformation adopted by the PABPN cluster on the poly(A) tail that may displace the CPSF-cPAP-PABPN-mRNA complex (Keller *et al.*, 2000; Kühn*et al.*, 2009).

Besides its roles as a molecular ruler regulating the length of poly(A) extension during polyadenylation, PABPN has important functions within the nucleus and is an essential protein in higher eukaryotes (reviewed in Banerjee *et al.*, 2013). Notably, PABPN has a dual role in RNA stability. While the binding of the PABPN protects the 3' end from exonucleolytic decay,

PABPN is involved in RNA surveillance that mediates decay of faulty transcripts. Together with the nCBC, PABPN interacts with the PAXT complex, and triggers nuclear exosome-mediated decay of faulty pre-mRNAs, preventing their export from the nucleus (Meola *et al.*, 2016; Ogami *et al.*, 2017).

After processing, the fully mature mRNA can be exported from the nucleus to the cytoplasm (reviewed in Stewart, 2019 and Xie & Ren, 2020). Among other factors, nuclear export relies on the interaction between the nCBC and the ALY subunit of the TRanscription-EXport (TREX) complex. TREX complex mediates the translocation of bound mRNA through the nuclear pore complex. This interaction with nCBC, along with other components of pre-mRNA processing machinery, is thought to ensure that only properly processed mRNAs are exported to the cytosol (reviewed in Xie & Ren, 2019). Interestingly, the presence of a poly(A) tail of sufficient length is enough to trigger transcript export, indicating that the poly(A) tail is an important feature needed for proper mRNA export (Fuke & Ohno, 2008).

1.3. mRNP remodelling following nuclear export

Upon translocation to the cytoplasm, the composition of the exported mRNP is remodelled to prevent its re-entry into the nucleus. In yeast, mRNP remodelling upon nuclear export is catalysed by the DEAD-box RNA helicase Dbp5 (Tran *et al.*, 2007) Alternatively (or additionally), mRNPs can be remodelled by a pioneer round of translation involving the nCBC and PABPN, as shown in mammals (Ishigaki *et al.*, 2001; Chiu *et al.*, 2004; Saato & Maquat, 2009). This pioneer translation may facilitate the transition from a “nuclear” mRNP to a “cytosolic” mRNP adapted cytoplasmic processes, and serves as a final quality control step before mRNA enters bulk translation (reviewed in Maquat *et al.*, 2010). This mRNP remodelling involves replacing PABPN by its cytoplasmic counterpart, PABPC. Similarly, the nCBC is displaced and replaced by the eIF4F cap-binding complex.

1.3.1. The eIF4F cap-binding complex

The eIF4F cap-binding complex comprises mainly three core components: eIF4E, eIF4G, and eIF4A (reviewed in Merrick, 2015). eIF4E is the actual cap-binding protein, recognising and binding to the 5' cap structure of mRNAs. eIF4G acts as a scaffold protein, interacting with eIF4E and other initiation factors such as eIF3 and eIF4A, facilitating the assembly of the complete translation initiation complex. eIF4A, an RNA helicase, unwinds secondary structures in the 5' UTR of mRNAs, helping the ribosome in scanning for the start codon.

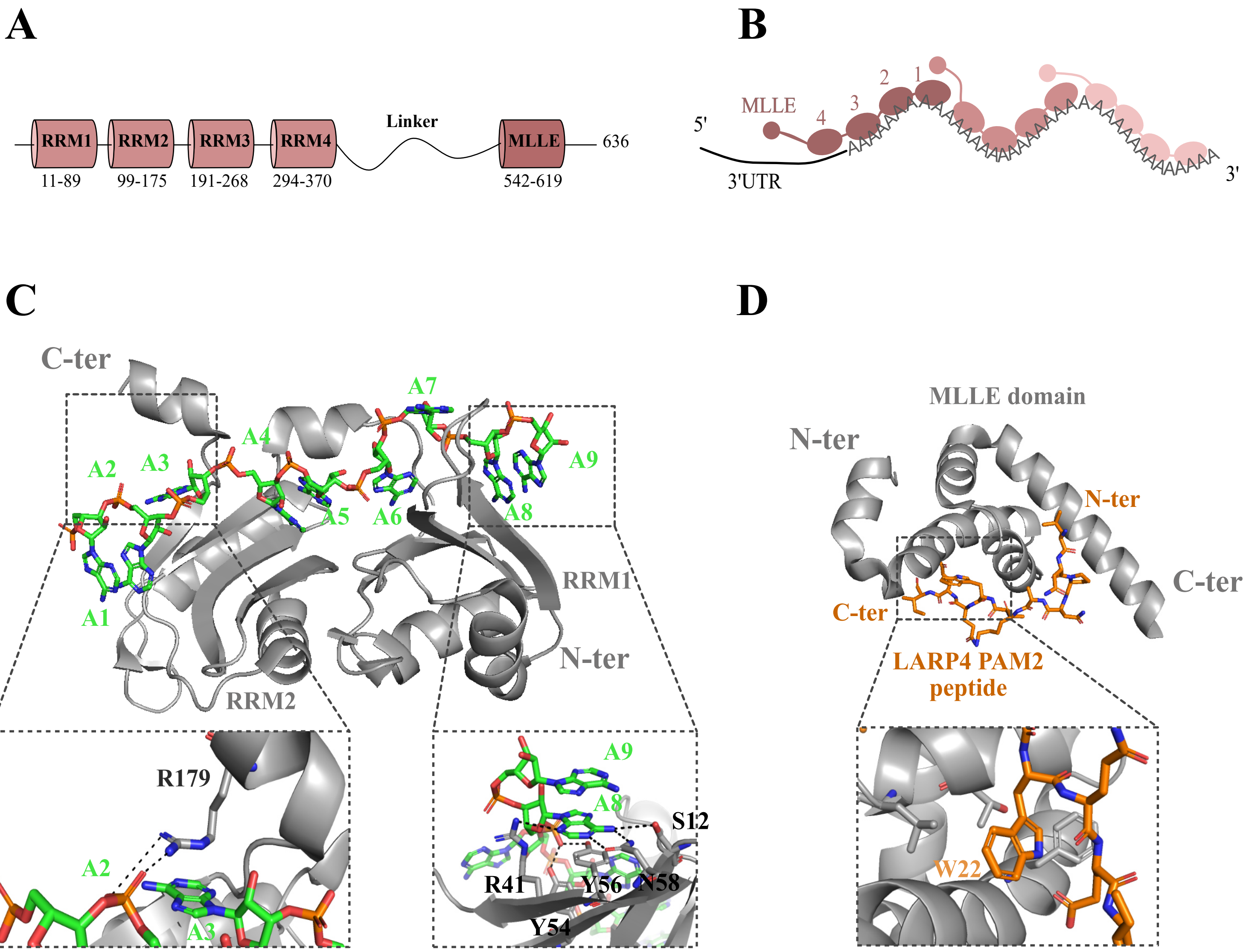

Figure 3. Molecular basis of PABPC interactions.

A) Domain organisation of human PABPC1. Its N-terminal region is composed of 4 consecutive RRM domains. Its C-terminal region consists of a proline-rich linker involved in PABPC multimeristation and a C-terminal domain containing the MLLE domain involved in the interaction with PAM2 motifs of PABPC-interacting proteins. **B)** Schematic of the organisation of PABPC1 binding on the polyadenylated mRNA. Consecutive binding of PABPCs on the poly(A) tail and oligomerisation creates a succession of arches. The relaxed specificity of RRM3-RRM4 enables the PABPC1 to bind AU-rich sequences within the 3'UTR. Modified from Schäfer *et al*., 2019. **C)** Crystal structure of RRM1-2 of PABPC1 (grey cartoon) in complex with an oligo(A) RNA (green sticks). Interactions between the PABPC and the oligo(A) are multipartite. The linkers connecting the RRM domains form α-helices (left inset) that, together with the β-sheets present in each RRM domain (right inset), create a clamp-like structure that binds and holds the RNA. Putative hydrogen bonds are represented as dashed black lines. Structure from Safaee et al., 2012 (PDB: 4F02). D**)** Crystal structure of MLLE domain of PABPC1 (grey cartoon) in complex with the PAM2 motif of LARP4 (orange sticks). The PAM2 peptide wraps around the MLLE domain of PABPC1 through multiple hydrophobic interactions. Particularly, a tryptophan residue (inset) replaces a phenylalanin highly conserved in PAM2 motifs of other proteins, and is embedded in a hydrophobic pocket within the PABPC1 MLLE domain. Structure from Yang et al., 2010 (PDB: 3PKN).

In plants, these components have several isoforms, which add a layer of complexity and regulation to the translation initiation process (Patrick & Browning, 2012). For instance, multiple isoforms of eIF4E and its variant eIFiso4E are found. These isoforms differ in their affinity for the cap structure and their interaction with other initiation factors (Kropiwnicka *et al*., 2015). The eIF4G and eIFiso4G isoforms also exhibit distinct interaction patterns and functional roles, further diversifying the regulatory mechanisms of translation initiation in plants. This diversity allows plants to finely tune translation in response to various cellular signals and stress conditions (Gallie & Browning, 2001; Wang et al., 2022).

1.3.2. The cytoplasmic PABPC

Domain organisation

The N-terminal region of PABPC contains four RNA Recognition Motif (RRM, **Figure 3A**), which are essential motifs involved in the poly(A) tail binding (Baer & Kornberg, 1983). While the footprint of the yeast PABPC Pab1 is 27 nucleotides, poly(A) tail as short as 12As can be bound by the module composed of RRM1-RRM2 (Baer & Kornberg, 1980; Sachs *et al*., 1987, Deo *et al*., 1999, Safaee *et al*., 2012). Interestingly, PABPC can bind to AU-rich sequences due to the relaxed specificity of RRM3-RRM4 towards oligo(A) sequences (**Figure 3B**) (Sladic *et al*., 2004; Kini *et al*., 2016; Webster *et al*., 2018). Because the 3' UTR is enriched in AU-rich sequences, the relaxed specificity of RRM3-RRM4 may allow PABPC binding within the 3' UTR, particularly upon shortening of the poly(A) tail (Webster *et al*., 2019). This non-canonical binding may hide 3'UTR *cis*-elements, thereby hindering their recognition by RNA Binding proteins (RBP). Currently, there is no available structure for the entire PABPC in complex with a poly(A) tail, and the full comprehension of the interactions involved in poly(A) tail binding remains incomplete. Nevertheless, the crystal structure of RRM1-2 in association with a short oligo(A) revealed that poly(A) specificity is mediated by multiple binding interfaces (**Figure 3C**). Both the RRM and the linkers connecting them are able to establish substantial contacts with the RNA phosphate backbone and/or adenine base. These interactions involve hydrogen bonds and base stacking, with the latter occurring between the adenine base and aromatic amino acids present in the RRM domain of PABPC. Besides binding the poly(A) tail, PABPC RRM1-2 bridge the 3' end to the 5' end by directly interacting with the eIF4F cap-binding complex (Imataka *et al*., 1998).

The C-terminal region of PABPC contains a conserved Mademoiselle (MLLE, **Figure 3A**) domain. This domain is recognised by proteins with a PAM2 motif (poly(A)-binding protein

interacting motif 2, reviewed in Xie *et al.*, 2014) (**Figure 3D**). In between the MLLE domain and the RRMs, an unfolded linker contains a proline rich sequence that mediates oligomerisation of PABPC on the poly(A) tail (Sawazaki *et al.*, 2018). The oligomerisation of PABPC creates a series of consecutive arches, and this architecture can be bound by *trans*-acting factors such as the PAN2-PAN3 deadenylase complex (Schäfer *et al.*, 2019).

PABPC isoforms

In yeast and *Drosophila*, the genome encodes a single PABPC (Pab1 and PABP, respectively), while humans and plants have undergone significant *PABPC* gene duplication (Gallie & Liu, 2014; Smith *et al.*, 2014). Human PABPC includes PABPC1, X-linked PABP, iPAB, the testis-specific tPABP, and the embryonic ePAB. PABPC1 is the most abundant and is expressed in somatic cells, and its molecular functions are particularly well characterised. Similarly, ePAB is an important regulator of translational control, and its role in regulating cytoplasmic polyadenylation has been extensively studied in *Xenopus laevis* oocytes (Ozturk *et al.*, 2019). Plant PABPCs have been sorted into 4 different classes (Belostotsky, 2003). Class I PAB3 and PAB5 expression is limited to reproductive tissues. Class II PAB2, PAB4 and PAB8 are highly and ubiquitously expressed and are proposed to serve as the main PABPCs. Class III PAB6 and PAB7 are specifically expressed and temporally regulated in maturing pollen, with an expression maximum in mature pollen (Honys & Twell, 2004). Finally, Class IV PAB1 is barely expressed and was denoted as an "orphan gene". Interestingly, PAB3, PAB6 and PAB7 are specifically expressed in the male gametophyte, while PAB5 is expressed during both male and female gametophytes, but is preferentially expressed in pollen (Belostotsky & Meagher, 1996; Belostotsky, 2003, Honys & Twell, 2004). Particularly, PAB3 is highly expressed in the tapetum, a cell layer inside the anthers that provides nutrients and produces substances essential for pollen development and maturation (reviewed in Ariizumi & Toriyama, 2011 and Ma *et al.*, 2021). Conversely, expression of ubiquitous PAB2/4/8 decreases upon pollen maturation (Honys & Twell, 2004). Given the redundancy in PABPC expression in *Arabidopsis* pollen, the implications of such an intricate expression pattern on the modulation of poly(A) tail length and, more broadly, on mRNA metabolism, are intriguing.

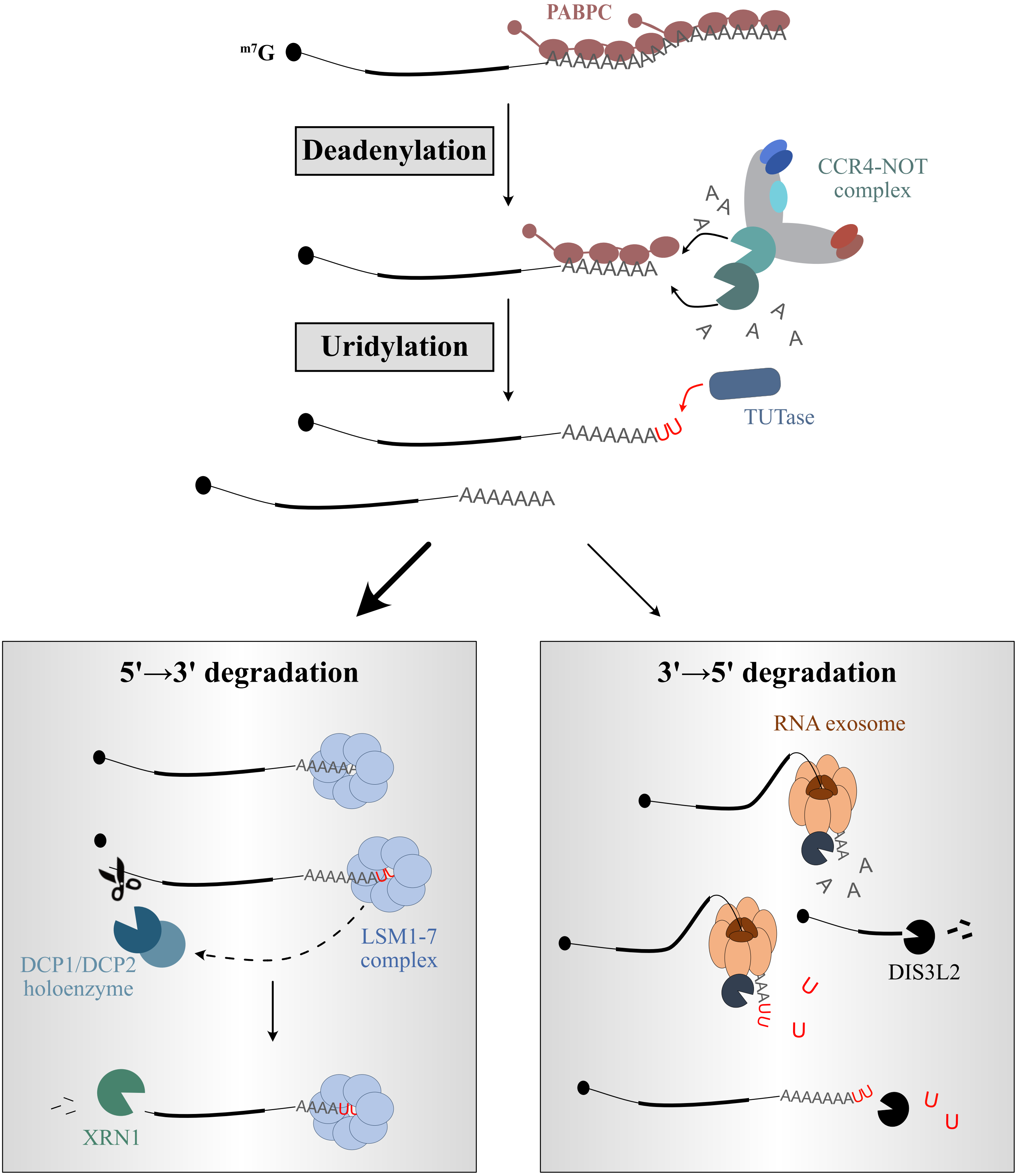

Figure 4. Overview of the cytoplasmic bulk mRNA degradation in humans.
In the cytoplasm, mRNA can be deadenylated, a step mainly catalysed by the CCR4-NOT complex. Oligoadenylated 3' ends can be uridylated at this step, and this event will further affect mRNA metabolism. Whether or not they are uridylated, oligoadenylated mRNAs can be degraded either by the 5' end or by the 3' end. The 3'→5' decay pathway is minor and catalysed by the RNA exosome and its cofactors. mRNA uridylation can enhance the recruitment of the RNA exosome and other factors such as DIS3L2. The main decay pathway is triggered by the recruitment of the heptameric LSM1-7 complex, that binds the oligo(A) tail, and has a higher affinity for uridylated ones. Through a network of interaction, LSM1-7 recruits the decapping complex, which will hydrolyse the 5' cap. Uncapped mRNAs are quickly degraded by the 5'→3' exoribonuclease XRN1.

2. Deadenylation is an essential process regulating mRNA fate

Deadenylation, *i.e.*, the shortening of the poly(A) tail, is critical for controlling gene expression and may represent a rate-limiting step in the decay of many mRNAs (Herrick *et al.*, 1990; Decker & Parker, 1993; Goldstrohm & Wickens, 2008; Eisen *et al.*, 2020; Audebert *et al.*, 2023; Pavanello *et al.*, 2023). By systematically shortening the poly(A) tail, deadenylation affects mRNA stability and the ability of the translation machinery to recognise and translate the mRNA into proteins. Deadenylation is carried out by specialised enzymes known as deadenylases, which efficiently trim the poly(A) tail. In this chapter, I will introduce the consequences of mRNA deadenylation, *i.e.*, the initiation of mRNA decay, and will briefly review the proteins involved in mRNA deadenylation, their inherent specificities, their biological functions and their regulations.

2.1. Cytosolic mRNA turnover is initiated by deadenylation

In mammals and yeast, deadenylation typically occurs as a biphasic process (Tucker *et al.*, 2001; Yamashita *et al.*, 2005; Yi *et al.*, 2018). In the first phase, mRNAs undergo a rapid and sequential shortening of their poly(A) tails. This is followed by a second phase in which the length of the poly(A) tails varies greatly, due to progressive deadenylation and dissociation of PABPCs. The transition to the second phase is crucial, as it is thought to disrupt the closed loop structure that connects the 5' and 3' ends of the mRNA, thus exposing the mRNA to decapping and exonucleolytic degradation (**Figure 4**). Additionally, the displacement of PABPC leaves the mRNA vulnerable to 3'→5' decay.

2.1.1. 5'→3' degradation results from a strong interplay between deadenylation and decapping

5'→ 3' degradation is regarded as the main pathway for bulk mRNA decay in eukaryotes. The key steps are the removal of the ^{m7}G cap, or decapping, followed by the 5'→3' degradation of uncapped and unprotected transcripts. Decapping is catalysed by the hydrolase DCP2. DCP2 displays very weak activity by itself and needs to interact with DCP1 to form the active DCP1/ DCP2 holoenzyme. In general, activity of the DCP1/DCP2 holoenzyme is intricately modulated by a host of decapping activators and translation inhibitors that are conserved in eukaryotes (see **Table1**) (reviewed in Vidya & Duchaine, 2022). In metazoans and plants, DCP1 and DCP2 only weakly interact together and need to associate with the decapping activator EDC4 (VCS in plants) to form a stable trimeric complex with robust decapping activity (Xu *et al*., 2006; reviewed in Xu & Chua, 2011 and Arribas-Layton *et al*., 2013). Other essential decapping activators are LSM1-7 and PAT1. Early results revealed a coupling between deadenylation and decapping (Decker & Parker, 1993; Hsu & Stevens, 1993; Muhlrad *et al*., 1994). Indeed, targets of 5'→3' decay are often mRNAs with short poly(A) tails that arise from deadenylation. This indicates that deadenylation precedes decapping. Later, it was proposed that two factors, PAT1 and the LSM1-7 complex, accounted for the coupling between deadenylation and decapping. Indeed, depletion of either PAT1 or the LSM1-7 strongly inhibits decapping and triggers the accumulation of capped and deadenylated mRNAs (Bouveret *et al*., 2000; Tharun *et al*., 2000). This coupling is readily explained by the fact that the LSM1-7 preferentially associates with deadenylated mRNAs and that it interacts with the scaffold protein PAT1, which in turn recruits the decapping holoenzyme DCP1/DCP2. Of note, the LSM1-7 complex has more affinity for uridylated oligo(A) tails, functionally linking uridylation to decay (Chowdhury *et al*., 2007; Song & Kiledjian, 2007). PAT1 also interacts with the RNA helicase and translation inhibitor/decapping activator DDX6/Scd6. Interestingly, DDX6 interacts with NOT1, the scaffold subunit of the CCR4-NOT deadenylase complex, and this may serve as an alternative platform to couple deadenylation to decapping (Vidya & Duchaine, 2022).

In addition to the recruitment of the decapping holoenzyme, yeast and human PAT1 recruits the 5'→3' exoribonuclease XRN1 that rapidly degrades 5' unprotected mRNAs (Nissan *et al*., 2010; Charenton *et al*., 2017). XRN1 belongs to the XRN family, which is characterised by the presence of one cytoplasmic member, XRN1/Pacman, and one or more nuclear members, namely XRN2 and XRN3 (Nagarajan *et al.,* 2013). While XRN1 is known for its role in bulk mRNA decay and turnover of various ncRNAs, XRN2 and XRN3 are primarily involved in rRNA processing and the decay of nuclear ncRNAs. Interestingly, higher plants lack an XRN1 ortholog, but the *Arabidopsis* genome contains three homologs of XRN2, namely XRN2, XRN3 and XRN4 (Kastenmayer & Green, 2000). Notably, XRN4, despite being a homolog of XRN2, does not complement the *xrn2* mutation in yeast. Instead, it effectively complements a *xrn1* mutation, suggesting that while structurally similar to yeast Xrn2, XRN4 functions as a homolog of yeast Xrn1 (Kastenmayer *et al*., 2001). Taken together, the interaction between the deadenylated mRNAs, the PAT1-LSM1-7 complex and the 5'→3' decay machinery efficiently bridges deadenylation to decapping and rapid decay.

Data from high-throughput sequencing of 5’ uncapped mRNAs in yeast, humans and plants revealed that decay intermediates have a 3-nucleotides periodicity, and that XRN1/4 are involved in this pattern (Pelechano *et al*., 2015; Yu *et al*., 2016, Carpentier *et al*., 2020). These data suggest that XRN1/4 proteins follow the last translating ribosome and are involved in co-translational decay. Such mechanism was observed in *S. cerevisiae*, *S. pombe* and *A. thaliana*, and is likely conserved in all eukaryotes. Thus, the 5’→3’ polarity of decay may be essential to ensure that the last translocating ribosome can complete translation, preventing the formation of truncated proteins.

2.1.2. 3’→5’ degradation is a more specialised pathway of mRNA decay

Unprotected mRNA 3’ends, whether they arise from endonucleolytic cleavage or deadenylation, are a substrate for 3’→5’ exoribonucleases (reviewed in Janyuszyk & Lima, 2014 and Lange & Gagliardi, 2022). The RNA exosome complex is structured around a core of nine RNase PH-like proteins, forming what is known as Exo9. This Exo9 core is present in both the cytoplasm and the nucleus, associating with distinct cofactors inherent to each compartment. Initially, due to its resemblance to bacterial polynucleotide phosphorylase (PNPases), the Exo9 core was thought to be catalytically active in eukaryotes. Recombinant proteins from the Exo9 core even demonstrated 3’→5’ exoribonuclease activity (Mitchell *et al*., 1997). However, it was later found that most of the residues necessary for functional catalytic activity are missing, and further studies have invalidated the activity of Exo9 in human and yeast cells (Liu *et al*., 2006; Dziembowsky *et al*., 2007). In contrast, in plants, the Exo9 protein RRP41 has a phosphorolytic activity and Exo9 is able to degrade RNA (Sikorska *et al*., 2017). Despite this plant specificity, the main catalytic activity of the exosome is provided by exoribonucleases recruited to the core Exo9, namely RRP6, RRP44 (DIS3), and DIS3L, the latter being conserved only in mammals. RRP6 and RRP44 are mostly associated with the nuclear Exo9 and involved in various nuclear RNA decay processes (reviewed in Kilchert *et al*., 2016), while DIS3L is associated to the cytoplasmic exosome (Staals *et al*., 2010; Tomecki *et al*., 2010).

Both nuclear and cytoplasmic exosome functions in collaboration with targeting complexes that promotes the recruitment of the exosome to its targets. In the cytoplasm, the SKI complex is essential for the activities of the exosome (Anderson & Parker, 1998; Van Hoof *et al*., 2000; Araki *et al*, 2001; Halbach *et al*, 2013). Together, the cytoplasmic exosome and the SKI complex are involved in mRNA turnover and are critical actors of co-translational surveillance pathways of the nonsense-mediated decay (NMD), non-stop decay (NSD) and no-go decay

(NGD) (reviewed in Shoemaker & Green, 2012 and Roy & Jacobson, 2013; Tuck *et al.*, 2020; Kögel *et al.*, 2022). Loss of SKI components has no major impact of mRNA steady state levels, yet mutations in SKI2 and the 5'→3' exoribonuclease XRN1 are synthetic lethal, suggesting functional redundancy between the 5'→3' and the 3'→5' decay pathways (Johnson & Kolodner, 1994). Results from our lab and others, suggest the importance of the exosome in degrading mRNA decay intermediates to prevent the production of illegitimate small interfering RNAs (siRNAs) (Lam *et al.*, 2015; Zhao & Kunst, 2016; Lange *et al.*, 2019). Additionally, transcriptome-wide analysis suggest that the exosome is involved in the degradation of uridylated transcripts in human cells (Lim *et al.*, 2014).

DIS3L2 is a homolog of DIS3 that lacks the PIN domain necessary for the interaction with Exo9 and thereby does not interact with the core exosome. DIS3L2 is present in fission yeast and metazoans, and multiple studies investigated its role as a 3′→5′ exoribonuclease targeting mRNAs (Malecki *et al.*, 2013; Lubas *et al.*, 2013; Lim *et al.*, 2014; Thomas *et al.*, 2015; Da Costa *et al.*, 2019; Wu *et al.*, 2023). Besides its roles in mRNA degradation, DIS3L2 plays a pivotal role in the quality control of non-coding RNAs, including unprocessed and highly structured RNAs (Chang *et al.*, 2013; Faehnle *et al.*, 2014; Eckwahl *et al.*, 2015; Łabno *et al.*, 2016; Pirouz *et al.*, 2016; Reimão-Pinto *et al.*, 2016; Ustanienko *et al.*, 2016; Pirouz *et al.*, 2019; Pirouz *et al.*, 2020). The activity of DIS3L2 is enhanced by 3' uridylation, both for non-coding RNAs and mRNAs. It is interesting to note that DIS3L2 is absent from *S. cerevisiae*, which is the only known eukaryote to date where uridylation is not present.

The ability of the plant ortholog of DIS3L2 to degrade mRNAs was identified more than 15 years ago (Zhang *et al.*, 2010). SUPPRESSOR OF VARICOSE (SOV) is a 3'→5' exoribonuclease and was initially discovered as a suppressor of the developmental phenotype caused by a mutation in the decapping factor VARICOSE (VCS), the plant ortholog of EDC4 (Zhang *et al.*, 2010). The study noted severe phenotypic defects in *Arabidopsis* from the Col-0 ecotype mutated in *VCS*, whereas those from the Landsberg (Ler) accession displayed milder phenotypes. The study revealed the presence of a point mutation in *SOV* of Col-0, likely affecting the function of the protein. SOV activity is redundant with both the exosome and the 5'→3' decay pathway (Sorenson *et al.*, 2018). Whether the activity of SOV is stimulated by uridylation of its target RNAs, as is DIS3L2, is not yet known.

While involved in more specialised processes, the 3′→5′ decay represents an important layer of mRNA degradation. Redundancy among cytoplasmic decay pathways, including 5′→3′ decay mediated by XRN1/XRN4, 3′→5′ exoribonuclease DIS3L2/SOV, and the cytoplasmic exosome along with the SKI complex, plays a pivotal role in the swift and proper elimination of mRNAs following the initiation of their decay by processes such as decapping, deadenylation, or endonucleolytic cleavage. In plants, this redundancy prevents the triggering of post-transcriptional silencing (PTGS) (Zhang *et al.*, 2015).

2.2. Overview of "secondary" roles in deadenylation

The CCR4-NOT complex is the main complex involved in mRNA deadenylation, and will be described later (see **Introduction 2.3**). In contrast, we designate other proteins with the capacity to degrade poly(A) tails as "secondary" deadenylases. This distinction sets the stage for a comprehensive overview, in which the secondary roles in deadenylation emerge as important contributors beyond the primary CCR4-NOT complex.

2.2.1. PARN

The Poly(A) RiboNuclease (PARN) deadenylase is a member of the DEDD exonuclease family, characterised by the presence of three aspartic acids and a glutamic acid as catalytic residues (Zuo & Deutscher, 2001; Goldstrohm & Wickens, 2008). PARN was one of the very first deadenylase identified, and is present in most eukaryotes, with the notable exceptions of *Saccharomyces cerevisiae* and *Drosophila melanogaster* (Parker & Song, 2004).

PARN functions as a homodimer, a formation that is obligatory for its structural (*e.g.*, RNA-binding) and catalytic activities (Wu *et al.*, 2005), and is found both in the cytoplasm and the nucleus, with a predominance in the nucleolus (Yamashita *et al.*, 2005; Berndt *et al.*, 2012). Interestingly, PARN has a high affinity for the ^{m7}G-cap, and this interaction stimulates the processivity of PARN. However, the presence of cap-binding complexes or PABPs inhibits its activity (Körner & Wahle, 1997; Körner *et al.*, 1998; Dehlin *et al.*, 2000; Gao *et al.*, 2000; Martînez *et al.*, 2001; Balatsos *et al.*, 2006). Initially thought to regulate bulk mRNA deadenylation due to its cap-binding capacity, further studies in mammalian systems revealed that PARN does not participate in the global deadenylation of mRNAs (Yamashita *et al.*, 2005; Lee *et al.*, 2012; Son *et al.*, 2018; Yi *et al.*, 2018). This suggests a more nuanced role for PARN in mRNA deadenylation, likely dependent on specific mRNA targets and cellular conditions. Instead, the primary substrates for PARN are non-coding RNAs (ncRNAs) (Son *et al.*, 2018). PARN is involved in the processing of a plethora of ncRNA species, including 18S rRNAs, small nucleolar RNAs (snoRNAs), the human telomerase RNA component (hTR), small Cajal body-specific RNAs (scaRNAs), PIWI-interacting RNAs (piRNAs), Y RNAs, and microRNAs (miRNAs) (Berndt *et al.*, 2012; Yoda *et al.*, 2013; Dhanraj *et al.*, 2015; Moon *et al.*, 2015; Nguyen *et al.*, 2015; Tseng *et al.*, 2015; Boyraz *et al.*, 2016; Izumi *et al.*, 2016; Shukla *et al.*, 2016; Tang *et al.*, 2016; Montellese *et al.*, 2017; Shukla and Parker, 2017; Tseng *et al.*, 2018).

In *Arabidopsis thaliana*, two PARN-like proteins are encoded, namely AtPARN/AHG2 and RRD1. AHG2 is crucial for the initial stages of development and was proposed to selectively deadenylates a small subset of embryo-specific mRNAs (Chiba *et al.*, 2004; Reverdatto *et al.*, 2004). Yet, the suppression of the mitochondrial poly(A) polymerase AGS1 rescued all the phenotypes of an *ahg2* hypomorphic mutant, suggesting that a role in mitochondrial mRNA deadenylation, rather than cytoplasmic mRNA deadenylation, was responsible for the embryo-lethality phenotype (Hirayama *et al.*, 2014, Kanazawa *et al.*, 2020). RRD1, the second PARN-like deadenylase, is not embryo-lethal but is also involved in mitochondrial mRNA deadenylation (Hirayama, 2021; Otsuka *et al.*, 2021). Consistent with this, AHG2 and RRD1 are both efficiently targeted to mitochondria. Hence, PARN-like proteins and AGS1 cooperate and directly influence the poly(A) tail length of mRNA in plant mitochondria, where poly(A) signals function as a degradation tag. To date, a direct role in the deadenylation of cytosolic transcripts has not been shown.

2.2.2. The PAN2-PAN3 complex

Rather counterintuitively, depletion or inactivation of the yeast Pab1/PABPC results in mRNAs with an increased average poly(A) tail length (Sachs & Davis, 1989; Caponigro & Parker, 1995; Boeck *et al.*, 1996; Mangus *et al.*, 2004; Wolf & Passmore, 2014). This suggests a deadenylation activity dependent on the presence of the PABPC. This PABPC-enhanced deadenylase activity was later found to be catalysed, at least in part, by a complex composed of PAN2 and PAN3 (Boeck *et al.*, 1996; Brown *et al.*, 1996, Schäfer *et al.*, 2019).

PAN2 and PAN3 form a heterotrimeric complex in a 1:2 stoichiometry (Jonas *et al.*, 2014; Schäfer *et al.*, 2014; Wolf *et al.*, 2014). In this complex, PAN2 serves as the catalytic subunit, featuring a conserved DEDD catalytic domain. PAN3, on the other hand, imparts poly(A) tail and PABPC specificity. It achieves this through direct binding to the poly(A) tail via its zinc finger domain and by linking the MLLE domain of PABPC with its PAM2 motif (Wolf *et al.*, 2014, Schäfer *et al.*, 2019). Intriguingly, the intrinsic structural conformation of the poly(A) tail within PAN2's active site further mediates the complex's specificity for poly(A) tails (Tang & Passmore, 2019). PAN2-PAN3 is often regarded as the initiator of the biphasic deadenylation process, as it targets mainly long poly(A) tailed mRNAs (Yamashita *et al.*, 2005, Wolf &

Passmore, 2014; Yi *et al*., 2018). The substrate specificity of PAN2-PAN3 is explained by its interaction with oligomerised PABPC. The necessity of PABPC oligomerisation for recruiting PAN2-PAN3 suggests a preference for long poly(A)-tailed mRNA, which can bind two or more PABPCs (Schäfer *et al.*, 2019).

The PAN2-PAN3 complex is present across higher eukaryotes, with the exception of flowering plants, and is not essential in any of the organisms studied so far (Parker & Song, 2004; Pavlopoulou *et al*., 2013; Wahle & Winkler, 2013; Wolf & Passmore, 2014). Moreover, inactivating PAN2-PAN3 in humans has only a limited impact on the accumulation of poly(A) tails longer than 150As, and has no major impact on mRNA steady-state levels (Yi *et al*., 2018). This suggests that other factors account for bulk mRNA deadenylation.

2.2.3. CAF1-like and CCR4-like proteins

Bulk mRNA deadenylation is catalysed by the CCR4-NOT complex. The deadenylation activity of the complex is mediated by CCR4 and CAF1 proteins that associate to form the nuclease module of the CCR4-NOT complex. Various CAF1-like and CCR4-like homologs have been identified based on their homology with the canonical CAF1 and CCR4 proteins (Dupressoir *et al*., 2001; Tucker *et al*., 2001; Pavlopoulou *et al*., 2013), and their roles as deadenylases are actively studied.

CAF1z/TOE1, a distant homolog of yeast Caf1, exhibits deadenylation activity *in vitro* (Wagner *et al*., 2007). However, functionally, it is more closely related to PARN than to CAF1 and does not affect mRNA deadenylation. Instead, CAF1z/TOE1 is involved in the maturation of ncRNAs, including snRNAs, snoRNAs, and hTR (Lardelli *et al*., 2017; Son *et al*., 2018; Lardelli & Lykke-Andersen, 2020).

Higher eukaryotes also have three paralogs that share conserved features with the canonical CCR4 proteins: PDE12, Angel, and Nocturnin (Dupressoir *et al*., 2001). PDE12 displays *in vitro* deadenylase activity, efficiently targeting and deadenylating mitochondrial RNAs (Rorbach *et al*., 2011; Pearce *et al*., 2017). Its *Drosophila* ortholog, named 3635, does not associate with the core proteins of the CCR4-NOT complex and is not involved in mRNA deadenylation (Temme *et al*., 2010).

In contrast, human ANGEL2 forms a heterodimer with deadenylase activity when it associates with CAF1z. This activity, however, is not inherent to ANGEL2 itself, as purified recombinant ANGEL2 does not show deadenylation activity *in vitro* (Wagner *et al*., 2007; Temme *et al*., 2010; Pinto *et al.*, 2020). Instead, Angel proteins exhibit 2’-3’ cyclic phosphatase activity and are involved in the non-canonical processing of various RNA species (Pinto *et al.*, 2020; Clemente *et al.*, 2022).

Identified as a circadian clock-regulated gene in *Xenopus*, Nocturnin (NOCT) displays a peak of expression at night (Green & Besharse, 1996). Early studies demonstrated NOCT's catalytic activity and its preference for poly(A) substrates (Baggs & Green, 2003), which was later confirmed in mice (Garbarino-Pico *et al.*, 2007; Niu *et al.*, 2011). In *Drosophila*, NOCT was found to be stably associated with the core CCR4-NOT complex (Temme *et al.*, 2010), leading to the hypothesis that it forms an alternative CCR4-NOT complex, with a rhythmic activity regulated by the circadian clock. While NOCT's involvement in key metabolic and developmental functions is well documented (reviewed in Hughes *et al.*, 2018), its direct mRNA targets have not been formally identified. The notion of NOCT as a cytoplasmic mRNA deadenylase was recently challenged by studies showing that recombinant NOCT lacks deadenylation activity *in vitro*, is targeted to the mitochondria, possesses 2′-phosphatase activity and has NADP+ and NADPH as its primary substrates (Abshire *et al.*, 2018; Estrella *et al.*, 2018; Estrella *et al.*, 2019; Laothamatas *et al.*, 2020). In *Arabidopsis*, the orthologue of NOCT, named HESPERIN (HESP) regulates the mRNA steady-state levels of circadian clock genes and the recombinant protein was proposed to have deadenylation activity *in vitro* (Delis *et al.*, 2016). However, no catalytic mutant was used as a negative control in those assays and given the recent discoveries on NOCT activity, the role of HESP in mRNA deadenylation may have to be reassessed with an experimental framework that undoubtedly characterises its activity.

Altogether, recent advancements in the study of CAF1-like and CCR4-like proteins have revealed that, despite the relative conservation of canonical domains involved in poly(A) tail removal, they are not major, if at all, regulators of cytoplasmic mRNA deadenylation. Rather, the canonical CAF1 and CCR4 account for the majority of deadenylation occurring in eukaryotes.

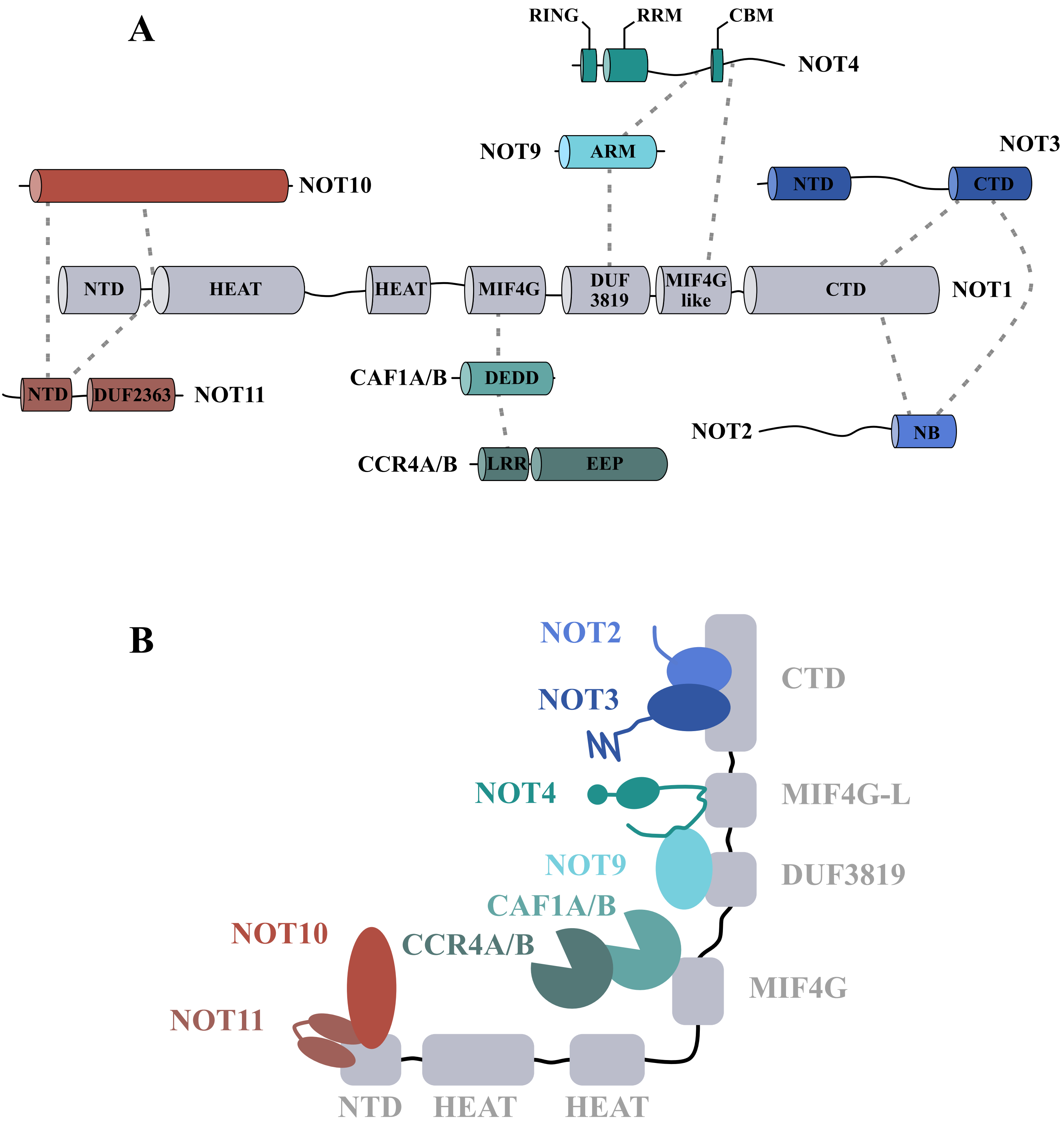

Figure 5. Domain organisation and architecture of the human CCR4-NOT complex. **A)** Representation of the interaction networks between CCR4-NOT subunits in humans. Interactions are indicated as grey dashed lines. Black lines represent intrinsically disordered regions (IDRs) contributing to structural flexibility of the proteins. Coloured boxes represent the functional modules and folded domains. The human 433 first amino acid of NOT4 binds to the C-terminal sequence of NOT1 in an unknown fashion (Albert *et al*., 2000). Because an IDR in yeast NOT4 binds the first HEAT-repeat unit of the NOT1 C-terminal region (Bhaskar *et al*., 2015), a similar interaction is depicted although it has not been experimentally validated. **B)** Cartoon representation of the assembled CCR4-NOT complex in humans. IDR are represented as black or colored lines. Figures are adapted from Collart, 2016 and Pavanello *et al*., 2023.

2.3. The CCR4-NOT complex is the main deadenylase

2.3.1. Composition and organisation of the CCR4-NOT complex

The CCR4-NOT complex is assembled around NOT1, the central scaffold protein (**Figure 5A**). NOT1 is composed of several structured domains separated by intrinsically disordered regions (IDRs) that promote flexibility of the protein, necessary to connect its factors and to position the mRNA optimally (Raisch *et al.*, 2019). This high intrinsic flexibility explains the difficulty to obtain high-resolution structures of the full CCR4-NOT complex (Ukleja *et al.*, 2016). Nonetheless, consequent efforts were made to characterise the overall structure of the CCR4-NOT complex by individually resolving the structure of its folded domains (reviewed in Pavanello *et al.*, 2023). NOT2 and NOT3 associate together via their NOT-box domain and bind NOT1's C-terminal domain (Boland *et al.*, 2013; Chen *et al.*, 2014; Mathys *et al.*, 2014; Bhaskar *et al.*, 2015). This ternary complex forms the NOT module. The NOT9/CAF40 subunit associates with CCR4-NOT by binding the DUF3819 with a conserved ARM domain (Chen *et al.*, 2014; Mathys *et al.*, 2014). The N-terminal module is composed of the NOT10 and NOT11 proteins closely bound together by two helical structures of the N-terminal domain (NTD) of NOT1 (Bawankar *et al.*, 2013; Mauxion *et al.*, 2013; Mauxion *et al.*, 2023). It was previously thought that the DUF2363 of NOT11 played a role in the interaction with NOT1, but in fact, it lies outside of the binding interface as a flexible antenna and mediates protein-protein interactions with other partners (Mauxion *et al.*, 2023). CAF1 contains a DEDD nuclease domain that directly interacts with the N-terminus leucine-rich repeat (LRR) domain of CCR4 (Basquin *et al.*, 2012; Chen *et al.*, 2021). This domain is connected to CCR4's C-terminal EEP (exonuclease, endonuclease, phosphatase) nuclease domain. The association between CAF1 and CCR4 forms the nuclease module of the CCR4-NOT complex. CAF1 interacts directly with NOT1 by binding to its MIF4G domain, thereby connecting the nuclease module to the rest of the complex (Petit *et al.*, 2012, Zhang *et al.*, 2021). Electron microscopy experiments demonstrated an L-shaped structure of the CCR4-NOT complex in yeast (**Figure 5B**), which, given the remarkable conservation of its components in eukaryotes, is expected to be similar in other organisms (Nasertorabi *et al.*, 2011).

Despite the conservation of core proteins within the CCR4-NOT, some divergence in the composition of the complex across eukaryotes can be observed. Specifically, *S. cerevisiae* lacks a functional homolog of the NOT10-NOT11 proteins, but rather contains an additional subunit, Caf130, which is not conserved in metazoans (Chen *et al.*, 2001). The yeast complex also

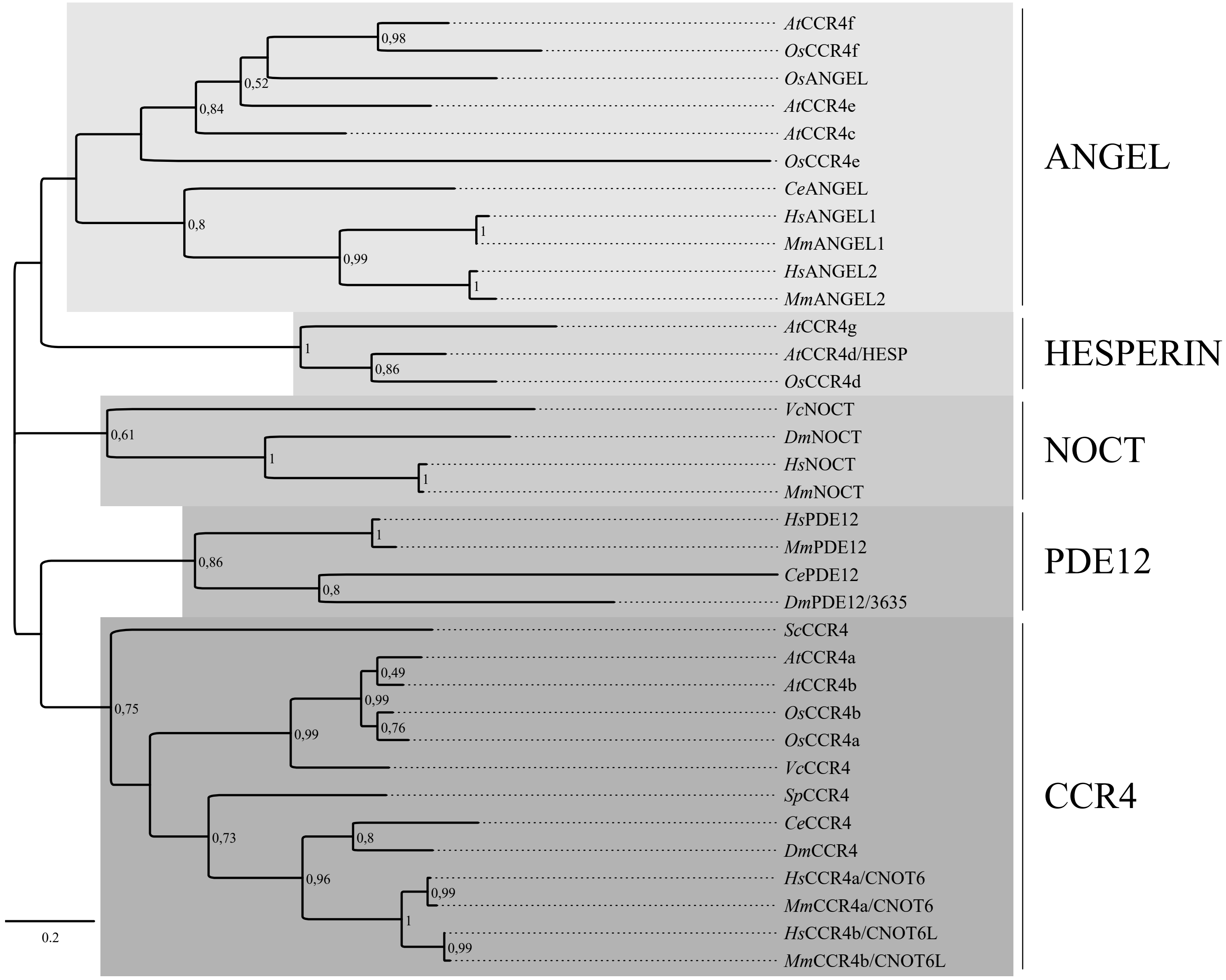

Figure 6. Phylogenetic relationship of CCR4-like proteins.
Cladogram of 35 CCR4-like proteins across eukaryotes. Full-length protein sequences were aligned using the MUSCLE algorithm implemented in MEGA (v.11, Tamura *et al.*, 2021). The maximum-likelihood tree, built in MEGA using the JTT substitution model with 100 bootstrap replicates, was further edited with FigTree (v.1.4.4, available at http://tree.bio.ed.ac.uk/software/figtree/). The scale bar indicates the number of substitutions per amino acid site. Bootstrap values greater than 50 are displayed at each node. Protein accessions used to construct the tree are provided in **Table S1**. *At*: *Arabidopsis thaliana*; *Ce*: *Caenorhabditis elegans*; *Dm*: *Drosophila melanogaster*; *Hs*: *Homo sapiens*; *Os*: *Oryza sativa*; *Mm*: *Mus musculus*; *Sc*: *Saccharomyces cerevisiae*; *Sp*: *Schizosaccharomyces pombe*; *Vc*: *Volvox carteri*

contains two orthologs of NOT3, named Not3 and Not5. Additionally, yeast Not4 is a stable component of the Ccr4-Not and associates with the CTD of Not1 (Bhaskar *et al.*, 2015). In humans and *Drosophila*, NOT4 is conserved but is only weakly associated with the complex, and is not thought to be part of the core complex (Lau *et al.*, 2009; Temme *et al.*, 2010; Keskeny *et al.*, 2019). In *Trypanosoma brucei*, the only CCR4-like protein that shares some homology with the canonical CCR4, lacks an LRR. As a consequence, it does not associate with CAF1 and the rest of the core complex. Thus, the complex in *Trypanosoma* was termed as CAF1-NOT complex (Schwede *et al.*, 2008; Erben *et al.*, 2014).

More importantly, vertebrates contain two paralogs of CCR4 and CAF1 proteins, named CCR4a/CCR4b and CAF1a/CAF1b respectively. Interestingly, despite high similarity, mouse CAF1a (CNOT7) is more stably associated with NOT1 than its paralog CAF1b (CNOT8) (Stoney *et al.*, 2022). This finding highlights the existence of different CCR4-NOT complexes that vary in their composition, and that may affect mRNA metabolism in distinct ways.

In plants, the gene expansion is even more important (Pavlopoulou *et al.*, 2013). 7 copies of CCR4 are present in *Arabidopsis* (CCR4a to CCR4g). Phylogenetic analysis based on 35 CCR4-like proteins in eukaryotes shows that only *At*CCR4a and *At*CCR4b cluster within the monophyletic group containing all the canonical CCR4 proteins known to be involved in bulk mRNA deadenylation (**Figure 6**). Other *Arabidopsis* CCR4 subunits cluster within the ANGEL family, suggesting that only *At*CCR4a and *At*CCR4b are involved in mRNA deadenylation. Curiously, *At*CCR4a and *At*CCR4b lack the LRR essential for the interaction with CAF1 in yeasts and humans (Dupressoir *et al.*, 2001). For this reason, CCR4 subunits in *Arabidopsis* were thought not to associate with the core CAF1-NOT complex as was described previously in *Trypanosoma*. However, this hypothesis was recently challenged. Studies of the CCR4-NOT architecture in *Oryza sativa* confirmed the loss of the essential LRR in plants (Chou *et al.*, 2017). Despite this, *Os*CCR4 and *Os*CAF1 directly interact through a conserved MYND-like domain within the N-terminal region of *Os*CCR4, which binds a PxLxP motif in *Os*CAF1. The MYND-like domain is conserved in *At*CCR4a/b, but no PxLxP motif is found in the *At*CAF1 orthologs. Nonetheless, *At*CCR4 associates with several *At*CAF1 paralogs in yeast-two-hybrid and co-immunoprecipitation experiments, suggesting the existence of a yet unknown binding interface bridging the nuclease together (Arae *et al.*, 2019). Similarly to CCR4, the CAF1 gene family presents an important gene duplication in plants, as 11 CAF1 paralogs were identified in *Arabidopsis.* They can be classified into 3 distinct clades that are proposed

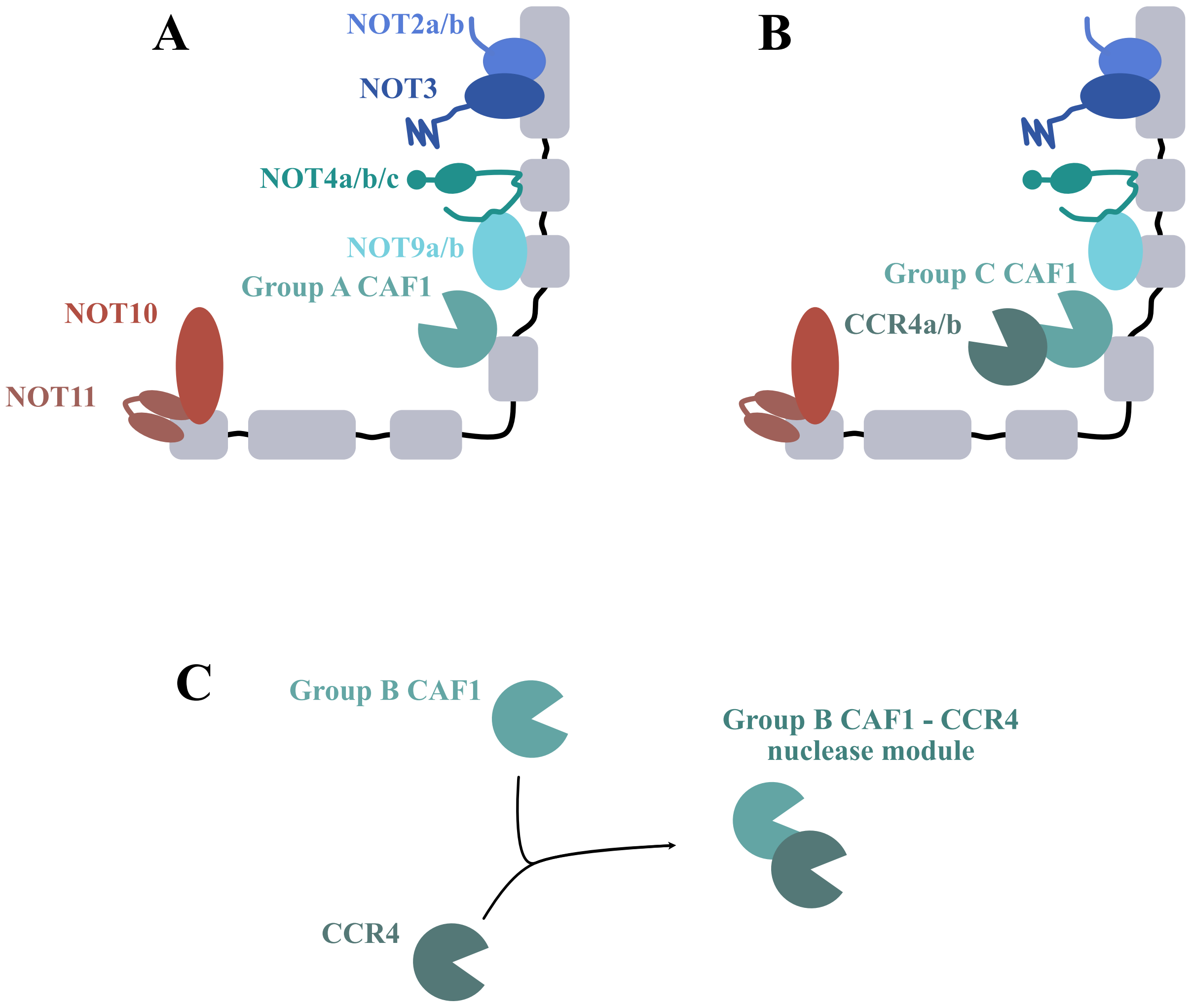

Figure 7. Possible diversity of the CCR4-NOT complex in plants.
Cartoon representation of the putative CCR4-NOT complex in plants. **A)** Group A CAF1 (CAF1a/b) associates with NOT1 but not with CCR4, and therefore may form a comparable CAF1-NOT complex similar to the one described in *Trypanosoma brucei*. **B)** Group C CAF1 (CAF1h/i/j/k) co-purifies with NOT1 and CCR4b in respective co-IPs (Arae *et al.*, 2019; Zhou *et al.*, 2020) and may form the main deadenylase complex together with CCR4a/b. **C)** Group B CAF1 (CAF1c/d/e/f/g) does not bind to NOT1, and may therefore act as a standalone deadenylase module, independantly of together with CCR4 proteins. However, the association between group B CAF1 and CCR4 was not studied so far. Many of the binding interfaces between NOT1 and its partners are not defined in plants, and are represented here as they occur in other eukaryotes (see **Figure 5**).

to be evolutionarily and functionally divergent from one another (Chou *et al.*, 2017; Arae *et al.*, 2019):

- group A includes CAF1a and CAF1b, which associates with NOT1 but not with the canonical CCR4 paralogs CCR4a/b. As they are not constitutively expressed, group A CAF1 are thought to associate with the CCR4-NOT complex only in certain specific conditions;
- group B includes CAF1c, CAF1d, CAF1e, CAF1f and CAF1g. They do not associate with NOT1 and might form, either together with CCR4 or independently, a standalone deadenylase module;
- group C includes CAF1h, CAF1i, CAF1j and CAF1k. The CAF1 paralogs within group C can interact with both NOT1 and CCR4a/b and are expected to form the main complex involved in bulk mRNA deadenylation.

In addition, *Arabidopsis* has 2 paralogs of NOT2, named NOT2a and NOT2b; 3 paralogs of NOT4 named NOT4a, NOT4b, NOT4c; 3 paralogs of NOT9a, NOT9b, NOT9c. Many of these proteins were found to be incorporated within the CCR4-NOT complex (Arae *et al.*, 2019; Zhou *et al.*, 2020; Schwenk *et al.*, 2021). Altogether, it indicates a surprising diversity and complexity in the organisation of the CCR4-NOT complex in *Arabidopsis* (**Figure 7**). This diversity may be functionally important as it provides potential for differential regulation and specialisation of the CCR4-NOT complex in various cellular processes.

While single mutants have barely any detrimental effects in yeasts, double mutants of various subunits are lethal (Collart, 2016). Most of all, the knock-out of the NOT1 subunit, the scaffold protein, is lethal in all organisms. This suggest that the formation of the complex and the processes regulated by its different subunits are essential for the eukaryotic development.

2.3.2. Other functions of the CCR4-NOT complex

While the most studied function of the CCR4-NOT complex is the deadenylation of mRNAs, its functions extend beyond this. Particularly, the complex is expressed both in the cytoplasm and in the nucleus, and is involved in numerous aspects of mRNA metabolism (reviewed in Collart, 2016 and Chalabi Hagkarim & Grand, 2020). In the nucleus, it modulates epigenetic factors and is an important regulator of the chromatin status (Peng *et al.*, 2008; Mersman *et al.*, 2009; Zhou *et al.*, 2020). The CCR4-NOT also controls transcription by interacting both with transcription factors, modulating their recruitment to

promoter regions, and RNA polymerases (Winkler *et al*., 2006; Kruk *et al*., 2011; Wang *et al*., 2013). In plants, the CCR4-NOT complex is involved in co-transcriptional processing, notably in miRNA processing and in the alternative splicing in response to light signals (Wang *et al*., 2013; Schwenk et al., 2021). Additionally, it contributes to nuclear RNA quality control and export by promoting the nuclear exosome assembly and by interacting with numerous components of the nuclear export pathway (Azzouz *et al.,* 2009; Assenholt *et al*., 2011; Kerr *et al.,* 2011).

2.3.3. *The complex role of deadenylation by CCR4-NOT*

The study of respective functions and targets of both deadenylases is complicated by the requirement of CAF1 for CCR4 to associate with the rest of the CCR4-NOT complex. Yet, there is growing evidence that CCR4 and CAF1 have distinct activities that contribute to the deadenylase function of the CCR4-NOT. In yeast, CCR4 is considered the major deadenylase as its deletion led to longer global poly(A) tails (Tucker *et al*., 2001; Tucker *et al*., 2002). However, CCR4 is non-essential, suggesting functional redundancy with other deadenylases or compensation from other decay pathways. On the other hand, deadenylase activity of CAF1 was deemed less important than that of CCR4 as its deletion did not greatly affect poly(A) tail length, and CAF1 catalytic mutants could complement its deletion (Tucker *et al*., 2001; Viswanathan *et al*., 2003; Bianchin *et al*., 2005). Knock-out of mice CAF1a (CNOT7 in the study) induce male sterility without effects on female gametogenesis (Berthet *et al*., 2004), while single and double mutans of CCR4a and CCR4b (CNOT6 and CNOT6L, respectively) induce female sterility without affecting spermatogenesis (Sha *et al*., 2018; Dai *et al*., 2021). These results support the idea that both deadenylase are involved in distinct pathways. The contributions of either deadenylase in mRNA metabolism may also depend on the organism and the cellular context.

Using a reconstituted CCR4-NOT complex in *S. pombe*, the team of Lori Passmore performed different assays on poly(A) tail removal by the two catalytic subunits (Webster *et al*., 2018). *In vitro*, CCR4 is able to readily degrade the poly(A) tail whether it is bound by PABPC or not. Interestingly, the removal of the poly(A) tail by CCR4 is characterised by increments of 8 nucleotides. These particular increments correspond to the number of adenosines bound by individual RRM of PABPC. Individually, each RRM interact with the poly(A) tail with low affinity. Hence, the authors propose that CCR4 can displace the RRM and degrade the now unprotected poly(A) tail. In contrast, CAF1 is inhibited by PABPC and cannot efficiently

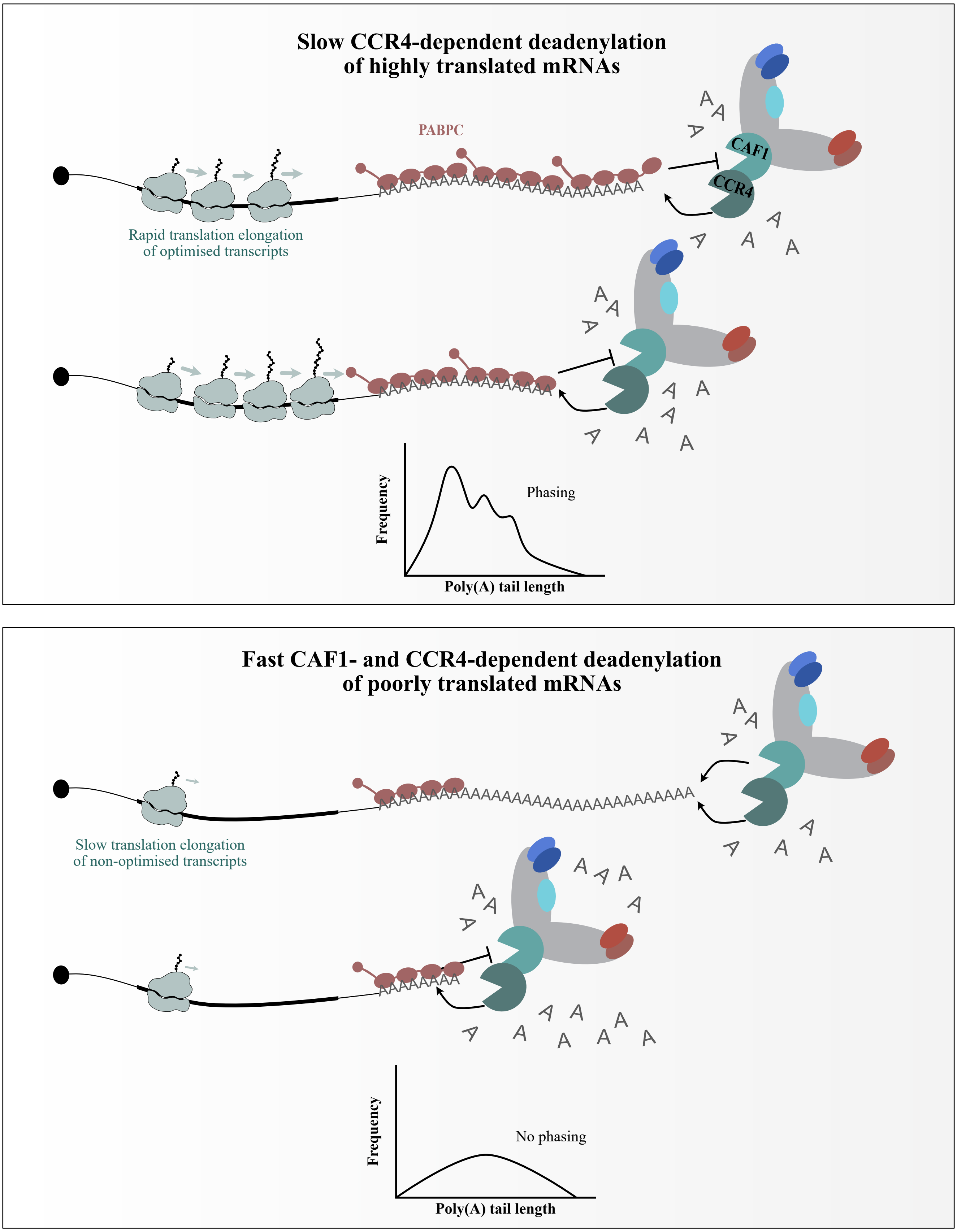

Figure 8. Distinct activities of CCR4 and CAF1 in deadenylation.
Top panel: highly translated mRNAs with codon-optimality have higher PABPC coverage. The presence of PABPC inhibits CAF1's activity, but CCR4 is able to displace the individual RRM to remove PABPC and deadenylate the poly(A) tail. The stepwise deadenylation caused by the presence of PABPC on these mRNAs leads to the appearance of a phased pattern in their poly(A) tails. Lower panel: mRNAs with non-optimal codon have low translation rates and have less PABPC coverage. The concerted action of CCR4 and CAF1 leads to rapid deadenylation of the free poly(A) tail. When a PABPC is reached, CAF1 is inhibited and the activity of CCR4 prevails. The deadenylation of these transcripts is fast and is barely hindered by PABPC. Thus, they display no apparent phasing.

remove PABPC-bound poly(A) tail *in vitro* (Webster *et al.*, 2018). Consistent with these observations, the depletion of CCR4 in yeast significantly stabilises a reporter transcript with either high or low codon optimality (which is a proxy of translation efficiency and PABPC binding, as mRNAs with more optimal codon in their coding sequence tend to be more associated with PABPC). Conversely, the depletion of CAF1 only stabilised the reporter transcript with low codon optimality and had no effect on the reporter with high codon optimality. These results suggest that CAF1 is mainly involved in the decay of low-PABPC occupancy mRNAs, while CCR4 is involved in the decay of both bound and unbound mRNAs (**Figure 8**). Consistent with this, the coupling between codon usage and decay-rate at the level of the transcriptome in yeast mostly rely on CCR4 rather than CAF1 (Cheng *et al.*, 2017). Such discrepancies in the activity of both CAF1 and CCR4, as well as the specific role of CCR4 in deadenylating PABPC-bound mRNA, were also observed in humans (Yi *et al.*, 2018). In contrast, the group of Elmar Wahle observed, using *in vitro* reconstituted *Drosophila* CCR4-NOT complex, that both CCR4 and CAF1 are able to degrade PABPC-bound poly(A) tails, although CCR4 is slightly more efficient (Pekovic *et al.*, 2023). This contrasting result may reflect species-specific differences in the activity of the complex, or that CAF1 is more sensitive to reaction conditions, and that *in vitro* experiments may not fully replicate the physiological catalytic activities of the CCR4-NOT complex.

According to the canonical model of mRNA decay, deadenylation induces poly(A) shortening followed by decapping and rapid decay. Hence, one would expect that mRNAs with short poly(A) tails are less abundant and less translated. However, results from new high-throughput sequencing methods contrast with this postulate. Indeed, mRNAs encoding ribosomal proteins and housekeeping genes have considerably shorter poly(A) tails than that of mRNAs encoding proteins with regulatory functions (Chang *et al.*, 2014; Subtelny *et al.*, 2014; Lima *et al.*, 2017; Jia *et al.*, 2022). Moreover, an inverse correlation between poly(A) tail length and half-life was observed (*i.e.*, mRNAs with short half-life have longer poly(A) tails, and inversely). A similar albeit less important negative correlation was also found between poly(A) tail length and translation efficiency (Lima *et al.*, 2017). However, the mechanisms behind these observations remained obscure. Various factors were later proposed to explain this counter-intuitive phenomenon: the distinct activities of the CCR4-NOT complex (that I previously addressed), PABPC and the PABPC-interacting protein LARP1.

First, the binding of PABPC correlates with translation efficiency using codon optimality as a proxy (Webster *et al.*, 2018). mRNAs with more optimal codons in their coding sequence tend

to be more associated with PABPC. By integrating previous reports, it means that mRNAs with longer poly(A) tails, despite having more possible PABPC-binding sites, are less associated with PABPC. In line with this, mRNAs with short poly(A) tails (*e.g.*, mRNAs of housekeeping genes and ribosomal proteins, which are often highly translated) display a phasing pattern of ~ 30 As in their poly(A) tails, which are associated with footprints of PABPC (Lima *et al*., 2017; Jia *et al*., 2022). Conversely, mRNAs with long poly(A) tails do not have such a pattern and display a flat poly(A) tail distribution. Of the few hypotheses that may explain this pattern, one can suggest that highly translated mRNAs with high PABPC coverage are deadenylated in a stepwise manner, with each PABPC hindering deadenylation. Conversely, less translated mRNAs are less bound by PABPC and are more rapidly degraded. This hypothesis fits particularly well with the step-wise removal of PABPC-bound mRNAs by CCR4 and the swift removal of unbound mRNAs by the joint activities of CAF1 and CCR4 (**Figure 8**).

The work of Narry Kim's lab on human LARP1 was also important to understand why mRNAs with short poly(A) tails are so stable (Park *et al*., 2023). LARP1 is an RNA binding protein that forms a ternary complex by interacting both with the 3'terminal of the poly(A) tail (Aoki *et al*., 2013) and with the PABPC1 through the binding of the PABPC1 MLLE domain with its PAM2 motif (Mattijssen *et al*., 2021). LARP1 associates with mRNAs bearing short tails (~30-60As), and depletion of LARP1 in human cells leads to rapid degradation of this short poly(A) tail population (Park *et al*., 2023). *In vitro* experiments demonstrated the protective role of LARP1 on the deadenylation by the CCR4-NOT complex. LARP1's effect on the stability of mRNAs with short poly(A) tails is global, although it associates more preferentially with 5'Terminal OligoPyrimidine (5'TOP)-motif containing mRNAs, which encodes proteins involved in housekeeping functions, further explaining the relative stability of such mRNAs despite their short poly(A) tails. Altogether, the coverage of PABPC on the poly(A) tail, the presence of PABPC-stabilising factors such as LARP1, and the differential activity of the CCR4-NOT complex explain the seemingly counterintuitive stability of short poly(A) tail mRNAs.

Still, this model of deadenylation does not explain why unstable transcripts accumulate with long poly(A) tails (as seen in Chang *et al*., 2014; Subtelny *et al*., 2014; Lima *et al*., 2017; Jia *et al*., 2022), as we would expect unstable transcripts to be quickly degraded, hence heavily deadenylated. However, the experiments in these studies analysed poly(A) tail distribution at the steady-state of whole cell extracts. Consequently, the observed pool of short-lived transcripts with long poly(A) tails likely includes a significant proportion of neo-transcribed mRNAs that are either still nuclear (where poly(A) tails are inherently longer) (Jia *et al*., 2022)

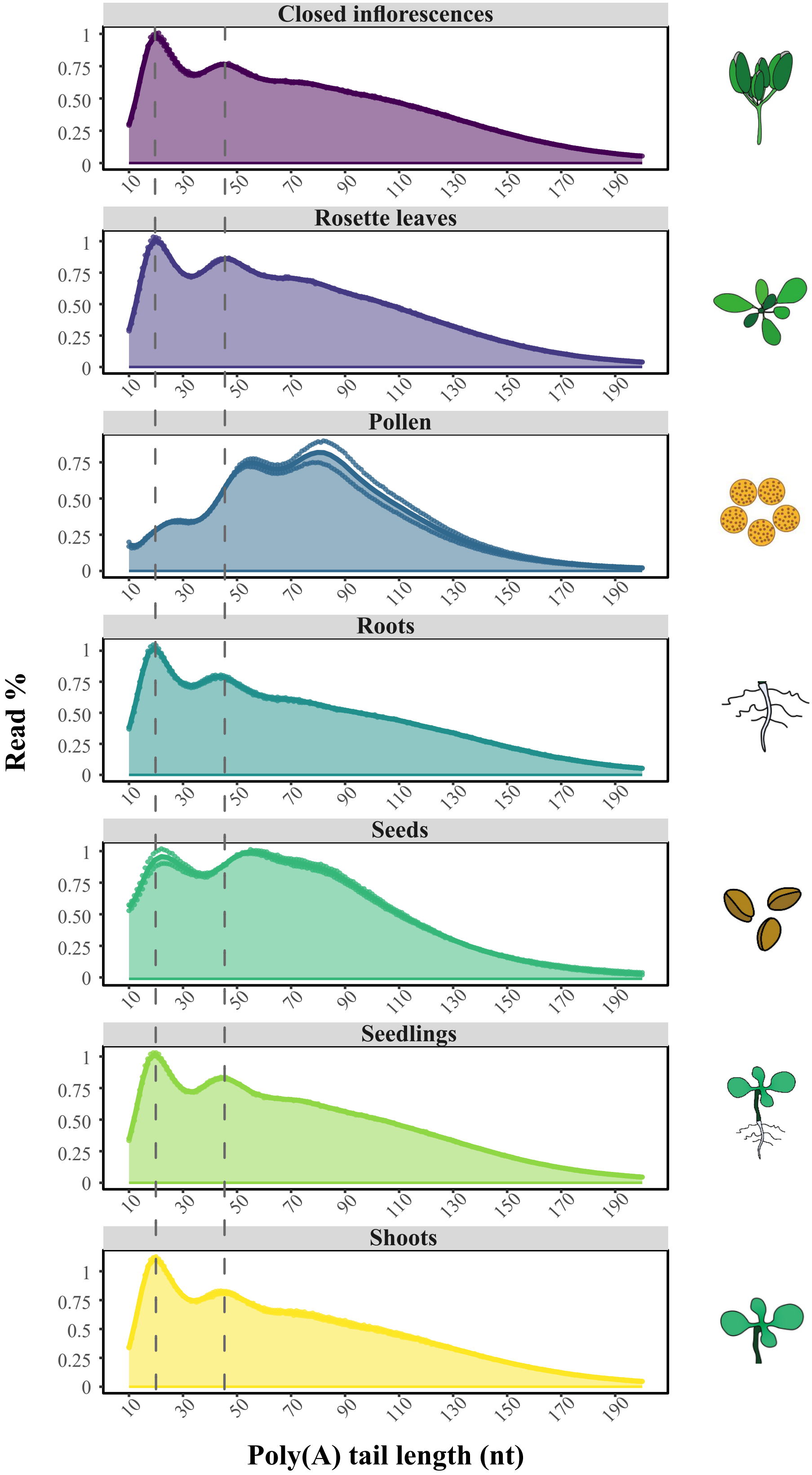

Figure 9. Global poly(A) tail distribution in different *Arabidopsis thaliana* tissues.
Bulk poly(A) tail distribution of mRNAs extracted from closed inflorescences (dark purple), rosette leaves (light purple), pollen (blue), roots (turquoise), seeds (dark green) whole seedlings (light green), shoot (yellow) of *Arabidopsis* wild-type plants. Individual points are shown for two biological replicates and the respective average is indicated as a colored area. Only poly(A) tails between 10-200As are plotted. The putative phasing of the Arabidopsis PABPCs is indicated by a dashed grey line. Other groups identified a modified phasing in *C. elegans* and humans cells (Lima *et al.*, 2017; Yi *et al.*, 2018). Data from Jia *et al.*, 2022.

or that have only recently entered the cytoplasm and thus have not been subjected to deadenylation yet. In support of this, a study examining the kinetics of deadenylation, instead of steady-state poly(A) tail length, shows that short-lived transcripts reach their steady-state abundance and poly(A) tail size distribution much more rapidly than long-lived transcripts (Eisen *et al*., 2020). In other words, less stable mRNAs are quickly deadenylated and degraded, likely because they are poorly bound by PABPC, whereas deadenylation rate of stable transcripts reflects their PABPC occupancy.

Interestingly, poly(A) tails in human cells lack the typical phasing of PABPC. This phasing appears when CCR4 is depleted, which is consistent with its role in clearing PABPC-bound poly(A) tails (Yi *et al*., 2018). Similarly, the phasing appears when transcription is inhibited which can be explained by a denser packing of poly(A) tails when the total mRNA pool decreases (Eisen *et al*., 2020). In other systems however, such as in plants and *C. elegans*, this pattern is constitutive (Lima *et al*., 2017; Parker *et al*., 2020; Jia *et al*., 2022). This pattern is well defined in plants, and can widely vary depending on the tissue (**Figure 9**). Particularly, the phasing of the PABPC peaks in pollen and seeds differs markedly from that of other tissues. Interestingly, *Arabidopsis thaliana* has a set of PABPC that are highly expressed and specific to pollen (see **Introduction chapter 1.3.2**). Because the phasing pattern is dependent on the interplay between PABPC, its putatively associated factors, and CCR4, it is unclear what governs the unique pattern of poly(A) tail distribution in *Arabidopsis* pollen.

2.3.4. The activity of the CCR4-NOT complex is modulated by RNA-binding proteins

The study of CCR4-NOT recruitment to its mRNA targets has been an especially active and exciting topic, with numerous discoveries in metazoans (reviewed in Inada *et al*., 2014; Shirai *et al*., 2014; Raisch & Valkov, 2022). The impressive diversity of mechanisms that mediate the recruitment of the CCR4-NOT complex to its target transcripts emphasises the importance of the fine-tuning needed to precisely modulate deadenylation (**Figure 10**). Particularly, sequences and structures within the 3′UTRs of various mRNAs are known to play determining roles in the recruitment of the CCR4-NOT. This recruitment is mediated by RBPs that act as adapters to bridge the CCR4-NOT complex to mRNAs bearing their specific recognition sequence. Widely studied examples include the Pumilio/Fem-3 mRNA binding Factor (PUF) family proteins that recognise the Pumilio-response elements (**Figure 10A**) (reviewed in Goldstrohm *et al*., 2018 and Nishanth & Simon, 2020). PUM proteins interact directly with the CCR4-NOT complex through multiple binding interfaces and are

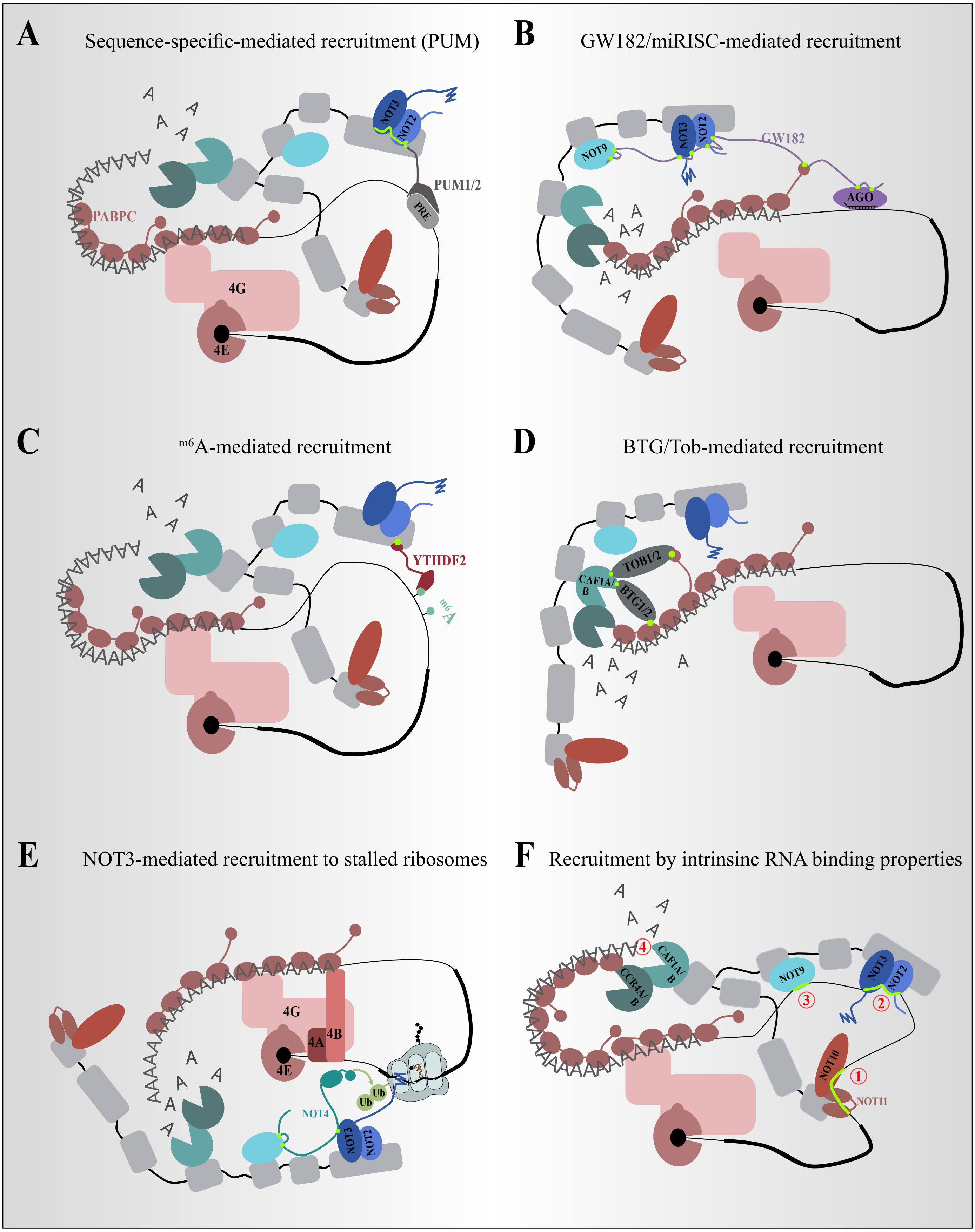

Figure 10. Overview of the recruitment of the CCR4-NOT complex to its target mRNAs. The recruitment of the CCR4-NOT complex to mRNAs involves numerous partners and binding interfaces. Binding motifs in *cis* of the mRNA such as **A)** a sequence recognition motif, **B)** miRNA sites or **C)** ^{m6}A methylation can recruit factors in *trans* that bridge the CCR4-NOT to the mRNA. Some factors such as **D)** the BTG/Tob family proteins and **E)** the NOT3 subunit directly interact with protein factors of the mRNP and recruit the CCR4-NOT complex. **F)** The CCR4-NOT complex has intrinsic RNA binding properties and can directly interact with the mRNA. To simplify the model of recruitment, only the interactions mediated by the described factors are displayed, but the interactions are multipartite, and can be both cooperative and exclusive. Interaction between the factors are highlighted in green.

involved in the repression of a significant proportion of the transcriptome (Enwerem *et al.*, 2021; Haugen *et al.*, 2022). Other RBPs such as Tristetraprolin (TTP) and Nanos act in a similar fashion by recruiting the complex to mRNAs with AU-rich element (ARE) or Nanos Response Element (NRE), respectively (Fabian *et al.*, 2013; Raisch *et al.*, 2016). miRNA binding sites within the 3'UTR are other *cis* elements known to promote deadenylation, and the GW182 protein is an essential factor of this miRNA-mediated recruitment (**Figure 10B**) (Behm-Ansmant *et al.*, 2006). This adapter protein has multiple short linear motifs (SLiMs) that efficiently and specifically bridge the CCR4-NOT complex, the RISC and the PABPC together to promote efficient translational repression and mRNA degradation (Zekri *et al.*, 2009; Jinek *et al.*, 2010; Braun *et al.*, 2011; Chen *et al.*, 2014; Mathys *et al.*, 2014). Another category of *cis* element that mediates recruitment of the CCR4-NOT is mRNA modification, and specifically ^{m6}A methylation (**Figure 10C**) (Du *et al.*, 2016; Lee *et al.*, 2020). The YTHDF2 protein associates with methylated mRNAs and recruits the CCR4-NOT complex by interacting with the C-terminal domain of NOT1 (Du *et al.*, 2016). Interestingly, many mRNAs contain several *cis* elements that are recognised by different RBPs that may compete or cooperate to interact with components of the CCR4-NOT complex, further complexifying the processes of recruiting the complex to target transcripts.

The recruitment of the CCR4-NOT complex to the mRNA can also be mediated by interactions that do not rely on the recognition of *cis* elements on the mRNA. For example, the BTG/Tob family proteins associate with the PABPC, and connects the CCR4-NOT complex through interactions with the CAF1 subunit and promotes deadenylation and turnover of PABPC-bound mRNAs (**Figure 10D**) (Ezzeddine *et al.*, 2007; Mauxion *et al.*, 2008; Stupfler *et al.*, 2016). More recently, the NOT3 subunit (Not5 in yeast) was found to connect stalled ribosomes to the CCR4-NOT complex (**Figure 10E**) (Buschauer *et al.*, 2020; Absmeier *et al.*, 2023). A triple-helix at the N-terminus of the NOT3 subunit is inserted into the E-site of stalled ribosomes (*i.e.*, when both the E-site and A-site are empty). This locks the ribosomes into position and further inhibits translation elongation, and allows ribosome ubiquitination and recycling by the NOT4 subunit. This mechanism is likely to be an important layer that connects mRNA decay and translation efficiency (reviewed in Bae & Coller, 2022).

Interestingly, the CCR4-NOT complex itself can bind its target mRNAs. Numerous structure studies and *in vitro* reconstitution of the whole complex emphasised the essential roles of intrinsic RNA binding properties of several of its subunits (Bhaskar *et al.*, 2013; Raisch *et al.*, 2019; Tang *et al.*, 2019; Chen *et al.*, 2021; Poetz *et al.*, 2021).

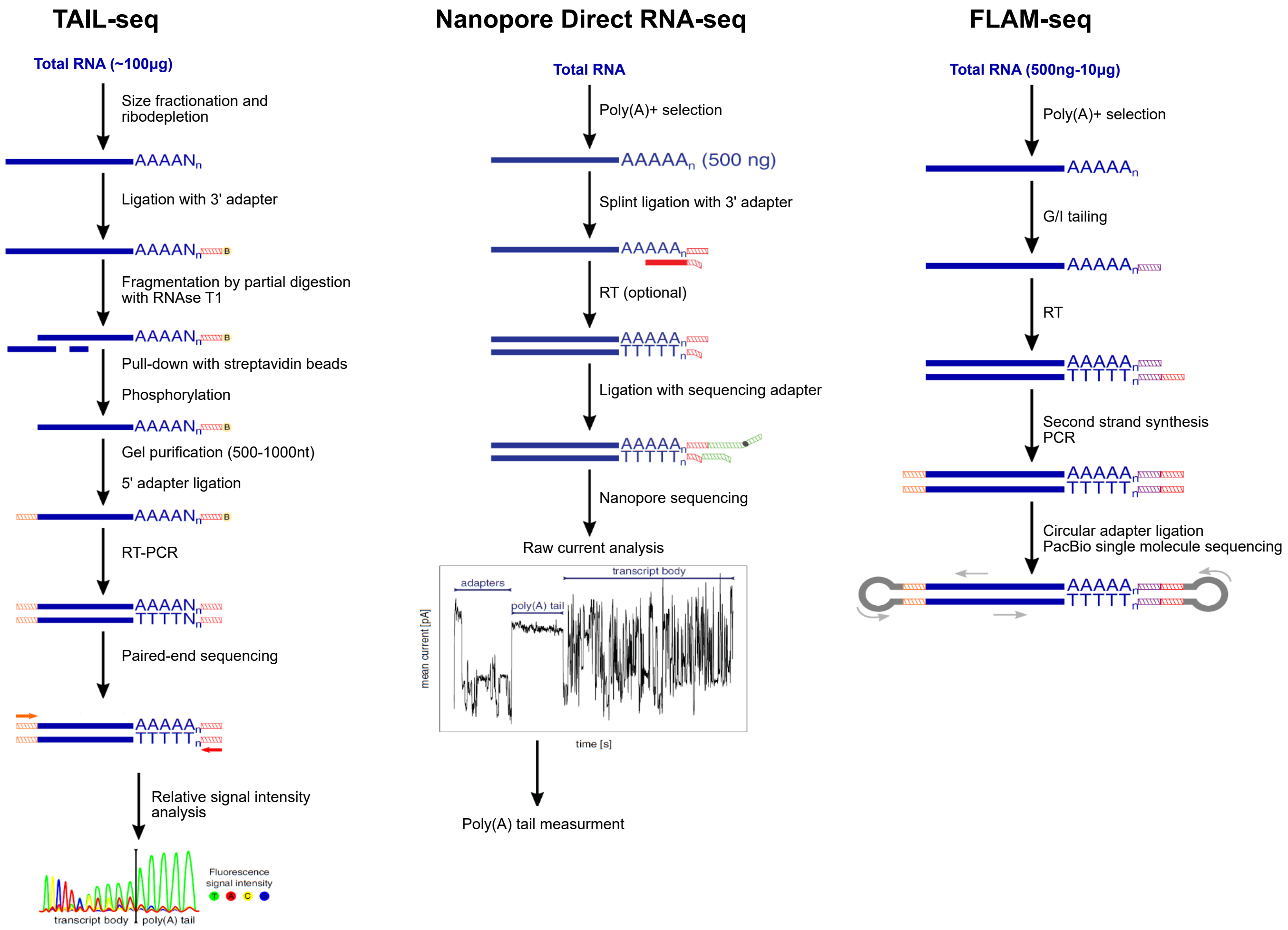
TAIL-seq

Nanopore Direct RNA-seq

FLAM-seq

Figure 11. Overview of poly(A) tail sequencing techniques.

Most poly(A) tail sequencing methods use relatively similar workflow including mRNA enrichment and 5' and 3' adapter ligation. Protocol variability between the techniques arise from the respective platform used. Orange dashed lines indicate the 5' adapter sequence. Red dashed lines represent the 3' adapter sequence. The red line indicates the oligo(dT) sequence. Green dashed lines indicate the sequencing adapter harbouring the motor protein. Violet dashed lines represent the G/I tag sequence. Figures and legends modified from Brouze et al., 2022.

Together, the NOT10-NOT11 module, the NOT2-NOT3/5 module, the NOT9 subunit, and the nuclease module cooperate to bind RNA (**Figure 10F**), which may modify the activity of the complex by correctly placing the different subunits for a better processivity and activity.

2.3.5. Methods to measure poly(A) tail length

As has been presented throughout this chapter, the regulation of poly(A) tail length by deadenylation is crucial for gene expression. Thus, a precise profiling of transcriptome poly(A) tails is essential for understanding the impact of deadenylation rates on mRNA metabolism. Many methods were specifically developed to measure poly(A) tails (reviewed in Brouze *et al.*, 2023).

Historically, the initial approaches involved hybridising the poly(A) tail with oligo(dT) probes, followed by RNase H cleavage, gel electrophoresis, and Northern blot (Sippel *et al.*, 1974). Alternatively, PCR-based amplification of poly(A) tails using both oligo(dT) and gene-specific primers provided information on the relative poly(A) tail size of target transcripts (Sallés& Strickland, 1995). However, these early methods were limited by the poor resolution of electrophoresis which only allows the observation of polyadenylation profiles rather than subtle changes. They did not provide information about poly(A) tail length and were low throughput. Although microarray assays increased knowledge of poly(A) tail length regulation at a broader level, they lacked an accurate readout on poly(A) tail size and were confined to genes with probes on the array (Brouze *et al.*, 2023). This prompted the development of novel methods for more accurate and higher throughput analyses.

The advent of RNA-seq was pivotal in understanding poly(A) tail metabolism. Techniques using the Illumina platform like TAIL-seq and PAL-seq were developed to measure poly(A) tail length at the transcriptome level with nucleotide resolution (**Figure 11**) (Chang *et al.*, 2014; Subtelny *et al.*, 2014). TAIL-seq and PAL-seq differ in sequencing procedures and computational approaches. TAIL-seq uses Hidden Markov Models to monitor fluorescence at the transition from the poly(A) tail to the mRNA body (Chang *et al.*, 2014), whereas PAL-seq calculates poly(A) tail lengths using the fluorescence of labelled streptavidin, which binds to biotinylated dUTP spike-ins (Subtelny *et al.*, 2014). Together, TAIL-seq, PAL-seq and their derivatives were critical to our understanding of mRNA 3’ end metabolism (Brouze *et al.*, 2023). These studies confirmed that poly(A) tails are highly heterogeneous in length and are shorter than previously expected, with a median of 60-95 nucleotides, depending on tissues and techniques (Chang *et al.*, 2014; Subtelny *et al.*, 2014).

Interestingly, median tail lengths vary greatly depending on species but remain conserved for orthologous genes (Subtelny *et al.*, 2014; Lima *et al.*, 2017). TAIL-seq was the first high-throughput sequencing method that allowed the detection of 3' terminal nucleotides, shedding light on the pervasive occurrence of 3'terminal uridylation and the enrichment of guanosines near the 3' end (Chang *et al.*, 2014; Zuber *et al.*, 2016). Despite its central role in the study of the 3' terminome, the Illumina platform inevitably introduces biases, such as fluorescence carryover during PCR amplification cycles leading to poly(A) tail overestimation (Chang *et al.*, 2014). Additionally, sequencing DNA spike-in standards with long poly(A) tails results in a consistent decline in read recovery compared to spike-in with short tails, creating a bias towards shorter poly(A) tails (Morgan *et al.*, 2017). These biases complicate poly(A) tail length estimation, making the Illumina-based methods less suitable for poly(A) profiling compared to third-generation sequencing-based methods.

Particularly, nanopore-sequencing emerges as a reliable technology for poly(A) tail profiling (Brouze *et al.*, 2023). Unlike with Illumina-based methods, nanopore-based methods to measure poly(A) tail do not rely on nucleotide basecalling to assess the poly(A) tail length. Rather, the poly(A) length is inferred based on the persistence of the adenine current during its translocation through the nanopore. This allows to overcome the bias introduced by the basecalling of homopolymeric sequences and provides a precise measurement of the poly(A) tail of full-length transcripts. Among the various methods developed on the nanopore platform, direct RNA sequencing (DRS) has emerged as a key technique in the poly(A) tail study (**Figure 11**) (Garalde *et al.*, 2018). This method enables real-time sequencing of single RNA molecules, eliminating the need for a retro-transcription step and PCR amplification. These steps, when present, can introduce biases leading to underestimations of the length of poly(A) tails. We and others successfully used DRS to accurately measure poly(A) tails in a variety of organisms and tissues (Bilska *et al.*, 2020; Lorenz *et al.*, 2020; Maier *et al.*, 2020; Parker *et al.*, 2020; Scheer *et al.*, 2021; Tudek *et al.*, 2021). However, the use of DRS is limited by the large amount of RNA needed for library preparation, and thus it is not suitable for all applications.

Jia and colleagues developed FLEP-seq2, a cDNA-sequencing method that provides full-length transcript information and poly(A) profiling at the transcriptome level using a minimal amount of mRNA (Jia *et al.*, 2022). Despite the need for an RT step and PCR amplification, the median poly(A) tail lengths obtained with FLEP-seq2 are highly correlated with those of DRS in similar samples, making it a suitable alternative (Jia *et al.*, 2022).

Additionally, and unlike most other poly(A) sequencing techniques, FLEP-seq2 has the advantage of bypassing the need for a poly(A) enrichment step and the use of oligo(dT) adapters for library preparation, as these are known to counterselect short poly(A) tails and introduce a selection bias for longer poly(A) tails. Recently, we adapted FLEP-seq2 to develop the Nano3'-RACE, which is suited to perform in-depth analysis of the 3' end of specific transcripts of interest (Giraudo *et al*., 2023).

The PacBio platform was successfully used to study poly(A) tail length in various tissues and organisms using two highly similar approaches namely FLAM-seq (**Figure 11**) (Legnini *et al*., 2019) and PAIso-seq (Liu *et al*., 2019; Liu *et al*., 2023). The use of circular consensus sequencing, which involves the multiple passing of a single template molecule generates long, high-fidelity reads with high accuracy (up to 99.8%; Wenger *et al*., 2019). Because of this inherent specificity, the PacBio platform can handle homopolymers better than Illumina, enabling the sequencing of the entire polyadenylated RNA molecules and the study of the internal composition of poly(A) tails, which were impossible with previous approaches (Legnini *et al*., 2019; Liu *et al*., 2019; Liu *et al*., 2023).

This diversification in methodologies reflects the ongoing effort to improve accuracy and applicability in the study of poly(A) tail length. In addition to having broadened our understanding of the poly(A) tail size in eukaryotes, NGS-based methods of poly(A) tail sequencing have uncovered the relative heterogeneity of poly(A) tails, which is a critical factor in mRNA metabolism (Chang *et al*., 2014; Zuber *et al*., 2016; Legnini *et al*., 2019; Liu *et al*., 2019; Scheer *et al*., 2021; Liu *et al*., 2023).

3. Tail modifications represent an additional layer of mRNA stability regulation

3.1. The poly(A) tail heterogeneity directly impacts deadenylation

Because deadenylation inherently targets stretches of adenosines, the variation in nucleotide composition of the poly(A) tail can play a crucial role in mRNA metabolism. This aspect is only now beginning to be fully recognised.

An unusual mechanism where poly(A) tail heterogeneity regulates deadenylation occurs to the *Trypanosoma brucei* Variant Surface Glycoprotein (VSG) mRNA, as discovered by Viegas and colleagues (Viegas *et al.*, 2022). VSG is a major surface component of the protozoan parasite *T. brucei* while it resides in the bloodstream of its mammalian host, and is essential for evading host immunity (Engstler *et al.*, 2007). The *VSG* mRNA is highly stable, and this stability was found to be caused by extensive ^{m6}A methylation. This methylation is rather intriguing because it occurs only in the poly(A) tail and not in the transcript body. The presence of ^{m6}A in the poly(A) tail inhibits the activity of CAF1 in the cytoplasm, reducing deadenylation and thus contributing to *VSG* mRNA stability. In the insect vector, *T. brucei* undergoes significant changes to adapt to its host, and the VSG coat is replaced by other coat proteins (Matthews, 2005). This replacement is caused by transcriptional arrest of VSG genes, but also by the removal of ^{m6}A from the poly(A) tail, promoting rapid deadenylation and decay of *VSG* mRNAs.

The fact that ^{m6}A methylation slows down deadenylation is rather interesting. The inhibition of deadenylation caused by this methylation could be due to a factor recruited to the methylated poly(A) tail, and/or by steric hindrance caused by the ^{m6}A moiety within the CAF1 catalytic domain. Indeed, the succession of non-adenosines nucleotides was found to efficiently inhibit the activity of the nuclease module (Chen *et al.*, 2021). Because of the significant amount of ^{m6}A in the poly(A) tail of *T. brucei VSG* mRNA, it is possible that the succession of ^{m6}A residues within the catalytic site of CAF1 hinders mRNA deadenylation.

While ^{m6}A methylation in the poly(A) tail is, to date, limited to *T. brucei*, it is now recognised that the poly(A) tail is not a strict homopolymer of adenosines. The use of transcriptome wide poly(A) tail profiling characterised a relative heterogeneity on poly(A) tails, with numerous tails harbouring internal and 3' terminal non-adenosine residues (Chang *et al.*, 2014; Zuber *et al.*, 2016; Legnini *et al.*, 2019; Liu *et al.*, 2019; Scheer *et al.*, 2022; Liu *et al.*, 2023).

Extensive and conserved mechanisms mediate the untemplated addition, or tailing, of non-adenosine nucleotides within the poly(A) tail, thereby contributing to the synthesis of a heteropolymeric poly(A) tail that efficiently modulates deadenylation.

More specifically, Narry Kim's lab identified the importance of 3' terminal guanosine in human cells. By developing and using TAIL-seq, they showed that guanosines were more frequently detected at the 3' terminal or penultimate positions of the poly(A) tail (Chang *et al*., 2014). Further investigations revealed that non-canonical poly(A) polymerases (ncPAPs) TENT4A and TENT4B are responsible for this mixed tailing (Lim *et al*., 2018). TENT4A/B can incorporate non-adenosine residues, the most common of which is guanosine, during re-polyadenylation events. The enrichment of guanosine at the 3' terminal residue is explained by the stalling effect of a single guanosine nucleotide on deadenylation by recombinant CCR4 and CAF1 (Lim *et al*., 2018; Tang & Passmore, 2019; Chen *et al*., 2021). Upon knock-down of TENT4A/B, half-life and abundance of highly guanylated transcripts are significantly reduced. Therefore, guanylation plays a critical role in stabilising mRNA by impeding deadenylation.

About 20% of mRNA species contain 3' terminal guanosines at a frequency higher than 5%. Uridylation, the untemplated addition of uridines at the 3' end of the poly(A) tail, is more widespread in humans, as about half the transcriptome is uridylated at a frequency exceeding 5% in human cells (Chang *et al*., 2014), with similar observations in *Arabidopsis* (Zuber *et al*., 2016).

3.2. RNA uridylation is catalysed by a family of TNTases

Uridylation is the second most frequent 3' terminal modification detected for eukaryotic RNAs, behind polyadenylation, and is involved in the metabolism of both coding and non-coding RNAs. Although uridylation of non-coding RNAs has been extensively studied and linked to numerous crucial biological processes, playing a role in various steps of RNA metabolism, from maturation to decay, it will not be addressed in this introduction (for reviews, see De Almeida *et al*., 2018; Zigáčková & Vaňáčová, 2018; Yu & Kim, 2020).

To date, RNA uridylation has been found in all eukaryotes tested, with the notable exception of *S. cerevisiae*. Uridylation is catalysed by a family of terminal-nucleotidyltransferases (TNTases) named terminal-uridylyltransferases (TUTases). These enzymes modify RNAs post-transcriptionally to regulate RNA stability and activity. The TUTases are organised around a Catalytic Core Domain (CCD), composed of a nucleotidyltransferase domain (NTD)

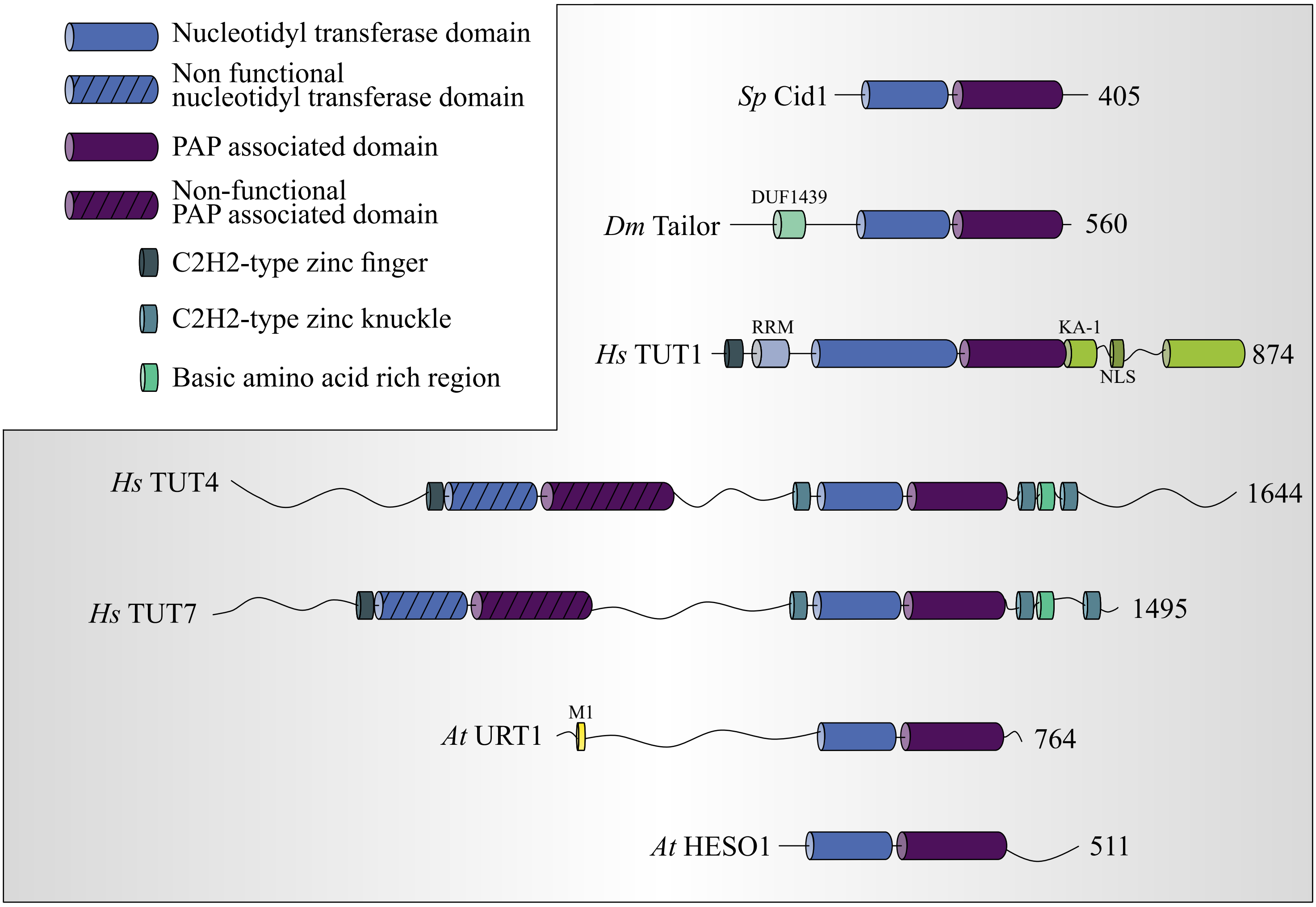

Figure 12. Domain organisation of TUTases.
Structural organisation of TUTases from *S. pombe* (*Sp*), *D. melanogaster* (*Dm*), *Homo sapiens* (*Hs*) and *A. thaliana* (*At*). Intrinsically disordered regions are represented as curved lines. Adapted from De Almeida *et al.*, 2018.

responsible for catalytic activity, and a poly(A) polymerase (PAP) associated domain, involved in nucleotide binding (**Figure 12**) (De Almeida *et al.*, 2018). This CCD is the minimal module for catalytic activity, as some TUTases like Cid1 in *S. pombe* consist only of the CCD. Nonetheless, the majority of TUTases have more complex organisation and often contain multiple folded domains that mediate protein-protein or protein-RNA interactions and are essential for their functions. Human TUT4 and TUT7 even possess a duplication of a CCD, which, although lacking catalytic activity, remains essential for their functions (Faehnle *et al.*, 2017). Interestingly, most TUTases have intrinsically disordered regions (IDR). These IDRs correspond to sequences enriched in charged and polar amino acids, but poor in hydrophobic amino acids. The enrichment of IDRs in TUTases may reflect their evolutionary adaptation for versatile interactions with diverse molecular targets, enabled by the presence of short linear motifs (SLiMs), which are involved in specific interactions with folded domains. In *Arabidopsis*, a helical leucine-rich motif (HLM) in the N-terminal IDR of URT1 has been shown to directly connect the LSm domain of DCP5/LSM14 and mediate the interaction of URT1 with numerous decay factors (Scheer *et al.*, 2021).

3.3. Uridylation is a conserved regulator of mRNA turnover in eukaryotes

mRNA uridylation plays complex roles in mRNA metabolism, and depends on the organism, cellular context, and the mRNA type. For instance, uridylation is implicated in the clearance of 5’ RISC-cleaved fragments in mammals and plants, in regulating the translation efficiency of mitochondrial mRNAs in Trypanosomatids, and is believed to both stabilise and induce decay of replication-dependent histone mRNAs (reviewed in Marzluff *et al.*, 2008; Scheer *et al.*, 2016; De Almeida *et al.*, 2018; Zigáčková *et al.*, 2018). However here, I will focus on uridylation of polyadenylated mRNAs and discuss how uridylation is an integral step during their turnover. Studies on polyadenylated mRNA uridylation indicate a strong link between deadenylation and decay, as mostly deadenylated mRNAs with short poly(A) tails (<20As) are preferentially uridylated. Of note, however, mRNA uridylation in *S. pombe* does not necessarily require a first step of deadenylation, as the median tail length is rather short in this organism with a median size of ~28 adenosines (Subtelny *et al.*, 2014).

The influence of mRNA uridylation on decay was first described in *S. pombe*, where it is catalysed by Cid1 (Rissland & Norbury, 2009). Upon mutation of the TUTase, the half-life of transcripts that are usually uridylated is significantly increased, suggesting a decay-promoting role of uridylation. This stimulatory effect on decay is due to the increased affinity of the Lsm1-7 complex for oligo-uridylated mRNAs. Indeed, this complex binds more efficiently to oligo-uridylated tails and promotes decapping *in vitro* (Song & Kiledjian, 2007). Consistent with this, depletion of the Lsm1 subunit leads to the accumulation and stabilisation of uridylated transcripts (Rissland & Norbury, 2009). This indicates that uridylation triggers 5’→3’ decay by promoting the recruitment of the Lsm1-7 complex to uridylated mRNAs, leading to subsequent decapping and degradation by 5’→3’ exoribonucleases. mRNA uridylation in *S. pombe* also favour 3’→5’ decay, as mutants for Dis3l2 accumulate uridylated transcripts (Malecki *et al.*, 2013).

Similar reports were made upon transcriptome-wide profiling of the poly(A) tail with TAIL-seq (Lim *et al.*, 2014). In humans, mRNA uridylation is catalysed by TUT4/7. Highly uridylated transcripts have shorter half-lives and are quickly degraded. While the knock-down of TUT4/7 slows down mRNA decay, depleting key components of the 5’→3 or the 3’→5’ decay pathways leads to accumulation of uridylated transcripts. Together, these results suggest a conserved role for uridylation in triggering decay across eukaryotes (Lim *et al.*, 2014).

This phenomenon has been extensively studied in animals, where uridylation significantly influences transcriptome remodelling in response to cellular or developmental stimuli (Thomas *et al.*, 2015; Morgan *et al.*, 2017; Chang *et al.*, 2018; Morgan *et al.*, 2019). A notable example of this occurs during gametogenesis and early embryogenesis, where widespread mRNA uridylation by TUT4/7 is closely associated with extensive transcriptome remodelling. This process predominantly leads to decay of the uridylated transcripts (Morgan *et al.*, 2017; Chang *et al.*, 2018; Morgan *et al.*, 2019).

However, the impact of uridylation varies considerably depending on the cellular context. For instance, in mouse oocytes, TUT4/7 are essential to sculpt the maternal transcriptome *via* bulk mRNA uridylation and subsequent decay (Morgan *et al.*, 2017). This is in contrast to *Tut4-Tut7* knock-out mice, which are viable and show no significant alterations in gene expression across various cell types, highlighting a differential response to uridylation between somatic and germline cells (Morgan *et al.*, 2017).

Additionally, the role of uridylation during the oocyte-to-embryo transition (OET) offers a particularly striking contrast. In this phase, approximately two-thirds of the transcriptome undergoes uridylation after deadenylation (Liu *et al.*, 2023). However, these uridylated transcripts remain stable and are subjected to cytoplasmic polyadenylation. The stability of uridylated transcripts during OET is in marked contrast to the decay-inducing role of uridylation observed in the subsequent maternal-to-zygotic transition (MZT) (Chang *et al*., 2018), underscoring the complexity and context-dependency of uridylation.

3.4. mRNA uridylation in plants

3.4.1. Plant mRNAs are uridylated by URT1

In *Arabidopsis*, our team has made significant contributions to investigating the mechanisms related to RNA uridylation. URT1 has been identified as the primary TUTase responsible for mRNA uridylation (Sement *et al*., 2013; Zuber *et al*., 2016; Scheer *et al*., 2021). In a knock-out *urt1* mutant, mRNA uridylation drops by 70–80%. Residual uridylation suggests the presence of another TUTase capable of uridylating mRNAs. HESO1, the other identified TUTase in *Arabidopsis*, was proposed to provide this additional activity (Zuber *et al*., 2016). Consequently, uridylation is close to background levels in a *urt1 heso1* double mutant (unpublished data). Similarly, residual uridylation of HESO1 targets, such as siRNAs, miRNAs, and 5' RISC-cleaved transcripts, is observed in *heso1* (or *hen1 heso1*) null mutants, with URT1 being responsible for this residual uridylation (Ren *et al*., 2012; Zhao *et al*., 2012; Ren *et al*., 2014; Tu *et al*., 2015; Wang *et al*., 2015; Zuber *et al*., 2018). However, in wild-type plants, the propensity of HESO1 to uridylate URT1 targets (and *vice versa*) is low and only becomes evident in knock-out mutants.

As previously stated, URT1 is the main TUTase involved in mRNA uridylation. As in humans, uridylation in plants preferentially targets mRNAs that have undergone prior deadenylation, as most uridylated mRNAs bear short poly(A) tails (Sement *et al*., 2013; Zuber *et al*., 2016; Scheer *et al*., 2021). The study of a model mRNA demonstrated that uridylation is particularly detected in transcripts lacking a 5' cap, and that uncapped uridylated mRNAs accumulate in a mutant of XRN4 (Sement *et al*., 2013), the ortholog of human XRN1, which is involved in the clearance of uridylated mRNAs (Lim *et al*., 2014). This observation indicates that in plants, as in mammals and *S. pombe*, uridylation marks mRNAs that undergo 5'→3' decay. Interestingly, a comparison of transcriptome-wide uridylation levels with datasets reporting mRNA half-lives in *Arabidopsis* reveals a clear correlation: mRNAs with the highest levels of uridylation tend to have the shortest half-lives, and *vice versa* (Zuber *et al*., 2016). Overall, these data suggest that mRNA uridylation may destabilise mRNA, and trigger their decay by the 5' end. However, these half-life data were not generated in a *urt1* background, and a direct role of uridylation by URT1 in the induction of mRNA decay has yet to be established.

While a direct role of mRNA uridylation in plants has not formally been linked to degradation, several lines of evidence indicate that mRNA uridylation by URT1 protects the 3' end of mRNAs from excessive deadenylation:

- Uridylation of deadenylated mRNAs re-establishes a 16 nt size distribution, mirroring that of non-uridylated reads. These uridylated mRNAs are bound *in vivo* by a PABPC. *In vitro,* the presence of a PABPC dictates the number of uridines added by URT1 on a synthetic RNA (Zuber *et al*., 2016). Hence, URT1 and PABPC cooperate to "repair" poly(A) tails to a length that is similar to non-uridylated transcripts and that allows binding by a PABPC. The presence of the PABPC may therefore impede accessibility of the 3' end to decay factors.
- Second, the addition of a single uridine at the 3' end of an oligoadenylated RNA impedes deadenylation of a recombinant CAF1b *in vitro* (Scheer *et al*., 2021).
- Third, uridylation by URT1 shapes the poly(A) tail distribution. Indeed, a knock-out *urt1* mutant display an accumulation of highly deadenylated mRNAs (Sement *et al*., 2013; Zuber *et al*., 2016., Scheer *et al*., 2021). Given that uridylation hinders deadenylation *in vitro*, it is likely that the shortening of poly(A) tails in *urt1* is caused by a more important deadenylation. Conversely, overexpression of URT1 in *Nicotiana benthamiana* drastically increases the length of poly(A) tails, and this may result from the impediment of deadenylation by 3' terminal uridines (Scheer *et al*., 2021).

In plants, excessively deadenylated mRNAs are substrates for RDR6, an RNA-dependent RNA polymerase involved in the biogenesis of siRNAs (Baeg *et al*., 2017). A *urt1 xrn4* mutant has many detrimental effects caused by the accumulation of spurious siRNAs, which are more prominently directed towards mRNAs that are highly uridylated in wild-type plants (Scheer *et al*., 2021). Hence, the hypothesis is that mRNAs that are normally uridylated at high frequencies and protected at their 3'end, are not anymore in *urt1 xrn4,* and accumulate because of the *xrn4* background. These mRNAs are then preferred targets of RDR6 that induces the production of illegitimate siRNAs directed towards these highly deadenylated mRNAs. Consistent with this hypothesis, the adverse effects observed in the *urt1 xrn4* mutant are readily reversed by mutating key factors of the siRNA biogenesis pathway (Scheer *et al*., 2021).

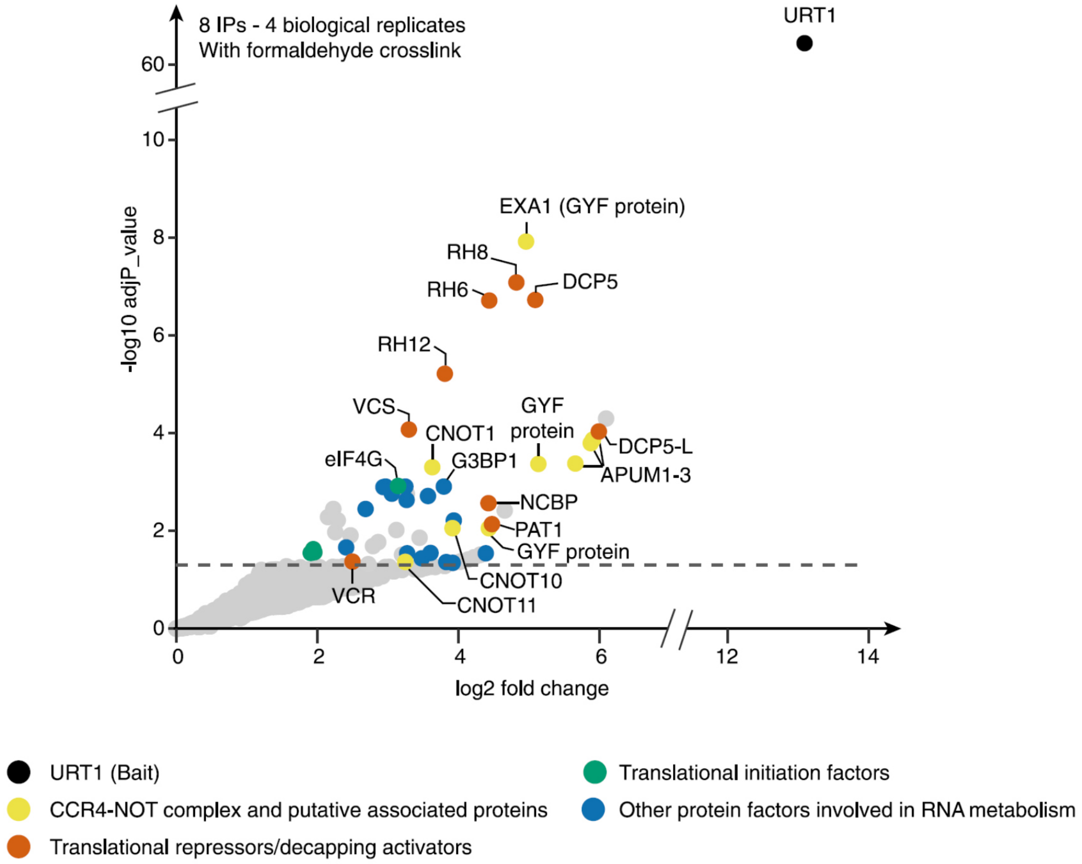

Figure 13. URT1 co-purifies with numerous decay factors.
Semi volcano plot showing proteins enriched in myc-URT1 or YFP-URT1 IPs following formaldehyde crosslink. The horizontal dashed line indicates the significant threshold (adjusted *p*value < 0.05, quasi-likelihood negative binomial generalised log-linear model with Benjamini-Hochberg correction). Figure and legends from Scheer et al., 2021.

3.4.2. Unravelling URT1's interaction network: connexion between uridylation, mRNA deadenylation and translational repression

Despite the strong relationship between uridylation and RNA decay, evidence for interactions between cytosolic TUTases and RNA decay factors remains scarce, with only three examples to date:

- First, the *Drosophila* TUTase Tailor interacts with the 3'→5' exoribonuclease Dis3l2 to form the Terminal RNA Uridylation-Mediated Processing (TRUMP) complex, implicated in the destabilisation of numerous ncRNAs (Reimão-Pinto *et al.*, 2016; Lin *et al.*, 2017).
- Second, human TUTases TUT4/7 interact with the RNA-binding protein Lin28, leading to the destabilisation of certain let-7 miRNA precursors (Faehnle *et al.*, 2017).
- Third, we demonstrated in *Arabidopsis* a direct interaction between URT1 and DCP5 (ortholog of human LSM14 and *Drosophila* Tral) (Scheer *et al.*, 2021). This is the first reported interaction between a TUTase and a decapping activator/translational inhibitor.

The URT1-DCP5 interaction mediates the recruitment of other decapping activators/ translation inhibitors, such as RH6-8-12 (orthologs of human DDX6 and *Drosophila* Me31B) and VCS (ortholog of human EDC4 and *Drosophila* Ge-1). We propose that the interaction between URT1 and DCP5 facilitates the recruitment of RH6-8-12 and VCS to deadenylated mRNAs, triggering their decay (Scheer *et al.*, 2021). This interaction was initially detected after the resolution of URT1's interactome using co-immunoprecipitation experiments followed by mass-spectrometry identification (co-IP/MS). Interestingly, numerous proteins significantly co-purifying with URT1 are involved in decapping activation/translational repression or are proteins of the CCR4-NOT complex or putatively associated with it (**Figure 13**). This observation further confirms the link between uridylation and mRNA decay, and most interestingly, mRNA deadenylation.

In this experiment, EXA1 was found to be the most significantly enriched protein, potentially indicating a robust interaction with URT1. EXA1 is an adaptor protein containing a GYF (Glycine-Tyrosine-Phenylalanine) domain, a highly conserved domain in eukaryotes that binds proline-rich motifs (Kofler *et al.*, 2005; Kofler & Freund, 2006). EXA1 was identified as a susceptibility factor necessary for infection by a Potexvirus (Hashimoto *et al.*, 2016). This susceptibility is likely caused by the translational repression of immune response genes by EXA1 (Wu *et al.*, 2017).

EXA1 is the ortholog of GIGYF proteins in humans and *Drosophila*, and GYF-1 in *C.elegans*. GIGYF proteins are decapping activators/translational inhibitors that connect different translational repressors such as 4EHP, DDX6 and PAT1 (Morita *et al*., 2012; Peter *et al*., 2017; Amaya-Ramirez *et al*., 2018; Peter *et al*., 2019; Ruscica *et al*., 2019; Hickey *et al*., 2020; Weber *et al*., 2020; Mayya *et al*., 2021). GIGYF proteins also interact with the CCR4-NOT complex by directly binding CAF1a and NOT1 (Amaya-Ramirez *et al*., 2018; Ruscica *et al*., 2019) as well as NOT9 (Ajiro *et al*., 2010). Interestingly, orthologs of all these factors are found in URT1 IPs, suggesting that such an interaction network is conserved in *Arabidopsis*.

The GYF domain of EXA1 specifically interacts with proline-rich sequences containing a PPGF motif (Proline-Proline-Glycine-Phenylalanine) (Kofler *et al*., 2005). Interestingly, URT1 contains such a motif located in the IDR of the N-terminal region. Phylogenetic analyses have demonstrated the important conservation of this PPGF motif in land plants (Scheer *et al*., 2021). The widespread presence of this motif in the IDR of URT1 orthologs suggests a fundamental role in the functions of the TUTase, possibly in its interaction with EXA1.

These findings, combined with general knowledge of EXA1 orthologs in metazoans, suggest a direct interaction between URT1/EXA1 and EXA1/CCR4-NOT, enabling the recruitment of the TUTase to mRNAs. In line with this hypothesis, yeast two-hybrid experiments using EXA1 as a bait retrieved NOT4 as an interactant (Kofler *et al*., 2005).

Thus, by interacting with the CCR4-NOT complex, EXA1 could recruit URT1 to the 3' end of mRNAs undergoing deadenylation. The TUTase would then be able to uridylate these mRNAs, preventing excessive deadenylation and promoting their 5'→3' degradation through the recruitment of the decapping activator DCP5. This model is supported by our previous observations and herlps clarify the functional link between uridylation and deadenylation (Scheer *et al*., 2021).

Thesis objectives

Thesis objectives

Deadenylation is a pivotal step of mRNA degradation, and the CCR4-NOT complex emerges as the main actor in poly(A) tail removal. Particularly, in yeast and mammals, CCR4 is described as the main deadenylase, as it is able to displace the PABPC from the poly(A) tail to efficiently catalyse poly(A) tail shortening (Webster *et al.*, 2018; Yi *et al.*, 2018). Deadenylation is a tightly regulated mechanism that is interconnected with numerous other mRNA decay pathways. We, along with others, have contributed to unravelling the intricate connections between uridylation and deadenylation: uridylation targets mostly deadenylated mRNAs (Sement *et al.*, 2013; Lim *et al.*, 2014; Zuber *et al.*, 2016; Scheer *et al.*, 2021); uridylation hinders the activity of CAF1b and prevents excessive deadenylation (Scheer *et al.*, 2021); a *urt1* knock-out mutant accumulates deadenylated mRNAs (Scheer *et al.*, 2021).

Altogether, these results suggest a strong coupling between uridylation and deadenylation.

However, to what extent the deadenylation step is important for subsequent uridylation remains unknown. Another open question is how URT1 is recruited to the deadenylated mRNAs. URT1 has no characterised mRNA binding motifs and is thought to be recruited to mRNAs by interacting with partner proteins. Because of the coupling between deadenylation and uridylation that we observed *in vivo*, one may hypothesise that there is a physical connection between the factors involved in both mechanisms. This hypothesis is supported by our recent mass-spectrometry data characterising proteins of the CCR4-NOT complex as co-purifying with URT1 (Scheer *et al.*, 2021). It possible that certain proteins that interact both with URT1 and the CCR4-NOT complex may bridge uridylation and deadenylation, and the GYF-domain protein EXA1 is a candidate.

> **The purpose of my thesis was to better understand the roles of the deadenylation by the CCR4-NOT complex and its interplay with uridylation in *Arabidopsis thaliana*.**

In the first chapter of this manuscript, I present an in-depth phenotypic and molecular analysis of a double knock-out mutant of the CCR4a and CCR4b deadenylases in *Arabidopsis*. In particular, I focused on the links between phenotypic defects and alterations in the metabolism of biologically significant transcripts using various sequencing and proteomics experiments. A key aspect of this chapter was the use of the FLEP-seq2 sequencing method that I was involved in optimising and setting up in the lab.

The second chapter of this manuscript focuses on the study of the functional links between uridylation and deadenylation, first by determining the impact of the mutations of the CCR4 deadenylases on uridylation profiles, and then by characterising the physical links that were initially thought to bridge uridylation and deadenylation. The characterisation of the interactome of EXA1 and its association with URT1 was a key aspect of this chapter.

The work conducted during my PhD seeks to characterise the main factors involved in deadenylation, their biological functions, and their targets, as these aspects remain largely unknown in *Arabidopsis*. This work also continue previous studies conducted by the team, aiming to uncover the roles and regulations of uridylation and its connections with deadenylation.

Results

1. Defining the biological functions and molecular consequences of deadenylation by CCR4a and CCR4b in *Arabidopsis*

Deadenylation by the CCR4-NOT complex plays an essential role in regulating the mRNA life cycle. Among the two deadenylases in the complex, CCR4 can remove PABPC to trim poly(A) tails, while the action of CAF1 is hindered by the presence of PABPC (Webster *et al*., 2018; Yi *et al*., 2018). Since PABPC can control the number of uridines added (Zuber *et al*., 2016; Yi *et al*., 2018), and because uridines impede deadenylation (Scheer *et al*., 2021), studying the extent of the actions of CCR4 proteins is critical to understand the links between uridylation and deadenylation in *Arabidopsis thaliana*.

1.1. Generation of a homozygous *ccr4a ccr4b* mutant line

Arabidopsis has two homologs of CCR4, CCR4a and CCR4b, and their biological functions remain largely unexplored. CCR4a and CCR4b arose from a recent gene duplication, and share 76% sequence identity (Suzuki *et al*., 2015). Consequently, it is plausible that they retain overlapping or redundant functions, posing a challenge for functional studies. Indeed, the *CCR4a* and *CCR4b* genes are only 6.3kb apart in the genome, and therefore generating a double KO line is not possible by crossing the single mutants. Suzuki and colleagues used a T-DNA insertion line for one gene in combination with an RNAi cassette designed to knock-down the expression of the second gene. These mutants were useful to uncover the roles of CCR4a and CCR4b in regulating the poly(A) tail length of a gene involved in starch metabolism (Suzuki *et al*., 2015). However, the lack of a proper double KO mutant hinders the study of the effects of CCR4 proteins on mRNA metabolism in *Arabidopsis* at a global scale. As the RNAi cassette may not fully suppress the expression of either *CCR4a* or *CCR4b*, the remaining expression of one or the other of these closely related paralogs could influence deadenylation of mRNAs targeted by both enzymes.

In this context, former PhD student of the team Caroline de Almeida in collaboration with Anthony Gobert from the "Genome Editing" facility of our institute, designed guide RNAs to mutate *CCR4a* and *CCR4b* genes using the CRISPR-Cas9 technology. During my PhD, I identified different alleles of *ccr4a/b* double mutants. First using High Resolution Melting (HRM) on amplification products of the sequences targeted by the gRNAs, I isolated several

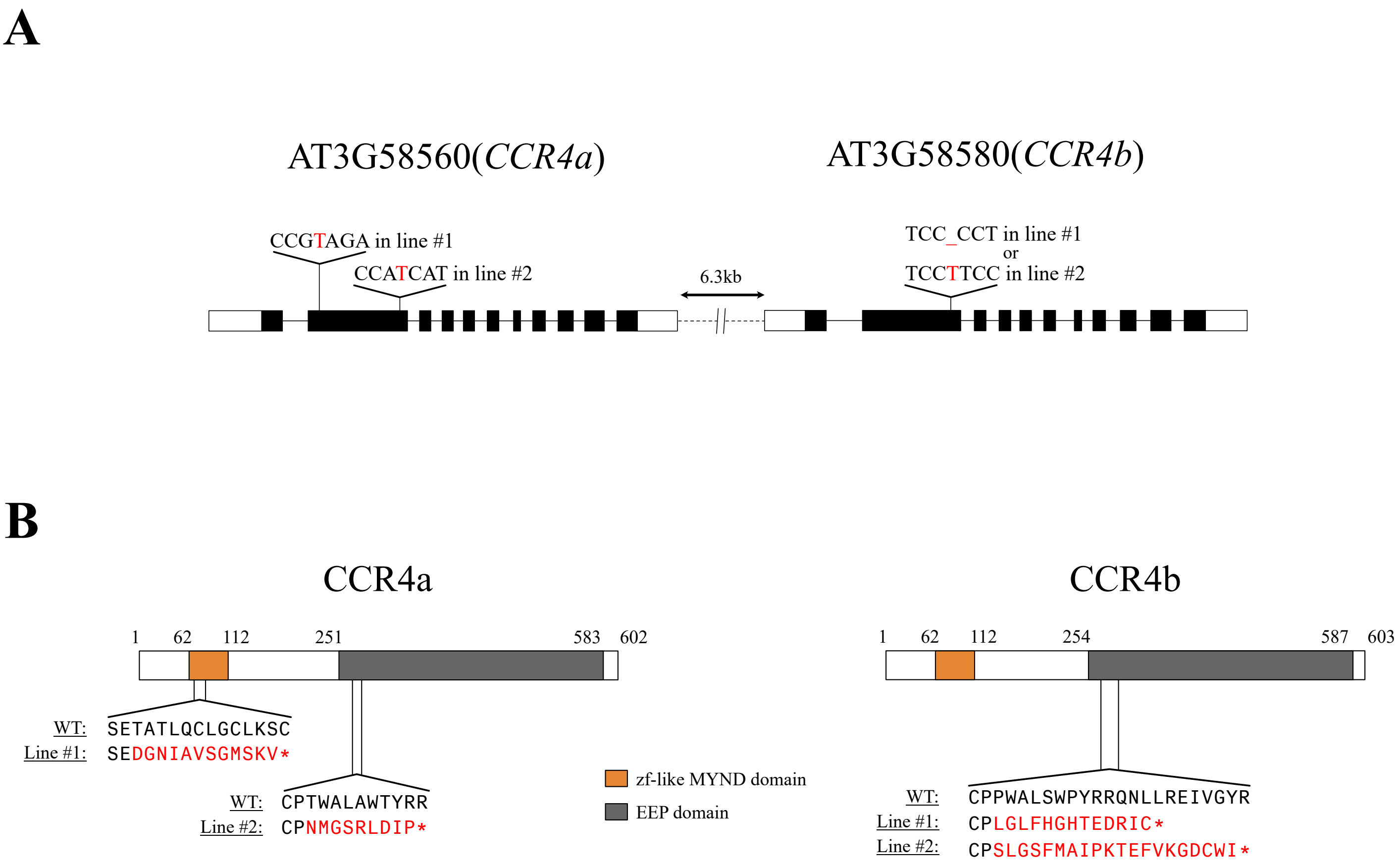

Figure 14. Description of *ccr4a ccr4b* mutagenesis.
A) Diagram of the AT3G58560-AT3G58580 locus encoding the *CCR4a* and *CCR4b* genes, respectively. Black boxes represent CDS, white boxes represent UTR, black lines represent introns, dashed lines represent the intergenic region. Insertions indicate the position of the 1 nt frameshift introduced in both genes for two alleles named line #1 and line #2. The mutation is highlighted in red in the sequence above. **B)** Domain organisation of CCR4a and CCR4b proteins. Both proteins contain a zf-like MYND domain essential for the recruitment to the CCR4-NOT complex, and a EEP domain responsible for the catalytic activity. Below the protein representation are the sequence alignment between wild-type (WT) and mutated sequences for both alleles. Letters in red highlight the amino acid substitution caused by the 1 nt frameshift, until the appearance of a STOP codon represented by a *.

plants with heterozygous profiles for both *CCR4* amplification products. Upon self-fertilisation and Sanger sequencing of the genomic DNA, two independent lines were selected, both homozygous for the mutation of *CCR4a* and *CCR4b* genes.

In line #1, a thymidine is inserted at the beginning of the second exon of *CCR4a*, causing a +1 frameshift in the coding sequence (**Figure 14A**). Upon translation of the mutated gene, this would change the amino acid sequence starting from Tyr62 until the introduction of a STOP codon in place of Cys85 (**Figure 14B, left panel**). Because the STOP codon is inserted at the beginning of the protein, we expect that the translated protein, if existing, is non-functional. As for *CCR4b,* I observed a deletion of a thymidine at the end of the second exon, causing a -1 frameshift in the coding sequence (**Figure 14A**). This frameshift would introduce mutations in the protein sequence of CCR4b, starting from Pro274 until the insertion of a STOP codon in place of Lys287 (**Figure 14B, right panel**). Here, the STOP codon is inserted at the beginning of the EEP domain, before the amino acids known to be necessary for the catalytic activity of the protein. Hence, if a protein is translated upon mutation of the *CCR4b* gene, it would only contain the MYND domain and would not have any catalytic activity.

In line #2, a thymidine is inserted at the end of the second exon of *CCR4a*, again causing a +1 frameshift. This mutation affects the potentially translated protein and introduces a Cys269 → STOP mutation. Similarly, the +1 frameshift in the *CCR4b* sequence in line #2 introduces an early STOP codon in place of Arg294. Hence, both proteins in line #2 will not have a complete EEP domain and therefore will not be fully functional. The effectiveness of the CRISPR-Cas9 mutation on the expression of the *CCR4a* and *CCR4a* genes both at the transcript and protein level will be discussed in **Results 1.2.1** and **1.3.6**, respectively.

1.2. Phenotypic and molecular consequences of deadenylation defects in *Arabidopsis* rosette

1.2.1. ccr4a ccr4b plants undergo constitutive stress response

To determine the effects of the mutation of *CCR4* genes on *Arabidopsis*' phenotype, CRISPR-Cas9 mutants were grown alongside WT plants, and the two lines generated by Suzuki and colleagues (Suzuki *et al.*, 2015). In *ccr4a/bi*, the *CCR4a* is knocked-out by a T-DNA insertion and *CCR4b* expression is knocked-down by an RNAi cassette. In *ccr4ai/b*, *CCR4a* is knocked-down by RNAi, and *CCR4b* is knocked-out by a T-DNA insertion.

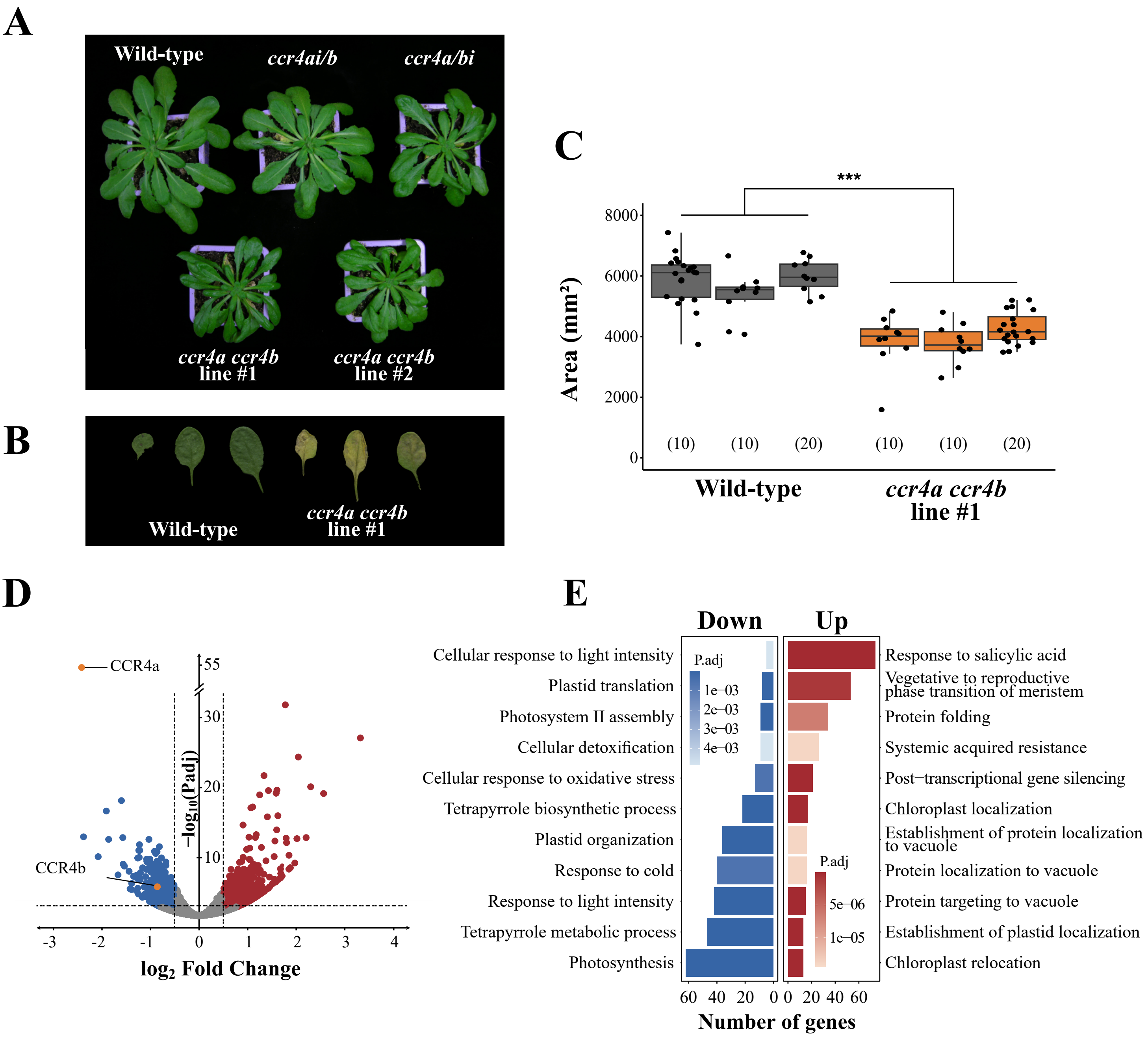

Figure 15. *ccr4a ccr4b* double mutant plants display auto-immune phenotype. A) Phenotype comparison between wild-type, RNAi lines (*ccr4a/bi*: *CCR4a* KO, *CCR4b* RNAi; *ccr4ai/b*: *CCR4a* RNAi, *CCR4b* KO), and the two CRISPR/Cas9 alleles line #1 and line #2. Phenotype was assessed on 6 week-old plants. **B)** Representative image of the 3 oldest leaves of 6 week-old wild-type (left) and *ccr4a ccr4b* line #1 (right) plants. **C)** Quantification of the leaf area for wild-type (WT) and line #1 (*ccr4a ccr4b*). Individual replicates are plotted separately. Each dot represents an individual plant. Number of plants n is indicated in parentheses. Each boxplot represents a biological replicate. The horizontal line in each box represents the median, and lower and upper hinges indicate first and third quartiles respectively. *p*-value was calculated using a Student's t-test, ***: $p < 0.001$. **D)** Volcanoplot depicting differentially expressed genes in *ccr4a ccr4b* double mutant. *p*-value is corrected using Benjamini-Hochberg correction and is depicted as -$\log_{10}$(Padj) in the Y-axis. Dots represent individual genes. Red and blue dots represent genes significantly upregulated ($\log_2$ Fold Change > 0.5 and adjusted *P*-value < 0.05) and downregulated ($\log_2$ Fold Change < -0.5 and adjusted *P*-value < 0.05) in *ccr4a ccr4b* compared to wild-type, respectively. Grey dots show no significant difference. CCR4a and CCR4b are displayed as orange dots. **E)** Over-representation analysis of GO terms in downregulated (left panel) and upregulated (right panel) genes in *ccr4a ccr4b* compared to wild-type identified in RNA-seq. The length and color of bars represent respectively the number of genes and significance calculated using hypergeometric test with Benjamini-Hochberg correction.

At 6 weeks, both the RNAi lines and CRISPR-Cas9 mutant plants grow smaller and have curly leaves (**Figure 15A**). Early leaf senescence can also be observed on older leaves (**Figure 15B**). The phenotype seems stronger in *ccr4a/bi* compared to *ccr4ai/b*. This is likely explained because of the higher level of expression of *CCR4a* as compared with *CCR4b*. Alternatively, *CCR4b* could be more efficiently silenced by RNAi in *ccr4a/bi*, than *CCR4a* in *ccr4ai/b*.

Interestingly, the phenotype is stronger in CRISPR-Cas9 generated lines compared to *ccr4a/bi*, suggesting that the RNAi does not completely silence the expression of *CCR4b*, and that this remaining expression partially complement the phenotype.

As the point mutation occur further upstream in *CCR4a* in line #1 as compared to line #2, I decided to use this line for all subsequent experiments. Hence, line #1 will hereafter be termed as *ccr4a ccr4b*. The quantification of the leaf area is shown in **Figure 15C**, and this analysis reveals a decrease of 31% of the median leaf area in *ccr4a ccr4b* compared to wild-type plants.

Dwarfism, leaf chlorosis and early senescence are typical phenotypes of auto-immunity (van Wersch *et al.*, 2016; Freh *et al.*, 2021). Hence, I wondered if the phenotype in *ccr4a ccr4b* would be correlated to transcriptomic changes for genes related to immunity. To address this question, I analysed the transcriptome of whole rosettes by RNA-seq. But because phenotypes observed at 6 weeks are significant, I assumed that the analysis of RNA-seq datasets on such samples would be complicated by pleiotropic changes caused by the phenotypes rather than direct effects caused by the *ccr4a ccr4b* mutation. For this reason, I performed RNA-seq on whole rosettes of 24-day-old plants, before aggravated phenotypes appear. Additionally, because we can expect an increase in poly(A) tail size in *ccr4a ccr4b*, I decided not to use oligo-(dT) mRNA enrichment for library preparation. Indeed, mRNAs with longer poly(A) tails have more potential binding sites for oligo-(dT) probes and therefore would be enriched compared to mRNAs with shorter poly(A) tails, hence introducing a bias towards mRNAs deadenylated by CCR4a and CCR4b in the wild-type controls. Rather, I decided to use ribodepletion to enrich mRNAs before library preparation.

Upon sequencing of triplicates for each genotype, more than 36 million 50-bp single-end reads per sample were obtained. Following differential gene expression analysis, 1377 genes are significantly upregulated and 1037 genes are downregulated in *ccr4a ccr4b* using a cut-off of $|\log_2 FC| > 0.5$ (**Figure 15D**). Among the downregulated genes, *CCR4a* and *CCR4b* expression is respectively around 5.35x (-2.42 $\log_2$FC) and 2x (-0.9 $\log_2$FC) lower in *ccr4a ccr4b* compared to WT plants. This suggests that point mutations, in addition to potentially

introducing frame-shifts that likely impede the production of functional proteins, also lead to the downregulation of the corresponding mRNA. This downregulation may occur through the NMD pathway, triggered by the creation of premature termination codons (PTCs) (Popp & Maquat, 2016). However, it is important to note CRISPR/Cas9-induced mutations do not completely eliminate the expression of the transcripts.

To characterise up- and downregulated transcripts in *ccr4a ccr4b* plants, I performed over-representation analysis based on Gene Ontology (GO) terms (Yu *et al.*, 2012). GO terms significantly enriched among upregulated genes correspond to immune response and protein catabolism (**Figure 15E**). This reflects important transcriptomic changes essential to orchestrate a shift in the metabolism towards defence response. This shift is necessary to allocate resources to defence response and implicates a strong downregulation of genes involved in primary metabolism (Bilgin *et al.*, 2010; Huot *et al.*, 2014). Consequently, GO terms over-represented in downregulated genes correspond mostly to genes related to photosynthesis (**Figure 15E**).

Taken together, these results suggest that *ccr4a ccr4b* plants undergo a constitutive stress response which may explain the autoimmune phenotype observed in mutant plants.

1.2.2. Presentation of FLEP-seq2

To determine the contribution of CCR4a and CCR4b in shaping the poly(A) tails in *Arabidopsis*, we needed a transcriptome-wide method to accurately measure poly(A) tail length. Nanopore sequencing, such as direct RNA sequencing (DRS) offers many advantages over Illumina sequencing for this purpose and emerges as a method of choice to measure poly(A) tails (Parker *et al.*, 2020; Scheer *et al.*, 2021; Brouze *et al.*, 2023). DRS was previously used by our team in collaboration with the team of Andrzej Dziembowski to uncover the global effect of uridylation by URT1 in shaping the poly(A) tail distribution of mRNAs (Scheer *et al.*, 2021). One of the main interest of DRS is that it provides information about RNA modifications, including ^{m6}A. Such information is relevant in the study of deadenylation processes mediated by the CCR4-NOT complex, as ^{m6}A triggers deadenylation (Du *et al.*, 2016). However, a major drawback of DRS is its relatively low depth as compared to Nanopore cDNA sequencing methods. Additionally, the use of a splint ligation in the DRS protocol prevents the obtention of data of 3’ end modifications, such as uridylation. Because this information on mRNA tailing is essential for my thesis project, we decided to explore other Nanopore-based sequencing methods

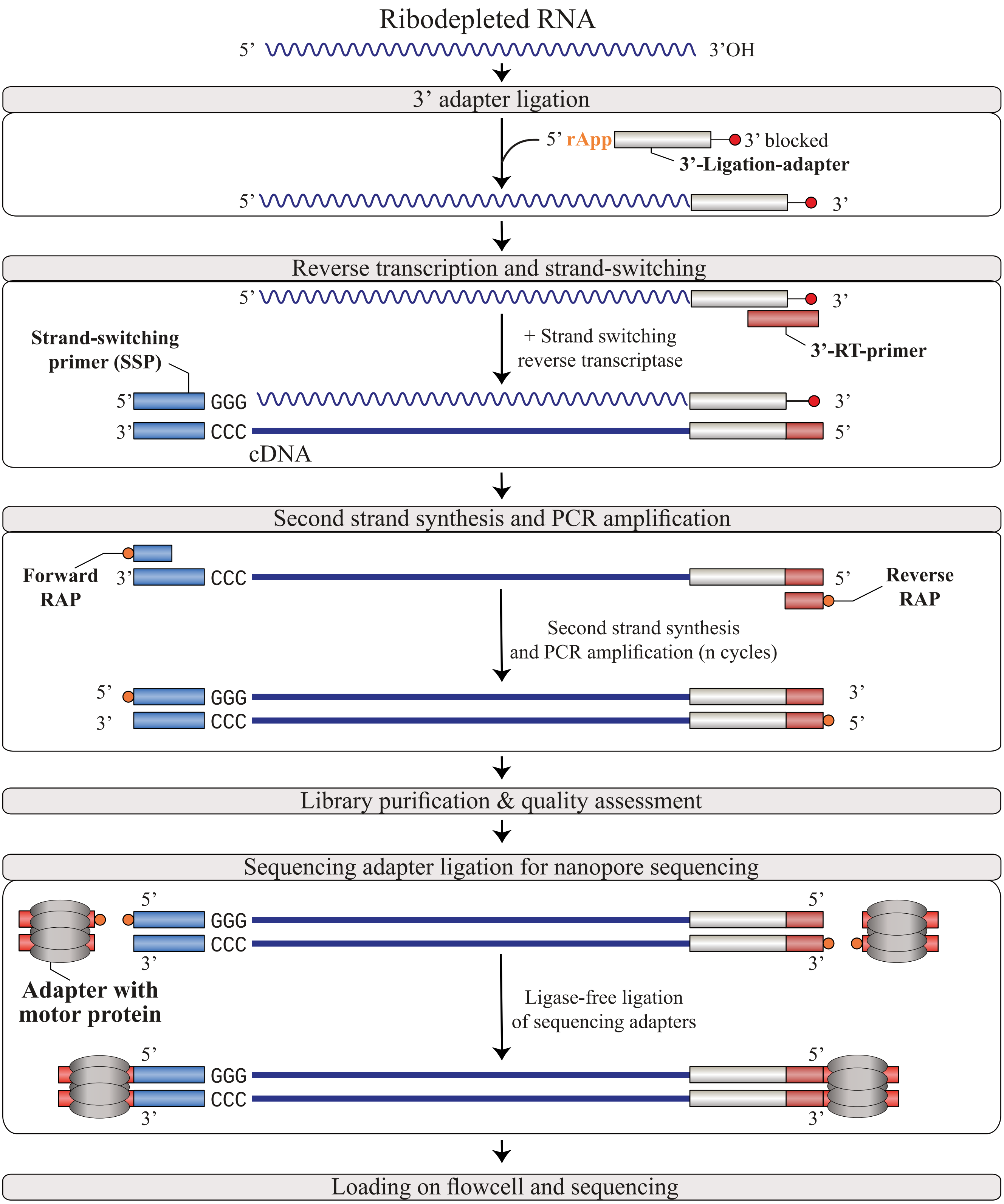

Figure 16. FLEP-seq2 workflow.

After total RNA extraction, mRNAs are enriched by ribodepletion. Next, a 3' adapter is ligated on the remaining RNAs. A primer complementary to the adapter is added and allows the strand-switching reverse-transcriptase (RT) to start the reaction. This specific RT adds a CCC overhang at the 3' extremity of the cDNA strand. The overhang is complementary to the strand-switching primer (SSP). The pairing of the two extends the template. The RT then switches template and synthesises the full length cDNA end. After PCR amplification, the library is purified and quality control is conducted. The rapid adapters (RAP) used to amplify the library by PCR contain the barcoding sequence necessary for multiplexing on the flow-cell and carry a proprietary modification that is needed for the ligase-free ligation of sequencing adapters containing the motor protein.

FLEP-seq2 is a recently developed PCR-based cDNA-sequencing method that provides full-length transcript information and poly(A) profiling at the transcriptome level (Jia *et al.*, 2022). FLEP-seq2 starts with depletion of rRNAs, followed by 3' adapter ligation on the ribodepleted RNAs (**Figure 16**). A primer complementary to the adapter is added and serves as an anchor to initiate cDNA synthesis. The strand-switching retro-transcriptase (RT) used adds an untemplated CCC overhang at the 3' extremity of the cDNA strand. Part of the strand-switching primer (SSP) base-pairs to the CCC overhang, creating an extended template. The RT then switches templates and synthesises the complementary strand until it reaches the end of the SSP. The resulting full-length cDNA strand is then amplified by PCR using rapid attachment primers (RAP) complementary to 5' and 3' sequences. These RAP contain the barcoding sequence necessary for multiplexing on the flow-cell and carry a modification that is needed for the ligase-free ligation of sequencing adapters containing the motor protein. Upon loading of the library onto the nanopore flow-cell, the motor protein binds a pore and actively translocates the cDNA strand through the pore. The poly(A) length is measured based on the basecalling sequence and corrected using the raw current intensity signal of the poly(A) region. Recent advances in our lab have shown that FLEP-seq2 can accurately measure poly(A) tail length and uridylation levels of custom spike-ins, making it a method of choice for my thesis project (**Figure S1**).

1.2.3. Global poly(A) tail size is increased in rosette of ccr4a ccr4b plants

Rosette samples used to prepare Illumina RNA-seq libraries were also used for FLEP-seq2 library construction. Following sequencing, basecalling and mapping, mitochondrion- and chloroplast-encoded mRNAs were removed, along with mRNAs with tails shorter than 10As or longer than 200As. We chose to use these thresholds to generate global poly(A) tail distribution profiles since there are several highly expressed non-coding RNAs that are annotated as nuclear protein-coding genes. These RNAs are not polyadenylated, but during sequencing, a short poly(A) tail of fewer than 5 adenosines is inferred. Due to their high expression levels, the global poly(A) distribution profile, spanning from 1 to 200 As, exhibits a prominent peak at tail lengths below 10 As. These shorter tail lengths are primarily associated with transcripts that are not polyadenylated, hence the threshold selection. In total, I obtained more than 10.3 million of nuclear encoded poly(A)+ mRNAs. 2613 genes had more than 50 reads per sample; 922 had more than 200 reads; 414 had more than 500 reads; 210 had more than 1000 reads. However, because of PCR amplification of the library, the absence of a unique molecular identifier, and of the workflow of the nanopore kit used, PCR duplicates and both strands of the PCR products are sequenced and artificially increase sequencing depth.

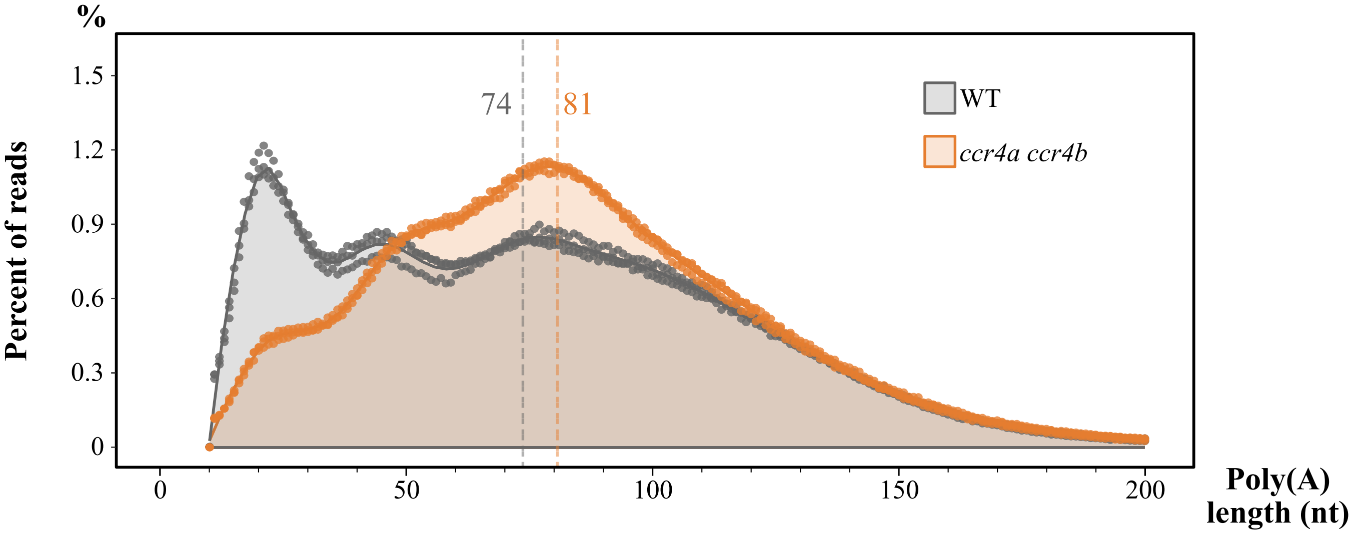

Figure 17. Global poly(A) tail distribution is longer in *ccr4a ccr4b*.
Bulk poly(A) distribution for WT (grey) and *ccr4a ccr4b* (orange) samples. Individual points are shown for three biological replicates and the respective average is indicated as a colored area. Median poly(A) tail size per genotype are represented as dashed lines.

To obtain a global overview of poly(A) tail length, data for all mRNAs in each genotype were combined and plotted as the average size distribution of all poly(A) tails (**Figure 17**). As evident from the point distribution, which represents the poly(A) tail size for the various replicates, we observe remarkably similar poly(A) distribution profiles across the replicates. In wild-type samples, the size distribution had clear peaks at 22, 45, and 75 nucleotides. The phasing between these peaks is 23-30 nucleotides, which is consistent with the footprint of one PABPC protein (Baer & Kornberg, 1983; Smith *et al.*, 1997; Wang *et al.*, 1999). Upon mutation of *CCR4a* and *CCR4b*, we observe an increase in global poly(A) tail size distribution, with the median size shifting from 74 As in wild-type to 81 As in *ccr4a ccr4b*. Interestingly, the main peak at 23 As is the most affected by the mutation. Between 10 and 45 As, the percentage of reads is lower in *ccr4a ccr4b*. Consequently, poly(A) tails between 45 and 120 As accumulate in the mutant. Here, we see that poly(A) tail sequencing by FLEP-seq2 is reproducible and allows us to accurately measure poly(A) tails. Our analysis using FLEP-seq2 to profile poly(A) tails in *ccr4a ccr4b* mutants provides the first transcriptome-wide evidence of a role for both CCR4a and CCR4b as deadenylases in *Arabidopsis*.

1.2.4. Upregulated mRNAs in ccr4a ccr4b rosette have longer poly(A) tails

Of the 1037 downregulated genes detected in RNA-seq, 877 were detected by FLEP-seq2, for a total of more than 3.6 million reads. 406 of these genes had more than 50 reads per sample. Similarly, 1331 of the 1377 upregulated genes were detected by FLEP-seq2. Yet, the total number of reads for these genes is about 167 000 reads, with only 46 of these genes having more than 50 reads in each sample. Defence response genes are not highly expressed in normal conditions, which complicates their detection by nanopore sequencing. Conversely, genes involved in photosynthesis, which corresponds to downregulated genes, are among the most highly expressed genes.

To determine whether the up- or downregulation of genes observed in Illumina RNA-seq could be related to changes in deadenylation, I plotted the poly(A) tail size distribution from 1 to 200 As of all mRNAs that were detected as up- or downregulated (**Figure 18**). Because highly expressed genes can influence the global poly(A) profile, we introduced a normalisation step before drawing the plots. To normalise, I calculated the percentage of reads at each poly(A) tail size for each mRNA in all biological replicates. Bins of 2As were used to draw poly(A) distribution for tails 1 to 200 As. To reduce variability during normalisation, I selected mRNAs with at least 10 reads per sample. Additionally, here, I included poly(A) lower than 10 As.

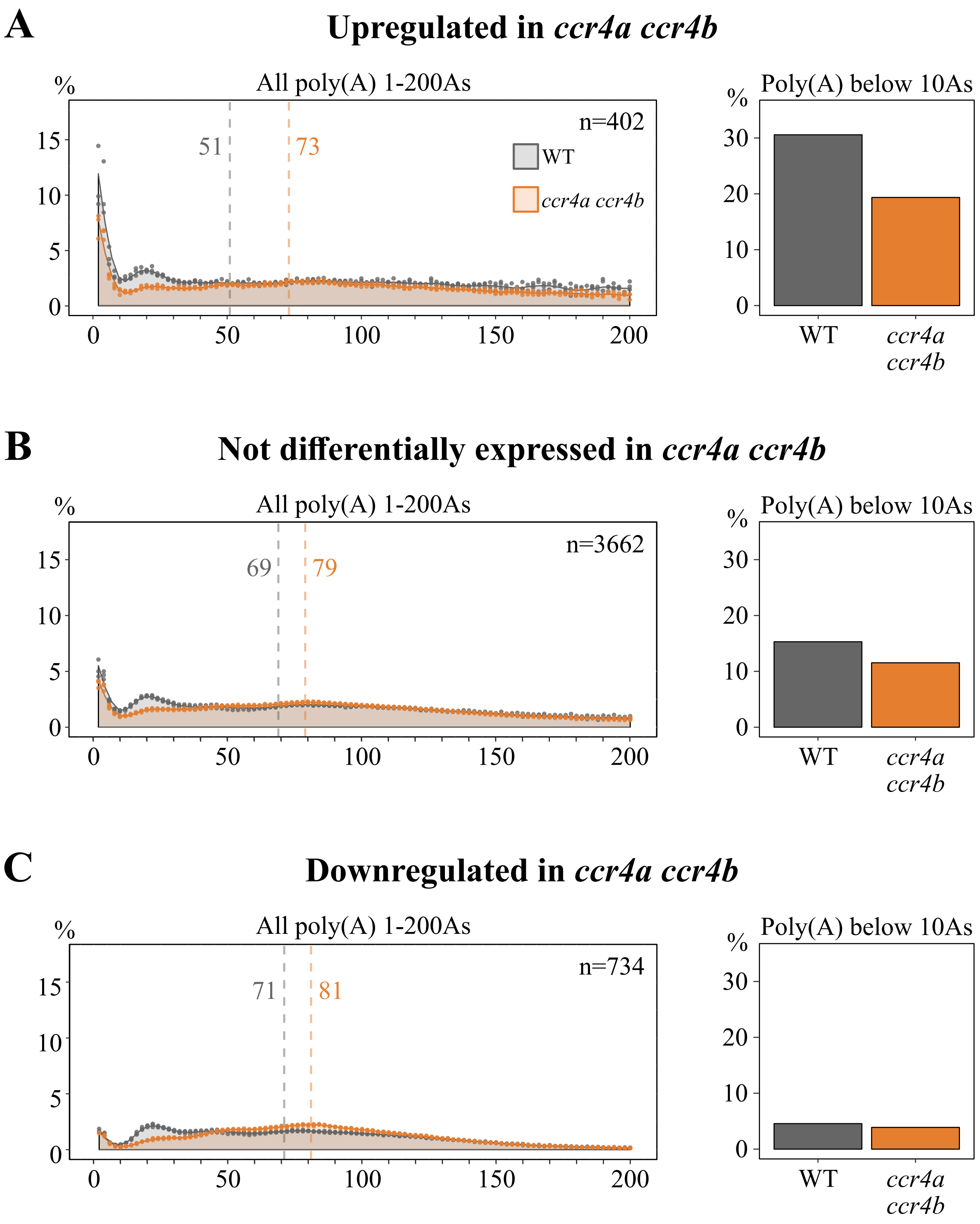

Figure 18. Upregulated genes are less deadenylated in *ccr4a ccr4b*.
Normalised poly(A) distribution for **A)** upregulated genes, **B)** not differentially expressed genes and **C)** downregulated genes for poly(A) tails 1-200As. Histograms on the right represent the percentage of reads with poly(A) tails shorter than 10As. To normalise, I calculated the percentage of reads for all poly(A) tail size (bins of 2 nucleotide) for each mRNA in all biological replicates. Dots represent the median percentage of reads per poly(A) tail size across biological replicates, while the colored lines represent the mean of this median across genotypes. To limit variability when normalising, I selected mRNAs that had at least 10 reads per sample. Number (n) of mRNAs used to draw the plots is indicated in upper right corner. Normalised median poly(A) tail size for all reads are represented as grey (wild-type) and orange (*ccr4a ccr4b*) dashed lines.

Because we normalise the poly(A) tail length per mRNA, the presence of non-coding transcripts has minimal impact on the normalised poly(A) profiles compared to the global poly(A) profiles, ensuring that no bias is introduced towards shorter poly(A) tails.

First, when examining at the poly(A) tail distribution across the three categories (downregulated, not differentially expressed and upregulated) irrespective of the genotype, we observe markedly different distributions. Indeed, upregulated mRNAs accumulate more oligoadenylated isoforms (below 10 As, **Figure 18A**) than mRNAs that are not differentially expressed (**Figure 18B**) or that are downregulated (**Figure 18C**). This suggests that upregulated mRNAs are more intensely deadenylated. This is consistent with the idea that this category is enriched in stress-response genes, whose transcripts are known to be short-lived and deadenylate faster (Chantarachot *et al.*, 2020; Eisen *et al.*, 2020).

When comparing genotypes, we observe an increase in the median poly(A) tail length across all categories in *ccr4a ccr4b*. For upregulated genes in particular, it increases by 22 As (**Figure 18A, left panel**). This effect is most likely caused by a reduction of the proportion of highly deadenylated mRNAs as they accumulate to a lesser extent in *ccr4a ccr4b* compared to wild-type samples (**Figure 18A, right panel**). For not differentially expressed genes and downregulated genes, the lengthening of poly(A) tails in *ccr4a ccr4b* is of 10As (**Figure18B and C, left panels**). We also observe a diminution of the proportion of oligoadenylated mRNAs in these categories upon mutation, but the decrease is not as important as for upregulated genes.

Here, our data suggest that CCR4a and CCR4b act as broad deadenylases that are able to deadenylate most, if not all, transcripts, whether they are differentially expressed in the *ccr4a ccr4b* mutant or not, as shown by the lengthening of the poly(A) tails in all categories. The impact of the mutation however, is best seen for upregulated mRNAs. This category is composed of stress-response genes. In humans and plants, these transcripts are actively deadenylated and short-lived (Chantarachot *et al.*, 2020; Eisen *et al.*, 2020). Consistent with this, in our dataset, they accumulate short oligo(A) isoforms in wild-type, implying that they are actively deadenylated. In *ccr4a ccr4b*, the proportion of these short tails largely decreases, and restores a median poly(A) tail length that resembles the ones in wild-type samples for the other categories. Altogether, this suggests that CCR4a and CCR4b may play a role in the extensive deadenylation of these mRNAs.

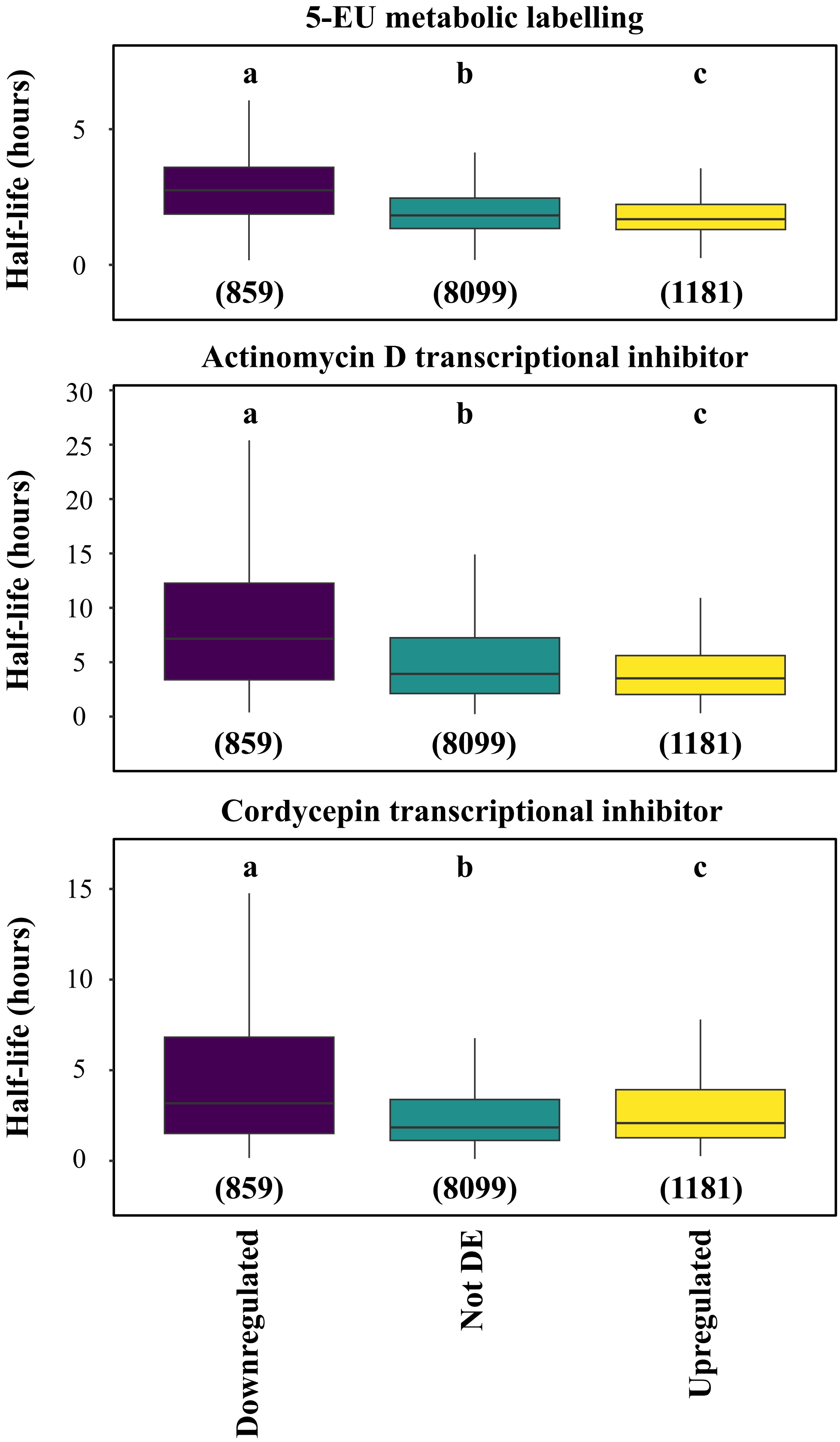

Figure 19. Upregulated genes in *ccr4a ccr4b* are short lived transcripts.
Boxplot analysis comparing mRNA half-lives as determined by 5-EU metabolic labeling (upper panel), or by actinomycin D (middle panel) and cordycepin (lower panel) transcription inhibitors vs. the differential expression in *ccr4a ccr4b* determined by RNA-seq. Genes commonly found in the 3 different decay rate experiments were used to determine half-lives of genes analysed by RNA-seq. Numbers in parentheses represent the number of genes used to draw the respective boxplots.The horizontal line in each box represents the median, and lower and upper hinges indicate first and third quartiles, respectively. Letters above the boxplots represent the significant statistical *p*-values calculated using two-tailed Wilcoxon rank-sum test.

1.2.5. Upregulated mRNAs in ccr4a ccr4b rosette have shorter half-lives

Upregulated mRNAs accumulate a substantial amount of highly deadenylated mRNAs with poly(A) tail shorter than 10 As. Such a short poly(A) tail is not sufficient for PABPC binding, making the mRNA more susceptible to rapid degradation. Hence, we wondered whether differential expression of mRNAs in *ccr4a ccr4b* correlated with half-life. To this end, I compared the differentially expressed genes in *ccr4a ccr4b* with three independent datasets reporting transcriptome-wide mRNA half-lives in *Arabidopsis* (Narsai *et al.*, 2007; Sorenson *et al.*, 2018; Szabo *et al.*, 2020).

We found that mRNA half-life correlated with the changes in steady-state in *ccr4a ccr4b* for the datasets using either 4-EU metabolic labeling or actinomycin D as a transcriptional inhibitor (**Figure 19, upper and mid panels**). This suggests that stable mRNAs are downregulated, whereas unstable transcripts accumulate in *ccr4a ccr4b*. Hence, we can hypothesise that in a wild-type background, CCR4a and CCR4b may be, at least in part, involved in the rapid turnover of unstable mRNAs. Upon mutation of both deadenylases, these mRNAs would be stabilised and accumulate to higher levels. This is consistent with the fact that upregulated mRNAs show a significant difference in poly(A) tail length between WT and *ccr4a ccr4b*, compared to the smaller difference observed between genotypes in downregulated or not differentially expressed genes.

Intriguingly, this correlation is absent in the dataset generated using cordycepin as a transcriptional inhibitor (**Figure 19, lower panel**). Cordycepin is an analog of ATP and incorporates into nascent RNA during transcription and polyadenylation. Due to the absence of a 3'OH group, the incorporation of cordycepin inhibits elongation and induces transcriptional arrest. This interference likely affects poly(A) tail elongation more than mRNA transcription, as ATP is in greater demand during poly(A) tail synthesis than during mRNA transcription. As a result, cordycepin could disproportionately affect polyadenylation, leading to an imbalance in which mRNA molecules might be transcribed but not properly polyadenylated, thereby affecting their metabolism during half-life determination Additionally, cordycepin inhibits deadenylation by the deadenylase PARN, suggesting that the absence of a 3'OH impedes deadenylation, at least for this deadenylase (Aström *et al.*, 1991).

For these reasons, the effects of cordycepin on poly(A) synthesis and protection against deadenylation may introduce significant bias for mRNAs whose turnover is regulated by deadenylases, which may explain the loss of correlation between decay rates and genes upregulated in *ccr4a ccr4b*.

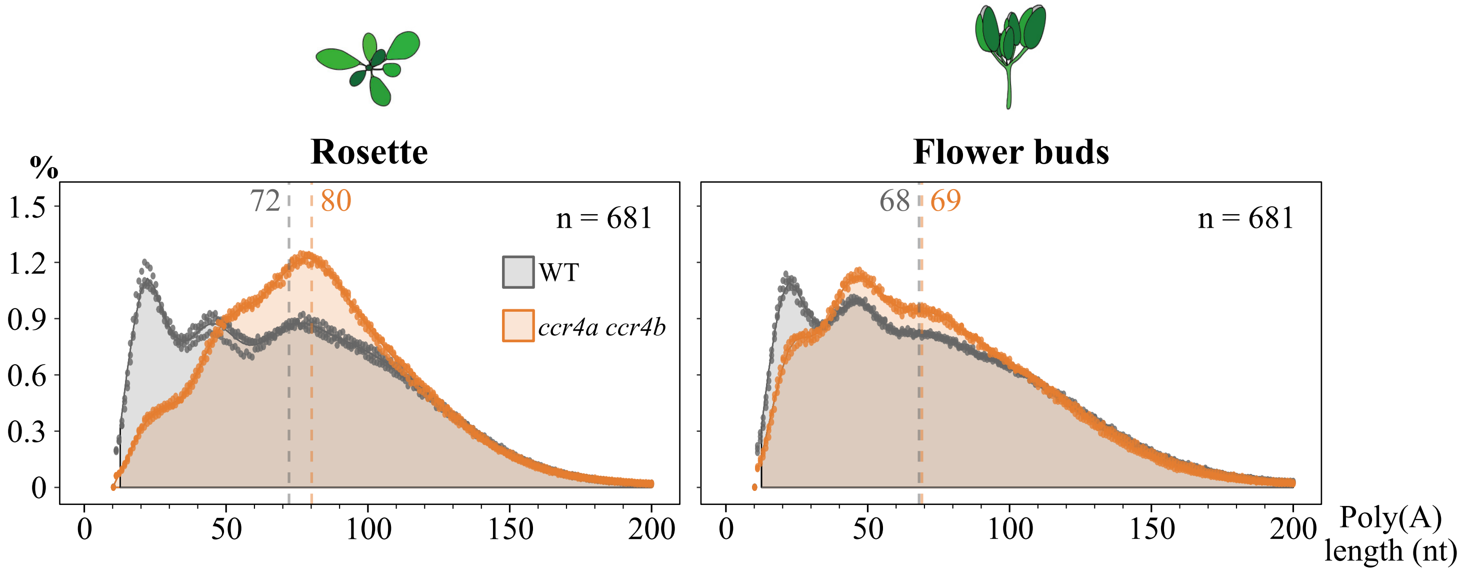

Figure 20. Tissue specific regulation of poly(A) tail length mediated by CCR4a and CCR4b. Bulk poly(A) distribution for WT (grey) and *ccr4a ccr4b* (orange) in leaves (left panel) and flower buds (right panel). Individual points are shown for three biological replicates and the respective average is indicated as a colored area. Number (n) of mRNAs used to draw the plots is indicated in the upper right corner. Median poly(A) tail size per genotype are represented as dashed lines.

1.3. Phenotypic and molecular consequences of deadenylation defects in *Arabidopsis* flowers

1.3.1. Poly(A) tail distribution and deadenylation by CCR4a and CCR4b are differently regulated across development

To gain a broader understanding of the roles of CCR4a and CCR4b in mRNA deadenylation across different *Arabidopsis* tissues, I compared poly(A) profiles from whole rosettes and unopened flower buds. Biological triplicates were prepared from flower buds of wild-type and *ccr4a ccr4b* plants. I applied the same filters as for the rosette FLEP-seq2 analysis, and removed chloroplastic and mitochondrial mRNAs, as well as excessively short and long poly(A) tails. To improve comparability between tissues limit variability, I applied a threshold to select mRNAs with more than 200 reads in each of the 12 rosette and flower bud samples. 681 genes were selected according to these criteria. In total, 3.5 and 3.5M reads were used to generate bulk poly(A) distributions for wild type and *ccr4a ccr4b* in rosette respectively; 2.6M and 2.7M reads were used to draw bulk poly(A) distribution for wild-type and *ccr4a ccr4b* in flower buds respectively (**Figure 20**).

While the role of CCR4a and CCR4b in regulating the accumulation of short poly(A) tails is also conserved in flower buds, its effect is limited to the 10-30 As population and is less prounounced compared to rosettes. Consequently, the median poly(A) size in *ccr4a ccr4b* increases, but not to the same extent as in rosette leaves.

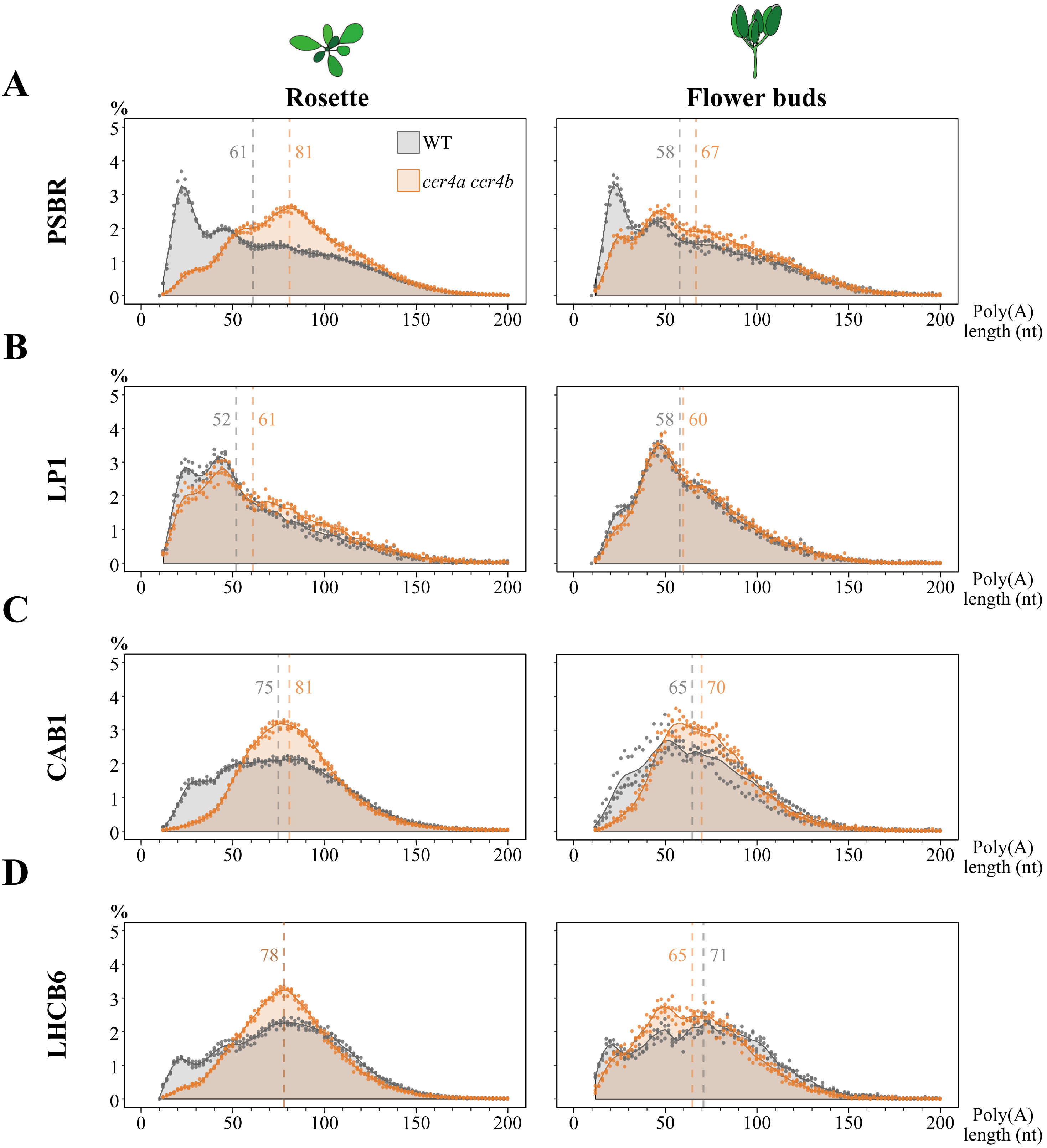

Figure 21. Poly(A) tail regulation is specific to both the tissue, and the mRNA species. Bulk poly(A) distribution for WT (grey) and *ccr4a ccr4b* (orange) in rosette (left panels) and flower buds (right panels) for **A)** PSBR, **B)** LP1, **C)** CAB1 and **D)** LHCB6 mRNAs. Individual points are shown for three biological replicates and the respective average is indicated as a colored area. Median poly(A) tail size per genotype are represented as dashed lines.

Next, we wondered whether genes expressed in both tissues exhibit different poly(A) distribution, and whether the mutation affects the profiles differently. I selected four of the most highly expressed genes common to both rosette and flower buds (**Figure 21**). The wild-type poly(A) tail distribution of PSBR mRNA is similar between rosette and flower buds, with only a slight reduction in the median poly(A) tail size in flower bud-expressed mRNAs (**Figure 21A, grey lines**). However, the profiles observed in *ccr4a ccr4b* vary considerably depending on whether the mRNA is expressed in rosette or in flower buds (**Figure 21A, orange lines**). Conversely, the profile of LP1 in wild-type samples varies depending on whether the mRNA is expressed in rosette or flower buds (**Figure 21B**), as the proportion of reads around 20 As is lower in flowers. This indicates that deadenylation activity is specifically modulated by factors inherent to the tissue of expression. This modulation of the deadenylation implicates, at least in part, CCR4a and CCR4b, because we observe changes in the distribution upon mutation.

Poly(A) tail distribution of CAB1 in wild-type samples is slightly different between rosette and flower buds (**Figure 21C**). Yet, we do not observe a different lengthening poly(A) tails in *ccr4a ccr4b* whether the mRNA is expressed in rosette or in flowers. This suggests that the processes regulating the poly(A) tail length of CAB1 are conserved in both rosette and flower buds.

For LHCB6, the proportion of mRNAs with small poly(A) tail < 40 As is lower in *ccr4a ccr4b* compared to wild-type in rosette and flowers, as for all profiles observed so far (**Figure 21D**). However, the median poly(A) tail length is not increased. Interestingly, the median poly(A) tail length is equivalent in rosette, and is smaller in *ccr4a ccr4b* flowers compared to wild-type samples. This effect on the median poly(A) tail length is caused by a loss of long poly(A) tails in *ccr4a ccr4b*. A potential compensation by the expression of other deadenylases may explain this intricate effect on long poly(A) tails. Yet, we did not observe any upregulation of deadenylases in rosette of *ccr4a ccr4b* plants (**Table S2**). Additionally, it is possible that the loss of CCR4 proteins modifies the activity and substrate recognition of CAF1 proteins, as was demonstrated for human CAF1 *in vitro* (Chen *et al.*, 2021).

Altogether, our data indicate that CCR4a and CCR4b act as deadenylases in two distinct tissues. Interestingly, their activity is defined by both the mRNA species and the tissue it is expressed in, thereby potentially involving tissue-specific factors.

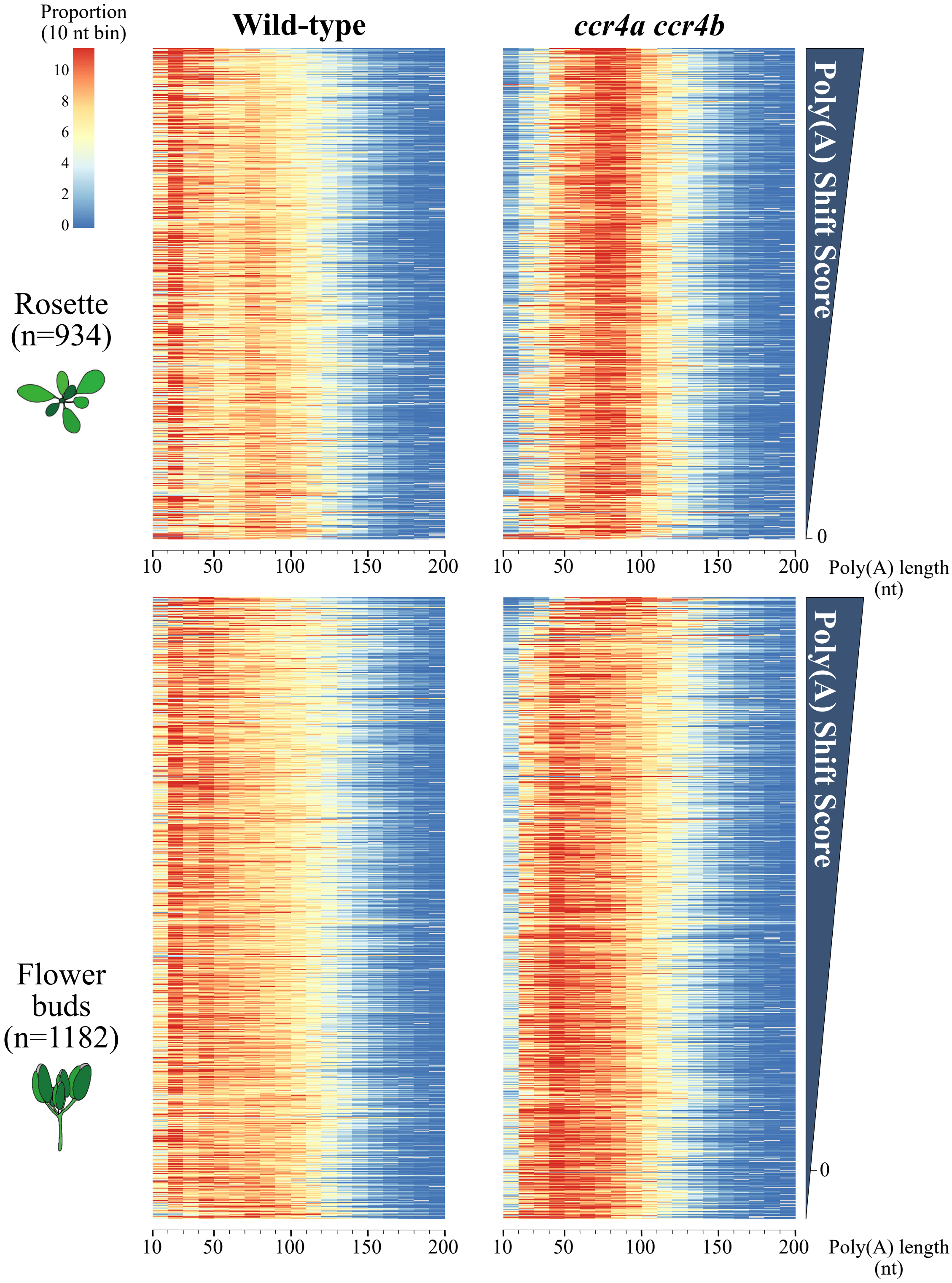

Figure 22. Widespread impact of CCR4a CCR4b in shaping the poly(A) profiles of mRNAs in rosette and flowers.
Heatmap showing the poly(A) tail length distribution of wild-type (left heatmaps) and *ccr4a ccr4b* (right heatmaps) in rosette (upper heatmaps) and flower buds (lower heatmaps). Frequencies of reads for each bin of poly(A) tail sizes (bins of 10As) are shown by a color scale with each row representing one gene. Only genes with at least 200 reads in each replicate and genotype were used to draw the plot. The number of genes is shown to the left of heatmaps. Genes are sorted by their Poly(A) Shift Score (PASS), in descending order from top to bottom.

1.3.2. The poly(A) tail size of a small mRNA population in flowers is largely regulated by CCR4a and CCR4b

Analysis of the poly(A) tail patterns of specific mRNAs has revealed a direct influence of tissue-specific expression and the activity of CCR4a/CCR4b deadenylases. Furthermore, the poly(A) tail of some mRNAs is more significantly lengthened upon mutation of the deadenylases, suggesting either that the CCR4a/CCR4b defect is not efficiently compensated for by alternative deadenylases such as CAF1 proteins, or that CCR4a/CCR4b preferentially target mRNAs under unstressed growth conditions. To identify mRNAs that are preferentially targeted by CCR4a and CCR4b, I calculated the poly(A) shift score (PASS) of all mRNAs in wild-type and *ccr4a ccr4b* in rosette and flowers. PASS is a metric that measures the discordance between two cumulative curves representing the distribution of tail length (Ogami *et al.*, 2022). When applied to individual mRNAs, PASS represents the shifting of the poly(A) tail of the mRNA between two conditions, here the genotype. PASS can be positive or negative: a positive score indicates poly(A) tail lengthening in *ccr4a ccr4b* compared to wild-type, whereas a negative score indicates the opposite trend. To emphasise the changes in poly(A) distribution in *ccr4a ccr4b*, I calculated PASS for poly(A) tails ranging from 10 to 120 As, as the distributions of wild-type and *ccr4a ccr4b* converge at approximately 120 As in both rosette and flower buds (**Figure S2**). I used a threshold of 200 reads per sample, and calculated the PASS for 934 and 1182 mRNAs in rosette and flower buds, respectively (**Table S3**). In rosette, 931 mRNAs had positive PASS while only 3 mRNAs had negative PASS. In flower buds, 1089 mRNAs had positive PASS and 93 had negative PASS, indicating that the depletion of long poly(A) tails in the mutant (as observed for *LHCB6* mRNA, **Figure 21D**) is stronger in flower buds.

Figure 22 shows the heatmap of poly(A) distribution of mRNAs sorted by their PASS score. Bins of 10 As were used to draw poly(A) distribution for tails ranging from 10 to 200 As. Genes with the highest PASS are at the top while those with the lowest PASS are at the bottom of each heatmap. First, we observe that all analysed mRNAs, irrespective of their PASS score, lose a proportion of the short poly(A) tail population in *ccr4a ccr4b*, confirming the global role of CCR4a and CCR4b in shaping the poly(A) profiles of the transcriptome (**Figure 22**). This effect is also evident for mRNAs with negative PASS in flower buds (**Figure 22, lower heatmaps**), indicating that these mRNAs also lose a substantial proportion of longer poly(A) tail which ultimately compensates for the loss of the short poly(A) tail population and shifts the PASS towards negative values. Importantly, the loss of the short poly(A) tail population is exacerbated in flowers for the population

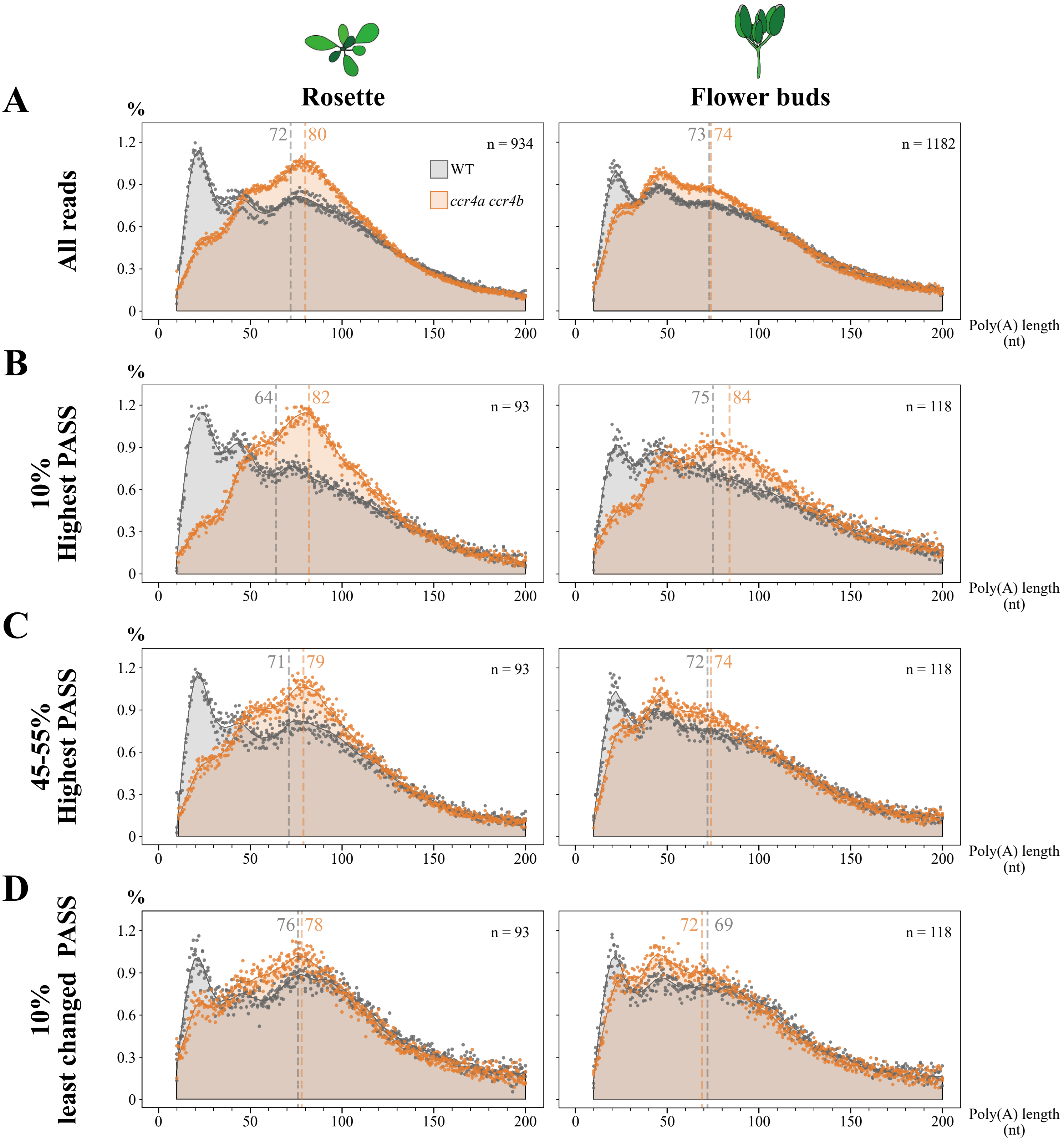

Figure 23. Some mRNAs are more prone to deadenylation by CCR4a and CCR4b. Normalised poly(A) distribution for **A)** all mRNAs, **B)** the 10% highest PASS mRNAs, **C)** mRNAs withing the range of 45-55% highest PASS, **D)** the 10% lowest PASS mRNAs in rosette (left panels) and flower buds (right panels). To normalise, I calculated the percentage of reads at all poly(A) tail size (bins of 1 nucleotide) for each mRNA in all biological replicates. Dots represent the median percentage of reads per poly(A) tail size across biological replicates, while the colored areas represent the mean of this median accross genotypes. To limit variability when normalising, I selected mRNAs that had at least 200 reads per sample. Number (n) of mRNAs used to draw the plots is indicated in upper right corner. Normalised median poly(A) tail size for all reads are represented as grey (wild-type) and orange (*ccr4a ccr4b*) dashed lines.

with the highest PASS, as compared to the rest of the flower transcriptome. Therefore, CCR4A and CCR4b appear to play a prominent role in shaping poly(A) tails of a subset of mRNAs detected in flower buds.

Another way to observe the global impact of the *ccr4a ccr4b* mutation on poly(A) tails is by doing subsets of mRNAs based on their PASS. **Figure 23** shows normalised distribution for all mRNAs, the 10% mRNAs with the highest PASS, mRNAs within the range of 45-55% highest PASS, and the 10% least changed PASS mRNAs. For the top 10% of mRNAs with the highest PASS, the accumulation of poly(A) tails of 10-50 As is diminished in *ccr4a ccr4b* (**Figure 23B**). Furthermore, the difference in accumulation of the 10-50 As population between WT and *ccr4a ccr4b* is relatively similar in rosettes and in flower buds. For mRNAs within the 45-55% highest PASS range, there remains a significant distinction in the accumulation of short poly(A) tails between wild-type and *ccr4a ccr4b* in rosettes, though the difference is less pronounced compared to the top 10% highest PASS mRNAs (**Figure 23C**). However, in flower buds, the accumulation of short poly(A) tails is still lower in *ccr4a ccr4b* compared to the wild-type, but the difference between the two is not as prominent as observed in the top 10% of highest PASS mRNAs.

As observed in the **Figure 22**, even mRNAs whose PASS is close to 0 lose to some extent the short poly(A) population, both in rosette and in flowers (**Figure 23D**). However, the differential accumulation of short poly(A) tails between wild-type and *ccr4a ccr4b* is even more subtle in flowers, and the median poly(A) tail is shorter in *ccr4a ccr4b*. As hypothesised, this is caused by a slight but consistent reduction in the long poly(A) tail population. We consistently observe fewer long poly(A) tails in *ccr4a ccr4b* mutants in both rosette and flowers. In flowers, the effect is easily seen as it shifts the median poly(A) tail size, due to a less significant loss of the short poly(A) population in *ccr4a ccr4b*. This implies that mRNAs with mid to low PASS do not exhibit a global increase in poly(A) tails across all sizes, but rather a narrowing of the distribution. This effect is not seen for the 10% of mRNAs with the highest PASS, suggesting that only mRNAs that are not highly deadenylated by CCR4a and CCR4b are more prone to it.

Taken together, our data indicate that the reduction in short poly(A) tail accumulation in *ccr4a ccr4b* is conserved for all mRNAs in rosette and flower buds. As the depletion of the short poly(A) tail population occurs even for genes with low or negative PASS, it suggests that virtually all mRNAs are potentially deadenylated by CCR4a and CCR4b. Nonetheless, we identified a specific mRNA population in flowers that seems to be more affected by the loss of CCR4 proteins. One of the most straightforward explanations for this observation is that these mRNAs are preferential targets of CCR4a and CCR4b in flowers.

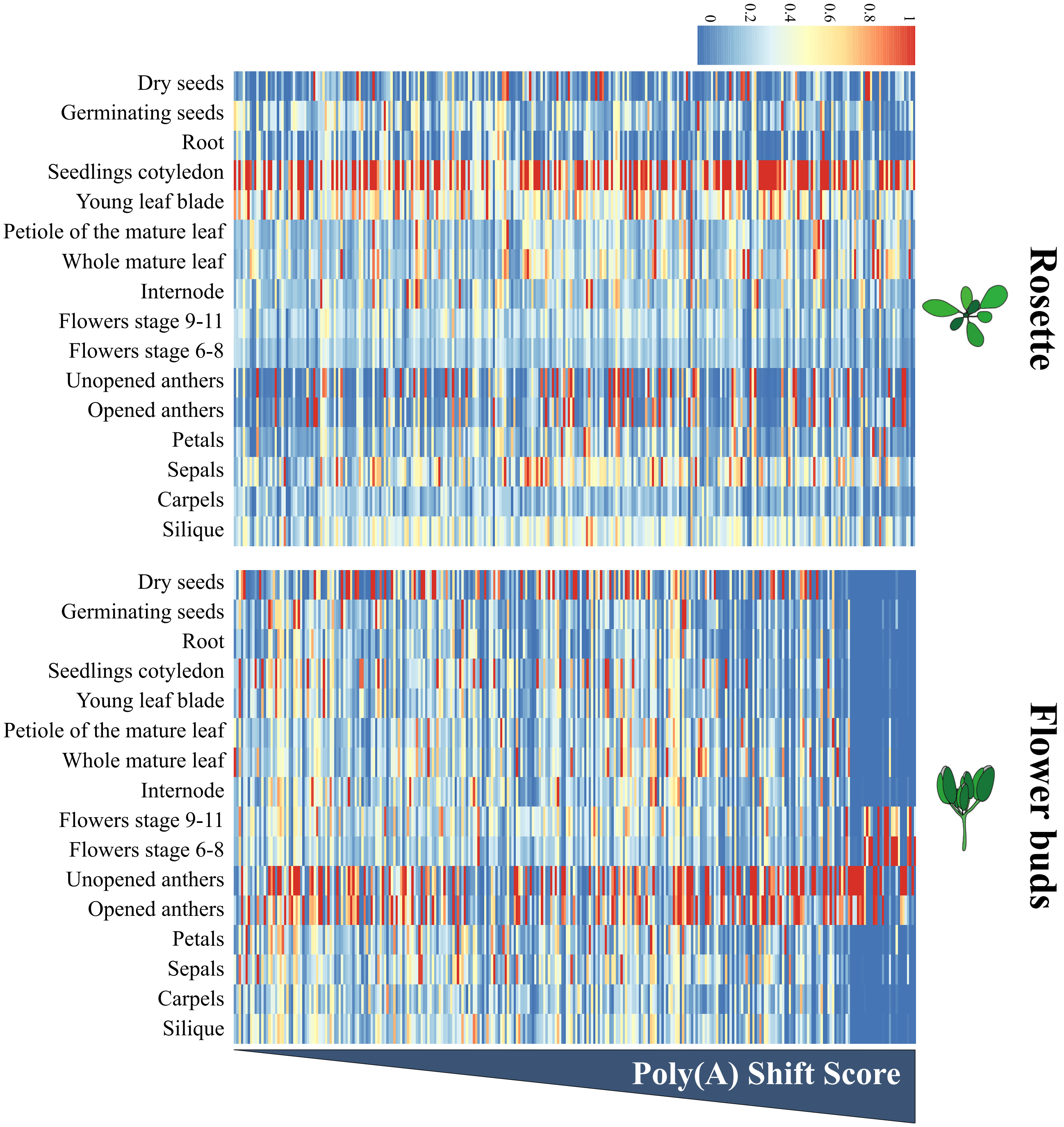

Figure 24. mRNAs mainly deadenylated by CCR4 proteins in flowers are exclusively expressed in specific developmental stages.
Gene expression heatmap of the 300 genes with the highest PASS in rosette (upper panel) and flower buds (lower panel). Relative expression level in selected representative tissues (rows) are shown by a color scale for each gene. For each gene, relative read counts (RNA-seq) normalised with median-of-ratio method were downloaded from TraVA (Klepikova *et al.*, 2016; http://travadb.org, accessed on 28 August 2023). Genes are sorted by their PASS in ascending order from left to right.

1.3.3. mRNAs with high PASS in flowers are expressed in specific tissues

Next, we wondered in which biological processes genes with the highest PASS were involved. We noticed that many mRNAs with high PASS in flowers are specifically expressed at distinct developmental stages. To determine if the PASS can be correlated with expression during a specific developmental stage, I plotted the gene expression profile of all mRNAs sequenced with more than 200 reads per sample (**Figure 24**). Genes on the right-most part of the heatmap have the highest PASS. Each column is an individual mRNA, while each row is a specific developmental stage. I selected 14 different tissues/ developmental stages that are representative of the full size heatmaps shown in **Figure S3 and S4**. Additionally, only the 300 mRNAs with the highest PASS were plotted.

Interestingly, most mRNAs with high PASS in flowers are specifically expressed in distinct developmental stages of flowers (particularly at stages 6-8, see below for a description of stages) or in maturing and mature anthers (**Figure 24, lower panel**). The coupling between PASS and expression pattern is lost for mRNAs with lower PASS and is does not exist in rosette (**Figure 24, upper panel**). The fact that such a coupling is detected in flower buds implies a potential role for CCR4a and CCR4b in shaping the poly(A) tails of transcripts expressed in developing and mature anthers and flowers of the corresponding developmental stage.

In the gene expression database nomenclature, “Flowers stage 6-8” and “Flowers stage 9-11” corresponds to stages 10-12 described by Smyth and colleagues (Smyth *et al.*, 1990). The developing anthers within these flowers correspond to anther stage 8-11 described by Sanders and colleagues (Sanders *et al.*, 1999). The “Unopened anthers” stage used in the database corresponds to mature anthers of unopened flowers and correspond to anther stage 11-12.

Anthers stage 8-12 corresponds to pollen stage 5-10 (Sanders *et al.*, 1999) which is, among other crucial processes, characterised by the formation of the pollen wall (Ariizumi &Toriyama, 2011; Ma *et al.*, 2021).

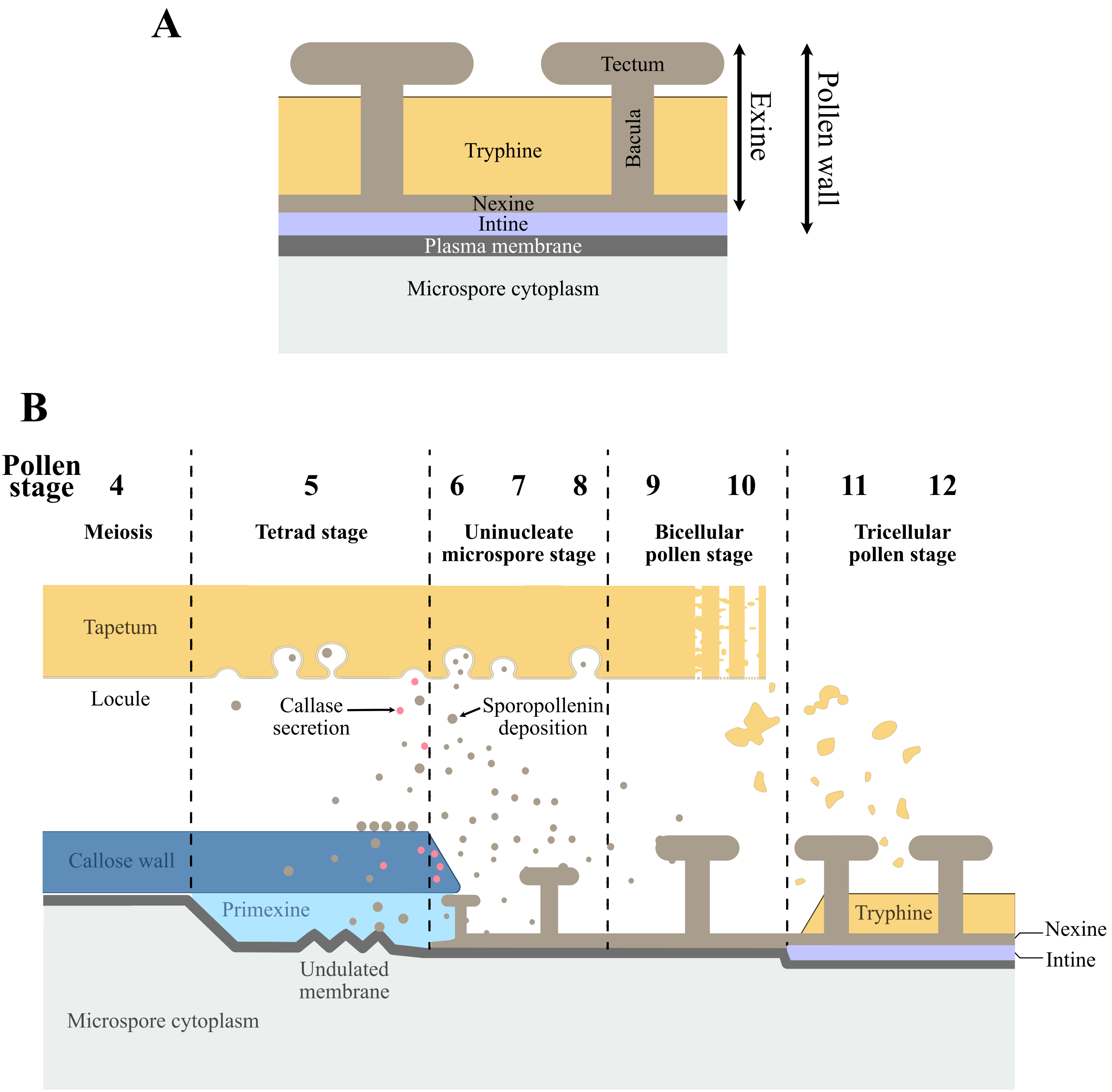

Figure 25. Organisation and synthesis of the pollen wall.
A) Structure of the pollen wall of the mature microspore. Exine is composed of the bacula, tectum, and the nexine layer. The pollen wall is composed of the exine and intine layers, and of the tryphin layer, or pollen coat, applied upon programmed cell death of the tapetal cells. **B)** Synthesis of the pollen wall. After the first meiosis, the tetrad is wrapped in a thick callose layer. Between the 5 and 6 pollen stages, the tapetum synthesises and secretes callase to degrade the callose layer and release the microspore. Following the decay of the callose layer, the sporopollenin secreted by the tapetal cells in the anther locule is deposited onto the primexine. The deposition forms the sculptured exine layer. Undulation of the plasma membrane defines the patterned structure of the exine layer. At the bicellular stage, the tapetum undergoes programmed cell death. Debris generated from the tapetum degeneration fill the exine cavities and form the tryphine layer. At the tricellular stage, the microspore synthesises the intine layer, eventually forming the mature pollen wall. Adapted from Ma *et al.*, 2021.

The pollen wall consists of several distinct layers, with two main components: the intine and the outermost layer called the exine (**Figure 25A**) (Gómez *et al.*, 2015; Ma *et al.*, 2021). The exine layer begins to take shape through a series of intricate steps (**Figure 25B**). Initially, callose is deposited on the outer surface of the microspore. Following this deposition, callose undergoes degradation. An essential tissue in this process are the tapetal cells, which play a pivotal role in exine layer formation (Ariizumi & Toriyama, 2011). These specialised cells secrete an enzyme called callase, which is responsible for breaking down the callose layer surrounding the microspore. Once the callose layer around the microspore is degraded, it creates a receptive surface on the microspore. The secretion by tapetal cells of sporopollenin precursors, lipids and proteins onto the microspore surface builds a patterned exine layer. The final steps of exine formation are initiated by programmed cell death of tapetal cells. Tapetum degenerative debris is composed mostly of lipids and proteins, and is deposited on the exine surface and its gaps. Intine, the innermost layer of the pollen cell wall, is produced by the microspore and is mostly composed of pectin, cellulose, hemicellulose and proteins. The protein composition and their metabolic activities in both intine and exine are essential for proper pollen function.

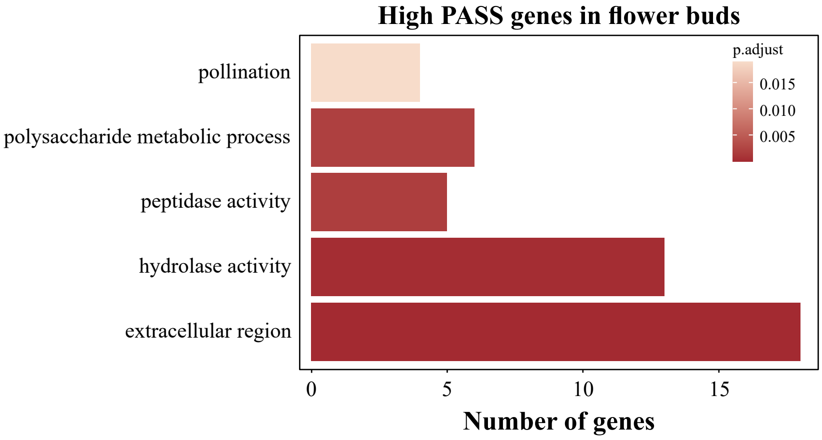

Figure 26. Genes with high PASS are enriched in GO terms related to pollen cell wall formation.

Over-representation analysis of GO terms for the 30 genes with the highest PASS. The length and color of bars represent respectively the number of genes and significance calculated with a hypergeometric test with Benjamini-Hochberg correction.

Interestingly, GO analysis of the 30 genes with the highest PASS showed an enrichment in GO terms related to secreted proteins, pollination, and metabolic functions directly linked to pollen cell wall formation (**Figure 26**). Upon further inspection, I found that 10/30 genes with the highest PASS, or their orthologs in other plants, have functions that were identified as important for pollen development (**Table S4**). Among them are proteins of the exine layer that are essential for proper pollen hydration upon reaching the stigma, which is a critical step towards pollen tube germination (Mayfield & Preuss, 2000; Updegraff *et al.*, 2009). Other proteins located in the intine layer are involved in the reshaping of the pectin web to ensure plasticity for cell wall remodelling during pollen tube growth (Jiang *et al.*, 2005; Tian *et al.*, 2006; Leroux *et al.*, 2015).

Interestingly, genes related to pollen development are differentially expressed in a *not1* heterozygous mutant (Motomura *et al.*, 2020; Pereira *et al.*, 2020). The CCR4-NOT complex has several cellular functions beyond deadenylation (see **Introduction 2.3.2**; Collart, 2016), and consequently, the phenotypes observed in the *not1*$^{+/-}$ mutant may not be solely attributable to defects in deadenylation. However, among the differentially expressed genes in *not1*$^{+/-}$, several have been identified with high PASS in my data. This observation led us to question whether changes in the poly(A) tail length of these genes in *ccr4a ccr4b* mutants could affect pollen functions.

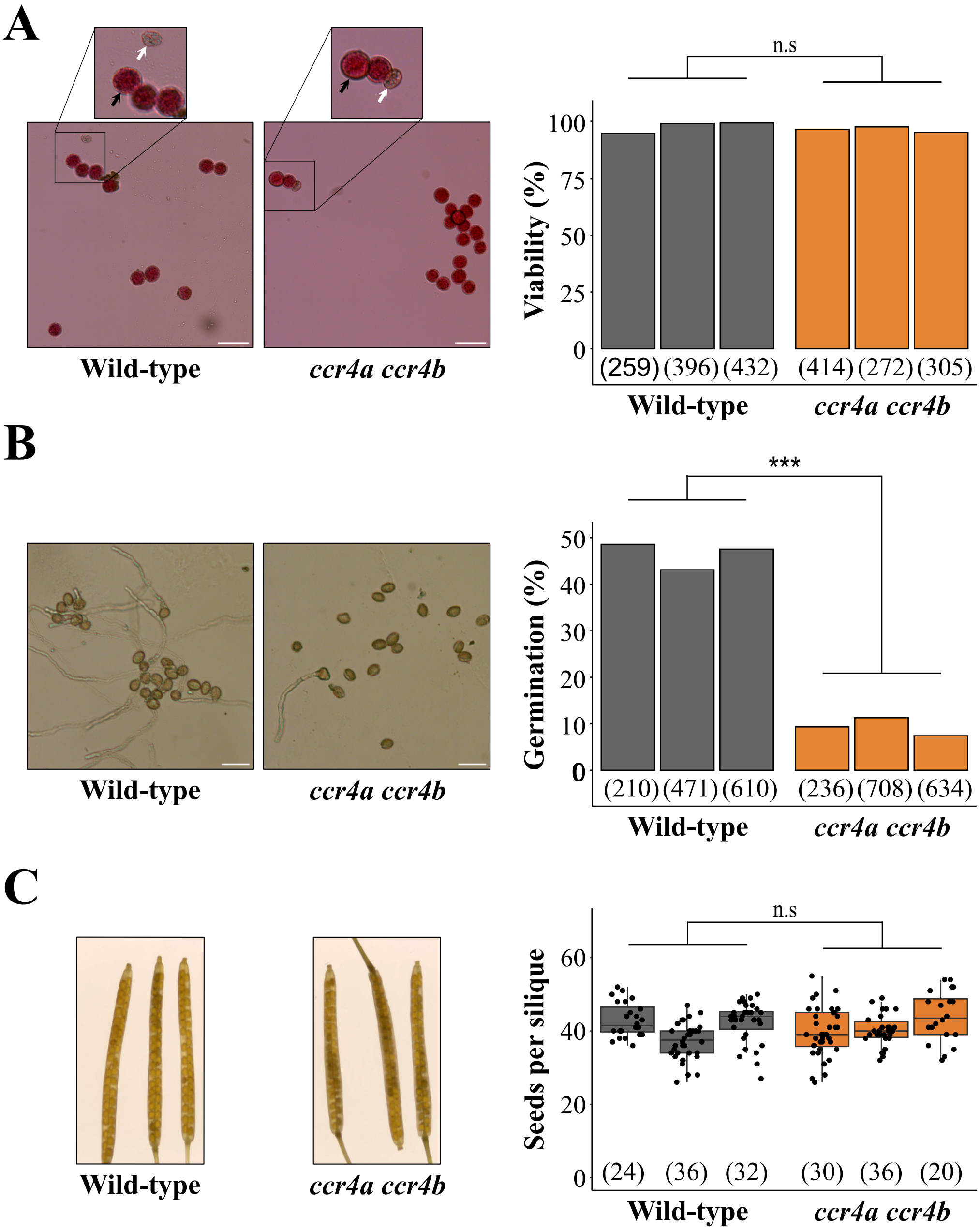

Figure 27. Pollen tube germination is impaired *in vitro* for *ccr4a ccr4b* pollen grains.
A) Pollen viability of wild-type and *ccr4a ccr4b* pollen. Pollen viability was assessed by Alexander staining. Left panel shows representative pictures of wild-type and double mutant pollen grains. Magnified views show viable pollen grains (black arrow), which appear pink, and aborted pollen grains (white arrow), which appear green. Scale bar = 20µm. Right panel shows percentages of pollen viability for each genotype. Individual biological replicates are plotted separately. Number of pollen grain is indicated below each bar in parentheses. **B)** Pollen tube germination of wild-type and *ccr4a ccr4b* pollen. Pollen grains from wild-type and double mutant plants were added to a semi-solid pollen germination medium. Left panel shows representative pictures of wild-type and double mutant pollen grains 3h after incubation on the germination medium. Scale bar = 20µm. Right panel shows the percentage of pollen germination. Individual replicates are plotted separately. Number of pollen grain is indicated below each bar in parentheses. **C)** Seed packing of wild-type and *ccr4a ccr4b* siliques. Left panel shows representative picture of wild-type and double mutant siliques. Right panel shows the quantification of seeds per silique for wild-type and double mutant plants. Each dot represents an individual silique. Number of siliques is indicated below each box in parentheses. Each box represents a biological replicate. The horizontal line in each box represents the mean, while lower and upper hinges indicate first and third quartiles, respectively. For all the plots, *P*-values were calculated using a General Linear Model with a binomial distribution. n.s: non-significant; ***: $P < 0.0001$.

1.3.4. *ccr4a ccr4b pollen grains have defects in tube germination in vitro*

First, I assessed pollen viability using Alexander staining (Alexander, 1969). It uses Orange-G as a cytoplasmic dye in combination with Malachite-green, which highlights the exine layer and imparts a greenish colour. Hence, viable pollen appears pink with a faint green outer layer, while aborted pollen grains, with no cytoplasm, appear only transparent/green. Colouration of pollen grains from wild-type and *ccr4a ccr4b* as well as the counting of viable pollen grains are shown in **Figure 27A**. I observed no major changes in pollen viability with 98.3% and 96.5% viability in wild-type and *ccr4a ccr4b* pollen, respectively. Similarly, I observed pollen grains under a scanning electron microscope and did not observe changes in the apparent shape of the pollen grains and patterning of the pollen coat (**Figure S5**). Therefore, CCR4a and CCR4b do not seem to be involved in the viability and patterning of pollen grains.

Next, I addressed the potential effects on pollen germination by using an *in vitro* germination medium that promotes pollen tube growth. Briefly, pollen grains of wild-type and *ccr4a ccr4b* plants were deposited on a semi-solid agar medium containing essential nutrients to trigger pollen tube germination and growth (Boavida & McCormick, 2007). Pollen grains were incubated in high humidity in the dark during 3h, and were observed under a microscope (**Figure 27B**). Interestingly, we observe a significant decrease in pollen germination in *ccr4a ccr4b* with only 9.4% of pollen grains germinating compared to 46.1% in wild-type pollen. Similar effects on *in vitro* pollen germination were found for mutants of multiple genes among the ones with high PASS, further suggesting that the changes in their poly(A) tail may alter their metabolism and subsequent functions (Tian *et al.*, 2006; Jian *et al.*, 2014; Leroux *et al.*, 2015).

Intriguingly, we did not observe changes in seed packing between wild-type and double mutant siliques, indicating that despite the significant effect on pollen germination of the *ccr4a ccr4b* mutation, it does not affect fertilisation of ovules (**Figure 27C**). Three non-mutually exclusive hypotheses to explain this discrepancy can be addressed:

- the germination of pollen grains is delayed in *ccr4a ccr4b*, rather than partially suppressed. This delay may be emphasised after a short 3-hour incubation, but longer incubation periods could potentially reduce the difference in pollen germination percentages between wild-type and *ccr4a ccr4b* mutant;
- *in vivo*, hundreds of pollen grains are deposited on the stigma. Thus, despite an important effect in pollen germination, sufficient number of pollen tubes can reach and fertilise ovules;

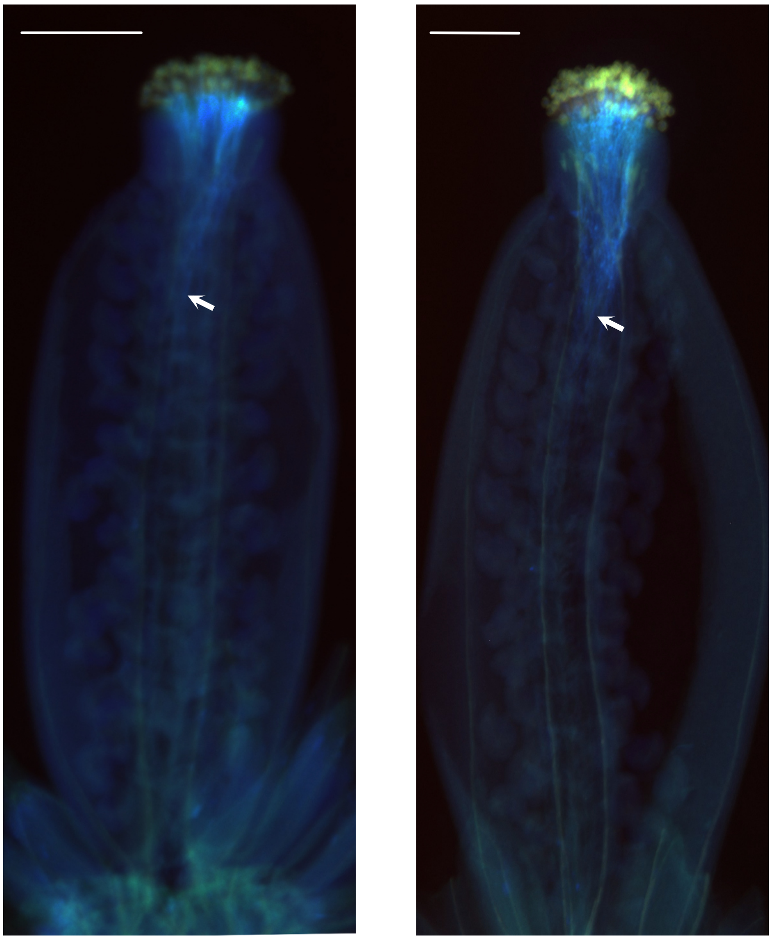

♂ **wild-type**
♀ **wild-type**

♂ ***ccr4a ccr4b***
♀ **wild-type**

Figure 28. *In vivo* germination does not seem to be affected for *ccr4a ccr4b* pollen grains. Representative images of aniline blue staining of wild-type pistils 6h after hand-pollination with wild-type (left panel) and *ccr4a ccr4b* (right panel) pollen. White arrows indicate pollen tubes furthest from the stigma. Scale bar: 200µm.

- *in vivo* germination is more efficient for pollen germination. The *in vitro* medium may lack certain essential compounds required for optimal pollen germination of *ccr4a ccr4b* pollen grains, whereas these compounds are naturally present when pollen germinates onto the stigma.

To test the latter hypothesis, I performed *in vivo* pollen germination. Briefly, pollen from wild-type and *ccr4a ccr4b* plants was applied to the stigma of emasculated wild-type flowers. After 6h of incubation, pistils were harvested, fixed, and stained with aniline blue which stains callose deposition, particularly present in the pollen tube. Because it is impossible to control the number of pollen grains applied to the stigma and discriminate individual pollen tubes inside the style, this technique is not best suited to score pollen germination. Yet, I hypothesised that if the difference in germination between wild-type and mutant pollen observed *in vitro* is equally significant *in vivo*, I would be able to discern the impact of the *ccr4a ccr4b* mutation on *in vivo* germination. In these preliminary experiments, I did not identify any visible variation in pollen tube length between genotypes, and the proportion of germinated pollen grains appeared to be similar in both genotypes (**Figure 28**).

1.3.5. CCR4a and CCR4b are not major regulators of translation efficiency in flowers

The roles of poly(A) tail metabolism in controlling gene expression are complex and largely depend on the cellular context and the organism (Passmore & Coller, 2022). Observing such pronounced poly(A) tail lengthening for mRNAs specifically expressed in young flowers and maturing anthers, and linking their biological functions to defects in pollen tube germination *in vitro*, prompted us to investigate potential changes in the metabolism of these mRNAs. While deadenylation is a major regulator of mRNA degradation, we were unable to measure changes in mRNA half-lives due to the absence of a reliable method for studying decay rates in flower buds. However, performing Illumina sequencing of total RNA and polysomal fractions would allow us to both assess alterations in the steady-state levels of flower buds mRNA in *ccr4a ccr4b*, and estimate variations in translation efficiency by analysing the enrichment or depletion of mRNAs purified from polysomal fractions.

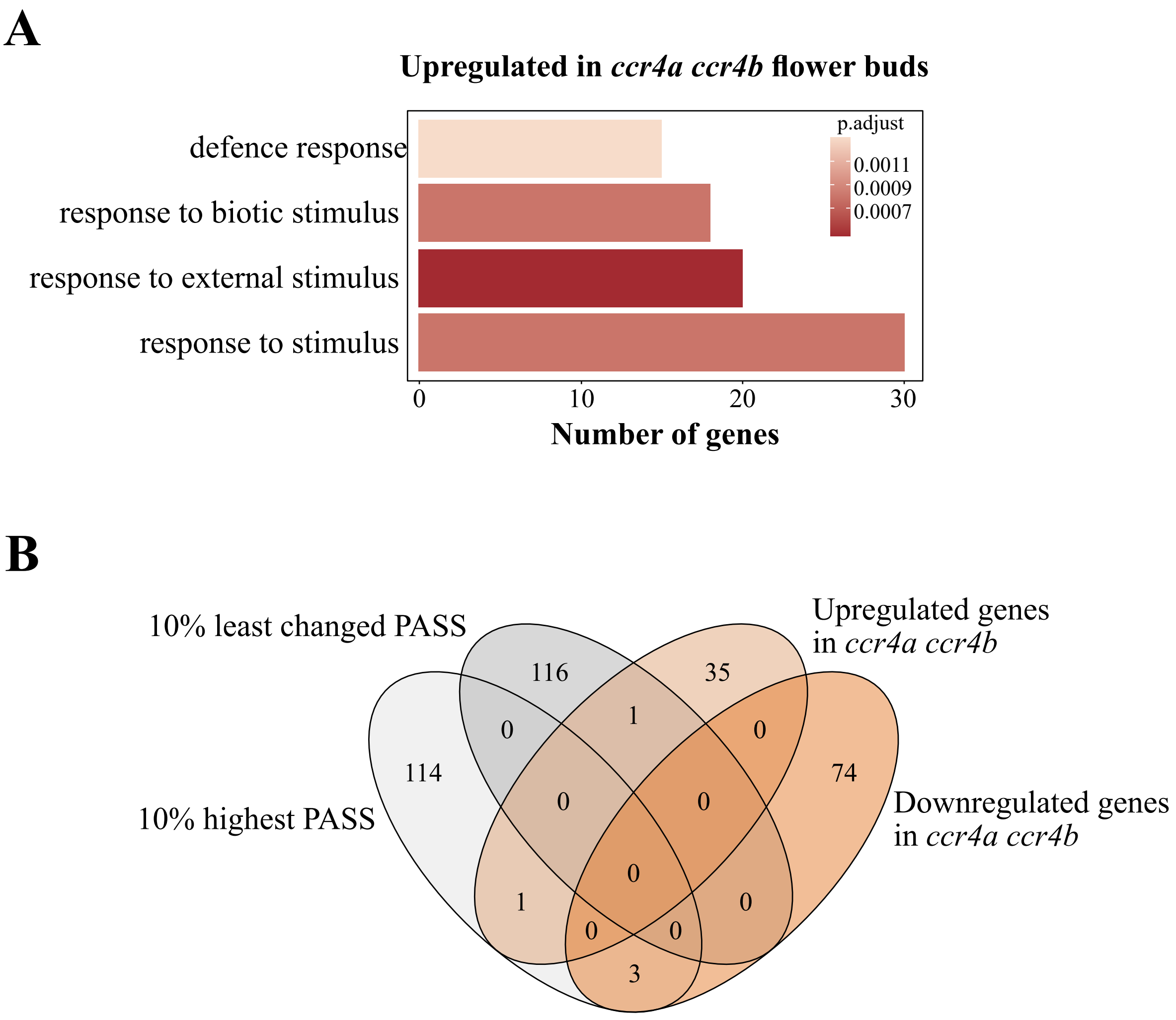

Figure 29. Upregulated genes in *ccr4a ccr4b* flower buds are enriched in GO terms related to defence response, but are not linked with changes in PASS. A) Over-representation analysis of GO terms for upregulated genes with a $\mathrm{Log_2FC} > 0.5$ in *ccr4a ccr4b* flower buds. The length and color of bars represent respectively the number of genes and significance calculated with a hypergeometric test with Benjamini-Hochberg correction. **B)** Venn diagram showing the overlap between mRNAs with high PASS or least changed PASS (determined previously using FLEP-seq2) and differentially expressed genes in *ccr4a ccr4b* flower buds (using $|\mathrm{Log_2FC}| > 0.5$ as a threshold).

Thus, I first characterised differential gene expression in total RNAs extracted from flower buds. Following RNA extraction, ribodepletion and sequencing of biological triplicates, more than 18 million 150-bp paired-end reads per sample were obtained. 77 genes are upregulated and 37 genes are downregulated in *ccr4a ccr4b*, using a cut-off of $|\log_2 FC| > 0.5$. As in rosette samples, I did not observe any misregulation of other deadenylases (**Table S5**). Interestingly, there is a clear diminution of the number of genes differentially expressed in *ccr4a ccr4b* in flower buds compared to rosette (see **Figure 15D**). Possibly, the differential gene expression observed in rosette is largely caused by pleiotropic effects, as a global stress response was observed. Nonetheless, GO term analysis showed that in flower buds, upregulated genes are enriched in processes related to defence response (**Figure 29A**). This further suggests that the accumulation of stress response genes at the steady-state is regulated by CCR4a and CCR4b. The number of mRNAs in common between FLEP-seq2 and differentially expressed genes found in Illumina sequencing is not enough to draw reliable poly(A) distributions; however, I did not observe significant overlap between the 10% highest or least changed PASS, and the up- or downregulated genes in flower buds (**Figure 29B**). This is in contrast to what we observed for rosette, where upregulated genes were significantly lengthened upon the *ccr4a ccr4b* mutation.

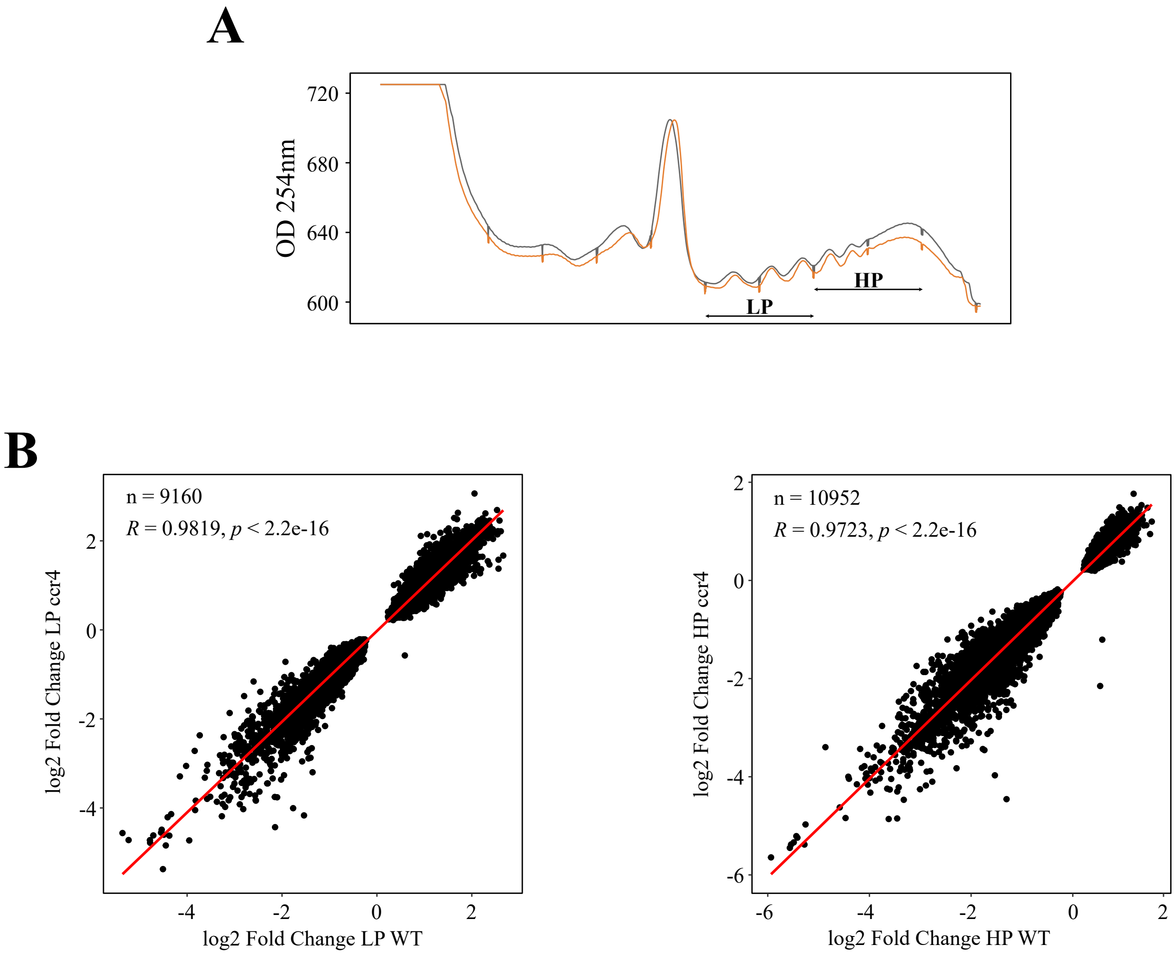

Figure 30. No effect on global mRNA polysomal association in *ccr4a ccr4b* flower buds. **A)** Polysomal extracts from WT (grey line) and *ccr4a ccr4b* (orange line) flower buds. Raw extracts were fractionated on a 15-60% sucrose gradient and absorbance was measured at 254nm. Fractions corresponding to low molecular weight polysomes were pooled together to create the "light polysomes" fraction (LP) and fractions corresponding to high molecular weight polysomes were pooled together to create the "heavy polysomes" fraction (HP). **B)** Scatter plot comparing fold change enrichment between WT (x-axis) and *ccr4a ccr4b* (y-axis) LP fractions (left panel) and HP fractions (right panel). Fold change enrichment was calculated using DESeq2 by comparing normalised counts in polysomal fraction to normalised counts in total RNA, for each condition. Correlation were calculated between the $\log_2$ fold change in WT and mutant polysomal fractions ($R > 0.95$, Spearman's test p-value < 2.2e-16). n represents the number of genes used to calculate the correlation.

A

10% highest PASS

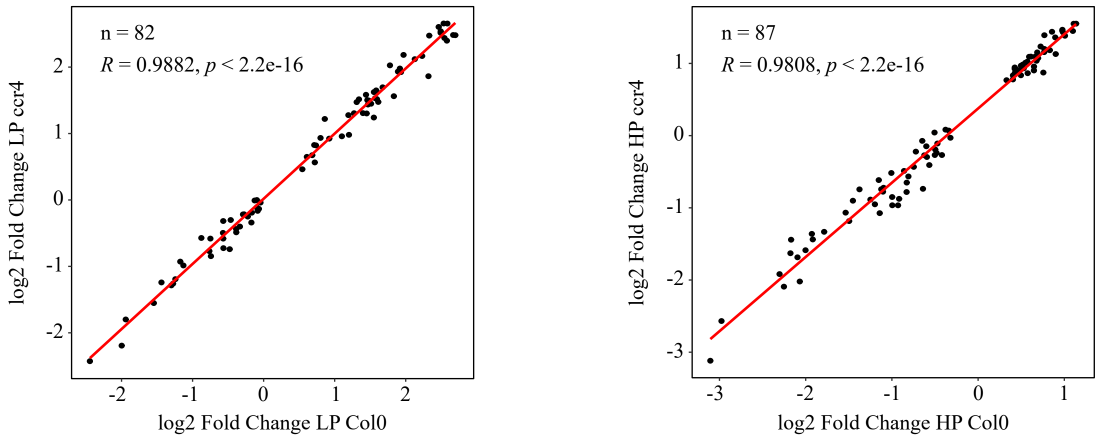

B

10% least changed PASS

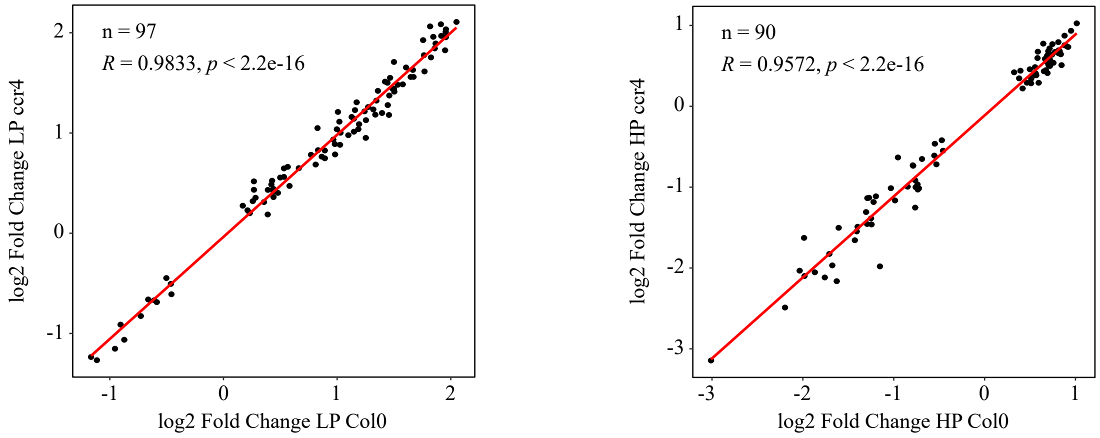

Figure 31. Changes in poly(A) size in *ccr4a ccr4b* do not influence mRNA translation efficiency.
Correlation of fold change enrichment between WT and *ccr4a ccr4b* LP fractions (left panels) and HP fractions (right panels) for **A)** the 10% mRNAs with the highest PASS and **B)** the 10% mRNAs with the least changed PASS. Fold change enrichment was calculated using DESeq2 by comparing normalised counts in polysomal fraction to normalised counts in total RNA, for each condition. Correlations were calculated between the $\log_2$ fold change in WT and mutant polysomal fractions (R > 0.95, Spearman's test p-value < 2.2e-16). n represents the number of genes used to calculate the correlation.

To determine the impact of the *ccr4a ccr4b* mutation on translation efficiency, raw extracts from flower buds were purified on sucrose gradients and were fractionated to isolate polysomes (**Figure 30**). Interestingly, the loss of CCR4a and CCR4b does not significantly impact the global polysome profiles, potentially indicating a modest effect of the mutation (**Figure 30A**). Hence, we may expect to observe mRNAs whose translation is diminished rather than completely abolished. These mRNAs could shift from heavy polysomal fractions to lighter polysomal fractions instead of being completely depleted from polysomes. Thus, pooling all polysomal fractions together may hide a mild effect of the mutation on translation efficiency. To address this concern, I pooled fractions corresponding to disomes, trisomes and tetrasomes into a light polysome fraction (LP), and pooled fractions corresponding to pentasome, hexasome and heavier fractions into a heavy polysome fraction (HP).

Upon sequencing the polysomal fractions and determining translation efficiency, I first compared fold change for each polysomal fraction relative to total RNA. Next, I plotted the fold change of wild-type and *ccr4a ccr4b* polysomal fractions for mRNAs commonly detected. By doing so, we can determine if the enrichment/depletion of mRNAs in the polysomal fractions is comparable between genotypes. If the loss of CCR4 proteins affects the overall translation rate, we would observe a decorrelation of the fold change enrichment between wild-type and *ccr4a ccr4b* polysomal fractions. Here, we observe a clear correlation, indicating that the loss of CCR4a and CCR4b does not have a major global effect on translation (**Figure 30B**). This can be observed in both LP and HP fractions. Similarly, we did not observe any change in translation efficiency for mRNAs with high or least changed PASS (**Figure 31**). Altogether, these observations suggest that CCR4a and CCR4b and their roles in deadenylating mRNAs are not major modulators of translation efficiency in flower buds. This is consistent with recent transcriptome-wide experiments where translation efficiency and poly(A) tail length are only correlated in specific cell types (Subtelny *et al.*, 2014; Eichhorn *et al.*, 2016; Xiang & Bartel, 2021; Eisen *et al.*, 2022).

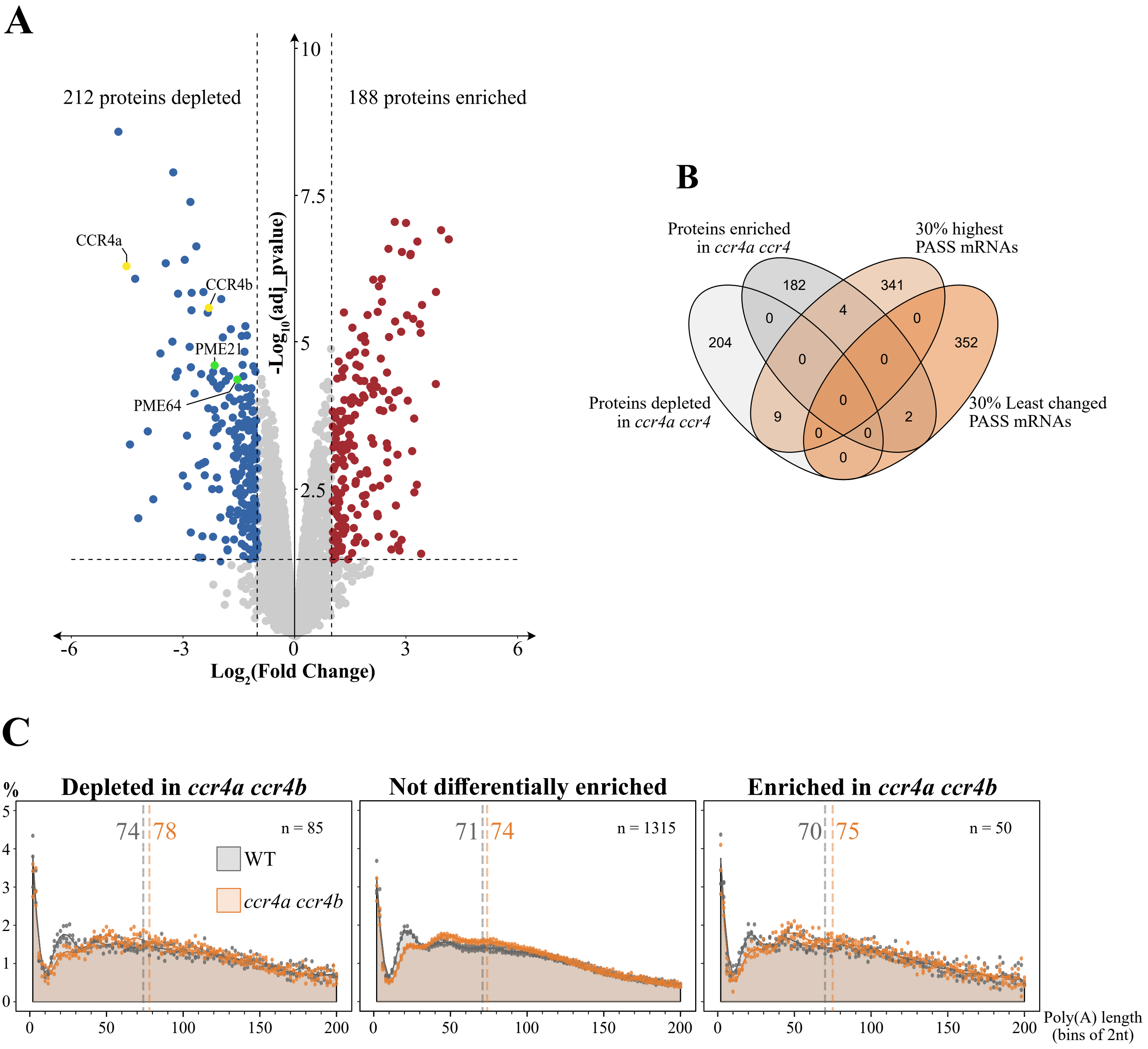

Figure 32. Differentially enriched proteins are not particularly regulated by CCR4a and CCR4b.

A) Volcano plot showing proteins differentially depleted ($\log_2$ fold change < -1, blue dots) or enriched ($\log_2$ fold change > 1, red dots) in *ccr4a ccr4b* pollen proteomics vs WT pollen proteomics. Vertical dashed lines delimits the arbitrarily chosen threshold for the enrichment/ depletion. The horizontal dashed line indicates the significant threshold (adjusted *p*-value < 0.05, quasi-likelihood negative binomial generalised log-linear model). **B)** Venn diagram showing the intersect between mRNAs coding differentially enriched proteins in *ccr4a ccr4b* pollen (using $|\text{Log}_2\text{FC}| > 1$ as a threshold) and mRNAs with the highest or the least changed PASS in flower buds **C)** Normalised poly(A) distribution of flowers buds extracted RNAs for genes coding proteins depleted in *ccr4a ccr4b* pollen (left panel), for genes coding proteins not differentially enriched (middle panel) or for genes coding proteins enriched (right panel) in *ccr4a ccr4b* pollen. To normalise, I calculated the percentage of reads at all poly(A) tail size (bins of 2 As) for each mRNA in all biological replicates. Dots represent the median percentage of reads per poly(A) tail size accross biological replicates, while the line represents the mean of this median across genotypes. To limit variability when normalising, I selected mRNAs that had at least 50 reads per sample. Number n of mRNAs used to draw the plots are indicated in upper right corner. Normalised median poly(A) tail size for all reads are represented as grey (wild-type) and orange (*ccr4a ccr4b*) dashed lines.

1.3.6. *Changes in pollen proteome are not correlated with poly(A) tail changes in ccr4a ccr4b*

I did not observe an effect of poly(A) tail lengthening on translation efficiency. Yet, I still observed reproducible defects in *ccr4a ccr4b* pollen tube germination *in vitro*. Hence, I wondered whether we would observe differential protein accumulation in *ccr4a ccr4b* pollen, despite seeing no obvious changes in translation efficiency in flower buds.

Hence, I performed a comprehensive study of the changes in the pollen proteome profiles upon mutation of the CCR4a and CCR4b deadenylases. Here, I isolated pollen grains from both wild-type and *ccr4a ccr4b* flowers. I extracted total proteins using a highly denaturing buffer in order to solubilise proteins that are embedded in the pollen coat, which is known to be highly resistant to chemical, physical, and biological degradation. After purification, total proteins were analysed by LC-MS/MS. Out of the 5082 proteins identified, 212 are significantly depleted (log2FC < -1, *p*-value < 0.05) and 188 are significantly enriched (log2FC > 1, *p*-value < 0.05) in *ccr4a ccr4b* pollen (**Figure 32A, Table S6**). We did not identify any spectra for either CCR4a or CCR4b in *ccr4a ccr4b* pollen, further confirming the KO of both deadenylases in the CRISPR-Cas9 line.

Among the significantly depleted proteins in *ccr4a ccr4b* pollen are PME21 and PME64, which belong to the pectin methylesterase inhibitors (PMEI) family. PMEIs inhibit the enzymatic activity of pectin methylesterases (PMEs) which catalyse the specific de-methylesterification of pectins. This modification determines the plasticity of the cell wall and regulates numerous biological processes, including pollen germination and pollen tube growth (Wormit & Usadel, 2018). PME21 and PME64 are highly and specifically expressed in pollen. Hence, the depletion of these PMEIs in *ccr4a ccr4b* pollen may disrupt the homeostasis regulating the activity of PME, which would result in their overactivation, and consequential changes in pollen cell wall plasticity.

While the depletion of PMEIs may explain the phenotype, one might wonder whether the likelihood of stumbling upon a protein specifically related to pollen functions, just by random sampling or experimentation in pollen tissues, could be high. Hence, further experimental data are needed to formally link the *ccr4a ccr4b* phenotype to changes in protein content in pollen grains.

Additionally, there is no significant overlap between proteins differently enriched in *ccr4a ccr4b* pollen and mRNAs with high or least changed PASS in flower buds (**Figure 32B**).

Likewise, mRNAs coding for proteins that are depleted, enriched, or not differentially enriched do not exhibit specific deadenylation patterns in flower buds upon mutation (**Figure 32C**).

To conclude, while the ccr4a ccr4b pollen proteomics may help explain the in vitro germination phenotype, we could not establish a formal link between the proteins differentially expressed in mature pollen and the mRNAs highly deadenylated by CCR4a and CCR4b in maturing anthers and flower buds. This lack of connection might be attributed to specific regulation mediated by CCR4a and CCR4b in mature pollen, rather than during pollen maturation in anthers. Despite the in-depth remodelling of the poly(A) tail of specific genes involved in pollen functions, our experimental data suggest that the loss of CCR4a and CCR4b deadenylases does not significantly influence mRNA translation efficiency and steady-state levels in flower buds.

Hence, the biological relevance of such an intricate deadenylation profile for mRNAs specifically expressed in flower buds and involved in pollen functions is yet to be deciphered, but it will be discussed later in the manuscript.

2. Characterising the molecular interplay between uridylation and deadenylation

2.1. Functional links between uridylation and deadenylation

The main objective of my thesis was to determine the functional and physical links between uridylation and deadenylation. Previous results from our group have shown that uridylation and deadenylation are intricately linked. The addition of a single U at the 3'end of a synthetic RNA can slow down the action of the CAF1b deadenylase *in vitro* and can prevent excessive deadenylation *in planta* (Scheer *et al.,* 2021). Interestingly, uridylation by URT1 targets mostly deadenylated mRNAs with poly(A) tails of 10-25 As (Sement *et al.*, 2013; Zuber *et al.*, 2018; Scheer *et al.,* 2021), indicating that URT1 and the deadenylation machinery may compete for the same substrate, *i.e.* mRNAs that are actively deadenylated. Hence, we wondered whether the suppression of CCR4a/b-mediated deadenylation would affect mRNA uridylation.

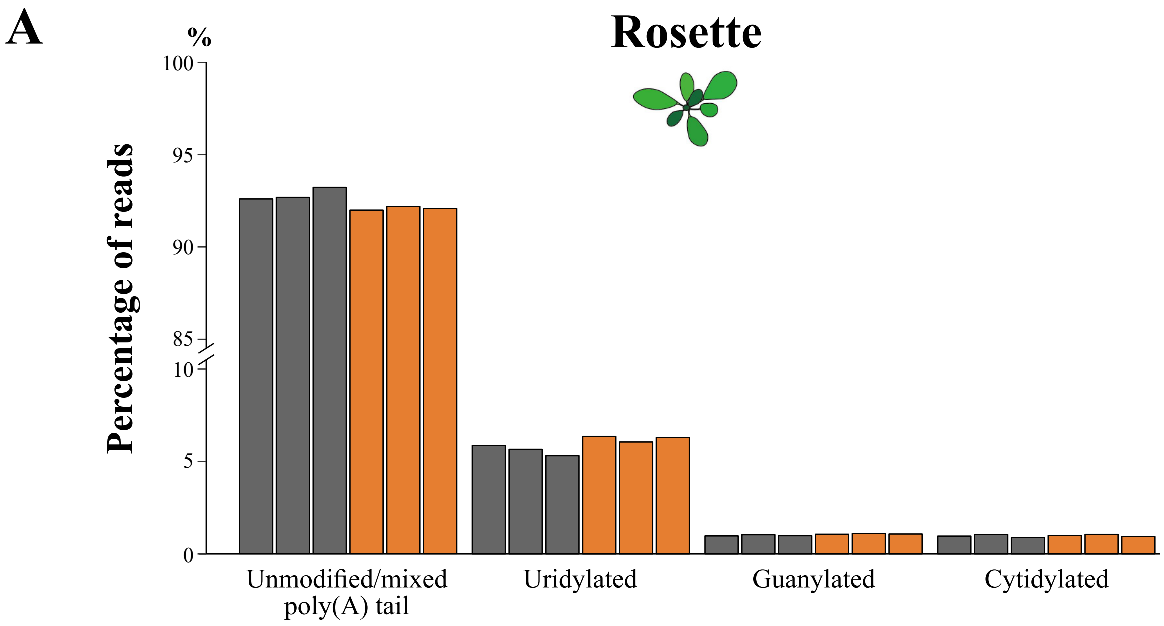

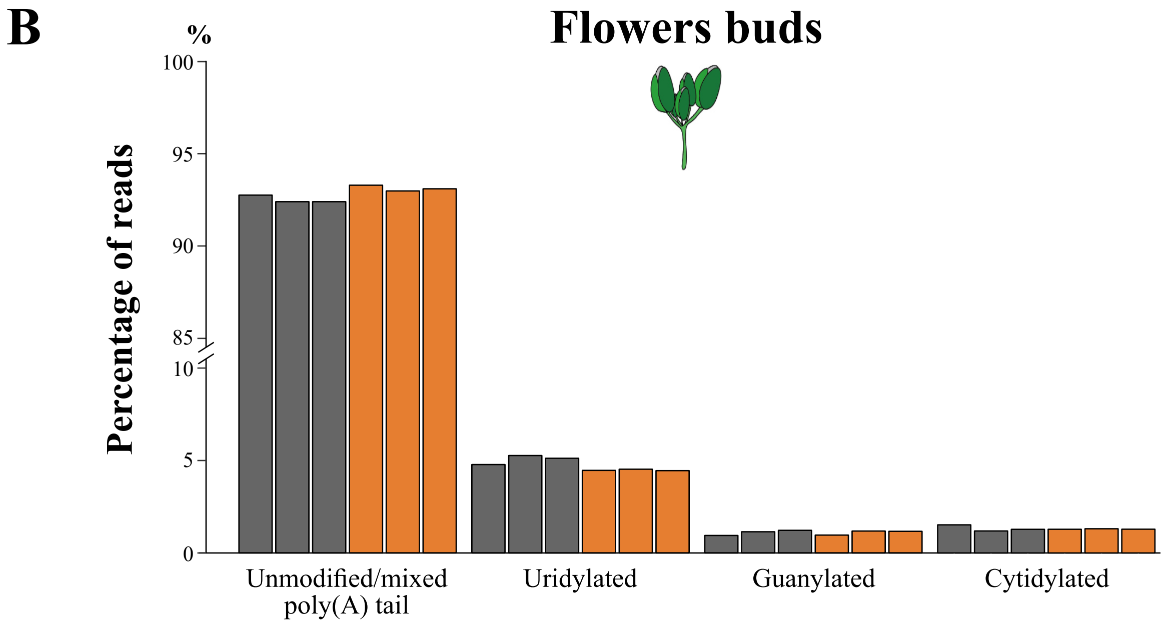

Figure 33. Uridylation is the most widespread 3' terminal modification of mRNAs. Composition of the additional tail **A)** for rosette or **B)** flower buds samples. Uridylated, guanlyated and cytidylated reads must have additional tails composed at least by 70% of uridines, guanines or cytidines respectively. Reads with additional tails containing no more than 70% of a single nucleotide are pooled as unmodified/mixed poly(A) tail.

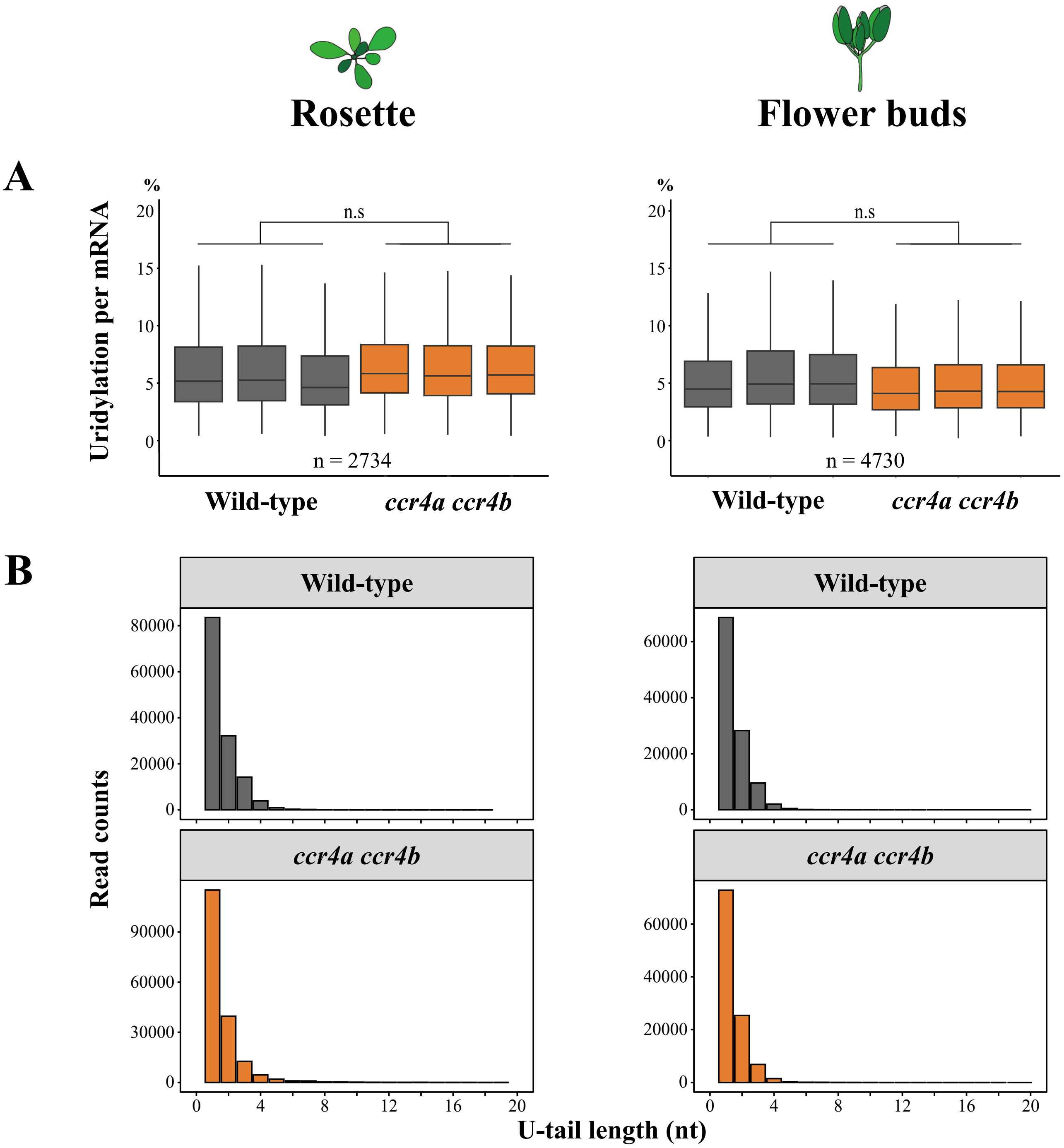

Figure 34. Loss of CCR4a and CCR4b does not significantly influence total mRNA uridylation.

A) Percentage of uridylation per mRNA in rosette (left panel) or flowers buds (right panel). To limit variability, I selected mRNAs that had at least 50 reads per sample. All reads with poly(A) tails between 1-200As were used. n is the number of mRNAs used to draw the boxplots. Each boxplot represents a biological replicate. The horizontal line in each box represents the median, and lower and upper hinges indicate first and third quartiles, respectively. *P*-values were calculated using General Linear Model with binomial distribution. n.s: non-significant. **B)** U-tail length for all uridylated reads in wild-type (upper panels) and *ccr4a ccr4b* (lower panels) in rosette (left panels) or flower buds samples (right panels). Uridylated reads from all biological replicates are pooled together.

2.1.1. *mRNAs are not more uridylated in ccr4a ccr4b*

In the original article presenting FLEP-seq2, the authors did not address 3' terminal nucleotide addition, therefore the analysis pipeline was not adapted to study uridylation (Jia *et al.*, 2022). To overcome this, Dr. Hélène Zuber and Dr. Jackson Peter modified the pipeline by searching the mapping files for unmapped sequences corresponding to the region between the mapped read and the 3'-FLEP-seq2 adapter. These unmapped sequences correspond to untemplated nucleotide additions, such as the poly(A) tail and 3'-terminally added nucleotides. Nucleotide sbetween the poly(A) tail and the 3' adapter were designated as the additional tail. Using this modified analysis pipeline, we were able to determine the percentage of 3' modified reads. The percentage threshold chosen to classify whether reads are uridylated, cytidylated, or guanylated is 70% (70% of the read's additional tail must consist of solely uridines, cytidines, or guanines, respectively). Unmodified reads and reads with mixed tails (*i.e.* reads with an additional tail composed of various nucleotides, with none comprising 70% or more of the tail) were pooled together as unmodified/mixed reads.

Unsurprisingly, the majority of reads are unmodified/mixed, both in rosettes and flowers, with ~92.5% of reads not being 3' terminally modified (**Figure 33**). ~5.2% of all polyadenylated transcripts are uridylated, compared to ~1.1% for cytidylated and ~1.1% for guanylated reads. This is consistent with previous work from Narry Kim's group and our group, which used TAIL-seq to define uridylation as the most widespread 3' terminal modification (Chang *et al.*, 2014; Zuber *et al.*, 2016). We do not observe significant changes in uridylation levels per mRNA between flowers and rosettes (**Figure 34A**). This suggests that the processes regulating mRNA uridylation are conserved in both tissues. Surprisingly, we do not observe major differences in uridylation levels between wild-type and *ccr4a ccr4b*, indicating that at the global level, altering deadenylation has little to no impact on uridylation levels. This was unexpected, given that uridylated mRNAs typically have short poly(A) tails of 15-20 As, and our work demonstrated that this population is significantly reduced in *ccr4a ccr4b* mutants, particularly in rosette samples. Consequently, we had anticipated a decrease in uridylation levels in the *ccr4a ccr4b* mutants due to the depletion of the short poly(A) tail population. Similarly, the mutation of CCR4 deadenylases has no impact on the length of the U extensions, as the majority of uridylated mRNAs bear an extension of 1-4 uridines (**Figure 34B**).

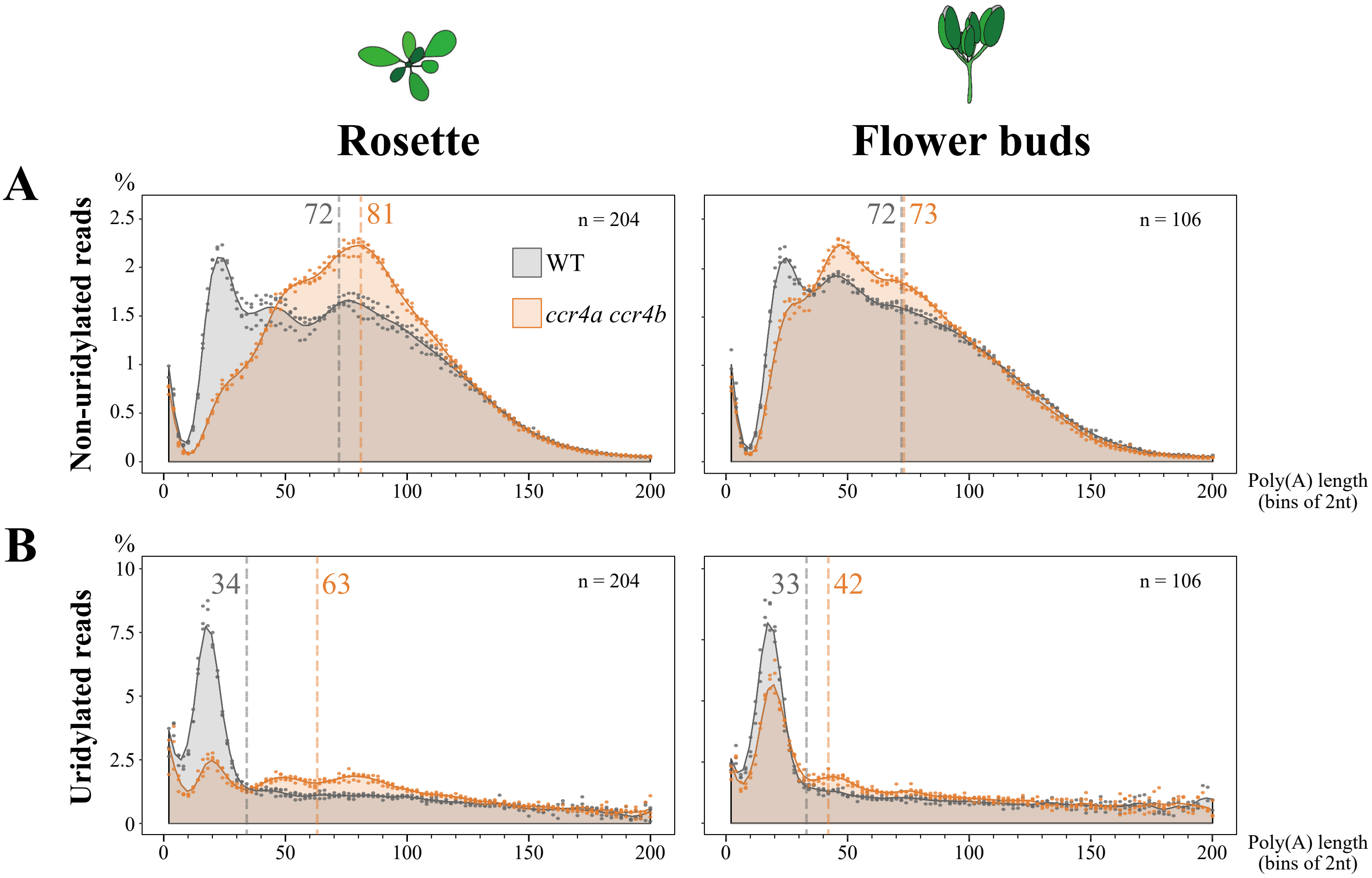

Figure 35. Uridylated poly(A) tails are longer in *ccr4a ccr4b*.
Normalised poly(A) distribution for **A)** non-uridylated and **B)** uridylated reads in rosettes (left panels) and flower buds (right panels). To normalise, I calculated the percentage of reads at all poly(A) tail size (bins of 2 nucleotides) for each mRNA in all biological replicates. Dots represent the median percentage of reads per poly(A) tail size across biological replicates, while the coloured area represents the mean of this median accross genotypes. To limit variability when normalising, I selected mRNAs that had at least 50 uridylated reads per sample. Number n of mRNAs used to draw the plots are indicated in upper right corner. Normalised median poly(A) tail size for all reads are represented as grey (wild-type) and orange (*ccr4a ccr4b*) dashed lines.

2.1.2. Deadenylation by CCR4a and CCR4b is a major regulator of uridylated poly(A) profiles in Arabidopsis

Given that the short poly(A) tail population is depleted in *ccr4a ccr4b* mutants without affecting uridylation levels, we were intrigued by a potential change in the poly(A) tail distribution of uridylated reads in the mutant. **Figure 35** shows the poly(A) profiles for uridylated and non-uridylated reads, normalised per mRNA. Because only 5% of the reads per mRNA are uridylated, we observed significant variability in the distribution of uridylated poly(A) tails caused by limited sequencing depth. To limit this variability, I selected mRNAs that had at least 50 uridylated reads in wild-type and *ccr4a ccr4b* samples, and bins of 2 As were used to draw the poly(A) distribution for tails ranging from 1 to 200 As. In wild-type plants, and as previously observed using TAIL-seq, uridylated mRNAs have much shorter poly(A) tails compared with non-uridylated mRNAs, both in rosette and flower samples (**Figure 35, grey lines**). This confirms that uridylation targets mainly deadenylated mRNAs. Surprisingly, in *ccr4a ccr4b*, we observe an increase in the length of uridylated poly(A) tails (**Figure 35B**). The increase in the population of long uridylated poly(A) tails is much more pronounced in rosette than in flower buds, and is in clear correlation with the global shift towards longer poly(A) tails observed in *ccr4a ccr4b* rosette samples. Because we observe lengthening of uridylated poly(A) tails without a drop in uridylation levels, this suggests that URT1 does not solely target deadenylated transcripts of ~20As, but can rather efficiently uridylate longer poly(A) tails, up to 90As in my dataset. It indicates that CCR4 proteins are essential regulators of the size of uridylated reads. Their impairment is not compensated by other deadenylases.

Despite the marked reduction of the short poly(A) tail population, it is still proportionally the most uridylated population, suggesting that factors other than CCR4a/CCR4b-mediated deadenylation regulate the size of uridylated poly(A) tails. Potentially, the activity of other deadenylases (*e.g.*, CAF1) may be involved in the particular distribution of uridylated reads upon the mutation of CCR4 proteins.

Another likely candidate for the modulation of uridylated poly(A) profiles is PABPC. Indeed, in *ccr4a ccr4b*, we observe the appearance of peaks corresponding to PABPC footprint. This observation supports the hypothesis that PABPC-bound poly(A) tails can be uridylated, as was previously shown *in vitro* (Zuber *et al.*, 2016), and confirms that the presence of PABPC is a modulator of the length of uridylated tails as was shown in humans (Yi *et al.*, 2018).

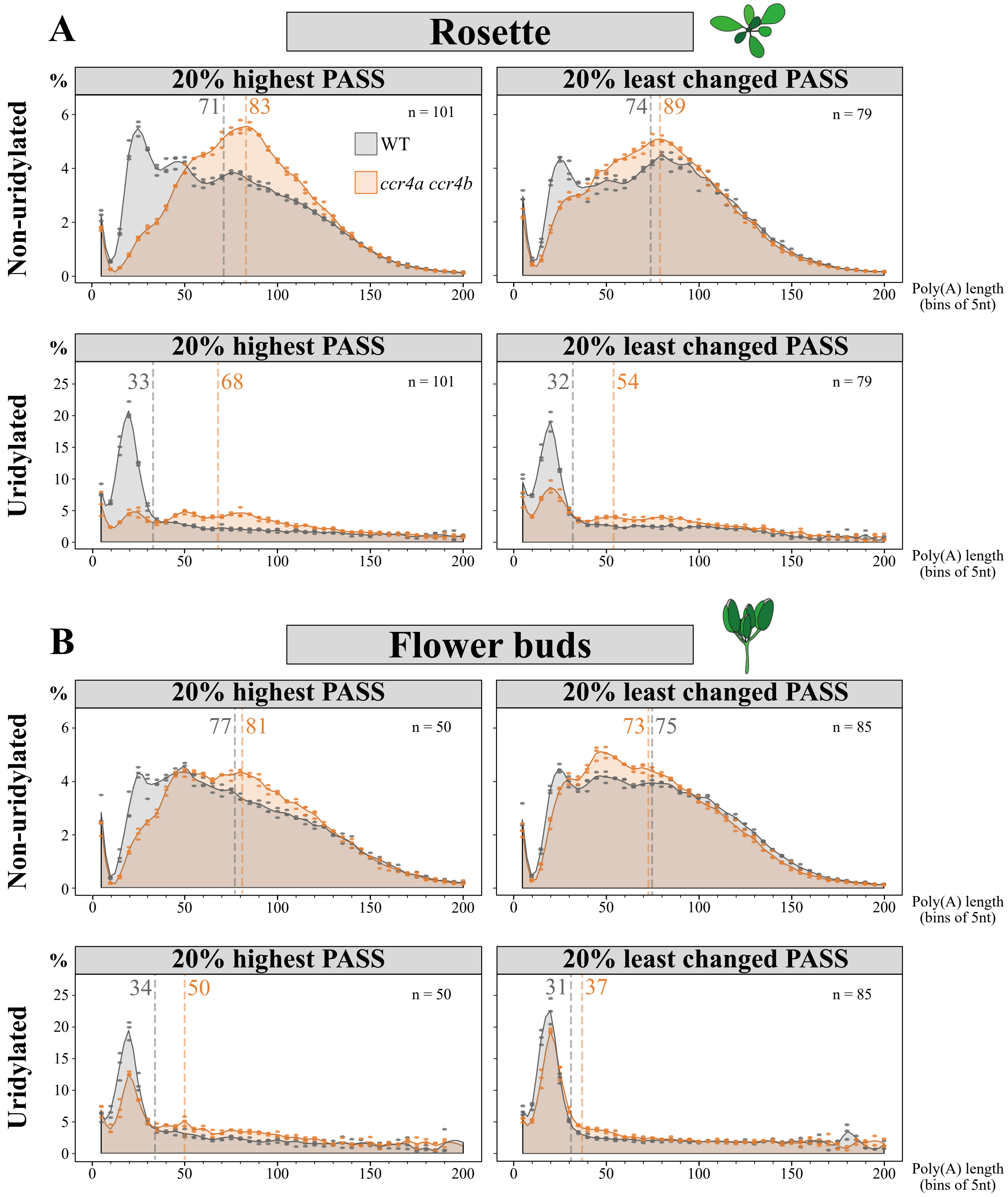

Figure 36. Size of uridylated tails is directly influenced by the poly(A) tail lengthening in *ccr4a ccr4b*.

Normalised poly(A) distribution for the 20% mRNAs with the highest PASS (left panels) or the 20% mRNAs with the least changed PASS (right panels) for non-uridylated reads (upper panels) or uridylated reads (lower panels) for **A)** rosette and **B)** flower buds. To normalise, I calculated the percentage of reads at all poly(A) tail size (bins of 5 nucleotides) for each mRNA in all biological replicates. Dots represent the median percentage of reads per poly(A) tail size across biological replicates, while the coloured area represents the mean of this median across genotypes. To limit variability when normalising, I selected mRNAs that had at least 20 uridylated reads per sample. Number (n) of mRNAs used to draw the plots are indicated in upper right corner. Normalised median poly(A) tail size for all reads are represented as grey (wild-type) and orange (*ccr4a ccr4b*) dashed lines.

2.1.3. *Actively deadenylated mRNAs are more uridylated in ccr4a ccr4b and have longer uridylated poly(A) tails*

The lengthening of uridylated poly(A) tails in rosette is much more pronounced than in flower buds, suggesting that the impact of the mutation of CCR4 deadenylases on poly(A) tail profiles directly impacts uridylation profiles. We hypothesised that the presence of CCR4 proteins determines the length of uridylated poly(A) tails; thus, the more mRNAs are deadenylated by CCR4a and CCR4b, the longer their uridylated poly(A) tails become in the *ccr4a ccr4b* mutant. To test this hypothesis, I analysed the poly(A) tail distribution of uridylated and non-uridylated reads for mRNAs with high PASS in rosettes and flower buds. **Figure 36** shows the normalised poly(A) distribution profiles for uridylated and non-uridylated reads for mRNAs with high PASS or the least changed PASS. To limit variability, I selected the top 20% mRNAs of each category, and selected only mRNAs that had at least 20 uridylated reads in wild-type and *ccr4a ccr4b* samples. Strikingly, long uridylated poly(A) tails clearly accumulate for mRNAs with the top 20% highest PASS, both in rosettes and flower buds, particularly when compared to the 20% least changed PASS. This accumulation of long uridylated poly(A) tails is directly related to the global lengthening of the poly(A) tails. Interestingly, high PASS mRNAs in rosette are significantly more uridylated in *ccr4a ccr4b*, albeit to a small extent (**Figure 37A**). By contrast, we do not observe such an increase for high PASS mRNAs in flower buds (**Figure 37B**).

Because mRNAs with high PASS accumulate longer uridylated poly(A) tails compared to the least changed PASS mRNAs in both rosette and flower buds, this confirms that the deadenylation activity of CCR4a and CCR4b largely shapes uridylation profiles in *Arabidopsis*. Taken together, our data further suggest a strong interplay between uridylation and deadenylation. While the full relationship between uridylation and deadenylation remains elusive, some hypotheses addressing the mechanistic functions linking these two mechanisms together can be proposed based on our experimental findings:

- In wild-type conditions, URT1 is able to uridylate all poly(A) sizes, but the action of CCR4 (and other deadenylases) removes the poly(A) tail and its uridine extensions, albeit inefficiently (Lim *et al.*, 2018; Chang *et al.*, 2021; Scheer *et al.*, 2021). When the poly(A) tail shortens, the activity of the CCR4-NOT complex becomes distributives and it loses its affinity for the poly(A) tail (Viswanathan *et al.*, 2003). Hence, only short poly(A) tails that are less degraded by CCR4 deadenylases accumulates uridylated tails. In *ccr4a ccr4b*, the removal of uridylation is less efficient

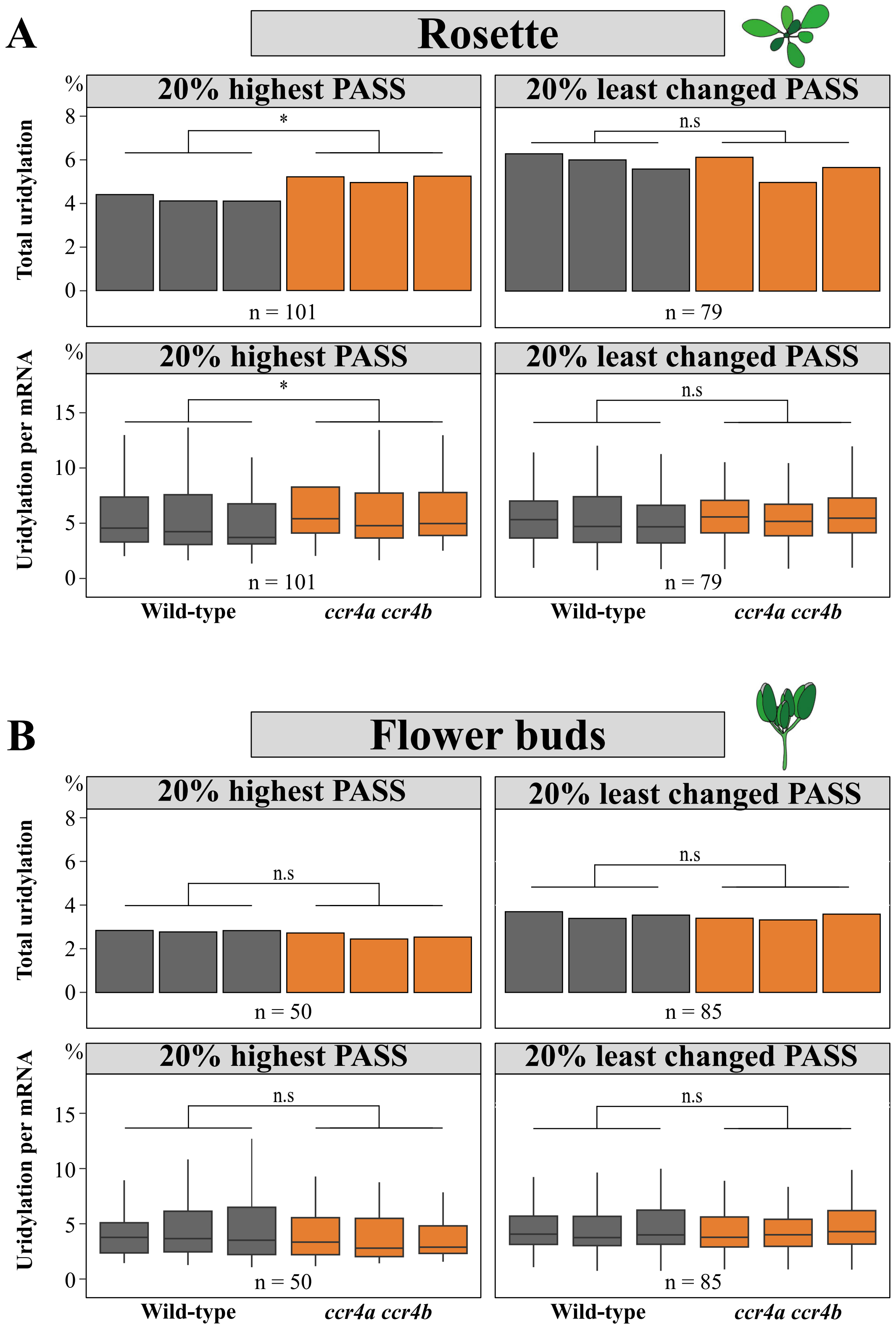

Figure 37. Changes in poly(A) tail length affects uridylation levels of actively deadenylated mRNAs.

Total uridylation percentage (upper panels) and uridylation percentage per mRNA (lower panels) for the 20% mRNAs with the highest PASS (left panels) or the 20% mRNAs with the least changed PASS (right panels) for **A)** rosette or **B)** flower buds mRNAs, that had at least 20 uridylated reads per sample. Each boxplot or barplot represents a biological replicate. The horizontal line in each box represents the median and lower and upper hinges indicate first and third quartiles, respectively. n is the number of mRNAs used to draw the plots. For all the plots, *P*-values were calculated using General Linear Model with binomial distribution. N.s: non-significant. *: $P < 0.05$.

and uridylated mRNAs with longer tail accumulates.

- CCR4 proteins and URT1 competes for the same substrate, *i.e.* actively deadenylated transcripts. When the activity of the CCR4-NOT complex becomes distributive, URT1 is able to bind the poly(A) tail of deadenylated mRNAs, catalysing the uridylation of this population of mRNAs with short poly(A) tails of 15-20As. In *ccr4a ccr4b*, we observe an overall decrease of the deadenylation. Hence, in absence of competitors, URT1 can more often bind mRNAs 3'ends, catalysing the addition of uridines on longer transcripts. This is coherent with the increase in uridylation level for mRNAs highly deadenylated by CCR4a/CCR4b in rosettes, while high PASS mRNAs in flowers are not as actively targeted by CCR4a/CCR4b.

2.2. Physical links bridging uridylation and deadenylation

URT1 has no RNA-binding motif, and how it is recruited to target mRNAs remains elusive. A physical interaction between URT1 and the CCR4-NOT complex could explain how URT1 recognises its substrates, *i.e.* mRNAs being deadenylated by the CCR4-NOT complex. Consistent with this hypothesis, several components of the CCR4-NOT complex, including the main scaffold protein NOT1, co-purify with URT1 in co-IP LC-MS/MS experiments. Indeed, the resolution of URT1's interactome shed light on its involvement in an intricate network of interactions with various proteins related to mRNA decay and translation inhibition (Scheer *et al.*, 2021). Notably, URT1 co-precipitated with several decapping activators/translational inhibitors such as the cap-binding protein NCBP (ortholog of 4E-HP), RNA helicases RH6/8/12 (orthologs of DDX6), decapping activators PAT1, VCS (ortholog of EDC4), and DCP5 (ortholog of LSM14A). Significantly, the study demonstrated that the direct interaction between URT1 and DCP5 was important for the co-precipitation of such factors. Indeed, the mutation of two conserved leucines in the intrinsically disordered region of URT1 not only abolished the direct interaction between URT1$^{L21/25N}$ and DCP5 in a pull-down experiment, but also led to the depletion of RH6-8-12, PAT1, and VCS in co-IP experiments, all of which are known to directly interact with DCP5 in other organisms. This experiment effectively unravelled the intricate chains of interactions linking URT1 to translational repressors/decapping activators. However, because the depletion of these factors was not complete upon the disruption of the URT1-DCP5 interaction, it is likely that other proteins are involved in the connection between URT1 and the decay machinery.

Hence, even though RH/DDX6 is a known partner of the CCR4-NOT complex in metazoans, the depletion of its orthologs in URT1$^{L21/25N}$ co-IPs does not lead to a depletion of components of the CCR4-NOT complex. This indicates that other proteins are involved in the connection between URT1 and the CCR4-NOT complex.

2.2.1. EXA1 is a central component of the mRNA decay machinery

One potential candidate is the GYF domain protein EXA1, which is the most significantly enriched protein co-purifying with URT1. GYF domain proteins serves as molecular adaptors that are able to bind and connect different protein factors (Kofler & Freund, 2006). Direct interactants of GIGYF proteins, the orthologs of EXA1 in humans and in *Drosophila*, include 4E-HP, DDX6/Me31B, and PAT1 (Morita *et al.*, 2012; Peter *et al.*, 2017; Peter *et al.*, 2019; Ruscica *et al.*, 2019; Hickey *et al.*, 2020). Orthologs of all these factors are detected in URT1 IPs. Therefore, such an interaction network could be conserved in *Arabidopsis* and may partially overlap with the DCP5 interactome. Additionally, GIGYF proteins directly connect to CNOT1, the ortholog of *Arabidopsis* NOT1 (Amaya-Ramirez *et al.*, 2018; Ruscica *et al.*, 2019). Therefore, we hypothesised that the interaction between EXA1 and the CCR4-NOT complex may be conserved in *Arabidopsis*. In line with this theory, EXA1 was initially discovered through a yeast two-hybrid screen as a direct interactant of NOT4C, the ortholog of human and yeast NOT4 (Kofler *et al.*, 2005).

The GYF domain of EXA1 recognises a PPGF motif, a sequence that is evolutionarily conserved in URT1 of flowering plants (Scheer *et al.*, 2021). Based on this observation, we hypothesised that URT1 and EXA1 may directly interact and that this interaction could potentially recruit URT1 to EXA1's partners. This interaction might serve as a bridge, linking uridylation to deadenylation through the URT1/EXA1/CCR4-NOT network.

Intrigued by the potential direct interaction between URT1 and EXA1, we conducted a comprehensive analysis to explore the molecular connections within the URT1/EXA1/CCR4-NOT network by LC-MS/MS. Proteins involved in mRNA metabolic processes often contain large intrinsically disordered regions (IDRs) mediating protein-protein or protein-RNA interactions thanks to short linear interspersed motifs (SLiMs) (Jonas & Izaurralde, 2013; Zamora-Briseño *et al.*, 2021). These SLiMs provide low-affinity interactions, which might go undetected by mass spectrometry (Davey *et al.*, 2011; Blikstad & Ivarsson, 2015). Therefore, we wondered whether EXA1 contains IDRs, and consequently, potential SLiMs, as this would influence our workflow for detecting its interacting partners. Using the disorder prediction tool

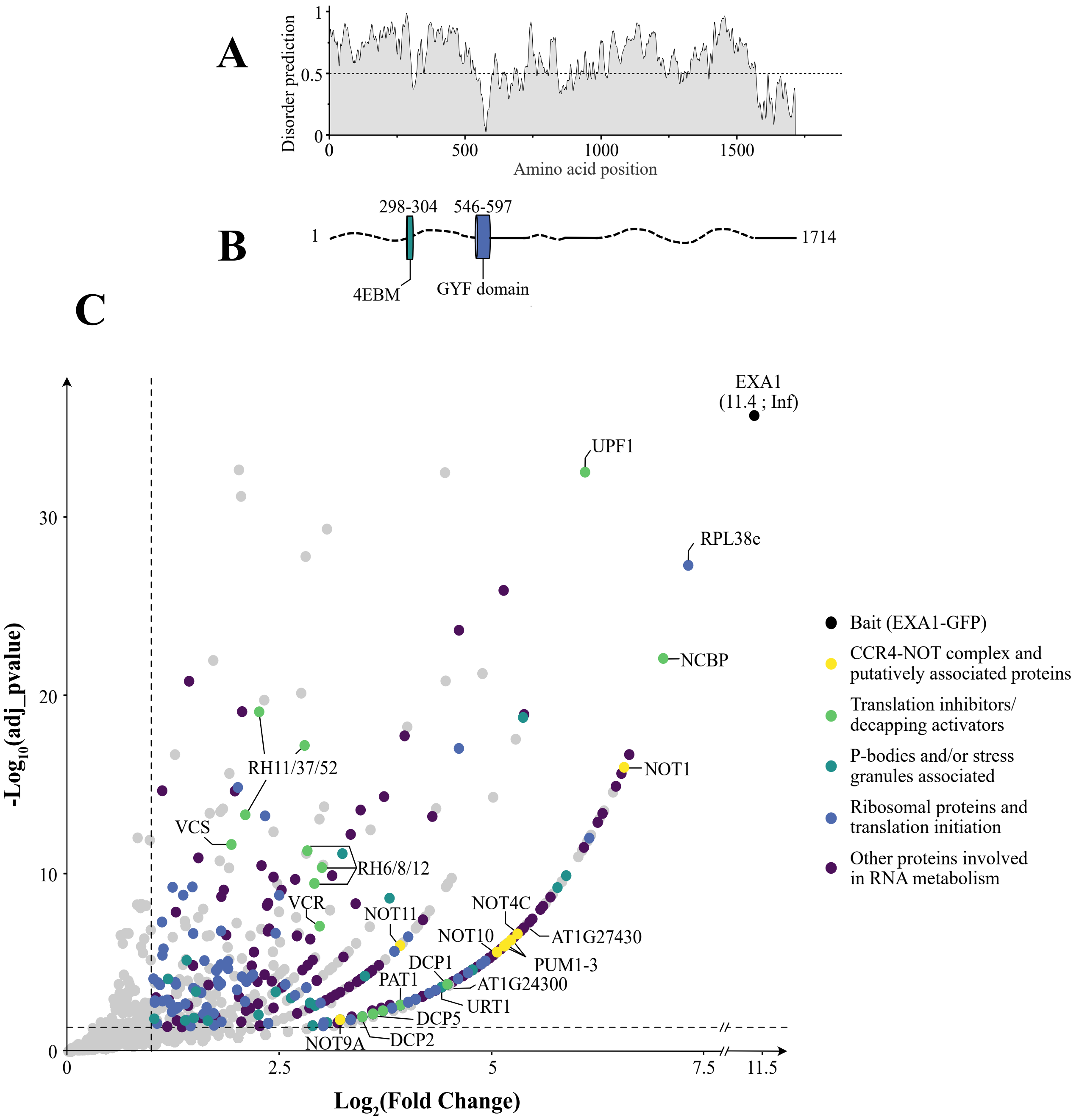

Figure 38. EXA1 is involved in a large interaction network revolving around mRNA metabolism.

A) Disorder prediction of EXA1 using IUPred3 algorithm (https://iupred3.elte.hu/). Dashed line represents the threshold delimiting order and disorder prediction **B)** Domain organisation of EXA1. Dashed line represents the intrinsically disordered region (IDR) of EXA1. Straight lines represent predicted ordered structures with no annotated domains. Boxes represent folded domains and conserved motifs previously identified (Kofler *et al.*, 2005; Hashimoto *et al.*, 2016). 4EBM: eIF4E-binding motif. GYF: Glycine-Tyrosine-Phenylalanine. **C)** Semi volcano plot showing proteins differentially enriched (arbitrary threshold of $\log_2$ fold change > 1, delimited by the vertical dashed line) in EXA1-GFP IPs versus control IPs. The horizontal dashed line indicates the significant threshold (adjusted *p*- value < 0.05, quasi-likelihood negative binomial generalised log-linear model with Benjamini-Hochberg correction). The point color code was attributed both manually and using GO terms as follows. P-bodies and/or stress granules associated: p-body (GO:0000932); p-body assembly (GO:0033962); stress granules (GO:0010494). Ribosomal proteins and translation initiation: structural constituent of ribosome (GO:0003735); formation of translation initiation complex (GO:0001732); eukaryotic translation initiation 4F complex (GO:0016281). Other proteins involved in RNA metabolism: RNA binding (GO:0003724); mRNA binding (GO:0003729). Point colors for "Translation inhibitors/decapping activators" and "CCR4-NOT complex and putatively associated proteins" were attributed manually.

IUPred3 (Erdős *et al.*, 2021), I found that EXA1 is an intrinsically disordered protein (**Figure 38A**). More than 75% of its amino acids are predicted to be disordered, with a disorder score > 0,5. Interestingly, the 4E-binding motif (4EBM), a SLiM involved in the binding of 4E-HP (Nishikawa *et al.*, 2023), is embedded in a large IDR (**Figure 38B**). As EXA1 is an adaptor protein largely intrinsically disordered, we can imagine that many of its partners are bound by SLiMs, which may make their interaction difficult to detect by mass spectrometry. Cross-linking can be employed to covalently bind closely interacting proteins and is particularly effective in stabilising transient interactions mediated by SLiMs (Gingras *et al.*, 2007). In our hands, formaldehyde cross-linking was successfully employed to determine a larger URT1 interactome compared to when omitting the cross-link. Therefore, we decided to utilise the same protocol to explore EXA1's interactome.

Cross-linked co-IP LC-MS/MS were performed using flower buds of *exa1-2* plants expressing EXA1-GFP under the control of the *EXA1* promoter (Wu *et al.*, 2017), and compared to control cross-linked co-IPs performed from flower buds of wild-type plants expressing no transgene. Three biological replicates were prepared per condition, and each biological replicate was split into 2 technical replicates, both of which were injected into the mass spectrometer. The results are presented in **Figure 38C**. Out of the 3008 total proteins identified, 1047 were significantly enriched ($\text{Log}_2\text{FC} > 2$; adjusted p-value < 0.05), of which 380 were identified with an average of 5 spectra or more in all 3 IPs (**Table S7**).

Observing that 1/3 of all identified proteins significantly co-precipitate with EXA1-GFP is rather intriguing. This phenomenon can be explained by 2 non-mutually exclusive hypotheses:

- The first explanation is technical. The control condition (3 co-IP fractions of flower buds from wild-type plants not expressing any transgene) is not stringent enough to clean potential contaminants. Indeed, only an average of 995 proteins were identified in all 3 control co-IPs, compared to the average of 2958 proteins identified in the EXA1-GFP co-IPs. Hence, finding an appropriate control, such as a GFP-fused bait protein that is not involved in any of the processes EXA1 is linked to, may be more useful for clearing potential contaminants.
- The second explanation is biological. EXA1 is an adaptor protein possibly implicated in the binding and connection of different factors. Studies in *Arabidopsis* have shown that it interacts with the ribosome (Wu *et al.*, 2017), components of the NMD (Matsui *et al.*, 2017), cap-binding proteins (Nishikawa *et al.*, 2023) and the CCR4-NOT complex (Kofler *et al.*, 2005). Hence, the interactome of EXA1 may be

important, revolving around critical mRNA metabolic pathways, often associated with large protein complexes.

Consistent with the latter hypothesis, the most enriched molecular function associated with EXA1 co-purifying proteins is mRNA binding (GO:0003723) (Fischer's exact test with Benjamini–Hochberg correction, adjusted *p*-value 2.5×10^{-6}). Particularly, EXA1 co-precipitates with a large number of ribosomal proteins, and RPL38e is the most enriched protein. Interestingly, RPL38e possesses a PPGL motif that can be bound by GYF domains (Kofler *et al.*, 2005). An interaction between EXA1 and the ribosome was already reported and is thought to be involved in the repression of plant immune genes (Wu *et al.*, 2017). Interestingly, a complex network of proteins revolving around translation inhibition co-precipitates with EXA1. NCBP/4EHP is the second most enriched protein, alongside various proteins involved in mRNA translation inhibition and decapping. Particularly, all proteins belonging to the decapping complex are present in EXA1 IPs, including DCP1, DCP2, DCP5/LSM14A, PAT1, VCS/EDC4 and its paralog VCR. DDX6 homologs RH6, RH8, RH12, as well as DDX3 homologs RH11, RH37, RH52, are co-precipitating with EXA1. DDX3 and DDX6 are essential components of processing bodies (P-bodies) and stress granules, just like many other proteins identified in EXA1's interactome. They play a complex yet conserved role in mRNA translational repression (Ostareck *et al.*, 2014; Park & Oh, 2022). The fact that orthologs of DDX3 and DDX6 co-purify with EXA1 reinforces the hypothesis regarding EXA1's involvement in translational repression.

UPF1, UPF2, UPF3, and SMG7, which are all components of the plant NMD pathway, have been observed to co-precipitate with EXA1. This indicates a physical connection between EXA1 and NMD. Our experimental data aligns with previous research showing a direct interaction between the GYF domain of EXA1 and the PPGF motif of SMG7 (Matsui *et al.*, 2017). Likewise, GIGYF2 was found in humans to be responsible for the translational repression of NMD targets (Zinshteyn *et al.*, 2021). Hence, EXA1 likely plays a conserved role in the translational repression of mRNAs targeted by the NMD.

Our co-immunoprecipitation experiments also revealed a significant association between EXA1 and members of the CCR4-NOT complex. NOT9A, NOT10, NOT11, NOT4C, and NOT1 co-precipitates with the GYF domain protein. Particularly, NOT1 is the 4th most enriched protein in EXA1 IPs. The enrichment of core components of the CCR4-NOT complex is consistent with direct interactions previously observed between EXA1 and the CCR4-NOT complex in *Arabidopsis* and animals (Kofler *et al.*, 2005; Ajiro *et al.*, 2010; Amaya-Ramirez *et al.*, 2018;

Ruscica *et al.*, 2019). Additionally, proteins associated with the CCR4-NOT complex co-precipitate with EXA1. APUM1-3 are orthologs of Pumilio proteins found in humans, *Drosophila*, and budding yeast, known as PUM1, Pumilio, and Puf3p, respectively. These proteins are involved in mRNA decay through the recruitment of the CCR4-NOT complex to mRNAs containing Pumilio-response elements (PRE) in their 3'UTR (Olivas & Parker, 2000; Morris *et al.*, 2008; Tam *et al.*, 2010; Goldstrohm *et al.*, 2018; Arvola *et al.*, 2020). Their association with EXA1 and the core components of the CCR4-NOT complex in our dataset suggests a conserved role for the APUM1-3 proteins in regulating functions of the CCR4-NOT complex through binding of mRNAs, as was previously suggested by Arae and colleagues in *Arabidopsis* (Arae *et al.*, 2019).

In conclusion, EXA1 is involved in a complex interactome revolving around translational inhibition and mRNA degradation. Many of the interactants identified in our dataset are supported by independent interaction assays in *Arabidopsis* and other organisms, backing the idea that the intricate interactome we identified accurately represents EXA1's functions. Moreover, all components of the CCR4-NOT complex present in URT1 IPs co-precipitate with EXA1, further indicating that EXA1 may be responsible for the presence of the CCR4-NOT complex in the URT1 interactome.

2.2.2. URT1 associates with EXA1 through its PPGF motif

One way to determine if EXA1 is involved in bridging together uridylation and deadenylation by interacting with both URT1 and the CCR4-NOT complex would be to disrupt the interaction between URT1 and EXA1. This could be achieved either by mutating the GYF domain of EXA1 or the PPGF motif of URT1, as we suppose that these motifs are involved in a direct binding interface. However, mutating the GYF domain of EXA1 would likely disrupt the interaction between EXA1 and other PPGF-containing proteins besides URT1. Hence, mutating the PPGF motif of URT1 appears to be a more precise method to study the URT1-EXA1 interaction. Additionally, mutating the PPGF motif of URT1 has the advantage of disrupting potential interactions with other GYF domain proteins. Indeed, 2 other GYF domain proteins, AT1G24300 and AT1G27430, are significantly enriched in EXA1 IPs and also co-precipitate with URT1 (**Figure 38C**) (Scheer *et al.*, 2021). AT1G24300 and AT1G27430 arose from a recent gene duplication and are highly similar to one another, with their GYF domain resembling the GYF domain of EXA1:

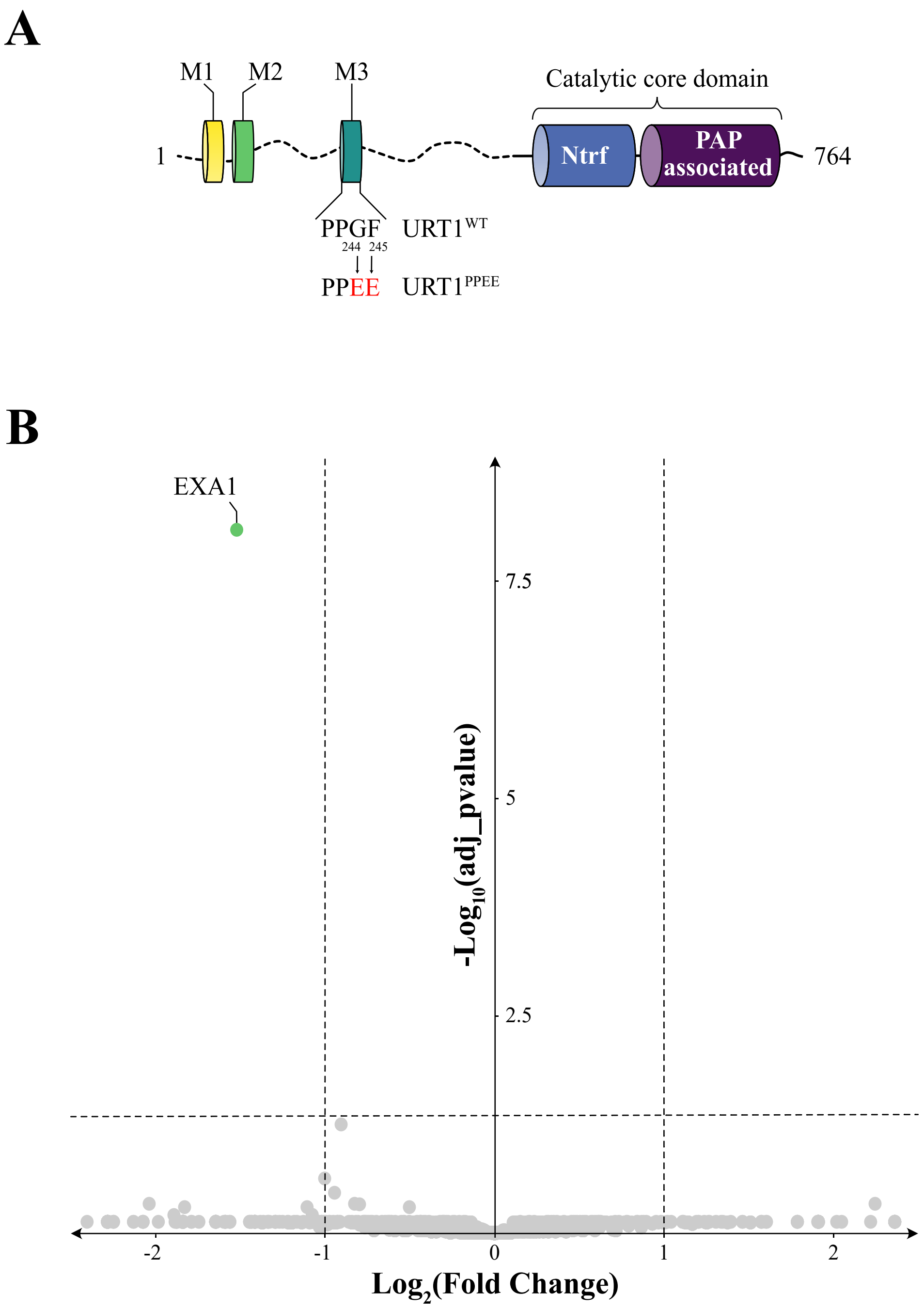

Figure 39. URT1 interacts with EXA1 through its PPGF motif.

A) Domain organisation of URT1. Dashed lines represent the IDR of URT1. Straight lines represent predicted ordered structures with no annotated domains. Boxes represent folded domains and conserved motifs previously identified (Scheer *et al*., 2021). M3 motif is a proline rich sequence containing a PPGF (Proline-Proline-Glycine-Phenylalanine) motif. In the mutated construct URT1^{PPEE}, G244E and F245E mutations are inserted. Ntfr: nucleotidyl-transferase; PAP-associated: poly(A) polymerase β associated domain. **B)** Volcano plot showing proteins differentially enriched ($\log_2$ fold change > 1) or depleted ($\log_2$ fold change < -1) in GFP-tagged URT1^{PPEE} versus GFP-tagged URT1^{WT} IPs. Vertical dashed lines delimit the arbitrarily chosen threshold for the enrichment/depletion. The horizontal dashed line indicates the significant threshold (adjusted *p*-value < 0.05, quasi-likelihood negative binomial generalised log-linear model).

- AT1G24300 and AT1G27430 share 76,1% identity between their full-length sequence; 96,2% identity between their GYF domain.
- EXA1 and AT1G24300 share 22,9% identity between their full-length sequence; 63,5% identity between their GYF domain.
- EXA1 and AT1G27430 share 18,9% identity between their full-length sequence; 67,3% identity between their GYF domain.

Therefore, their functions in mRNA metabolism and their interaction network may be conserved, and to some extent, acting redundantly to EXA1, and thus maybe directly interacting with URT1.

Phage display experiments have shown the preferential recognition of the GYF domain of EXA1 to bind a PPGΦ motif (where Φ is a hydrophobic amino acid) (Kofler *et al.*, 2005). In this motif, the glycine was deemed essential as a single amino acid switch impaired its recognition by the GYF domain. Additionally, the crystal structure of the GYF domain of Smy2 in complex with a PPGL motif indicates that the entire motif is embedded in a hydrophobic pouch within the GYF domain (Ash *et al.*, 2010). Hence, we hypothesised that replacing the glycine and phenylalanine within the PPGF motif of URT1 with charged amino acid such as glutamic acid would disrupt the EXA1-URT1 interaction and other putative URT1-GYF domain protein interactions.

urt1-1 plants were transformed with a cassette expressing either the WT or mutated version of URT1, tagged with GFP at the C-terminus. To generate the cassette expressing the mutated URT1, I performed PCR directed mutagenesis to introduce changes in the CDS of URT1, which would result in Gly244Glu and Phe245Glu mutations (**Figure 39A**). Because prior co-IP experiments conducted by the team revealed the necessity of overexpressing URT1 to identify its partners through LC-MS/MS analysis, the construct is driven by the *UBIQUITIN10* promoter, which is stronger than the endogenous *URT1* promoter.

Co-IPs prepared from flower buds of URT1^{PPEE}-GFP overexpressing plants were compared to control co-IPs of URT1^{WT}-GFP overexpressing plants. 6 co-IPs representing 3 biological replicates were compared. Strikingly, out of the 3345 proteins identified, only EXA1 was significantly depleted upon mutation of the PPGF motif (**Figure 39B**). Co-IP LC-MS/MS experiments are not designed to determine direct protein-protein interactions, yet, here, it strongly suggests that URT1 and EXA1 directly interact together through a PPGF motif-GYF domain interaction. Interestingly, both AT1G24300 and AT1G27430 are not significantly

depleted, indicating that they may not be direct partners of URT1, or at least not through a PPGF motif-GYF domain interaction. Additionally, we do not observe depletion of any previously identified EXA1 partners in URT1^{PPEE}-GFP. No subunit of the CCR4-NOT complex is significantly depleted. Although we observed fewer spectra corresponding to top EXA1 interactants such as NCBP and NOT1 in URT1^{PPEE}-GFP co-IPs, their depletion is not significant. This can be explained by several non-mutually exclusive hypotheses:

- First, EXA1 is not the sole means of recruiting URT1 to the CCR4-NOT complex and other partners. It is likely that within the large protein network shared by EXA1 and URT1, interaction interfaces are multiple and redundant, serving as additional paths linking uridylation and deadenylation.
- Second, the cross-linking may stabilise these interactions. Here, the cross-link is essential for strengthening the interaction bridging URT1 and EXA1 together. Yet, it also reinforces other interaction interfaces that may bridge URT1 to other components of the EXA1 interactome, such as the CCR4-NOT complex.
- Finally, the analysis by LC-MS/MS is not sensitive enough to detect the limited depletion of URT1's secondary partners.

Altogether, our data strongly suggest that EXA1 and URT1 are direct partners, and that this interaction is mediated by the PPGF motif of URT1. Although we were able to precisely disrupt the interaction between URT1 and EXA1, we could not identify depletion of secondary partners of URT1 caused by the loss of EXA1. Hence, the chain of interactions linking URT1 to the CCR4-NOT complex and other partners of the RNA decay machinery has yet to be fully elucidated. However, this result may be due to low sensitivity in detecting interactants with MS, while *in vivo*, the disruption of the interaction impacts mRNA and poly(A) tail metabolism.

2.2.3. Prospects into the role of URT1-EXA1 interaction in shaping mRNA poly(A) tails

To determine whether we observe changes in mRNA 3'end metabolism upon disruption of the URT1-EXA1 interaction, we decided to adopt an exploratory approach through FLEP-seq2 sequencing of an *exa1* knock-out mutant and both the URT1^{WT} and the URT1^{PPEE} over-expressing lines. With this experimental setup, we wanted to check whether modified uridylation levels and poly(A) profiles are observed in *exa1* and whether changes in uridylation

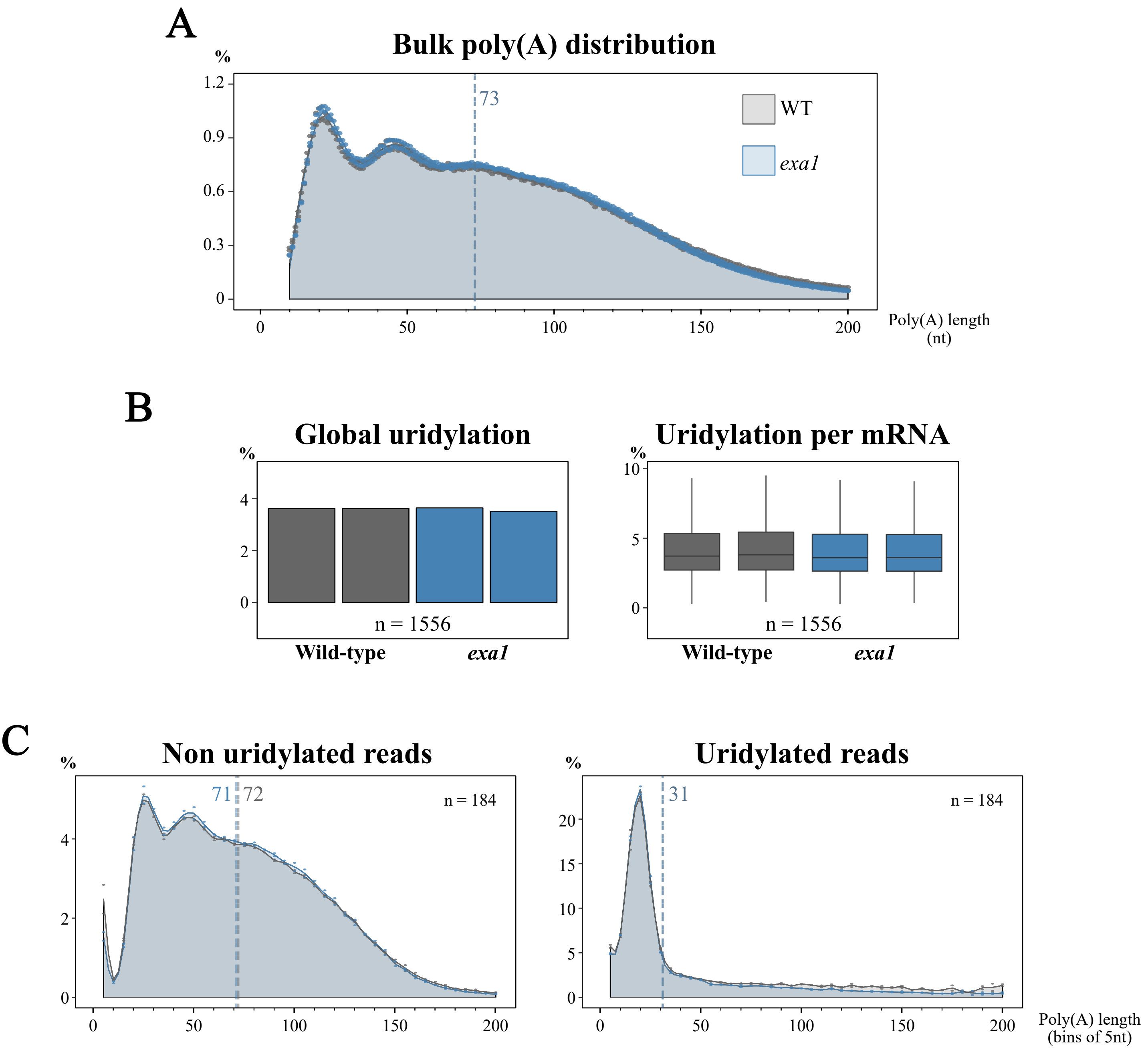

Figure 40. EXA1 does not shape the 3'end of the transcriptome.
A) Bulk poly(A) distribution for WT (grey) and *exa1* (blue) samples. Individual points are shown for two biological replicates and the respective average is indicated as a colored area. Median poly(A) tail size per genotype are represented as dashed lines. **B)** Global uridylation (left panel) or uridylation per mRNA (right panel) for mRNAs with more than 200 reads per sample. **C)** Normalised poly(A) distribution for non uridylated (left panel) and uridylated reads (right panel). To normalise, I calculated the percentage of reads at all poly(A) tail size (bins of 5 nucleotides) for each mRNA in all biological replicates. Dots represent the median percentage of reads per poly(A) tail size across biological replicates, while the line represents the mean of this median across genotypes. To limit variability when normalising, I selected mRNAs that had at least 50 uridylated reads per sample. Normalised median poly(A) tail size for all reads are represented as grey (wild-type) and blue (*exa1*) dashed lines. For all plots, n is the number of mRNAs used to draw the plots.

would be confirmed by comparing the URT1^{PPEE} over-expressing line to the URT1^{WT} over-expressing line. Because those questions remain quite hypothetical, I first analysed only two biological replicates of the *exa1* mutant and their associated controls, and one biological replicate of the URT1 over-expressing line was sequenced. Therefore, the data shown hereafter are preliminary.

Figure 40 shows the analysis of FLEP-seq2 *exa1* mutant. The bulk poly(A) size distribution for poly(A) tails 10-200 As is identical in the wild-type and *exa1* samples (**Figure 40A**). Additionally, when refining the analysis for the most expressed genes, we did not observe an increase in uridylation levels, either in global uridylation or for individual mRNAs (**Figure 40B**). Finally, when plotting the poly(A) distribution of uridylated and non-uridylated tails, we did not identify any difference in the poly(A) profiles between wild-type and *exa1*. Altogether, our data suggest that EXA1 is not a major determinant of the transcriptome's poly(A) tail metabolism through the modulation of poly(A) profiles and uridylation levels.

Overexpression of either URT1^{WT} or URT1^{PPEE} only slightly affects the bulk poly(A) tail profiles, yet the uridylation level is increased in both over-expressing lines (**Figure 41A and B**). We observe a lengthening of uridylated poly(A) tails (**Figure 41C**). Interestingly, the increase in uridylated poly(A) tail size is comparable to the one observed in *ccr4a ccr4b* flower buds (**Figure 35B, right panel**) By overexpressing URT1, we disrupt the balance regulating access to the poly(A) tail for the different components involved in mRNA 3'end metabolism. Because the effect of the overexpression of URT1 resembles the effect that the depletion of CCR4a/CCR4b has on uridylated poly(A) tail size, it reinforces the hypothesis of a competition between the CCR4-NOT complex and URT1 for access to the poly(A) tail.

More replicates are needed to confirm whether uridylation levels drop in URT1^{PPEE} as compared to URT1^{WT}, suggesting that the mutation of the PPGF motif could affect the uridylation capacity of URT1. However, in the FLEP-seq2, we identified fewer reads of URT1 mRNA in the URT1^{PPEE}-GFP line thhan in the URT1^{WT}-GFP line. As a different level of expression of URT1 is likely to influence uridylation levels, more lines and more replicates are needed to reliably assess whether mutating the PPGF motif of URT1 affects uridylation of mRNAs *in vivo*.

Despite the limited number of replicates analysed, several conclusions can be drawn here:

- We observed no changes in global poly(A) tail length or global uridylation level in *exa1*. This suggests that EXA1 is not a major, if at all, regulator of mRNA 3'end shaping and

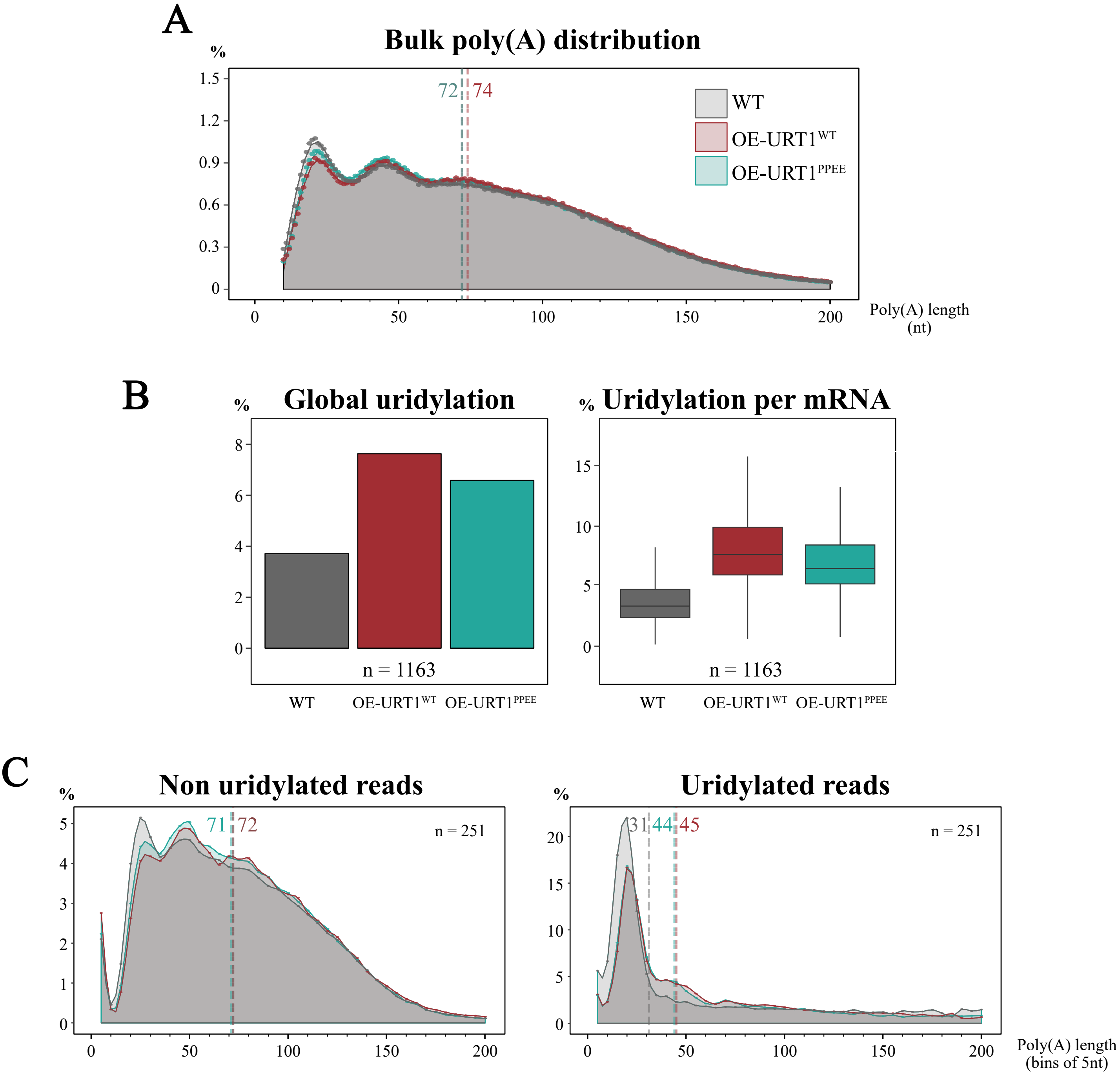

Figure 41. URT1 overexpression increases uridylation levels and lengthens the poly(A) tail. **A)** Bulk poly(A) distribution for WT (grey), OE-URT1^{WT} (red) and OE-URT1^{PPEE} (green). Individual points are shown for two biological replicates and the respective average is indicated as a colored area. Median poly(A) tail size per genotype are represented as dashed lines. **B)** Global uridylation (left panel) or uridylation per mRNA (right panel) for mRNAs with more than 200 reads per sample. **C)** Normalised poly(A) distribution for non uridylated (left panel) and uridylated reads (right panel). To normalise, I calculated the percentage of reads at all poly(A) tail size (bins of 5 nucleotides) for each mRNA in the single biological replicate. Dots and line represent the median percentage of reads per poly(A) tail size in this biological replicate. To limit variability when normalising, I selected mRNAs that had at least 50 uridylated reads per sample. Normalised median poly(A) tail size for all reads are represented as grey (WT), red (OE-URT1^{WT}) and green (OE-URT1^{PPEE}) dashed lines. n is the number of mRNAs used to draw the plots.

that it may not be required for the recruitment of URT1 to its target mRNAs. This will be further discussed in in the manuscript.

- We proposed that overexpression of URT1 promotes the accumulation of longer poly(A) tails by promoting decay of short oligoadenylated mRNAs, combined with the impediment of deadenylation due to the addition of uridines on poly(A) tails, (Scheer *et al.*, 2021). Although there may be a slight decrease in uridylation levels upon overexpression of URT1 mutated for the PPGF motif, the poly(A) profiles remain largely the same whether the PPGF motif is mutated or not. Altogether, our data do not suggest a major role for the PPGF motif in the uridylation capacity of URT1 and its propensity to shape the poly(A) tail profile of the transcriptome.

Discussion & perspectives

1. URT1 interacts with a GYF domain protein that may connect decay factors

My data provide the interactome of EXA1, the first available interactome of a GYF domain protein in eukaryotes. GYF domain proteins are adapter proteins involved in connecting various metabolic pathways. Accordingly, the interactome of EXA1 revolves around well-known complexes involved in mRNA decay or translational inhibition such as the CCR4-NOT complex, the NMD machinery, proteins of the decapping complex, and associated translational inhibitors. The involvement of EXA1 in these critical metabolic functions is described in *Arabidopsis* (Matsui *et al*., 2017; Wu *et al*., 2017; Nishikawa *et al*., 2023), and is evolutionarily conserved, as orthologs in metazoans are involved in connecting similar factors (Ajiro *et al*., 2010; Morita *et al*., 2012; Peter *et al*., 2017; Amaya-Ramirez *et al*., 2018; Peter *et al*., 2019; Ruscica *et al*., 2019; Hickey *et al*., 2020; Weber *et al*., 2020; Mayya *et al*., 2021).

The TUTase URT1 is also identified in the EXA1 interactome, and previous reverse IPs demonstrated the co-purification of EXA1 with URT1 (Scheer *et al*., 2021). I have shown the importance of the conserved PPGF of URT1 motif in the interaction with EXA1. While our experimental framework cannot definitely confirm the direct nature of this interaction, the exclusive depletion of EXA1 among proteins argues in favour of its specificity. This demonstrates a unique interaction, in which a TUTase is connected to an adaptor GYF-domain protein. Yet, while we initially hypothesised that the connection between URT1 and EXA1 would be of importance for the function of either protein, particularly concerning URT1's recruitment to mRNAs, I was unable to determine the molecular function of this interaction. However, establishing an appropriate experimental setup may help clarify its purpose.

Because of the overlap between URT1 and EXA1 interactomes, particularly in regard of proteins involved in translational repression such as DCP5, VCS, VCR, RH6-8-12 and NCBP (**Figure 13 and 38**), it is tempting to suppose a network of interaction including all these factors. EXA1 and NCBP associate together (Nishikawa *et al*., 2023), likely to promote translational repression of mRNA targets as described in metazoans (Morita *et al*., 2012; Peter *et al*., 2017; Amaya-Ramirez *et al*., 2018; Peter *et al*., 2019; Ruscica *et al*., 2019; Hickey *et al*., 2020; Weber *et al*., 2020). One can hypothesise that URT1 is recruited to mRNA targets of EXA1-NCBP that need to be translationally repressed. The presence of URT1 could facilitate the recruitment of DCP5 and associated decay factors to promote the formation of an mRNP necessary to induce

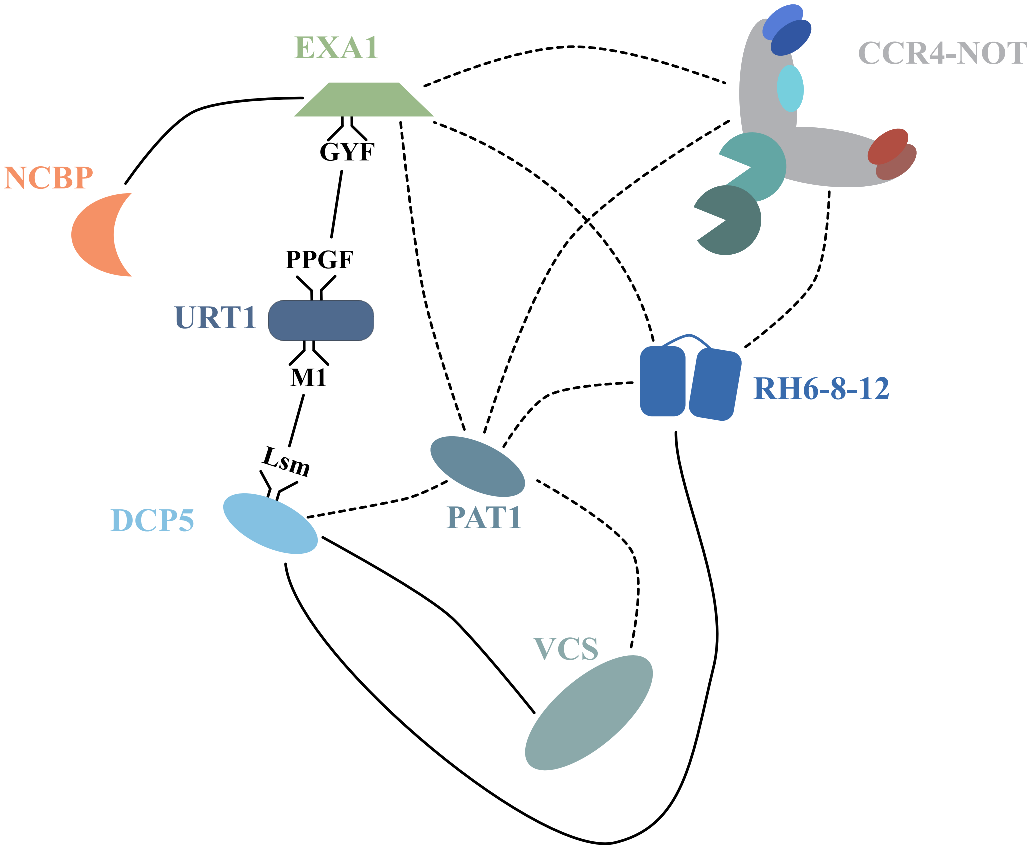

Figure 42. Extensive redundancy in the interactions of the URT1-EXA1 network. Known interactions in *Arabidopsis* are displayed as straight lines. Interactions demonstrated in orthologs of the respective factors in other eukaryotes are represented as dashed lines. The role of the mRNA as a scaffold for the interactions with proteins of the network is not represented but is essential. Interactions interfaces were inferred from Ajiro *et al.*, 2010; Morita *et al.*, 2012; Peter *et al.*, 2017; Amaya-Ramirez *et al.*, 2018; Peter *et al.*, 2019; Ruscica *et al.*, 2019; Hickey *et al.*, 2020; Weber *et al.*, 2020; Mayya *et al.*, 2021; Scheer *et al.*, 2021; Vidya *et al.*, 2022; Nishikawa *et al.*, 2023.

efficient translational inhibition and, eventually, further decay. Whether uridylation plays a role in this process is an interesting hypothesis, but it would need to be formally determined. The identification of target mRNAs of NCBP-EXA1 would provide candidates to address this hypothesis. EXA1 is involved in the translational repression of NB-LRR proteins, and putative targets were already described (Wu *et al*., 2017). Yet, FLEP-seq2 is not adapted to capture the poly(A) tail of transcripts expressed at such low levels. We adapted the FLEP-seq2 to develop the Nano3'-RACE, that is suited to perform high depth sequencing of target transcripts (Giraudo *et al*., 2023). Nano3'-RACE may be a useful tool to determine the role of the putative NCBP-EXA1-URT1 interaction at the 3'end of specific targets.

The mutation of the motif in URT1 did not lead to the depletion of other putative secondary interactants. A plausible explanation for this lack of depletion could be the redundancy of interactions between decay factors identified in both URT1 and EXA1 IPs (**Figure 42**). Combining mutations in both the M1 motif and the PPGF motif may be useful to disrupt redundant interactions and identify unique factors depleted upon the loss of both DCP5 and EXA1.

Nonetheless, it is also likely that other unidentified motifs exist and may provide an additional layer connecting URT1 to decay factors in addition to the M1 and the PPGF motifs. The presence of such motifs is highly probable. Ectopic overexpression of URT1 truncated in different parts of its N-terminal region demonstrated that the initial 162 amino acids of URT1, encompassing three conserved motifs including the M1 motif, are dispensable for its targeting to P-bodies (Ferrier, 2013). Conversely, a region between the 163rd and 418th residues was deemed essential for proper targeting to P-bodies. This region encompasses not only the PPGF motif but is also enriched in specific amino acids, namely proline, glutamine, asparagine and histidine (Ferrier, 2013; Scheer, 2018; Scheer *et al*., 2021). Importantly, this enrichment is evolutionarily conserved among URT1 orthologs in land plants, suggesting selective pressure to maintain this amino acid composition due to its potential significance for URT1's functions. Interestingly, sequences enriched in glutamine and asparagine are responsible for the aggregation into P-bodies of Ccr4, Caf1 and Dhh1 in yeast (Reijns *et al*., 2008). Further experiments are needed to address the actual role of this region in shaping the interactome of URT1, and to possibly determine the molecular determinants of the interaction between URT1 and the CCR4-NOT complex.

2. CCR4a CCR4b are broad deadenylases involved in multiple processes throughout development

A recent article provided the first insight into the role of CCR4a as a key cellular factor involved in mRNA deadenylation in *Arabidopsis* (Wang *et al*., 2023). Using nanopore Direct RNA sequencing, the authors demonstrated that CCR4a is involved in bulk mRNA deadenylation, and that it represses a specific subset of transposable elements, likely through deadenylation-dependent decay. However, because the authors used a *ccr4a* mutant to define the poly(A) tail profiles, it is likely that the decrease in deadenylation is compensated to some extent by the other paralog CCR4b. Furthermore, the authors purified mRNAs using oligo(dT) beads prior to nanopore library preparation. The use of oligo(dT) beads introduces a bias towards selecting long poly(A) tails, especially when deadenylation is impaired, because it inherently increases poly(A) tail size. In this context, the experimental workflow I employed, using a *ccr4a ccr4b* double mutant and FLEP-seq2, is more adapted to accurately capture the importance of mRNA deadenylation by CCR4 proteins in *Arabidopsis*.

I provide evidence that CCR4a and CCR4b act as broad deadenylases that largely shape the poly(A) tail profile in two distinct developmental stages. Indeed, 931/934 and 1089/1182 mRNAs displayed positive PASS in rosette and flower buds, respectively (**Figure 22**). We propose that virtually all mRNAs are deadenylated by CCR4a and CCR4b in *Arabidopsis*. While we cannot rule out any possible indirect effect of the mutation, we do not favour such a hypothesis given the conserved role of CCR4 proteins in deadenylation across eukaryotes, likely explaining the changes observed for poly(A) tail profiles in *ccr4a ccr4b*. GO term analysis suggests that CCR4 proteins may be involved in modulating immunity both in rosettes and flower buds (**Figure 15E** and **29A**), likely by triggering the decay of mRNAs encoding stress-response genes. While we cannot rule out that the transcriptomic changes observed using Illumina and nanopore sequencing are caused by an indirect activation of defence response in the *ccr4a ccr4b* mutant, we do not favour such a hypothesis. Indeed, in humans, mRNAs encoded by stress-response genes are short-lived and accumulate highly deadenylated species (Eisen *et al*., 2020). Accordingly, I observed a clear increase in poly(A) tail size in *ccr4a ccr4b*, particularly regarding short oligo(A) isoforms of stress-response genes (**Figure 18A**). I also observed a significant correlation between the half-life of stress-response genes and their steady-state accumulation in *ccr4a ccr4b* in two datasets of mRNA half-life measurements (**Figure 19**). Consistent with a role of deadenylation in immunity, *Arabidopsis* CAF1a and CAF1b are induced upon various biotic and abiotic stresses, and their deadenylation activity is essential to promote an efficient response to stress (reviewed in Walley *et al.*, 2010). Additionally, knock-out mutants *caf1a* and *caf1b* are sensitive to infection by *Pseudomonas syringae* (Liang *et al.*, 2008). Altogether, it suggests that deadenylation is essential in controlling plant immunity. This encourages us to investigate how *ccr4a ccr4b* mutants respond to stress conditions.

Rather interestingly, I identified a specific population of mRNAs in flower buds whose poly(A) tail distribution is largely lengthened in *ccr4a ccr4b* (**Figure 22**). We propose that this particular population is highly regulated by CCR4a and CCR4b in normal conditions. These mRNAs are exclusively expressed in tissues related to maturing or mature pollen, and encode proteins that are deemed essential for pollen germination and tube growth. Accordingly, we observed a significant decrease in pollen tube growth in *ccr4a ccr4b* pollen grains *in vitro* (**Figure 27B**). Such a phenotype was previously observed in a *not1* heterozygous mutant, which suggests the importance of the CCR4-NOT complex for pollen maturation (Motomura *et al.*, 2020; Pereira *et al.*, 2020). My data provide evidence that the effects observed in *not1* $^{+/-}$ pollen are caused, at least in part, either by CCR4-mediated deadenylation or by its structural functions in the complex. Yet, we cannot rule out that other metabolic processes mediated by CCR4-NOT and unrelated to deadenylation also play a role in the pollen phenotype in *not1*$^{+/-}$.

Pollen development involves two distinct and sequential gene expression programs, classified based on their occurrence during pollen development (reviewed in Twell *et al.*, 2006 and Rafinska *et al.*, 2014). Early genes are transcribed shortly after meiosis, and their levels decrease significantly as the pollen grains mature. In contrast, late genes transcripts are only detected after the first mitotic division, and accumulate as the pollen grain matures until complete maturity. The transcripts of these late genes constitute a pool of highly stable and translationally repressed mRNAs that are stored in mRNPs. The transition from a translationally dormant transcriptome to an actively translating one is crucial for pollen germination (Honys & Twell, 2004), and the composition of the mRNPs is likely essential for the shift from a repressed to an active state (Billey *et al.*, 2021). Late gene transcripts start to accumulate starting from pollen stage 8-9, and numerous mRNAs that I identified as highly deadenylated by CCR4 are expressed in these stages, and thus belong to this late gene transcriptional program (**Figure 24, lower panel**). It is then likely that they are stored in a quiescent state, explaining why we did not observe effects on translation and protein accumulation in *ccr4a ccr4b*. Mature pollen is a rather unique developmental stage in regard to poly(A) tail profiles in *Arabidopsis* (**Figure 9**; Jia *et al.*, 2022), where both the length and the PABPC phasing are different other developmental stages. This intricate profile implies a specific regulation of the poly(A) tail, that may be essential for the correct definition of a functional mRNP.

Due to their activity during gametophyte maturation (and/or in mature pollen), CCR4 proteins may play a role in shaping the 3' end of a functional transcriptome in mature pollen, where the precise poly(A) length is crucial for proper mRNP formation and, potentially, composition. It is plausible that in *ccr4a ccr4b* mature pollen, the transcriptome undergoes significant poly(A) lengthening. My data support this proposition: CCR4 and CCR4b are involved in deadenylation in two distinct developmental stages; late gene transcripts are specifically lengthened in *ccr4a ccr4b*. Defects in the precise definition of the poly(A) tail in mature pollen could affect the binding of *trans* factors, such as specific pollen PABPCs. Excessive binding may alter the composition of pollen mRNPs, potentially altering its functions or leading to aggregates that are not reversible upon pollen hydration.

An alternative, non-concurrent hypothesis to explain defects in pollen germination in *ccr4a ccr4b* could be that, upon pollen hydration, CCR4 proteins play an essential role in initiating the degradation of a specific subset or potentially numerous transcripts. This process is proposed to facilitate the transition from a translationally quiescent state to an active state, promoting pollen germination.

These hypotheses will drive subsequent investigations aimed at characterising the molecular basis of CCR4-mediated regulation in pollen germination. Specifically, elucidating the extent of deadenylation defects in both mature and early germinating pollen would yield valuable insights into the roles of the CCR4-NOT complex in this crucial process.

3. The balance between factors regulating uridylation and deadenylation shapes the poly(A) tail profile

3.1. URT1 uridylates long poly(A) tails when overexpressed

The main aspect of my thesis and a recurrent research topic of our team is the study of the interplay between uridylation and deadenylation. It was initially thought that URT1 targets only mRNAs with short oligoadenylated tails and that deadenylation was a necessary step prior to uridylation (Sement *et al.*, 2013; Zuber *et al.*, 2016). However, transient overexpression of URT1 in *Nicotiana benthamiana* leaves coupled with 3'RACE-seq demonstrated that URT1 can uridylate much longer poly(A) tails of both endogenous and reporter mRNAs, indicating that the catalytic activity of URT1 is not restricted to a particular poly(A) tail size (Scheer *et al*., 2021). The global increase in poly(A) length is likely caused by the protective effect resulting from extensive uridylation. We and others have demonstrated the protective role of 3' terminal uridines in preventing deadenylation by impeding deadenylases (Lim *et al*., 2018; Zuber *et al*., 2018; Tang *et al*., 2019; Chen *et al*., 2021). The use of nanopore sequencing with FLEP-seq2 allowed me to confirm these observations at the level of the transcriptome in *Arabidopsis* using a stable transformed line overexpressing URT1.

While URT1 can uridylate longer poly(A) tails, and despite its overexpression, we still observe fewer long uridylated poly(A) tails compared to uridylated tails shorter than 25-30As (**Figure 41C**). This was also observed at high levels of overexpression during transient expression in *N. benthamiana* (Scheer *et al*., 2021). This implies that additional mechanisms modulate URT1's activity/ability to catalyse uridylation on short poly(A) tails. Such mechanisms may be caused by intrinsic properties of URT1 and its possible preference for short oligo(A) tails, as observed for TUT4/7 in humans, where oligo(A) tails of 0-10As were more efficiently uridylated *in vitro* than poly(A) tails of 25-50As (Lim *et al*., 2014). Alternatively, or simultaneously, other factors may be responsible for the preferential uridylation of short poly(A) tails. We hypothesised that one such factor could be the CCR4-NOT complex. Indeed, the CCR4-NOT complex, and particularly CCR4, is suggested to be a processive enzyme on poly(A) tails longer than 44As (Viswanathan *et al*., 2003). These tails are efficiently bound and degraded by the complex, thus making them less accessible for URT1, which would explain the lack of uridylation for mRNAs with long poly(A) tails.

3.2. CCR4-NOT and the PABPCs regulate the size of uridylated tails

The analysis of mRNA 3' ends using FLEP-seq2 in the *ccr4a ccr4b* double mutant revealed drastic changes in uridylation patterns. It clearly demonstrated that deadenylation by CCR4 proteins is not a necessary step preceding uridylation. No drop in uridylation percentage was observed, contrary to the expected outcome if deadenylation were mandatory. Rather, we observed a slight increase in uridylation percentages for mRNAs with high PASS in rosette, *i.e.* mRNAs that are more prone to deadenylation by CCR4a/CCR4b in wild-type conditions (**Figure 37A, left panels**). The idea that mRNAs efficiently deadenylated by CCR4a and CCR4b are significantly more uridylated in *ccr4a ccr4b* supports the hypothesis that active deadenylation blocks the addition of uridines. However, the mechanism behind such a process remains unclear. A possible explanation is that the processivity of the CCR4-NOT complex and of CCR4 proteins may hinder the access of long poly(A) tails to URT1. Thus, poly(A) tails become accessible only when the activity of the complex becomes distributive, *i.e.*, on short poly(A) tails. Alternatively, or concurrently, the CCR4-NOT complex may more efficiently remove uridines from longer poly(A) tails than from short poly(A) tails.

Moreover, we observe a peak of uridylated poly(A) tails centered at 20 As (**Figure 35B, grey lines**). This implies that yet another factor is involved in defining the size at which uridines can be stably incorporated (or less efficiently removed) at the 3' end of the poly(A) tail. Such a factor is likely to be the PABPC. Our team demonstrated that *Arabidopsis* PABPC PAB2 is able to bind uridylated poly(A) tails of such size *in vivo* (Zuber *et al.*, 2016). *In vitro* experiments demonstrated that PAB2 could bind short poly(A) tails and control the number of uridines added, likely by covering the 3' end after uridylation reconstitutes a sufficient size for a stable PAB2 binding. Here, PAB2 acts as a molecular ruler that determines the extent of the uridine extension. In line with this, depletion of PABPC1 in human cells leads to an increase in global uridylation levels and in the size of uridine extensions (Yi *et al.*, 2018). Interestingly, upon mutation of *ccr4a ccr4b*, fewer uridylated poly(A) tails accumulate at 20As, while longer tails accumulate at 50As and 80As (**Figure 35B, orange lines**). Because PABPC protein protects a size of ~27As, such a phasing pattern could represent serial binding of PABPC to uridylated poly(A) tails. This indicates that in the absence of CCR4 proteins, PABPC can bind much longer uridylated poly(A) tails than expected. Recently, *Ph*D student Pietro Giraudo conducted FLEP-seq2 on combinations of the main cytoplasmic PABPCs (PAB2, PAB4, and PAB8) mutants in *Arabidopsis* seedlings. A somewhat similar effect to that in *ccr4a ccr4b* rosette was observed, with increased uridylation levels and lengthening of uridylated and non-uridylated poly(A) tails. Interestingly, the identity of the PABPC that is depleted is important, as the different PABPC mutants display different poly(A) tail distributions and uridylation patterns. Moreover, the extent of the effects observed on poly(A) profiles correlates to the level of expression of the PABPC depleted. While we cannot rule out specific and distinct roles of the different PABPCs in this process, this observation is in line with our hypothesis that shifting the equilibrium for the access to the 3'end is an important modulator of uridylation. Altogether, these results support the idea that PABPC proteins are important regulators of uridylation in *Arabidopsis*.

The emergence of defined uridylated peaks at 50As and 80As in *ccr4a ccr4b* is directly associated with the extent of deadenylation. Indeed, distribution of uridylated reads in rosette (where the KO of CCR4a and CCR4b particularly impacts poly(A) tail distribution) exhibits a clearer phasing pattern compared to flower mRNAs (**Figure 35B, orange lines**). Accordingly, high PASS mRNAs show better-defined peaks than those with low PASS (**Figure 36, orange lines**). This emphasises the prominent role of deadenylation by CCR4a and CCR4b in shaping the uridylation profiles.

Interestingly, in rosette mRNAs of *ccr4a ccr4b* plants, the proportion of uridylated reads for the peaks at 20 As, 50 As and 80 As is relatively similar, with a slightly higher proportion for the peak at 20 As (**Figure 35B, left panel, orange line)**. However, the poly(A) tail distribution for all rosette mRNAs in *ccr4a ccr4b* does not follow the same pattern. Indeed, we observe that the proportion of reads with poly(A) tails of ~20 As is largely smaller than that of the peaks at 50 As and 80 As (**Figure 21A, left panel, grey line**). Altogether, it indicates that despite the increase in the length of uridylated poly(A) tails in *ccr4a ccr4b* compared to wild-type, uridylation of short poly(A) tails is still proportionally preferred over longer tails. As discussed previously, this may be explained at least in part by the distributive activity of CCR4-NOT when reaching short poly(A) tails. Uridylated poly(A) tails of ~20 As may then be more accessible than uridylated tails of 50 As and 80 As. Moreover, in line with recent findings about the specific role of LARP1 that binds and stabilises short poly(A) tails (Yi *et al.*, 2018), we cannot exclude that there exists a yet unknown factor that specifically stabilise short uridylated poly(A) tails of ~20 As.

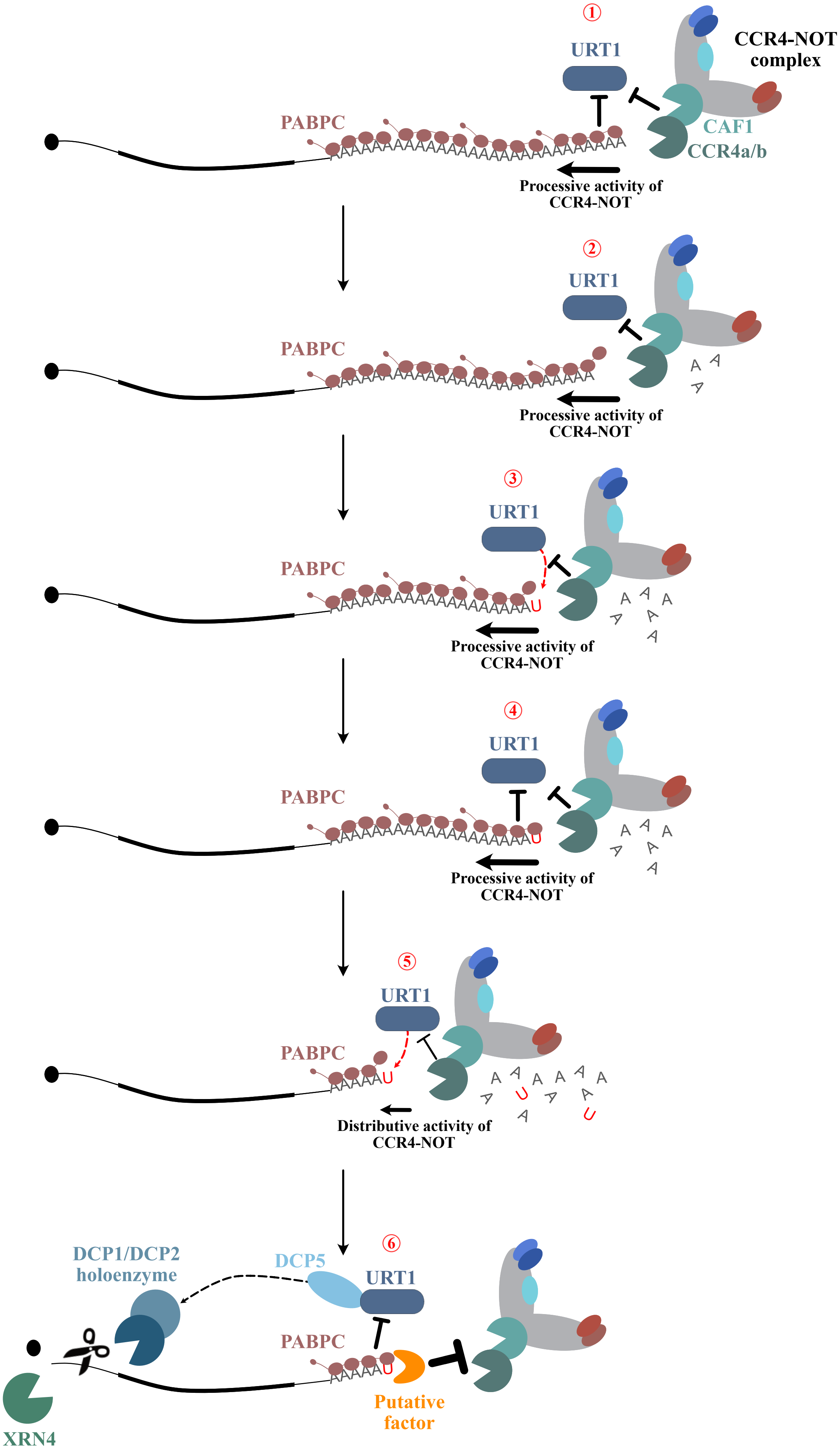

Figure 43. Model of the interplay between uridylation and deadenylation.
For legend, see text

4. General conclusions

The purpose of my thesis was to better understand the roles of deadenylation by the CCR4-NOT complex and its interplay with uridylation in *Arabidopsis thaliana*. To achieve this goal, I combined biochemical and sequencing approaches to provide an accurate analysis of their functions. Using the recently developed FLEP-seq2, I identified CCR4a and CCR4b as important deadenylases that are involved in bulk mRNA deadenylation in two different developmental stages. Interestingly, we observed specific deadenylation patterns that are dictated both by the tissue of expression and the mRNA species, and further work is needed to decipher the molecular purpose of such targeted deadenylation.

Altogether the extensive use of FLEP-seq2 significantly improved our understanding of the interplay between factors that shape both the size and composition of the poly(A) tail. Our current model is that URT1 is able to target and uridylate both short and long poly(A) tails and that its activity is modulated by factors competing for the access to the 3’ end (**Figure 43, numbers in the main text correspond to the figure legend**). **(1)** The processive activity of the CCR4-NOT complex likely impedes URT1's ability to efficiently bind and uridylate mRNAs with long poly(A) tails. In addition, the PABPC may completely cover the 3’ terminal of the poly(A) tail, blocking the access for uridylation by URT1. **(2)** The stepwise removal of each RRM of the PABPC by CCR4 and further deadenylation readily shortens the poly(A) tail (Webster *et al*., 2018). **(3)** At some point in this process ,when one or more RRMs of the PABPC are disengaged, URT1 may be able to access the 3’ end of the mRNA and catalyse the addition of enough uridines to restore a binding site for the PABPC. **(4)** The complete binding of the PABPC to the repaired 3’end likely impedes the addition of more uridines by URT1. Because the CCR4-NOT is processive on long poly(A) tail, it is likely that it is still able to degrade the uridine extension to further remove the PABPC and shorten the poly(A) tail. This would explain the absence of uridylation on long poly(A) tails in wild-type plants. **(5)** When the poly(A) tail shortens and reaches < 25As, the activity of the CCR4-NOT switches from processive to distributive (Viswanathan *et al*., 2003). Thereby, the equilibrium between URT1, PABPC and CCR4-NOT shifts, and URT1 is able to access the deadenylated 3’end, catalyses uridylation until the nucleotide extension is long enough to promote PABPC binding which blocks uridylation by URT1 **(6)** The combined effects of the presence of a PABPC stably bound on the short poly(A) tail, of uridines at the 3’ extremity, and potentially other factors that may stabilise the uridylated short poly(A) tail, effectively hinder excessive deadenylation. The 3’ stability conferred by URT1-mediated uridylation together with the recruitment of the decapping activator/translation inhibitor DCP5 could promote the 5’→3’ polarised degradation, likely essential in the case of co-translational decay to prevent the production of truncated proteins.

In summary, our findings underscore the precise regulation of uridylation in plants, finely orchestrated through a complex interplay among essential mRNA metabolism factors competing for access to the 3' end.

Material & methods

1. Material

1.1. Plant material and growth conditions

The *Arabidopsis thaliana* plants used during my thesis were of the Columbia accession (Col-0). Plants were grown on soil at 21/18°C in short days light condition (12h day / 12h night) during 5 weeks, and latter placed in long days condition (16h day / 8h night) until flowering. Lighting was provided by neon bulbs (for the Illumina RNA-seq experiment on rosette leaves) or LEDs (for all other experiments).

1.2. Mutants and accession

T-DNA insertion lines *urt1-1* (SALK_087647C), *exa1-1* (SALK_005994C) were used. The *ccr4a/bi* and *ccr4ai/b* were previously described (Suzuki *et al*., 2015) and were kindly provided by Yukako Chiba. The EXA1-GFP line used for the LC-MS/MS experiment was previously described (Wu *et al*., 2017) and was kindly provided by Xin Li. URT1^{WT}-GFP and URT1^{PPEE}-GFP overexpressing lines were obtained by *Agrobacterium*-mediated transformation of homozygous *urt1-1* plants with binary vectors containing either the WT or mutated version of the genomic URT1 (see **Methods 2.2**). URT1^{WT}-GFP, URT1^{PPEE}-GFP and EXA1-GFP expressing lines were selected upon their expression of the recombinant protein by western blot (see **Methods 2.3**).

The ccr4a ccr4b double mutant was generated using the CRISPR-Cas9 technology on wild-type plants (see Methods, chapter xxx).

1.3. Bacterial strains

Chemically competent *Escherichia coli* TOP10 cells were used for plasmid amplification.

Chemically competent *Agrobacterium tumefaciens* GV3101 (Gentamicin and Rifampicine resistance) were used for *Arabidopsis* stable transformation.

1.4. Vectors

pDONR207 (Gentamycin resistance, *ccdB* marker) is a Gateway donor vector with *attP1* and *attP2* sites used for Gateway cloning. This plasmid was used for the cloning of the URT1^{WT}-GFP construct into the pUBC-GFP destination vector. It was also used for site directed mutagenesis in order to create the vector with the URT1^{PPEE}-GFP cassette (see **Methods 2.1.4**) and subsequent recombination into the pBlevins1 destination vector.

pEN-Chimera (Ampicilin resistance) is an entry Gateway vector with *attL1* and *attL2* sites used for recombination with Gateway destination vectors. This plasmid is used to generate the desired sgRNA needed for CRISPR-Cas9-mediated mutagenesis. The entry vector pEN-Chimera_2X has 2 different sgRNA backbone under the control of the *At*U6-26 promoter and can then accommodate the insertion of 2 different protospacers at a time. This plasmid was used for cloning the 2 sgRNAs targeting the *CCR4a* and *CCR4b* genes into the gateway destination vector.

pUBC-GFP (Spectinomycin and glufosinate resistance, *ccdB* marker) is a destination Gateway vector with *attR1* and *attR2* sites used for recombination with Gateway entry vectors. This plasmid contains left border (LB) and right border (RB) sequences needed for Agrobacterium-mediated plant transformation. This plasmid is used to express sequences of interest fused to the green-fluorescent protein (GFP) in C-terminal. The construct is expressed under the control of the ubiquitin-10 promoter. In this work, this plasmid was used to generate pUBC-gURT1^{WT}-GFP and pUBC-gURT1^{PPEE}-GFP plasmids used to transform plants so that they express URT1^{WT}-GFP and URT1^{PPEE}-GFP, respectively.

pBlevins1 (Kanamycin resistance, ccdB marker) is a modified Gateway destination vector with attR1 and attR2 sites used for recombination with Gateway entry vectors. This plasmid contains left border (LB) and right border (RB) sequences needed for Agrobacterium-mediated plant transformation. This plasmid is used to for site-directed mutagenesis by the CRISPR-Cas9 technology. This plasmid contains the coding sequence of Streptococcus pyogenes Cas9 fused with an N-terminal NLS and under the control of the egg-cell specific promoter EC1.2. It also contains a GFP under the control of the At2S3 promoter, a seed-coat specific primer, used to facilitate screening of transformed seeds.

1.5. Antibodies

Anti-URT1 antibody is a rabbit polyclonal antibody produced by our team. It is used at a dilution of 1/10000 and is recognised by a secondary anti-goat antibody.

Anti-GFP-HRP antibody is a monoclonal antibody obtained from Miltenyi Biotec. It is used at a dilution of 1/10000 and does not need a secondary antibody.

1.6. Primers

1.6.1. Primers used for cloning

Target	Primer sequence (5'-3')	Description
URT1 (AT2G45620)	GGGGACAAGTTTGTACAAAAAAGCAGGCTCATTGTAAGATCTTCGACTTGGC	Reverse primer in 5'UTR with attB1 site, for C-ter cloning
	GGGGACCACTTTGTACAAGAAAGCTGGGTAGTTGTGGCCTTGTCCATTATTAT	Reverse primer without stop codon with attB1 site, for C-ter cloning
	CCTCCTCCTCCTCCTGAAGAATCGAGTAACCAAAGAG	Forward primer for URT1 mutagenesis (G244E and F245E mutation)
	CTCTTTGGTTACTCGATTCTTCAGGAGGAGGAGGAGG	Reverse primer for URT1 mutagenesis (G244E and F245E mutation)
CCR4a (AT3G58560)	ATTGTAGTGTGCATCCATCCGAGA	Forward primer for sgRNA 1 on CCR4a
	AAACTCTCGGATGGATGCACACTA	Reverse primer for sgRNA 1 on CCR4a
	ATTGATACAGTTACTGCCCCACAT	Forward primer for sgRNA 2 on CCR4a
	AAACATGTGGGGCAGTAACTGTA	Reverse primer for sgRNA 2 on CCR4a
CCR4b (AT3G58580)	ATTGTCTACAGTTACTGTCCTCCT	Forward primer for sgRNA 3 on CCR4b
	AAACAGGAGGACAGTAACTGTAGA	Reverse primer for sgRNA 3 on CCR4b

1.6.2. Primers used for genotyping and sequencing

Target	Primer sequence (5'-3')	Description
URT1 (AT2G45620)	ACCTGTGGATGTCATTTCGAC	Foward primer on the genomic URT1 for genotyping of the urt1-1 mutant
	CCGTCAATAATCCTTTTCCTCCG	Reverse primer on the genomic URT1 for genotyping of the urt1-1 mutant
EXA1 (AT5G42950)	GGAATTCCATATGATGCAGGGAAATGCTCATGTT	Foward primer on the genomic EXA1 for genotyping of the exa1-1 mutant
	CCGCTCGAGGACCCCAAAGGGAATTTGC	Reverse primer on the genomic EXA1 for genotyping of the urt1-1 mutant
CCR4a (AT3G58560)	ACAGAGTGATAAGAAAGTTGCGATT	Forward primer for HRM genotyping of ccr4a g1
	ACTTTAGACATCCCAGACACTGC	Reverse primer for HRM genotyping of ccr4a g1
	TGTCTGATACATATGCTAGCAGCG	Forward primer for HRM genotyping of ccr4a g2
	ACAAATTCTGTCTACGGTATGTCCA	Reverse primer for HRM genotyping of ccr4a g2
	AGGGTTCATCCATGCTGTCG	Forward primer for PCR amplificiation of CCR4a for genotyping of ccr4a g1
	CCTTCTGTAGCAGCACTGG	Reverse primer for PCR amplificiation of CCR4a for genotyping of ccr4a g1
	AGCCATAACTCAAAAGACCG	Forward primer for PCR amplificiation of CCR4a for genotyping of ccr4a g2
	GCACCCATCAATTGTGTTTGT	Reverse primer for PCR amplificiation of CCR4a for genotyping of ccr4a g2
	GTAGGGTTTATAAGTCTCCAGTC	For sequencing of PCR product for ccr4a g1 genotyping
	GGAACATTCACTGTGCTGTCC	For sequencing of PCR product for ccr4a g2 genotyping
CCR4b (AT3G58580)	TTGTCTGATACTTCTGCAAGTAGCG	Forward primer for HRM genotyping of ccr4b g3
	CTGTCTTCGGTATGGCCATGA	Forward primer for HRM genotyping of ccr4b g3
	CCAACGGAACAAGCTACTTTACAG	Forward primer for PCR amplificiation of CCR4b for genotyping of ccr4b g3
	GCTCTATATCCAACAATCTCCCT	Reverse primer for PCR amplificiation of CCR4b for genotyping of ccr4b g3
	GACTTCACGGGTTATTCCTGC	For sequencing of PCR product for ccr4b g3 genotyping

pEN-Chimera_2X	GTACAAAAAAGCAGGCTC	Forward primer for screening of the pEN-Chimera_2X plasmids
T-DNA	ATTTTGCCGATTTCGGAAC	Reverse primer for genotyping SALK T-DNA lines (*urt1-1* and *exa1-1*)

1.6.3. Primers used for FLEP-seq2 sequencing

Primer sequence (5'-3')	**Description**
ACTTGCCTGTCGCTCTATCTTCATTGATGGTGCCTACAG	FLEP_seq2_RT_primer for cDNA synthesis
ATCGCCTACCGTGACAAGAAAGTTGTCGGTGTCTTTGTGACTTGCCTGTCGCTCTATCTTC	Forward primer for PCR optimisation
ATCGCCTACCGTGACAAGAAAGTTGTCGGTGTCTTTGTGTTTCTGTTGGTGCTGATATTGC	Reverse primer for PCR optimisation

2. Methods

2.1. Gateway cloning

To construct the pUBC-URT1-GFP destination vector I used the gateway cloning technology. It is based on site-specific recombination between bacteriophage lambda sequences present in the desired PCR product, the donor and the destination vectors. First by enzymatic recombination with the BP clonase, *attB* sites flanking the desired PCR product recombines with the *attP* sites of the donor plasmid (here p207). The product of the recombination is an entry vector with *attL* sites flanking the inserted sequence. Next, LR clonase is used to recombines the *attL* sites of the entry vector with the *attR* sites in the destination vector (here pUBC-GFP).

2.1.1. PCR amplification of the sequence of interest

To clone the pUBC-gURT1^{WT}-GFP, the genomic sequence of *URT1* with the 5'UTR, but without the stop codon and 3'UTR was amplified by polymerase chain reaction (PCR) using the Phusion DNA polymerase (Thermo Scientific) and gene-specific primers with *attB1* (forward primer) and *attB2* (reverse primer) sequences. PCR was performed on genomic DNA (gDNA) extracted from wild-type *Arabidopsis*. The reaction is performed in 20µL with 0.5µM of each primer, 1X Phusion Master Mix (Thermo Scientific) and around 100 ng of gDNA. The program for PCR amplification is as follows: 2min initial denaturation at 98°C; 35 cycles of 30s denaturation at 98°C, 45s primer annealing at the calculated temperature, 1min30 elongation at 72°C; 5min final elongation at 72°C. Resulting PCR products were purified using NucleoSpin Gel and PCR clean-up kit (Macheny-Nagel) according to the manufacturer's protocol.

2.1.2. Gateway BP

For the BP reaction, a mix of 100ng of purified PCR product, 100ng of the p207 donor vector and 1µL of the BP Clonase II reaction mix (Invitrogen) is assembled in a final volume of 5µL and incubated overnight at room temperature. The reaction is stopped by adding 0.2µg/µL of proteinase K followed by a 10min incubation at 37°C.

2.1.3. TOP10 bacterial transformation by heat shock

50µL of chemocompetent TOP10 cells were added to the BP reaction and incubated 30min on ice. The heat shock was done by incubating the bacteria 30s at 42°C in a water bath, followed by 1min on ice. Next, 1mL of LB medium was added and the suspension was incubated 1h at 37°C for recovery. 100µL of the suspension was plated on LB agar medium complemented with gentamycin. Next, p207-gURT1^{WT} entry plasmid was purified using the NucleoSpin Plasmid QuickPure kit (Machery-Nagel) following manufacturer's instructions before rapidly. At this step, either the plasmid is used for further cloning (see **Methods 2.1.5**), or is used for site-directed mutagenesis (see **Methods 2.1.4**) to introduce the mutation on the sequence coding the PPGF motif.

2.1.4. Site-directed mutagenesis

The URT1^{PPEE} mutation (G244E/F245E) was introduced using site-directed mutagenesis. In this method mostly-overlapping primers carrying the wanted mutation (in the forward and reverse primer) are used to amplify the plasmid. The resulting PCR product corresponds to the plasmid sequence with the selected mutation. The primers were designed using the primer web program (http://www.bioinformatics.org/primerx/) and are listed in **Material 1.6.1**.

A mix of 2.5 units of Pfu polymerase (Promega) in 1x of reaction buffer, 2.5pmole of forward and reverse primers carrying the mutation, and 5nM of dNTP is assembled in a final volume of

25µL. The program for PCR amplification is as follows: 5 min initial denaturation at 95°C; 18 cycles of 50 s denaturation at 95°C, 50 s primer annealing at 60°C, 5min elongation (1min/kb) elongation at 68°C; 30s final elongation at 72°C. To remove the template plasmid, PCR product is incubated with 10 units of *DpnI* enzyme (Promega) for 1h at 37°C. The treated PCR product is then transformed into competent TOP10 bacteria (see **Methods 2.1.3**).

2.1.5. Gateway LR

For the LR reaction, a mix of 100ng of entry plasmid, 100ng of the pUBC destination vector and 1µL of the LR Clonase II reaction mix (Invitrogen) is assembled in a final volume of 5µL and incubated 1h at room temperature. The reaction is stopped by adding 0.2µg/µL of proteinase K followed by a 10min incubation at 37°C. The reaction mix is used to transform competent TOP 10 cells for plasmid amplification (see **Methods 2.1.3**).

2.2. Transformation of *Arabidopsis* thaliana

2.2.1. Agrobacterium transformation by heat shock

50µL of chemocompetent *A. tumefaciens* GV3101 cells were added to 100ng of expression plasmid (pUBC-gURT1$^{WT/PPEE}$ plasmids) and incubated 30 minutes on ice. The heat shock was done by incubating the bacteria 5min at 37°C in a water bath, followed by 2min on ice. Next, 1mL of LB medium was added and the suspension was incubated 2h at 28°C for recovery. 100mL of the suspension was plated on LB agar medium complemented with rifampicin, gentamycin and spectinomycin.

2.2.2. Plant transformation by flower dipping

Flowering *Arabidopsis thaliana* are transformed according to the method described by Zhang et al., 2006. *A. tumefaciens* transformed with the binary vector are grown in a pre-culture of 10mL LB medium supplemented with antibiotics for 24h at 28°C on a shaker. The following day, 100mL of LB medium supplemented with antibiotics is inoculated with 100µL of the pre-culture and incubated for 16h at 28°C on a shaker. The following day, bacteria are pelleted for 10 min at 5000g and resuspended in infiltration medium (2g/L MS medium M0222; 5% sucrose (w/v); 0.005% Silwet L-77 (v/v); 200µM acetosyringone) to an OD of 0.8. Next, the cells are incubated for 1h in the dark. During this time, siliques and opened flowers are trimmed from the plants to decrease the number of untransformed seeds in the end. After trimming, aerial parts are dipped 30 s into the resuspended bacteria, and plants are placed in the dark in a humidity chamber for 24h. The next day, the plants are put back in growth chambers still in the humidity chamber for another 24h. The seeds of these plants are harvested to screen the positive transformants.

2.2.3. Screening of transformants

The transformants plants are selected according to insertion of the T-DNA cassette. This T-DNA contains a gene conferring glufosinate resistance. 10 days old seedlings grown on trays are sprayed three time with 0.002% (v/v) glufosinate. Resistant plants are transferred into individual pots, and the expression of the transgene is assessed on flowers tissues by western blot. The T1 plants expressing the transgene are further selected on agar medium by sowing their seeds on agar medium supplemented with glufosinate. Rounds of selection are performed until the transgene is stable and does not segregate anymore.

2.3. Western blot analysis

2.3.1. Protein extraction

Flower tissues were harvested in microcentrifuge tubes and flash-frozen in liquid nitrogen. Glass beeds (4mm diameter) are added to the tubes and samples are grinded using Silamat S6 (Ivoclar Vivadent). 100µL SDS-Urea-DTT buffer (62.5mM Tris pH 6.8; 4M urea; 2% (w/v) SDS; 10% glycerol (w/v); 100mM DTT) is added to tubes and the tissues are further grinded 20s with Silamat S6. Samples are heated for 10min at 95°C to denature proteins, spined down to pellet debris.

2.3.2. SDS-PAGE

Protein extracts are separated by SDS-PAGE. The gel is composed of two layers. The lower layer is a 10% separation gel (375mM Tris-HCl, pH 8.8; 0.1% (w/v) SDS; 10% (v/v) polyacrylamide/N,N' methylene bisacrylamide 37.5/1). The upper layer is a 4% stacking gel (125mM Tris-HCl, pH 6.8; 0.1% (w/v) SDS; 10% (v/v) polyacrylamide/N,N' methylene bisacrylamide 37.5/1). The gel is polymerised by the addition of ammonium persulfate (APS) and tetramethylethylenediamine (TEMED). 5-10µL protein extracts are loaded on the gel and the separation is done at 25mA for 1h in a tank filled with migration buffer (25mM Tris, pH 8.5; 250mM glycine; 0.1% (w/v) SDS).

2.3.3. Western blot

Proteins are transferred to an ethanol activated 0.45µM Immobilon-P PVDF membrane (Millipore) by a liquid transfer in transfer buffer (48mM Tris; 39mM glycine; 15% (v/v) EtOH) at 4°C for 1h at 250mA. The membrane is incubated in TBS-T solution (20mM Tris-HCl, pH 7.4; 150mM NaCl; 0.2% (v/v) Tween-20) supplemented with 5% milk powder for 30min at room temperature for saturation. The solution is then discarded and the membrane is incubated overnight at 4°C with the primary antibodies diluted to 1/10000 in TBS-T supplemented with 2% (w/v) milk powder. The membrane is then washed 5 times for 5min using TBS-T and incubated (if needed) with the secondary antibody for 30min at room temperature. The membrane is washed 5 times for 5 minutes before protein detection by chemiluminescence using Lumi-Light Western Blotting Substrate (Roche) and a Fusion FX imager.

2.3.4. Coomassie staining

To control the loading, the membrane is incubated with Coomassie staining solution (0.0025% Coomassie Brilliant Blue R-250 (w/v), 50% ethanol (v/v), 9% acetic acid (v/v)) for 30 min. Destaining is performed using destain solution (50% ethanol (v/v), 9% acetic acid (v/v)).

2.4. CRISPR-Cas9 mutagenesis of CCR4a and CCR4b genes

CRISPR/Cas9 mutagenesis uses the plant's innate DNA repair mechanism, Non-Homologous End Joining (NHEJ), to introduce insertions or deletions at targeted genomic sequences. In this process, Cas9, here derived from *Streptococcus pyogenes*, is directed to the target gene by a guide RNA (gRNA). This gRNA is specifically designed to be complementary to the target genomic sequence, known as the protospacer. The presence of a protospacer-adjacent motif (PAM) downstream of the target sequence is needed for binding and cleavage by Cas9. For *Sp*Cas9, the PAM is an NGG sequence. The entry vector pEN-Chimera_2X has 2 different sgRNA backbone and can accommodate 2 different protospacers at a time (one directed towards *CCR4a*, the other targeted to *CCR4b*). For the mutagenesis of *CCR4a* and *CCR4b* genes, primer selection for gRNA design, plasmid construction and *Arabidopsis* transformation was performed by the Genome Editing platform and former *Ph*D student Caroline De Almeida, and I was involved in the selection process.

2.4.1. sgRNA design

The protospacer sequences required for mutating *CCR4a* and *CCR4b* were selected using the CRISPOR website (http://crispor.tefor.net/). After selecting the protospacers, overlapping primers corresponding to these sequences were ordered from Integrated DNA Technologies (IDT). Of note, 5’ overhang sequences must be included in the forward (5’-ATTG-3’) and reverse (5’-AAAC-3’) primer sequences to allow cloning into the pEN-Chimera_2X entry vector.

2.4.2. Cloning first protospacer into the pEN-Chimera_2X

The cloning begins by the insertion of the protospacer sequences into the sgRNA backbones contained in the entry vector, to create full-length sgRNA. Because we target two different genes, we need to insert the two protospacers, one at a time.

The entry vector (pEN-Chimera_2X) is first linearised by mixing 1µL *BpiI* (Thermo Scientific), 2µL of 10X FastDigest buffer (Thermo Scientific) to 1µg of entry vector in a final volume of 20µL. The mix is incubated at 37°C for 30min, and the linearised plasmid purified using NucleoSpin Plasmid QuickPure kit (Machery-Nagel) following manufacturer’s intructions. To create the double stranded DNA fragment containing the protospacer sequence, overlapping primers are mixed together at a final concentration of 45µM each, with 1.1µL 10X T4 DNA ligase buffer (Promega) in a final volume of 11.1µL. The mix is incubated at 70°C in a water bath for 10 minutes and then allowed to slowly cool down to room temperature while remaining in the water bath. Then, 40ng of linearised entry vector is mixed with equimolar amount of hybridised oligos and with 2.5µL of Rapid Ligase buffer 2X (Promega), 0.5µL of T4 DNA ligase (Promega) in a final volume of 5µL. The mix is incubated overnight at 4°C, and is used to transform competent TOP10 cells (see **Methods 2.1.3**).

2.4.3. Selection of positive colonies and sequencing of recombinant plasmid

50 colonies are screened by PCR to select colonies positive for the transformation of the recombinant vector. The PCR reaction (for 1 reaction) is performed in 10µL final volume with 0.2µM of forward pEN-Chimera_2X primer (see **Material 1.6.2**), 0.2µM of the reverse primer used for the hybridisation, 0.2mM of dNTP mix (10mM each), 1.5mM of MgCl2, 0.08µM of GoTaq G2 DNA polymerase (Promega), 2µM of GoTaq 5X buffer (Promega). The program for PCR amplification is as follows: 3min initial denaturation at 95°C; 35 cycles of 30s denaturation at 95°C, 30s primer annealing at the appropriate temperature, 30s elongation at 72°C; 5min

final elongation at 72°C. Positive colonies are inoculated in 3mL of LB with ampicillin antibiotic and grown overnight at 37°C on a shaker. Plasmids are extracted using NucleoSpin Plasmid QuickPure kit (Machery-Nagel) following manufacturer's instructions. Recombinant plasmids are sequenced by Sanger sequencing to assess the insertion of the protospacer sequence into the sgRNA backbone.

2.4.4. Cloning second protospacer into the pEN-Chimera_2X

The recombinant entry vector with the first protospacer inserted is linearised by mixing 1µL *Esp3I* (Thermo Scientific), 2µL of 10X FastDigest buffer (Thermo Scientific) to 1µg of entry vector in a final volume of 20µL. The mix is incubated at 37°C for 30min, and the linearised plasmid purified using NucleoSpin Plasmid QuickPure kit (Machery-Nagel) following manufacturer's intructions. To create the double stranded DNA fragment containing the protospacer sequence, overlapping primers are mixed together at a final concentration of 45µM each, with 1.1µL 10X T4 DNA ligase buffer (Promega) in a final volume of 11.1µL. The mix is incubated at 70°C in a water bath for 10 minutes and then allowed to slowly cool down to room temperature while remaining in the water bath. Then, 40ng of linearised entry vector is mixed with equimolar amount of hybridised oligos and with 2.5µL of Rapid Ligase buffer 2X (Promega), 0.5µL of T4 DNA ligase (Promega) in a final volume of 5µL. The mix is incubated overnight at 4°C, and is used to transform competent TOP10 cells for plasmid amplification. The resulting plasmid is pBlevins1-CCR4$^{X/b3}$, where X can be guide 1 or 2 targeting *CCR4a*. b3 is the guide 3 targeting *CCR4b*. Next, positive colonies are selected (see **Methods 2.2.3**) transformed into Agrobacterium for further stable *Arabidopsis* transformation (see **Methods 2.3**).

2.4.5. Selection of T-DNA transformed seeds

To ensure that we will screen for seeds that integrated the T-DNA expressing the *Sp*Cas9 upon floral dip, we use the selection cassette present in the T-DNA. It corresponds to GFP expressed under the control of a seed coat specific promoter (*pAt2S3::GFP*). GFP seeds are positive for the T-DNA insertion and were selected using a humidified toothpick under an AXIO Zoom V.16 (Zeiss) under UV light (358 nm). Positive seeds were then sowed on soil and grown for further characterisation by high-resolution melting (HRM).

2.4.6. Selection by high-resolution melting

HRM was used to screen for homozygous and heterozygous mutants of the *CCR4a* and *CCR4b* genes upon transformation of wild-type plants with the pBlevins1-CCR4$^{X/b3}$ vectors. By comparing the melting curve of short PCR products amplified from WT and transformed plants, it is possible to rapidly screen for mutants. Genomic sequences targeted by gRNAs were amplified by PCR using 1µL of gDNA extracted from control or transformed plants, 2.5µM of forward and reverse primer and 5µL of Precision Melt Supermix (BioRad) in a final volume of 10µL and loaded in a 386 wells microplate. The program for PCR amplification is as follows: 2min initial denaturation at 95°C; 45 cycles of 15s denaturation at 95°C, 10s primer annealing at 60°C, 20s elongation at 68°C; 30s final elongation at 68°C. PCR reaction and detection is performed on a LightCycler 480 (Roche). Melting curve analysis is performed using the LightCycler 480 built-in software. Putative mutants are confirmed by Sanger sequencing. Only double heterozygous mutants (*ccr4a*+/-; *ccr4b*+/-) mutants were obtained at the F1. Hence, positive double heterozygous plants were grown on soil until flowering and autofertilisation. The T-DNA containing the SpCas9 was counterselected from the seeds of the F2 by selecting non-fluorescent seeds using a humidified toothpick. F2 plants were next selected by Sanger sequencing directly, as ¼ of the F2 plants were double homozygous (as the *CCR4a CCR4b* genes are genetically linked, they segregate as a single locus).

2.5. Pollen Viability test

Dehiscent anthers were harvested and incubated in 100µL of Alexander staining (Alexander, 1969, kindly provided by Marie-Claire Criqui), incubated at room temperature for 1h, mounted in a slide and covered with a coverslip and observed under bright field microscope Leitz DMRB (Leica).

2.6. *In vitro* pollen germination

One-day-old flowers were harvested at 10 a.m and incubated over a wet tissue in a wet chamber to allow pollen hydration and prepare semi-solid pollen germination medium (PGM) (Boavida & McCormick, 2007). To prepare the semi-solid medium, 1% low-melting agarose (w/v) is added to 2mL of liquid PGM (0.01% $H3BO3$ (w/v); 5mM KCl; 5mM $CaCl2$; 1mM $MgSO4$; 10% sucrose (w/v); pH adjusted to 7.5-8 with KOH), and melted at 95°C for 5min using a block heater. Once melted, a thin coat of semi-solid PGM is added to a microscopy slide. Anthers are dabbed on cool semi-solid medium to release pollen grains, and a coverslip is placed on top of the medium and the slide is incubated in a humidity chamber at 22°C for 3h. Upon incubation, pollen grains and pollen tubes are observed under bright field microscope Leitz DMRB (Leica).

2.7. *In vivo* pollen germination

2.7.1. Flower emasculation and manual fertilisation

In vivo pollen germination was performed as described in Mori *et al*., 2006. Closed flower buds approaching dehiscence were emasculated and plants were put back in growth chamber for 24h to ensure the pistil from emasculated flowers is still viable and is receptive. Dehiscent anthers from Col-0 flowers were dabbed gently onto receptive pistil from either Col-0 or *ccr4a ccr4b* emasculated flowers, and plants were incubated 4h in growth chamber.

2.7.2. Pistil fixation and alkaline treatment

Pistils are then harvested and incubated in 1mL of a fixative solution (1V glacial acetic acid; 3V EtOH 100%) for 2h at room temperature. Fixative solution is then removed and replaced by 1mL of 70% EtOH (v/v) and incubated for 10min at room temperature. Same treatment is done again with 50%, then 30% EtOH solution and finally deionised water to fully rehydrate the pistils. Pistils are cleared by replacing water with 8M NaOH solution and incubation overnight at room temperature.

2.7.3. Aniline blue staining and observation

A solution of 0.1% of aniline blue (w/v) resuspended in 108mM K_3PO_4 pH11 is prepared and incubated at 4°C overnight. The staining solution is filtered through activated charcoal and glycerol is added to the filtrate for a final concentration of 2% (v/v). The following day, the alkaline solution is replaced by deionised water and pistils are incubated 1min at room temperature. Water is discarded and replaced with 500µL of DABS and incubated for 2h at room temperature in the dark. Upon incubation, pistils are placed on slide glass with extra DABS and covered by a coverslip with a gentle push to split the ovary walls. Picture were taken using a AXIO Zoom V.16 (Zeiss) under UV light (358 nm).

2.8. Scanning Electron Microscopy

Dehiscent anthers were dabbed on double-sided tape to release pollen grains, and their surface morphology was observed under the scanning electron microscope (SEM) Hitachi TM-1000.

2.9. Seed quantification

Greenish-yellowing siliques were harvested and incubated in 70% EtOH (v/v) for 8h, and silique filing is assessed under a stereomicroscope.

2.10. Pollen mass spectrometry

2.10.1. Pollen protein extraction

Pollen proteins were extracted using a protocol modified from Chang & Huang, 2017. Approximately 100 freshly opened flowers from wild-type or ccr4a ccr4b plants were harvested (at 10 a.m for consistency with other experiments) and pooled together in a microcentrifuge tube. 650µL of Phosphate Buffer Saline (PBS) 1X pH7.4 is added, and the tube is vortexed for 3 minutes at full rotation in order to separate the pollen from the flowers. Pollen is pelleted by centrifugation at 350g for 1min at 4°C. Supernatant is discarded and pollen is resuspended in 200µL of extraction buffer (7M Urea; 2M Thiourea; 4% CHAPS (v/v); 20mM Tris; 1mM PMSF), transferred into a screw-cap tube compatible with Precellys evolution grinder (Bertin technologies) and kept on ice. Small glass beads are added in the tube and the pollen is grinded using the Precellys grinder at 10000rpm, 2 cycles of 15sec with a pause of 30sec on ice in between to prevent sample from overheating. Lysate is centrifuged at 18000g for 20min at 4°C and the supernatant is transferred to a new clean microcentrifuge tube. This step is repeated 2 times to prevent the presence of debris in the protein extracts. Proteins are precipitated by adding 5V of 100% MeOH, 100mM ammonium acetate and incubated overnight at -20°C. The following day, the precipitates is pelleted by centrifugation at 12000g at 4°C for 1 min and washed two times using 200µL 80% MeOH, 100mM ammonium acetate.

2.10.2. Gel electrophoresis and Coomassie staining

10µL of proteins extracted from pollen were resuspended in SDS-urea sample buffer (62.5mM Tris pH6.8; 4M urea; 3% SDS (w/v); 10% glycerol (v/v); 0,01% bromophenol blue(w/v)) and separated by gel electrophoresis on a NuPAGE™ Bis-Tris (Invitrogen) precast gradient gel 4-12% with 1X MOPS running buffer (Invitrogen) for 1h40 under constant voltage at 110V. The gel is next incubated with Coomassie staining solution (0.0025% Coomassie Brilliant Blue R-250 (w/v), 50% ethanol (v/v), 9% acetic acid (v/v)) for 30 min. Destaining is performed using destain solution (50% ethanol (v/v), 9% acetic acid (v/v)).

2.10.3. Mass Spectrometry Analysis

Mass spectrometry analysis was performed at the Strasbourg-Esplanade Proteomic Platform. Purified pollen proteins were digested with sequencing-grade trypsin (Promega) and analysed by nanoLC-MS/MS on a TIMS-TOF Pro2 mass spectrometer coupled to an EASY-nanoLC-1000 (Thermo Fisher Scientific). Data are searched against the TAIR 10 with a decoy strategy. Prostar was used for the statistical analyses of the intensities. Partially observed values (POV) were imputed with structured least square adaptative regression (SLSA) method while values missing in the entire condition (MEC) were imputed with det quantile 1%. A LIMMA statistical test with a log (FC) threshold of 1 and a Benjamini-Hochberg correction were used to generate log2(FC) and adjusted p-values.

2.11. Immunonoprecipitation followed by Mass Spectrometry

2.11.1. Co-immunoprecipitation

For each IP, 150mg of closed flower buds were grinded for 10min at 4°C using a mortar and pestle after addition of ice-cold lysis buffer (50mM Tris-HCl pH8; 50mM NaCl; 5mM MgCl2; 1% Triton X-100; protease inhibitors (cOmplete, EDTA-free Protease Inhibitor Cocktail, Roche)) supplemented with 0.375% formaldehyde from crosslinking. Cross-linking was quenched by the addition of glycine at a final concentration of 200mM and mixing for 5min. Debris are pelleted by centrifugation at 10000g for 10min at 4°C and repeated once. Supernatant is incubated for 45min with 50µL of magnetic beads coupled with anti-GFP antibodies (Miltenyi) and processed according to manufacturer’s instructions, except that washes were performed with homemade wash buffer (50mM Tris-HCl pH7.5; 50mM NaCl; 5mM MgCl2; 0.1% Triton X-100; protease inhibitors (cOmplete, EDTA-free Protease Inhibitor Cocktail, Roche)). Proteins were eluted using the elution buffer from the beads manufacturer.

2.11.2. Mass Spectrometry Analysis

Mass spectrometry analysis was performed at the Strasbourg-Esplanade Proteomic Platform. Eluted proteins were digested with sequencing-grade trypsin (Promega) and analysed by nanoLC-MS/MS on a QExactive+ mass spectrometer coupled to an EASY-nanoLC-1000 (Thermo Fisher Scientific). Data are searched against involved matching against the TAIR10 database. Peptides are identified with Mascot algorithm (v 2.5.1) and Proline software (v 1.4). Proteins were validated on Mascot pretty rank equal to 1, and 1% FDR on both peptide spectrum matches (PSM score) and protein sets (Protein Set score). The aggregate spectral count was used to estimate protein abundance from at least six independent IPs and three independent biological replicates. To identify significantly enriched proteins in test IPs compared to control IPs, statistical analysis was performed using R package IPinquiry4 (v 0.4.7) (Kuhn *et al*., 2023) based on the negative binomial model implemented in edgeR (Robinson *et al*., 2010). Data were normalised according to the "median of ratios" method described in the Deseq2 package (Love *et al*., 2014). Fold-changes were calculated for each protein and p-values were adjusted using the Benjamini-Hochberg correction method.

2.12. RNA extraction

Plant tissues were harvested and flash-frozen in liquid nitrogen and grinded in mortar and pestle. ~200µL of powder are put in microcentrifuge tubes. To the powder, 800µL of TRI-Reagent (Molecular Research center) is added and the tubes are vortexed for 15s. Debris are pelleted by centrifugation at 12000g for 5min at 4°C. The supernatant is transferred to a new tube and 160µL of chloroform is added and the tubes are vortexed and incubated for 10min at room temperature. The phases are separated by centrifugation at 18000g for 10min at 4°C, and the aqueous upper layer is transferred in a new tube. RNA is precipitated by adding 0.5V of isopropanol and incubating 10min at room temperature. The RNA is pelleted by centrifugation at 18000g for 10min at 4°C, and the pellet is washed twice with ice-cold 75% EtOH. The pellet is resuspended in 150µL RNase-free water and re-extracted by adding 1V of phenol-chloroforme-isoamyl alcohol (25-24-1) mix. After vortexing, the phases are separated by centrifugation at 18000g for 10min at 4°C. The upper layer is transferred into a new tube, and 1/10V of sodium acetate (3M, pH 5.2), 2.5V of 100% EtOH, 0.5µL of Glycogen Blue (20 mg/µL, Invitrogen) are added and the sample is incubated at -80°C for 1h. RNA is pelleted by centrifugation at 18000g for 30min at 4°C, and the pellet is washed twice with ice-cold 75% EtOH and resuspended in RNase free water. RNA destinated to Nanopore sequencing are further purified by using RNeasy MinElute Cleanup Kit (QIAGEN) following manufacturer's instructions. The RNA is then quantified by spectrophotometry using Nanodrop 2000 (Thermo Scientific). RNA destinated to sequencing (either Illumina or Nanopore) are further quantified using the Qubit fluorometer (Invitrogen) and their quality is assessed using the Bioanalyzer 2100 system (Agilent).

2.13. FLEP-seq2

2.13.1. Ribosomal RNA depletion and ligation of 3' adapter

3µg of total RNA (extracted as in **Methods 2.12**) is ribodepleted using *Arabidopsis* riboPOOLs (siTOOLS Biotech) following manufacturer's instructions. To the ribodepleted RNA, 1µL of glycoblue (25mg/mL), 10µL 3M NaAc pH5.8 and 3V of EtOH 100% is added. The mix is precipitated 30min at -80°C and precipitate is pelleted by centrifugation at 18000g at 4°C for 30min. The pellet is washed twice with ice-cold EtOH 75% (v/v). EtOH is discarded and ribodepleted RNA is resuspended in 5µL. To the ribodepleted RNA, 50µM of Universal miRNA cloning linker (NEB) is added, and the mix is incubated 5min at 65°C and cooled on ice for 2min. Then, a mix of 2µL 10X T4 RNA ligase reaction buffer (NEB), 1µL RNAseOUT (Invitrogen), 1µL of T4 RNA ligase 2 truncated K227Q (NEB) and 10µL of 50% PEG8000 is added to the ribodepleted RNA and incubated 10h at 16°C. The ligated RNA is purified using the RNA Clean & Concentrator-5 kit (ZYMO) following manufacturer's instructions on the the removal of fragments smaller than 200bp. Purified RNA is eluted with 9µL of RNase-free water.

2.13.2. cDNA synthesis

9µL of ligated RNA is mixed with 1µL of FLEP_seq2_RT_primer (diluted to 2µM), 1µL of dNTP (10mM each) and is incubated 5min at 65°C and cooled on ice for 2 min. Next, a mix of 4µL of Maxima RT 5X Buffer (Thermo Scientific), 1µL of RNaseOUT (Invitrogen), 2µL of Strand-switching primer (Oxford Nanopore Technologies, ONT) and 1µL of RNase-free water is added to the RNA and heated to 42°C. When it is at temperature, 1µL of Maxima H minus Reverse Transcriptase (Thermo Scientific) is added and the mix is incubated on a thermocycler with the following program: initial incubation 90min at 42°C; 10 cycles of 2min at 50°C, 2min at 42°C; RT inactivation at 85°C for 10 min.

2.13.3. PCR optimisation

This step is needed to optimise the number of cycles to obtain the highest quality amplification possible without overamplification. Different amplification cycles are tested: 10, 12, 14, 16, 18 and 20 cycles. Because the commercial primers from ONT are expensive, we use for the PCR optimisation custom made oligos that have the same nucleotide sequence but that do not have the modification needed for sequencing primer anchoring. A master mix composed of 16.25µL RNase-free water, 5µL 5X PrimeSTAR GXL buffer (TakaraBio), 2µL of dNTP mix (2.5mM, TakaraBio), 0.75µL of custom-made cDNA primers (10µM each), 0.5µL of PrimeSTAR GXL

DNA polymerase (TakaraBio) is added to 0.5µL of cDNA. The program for PCR amplification is as follows: 30min initial denaturation at 98°C; 10 cycles of 10s denaturation at 98°C, 15s primer annealing at 65°C, 10min elongation at 68°C; 5min final elongation at 68°C. At this point, the PCR tube for the 10th cycle is withdrawn and the amplification cycles continues, and PCR reactions for the 12th, 14th, 16th, 18th and 20th PCR cycles are withdrawn at the appropriate cycles. 8µL of each PCR cycle is mixed with 2µL of 6x DNA loading dye (Thermo Scientific), and are loaded on a 1.5% agarose gel 1X TAE without EtBr and migrated for 30min at 135V. The gel is then incubated for 30min with SYBR Gold (diluted 1/10000, Thermo Scientific) in 1X TAE and revealed with UV. The optimal PCR condition should have a faint smear at around 1kb and no contaminant band.

2.13.4. Full scale PCR, quality control and loading on Nanopore flowcell

The cDNA is amplified in 12 PCR reactions of 25µL in the conditions optimised in the previous step, and by replacing the custom-made primers with the commercial barcoded primers. Upon PCR, the reactions of each barcode are pooled and and remaining primers are digested by incubating 6µL of Exonuclease I (NEB) during 15min at 37°C. Exo I is inactivated at 80°C during 15min. Next, PCR products are purified using NucleoMag NGS clean-up (Machery-Nagel) with 3 subsequent purifications with 0.8X volume of beads eluted in 80 µL of RNase-free water; 0.55X volume of beads eluted in 50µL of RNAse-free water; 0.55X volume of beads eluted in 12µL of elution buffer (ONT) following manufacturer’s instructions. The obtained libraries are quantified using the Qubit fluorometer (Invitrogen) and their quality is assessed using the Bioanalyzer 2100 system (Agilent) with DNA HS chip.

For samples loadeed on MinION (ONT) flowcells, libraries are pooled together for a total molarity of 100fmol in 11µL of final volume. For samples loaded on PromethION (ONT) flowcells, libraries are pooled together for a total molarity of 100fmol in 23µL of final volume. In both cases, 1µL of rapid adapter (ONT) harbouring the motor protein are added to the pool and incubated for 10 minutes at room temperature. Respective flowcells are primed according to manufacturer’s instructions. MinION flowcells R9.4.1 are run on a MinION Mk1B device. PromethION flowcells R9.4.1 are run on a PromethION P2.

2.13.5. Nanopore data processing and bioinformatic analysis

For poly(A) tail and uridylation analysis, the raw reads are processed using a pipeline based on the original FLEP-seq2 (Jia et al., 2022), and available on GitHub (https://github.com/jackson-peter/FLEPseq2/). Raw signals from nanopore sequencing were converted to base sequences by Guppy (v 6.4.2) with the default parameters (--c dna_r9.4.1_450bps_hac.cfg). Reads with a quality score lower than 7 were discarded. Kept reads were mapped to the *Arabidopsis* thaliana genome (TAIR10) using Minimap2 (Li *et al*., 2018; v .26-r1175) with the following settings: -ax splice --secondary=no -G 5000. Reads mapping to rRNA are discarded. 5' and 3' adapter sequences are searched in the aligned reads, and only reads corresponding to full-length amplicons are retained for the following analysis. The 3' unmapped portion of the read, between the mapped read and the 3' adapter, is labelled as the poly(A) tail with its terminal nucleotide addition. The length estimation is inferred based on the basecalling sequence corrected by the raw signal sequence corresponding to the poly(A) tail. At the same time, 3' terminal non-adenosines are detected using the basecalling sequence. The poly(A) shift score (PASS) calculation was defined as previously described (Ogami *et al*., 2022). In this study, it was defined as $\sum_i \{wt(i) - mut(i)\}$ where $wt(i)$ is the cumulative ratio at poly(A) length i for the wild-type sample and $mut(i)$ is the cumulative ratio at poly(A) length i for the mutant sample. Positive PASS indicates poly(A) tail is lengthened in the mutant compared to the wild-type, while a negative PASS indicates the opposite.

2.14. RNA-sequencing of rosette samples

2.14.1. RNA extraction, library preparation and sequencing

Total RNA of 24-days-old *Arabidopsis* rosette samples was extracted as in **Methods 2.13**. 20µg of total RNA is treated with 40 units of DNAse I (Thermo Scientific) following manufacturer's instructions. After treatment, RNA is purified using RNeasy MinElute Clean-Up Kit (Qiagen) following manufacturer's instructions. Library preparation was done using Illumina TruSeq Stranded Total RNA Total RNA Library Prep kit including Ribo-Zero rRNA depletion according to manufacturer's instructions. Single-end sequencing (1x50bp) was done on Illumina NextSeq 2000.

2.14.2. Data preprocessing and bioinformatic analysis

Raw reads from Illumina sequencing were trimmed with Cutadapt (v 3.4) (Martin, 2011) and the wrapper Trim_galore (v 0.6.7) using the following settings: trim_galore --fastqc --dont_gzip -q 30 --stringency 6 --max_n=5. Trimmed reads were mapped on the *Arabidopsis* thaliana genome (TAIR10) using Hisat2 (v 2.2.1) (Kim *et al*., 2019) using the following settings: hisat2 -p 4 -t --rna-strandness R --max-intronlen 2000 -q. Read assignment was performed on

Arabidopsis annotation file Araport11_GTF_genes_transposons.Feb2022.gtf using featureCounts (v 2.0.1) (Liao *et al*., 2014) and the following settings: featureCounts -s 2 -t gene,transposable_element -g gene_id --minOverlap 10. Differential gene expression analysis was performed on R (v 4.3.1) using Deseq2 (v 1.40.2) (Love *et al*., 2014). Low-expressing genes with less than 1 count per million mapped reads in any sample were discarded. |log2 FC| > 0.5 and adj*p*-value < 0.05 (*p*-value obtained with Benjamini-Hochberg correction) were used to identify DEGs.

2.15. Sequencing of polysomal fractions

2.15.1. Sucrose gradient preparation

Gradients for polysomes purifications are prepared by casting 4 different layers (60-45-30-15%) of sucrose gradient in a 13mL ultracentrifugation tube. Each sucrose gradient is prepared as follows with 10X Salts solution (0.4M Tris-HCl ph8.4, 0.2M KCl, 0.1M MgCl2):

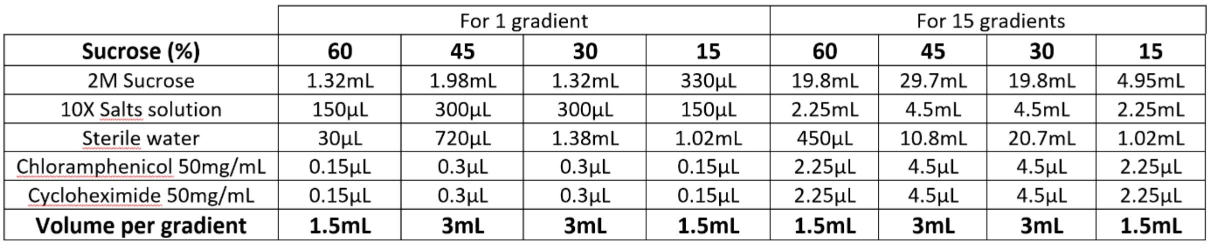

	For 1 gradient				For 15 gradients			
Sucrose (%)	**60**	**45**	**30**	**15**	**60**	**45**	**30**	**15**
2M Sucrose	1.32mL	1.98mL	1.32mL	330µL	19.8mL	29.7mL	19.8mL	4.95mL
10X Salts solution	150µL	300µL	300µL	150µL	2.25mL	4.5mL	4.5mL	2.25mL
Sterile water	30µL	720µL	1.38mL	1.02mL	450µL	10.8mL	20.7mL	1.02mL
Chloramphenicol 50mg/mL	0.15µL	0.3µL	0.3µL	0.15µL	2.25µL	4.5µL	4.5µL	2.25µL
Cycloheximide 50mg/mL	0.15µL	0.3µL	0.3µL	0.15µL	2.25µL	4.5µL	4.5µL	2.25µL
Volume per gradient	**1.5mL**	**3mL**	**3mL**	**1.5mL**	**1.5mL**	**3mL**	**3mL**	**1.5mL**

The 60% is cast first followed by other layers. In between each layer, the ultracentrifugation tube is placed 1h at -80°C for the sucrose layer to set. The day before the polysome purification, the sucrose gradient is thaw at 4°C. The ultracentrifugation rotor is put at 4°C as well.

2.15.2. Polysome purification and fractionation

Closed inflorescences are grinded using mortar and pestle in liquid nitrogen. 900µL of polysome extraction buffer (100mM Tris-HCl pH8.4; 200mM KCl; 1% (v/v) Sodium deoxycholate; 50mM EGTA; 2% (w/v) polyoxyethylene(10) tridecyl ether; 100mM MgCl2; 50mM DTT; 10µL of Enzymatic cocktail (Sigma-P9599, Sigma); 1% Brij-35 (w/v); 1% Triton X-100 (v/v); 1% Igepal (v/v); 1% Tween20 (v/v); 5mg/mL cycloheximide; 5mg/mL chloramphenicol) is added to 100mg of plant tissue and gently mixed. Debris are pelleted by centrifugation at 12000g at 4°C for 10min. 800µL of crude extract (90mg equivalent tissues) is carefully deposited on top of the sucrose gradient. Tubes are balanced with polysome extraction buffer and ultracentrifuged for 3h at 38000rpm with SW41 (Beckman Coulter) at 4°C, with slow acceleration and no brakes. Polysome profile analyses was performed with an ISCO absorbance detector at 254nm and sucrose gradients were collected into 11 fractions of 650µL. Fractions 8-9 corresponding to low molecular weigth polysomes (LP) and fractions 10-11corresponding to heavy molecular weight polysomes (HP) were pooled together.

2.15.3. RNA extraction, library preparation and sequencing

To each pool, 2V of 8M guanidinium and 3V of 100% EtOH is added, mixed and incubated overnight at -20°C. RNA is pelleted by centrifugation at 15000g for 45min at 4°C. Pellet is resuspended in 2000µL of Protect Reagant (Monarch) and is purified using Monarch Total RNA miniprep kit (Monarch) following manufacturer's instructions including DNase treatment. RNA was resuspended in RNase-free water and quantified using the Qubit fluorometer (Invitrogen). Quality was assessed using the Bioanalyzer 2100 system (Agilent) with RNA HS chip. RNA was diluted to 100ng/µL and sent to Genewiz (Azenta) for library preparation using Illumina TruSeq Stranded Total RNA Total RNA Library Prep kit including Ribo-Zero rRNA depletion followed by paired-end sequencing (2x150bp) on Illumina NovaSeq.

2.15.4. Data preprocessing and bioinformatic analysis

Raw reads from Illumina sequencing were trimmed with Cutadapt (v 3.4) (Martin, 2011) and the wrapper Trim_galore (v 0.6.7) using the following settings: trim_galore --paired --fastqc --dont_gzip -q 30 --max_n=5. Trimmed reads were mapped on the *Arabidopsis thaliana* genome (TAIR10) using Hisat2 (v 2.2.1) (Kim *et al.*, 2019) using the following settings: hisat2 -p 4 -t --dta --rna-strandness FR --max-intronlen 2000 -k 50 -q. Read assignment was performed on *Arabidopsis* annotation file Araport11_GTF_genes_transposons.Feb2022.gtf using featureCounts (v 2.0.1) (Liao *et al.*, 2014) and the following settings: featureCounts -F GTF -s 2 -p -t gene,transposable_element -g gene_id --minOverlap 10. Differential gene expression analysis was performed on R (v 4.3.1) using Deseq2 (v 1.40.2) (Love *et al.*, 2014). Low-expressing genes with less than 1 count per million mapped reads in any sample were discarded. $|\log2\ FC| > 0.5$ and adj*p*-value < 0.05 (*p*-value obtained with Benjamini-Hochberg correction) were used to identify DEGs.

Bibliography

Bibliography

Abshire, E.T., Chasseur, J., Bohn, J.A., Del Rizzo, P.A., Freddolino, P.L., Goldstrohm, A.C., and Trievel, R.C. (2018). The structure of human Nocturnin reveals a conserved ribonuclease domain that represses target transcript translation and abundance in cells. Nucleic Acids Research **46**: 6257–6270.

Absmeier, E., Chandrasekaran, V., O'Reilly, F.J., Stowell, J.A.W., Rappsilber, J., and Passmore, L.A. (2023). Specific recognition and ubiquitination of translating ribosomes by mammalian CCR4–NOT. Nat Struct Mol Biol **30**: 1314–1322.

Ajiro, M., Nishidate, T., Katagiri, T., and Nakamura, Y. (2010). Critical involvement of RQCD1 in the EGFR-Akt pathway in mammary carcinogenesis. Int J Oncol **37**: 1085–1093.

Akichika, S., Hirano, S., Shichino, Y., Suzuki, T., Nishimasu, H., Ishitani, R., Sugita, A., Hirose, Y., Iwasaki, S., Nureki, O., and Suzuki, T. (2019). Cap-specific terminal N 6-methylation of RNA by an RNA polymerase II-associated methyltransferase. Science **363**: eaav0080.

Albert, T.K., Lemaire, M., van Berkum, N.L., Gentz, R., Collart, M.A., and Timmers, H.Th.M. (2000). Isolation and characterization of human orthologs of yeast CCR4–NOT complex subunits. Nucleic Acids Research **28**: 809–817.

Alexander, M.P. (1969). Differential Staining of Aborted and Nonaborted Pollen. Stain Technology **44**: 117–122.

Alles, J., Legnini, I., Pacelli, M., and Rajewsky, N. (2023). Rapid nuclear deadenylation of mammalian messenger RNA. iScience **26**: 105878.

Amaya Ramirez, C.C., Hubbe, P., Mandel, N., and Béthune, J. (2018). 4EHP-independent repression of endogenous mRNAs by the RNA-binding protein GIGYF2. Nucleic Acids Res **46**: 5792–5808.

Andersen, P.R. et al. (2013). The human cap-binding complex is functionally connected to the nuclear RNA exosome. Nat Struct Mol Biol **20**: 1367–1376.

Anderson, J.S. and Parker, R.P. (1998). The 3' to 5' degradation of yeast mRNAs is a general mechanism for mRNA turnover that requires the SKI2 DEVH box protein and 3' to 5' exonucleases of the exosome complex. EMBO J **17**: 1497–1506.

Arae, T., Morita, K., Imahori, R., Suzuki, Y., Yasuda, S., Sato, T., Yamaguchi, J., and Chiba, Y. (2019). Identification of Arabidopsis CCR4-NOT Complexes with Pumilio RNA-Binding Proteins, APUM5 and APUM2. Plant and Cell Physiology **60**: 2015–2025.

Araki, Y., Takahashi, S., Kobayashi, T., Kajiho, H., Hoshino, S., and Katada, T. (2001). Ski7p G protein interacts with the exosome and the Ski complex for 3'-to-5' mRNA decay in yeast. EMBO J **20**: 4684–4693.

Ariizumi, T. and Toriyama, K. (2011). Genetic Regulation of Sporopollenin Synthesis and Pollen Exine Development. Annu. Rev. Plant Biol. **62**: 437–460.

Arribas-Layton, M., Wu, D., Lykke-Andersen, J., and Song, H. (2013). Structural and functional control of the eukaryotic mRNA decapping machinery. Biochim Biophys Acta **1829**: 580–589.

Arvola, R.M., Chang, C.-T., Buytendorp, J.P., Levdansky, Y., Valkov, E., Freddolino, P.L., and Goldstrohm, A.C. (2020). Unique repression domains of Pumilio utilize deadenylation and decapping factors to accelerate destruction of target mRNAs. Nucleic Acids Res **48**: 1843–1871.

Ash, M.-R., Faelber, K., Kosslick, D., Albert, G.I., Roske, Y., Kofler, M., Schuemann, M., Krause, E., and Freund, C. (2010). Conserved β-Hairpin Recognition by the GYF Domains of Smy2 and GIGYF2 in mRNA Surveillance and Vesicular Transport Complexes. Structure **18**: 944–954.

Assenholt, J., Mouaikel, J., Saguez, C., Rougemaille, M., Libri, D., and Jensen, T.H. (2011). Implication of Ccr4-Not complex function in mRNA quality control in Saccharomyces cerevisiae. RNA **17**: 1788–1794.

Aström, J., Aström, A., and Virtanen, A. (1991). In vitro deadenylation of mammalian mRNA by a HeLa cell 3′ exonuclease. The EMBO Journal **10**: 3067–3071.

Audebert, L., Feuerbach, F., Decourty, L., Namane, A., Permal, E., Badis, G., and Saveanu, C. (2023). Deadenylation rate is not a major determinant of RNA degradation in yeast.: 2023.01.16.524186.

Azzouz, N., Panasenko, O.O., Colau, G., and Collart, M.A. (2009). The CCR4-NOT Complex Physically and Functionally Interacts with TRAMP and the Nuclear Exosome. PLOS ONE **4**: e6760.

Babbarwal, V., Fu, J., and Reese, J.C. (2014). The Rpb4/7 Module of RNA Polymerase II Is Required for Carbon Catabolite Repressor Protein 4-Negative on TATA (Ccr4-Not) Complex to Promote Elongation*. Journal of Biological Chemistry **289**: 33125–33130.

Bae, H. and Coller, J. (2022). Codon optimality-mediated mRNA degradation: Linking translational elongation to mRNA stability. Molecular Cell **82**: 1467–1476.

Baeg, K., Iwakawa, H.-O., and Tomari, Y. (2017). The poly(A) tail blocks RDR6 from converting self mRNAs into substrates for gene silencing. Nat Plants **3**: 17036.

Baer, B.W. and Kornberg, R.D. (1980). Repeating structure of cytoplasmic poly(A)-ribonucleoprotein. Proc Natl Acad Sci U S A **77**: 1890–1892.

Baer, B.W. and Kornberg, R.D. (1983). The protein responsible for the repeating structure of cytoplasmic poly(A)-ribonucleoprotein. J Cell Biol **96**: 717–721.

Baggs, J.E. and Green, C.B. (2003). Nocturnin, a deadenylase in Xenopus laevis retina: a mechanism for posttranscriptional control of circadian-related mRNA. Curr Biol **13**: 189–198.

Bajczyk, M., Lange, H., Bielewicz, D., Szewc, L., Bhat, S.S., Dolata, J., Kuhn, L., Szweykowska-Kulinska, Z., Gagliardi, D., and Jarmolowski, A. (2020). SERRATE interacts with the nuclear exosome targeting (NEXT) complex to degrade primary miRNA precursors in Arabidopsis. Nucleic Acids Res **48**: 6839–6854.

Balatsos, N.A.A., Nilsson, P., Mazza, C., Cusack, S., and Virtanen, A. (2006). Inhibition of mRNA Deadenylation by the Nuclear Cap Binding Complex (CBC)*. Journal of Biological Chemistry **281**: 4517–4522.

Banerjee, A., Apponi, L.H., Pavlath, G.K., and Corbett, A.H. (2013). PABPN1: molecular function and muscle disease. The FEBS Journal **280**: 4230–4250.

Basquin, J., Roudko, V.V., Rode, M., Basquin, C., Séraphin, B., and Conti, E. (2012). Architecture of the nuclease module of the yeast Ccr4-not complex: the Not1-Caf1-Ccr4 interaction. Mol Cell **48**: 207–218.

Bawankar, P., Loh, B., Wohlbold, L., Schmidt, S., and Izaurralde, E. (2013). NOT10 and C2orf29/NOT11 form a conserved module of the CCR4-NOT complex that docks onto the NOT1 N-terminal domain. RNA Biology **10**: 228–244.

Behm-Ansmant, I., Rehwinkel, J., Doerks, T., Stark, A., Bork, P., and Izaurralde, E. (2006). mRNA degradation by miRNAs and GW182 requires both CCR4:NOT deadenylase and DCP1:DCP2 decapping complexes. Genes Dev **20**: 1885–1898.

Bélanger, F., Stepinski, J., Darzynkiewicz, E., and Pelletier, J. (2010). Characterization of hMTr1, a Human Cap1 2′-O-Ribose Methyltransferase*,. Journal of Biological Chemistry **285**: 33037–33044.

Belostotsky, D.A. (2003). Unexpected complexity of poly(A)-binding protein gene families in flowering plants: three conserved lineages that are at least 200 million years old and possible auto- and cross-regulation. Genetics **163**: 311–319.

Belostotsky, D.A. and Meagher, R.B. (1996). A pollen-, ovule-, and early embryo-specific poly(A) binding protein from Arabidopsis complements essential functions in yeast. Plant Cell **8**: 1261–1275.

Berndt, H., Harnisch, C., Rammelt, C., Stöhr, N., Zirkel, A., Dohm, J.C., Himmelbauer, H., Tavanez, J.-P., Hüttelmaier, S., and Wahle, E. (2012). Maturation of mammalian H/ACA box snoRNAs: PAPD5-dependent adenylation and PARN-dependent trimming. RNA **18**: 958–972.

Berthet, C., Morera, A.-M., Asensio, M.-J., Chauvin, M.-A., Morel, A.-P., Dijoud, F., Magaud, J.-P., Durand, P., and Rouault, J.-P. (2004). CCR4-Associated Factor CAF1 Is an Essential Factor for Spermatogenesis. Mol Cell Biol **24**: 5808–5820.

Bett, J.S., Ibrahim, A.F.M., Garg, A.K., Kelly, V., Pedrioli, P., Rocha, S., and Hay, R.T. (2013). The P-body component USP52/PAN2 is a novel regulator of HIF1A mRNA stability. Biochemical Journal **451**: 185–194.

Bhaskar, V., Basquin, J., and Conti, E. (2015). Architecture of the Ubiquitylation Module of the Yeast Ccr4-Not Complex. Structure **23**: 921–928.

Bhaskar, V., Roudko, V., Basquin, J., Sharma, K., Urlaub, H., Séraphin, B., and Conti, E. (2013). Structure and RNA-binding properties of the Not1–Not2–Not5 module of the yeast Ccr4–Not complex. Nat Struct Mol Biol **20**: 1281–1288.

Bianchin, C., Mauxion, F., Sentis, S., Séraphin, B., and Corbo, L. (2005). Conservation of the deadenylase activity of proteins of the Caf1 family in human. RNA **11**: 487–494.

Bilgin, D.D., Zavala, J.A., Zhu, J., Clough, S.J., Ort, D.R., and DeLucia, E.H. (2010). Biotic stress globally downregulates photosynthesis genes. Plant Cell Environ **33**: 1597–1613.

Billey, E. et al. (2021). LARP6C orchestrates posttranscriptional reprogramming of gene expression during hydration to promote pollen tube guidance. Plant Cell **33**: 2637–2661.

Bilska, A., Kusio-Kobiałka, M., Krawczyk, P.S., Gewartowska, O., Tarkowski, B., Kobyłecki, K., Nowis, D., Golab, J., Gruchota, J., Borsuk, E., Dziembowski, A., and Mroczek, S. (2020). Immunoglobulin expression and the humoral immune response is regulated by the non-canonical poly(A) polymerase TENT5C. Nat Commun **11**: 2032.

Bird, J.G. et al. (2016). The mechanism of RNA 5′ capping with NAD+, NADH, and desphospho-CoA. Nature **535**: 444–447.

Blikstad, C. and Ivarsson, Y. (2015). High-throughput methods for identification of protein-protein interactions involving short linear motifs. Cell Communication and Signaling **13**: 38.

Boavida, L.C. and McCormick, S. (2007). TECHNICAL ADVANCE: Temperature as a determinant factor for increased and reproducible in vitro pollen germination in Arabidopsis thaliana. The Plant Journal **52**: 570–582.

Boeck, R., Tarun, S., Rieger, M., Deardorff, J.A., Müller-Auer, S., and Sachs, A.B. (1996). The Yeast Pan2 Protein Is Required for Poly(A)-binding Protein-stimulated Poly(A)-nuclease Activity ∗. Journal of Biological Chemistry **271**: 432–438.

Boland, A., Chen, Y., Raisch, T., Jonas, S., Kuzuoğlu-Öztürk, D., Wohlbold, L., Weichenrieder, O., and Izaurralde, E. (2013). Structure and assembly of the NOT module of the human CCR4-NOT complex. Nat Struct Mol Biol **20**: 1289–1297.

Boulias, K., Toczydłowska-Socha, D., Hawley, B.R., Liberman, N., Takashima, K., Zaccara, S., Guez, T., Vasseur, J.-J., Debart, F., Aravind, L., Jaffrey, S.R., and Greer, E.L. (2019). Identification of the m6Am Methyltransferase PCIF1 Reveals the Location and Functions of m6Am in the Transcriptome. Mol Cell **75**: 631-643.e8.

Bousquet-Antonelli, C. and Deragon, J.-M. (2009). A comprehensive analysis of the La-motif protein superfamily. RNA **15**: 750–764.

Bouveret, E., Rigaut, G., Shevchenko, A., Wilm, M., and Séraphin, B. (2000). A Sm-like protein complex that participates in mRNA degradation. EMBO J **19**: 1661–1671.

Boyraz, B., Moon, D.H., Segal, M., Muosieyiri, M.Z., Aykanat, A., Tai, A.K., Cahan, P., and Agarwal, S. (2016). Posttranscriptional manipulation of TERC reverses molecular hallmarks of telomere disease. J Clin Invest **126**: 3377–3382.

Braun, J.E., Huntzinger, E., Fauser, M., and Izaurralde, E. (2011). GW182 Proteins Directly Recruit Cytoplasmic Deadenylase Complexes to miRNA Targets. Molecular Cell **44**: 120–133.

Brouze, A., Krawczyk, P.S., Dziembowski, A., and Mroczek, S. (2023). Measuring the tail: Methods for poly(A) tail profiling. WIREs RNA **14**: e1737.

Brown, C.E., S Z Tarun, J., Boeck, R., and Sachs, A.B. (1996). PAN3 encodes a subunit of the Pab1p-dependent poly(A) nuclease in Saccharomyces cerevisiae. Molecular and Cellular Biology **16**: 5744.

Buschauer, R. et al. (2020). The Ccr4-Not complex monitors the translating ribosome for codon optimality. Science **368**: eaay6912.

Caponigro, G. and Parker, R. (1995). Multiple functions for the poly(A)-binding protein in mRNA decapping and deadenylation in yeast. Genes Dev **9**: 2421–2432.

Carpentier, M.-C., Deragon, J.-M., Jean, V., Be, S.H.V., Bousquet-Antonelli, C., and Merret, R. (2020). Monitoring of XRN4 Targets Reveals the Importance of Cotranslational Decay during Arabidopsis Development. Plant Physiology **184**: 1251–1262.

Chalabi Hagkarim, N. and Grand, R.J. (2020). The Regulatory Properties of the Ccr4-Not Complex. Cells **9**: 2379.

Chang, H. et al. (2018). Terminal Uridylyltransferases Execute Programmed Clearance of Maternal Transcriptome in Vertebrate Embryos. Molecular Cell **70**: 72-82.e7.

Chang, H., Lim, J., Ha, M., and Kim, V.N. (2014). TAIL-seq: genome-wide determination of poly(A) tail length and 3’ end modifications. Mol Cell **53**: 1044–1052.

Chang, H.-M., Triboulet, R., Thornton, J.E., and Gregory, R.I. (2013). A role for the Perlman syndrome exonuclease Dis3l2 in the Lin28-let-7 pathway. Nature **497**: 244–248.

Chang, M. and Huang, S. (2017). Rapid Isolation of Total Protein from Arabidopsis Pollen. Bio Protoc **7**: e2227.

Chantarachot, T., Sorenson, R.S., Hummel, M., Ke, H., Kettenburg, A.T., Chen, D., Aiyetiwa, K., Dehesh, K., Eulgem, T., Sieburth, L.E., and Bailey-Serres, J. (2020). DHH1/DDX6-like RNA helicases maintain ephemeral half-lives of stress-response mRNAs. Nat Plants **6**: 675–685.

Charenton, C., Gaudon-Plesse, C., Fourati, Z., Taverniti, V., Back, R., Kolesnikova, O., Séraphin, B., and Graille, M. (2017). A unique surface on Pat1 C-terminal domain directly interacts with Dcp2 decapping enzyme and Xrn1 5′–3′ mRNA exonuclease in yeast. Proceedings of the National Academy of Sciences **114**: E9493–E9501.

Chen, J., Rappsilber, J., Chiang, Y.C., Russell, P., Mann, M., and Denis, C.L. (2001). Purification and characterization of the 1.0 MDa CCR4-NOT complex identifies two novel components of the complex. J Mol Biol **314**: 683–694.

Chen, Y., Boland, A., Kuzuoğlu-Öztürk, D., Bawankar, P., Loh, B., Chang, C.-T., Weichenrieder, O., and Izaurralde, E. (2014). A DDX6-CNOT1 Complex and W-Binding Pockets in CNOT9 Reveal Direct Links between miRNA Target Recognition and Silencing. Molecular Cell **54**: 737–750.

Chen, Y., Khazina, E., Izaurralde, E., and Weichenrieder, O. (2021). Crystal structure and functional properties of the human CCR4-CAF1 deadenylase complex. Nucleic Acids Res **49**: 6489–6510.

Cheng, J., Maier, K.C., Avsec, Ž., Rus, P., and Gagneur, J. (2017). Cis-regulatory elements explain most of the mRNA stability variation across genes in yeast. RNA **23**: 1648–1659.

Chi, B., Wang, Q., Wu, G., Tan, M., Wang, L., Shi, M., Chang, X., and Cheng, H. (2013). Aly and THO are required for assembly of the human TREX complex and association of TREX components with the spliced mRNA. Nucleic Acids Res **41**: 1294–1306.

Chiba, Y., Johnson, M.A., Lidder, P., Vogel, J.T., van Erp, H., and Green, P.J. (2004). AtPARN is an essential poly(A) ribonuclease in Arabidopsis. Gene **328**: 95–102.

Chiu, S.-Y., Lejeune, F., Ranganathan, A.C., and Maquat, L.E. (2004). The pioneer translation initiation complex is functionally distinct from but structurally overlaps with the steady-state translation initiation complex. Genes Dev **18**: 745–754.

Cho, E.-J., Takagi, T., Moore, C.R., and Buratowski, S. (1997). mRNA capping enzyme is recruited to the transcription complex by phosphorylation of the RNA polymerase II carboxy-terminal domain. Genes Dev **11**: 3319–3326.

Chou, W.-L., Chung, Y.-L., Fang, J.-C., and Lu, C.-A. (2017). Novel interaction between CCR4 and CAF1 in rice CCR4–NOT deadenylase complex. Plant Mol Biol **93**: 79–96.

Chowdhury, A., Mukhopadhyay, J., and Tharun, S. (2007). The decapping activator Lsm1p-7p-Pat1p complex has the intrinsic ability to distinguish between oligoadenylated and polyadenylated RNAs. RNA **13**: 998–1016.

Clemente, P. et al. (2022). ANGEL2 phosphatase activity is required for non-canonical mitochondrial RNA processing. Nat Commun **13**: 5750.

Collart, M.A. (2016). The Ccr4-Not complex is a key regulator of eukaryotic gene expression. WIREs RNA **7**: 438–454.

Colot, H.V., Stutz, F., and Rosbash, M. (1996). The yeast splicing factor Mud13p is a commitment complex component and corresponds to CBP20, the small subunit of the nuclear cap-binding complex. Genes Dev **10**: 1699–1708.

da Costa, P.J., Menezes, J., Saramago, M., García-Moreno, J.F., Santos, H.A., Gama-Carvalho, M., Arraiano, C.M., Viegas, S.C., and Romão, L. (2019). A role for DIS3L2 over natural nonsense-mediated mRNA decay targets in human cells. Biochemical and Biophysical Research Communications **518**: 664–671.

Daffis, S. et al. (2010). 2′-O methylation of the viral mRNA cap evades host restriction by IFIT family members. Nature **468**: 452–456.

Dai, X.-X., Jiang, Y., Gu, J.-H., Jiang, Z.-Y., Wu, Y.-W., Yu, C., Yin, H., Zhang, J., Shi, Q.-H., Shen, L., Sha, Q.-Q., and Fan, H.-Y. (2021). The CNOT4 Subunit of the CCR4-NOT Complex is Involved in mRNA Degradation, Efficient DNA Damage Repair, and XY Chromosome Crossover during Male Germ Cell Meiosis. Advanced Science **8**: 2003636.

Davey, N.E., Roey, K.V., Weatheritt, R.J., Toedt, G., Uyar, B., Altenberg, B., Budd, A., Diella, F., Dinkel, H., and Gibson, T.J. (2011). Attributes of short linear motifs. Mol. BioSyst. **8**: 268–281.

De Almeida, C., Scheer, H., Zuber, H., and Gagliardi, D. (2018). RNA uridylation: a key posttranscriptional modification shaping the coding and noncoding transcriptome. WIREs RNA **9**: e1440.

Decker, C.J. and Parker, R. (1993). A turnover pathway for both stable and unstable mRNAs in yeast: evidence for a requirement for deadenylation. Genes Dev **7**: 1632–1643.

Dehlin, E., Wormington, M., Körner, C.G., and Wahle, E. (2000). Cap-dependent deadenylation of mRNA. EMBO J **19**: 1079–1086.

Delis, C., Krokida, A., Tomatsidou, A., Tsikou, D., Beta, R.A.A., Tsioumpekou, M., Moustaka, J., Stravodimos, G., Leonidas, D.D., Balatsos, N.A.A., and Papadopoulou, K.K. (2016). AtHESPERIN: a novel regulator of circadian rhythms with poly(A)-degrading activity in plants. RNA Biology **13**: 68–82.

Deo, R.C., Bonanno, J.B., Sonenberg, N., and Burley, S.K. (1999). Recognition of polyadenylate RNA by the poly(A)-binding protein. Cell **98**: 835–845.

Devarkar, S.C., Wang, C., Miller, M.T., Ramanathan, A., Jiang, F., Khan, A.G., Patel, S.S., and Marcotrigiano, J. (2016). Structural basis for m7G recognition and 2’-O-methyl discrimination in capped RNAs by the innate immune receptor RIG-I. Proc Natl Acad Sci U S A **113**: 596–601.

Dhanraj, S. et al. (2015). Bone marrow failure and developmental delay caused by mutations in poly(A)-specific ribonuclease (PARN). J Med Genet **52**: 738–748.

Dominski, Z., Yang, X., and Marzluff, W.F. (2005). The Polyadenylation Factor CPSF-73 Is Involved in Histone-Pre-mRNA Processing. Cell **123**: 37–48.

Dp, M., Hn, D., Im, F., Pf, S., and Sd, B. (2009). Polyubiquitination of the demethylase Jhd2 controls histone methylation and gene expression. Genes & development **23**.

Du, H., Zhao, Y., He, J., Zhang, Y., Xi, H., Liu, M., Ma, J., and Wu, L. (2016). YTHDF2 destabilizes m6A-containing RNA through direct recruitment of the CCR4–NOT deadenylase complex. Nat Commun **7**: 12626.

Dupressoir, A., Morel, A.P., Barbot, W., Loireau, M.P., Corbo, L., and Heidmann, T. (2001). Identification of four families of yCCR4- and Mg2+-dependent endonuclease-related proteins in higher eukaryotes, and characterization of orthologs of yCCR4 with a conserved leucine-rich repeat essential for hCAF1/hPOP2 binding. BMC Genomics **2**: 9.

Dziembowski, A., Lorentzen, E., Conti, E., and Séraphin, B. (2007). A single subunit, Dis3, is essentially responsible for yeast exosome core activity. Nat Struct Mol Biol **14**: 15–22.

Eckwahl, M.J., Sim, S., Smith, D., Telesnitsky, A., and Wolin, S.L. (2015). A retrovirus packages nascent host noncoding RNAs from a novel surveillance pathway. Genes Dev **29**: 646–657.

Eichhorn, S.W., Subtelny, A.O., Kronja, I., Kwasnieski, J.C., Orr-Weaver, T.L., and Bartel, D.P. (2016). mRNA poly(A)-tail changes specified by deadenylation broadly reshape translation in Drosophila oocytes and early embryos. eLife **5**: e16955.

Eisen, T.J., Eichhorn, S.W., Subtelny, A.O., Lin, K.S., McGeary, S.E., Gupta, S., and Bartel, D.P. (2020). The Dynamics of Cytoplasmic mRNA Metabolism. Mol Cell **77**: 786-799.e10.

Eisen, T.J., Li, J.J., and Bartel, D.P. (2022). The interplay between translational efficiency, poly(A) tails, microRNAs, and neuronal activation. RNA **28**: 808–831.

Engstler, M., Pfohl, T., Herminghaus, S., Boshart, M., Wiegertjes, G., Heddergott, N., and Overath, P. (2007). Hydrodynamic flow-mediated protein sorting on the cell surface of trypanosomes. Cell **131**: 505–515.

Enwerem, I.I.I., Elrod, N.D., Chang, C.-T., Lin, A., Ji, P., Bohn, J.A., Levdansky, Y., Wagner, E.J., Valkov, E., and Goldstrohm, A.C. (2021). Human Pumilio proteins directly bind the CCR4-NOT deadenylase complex to regulate the transcriptome. RNA **27**: 445–464.

Erben, E., Chakraborty, C., and Clayton, C. (2014). The CAF1-NOT complex of trypanosomes. Front Genet **4**: 299.

Erdős, G., Pajkos, M., and Dosztányi, Z. (2021). IUPred3: prediction of protein disorder enhanced with unambiguous experimental annotation and visualization of evolutionary conservation. Nucleic Acids Research **49**: W297–W303.

Estrella, M.A., Du, J., Chen, L., Rath, S., Prangley, E., Chitrakar, A., Aoki, T., Schedl, P., Rabinowitz, J., and Korennykh, A. (2019). The metabolites NADP+ and NADPH are the targets of the circadian protein Nocturnin (Curled). Nat Commun **10**: 2367.

Estrella, M.A., Du, J., and Korennykh, A. (2018). Crystal Structure of Human Nocturnin Catalytic Domain. Sci Rep **8**: 16294.

Ezzeddine, N., Chang, T.-C., Zhu, W., Yamashita, A., Chen, C.-Y.A., Zhong, Z., Yamashita, Y., Zheng, D., and Shyu, A.-B. (2007). Human TOB, an antiproliferative transcription factor, is a poly(A)-binding protein-dependent positive regulator of cytoplasmic mRNA deadenylation. Mol Cell Biol **27**: 7791–7801.

Fabian, M.R., Frank, F., Rouya, C., Siddiqui, N., Lai, W.S., Karetnikov, A., Blackshear, P.J., Nagar, B., and Sonenberg, N. (2013). Structural basis for the recruitment of the human CCR4-NOT deadenylase complex by tristetraprolin. Nat Struct Mol Biol **20**: 735–739.

Faehnle, C.R., Walleshauser, J., and Joshua-Tor, L. (2014). Mechanism of Dis3l2 substrate recognition in the Lin28-let-7 pathway. Nature **514**: 252–256.

Faehnle, C.R., Walleshauser, J., and Joshua-Tor, L. (2017). Multi-domain utilization by TUT4 and TUT7 in control of let-7 biogenesis. Nat Struct Mol Biol **24**: 658–665.

Flaherty, S.M., Fortes, P., Izaurralde, E., Mattaj, I.W., and Gilmartin, G.M. (1997). Participation of the nuclear cap binding complex in pre-mRNA 3′ processing. Proceedings of the National Academy of Sciences **94**: 11893–11898.

Ferrier, E. (2013) Rôle et mode d'action de l'UTP:RNA uridylyltransferase URT1 dans l'uridylation et la dégradation des ARNm chez Arabidopsis thaliana (doctoral dissertation). University of Strasbourg, Strasbourg, France.

Freh, M., Gao, J., Petersen, M., and Panstruga, R. (2021). Plant autoimmunity—fresh insights into an old phenomenon. Plant Physiol **188**: 1419–1434.

Friend, K., Brook, M., Bezirci, F.B., Sheets, M.D., Gray, N.K., and Seli, E. (2012). Embryonic poly(A)-binding protein (ePAB) phosphorylation is required for Xenopus oocyte maturation. Biochem J **445**: 93–100.

Fuke, H. and Ohno, M. (2008). Role of poly (A) tail as an identity element for mRNA nuclear export. Nucleic Acids Res **36**: 1037–1049.

Gallie, D.R. and Browning, K.S. (2001). eIF4G functionally differs from eIFiso4G in promoting internal initiation, cap-independent translation, and translation of structured mRNAs. J Biol Chem **276**: 36951–36960.

Gallie, D.R. and Liu, R. (2014). Phylogenetic analysis reveals dynamic evolution of the poly(A)-binding protein gene family in plants. BMC Evolutionary Biology **14**: 238.

Galloway, A. and Cowling, V.H. (2019). mRNA cap regulation in mammalian cell function and fate. Biochim Biophys Acta Gene Regul Mech **1862**: 270–279.

Gao, M., Fritz, D.T., Ford, L.P., and Wilusz, J. (2000). Interaction between a poly(A)-specific ribonuclease and the 5’ cap influences mRNA deadenylation rates in vitro. Mol Cell **5**: 479–488.

Garalde, D.R. et al. (2018). Highly parallel direct RNA sequencing on an array of nanopores. Nat Methods **15**: 201–206.

Garbarino-Pico, E., Niu, S., Rollag, M.D., Strayer, C.A., Besharse, J.C., and Green, C.B. (2007). Immediate early response of the circadian polyA ribonuclease nocturnin to two extracellular stimuli. RNA **13**: 745–755.

Gingras, A.-C., Gstaiger, M., Raught, B., and Aebersold, R. (2007). Analysis of protein complexes using mass spectrometry. Nat Rev Mol Cell Biol **8**: 645–654.

Giraudo, P., Simonnot, Q., Pflieger, D., Peter, J., Gagliardi, D., and Zuber, H. (2024). Nano3′RACE: A Method to Analyze Poly(A) Tail Length and Nucleotide Additions at the 3′ Extremity of Selected mRNAs Using Nanopore Sequencing. In Deadenylation: Methods and Protocols, E. Valkov and A.C. Goldstrohm, eds, Methods in Molecular Biology. (Springer US: New York, NY), pp. 233–252.

Goeres, D.C., Norman, J.M.V., Zhang, W., Fauver, N.A., Spencer, M.L., and Sieburth, L.E. (2007). Components of the Arabidopsis mRNA Decapping Complex Are Required for Early Seedling Development. The Plant Cell **19**: 1549.

Goldstrohm, A.C., Tanaka Hall, T.M., and McKenney, K.M. (2018). Post-transcriptional Regulatory Functions of Mammalian Pumilio Proteins. Trends Genet **34**: 972–990.

Goldstrohm, A.C. and Wickens, M. (2008). Multifunctional deadenylase complexes diversify mRNA control. Nat Rev Mol Cell Biol **9**: 337–344.

Gómez, J.F., Talle, B., and Wilson, Z.A. (2015). Anther and pollen development: A conserved developmental pathway. Journal of Integrative Plant Biology **57**: 876–891.

Gonatopoulos-Pournatzis, T. and Cowling, V.H. (2014). Cap-binding complex (CBC). Biochem J **457**: 231–242.

Green, C.B. and Besharse, J.C. (1996). Identification of a novel vertebrate circadian clock-regulated gene encoding the protein nocturnin. Proc Natl Acad Sci U S A **93**: 14884–14888.

Gruber, J.J. et al. (2009). Ars2 links the nuclear cap binding complex to RNA interference and cell proliferation. Cell **138**: 328–339.

Gruber, J.J., Olejniczak, S.H., Yong, J., Rocca La, G., Dreyfuss, G., and Thompson, C.B. (2012). Ars2 promotes proper replication-dependent histone mRNA 3′ end formation. Mol Cell **45**: 87–98.

Halbach, F., Reichelt, P., Rode, M., and Conti, E. (2013). The yeast ski complex: crystal structure and RNA channeling to the exosome complex. Cell **154**: 814–826.

Hallais, M. et al. (2013). CBC-ARS2 stimulates 3’-end maturation of multiple RNA families and favors cap-proximal processing. Nat Struct Mol Biol **20**: 1358–1366.

Hao, H., Li, Y., Hu, Y., and Lin, J. (2005). Inhibition of RNA and protein synthesis in pollen tube development of Pinus bungeana by actinomycin D and cycloheximide. New Phytol **165**: 721–729.

Hashimoto, M., Neriya, Y., Keima, T., Iwabuchi, N., Koinuma, H., Hagiwara-Komoda, Y., Ishikawa, K., Himeno, M., Maejima, K., Yamaji, Y., and Namba, S. (2016). EXA1, a GYF domain protein, is responsible for loss-of-susceptibility to plantago asiatica mosaic virus in Arabidopsis thaliana. Plant J **88**: 120–131.

Haugen, R.J., Arvola, R.M., Connacher, R.P., Roden, R.T., and Goldstrohm, A.C. (2022). A conserved domain of Drosophila RNA-binding protein Pumilio interacts with multiple CCR4–NOT deadenylase complex subunits to repress target mRNAs. Journal of Biological Chemistry **298**.

Herrick, D., Parker, R., and Jacobson, A. (1990). Identification and comparison of stable and unstable mRNAs in Saccharomyces cerevisiae. Mol Cell Biol **10**: 2269–2284.

Hickey, K.L. et al. (2020). GIGYF2 and 4EHP Inhibit Translation Initiation of Defective Messenger RNAs to Assist Ribosome-Associated Quality Control. Mol Cell **79**: 950-962.e6.

Hirayama, T. (2014). A unique system for regulating mitochondrial mRNA poly(A) status and stability in plants. Plant Signal Behav **9**: e973809.

Hirayama, T. (2021). PARN-like Proteins Regulate Gene Expression in Land Plant Mitochondria by Modulating mRNA Polyadenylation. Int J Mol Sci **22**: 10776.

Ho, C.K., Lehman, K., and Shuman, S. (1999). An essential surface motif (WAQKW) of yeast RNA triphosphatase mediates formation of the mRNA capping enzyme complex with RNA guanylyltransferase. Nucleic Acids Res **27**: 4671–4678.

Ho, C.K., Schwer, B., and Shuman, S. (1998). Genetic, Physical, and Functional Interactions between the Triphosphatase and Guanylyltransferase Components of the Yeast mRNA Capping Apparatus. Molecular and Cellular Biology **18**: 5189–5198.

Honys, D. and Twell, D. (2004). Transcriptome analysis of haploid male gametophyte development in Arabidopsis. Genome Biol **5**: R85.

van Hoof, A., Staples, R.R., Baker, R.E., and Parker, R. (2000). Function of the Ski4p (Csl4p) and Ski7p Proteins in 3′-to-5′ Degradation of mRNA. Molecular and Cellular Biology **20**: 8230–8243.

Hsu, C.L. and Stevens, A. (1993). Yeast cells lacking 5’-->3’ exoribonuclease 1 contain mRNA species that are poly(A) deficient and partially lack the 5’ cap structure. Mol Cell Biol **13**: 4826–4835.

Hughes, K.L., Abshire, E.T., and Goldstrohm, A.C. (2018). Regulatory roles of vertebrate Nocturnin: insights and remaining mysteries. RNA Biology **15**: 1255–1267.

Huot, B., Yao, J., Montgomery, B.L., and He, S.Y. (2014). Growth–Defense Tradeoffs in Plants: A Balancing Act to Optimize Fitness. Mol Plant **7**: 1267–1287.

Iasillo, C., Schmid, M., Yahia, Y., Maqbool, M.A., Descostes, N., Karadoulama, E., Bertrand, E., Andrau, J.-C., and Jensen, T.H. (2017). ARS2 is a general suppressor of pervasive transcription. Nucleic Acids Res **45**: 10229–10241.

Imataka, H., Gradi, A., and Sonenberg, N. (1998). A newly identified N-terminal amino acid sequence of human eIF4G binds poly(A)-binding protein and functions in poly(A)-dependent translation. The EMBO Journal **17**: 7480–7489.

Inada, T. and Makino, S. (2014). Novel roles of the multi-functional CCR4-NOT complex in post-transcriptional regulation. Frontiers in Genetics **5**.

Ishigaki, Y., Li, X., Serin, G., and Maquat, L.E. (2001). Evidence for a Pioneer Round of mRNA Translation: mRNAs Subject to Nonsense-Mediated Decay in Mammalian Cells Are Bound by CBP80 and CBP20. Cell **106**: 607–617.

Izaurralde, E., Lewis, J., McGuigan, C., Jankowska, M., Darzynkiewicz, E., and Mattaj, I.W. (1994). A nuclear cap binding protein complex involved in pre-mRNA splicing. Cell **78**: 657–668.

Izumi, N., Shoji, K., Sakaguchi, Y., Honda, S., Kirino, Y., Suzuki, T., Katsuma, S., and Tomari, Y. (2016). Identification and Functional Analysis of the Pre-piRNA 3’ Trimmer in Silkworms. Cell **164**: 962–973.

Januszyk, K. and Lima, C.D. (2014). The eukaryotic RNA exosome. Curr Opin Struct Biol **0**: 132–140.

Jia, J., Lu, W., Liu, B., Fang, H., Yu, Y., Mo, W., Zhang, H., Jin, X., Shu, Y., Long, Y., Pei, Y., and Zhai, J. (2022). An atlas of plant full-length RNA reveals tissue-specific and monocots–dicots conserved regulation of poly(A) tail length. Nat. Plants **8**: 1118–1126.

Jia, Q.-S., Zhu, J., Xu, X.-F., Lou, Y., Zhang, Z.-L., Zhang, Z.-P., and Yang, Z.-N. (2015). Arabidopsis AT-hook Protein TEK Positively Regulates the Expression of Arabinogalactan Proteins for Nexine Formation. Molecular Plant **8**: 251–260.

Jiang, J., Yao, L., Yu, Y., Lv, M., Miao, Y., and Cao, J. (2014). PECTATE LYASE-LIKE10 is associated with pollen wall development in Brassica campestris. Journal of Integrative Plant Biology **56**: 1095–1105.

Jiang, L., Yang, S.-L., Xie, L.-F., Puah, C.S., Zhang, X.-Q., Yang, W.-C., Sundaresan, V., and Ye, D. (2005). VANGUARD1 Encodes a Pectin Methylesterase That Enhances Pollen Tube Growth in the Arabidopsis Style and Transmitting Tract. The Plant Cell **17**: 584–596.

Jiao, X., Chang, J.H., Kilic, T., Tong, L., and Kiledjian, M. (2013). A mammalian pre-mRNA 5′-end capping quality control mechanism and an unexpected link of capping to pre-mRNA processing. Mol Cell **50**: 104–115.

Jiao, X., Doamekpor, S.K., Bird, J.G., Nickels, B.E., Tong, L., Hart, R.P., and Kiledjian, M. (2017). 5′-end NAD+ cap in human cells promotes RNA decay through DXO-mediated deNADding. Cell **168**: 1015-1027.e10.

Jinek, M., Fabian, M.R., Coyle, S.M., Sonenberg, N., and Doudna, J.A. (2010). Structural insights into the human GW182-PABC interaction in microRNA-mediated deadenylation. Nat Struct Mol Biol **17**: 238–240.

Johnson, A.W. and Kolodner, R.D. (1995). Synthetic Lethality of sep1 (xrn1) ski2 and sep1 (xrn1) ski3 Mutants of Saccharomyces cerevisiae Is Independent of Killer Virus and Suggests a General Role for These Genes in Translation Control. Molecular and Cellular Biology **15**: 2719–2727.

Jonas, S. and Izaurralde, E. (2013). The role of disordered protein regions in the assembly of decapping complexes and RNP granules. Genes Dev **27**: 2628–2641.

Kanazawa, M., Ikeda, Y., Nishihama, R., Yamaoka, S., Lee, N.-H., Yamato, K.T., Kohchi, T., and Hirayama, T. (2020). Regulation of the Poly(A) Status of Mitochondrial mRNA by Poly(A)-Specific Ribonuclease Is Conserved among Land Plants. Plant Cell Physiol **61**: 470–480.

Kastenmayer, J.P. and Green, P.J. (2000). Novel features of the XRN-family in Arabidopsis: evidence that AtXRN4, one of several orthologs of nuclear Xrn2p/Rat1p, functions in the cytoplasm. Proc Natl Acad Sci U S A **97**: 13985–13990.

Kastenmayer, J.P., Johnson, M.A., and Green, P.J. (2001). Analysis of XRN orthologs by complementation of yeast mutants and localization of XRN-GFP fusion proteins. Methods Enzymol **342**: 269–282.

Kataoka, N., Ohno, M., Moda, I., and Shimura, Y. (1995). Identification of the factors that interact with NCBP, an 80 kDa nuclear cap binding protein. Nucleic Acids Res **23**: 3638–3641.

Keith, J.M., Ensinger, M.J., and Moss, B. (1978). HeLa cell RNA (2’-O-methyladenosine-N6-)-methyltransferase specific for the capped 5’-end of messenger RNA. J Biol Chem **253**: 5033–5039.

Keller, R.W., Kühn, U., Aragón, M., Bornikova, L., Wahle, E., and Bear, D.G. (2000). The nuclear poly(A) binding protein, PABP2, forms an oligomeric particle covering the length of the poly(A) tail11Edited by I. Tinoco. Journal of Molecular Biology **297**: 569–583.

Kerr, S.C., Azzouz, N., Fuchs, S.M., Collart, M.A., Strahl, B.D., Corbett, A.H., and Laribee, R.N. (2011). The Ccr4-Not Complex Interacts with the mRNA Export Machinery. PLOS ONE **6**: e18302.

Keskeny, C., Raisch, T., Sgromo, A., Igreja, C., Bhandari, D., Weichenrieder, O., and Izaurralde, E. (2019). A conserved CAF40-binding motif in metazoan NOT4 mediates association with the CCR4-NOT complex. Genes Dev **33**: 236–252.

Kilchert, C., Wittmann, S., and Vasiljeva, L. (2016). The regulation and functions of the nuclear RNA exosome complex. Nat Rev Mol Cell Biol **17**: 227–239.

Kim, D., Paggi, J.M., Park, C., Bennett, C., and Salzberg, S.L. (2019). Graph-based genome alignment and genotyping with HISAT2 and HISAT-genotype. Nat Biotechnol **37**: 907–915.

Kini, H.K., Silverman, I.M., Ji, X., Gregory, B.D., and Liebhaber, S.A. (2016). Cytoplasmic poly(A) binding protein-1 binds to genomically encoded sequences within mammalian mRNAs. RNA **22**: 61–74.

Klepikova, A.V., Kasianov, A.S., Gerasimov, E.S., Logacheva, M.D., and Penin, A.A. (2016). A high resolution map of the Arabidopsis thaliana developmental transcriptome based on RNA-seq profiling. The Plant Journal **88**: 1058–1070.

Kofler, M., Motzny, K., and Freund, C. (2005). GYF Domain Proteomics Reveals Interaction Sites in Known and Novel Target Proteins * S. Molecular & Cellular Proteomics **4**: 1797–1811.

Kofler, M.M. and Freund, C. (2006). The GYF domain. FEBS J **273**: 245–256.

Kögel, A., Keidel, A., Bonneau, F., Schäfer, I.B., and Conti, E. (2022). The human SKI complex regulates channeling of ribosome-bound RNA to the exosome via an intrinsic gatekeeping mechanism. Mol Cell **82**: 756-769.e8.

Konarska, M.M., Padgett, R.A., and Sharp, P.A. (1984). Recognition of cap structure in splicing in vitro of mRNA precursors. Cell **38**: 731–736.

Körner, C.G. and Wahle, E. (1997). Poly(A) tail shortening by a mammalian poly(A)-specific 3’-exoribonuclease. J Biol Chem **272**: 10448–10456.

Körner, C.G., Wormington, M., Muckenthaler, M., Schneider, S., Dehlin, E., and Wahle, E. (1998). The deadenylating nuclease (DAN) is involved in poly(A) tail removal during the meiotic maturation of Xenopus oocytes. EMBO J **17**: 5427–5437.

Kropiwnicka, A., Kuchta, K., Lukaszewicz, M., Kowalska, J., Jemielity, J., Ginalski, K., Darzynkiewicz, E., and Zuberek, J. (2015). Five eIF4E isoforms from Arabidopsis thaliana are characterized by distinct features of cap analogs binding. Biochem Biophys Res Commun **456**: 47–52.

Kruk, J.A., Dutta, A., Fu, J., Gilmour, D.S., and Reese, J.C. (2011). The multifunctional Ccr4–Not complex directly promotes transcription elongation. Genes Dev. **25**: 581–593.

Kuhn, J.M., Breton, G., and Schroeder, J.I. (2007). mRNA metabolism of flowering-time regulators in wild-type Arabidopsis revealed by a nuclear cap binding protein mutant, abh1. Plant J **50**: 1049–1062.

Kuhn, L., Vincent, T., Hammann, P., and Zuber, H. (2023). Exploring Protein Interactome Data with IPinquiry: Statistical Analysis and Data Visualization by Spectral Counts. Methods Mol Biol **2426**: 243–265.

Kühn, U., Buschmann, J., and Wahle, E. (2017). The nuclear poly(A) binding protein of mammals, but not of fission yeast, participates in mRNA polyadenylation. RNA **23**: 473–482.

Kühn, U., Gündel, M., Knoth, A., Kerwitz, Y., Rüdel, S., and Wahle, E. (2009). Poly(A) Tail Length Is Controlled by the Nuclear Poly(A)-binding Protein Regulating the Interaction between Poly(A) Polymerase and the Cleavage and Polyadenylation Specificity Factor*. Journal of Biological Chemistry **284**: 22803–22814.

Łabno, A., Warkocki, Z., Kuliński, T., Krawczyk, P.S., Bijata, K., Tomecki, R., and Dziembowski, A. (2016). Perlman syndrome nuclease DIS3L2 controls cytoplasmic non-coding RNAs and provides surveillance pathway for maturing snRNAs. Nucleic Acids Res **44**: 10437–10453.

Lam, P., Zhao, L., Eveleigh, N., Yu, Y., Chen, X., and Kunst, L. (2015). The Exosome and Trans-Acting Small Interfering RNAs Regulate Cuticular Wax Biosynthesis during Arabidopsis Inflorescence Stem Development. Plant Physiology **167**: 323–336.

Lange, H. et al. (2019). RST1 and RIPR connect the cytosolic RNA exosome to the Ski complex in Arabidopsis. Nat Commun **10**: 3871.

Lange, H. and Gagliardi, D. (2022). Catalytic activities, molecular connections, and biological functions of plant RNA exosome complexes. The Plant Cell **34**: 967–988.

Laothamatas, I., Gao, P., Wickramaratne, A., Quintanilla, C.G., Dino, A., Khan, C.A., Liou, J., and Green, C.B. (2020). Spatiotemporal regulation of NADP(H) phosphatase Nocturnin and its role in oxidative stress response. Proc Natl Acad Sci U S A **117**: 993–999.

Lardelli, R.M. et al. (2017). Biallelic mutations in the 3′ exonuclease TOE1 cause pontocerebellar hypoplasia and uncover a role in snRNA processing. Nat Genet **49**: 457–464.

Lardelli, R.M. and Lykke-Andersen, J. (2020). Competition between maturation and degradation drives human snRNA 3′ end quality control. Genes Dev. **34**: 989–1001.

Lau, N.-C., Kolkman, A., van Schaik, F.M.A., Mulder, K.W., Pijnappel, W.W.M.P., Heck, A.J.R., and Timmers, H.Th.M. (2009). Human Ccr4–Not complexes contain variable deadenylase subunits. Biochemical Journal **422**: 443–453.

Laubinger, S., Sachsenberg, T., Zeller, G., Busch, W., Lohmann, J.U., Rätsch, G., and Weigel, D. (2008). Dual roles of the nuclear cap-binding complex and SERRATE in pre-mRNA splicing and microRNA processing in Arabidopsis thaliana. Proc Natl Acad Sci U S A **105**: 8795–8800.

Lee, J.E., Lee, J.Y., Trembly, J., Wilusz, J., Tian, B., and Wilusz, C.J. (2012). The PARN deadenylase targets a discrete set of mRNAs for decay and regulates cell motility in mouse myoblasts. PLoS Genet **8**: e1002901.

Lee, Y., Choe, J., Park, O.H., and Kim, Y.K. (2020). Molecular Mechanisms Driving mRNA Degradation by m6A Modification. Trends in Genetics **36**: 177–188.

Legnini, I., Alles, J., Karaiskos, N., Ayoub, S., and Rajewsky, N. (2019). FLAM-seq: full-length mRNA sequencing reveals principles of poly(A) tail length control. Nat Methods **16**: 879–886.

Leroux, C. et al. (2015). PECTIN METHYLESTERASE48 is involved in Arabidopsis pollen grain germination. Plant Physiol **167**: 367–380.

Li, H. (2018). Minimap2: pairwise alignment for nucleotide sequences. Bioinformatics **34**: 3094–3100.

Liang, W., Li, C., Liu, F., Jiang, H., Li, S., Sun, J., Wu, X., and Li, C. (2009). The Arabidopsis homologs of CCR4-associated factor 1 show mRNA deadenylation activity and play a role in plant defence responses. Cell Res **19**: 307–316.

Liao, Y., Smyth, G.K., and Shi, W. (2014). featureCounts: an efficient general purpose program for assigning sequence reads to genomic features. Bioinformatics **30**: 923–930.

Lim, J., Ha, M., Chang, H., Kwon, S.C., Simanshu, D.K., Patel, D.J., and Kim, V.N. (2014). Uridylation by TUT4 and TUT7 Marks mRNA for Degradation. Cell **159**: 1365–1376.

Lim, J., Kim, D., Lee, Y.-S., Ha, M., Lee, M., Yeo, J., Chang, H., Song, J., Ahn, K., and Kim, V.N. (2018). Mixed tailing by TENT4A and TENT4B shields mRNA from rapid deadenylation. Science **361**: 701–704.

Lima, S.A., Chipman, L.B., Nicholson, A.L., Chen, Y.-H., Yee, B.A., Yeo, G.W., Coller, J., and Pasquinelli, A.E. (2017). Short Poly(A) Tails are a Conserved Feature of Highly Expressed Genes. Nat Struct Mol Biol **24**: 1057–1063.

Lin, C.-J., Wen, J., Bejarano, F., Hu, F., Bortolamiol-Becet, D., Kan, L., Sanfilippo, P., Kondo, S., and Lai, E.C. (2017). Characterization of a TUTase/RNase complex required for Drosophila gametogenesis. RNA **23**: 284–296.

Liu, Q., Greimann, J.C., and Lima, C.D. (2006). Reconstitution, Activities, and Structure of the Eukaryotic RNA Exosome. Cell **127**: 1223–1237.

Liu, Y. et al. (2023). Remodeling of maternal mRNA through poly(A) tail orchestrates human oocyte-to-embryo transition. Nat Struct Mol Biol **30**: 200–215.

Liu, Y., Nie, H., Liu, H., and Lu, F. (2019). Poly(A) inclusive RNA isoform sequencing (PAIso−seq) reveals wide-spread non-adenosine residues within RNA poly(A) tails. Nat Commun **10**: 5292.

Lorenz, D.A., Sathe, S., Einstein, J.M., and Yeo, G.W. (2020). Direct RNA sequencing enables m6A detection in endogenous transcript isoforms at base-specific resolution. RNA **26**: 19–28.

Love, M.I., Huber, W., and Anders, S. (2014). Moderated estimation of fold change and dispersion for RNA-seq data with DESeq2. Genome Biology **15**: 550.

Lu, J.-Y., Xiong, S.-X., Yin, W., Teng, X.-D., Lou, Y., Zhu, J., Zhang, C., Gu, J.-N., Wilson, Z.A., and Yang, Z.-N. (2020). MS1, a direct target of MS188, regulates the expression of key sporophytic pollen coat protein genes in Arabidopsis. Journal of Experimental Botany **71**: 4877–4889.

Lubas, M., Damgaard, C.K., Tomecki, R., Cysewski, D., Jensen, T.H., and Dziembowski, A. (2013). Exonuclease hDIS3L2 specifies an exosome-independent 3’-5’ degradation pathway of human cytoplasmic mRNA. EMBO J **32**: 1855–1868.

Ma, X., Wu, Y., and Zhang, G. (2021). Formation pattern and regulatory mechanisms of pollen wall in Arabidopsis. Journal of Plant Physiology **260**: 153388.

Maier, K.C., Gressel, S., Cramer, P., and Schwalb, B. (2020). Native molecule sequencing by nano-ID reveals synthesis and stability of RNA isoforms. Genome Res **30**: 1332–1344.

Malecki, M., Viegas, S.C., Carneiro, T., Golik, P., Dressaire, C., Ferreira, M.G., and Arraiano, C.M. (2013). The exoribonuclease Dis3L2 defines a novel eukaryotic RNA degradation pathway. The EMBO Journal **32**: 1842–1854.

Mangus, D.A., Evans, M.C., Agrin, N.S., Smith, M., Gongidi, P., and Jacobson, A. (2004). Positive and negative regulation of poly(A) nuclease. Mol Cell Biol **24**: 5521–5533.

Mangus, D.A., Evans, M.C., and Jacobson, A. (2003). Poly(A)-binding proteins: multifunctional scaffolds for the post-transcriptional control of gene expression. Genome Biol **4**: 223.

Mao, X., Schwer, B., and Shuman, S. (1995). Yeast mRNA cap methyltransferase is a 50-kilodalton protein encoded by an essential gene. Mol Cell Biol **15**: 4167–4174.

Maquat, L.E., Tarn, W.-Y., and Isken, O. (2010). The Pioneer Round of Translation: Features and Functions. Cell **142**: 368–374.

Marchese, F.P., Raimondi, I., and Huarte, M. (2017). The multidimensional mechanisms of long noncoding RNA function. Genome Biology **18**: 206.

Martin, M. (2011). Cutadapt removes adapter sequences from high-throughput sequencing reads. EMBnet.journal **17**: 10–12.

Martînez, J., Ren, Y.G., Nilsson, P., Ehrenberg, M., and Virtanen, A. (2001). The mRNA cap structure stimulates rate of poly(A) removal and amplifies processivity of degradation. J Biol Chem **276**: 27923–27929.

Marzluff, W.F., Wagner, E.J., and Duronio, R.J. (2008). Metabolism and regulation of canonical histone mRNAs: life without a poly(A) tail. Nat Rev Genet **9**: 843–854.

Mathys, H., Basquin, J., Ozgur, S., Czarnocki-Cieciura, M., Bonneau, F., Aartse, A., Dziembowski, A., Nowotny, M., Conti, E., and Filipowicz, W. (2014). Structural and Biochemical Insights to the Role of the CCR4-NOT Complex and DDX6 ATPase in MicroRNA Repression. Molecular Cell **54**: 751–765.

Matsui, H., Nomura, Y., Egusa, M., Hamada, T., Hyon, G.-S., Kaminaka, H., Watanabe, Y., Ueda, T., Trujillo, M., Shirasu, K., and Nakagami, H. (2017). The GYF domain protein PSIG1 dampens the induction of cell death during plant-pathogen interactions. PLoS Genet **13**: e1007037.

Matthews, K.R. (2005). The developmental cell biology of Trypanosoma brucei. J Cell Sci **118**: 283–290.

Mattijssen, S., Kozlov, G., Gaidamakov, S., Ranjan, A., Fonseca, B.D., Gehring, K., and Maraia, R.J. The isolated La-module of LARP1 mediates 3' poly(A) protection and mRNA stabilization, dependent on its intrinsic PAM2 binding to PABPC1. RNA Biol **18**: 275–289.

Mauer, J. et al. (2017). Reversible methylation of m6Am in the 5′ cap controls mRNA stability. Nature **541**: 371–375.

Mauxion, F., Basquin, J., Ozgur, S., Rame, M., Albrecht, J., Schäfer, I., Séraphin, B., and Conti, E. (2023). The human CNOT1-CNOT10-CNOT11 complex forms a structural platform for protein-protein interactions. Cell Rep **42**: 111902.

Mauxion, F., Faux, C., and Séraphin, B. (2008). The BTG2 protein is a general activator of mRNA deadenylation. EMBO J **27**: 1039–1048.

Mauxion, F., Prève, B., and Séraphin, B. (2013). C2ORF29/CNOT11 and CNOT10 form a new module of the CCR4-NOT complex. RNA Biol **10**: 267–276.

Maxwell, E. and Fournier, M. (1995). THE SMALL NUCLEOLAR RNAs. Annu. Rev. Biochem. **64**: 897–934.

Mayfield, J.A. and Preuss, D. (2000). Rapid initiation of Arabidopsis pollination requires the oleosin-domain protein GRP17. Nat Cell Biol **2**: 128–130.

Mayya, V.K., Flamand, M.N., Lambert, A.M., Jafarnejad, S.M., Wohlschlegel, J.A., Sonenberg, N., and Duchaine, T.F. (2021). microRNA-mediated translation repression through GYF-1 and IFE-4 in C. elegans development. Nucleic Acids Research **49**: 4803–4815.

McCracken, S., Fong, N., Rosonina, E., Yankulov, K., Brothers, G., Siderovski, D., Hessel, A., Foster, S., Program, A.E., Shuman, S., and Bentley, D.L. (1997a). 5′-Capping enzymes are targeted to pre-mRNA by binding to the phosphorylated carboxy-terminal domain of RNA polymerase II. Genes Dev **11**: 3306–3318.

McCracken, S., Fong, N., Yankulov, K., Ballantyne, S., Pan, G., Greenblatt, J., Patterson, S.D., Wickens, M., and Bentley, D.L. (1997b). The C-terminal domain of RNA polymerase II couples mRNA processing to transcription. Nature **385**: 357–361.

Melko, M., Winczura, K., Rouvière, J.O., Oborská-Oplová, M., Andersen, P.K., and Heick Jensen, T. (2020). Mapping domains of ARS2 critical for its RNA decay capacity. Nucleic Acids Research **48**: 6943–6953.

Meola, N., Domanski, M., Karadoulama, E., Chen, Y., Gentil, C., Pultz, D., Vitting-Seerup, K., Lykke-Andersen, S., Andersen, J.S., Sandelin, A., and Jensen, T.H. (2016). Identification of a Nuclear Exosome Decay Pathway for Processed Transcripts. Mol Cell **64**: 520–533.

Merret, R., Martino, L., Bousquet-Antonelli, C., Fneich, S., Descombin, J., Billey, É., Conte, M.R., and Deragon, J.-M. (2013). The association of a La module with the PABP-interacting motif PAM2 is a recurrent evolutionary process that led to the neofunctionalization of La-related proteins. RNA **19**: 36–50.

Merrick, W.C. (2015). eIF4F: A Retrospective. J Biol Chem **290**: 24091–24099.

Mitchell, P., Petfalski, E., Shevchenko, A., Mann, M., and Tollervey, D. (1997). The Exosome: A Conserved Eukaryotic RNA Processing Complex Containing Multiple 3′→5′ Exoribonucleases. Cell **91**: 457–466.

Montellese, C., Montel-Lehry, N., Henras, A.K., Kutay, U., Gleizes, P.-E., and O’Donohue, M.-F. (2017). Poly(A)-specific ribonuclease is a nuclear ribosome biogenesis factor involved in human 18S rRNA maturation. Nucleic Acids Res **45**: 6822–6836.

Moon, D.H., Segal, M., Boyraz, B., Guinan, E., Hofmann, I., Cahan, P., Tai, A.K., and Agarwal, S. (2015). Poly(A)-specific ribonuclease (PARN) mediates 3′-end maturation of the telomerase RNA component. Nat Genet **47**: 1482–1488.

Moraes, K.C.M. (2010). RNA Surveillance: Molecular Approaches in Transcript Quality Control and their Implications in Clinical Diseases. Mol Med **16**: 53–68.

Moreno, A.B., Martínez de Alba, A.E., Bardou, F., Crespi, M.D., Vaucheret, H., Maizel, A., and Mallory, A.C. (2013). Cytoplasmic and nuclear quality control and turnover of single-stranded RNA modulate post-transcriptional gene silencing in plants. Nucleic Acids Res **41**: 4699–4708.

Morgan, M. et al. (2019). A programmed wave of uridylation-primed mRNA degradation is essential for meiotic progression and mammalian spermatogenesis. Cell Res **29**: 221–232.

Morgan, M., Much, C., DiGiacomo, M., Azzi, C., Ivanova, I., Vitsios, D.M., Pistolic, J., Collier, P., Moreira, P., Benes, V., Enright, A.J., and O'Carroll, D. (2017). mRNA 3′ uridylation and poly(A) tail length sculpt the mammalian maternal transcriptome. Nature **548**: 347–351.

Mori, T., Kuroiwa, H., Higashiyama, T., and Kuroiwa, T. (2006). GENERATIVE CELL SPECIFIC 1 is essential for angiosperm fertilization. Nat Cell Biol **8**: 64–71.

Morita, M. et al. (2012). A novel 4EHP-GIGYF2 translational repressor complex is essential for mammalian development. Mol Cell Biol **32**: 3585–3593.

Morris, A.R., Mukherjee, N., and Keene, J.D. (2008). Ribonomic Analysis of Human Pum1 Reveals cis-trans Conservation across Species despite Evolution of Diverse mRNA Target Sets. Mol Cell Biol **28**: 4093–4103.

Motomura, K., Arae, T., Araki-Uramoto, H., Suzuki, Y., Takeuchi, H., Suzuki, T., Ichihashi, Y., Shibata, A., Shirasu, K., Takeda, A., Higashiyama, T., and Chiba, Y. (2020). AtNOT1 Is a Novel Regulator of Gene Expression during Pollen Development. Plant and Cell Physiology **61**: 712–721.

Muhlrad, D. and Parker, R. (1999). Recognition of Yeast mRNAs as "Nonsense Containing" Leads to Both Inhibition of mRNA Translation and mRNA Degradation: Implications for the Control of mRNA Decapping. Mol Biol Cell **10**: 3971–3978.

Narita, T., Yung, T.M.C., Yamamoto, J., Tsuboi, Y., Tanabe, H., Tanaka, K., Yamaguchi, Y., and Handa, H. (2007). NELF Interacts with CBC and Participates in 3′ End Processing of Replication-Dependent Histone mRNAs. Molecular Cell **26**: 349–365.

Narsai, R., Howell, K.A., Millar, A.H., O'Toole, N., Small, I., and Whelan, J. (2007). Genome-Wide Analysis of mRNA Decay Rates and Their Determinants in Arabidopsis thaliana. Plant Cell **19**: 3418–3436.

Nasertorabi, F., Batisse, C., Diepholz, M., Suck, D., and Böttcher, B. (2011). Insights into the structure of the CCR4-NOT complex by electron microscopy. FEBS Letters **585**: 2182–2186.

Neve, J., Patel, R., Wang, Z., Louey, A., and Furger, A.M. (2017). Cleavage and polyadenylation: Ending the message expands gene regulation. RNA Biology **14**: 865–890.

Nguema-Ona, E., Coimbra, S., Vicré-Gibouin, M., Mollet, J.-C., and Driouich, A. (2012). Arabinogalactan proteins in root and pollen-tube cells: distribution and functional aspects. Annals of Botany **110**: 383–404.

Nguyen, D., Grenier St-Sauveur, V., Bergeron, D., Dupuis-Sandoval, F., Scott, M.S., and Bachand, F. (2015). A Polyadenylation-Dependent 3' End Maturation Pathway Is Required for the Synthesis of the Human Telomerase RNA. Cell Rep **13**: 2244–2257.

Nishanth, M.J. and Simon, B. (2020). Functions, mechanisms and regulation of Pumilio/Puf family RNA binding proteins: a comprehensive review. Mol Biol Rep **47**: 785–807.

Nishikawa, M. et al. (2023). Interaction of EXA1 and eIF4E Family Members Facilitates Potexvirus Infection in Arabidopsis thaliana. Journal of Virology **97**: e00221-23.

Nissan, T., Rajyaguru, P., She, M., Song, H., and Parker, R. (2010). Decapping activators in Saccharomyces cerevisiae act by multiple mechanisms. Mol Cell **39**: 773–783.

Niu, S., Shingle, D.L., Garbarino-Pico, E., Kojima, S., Gilbert, M., and Green, C.B. (2011). The circadian deadenylase Nocturnin is necessary for stabilization of the iNOS mRNA in mice. PLoS One **6**: e26954.

Nogueira Júnior, A.F., Tränkner, M., Ribeiro, R.V., von Tiedemann, A., and Amorim, L. (2020). Photosynthetic Cost Associated With Induced Defense to Plasmopara viticola in Grapevine. Frontiers in Plant Science **11**.

Nourse, J., Spada, S., and Danckwardt, S. (2020). Emerging Roles of RNA 3′-end Cleavage and Polyadenylation in Pathogenesis, Diagnosis and Therapy of Human Disorders. Biomolecules **10**: 915.

Ogami, K. et al. (2022). mTOR- and LARP1-dependent regulation of TOP mRNA poly(A) tail and ribosome loading. Cell Rep **41**: 111548.

Ogami, K., Richard, P., Chen, Y., Hoque, M., Li, W., Moresco, J.J., Yates, J.R., Tian, B., and Manley, J.L. (2017). An Mtr4/ZFC3H1 complex facilitates turnover of unstable nuclear RNAs to prevent their cytoplasmic transport and global translational repression. Genes Dev. **31**: 1257–1271.

Oh, J.T.P.& S. (2022). The translational landscape as regulated by the RNA helicase DDX3. BMB Reports **55**: 125–135.

Olivas, W. and Parker, R. (2000). The Puf3 protein is a transcript-specific regulator of mRNA degradation in yeast. EMBO J **19**: 6602–6611.

Ostareck, D.H., Naarmann-de Vries, I.S., and Ostareck-Lederer, A. (2014). DDX6 and its orthologs as modulators of cellular and viral RNA expression. Wiley Interdiscip Rev RNA **5**: 659–678.

Otsuka, K. et al. Temperature-dependent fasciation mutants provide a link between mitochondrial RNA processing and lateral root morphogenesis. eLife **10**: e61611.

Ozturk, S. (2019). The translational functions of embryonic poly(A)-binding protein during gametogenesis and early embryo development. Molecular Reproduction and Development **86**: 1548–1560.

Park, J., Kim, M., Yi, H., Baeg, K., Choi, Y., Lee, Y., Lim, J., and Kim, V.N. (2023). Short poly(A) tails are protected from deadenylation by the LARP1–PABP complex. Nat Struct Mol Biol **30**: 330–338.

Park, J.T. and Oh, S. (2022). The translational landscape as regulated by the RNA helicase DDX3. BMB Rep **55**: 125–135.

Parker, M.T., Knop, K., Sherwood, A.V., Schurch, N.J., Mackinnon, K., Gould, P.D., Hall, A.J., Barton, G.J., and Simpson, G.G. (2020). Nanopore direct RNA sequencing maps the complexity of Arabidopsis mRNA processing and m6A modification. eLife **9**: e49658.

Parker, R. and Song, H. (2004). The enzymes and control of eukaryotic mRNA turnover. Nat Struct Mol Biol **11**: 121–127.

Passmore, L.A. and Coller, J. (2022). Roles of mRNA poly(A) tails in regulation of eukaryotic gene expression. Nat Rev Mol Cell Biol **23**: 93–106.

Patrick, R.M. and Browning, K.S. (2012). The eIF4F and eIFiso4F Complexes of Plants: An Evolutionary Perspective. International Journal of Genomics **2012**: e287814.

Pavanello, L., Hall, M., and Winkler, G.S. (2023). Regulation of eukaryotic mRNA deadenylation and degradation by the Ccr4-Not complex. Frontiers in Cell and Developmental Biology **11**.

Pavlopoulou, A., Vlachakis, D., Balatsos, N.A.A., and Kossida, S. (2013). A Comprehensive Phylogenetic Analysis of Deadenylases. Evol Bioinform Online **9**: 491–497.

Pearce, S.F., Rorbach, J., Van Haute, L., D'Souza, A.R., Rebelo-Guiomar, P., Powell, C.A., Brierley, I., Firth, A.E., and Minczuk, M. (2017). Maturation of selected human mitochondrial tRNAs requires deadenylation. Elife **6**: e27596.

Pekovic, F., Rammelt, C., Kubíková, J., Metz, J., Jeske, M., and Wahle, E. (2023). RNA binding proteins Smaug and Cup induce CCR4–NOT-dependent deadenylation of the nanos mRNA in a reconstituted system. Nucleic Acids Research **51**: 3950–3970.

Pelechano, V., Wei, W., and Steinmetz, L.M. (2015). Widespread Co-translational RNA Decay Reveals Ribosome Dynamics. Cell **161**: 1400–1412.

Peng, W., Togawa, C., Zhang, K., and Kurdistani, S.K. (2008). Regulators of Cellular Levels of Histone Acetylation in Saccharomyces cerevisiae. Genetics **179**: 277.

Pereira, P.A., Boavida, L.C., Santos, M.R., and Becker, J.D. (2020). AtNOT1 is required for gametophyte development in Arabidopsis. The Plant Journal **103**: 1289–1303.

Perry, K.L., Watkins, K.P., and Agabian, N. (1987). Trypanosome mRNAs have unusual "cap 4" structures acquired by addition of a spliced leader. Proc Natl Acad Sci U S A **84**: 8190–8194.

Peter, D., Ruscica, V., Bawankar, P., Weber, R., Helms, S., Valkov, E., Igreja, C., and Izaurralde, E. (2019). Molecular basis for GIGYF–Me31B complex assembly in 4EHP-mediated translational repression. Genes Dev **33**: 1355–1360.

Peter, D., Weber, R., Sandmeir, F., Wohlbold, L., Helms, S., Bawankar, P., Valkov, E., Igreja, C., and Izaurralde, E. (2017). GIGYF1/2 proteins use auxiliary sequences to selectively bind to 4EHP and repress target mRNA expression. Genes Dev. **31**: 1147–1161.

Petit, A.-P., Wohlbold, L., Bawankar, P., Huntzinger, E., Schmidt, S., Izaurralde, E., and Weichenrieder, O. (2012). The structural basis for the interaction between the CAF1 nuclease and the NOT1 scaffold of the human CCR4-NOT deadenylase complex. Nucleic Acids Res **40**: 11058–11072.

Pinto, P.H., Kroupova, A., Schleiffer, A., Mechtler, K., Jinek, M., Weitzer, S., and Martinez, J. (2020). ANGEL2 is a member of the CCR4 family of deadenylases with 2′,3′-cyclic phosphatase activity. Science **369**: 524–530.

Pirouz, M., Du, P., Munafò, M., and Gregory, R.I. (2016). Dis3l2-Mediated Decay Is a Quality Control Pathway for Noncoding RNAs. Cell Rep **16**: 1861–1873.

Pirouz, M., Munafò, M., Ebrahimi, A.G., Choe, J., and Gregory, R.I. (2019). Exonuclease requirements for mammalian ribosomal RNA biogenesis and surveillance. Nat Struct Mol Biol **26**: 490–500.

Pirouz, M., Wang, C.-H., Liu, Q., Ebrahimi, A.G., Shamsi, F., Tseng, Y.-H., and Gregory, R.I. (2020). The Perlman syndrome DIS3L2 exoribonuclease safeguards endoplasmic reticulum-targeted mRNA translation and calcium ion homeostasis. Nat Commun **11**: 2619.

Poetz, F., Corbo, J., Levdansky, Y., Spiegelhalter, A., Lindner, D., Magg, V., Lebedeva, S., Schweiggert, J., Schott, J., Valkov, E., and Stoecklin, G. (2021). RNF219 attenuates global mRNA decay through inhibition of CCR4-NOT complex-mediated deadenylation. Nat Commun **12**: 7175.

Popp, M.W. and Maquat, L.E. (2016). Leveraging Rules of Nonsense-Mediated mRNA Decay for Genome Engineering and Personalized Medicine. Cell **165**: 1319–1322.

Rafinska, K., Zienkiewicz, K., and Bednarska, E. (2010). Pollen Transcriptome and Proteome: Molecular and Functional Analysis. Medical Journal of Cell Biology **2**: 29–57.

Raisch, T., Bhandari, D., Sabath, K., Helms, S., Valkov, E., Weichenrieder, O., and Izaurralde, E. (2016). Distinct modes of recruitment of the CCR4–NOT complex by Drosophila and vertebrate Nanos. The EMBO Journal **35**: 974–990.

Raisch, T., Chang, C.-T., Levdansky, Y., Muthukumar, S., Raunser, S., and Valkov, E. (2019). Reconstitution of recombinant human CCR4-NOT reveals molecular insights into regulated deadenylation. Nat Commun **10**: 3173.

Raisch, T. and Valkov, E. (2022). Regulation of the multisubunit CCR4-NOT deadenylase in the initiation of mRNA degradation. Current Opinion in Structural Biology **77**: 102460.

Ramanathan, A., Robb, G.B., and Chan, S.-H. (2016). mRNA capping: biological functions and applications. Nucleic Acids Research **44**: 7511–7526.

Rambout, X. and Maquat, L.E. (2021). NCBP3: A Multifaceted Adaptive Regulator of Gene Expression. Trends Biochem Sci **46**: 87–96.

Rao, M.N., Chernokalskaya, E., and Schoenberg, D.R. (1996). Regulated nuclear polyadenylation of Xenopus albumin pre-mRNA. Nucleic Acids Res **24**: 4078–4083.

Regan, S. and Moffatt, B. (1990). Cytochemical Analysis of Pollen Development in Wild-Type Arabidopsis and a Male-Sterile Mutant. Plant Cell **2**: 877–889.

Reijns, M.A.M., Alexander, R.D., Spiller, M.P., and Beggs, J.D. (2008). A role for Q/N-rich aggregation-prone regions in P-body localization. J Cell Sci **121**: 2463–2472.

Reimão-Pinto, M.M., Manzenreither, R.A., Burkard, T.R., Sledz, P., Jinek, M., Mechtler, K., and Ameres, S.L. (2016). Molecular basis for cytoplasmic RNA surveillance by uridylation-triggered decay in Drosophila. The EMBO Journal **35**: 2417–2434.

Ren, G., Chen, X., and Yu, B. (2012). Uridylation of miRNAs by hen1 suppressor1 in Arabidopsis. Curr Biol **22**: 695–700.

Ren, G., Xie, M., Zhang, S., Vinovskis, C., Chen, X., and Yu, B. (2014). Methylation protects microRNAs from an AGO1-associated activity that uridylates 5' RNA fragments generated by AGO1 cleavage. Proc Natl Acad Sci U S A **111**: 6365–6370.

Reverdatto, S.V., Dutko, J.A., Chekanova, J.A., Hamilton, D.A., and Belostotsky, D.A. (2004). mRNA deadenylation by PARN is essential for embryogenesis in higher plants. RNA **10**: 1200–1214.

Rissland, O.S. and Norbury, C.J. (2009). Decapping is preceded by 3' uridylation in a novel pathway of bulk mRNA turnover. Nat Struct Mol Biol **16**: 616–623.

Robinson, M.D., McCarthy, D.J., and Smyth, G.K. (2010). edgeR: a Bioconductor package for differential expression analysis of digital gene expression data. Bioinformatics **26**: 139–140.

Rorbach, J., Nicholls, T.J.J., and Minczuk, M. (2011). PDE12 removes mitochondrial RNA poly(A) tails and controls translation in human mitochondria. Nucleic Acids Res **39**: 7750–7763.

Roy, B. and Jacobson, A. (2013). The intimate relationships of mRNA decay and translation. Trends Genet **29**: 10.1016/j.tig.2013.09.002.

Ruscica, V., Bawankar, P., Peter, D., Helms, S., Igreja, C., and Izaurralde, E. (2019). Direct role for the Drosophila GIGYF protein in 4EHP-mediated mRNA repression. Nucleic Acids Res **47**: 7035–7048.

RYAN, K., CALVO, O., and MANLEY, J.L. (2004). Evidence that polyadenylation factor CPSF-73 is the mRNA 3′ processing endonuclease. RNA **10**: 565–573.

Sachs, A.B. and Davis, R.W. (1989). The poly(A) binding protein is required for poly(A) shortening and 60S ribosomal subunit-dependent translation initiation. Cell **58**: 857–867.

Sachs, A.B., Davis, R.W., and Kornberg, R.D. (1987). A single domain of yeast poly(A)-binding protein is necessary and sufficient for RNA binding and cell viability. Mol Cell Biol **7**: 3268–3276.

Safaee, N., Kozlov, G., Noronha, A.M., Xie, J., Wilds, C.J., and Gehring, K. (2012). Interdomain Allostery Promotes Assembly of the Poly(A) mRNA Complex with PABP and eIF4G. Molecular Cell **48**: 375–386.

Saha, N., Schwer, B., and Shuman, S. (1999). Characterization of Human, Schizosaccharomyces pombe, and Candida albicans mRNA Cap Methyltransferases and Complete Replacement of the Yeast Capping Apparatus by Mammalian Enzymes *. Journal of Biological Chemistry **274**: 16553–16562.

Sallés, F.J. and Strickland, S. (1995). Rapid and sensitive analysis of mRNA polyadenylation states by PCR. PCR Methods Appl **4**: 317–321.

Sanders, P.M., Bui, A.Q., Weterings, K., McIntire, K.N., Hsu, Y.-C., Lee, P.Y., Truong, M.T., Beals, T.P., and Goldberg, R.B. (1999). Anther developmental defects in Arabidopsis thaliana male-sterile mutants. Sex Plant Reprod **11**: 297–322.

Sawazaki, R., Imai, S., Yokogawa, M., Hosoda, N., Hoshino, S., Mio, M., Mio, K., Shimada, I., and Osawa, M. (2018). Characterization of the multimeric structure of poly(A)-binding protein on a poly(A) tail. Sci Rep **8**: 1455.

Schäfer, I.B., Rode, M., Bonneau, F., Schüssler, S., and Conti, E. (2014). The structure of the Pan2-Pan3 core complex reveals cross-talk between deadenylase and pseudokinase. Nat Struct Mol Biol **21**: 591–598.

Schäfer, I.B., Yamashita, M., Schuller, J.M., Schüssler, S., Reichelt, P., Strauss, M., and Conti, E. (2019). Molecular Basis for poly(A) RNP Architecture and Recognition by the Pan2-Pan3 Deadenylase. Cell **177**: 1619-1631.e21.

Scheer, H. (2018) Rôle complexe de l'uridylation dans le métabolisme des ARNm chez *Arabidopsis thaliana* (doctoral dissertation). University of Strasbourg, Strasbourg, France.

Scheer, H. et al. (2021). The TUTase URT1 connects decapping activators and prevents the accumulation of excessively deadenylated mRNAs to avoid siRNA biogenesis. Nat Commun **12**: 1298.

Schwede, A., Ellis, L., Luther, J., Carrington, M., Stoecklin, G., and Clayton, C. (2008). A role for Caf1 in mRNA deadenylation and decay in trypanosomes and human cells. Nucleic Acids Res **36**: 3374–3388.

Schwenk, P., Sheerin, D.J., Ponnu, J., Staudt, A.-M., Lesch, K.L., Lichtenberg, E., Medzihradszky, K.F., Hoecker, U., Klement, E., Viczián, A., and Hiltbrunner, A. (2021). Uncovering a novel function of the CCR4-NOT complex in phytochrome A-mediated light signalling in plants. eLife **10**: e63697.

Sement, F.M., Ferrier, E., Zuber, H., Merret, R., Alioua, M., Deragon, J.-M., Bousquet-Antonelli, C., Lange, H., and Gagliardi, D. (2013). Uridylation prevents 3′ trimming of oligoadenylated mRNAs. Nucleic Acids Research **41**: 7115–7127.

Sha, Q. et al. (2018). CNOT6L couples the selective degradation of maternal transcripts to meiotic cell cycle progression in mouse oocyte. EMBO J **37**: e99333.

Shirai, Y.-T., Suzuki, T., Morita, M., Takahashi, A., and Yamamoto, T. (2014). Multifunctional roles of the mammalian CCR4–NOT complex in physiological phenomena. Frontiers in Genetics **5**.

Shoemaker, C.J. and Green, R. (2012). Translation drives mRNA quality control. Nat Struct Mol Biol **19**: 594–601.

Shukla, S. and Parker, R. (2017). PARN Modulates Y RNA Stability and Its 3′-End Formation. Molecular and Cellular Biology **37**: e00264-17.

Shukla, S., Schmidt, J.C., Goldfarb, K.C., Cech, T.R., and Parker, R. (2016). Inhibition of telomerase RNA decay rescues telomerase deficiency caused by dyskerin or PARN defects. Nat Struct Mol Biol **23**: 286–292.

Sikorska, N., Zuber, H., Gobert, A., Lange, H., and Gagliardi, D. (2017). RNA degradation by the plant RNA exosome involves both phosphorolytic and hydrolytic activities. Nat Commun **8**: 2162.

Sippel, A.E., Stavrianopoulos, J.G., Schutz, G., and Feigelson, P. (1974). Translational Properties of Rabbit Globin mRNA after Specific Removal of Poly(A) with Ribonuclease H. Proc Natl Acad Sci U S A **71**: 4635–4639.

Skuzeski, J.M., Lund, E., Murphy, J.T., Steinberg, T.H., Burgess, R.R., and Dahlberg, J.E. (1984). Synthesis of human U1 RNA. II. Identification of two regions of the promoter essential for transcription initiation at position +1. Journal of Biological Chemistry **259**: 8345–8352.

Sladic, R.T., Lagnado, C.A., Bagley, C.J., and Goodall, G.J. (2004). Human PABP binds AU-rich RNA via RNA-binding domains 3 and 4. Eur J Biochem **271**: 450–457.

Smith, B.L., Gallie, D.R., Le, H., and Hansma, P.K. (1997). Visualization of poly(A)-binding protein complex formation with poly(A) RNA using atomic force microscopy. J Struct Biol **119**: 109–117.

Smith, R.W.P., Blee, T.K.P., and Gray, N.K. (2014). Poly(A)-binding proteins are required for diverse biological processes in metazoans. Biochem Soc Trans **42**: 1229–1237.

Smyth, D.R., Bowman, J.L., and Meyerowitz, E.M. (1990). Early flower development in Arabidopsis. The Plant Cell **2**: 755–767.

Son, A., Park, J.-E., and Kim, V.N. (2018). PARN and TOE1 Constitute a 3′ End Maturation Module for Nuclear Non-coding RNAs. Cell Reports **23**: 888–898.

Song, M.-G. and Kiledjian, M. (2007). 3’ Terminal oligo U-tract-mediated stimulation of decapping. RNA **13**: 2356–2365.

Sorenson, R.S., Deshotel, M.J., Johnson, K., Adler, F.R., and Sieburth, L.E. (2018). Arabidopsis mRNA decay landscape arises from specialized RNA decay substrates, decapping-mediated feedback, and redundancy. Proceedings of the National Academy of Sciences **115**: E1485–E1494.

Staals, R.H.J., Bronkhorst, A.W., Schilders, G., Slomovic, S., Schuster, G., Heck, A.J.R., Raijmakers, R., and Pruijn, G.J.M. (2010). Dis3-like 1: a novel exoribonuclease associated with the human exosome. EMBO J **29**: 2358–2367.

Stewart, M. (2019). Polyadenylation and nuclear export of mRNAs. Journal of Biological Chemistry **294**: 2977–2987.

Stoney, P.N., Yanagiya, A., Nishijima, S., and Yamamoto, T. (2022). CNOT7 Outcompetes Its Paralog CNOT8 for Integration into The CCR4-NOT Complex. Journal of Molecular Biology **434**: 167523.

Struhl, K. (2007). Transcriptional noise and the fidelity of initiation by RNA polymerase II. Nat Struct Mol Biol **14**: 103–105.

Stupfler, B., Birck, C., Séraphin, B., and Mauxion, F. (2016). BTG2 bridges PABPC1 RNA-binding domains and CAF1 deadenylase to control cell proliferation. Nat Commun **7**: 10811.

Subtelny, A.O., Eichhorn, S.W., Chen, G.R., Sive, H., and Bartel, D.P. (2014). Poly(A)-tail profiling reveals an embryonic switch in translational control. Nature **508**: 66–71.

Sun, H., Li, K., Zhang, X., Liu, J., Zhang, M., Meng, H., and Yi, C. (2021). m6Am-seq reveals the dynamic m6Am methylation in the human transcriptome. Nat Commun **12**: 4778.

Suzuki, T., Tsunekawa, S., Koizuka, C., Yamamoto, K., Imamura, J., Nakamura, K., and Ishiguro, S. (2013). Development and disintegration of tapetum-specific lipid-accumulating organelles, elaioplasts and tapetosomes, in Arabidopsis thaliana and Brassica napus. Plant Science **207**: 25–36.

Suzuki, Y., Arae, T., Green, P.J., Yamaguchi, J., and Chiba, Y. (2015). AtCCR4a and AtCCR4b are Involved in Determining the Poly(A) Length of Granule-bound starch synthase 1 Transcript and Modulating Sucrose and Starch Metabolism in Arabidopsis thaliana. Plant Cell Physiol **56**: 863–874.

Szabo, E.X., Reichert, P., Lehniger, M.-K., Ohmer, M., de Francisco Amorim, M., Gowik, U., Schmitz-Linneweber, C., and Laubinger, S. (2020). Metabolic Labeling of RNAs Uncovers Hidden Features and Dynamics of the Arabidopsis Transcriptome[CC-BY]. The Plant Cell **32**: 871–887.

Tam, P.P., Barrette-Ng, I.H., Simon, D.M., Tam, M.W., Ang, A.L., and Muench, D.G. (2010). The Puf family of RNA-binding proteins in plants: phylogeny, structural modeling, activity and subcellular localization. BMC Plant Biol **10**: 44.

Tamura, K., Stecher, G., and Kumar, S. (2021). MEGA11: Molecular Evolutionary Genetics Analysis Version 11. Mol Biol Evol **38**: 3022–3027.

Tang, T.T., Stowell, J.A., Hill, C.H., and Passmore, L.A. (2019). The intrinsic structure of poly(A) RNA determines the specificity of Pan2 and Caf1 deadenylases. Nat Struct Mol Biol **26**: 433–442.

Tang, T.T.L. and Passmore, L.A. (2019). Recognition of Poly(A) RNA through Its Intrinsic Helical Structure. Cold Spring Harb Symp Quant Biol **84**: 21–30.

Temme, C., Zhang, L., Kremmer, E., Ihling, C., Chartier, A., Sinz, A., Simonelig, M., and Wahle, E. (2010). Subunits of the Drosophila CCR4-NOT complex and their roles in mRNA deadenylation. RNA **16**: 1356–1370.

Tharun, S., He, W., Mayes, A.E., Lennertz, P., Beggs, J.D., and Parker, R. (2000). Yeast Sm-like proteins function in mRNA decapping and decay. Nature **404**: 515–518.

Thomas, M.P., Liu, X., Whangbo, J., McCrossan, G., Sanborn, K.B., Basar, E., Walch, M., and Lieberman, J. (2015). Apoptosis Triggers Specific, Rapid, and Global mRNA Decay with 3’ Uridylated Intermediates Degraded by DIS3L2. Cell Rep **11**: 1079–1089.

Tian, B. and Manley, J.L. (2017). Alternative polyadenylation of mRNA precursors. Nat Rev Mol Cell Biol **18**: 18–30.

Tian, G.-W., Chen, M.-H., Zaltsman, A., and Citovsky, V. (2006). Pollen-specific pectin methylesterase involved in pollen tube growth. Developmental Biology **294**: 83–91.

Tomecki, R., Kristiansen, M.S., Lykke-Andersen, S., Chlebowski, A., Larsen, K.M., Szczesny, R.J., Drazkowska, K., Pastula, A., Andersen, J.S., Stepien, P.P., Dziembowski, A., and Jensen, T.H. (2010). The human core exosome interacts with differentially localized processive RNases: hDIS3 and hDIS3L. EMBO J **29**: 2342–2357.

Tran, E.J., Zhou, Y., Corbett, A.H., and Wente, S.R. (2007). The DEAD-box protein Dbp5 controls mRNA export by triggering specific RNA:protein remodeling events. Mol Cell **28**: 850–859.

Tseng, C.-K., Wang, H.-F., Burns, A.M., Schroeder, M.R., Gaspari, M., and Baumann, P. (2015). Human Telomerase RNA Processing and Quality Control. Cell Reports **13**: 2232–2243.

Tseng, C.-K., Wang, H.-F., Schroeder, M.R., and Baumann, P. (2018). The H/ACA complex disrupts triplex in hTR precursor to permit processing by RRP6 and PARN. Nat Commun **9**: 5430.

Tsukamoto, T., Shibagaki, Y., Murakoshi, T., Suzuki, M., Nakamura, A., Gotoh, H., and Mizumoto, K. (1998). Cloning and Characterization of Two Human cDNAs Encoding the mRNA Capping Enzyme. Biochemical and Biophysical Research Communications **243**: 101–108.

Tu, B. et al. (2015). Distinct and Cooperative Activities of HESO1 and URT1 Nucleotidyl Transferases in MicroRNA Turnover in Arabidopsis. PLOS Genetics **11**: e1005119.

Tuck, A.C., Rankova, A., Arpat, A.B., Liechti, L.A., Hess, D., Iesmantavicius, V., Castelo-Szekely, V., Gatfield, D., and Bühler, M. (2020). Mammalian RNA Decay Pathways Are Highly Specialized and Widely Linked to Translation. Molecular Cell **77**: 1222-1236.e13.

Tucker, M., Staples, R.R., Valencia-Sanchez, M.A., Muhlrad, D., and Parker, R. (2002). Ccr4p is the catalytic subunit of a Ccr4p/Pop2p/Notp mRNA deadenylase complex in Saccharomyces cerevisiae. EMBO J **21**: 1427–1436.

Tucker, M., Valencia-Sanchez, M.A., Staples, R.R., Chen, J., Denis, C.L., and Parker, R. (2001). The transcription factor associated Ccr4 and Caf1 proteins are components of the major cytoplasmic mRNA deadenylase in Saccharomyces cerevisiae. Cell **104**: 377–386.

Tudek, A., Krawczyk, P.S., Mroczek, S., Tomecki, R., Turtola, M., Matylla-Kulińska, K., Jensen, T.H., and Dziembowski, A. (2021). Global view on the metabolism of RNA poly(A) tails in yeast Saccharomyces cerevisiae. Nat Commun **12**: 4951.

Twell, D., Oh, S.-A., and Honys, D. (2006). Pollen Development, a Genetic and Transcriptomic View. In The Pollen Tube: A Cellular and Molecular Perspective, R. Malhó, ed, Plant Cell Monographs. (Springer: Berlin, Heidelberg), pp. 15–45.

Ukleja, M., Cuellar, J., Siwaszek, A., Kasprzak, J.M., Czarnocki-Cieciura, M., Bujnicki, J.M., Dziembowski, A., and M. Valpuesta, J. (2016). The architecture of the Schizosaccharomyces pombe CCR4-NOT complex. Nat Commun **7**: 10433.

Updegraff, E.P., Zhao, F., and Preuss, D. (2009). The extracellular lipase EXL4 is required for efficient hydration of Arabidopsis pollen. Sex Plant Reprod **22**: 197–204.

Ustianenko, D., Pasulka, J., Feketova, Z., Bednarik, L., Zigackova, D., Fortova, A., Zavolan, M., and Vanacova, S. (2016). TUT-DIS3L2 is a mammalian surveillance pathway for aberrant structured non-coding RNAs. The EMBO Journal **35**: 2179–2191.

Vidya, E. and Duchaine, T.F. (2022). Eukaryotic mRNA Decapping Activation. Frontiers in Genetics **13**.

Viegas, I.J., de Macedo, J.P., Serra, L., De Niz, M., Temporão, A., Silva Pereira, S., Mirza, A.H., Bergstrom, E., Rodrigues, J.A., Aresta-Branco, F., Jaffrey, S.R., and Figueiredo, L.M. (2022). N6-methyladenosine in poly(A) tails stabilize VSG transcripts. Nature **604**: 362–370.

Viswanathan, P., Chen, J., Chiang, Y.-C., and Denis, C.L. (2003). Identification of Multiple RNA Features That Influence CCR4 Deadenylation Activity*. Journal of Biological Chemistry **278**: 14949–14955.

Viswanathan, P., Ohn, T., Chiang, Y.-C., Chen, J., and Denis, C.L. (2004). Mouse CAF1 can function as a processive deadenylase/3’-5’-exonuclease in vitro but in yeast the deadenylase function of CAF1 is not required for mRNA poly(A) removal. J Biol Chem **279**: 23988–23995.

Wagner, E., Clement, S.L., and Lykke-Andersen, J. (2007). An Unconventional Human Ccr4-Caf1 Deadenylase Complex in Nuclear Cajal Bodies. Mol Cell Biol **27**: 1686–1695.

Wahle, E. and Winkler, G.S. (2013). RNA decay machines: Deadenylation by the Ccr4–Not and Pan2–Pan3 complexes. Biochimica et Biophysica Acta (BBA) - Gene Regulatory Mechanisms **1829**: 561–570.

Walley, J.W., Kelley, D.R., Savchenko, T., and Dehesh, K. (2010). Investigating the function of CAF1 deadenylases during plant stress responses. Plant Signaling & Behavior **5**: 802–805.

Walters, R.W., Matheny, T., Mizoue, L.S., Rao, B.S., Muhlrad, D., and Parker, R. (2017). Identification of NAD+ capped mRNAs in Saccharomyces cerevisiae. Proc Natl Acad Sci U S A **114**: 480–485.

Wang, F., Johnson, N.R., Coruh, C., and Axtell, M.J. (2016). Genome-wide analysis of single non-templated nucleotides in plant endogenous siRNAs and miRNAs. Nucleic Acids Research **44**: 7395–7405.

Wang, J., Zhang, X., Greene, G.H., Xu, G., and Dong, X. (2022). PABP/purine-rich motif as an initiation module for cap-independent translation in pattern-triggered immunity. Cell **185**: 3186-3200.e17.

Wang, L., Li, H., Lei, Z., Jeong, D.-H., and Cho, J. (2024). The CARBON CATABOLITE REPRESSION 4A-mediated RNA deadenylation pathway acts on the transposon RNAs that are not regulated by small RNAs. New Phytologist **241**: 1636–1645.

Wang, L., Song, X., Gu, L., Li, X., Cao, S., Chu, C., Cui, X., Chen, X., and Cao, X. (2013). NOT2 Proteins Promote Polymerase II–Dependent Transcription and Interact with Multiple MicroRNA Biogenesis Factors in Arabidopsis. The Plant Cell **25**: 715–727.

Wang, Y., Li, S., Zhao, Y., You, C., Le, B., Gong, Z., Mo, B., Xia, Y., and Chen, X. (2019). NAD+-capped RNAs are widespread in the Arabidopsis transcriptome and can probably be translated. Proc Natl Acad Sci U S A **116**: 12094–12102.

Wang, Z., Day, N., Trifillis, P., and Kiledjian, M. (1999). An mRNA stability complex functions with poly(A)-binding protein to stabilize mRNA in vitro. Mol Cell Biol **19**: 4552–4560.

Weber, R., Chung, M.-Y., Keskeny, C., Zinnall, U., Landthaler, M., Valkov, E., Izaurralde, E., and Igreja, C. (2020). 4EHP and GIGYF1/2 Mediate Translation-Coupled Messenger RNA Decay. Cell Reports **33**: 108262.

Webster, M.W., Chen, Y.-H., Stowell, J.A.W., Alhusaini, N., Sweet, T., Graveley, B.R., Coller, J., and Passmore, L.A. (2018). mRNA Deadenylation Is Coupled to Translation Rates by the Differential Activities of Ccr4-Not Nucleases. Mol Cell **70**: 1089-1100.e8.

Webster, M.W., Stowell, J.A., and Passmore, L.A. (2019). RNA-binding proteins distinguish between similar sequence motifs to promote targeted deadenylation by Ccr4-Not. eLife **8**: e40670.

Wei, S. and Ma, L. (2023). Comprehensive Insight into Tapetum-Mediated Pollen Development in Arabidopsis thaliana. Cells **12**: 247.

Wenger, A.M. et al. (2019). Accurate circular consensus long-read sequencing improves variant detection and assembly of a human genome. Nat Biotechnol **37**: 1155–1162.

Werner, M., Purta, E., Kaminska, K.H., Cymerman, I.A., Campbell, D.A., Mittra, B., Zamudio, J.R., Sturm, N.R., Jaworski, J., and Bujnicki, J.M. (2011). 2'-O-ribose methylation of cap2 in human: function and evolution in a horizontally mobile family. Nucleic Acids Res **39**: 4756–4768.

van Wersch, R., Li, X., and Zhang, Y. (2016). Mighty Dwarfs: Arabidopsis Autoimmune Mutants and Their Usages in Genetic Dissection of Plant Immunity. Frontiers in Plant Science **7**.

Winkler, G. and Balacco, D. (2013). Heterogeneity and complexity within the nuclease module of the Ccr4-Not complex. Frontiers in Genetics **4**.

Winkler, G.S., Mulder, K.W., Bardwell, V.J., Kalkhoven, E., and Timmers, H.T.M. (2006). Human Ccr4-Not complex is a ligand-dependent repressor of nuclear receptor-mediated transcription. The EMBO Journal **25**: 3089–3099.

Wolf, J. and Passmore, L.A. (2014). mRNA deadenylation by Pan2–Pan3. Biochemical Society Transactions **42**: 184–187.

Wormit, A. and Usadel, B. (2018). The Multifaceted Role of Pectin Methylesterase Inhibitors (PMEIs). International Journal of Molecular Sciences **19**: 2878.

Wu, D., Pedroza, M., Chang, J., and Dean, J. (2023). DIS3L2 ribonuclease degrades terminal-uridylated RNA to ensure oocyte maturation and female fertility. Nucleic Acids Research **51**: 3078–3093.

Wu, M., Reuter, M., Lilie, H., Liu, Y., Wahle, E., and Song, H. (2005). Structural insight into poly(A) binding and catalytic mechanism of human PARN. EMBO J **24**: 4082–4093.

Wu, Z., Huang, S., Zhang, X., Wu, D., Xia, S., and Li, X. (2017). Regulation of plant immune receptor accumulation through translational repression by a glycine-tyrosine-phenylalanine (GYF) domain protein. eLife **6**: e23684.

Xiang, K. and Bartel, D.P. (2021). The molecular basis of coupling between poly(A)-tail length and translational efficiency. eLife **10**: e66493.

Xiao, C. et al. (2023). Arabidopsis DXO1 activates RNMT1 to methylate the mRNA guanosine cap. Nat Commun **14**: 202.

Xie, J., Kozlov, G., and Gehring, K. (2014). The “tale” of poly(A) binding protein: The MLLE domain and PAM2-containing proteins. Biochimica et Biophysica Acta (BBA) - Gene Regulatory Mechanisms **1839**: 1062–1068.

Xie, Y. and Ren, Y. (2019). Mechanisms of nuclear mRNA export: A structural perspective. Traffic **20**: 829–840.

Xu, J. and Chua, N.-H. (2011). Processing bodies and plant development. Curr Opin Plant Biol **14**: 88–93.

Xu, J., Yang, J.-Y., Niu, Q.-W., and Chua, N.-H. (2006). Arabidopsis DCP2, DCP1, and VARICOSE Form a Decapping Complex Required for Postembryonic Development. Plant Cell **18**: 3386–3398.

Yamada-Okabe, T., Doi, R., Shimmi, O., Arisawa, M., and Yamada-Okabe, H. (1998). Isolation and characterization of a human cDNA for mRNA 5′-capping enzyme. Nucleic Acids Research **26**: 1700–1706.

Yamashita, A., Chang, T.-C., Yamashita, Y., Zhu, W., Zhong, Z., Chen, C.-Y.A., and Shyu, A.-B. (2005). Concerted action of poly(A) nucleases and decapping enzyme in mammalian mRNA turnover. Nat Struct Mol Biol **12**: 1054–1063.

Yang, J., Cao, Y., and Ma, L. (2021). Co-Transcriptional RNA Processing in Plants: Exploring from the Perspective of Polyadenylation. International Journal of Molecular Sciences **22**: 3300.

Yang, R., Gaidamakov, S.A., Xie, J., Lee, J., Martino, L., Kozlov, G., Crawford, A.K., Russo, A.N., Conte, M.R., Gehring, K., and Maraia, R.J. (2011). La-Related Protein 4 Binds Poly(A), Interacts with the Poly(A)-Binding Protein MLLE Domain via a Variant PAM2w Motif, and Can Promote mRNA Stability. Molecular and Cellular Biology **31**: 542–556.

Yang, Y., Dong, C., Yu, J., Shi, L., Tong, C., Li, Z., Huang, J., and Liu, S. (2014). Cysteine Protease 51 (CP51), an anther-specific cysteine protease gene, is essential for pollen exine formation in Arabidopsis. Plant Cell Tiss Organ Cult **119**: 383–397.

Yi, H., Park, J., Ha, M., Lim, J., Chang, H., and Kim, V.N. (2018). PABP Cooperates with the CCR4-NOT Complex to Promote mRNA Deadenylation and Block Precocious Decay. Molecular Cell **70**: 1081-1088.e5.

Yoda, M., Cifuentes, D., Izumi, N., Sakaguchi, Y., Suzuki, T., Giraldez, A.J., and Tomari, Y. (2013). Poly(A)-Specific Ribonuclease Mediates 3′-End Trimming of Argonaute2-Cleaved Precursor MicroRNAs. Cell Reports **5**: 715–726.

Yu, G., Wang, L.-G., Han, Y., and He, Q.-Y. (2012). clusterProfiler: an R package for comparing biological themes among gene clusters. OMICS **16**: 284–287.

Yu, S. and Kim, V.N. (2020). A tale of non-canonical tails: gene regulation by post-transcriptional RNA tailing. Nat Rev Mol Cell Biol **21**: 542–556.

Yu, X., Willmann, M.R., Anderson, S.J., and Gregory, B.D. (2016). Genome-Wide Mapping of Uncapped and Cleaved Transcripts Reveals a Role for the Nuclear mRNA Cap-Binding Complex in Cotranslational RNA Decay in Arabidopsis[OPEN]. Plant Cell **28**: 2385–2397.

Zamora-Briseño, J.A., Pereira-Santana, A., Reyes-Hernández, S.J., Cerqueda-García, D., Castaño, E., and Rodríguez-Zapata, L.C. (2021). Towards an understanding of the role of intrinsic protein disorder on plant adaptation to environmental challenges. Cell Stress Chaperones **26**: 141–150.

Zamudio, J.R., Mittra, B., Campbell, D.A., and Sturm, N.R. (2009). Hypermethylated cap 4 maximizes Trypanosoma brucei translation. Molecular Microbiology **72**: 1100–1110.

Zamudio, J.R., Mittra, B., Zeiner, G.M., Feder, M., Bujnicki, J.M., Sturm, N.R., and Campbell, D.A. (2006). Complete Cap 4 Formation Is Not Required for Viability in Trypanosoma brucei. Eukaryotic Cell **5**: 905–915.

Zekri, L., Huntzinger, E., Heimstädt, S., and Izaurralde, E. (2009). The silencing domain of GW182 interacts with PABPC1 to promote translational repression and degradation of microRNA targets and is required for target release. Mol Cell Biol **29**: 6220–6231.

Zhang, B. and Chen, S. (2021). CNOT4 suppresses non-small cell lung cancer progression and is required for effector cytolytic T lymphocytes cell responses to lung cancer cells. Mol Immunol **132**: 165–171.

Zhang, Q., Pavanello, L., Potapov, A., Bartlam, M., and Winkler, G.S. (2022). Structure of the human Ccr4-Not nuclease module using X-ray crystallography and electron paramagnetic resonance spectroscopy distance measurements. Protein Science **31**: 758–764.

Zhang, W., Murphy, C., and Sieburth, L.E. (2010). Conserved RNaseII domain protein functions in cytoplasmic mRNA decay and suppresses Arabidopsis decapping mutant phenotypes. Proceedings of the National Academy of Sciences **107**: 15981–15985.

Zhang, X. et al. (2015). Suppression of endogenous gene silencing by bidirectional cytoplasmic RNA decay in *Arabidopsis*. Science **348**: 120–123.

Zhang, X., Henriques, R., Lin, S.-S., Niu, Q.-W., and Chua, N.-H. (2006). Agrobacterium-mediated transformation of Arabidopsis thaliana using the floral dip method. Nat Protoc **1**: 641–646.

Zhao, L. and Kunst, L. (2016). SUPERKILLER Complex Components Are Required for the RNA Exosome-Mediated Control of Cuticular Wax Biosynthesis in Arabidopsis Inflorescence Stems. Plant Physiol **171**: 960–973.

Zhao, Y., Yu, Y., Zhai, J., Ramachandran, V., Dinh, T.T., Meyers, B.C., Mo, B., and Chen, X. (2012). The *Arabidopsis* Nucleotidyl Transferase HESO1 Uridylates Unmethylated Small RNAs to Trigger Their Degradation. Current Biology **22**: 689–694.

Zhou, H.-R., Lin, R.-N., Huang, H.-W., Li, L., Cai, T., Zhu, J.-K., Chen, S., and He, X.-J. (2020). The CCR4-NOT complex component NOT1 regulates RNA-directed DNA methylation and transcriptional silencing by facilitating Pol IV-dependent siRNA production. The Plant Journal **103**: 1503–1515.

Zigáčková, D. and Vaňáčová, Š. (2018). The role of 3’ end uridylation in RNA metabolism and cellular physiology. Philos Trans R Soc Lond B Biol Sci **373**: 20180171.

Zinshteyn, B., Sinha, N.K., Enam, S.U., Koleske, B., and Green, R. (2021). Translational repression of NMD targets by GIGYF2 and EIF4E2. PLOS Genetics **17**: e1009813.

Zuber, H., Scheer, H., Ferrier, E., Sement, F.M., Mercier, P., Stupfler, B., and Gagliardi, D. (2016). Uridylation and PABP Cooperate to Repair mRNA Deadenylated Ends in Arabidopsis. Cell Reports **14**: 2707–2717.

Zuber, H., Scheer, H., Joly, A.-C., and Gagliardi, D. (2018). Respective Contributions of URT1 and HESO1 to the Uridylation of 5′ Fragments Produced From RISC-Cleaved mRNAs. Front Plant Sci **9**: 1438.

Zuo, Y. and Deutscher, M.P. (2001). Exoribonuclease superfamilies: structural analysis and phylogenetic distribution. Nucleic Acids Research **29**: 1017–1026.

Supplementary material

Supplementary material

Species	Protein name	Uniprot accession number
Arabidopsis thaliana	AtCCR4a	Q8W0Z9
Arabidopsis thaliana	AtCCR4b	Q9M2F8
Arabidopsis thaliana	AtCCR4c	Q9LS39
Arabidopsis thaliana	AtCCR4d	A8MS41
Arabidopsis thaliana	AtCCR4e	Q0WKY2
Arabidopsis thaliana	AtCCR4f	Q8VYU4
Caenorhabditis elegans	Ce2'PDE	O18005
Caenorhabditis elegans	CeCCR-4	G5EE09
Caenorhabditis elegans	CeANGL-1	A0A0M9JJ86
Drosophila melanogaster	DmNOC	Q8MTZ6
Drosophila melanogaster	Dm2'PDE	Q8IP91
Drosophila melanogaster	DmCCR4	Q8IMX1
Homo sapiens	HsNOC	Q9UK39
Homo sapiens	Hs2'PDE	Q6L8Q7
Homo sapiens	HsCNOT6	Q9ULM6
Homo sapiens	HsCNOT6L	Q96LI5
Homo sapiens	HsANGEL1	Q9UNK9
Homo sapiens	HsANGEL2	Q5VTE6
Mus musculus	MmNOC	O35710
Mus musculus	Mm2'PDE	Q3TIU4
Mus musculus	MmCCR4	Q8K3P5
Mus musculus	MmCCR4L	Q8VEG6
Mus musculus	MmANGEL1	Q8VCU0
Mus musculus	MmANGEL2	Q8K1C0
Oryza sativa	OsCCR4a	Q338D5
Oryza sativa	OsCCR4b	Q10R99
Oryza sativa	OsCCR4c	A0A8I3B2E9
Oryza sativa	OsCCR4d	Q6I5Y3
Oryza sativa	OsCCR4e	Q33A95
Oryza sativa	OsCCR4f	A0A0N7KDB0
Saccharomyces cerevisiae	ScCCR4	P31384
Schizosaccharomyces pombe	SpCCR4	O74874
Volvox carteri	VcNOCT	D8UEL2
Volvox carteri	VcCCR4	D8U8M2

Table S1. List and accession of proteins used to construct the phylogenetic tree of CCR4 proteins (see Figure 6)

Homology	Gene name	AGI	baseMean	log2FoldChange	lfcSE	pvalue	padj
CAF1 homologs	**CAF1a**	AT3G44260	133.36	0.04	0.25	0.87	0.93
	CAF1b	AT5G22250	53.03	0.13	0.30	0.66	0.81
	CAF1c	AT1G27820	1.52	-0.27	0.19	0.15	1.00
	CAF1d	AT1G27890	0.30	0.04	0.10	0.67	1.00
	CAF1e	AT1G61470	26.20	-0.40	0.29	0.17	0.36
	CAF1f	AT3G44240	NA	NA	NA	NA	NA
	CAF1g	AT1G06450	45.64	-0.02	0.25	0.92	0.96
	CAF1h	AT1G15920	164.90	0.14	0.16	0.39	0.59
	CAF1i	AT5G10960	1563.06	0.07	0.12	0.59	0.76
	CAF1j	AT1G80780	425.02	0.26	0.15	0.10	0.25
	CAF1k	AT2G32070	432.69	-0.16	0.13	0.23	0.43
CCR4 homologs	**CCR4a**	AT3G58560	447.34	-2.42	0.15	0.00	0.00
	CCR4b	AT3G58560	174.97	-0.91	0.18	0.00	0.00
	CCR4c	AT3G18500	315.31	-0.26	0.15	0.07	0.20
	CCr4d	AT1G31500	243.35	-0.09	0.16	0.56	0.74
	CCR4e	AT1G73875	128.22	-0.04	0.18	0.84	0.92
	CCR4f	AT5G11350	141.19	0.00	0.18	0.99	0.99
	CCr4g	AT1G31530	NA	NA	NA	NA	NA

Upregulated
Downregulated

Table S2. Differential expression of proteins involved in deadenylation in *ccr4a ccr4b* rosette

Table S3. PASS score of rosette and flower buds. The 934 rosette mRNAs (left table) and the 1182 flower buds mRNAs (right table, orange) are sorted by their PASS.

mRNA	PASS_rep1	PASS_rep2	PASS_rep3	Mean
AT3G63160.1	25.82	25.21	22.35	24.46
AT3G44990.1	18.62	19.62	19.93	19.39
AT1G64720.1	18.10	19.62	17.76	18.49
AT2G21330.1	18.63	17.50	19.15	18.43
AT5G47435.1	18.99	17.50	18.28	18.26
AT4G26850.1	17.80	18.91	17.82	18.18
AT4G34620.1	17.08	19.11	18.17	18.12
AT5G54770.1	16.29	18.27	19.68	18.08
AT2G33855.1	22.28	18.37	13.40	18.02
AT5G15970.1	12.34	19.40	19.57	17.10
AT4G26530.1	18.09	14.98	17.15	16.74
AT1G62250.1	12.24	23.41	14.32	16.66
AT1G79040.1	15.16	17.37	16.76	16.43
AT5G19190.1	15.40	19.41	13.67	16.16
AT2G27402.1	17.82	16.28	14.26	16.12
AT3G01390.1	15.72	15.35	16.46	15.84
AT1G67865.1	15.18	16.35	15.74	15.76
AT3G14210.1	16.38	14.91	15.63	15.64
AT5G20700.1	15.35	13.04	18.23	15.54
AT4G13520.1	15.99	17.09	13.25	15.44
AT3G52230.1	17.18	14.74	13.94	15.29
AT1G08570.1	17.30	14.28	13.73	15.10
AT2G36870.1	14.05	14.80	16.35	15.06
AT3G08610.1	13.55	17.70	13.94	15.06
AT1G65930.1	15.08	13.95	16.05	15.03
AT3G47650.1	14.91	14.68	15.44	15.01
AT5G44580.1	13.77	14.45	16.51	14.91
AT1G64680.1	15.83	11.18	17.45	14.82
AT1G69530.3	13.71	17.13	13.22	14.69
AT3G24160.1	18.32	10.04	15.63	14.66
AT3G58610.1	14.68	11.47	17.54	14.56
AT2G04700.1	15.78	15.49	12.22	14.50
AT5G60360.3	13.56	15.04	14.86	14.49
AT5G46110.4	20.12	16.45	6.85	14.47
AT4G00810.1	14.85	13.88	14.50	14.41
AT1G56190.1	13.87	13.40	15.77	14.34
AT4G22310.1	19.65	11.08	12.30	14.34
AT1G02820.1	19.08	12.79	11.03	14.30
AT5G38410.3	12.98	15.17	14.74	14.30
AT3G47070.1	14.42	14.56	13.56	14.18
AT1G13440.1	14.74	12.69	14.50	13.98
AT5G26742.2	15.53	12.65	13.70	13.96
AT3G22890.1	14.74	16.01	11.09	13.95
AT1G56280.2	14.91	13.15	13.73	13.93
AT5G03455.1	12.39	13.99	15.41	13.93
AT1G62780.1	15.76	13.25	12.62	13.88
AT5G49480.1	11.95	14.96	14.71	13.87
AT1G48030.1	15.21	12.74	13.64	13.86
AT4G01150.1	13.58	14.79	13.20	13.86
AT1G10960.1	13.66	15.00	12.78	13.81
AT3G01500.2	11.14	16.89	13.34	13.79
AT1G60550.1	12.85	13.42	14.96	13.74
AT5G64350.1	15.66	12.92	12.52	13.70
AT5G01410.1	11.44	12.68	16.94	13.69
AT5G17560.1	17.29	13.09	10.55	13.64
AT3G23600.1	12.32	13.48	15.12	13.64
AT5G44190.1	9.55	12.70	18.56	13.60
AT2G26500.1	12.30	14.16	14.25	13.57
AT3G15640.1	14.83	12.38	13.46	13.56
AT2G38140.1	12.21	13.87	14.57	13.55
AT5G17870.2	11.88	14.93	13.73	13.51
AT3G48420.1	14.33	10.27	15.90	13.50
AT5G65220.1	11.66	14.84	13.92	13.47
AT1G05190.1	14.01	12.82	13.44	13.42
AT5G14740.1	15.56	11.47	13.20	13.41
AT4G38970.1	13.86	13.40	12.86	13.37
AT3G56910.1	12.75	12.85	14.21	13.27
AT2G05310.1	11.80	14.46	13.46	13.24
AT1G74880.1	11.82	14.18	13.40	13.13
AT3G03820.1	19.17	11.13	9.00	13.10
AT1G76200.1	12.37	15.13	11.70	13.07
AT5G59613.1	13.37	12.37	13.43	13.05
AT3G52360.1	13.84	10.74	14.53	13.04
AT4G19170.1	10.80	10.74	17.50	13.01
AT2G39730.1	12.84	12.18	13.92	12.98
AT1G80180.1	17.25	13.04	8.64	12.98
AT4G28025.1	10.57	14.40	13.85	12.94
AT2G21170.1	11.96	10.19	16.55	12.90

mRNA	PASS_rep1	PASS_rep2	PASS_rep3	Mean
AT5G07530.1	24.97	28.96	32.76	28.90
AT4G11760.1	23.51	20.22	17.23	20.32
AT5G07550.1	18.25	20.43	20.70	19.79
AT4G04460.1	19.20	20.25	18.85	19.43
AT1G69940.1	22.11	17.64	15.94	18.56
AT5G07410.1	18.87	17.56	17.91	18.11
AT5G61720.1	18.49	18.15	16.15	17.60
AT3G15400.1	16.98	18.41	16.17	17.19
AT2G31980.1	14.10	18.37	18.09	16.85
AT3G25050.1	16.19	18.37	13.98	16.18
AT4G33355.1	13.74	18.41	16.01	16.05
AT4G16190.1	12.02	18.49	16.66	15.72
AT1G66850.1	13.38	16.68	15.10	15.05
AT1G75940.1	15.54	15.40	10.43	13.79
AT3G45010.1	10.19	15.05	14.02	13.09
AT4G13230.1	14.40	11.12	12.26	12.59
AT1G75910.1	12.58	12.29	12.08	12.31
AT2G47040.1	11.38	13.71	11.85	12.31
AT3G20865.1	11.91	12.39	12.49	12.26
AT1G23240.4	6.62	13.49	16.09	12.07
AT1G06260.1	12.27	12.34	11.24	11.95
AT1G68875.1	11.89	12.24	11.30	11.81
AT2G23800.1	9.34	12.86	12.40	11.53
AT5G15960.1	12.31	12.07	9.79	11.39
AT3G01270.1	13.02	9.43	11.20	11.22
AT5G54095.1	8.67	12.01	12.45	11.04
AT5G38760.1	11.95	12.56	8.34	10.95
AT2G19770.1	12.89	10.34	9.57	10.93
AT2G41905.1	10.78	12.63	8.90	10.77
AT2G28840.1	15.21	7.70	8.61	10.51
AT3G51000.1	12.14	10.88	7.95	10.32
AT4G13560.1	9.40	11.36	9.66	10.14
AT3G10410.1	4.67	11.76	13.39	9.94
AT5G07440.1	7.54	11.05	11.21	9.94
AT1G67865.1	9.50	9.59	10.66	9.92
AT3G28750.1	12.09	8.29	8.99	9.79
AT1G63980.1	10.65	9.82	8.81	9.76
AT3G12120.1	9.38	11.76	7.96	9.70
AT1G71695.1	14.85	10.08	4.14	9.69
AT3G49540.1	11.62	10.84	6.35	9.60
AT3G01240.1	12.69	9.27	6.83	9.60
AT3G51950.1	11.45	11.37	5.15	9.33
AT1G14820.3	13.34	9.76	4.80	9.30
AT1G19000.1	3.63	10.94	13.25	9.27
AT3G28980.1	11.48	7.27	8.39	9.05
AT5G53820.1	9.93	8.74	8.31	9.00
AT1G28330.2	-3.58	11.79	18.65	8.96
AT1G65930.1	7.51	8.65	10.01	8.72
AT1G77370.2	7.00	7.56	11.49	8.68
AT5G54390.1	3.33	8.75	13.93	8.67
AT1G02840.1	8.63	4.70	12.38	8.57
AT5G57655.2	5.82	8.34	11.21	8.46
AT5G10450.4	8.07	6.00	11.26	8.45
AT1G61566.1	8.75	8.43	7.98	8.39
AT1G80460.1	9.49	7.19	8.26	8.31
AT3G57520.1	-3.50	15.56	12.69	8.25
AT5G39493.1	9.35	9.98	5.39	8.24
AT1G15360.1	4.52	9.58	10.42	8.17
AT5G10860.1	3.49	9.13	11.73	8.12
AT1G70830.1	7.82	9.44	7.01	8.09
AT3G02700.1	7.10	12.35	4.78	8.07
AT2G34520.1	5.75	8.18	10.11	8.01
AT4G24990.1	6.67	4.58	12.78	8.01
AT4G16520.1	2.89	9.19	11.76	7.94
AT3G22200.2	0.32	7.88	15.57	7.92
AT2G33810.1	9.12	6.45	8.12	7.90
AT5G47310.1	2.87	9.43	11.01	7.77
AT3G51730.1	-0.37	10.52	13.09	7.75
AT5G39730.1	7.16	10.24	5.62	7.67
AT5G67260.2	6.38	11.63	4.70	7.57
AT1G28270.1	9.94	7.99	4.69	7.54
AT2G02760.1	7.89	5.42	9.12	7.47
AT3G28830.1	3.23	9.76	9.05	7.35
AT5G60910.1	8.33	4.38	9.32	7.34
AT2G13360.1	7.52	8.19	6.28	7.33
AT5G25280.1	3.14	8.44	10.15	7.24
AT1G52410.2	5.32	8.05	8.33	7.23
AT4G32240.1	8.11	4.41	8.96	7.16

AT1G32080.1	13.71	10.34	14.56	12.87
AT1G75630.2	10.09	13.18	15.18	12.81
AT3G27090.1	15.30	12.65	10.46	12.80
AT1G67280.1	11.11	12.93	14.25	12.76
AT1G18730.1	13.21	12.90	12.17	12.76
AT5G07020.1	12.38	11.43	14.41	12.74
AT4G17560.1	10.22	12.80	15.14	12.72
AT2G47690.1	10.50	11.49	16.12	12.71
AT2G35370.1	12.75	12.98	12.34	12.69
AT3G15850.1	11.68	11.52	14.75	12.65
AT5G13630.1	10.82	15.14	11.91	12.62
AT2G44860.1	13.38	15.15	9.27	12.60
AT3G52590.1	13.27	10.89	13.52	12.56
AT3G55440.1	14.30	13.52	9.85	12.55
AT1G66820.1	10.02	13.49	14.12	12.54
AT4G38860.1	13.09	12.52	11.97	12.53
AT5G47700.1	14.70	10.04	12.83	12.52
AT3G48140.1	12.60	12.21	12.73	12.51
AT3G21670.1	12.25	13.86	11.42	12.51
AT4G34720.1	10.38	13.86	13.29	12.51
AT5G24930.1	14.12	10.96	12.41	12.50
AT1G07590.1	11.39	13.57	12.46	12.47
AT3G09390.1	10.02	13.40	13.97	12.47
AT2G29310.1	16.36	9.09	11.89	12.45
AT4G32590.3	14.46	11.14	11.72	12.44
AT1G72930.1	13.84	12.00	11.46	12.43
AT1G51650.1	12.15	12.43	12.65	12.41
AT4G28730.1	18.74	6.32	12.11	12.39
AT2G24090.1	11.04	12.80	13.26	12.37
AT1G14450.2	12.66	10.52	13.81	12.33
AT2G02510.1	8.21	14.45	14.24	12.30
AT3G15360.1	12.60	11.83	12.47	12.30
AT1G22630.1	14.79	12.83	9.22	12.28
AT4G10300.1	12.17	11.81	12.80	12.26
AT1G51200.1	8.80	16.24	11.62	12.22
AT5G23120.2	11.56	11.65	13.44	12.22
AT2G22430.1	14.90	9.78	11.82	12.17
AT2G38170.3	10.74	11.36	14.37	12.16
AT1G04420.1	13.98	11.15	11.33	12.16
AT5G17920.1	15.02	11.41	9.92	12.12
AT2G36835.1	14.29	11.69	10.28	12.09
AT5G14320.1	11.87	11.41	12.91	12.06
AT5G09650.1	11.36	11.49	13.29	12.05
AT2G05990.1	9.83	14.76	11.42	12.00
AT5G47190.1	11.45	12.09	12.39	11.98
AT4G34190.1	11.28	12.80	11.72	11.93
AT4G27310.1	15.21	9.28	11.30	11.93
AT5G54600.1	11.88	10.95	12.96	11.93
AT2G46390.1	12.25	10.69	12.81	11.92
AT5G47110.1	14.18	13.83	7.72	11.91
AT5G53650.1	13.29	10.73	11.67	11.90
AT5G45680.1	10.45	11.35	13.82	11.87
AT4G11150.1	12.01	12.76	10.83	11.87
AT1G69460.1	9.99	8.33	17.26	11.86
AT4G13615.1	13.30	10.39	11.85	11.85
AT3G16140.1	12.33	11.63	11.51	11.82
AT5G10450.4	12.61	10.15	12.66	11.81
AT3G04790.1	9.46	11.19	14.58	11.74
AT5G09660.4	14.13	8.54	12.54	11.74
AT3G23490.1	10.53	11.44	13.15	11.71
AT1G21770.1	10.69	13.89	10.53	11.70
AT3G60750.1	14.94	9.48	10.65	11.69
AT4G10920.1	17.17	9.85	8.06	11.69
AT4G02530.2	11.69	11.00	12.31	11.67
AT3G53420.1	13.01	10.12	11.85	11.66
AT3G58730.1	10.78	10.13	14.04	11.65
AT3G17210.1	14.44	11.19	9.24	11.63
AT1G54580.1	11.46	12.91	10.46	11.61
AT5G66190.1	11.50	10.79	12.40	11.56
AT3G54210.1	10.95	9.83	13.88	11.55
AT1G67090.1	9.74	12.27	12.64	11.55
AT2G44650.1	10.63	12.65	11.34	11.54
AT2G47710.1	10.40	9.64	14.56	11.53
AT1G12840.1	13.55	11.89	9.15	11.53
AT2G23090.1	12.00	11.59	10.98	11.52
AT4G15560.1	9.96	9.80	14.81	11.52
AT5G19855.1	12.93	9.87	11.75	11.52
AT1G60010.1	8.29	8.64	17.61	11.51
AT1G33810.1	13.50	8.43	12.60	11.51
AT3G03100.1	8.56	13.41	12.55	11.51
AT3G12780.1	9.79	10.97	13.74	11.50
AT5G05370.1	10.27	12.10	11.97	11.45
AT3G23000.1	13.35	8.32	12.66	11.44
AT4G22890.1	8.37	9.56	16.38	11.44
AT1G77710.1	9.88	12.57	11.84	11.43
AT3G22210.1	11.25	11.75	11.24	11.41
AT5G01600.1	10.36	11.15	12.68	11.40
AT1G71880.1	11.73	6.87	2.72	7.11
AT5G60640.1	7.69	3.25	10.28	7.08
AT1G61563.1	7.91	6.86	6.35	7.04
AT5G55160.2	7.21	5.91	7.93	7.02
AT5G16960.1	10.53	4.23	6.08	6.95
AT1G79040.1	6.84	7.10	6.83	6.92
AT1G02790.1	6.85	8.71	5.08	6.88
AT1G12780.1	2.28	9.77	8.57	6.87
AT5G60360.3	5.84	8.61	6.08	6.84
AT4G15560.1	2.54	11.73	6.09	6.79
AT5G09920.1	8.08	6.58	5.69	6.78
AT4G34620.1	7.70	10.22	2.31	6.74
AT2G31570.1	6.07	6.07	8.09	6.74
AT2G19830.2	7.96	4.13	8.05	6.71
AT1G75380.1	7.53	6.16	6.28	6.66
AT4G26530.1	11.62	9.41	-1.16	6.62
AT3G28940.1	-0.33	10.41	9.79	6.62
AT1G56220.3	2.47	5.94	11.45	6.62
AT5G15970.1	1.18	9.01	9.49	6.56
AT2G34560.2	10.52	1.08	8.08	6.56
AT4G31290.1	6.83	7.19	5.46	6.49
AT1G69510.1	8.76	2.42	8.26	6.48
AT5G03460.1	2.04	6.33	11.02	6.46
AT4G01610.1	4.61	6.22	8.52	6.45
AT1G04850.1	8.57	6.16	4.60	6.44
AT3G49870.1	5.46	8.24	5.59	6.43
AT5G51400.1	5.17	5.98	8.09	6.42
AT5G46020.1	5.87	6.75	6.59	6.41
AT2G28910.1	5.56	7.40	6.10	6.35
AT5G26360.1	8.12	7.58	3.23	6.31
AT1G55360.1	6.71	7.22	4.95	6.29
AT5G19140.1	6.29	4.70	7.88	6.29
AT1G22520.2	8.83	6.15	3.89	6.29
AT3G51590.1	5.84	6.44	6.57	6.28
AT1G02500.1	10.34	3.75	4.74	6.28
AT5G28640.1	9.09	5.94	3.73	6.25
AT4G25570.2	8.20	4.89	5.65	6.25
AT4G01897.1	4.77	9.96	4.00	6.24
AT1G75800.1	2.10	5.38	11.21	6.23
AT1G80920.1	2.66	8.01	7.99	6.22
AT1G62040.1	-0.23	5.53	13.27	6.19
AT3G04730.1	6.14	4.55	7.89	6.19
AT5G10360.1	8.61	5.49	4.34	6.15
AT5G03240.1	2.83	8.37	7.21	6.14
AT4G14615.1	4.17	7.28	6.95	6.14
AT2G17380.1	5.28	5.52	7.57	6.12
AT1G74470.1	6.65	6.60	5.04	6.09
AT3G16640.1	8.38	6.12	3.79	6.09
AT1G26470.1	5.86	8.73	3.63	6.07
AT3G42790.1	1.81	6.61	9.73	6.05
AT1G64230.4	6.96	4.87	6.32	6.05
AT1G60870.1	4.21	6.32	7.55	6.03
AT5G62575.2	6.22	5.97	5.87	6.02
AT1G76405.2	8.90	5.13	3.99	6.01
AT1G49300.1	1.78	7.05	9.08	5.97
AT3G56240.1	7.09	6.98	3.75	5.94
AT2G32090.1	1.24	5.07	11.38	5.89
AT5G24490.1	1.87	8.29	7.51	5.89
AT2G28800.1	2.56	7.33	7.72	5.87
AT4G22330.1	9.21	6.89	1.47	5.86
AT1G70650.2	2.56	6.22	8.69	5.82
AT1G51200.1	6.24	6.05	5.13	5.81
AT4G14110.1	14.22	1.40	1.79	5.80
AT1G28375.1	4.90	6.79	5.69	5.79
AT2G46280.1	1.22	7.83	8.33	5.79
AT3G62650.1	7.53	4.60	5.22	5.78
AT5G58330.1	3.86	8.05	5.40	5.77
AT1G33430.2	6.36	6.82	3.96	5.71
AT3G54890.1	6.76	4.98	5.32	5.69
AT1G18800.1	7.87	4.98	4.18	5.68
AT1G52400.1	5.02	6.06	5.95	5.68
AT4G10920.1	7.13	5.73	4.13	5.66
AT4G02890.3	4.18	7.35	5.45	5.66
AT1G07440.1	5.94	8.64	2.38	5.65
AT5G27430.1	3.10	7.96	5.83	5.63
AT3G01740.1	3.49	5.41	7.95	5.62
AT5G20230.1	3.58	6.18	7.03	5.60
AT1G53320.1	8.13	3.96	4.70	5.60
AT4G01150.1	4.73	8.13	3.93	5.59
AT2G47320.1	3.94	6.93	5.86	5.58
AT1G12840.1	4.30	6.60	5.78	5.56
AT5G09225.1	3.12	7.24	6.24	5.53
AT5G14240.1	1.42	7.65	7.50	5.52
AT2G21195.4	4.57	6.07	5.91	5.52
AT4G09800.1	5.63	6.75	4.13	5.50
AT1G23820.1	3.30	3.48	9.71	5.49
AT3G52560.4	4.62	6.02	5.83	5.49

AT4G32260.1	13.70	15.43	4.97	11.36	AT1G21770.1	4.36	7.01	5.06	5.47
AT4G37930.1	9.48	12.30	12.30	11.36	AT3G15850.1	6.30	2.12	7.90	5.44
AT3G63540.1	10.73	12.00	11.32	11.35	AT1G21400.5	0.38	8.94	6.97	5.43
AT1G15120.2	10.13	10.97	12.86	11.32	AT4G28395.1	5.20	5.54	5.56	5.43
AT1G21065.1	13.03	12.96	7.89	11.30	AT1G04290.1	3.87	8.75	3.65	5.42
AT2G27290.1	10.99	11.00	11.85	11.28	AT1G44760.2	-0.68	6.54	10.37	5.41
AT2G13360.1	9.89	10.79	13.03	11.24	AT5G01350.1	2.87	6.66	6.65	5.40
AT1G62180.1	14.18	8.73	10.74	11.22	AT4G15910.1	4.62	7.82	3.68	5.37
AT1G14150.1	10.74	8.72	14.03	11.16	AT3G09390.1	3.05	7.44	5.60	5.36
AT3G23390.1	11.76	10.50	11.22	11.16	AT5G15800.2	7.40	2.96	5.74	5.36
AT3G28900.1	12.26	9.14	12.03	11.14	AT5G03455.1	0.98	7.17	7.93	5.36
AT4G00430.1	8.48	14.75	10.16	11.13	AT4G34750.1	6.91	8.92	0.21	5.35
AT1G74670.1	10.11	12.38	10.84	11.11	AT5G52920.1	4.42	7.11	4.49	5.34
AT3G53890.1	10.54	11.39	11.37	11.10	AT3G47470.1	3.32	7.08	5.59	5.33
AT5G04590.1	10.64	11.97	10.67	11.09	AT2G20420.1	3.07	4.80	8.11	5.33
AT5G50920.1	13.10	5.92	14.20	11.07	AT1G21460.1	4.05	7.89	4.03	5.32
AT1G66240.1	8.25	11.48	13.45	11.06	AT3G23050.1	2.72	3.79	9.38	5.30
AT3G09820.1	9.68	9.74	13.73	11.05	AT4G21960.1	5.68	7.76	2.43	5.29
AT4G13940.1	10.99	11.19	10.94	11.04	AT1G45145.1	3.47	7.10	5.27	5.28
AT4G20150.1	9.40	9.81	13.80	11.00	AT1G07830.1	3.88	5.46	6.48	5.27
AT1G07610.1	9.10	12.54	11.31	10.98	AT4G28025.1	6.89	3.29	5.63	5.27
AT5G56710.1	12.01	9.89	10.96	10.96	AT1G75630.2	5.27	7.04	3.47	5.26
AT5G67590.1	12.84	11.58	8.43	10.95	AT5G62300.1	4.96	6.26	4.56	5.26
AT3G25920.1	11.11	9.66	12.05	10.94	AT5G59310.1	7.01	5.30	3.47	5.26
AT4G29390.1	16.77	13.18	2.85	10.93	AT1G65980.1	6.22	3.73	5.81	5.25
AT1G20340.1	10.74	11.20	10.78	10.91	AT5G52390.1	4.75	5.05	5.95	5.25
AT5G41520.1	12.63	9.91	10.17	10.90	AT1G29930.1	9.22	3.48	2.97	5.22
AT1G22520.2	10.72	12.68	9.26	10.89	AT3G57810.2	4.11	3.24	8.30	5.22
AT2G42210.2	9.64	10.34	12.66	10.88	AT1G11840.6	5.12	6.13	4.37	5.21
AT3G43810.2	9.83	13.30	9.51	10.88	AT3G17210.1	1.10	6.39	8.12	5.20
AT2G19310.1	10.16	13.78	8.60	10.85	AT4G34050.3	3.78	6.50	5.21	5.16
AT1G73060.1	13.29	9.19	10.03	10.84	AT4G34670.1	8.41	4.07	3.01	5.16
AT1G44000.1	8.29	13.53	10.64	10.82	AT1G74670.1	6.49	4.56	4.43	5.16
AT2G34860.1	12.73	9.41	10.30	10.81	AT3G27090.1	6.07	4.21	5.18	5.16
AT3G08740.1	13.50	7.87	11.02	10.80	AT2G34470.2	7.31	3.91	4.23	5.15
AT4G29350.1	11.43	10.80	10.05	10.76	AT5G23120.2	4.24	4.07	7.05	5.12
AT3G62530.1	9.84	10.37	12.04	10.75	AT3G57800.1	3.08	3.23	9.03	5.11
AT3G44010.1	10.88	10.90	10.40	10.73	AT3G45140.1	2.46	3.78	9.08	5.11
AT5G20090.1	11.06	12.35	8.68	10.69	AT5G03290.1	1.70	5.53	8.08	5.10
AT3G12345.1	5.96	12.40	13.70	10.69	AT4G16141.1	2.64	8.13	4.50	5.09
AT1G57860.1	13.89	8.36	9.79	10.68	AT5G51960.1	12.30	1.91	1.02	5.08
AT2G27730.1	8.63	11.25	12.14	10.68	AT3G23490.1	5.15	5.92	4.15	5.07
AT3G60210.1	6.63	11.79	13.61	10.68	AT3G46060.1	3.75	7.38	4.08	5.07
AT3G53020.1	12.56	7.86	11.60	10.67	AT5G24650.1	8.24	2.80	4.16	5.07
AT2G35830.2	10.65	11.17	10.19	10.67	AT5G46430.1	4.55	5.17	5.44	5.05
AT1G16080.1	16.16	5.64	10.18	10.66	AT2G29310.1	6.58	3.74	4.82	5.05
AT2G46820.1	8.81	11.90	11.23	10.64	AT1G43890.1	4.01	5.62	5.51	5.04
AT2G39010.1	7.92	9.88	14.10	10.63	AT1G11910.2	6.04	4.84	4.23	5.04
AT4G18730.1	12.47	9.10	10.26	10.61	AT1G31970.1	4.04	3.12	7.92	5.03
AT3G15190.1	6.79	12.45	12.59	10.61	AT3G62290.1	6.55	3.60	4.91	5.02
AT5G65480.1	9.61	13.61	8.59	10.61	AT1G65720.1	5.57	1.44	8.00	5.00
AT3G26650.1	11.52	9.86	10.38	10.59	AT4G13200.1	1.59	3.74	9.64	4.99
AT5G21430.1	13.10	9.52	9.08	10.56	AT5G04750.1	5.22	5.95	3.76	4.98
AT5G59880.1	11.11	10.99	9.51	10.54	AT1G68560.1	7.50	4.92	2.43	4.95
AT4G25570.2	7.35	9.18	14.96	10.50	AT4G35750.1	-0.37	2.57	12.60	4.93
AT2G47380.1	10.34	9.98	11.12	10.48	AT5G41210.1	4.40	9.93	0.41	4.91
AT5G11450.2	8.24	9.29	13.85	10.46	AT1G14400.1	2.51	4.90	7.33	4.91
AT3G16240.1	9.22	11.38	10.77	10.46	AT5G59890.1	6.72	3.71	4.30	4.91
AT4G39800.1	7.96	15.76	7.64	10.45	AT1G05720.1	1.73	5.76	7.24	4.91
AT1G75750.1	9.47	11.97	9.92	10.45	AT1G23960.1	6.71	5.97	2.03	4.90
AT5G35630.1	10.79	10.23	10.29	10.43	AT5G01800.1	6.16	4.56	3.98	4.90
AT4G30010.1	9.73	10.56	11.01	10.43	AT3G47833.1	1.34	6.13	7.22	4.90
AT5G24314.2	10.20	11.59	9.50	10.43	AT1G56280.2	7.46	5.17	2.04	4.89
AT5G40950.1	11.55	10.96	8.76	10.42	AT5G45350.1	6.35	5.21	3.07	4.88
AT2G01850.1	8.49	10.99	11.75	10.41	AT1G19120.1	3.39	1.16	10.07	4.87
AT4G18040.1	13.36	9.05	8.81	10.41	AT4G24690.1	2.94	6.48	5.19	4.87
AT2G47400.1	10.92	10.99	9.27	10.39	AT4G34720.1	6.10	4.26	4.20	4.85
AT2G40590.1	16.00	6.48	8.67	10.38	AT5G24420.1	3.72	4.02	6.80	4.85
AT5G28050.3	10.50	12.21	8.39	10.37	AT3G49560.1	4.88	2.36	7.31	4.85
AT1G67430.1	12.26	9.56	9.22	10.35	AT2G40110.1	2.96	3.79	7.76	4.84
AT4G25100.1	5.17	13.00	12.87	10.35	AT4G24820.1	6.90	2.19	5.41	4.83
AT5G40500.1	5.80	11.63	13.59	10.34	AT5G48300.1	4.00	1.67	8.82	4.83
AT4G18370.1	12.60	10.96	7.44	10.33	AT4G18970.2	4.74	3.88	5.87	4.83
AT4G14880.1	10.50	10.27	10.23	10.33	AT1G65820.3	4.49	3.98	5.98	4.82
AT3G10060.1	10.57	10.17	10.23	10.32	AT2G23090.1	4.41	5.66	4.37	4.81
AT4G14320.2	11.11	8.84	11.00	10.32	AT5G24780.1	0.06	9.27	5.10	4.81
AT1G32060.1	12.15	8.21	10.59	10.32	AT5G15230.1	4.47	5.11	4.79	4.79
AT1G48350.1	9.81	10.17	10.95	10.31	AT1G17455.1	3.98	9.41	0.93	4.78
AT1G04410.1	8.83	8.74	13.31	10.29	AT2G27385.1	5.00	4.10	5.19	4.76
AT4G35450.5	11.23	9.32	10.28	10.28	AT3G51600.1	4.33	4.34	5.62	4.76
AT1G64750.3	11.34	8.87	10.61	10.27	AT2G41410.1	4.12	3.59	6.58	4.76
AT4G20360.1	8.61	10.48	11.72	10.27	AT4G11220.1	3.78	6.38	4.12	4.76
AT2G43030.1	11.27	10.04	9.48	10.26	AT2G46170.1	4.64	8.15	1.44	4.74
AT2G43460.1	11.92	9.62	9.21	10.25	AT5G60790.1	6.01	3.65	4.56	4.74
AT3G04400.1	10.13	9.14	11.43	10.23	AT2G45820.1	3.13	5.92	5.15	4.73
AT1G42970.1	9.98	10.54	10.15	10.23	AT3G52220.1	5.99	6.32	1.87	4.73
AT4G26230.1	11.69	11.31	7.66	10.22	AT5G41520.1	4.63	4.80	4.68	4.70

AT4G01940.1	7.32	11.91	11.44	10.22
AT3G46430.1	10.07	11.28	9.31	10.22
AT5G62140.1	13.46	6.23	10.96	10.21
AT4G34700.1	10.25	10.37	10.00	10.20
AT3G59980.1	13.62	11.26	5.71	10.20
AT5G19510.1	10.15	9.78	10.62	10.19
AT5G20180.1	13.55	8.94	8.05	10.18
AT3G18410.1	11.60	6.34	12.58	10.17
AT5G62575.2	7.73	12.42	10.30	10.15
AT2G42590.3	8.99	9.06	12.39	10.15
AT1G74270.1	10.87	10.47	9.05	10.13
AT5G06980.4	16.26	7.27	6.80	10.11
AT4G22220.1	10.97	10.07	9.28	10.11
AT2G39470.1	9.48	11.75	9.05	10.10
AT3G54900.1	5.54	10.51	14.20	10.08
AT1G47128.1	10.38	9.30	10.54	10.07
AT4G27090.1	10.71	9.48	9.87	10.02
AT1G75350.1	11.09	9.12	9.84	10.02
AT1G35680.1	8.19	12.25	9.60	10.01
AT2G29180.1	8.60	8.28	13.09	9.99
AT2G27710.1	11.62	6.89	11.44	9.98
AT5G04800.1	12.93	5.81	11.20	9.98
AT3G27160.2	9.07	11.33	9.51	9.97
AT4G29905.1	11.44	9.55	8.90	9.96
AT1G70890.1	5.90	11.45	12.43	9.93
AT4G22570.1	6.09	8.83	14.82	9.92
AT1G26630.1	14.98	9.56	5.20	9.91
AT2G04039.3	9.78	7.78	12.09	9.89
AT3G22235.1	11.85	11.65	6.10	9.87
AT4G02620.1	8.90	11.63	9.04	9.85
AT5G67260.2	11.91	5.20	12.43	9.84
AT3G45050.2	7.42	10.58	11.51	9.84
AT5G08050.1	11.81	9.09	8.56	9.82
AT3G03920.1	15.07	5.55	8.82	9.81
AT1G32990.1	10.45	9.90	9.08	9.81
AT1G31812.1	9.41	10.60	9.41	9.81
AT1G19050.1	10.19	7.36	11.84	9.80
AT4G32470.1	5.06	7.79	16.51	9.79
AT3G62410.1	9.00	9.42	10.94	9.79
AT2G41090.1	11.28	9.85	8.17	9.76
AT5G22390.1	10.34	7.53	11.39	9.76
AT2G33800.1	8.51	12.68	8.07	9.75
AT1G76450.1	10.64	7.61	11.00	9.75
AT2G31490.1	3.01	17.62	8.60	9.75
AT4G39200.1	11.09	8.34	9.81	9.74
AT5G13120.1	13.03	5.45	10.75	9.74
AT3G04120.1	10.75	12.15	6.33	9.74
AT2G28000.1	7.80	9.51	11.91	9.74
AT5G42890.1	8.52	8.92	11.76	9.73
AT1G10470.1	9.24	6.99	12.96	9.73
AT1G73600.2	11.57	5.41	12.19	9.72
AT5G02960.1	11.09	8.63	9.44	9.72
AT5G59890.1	9.24	9.07	10.84	9.72
AT1G09690.1	9.57	8.72	10.76	9.69
AT3G15810.1	12.79	8.44	7.83	9.69
AT3G55240.1	10.44	7.28	11.27	9.66
AT1G56220.3	15.59	3.82	9.58	9.66
AT2G19740.1	13.75	5.75	9.46	9.65
AT5G42850.1	10.01	6.63	12.31	9.65
AT1G13360.1	8.84	12.22	7.83	9.63
AT2G39460.1	11.38	8.57	8.92	9.62
AT2G40510.1	11.49	6.93	10.40	9.61
AT1G37130.1	10.64	12.85	5.28	9.59
AT5G38420.1	6.55	11.01	11.21	9.59
AT2G20450.1	9.36	7.21	12.16	9.58
AT5G58330.1	3.55	11.82	13.35	9.57
AT2G35635.1	7.88	10.51	10.28	9.56
AT5G19370.1	9.44	12.64	6.59	9.56
AT2G47110.1	11.18	8.95	8.53	9.55
AT3G12630.1	8.43	8.91	11.30	9.55
AT2G33150.1	9.79	5.51	13.34	9.55
AT4G18100.1	11.05	8.78	8.76	9.53
AT2G30620.1	11.96	3.56	13.07	9.53
AT1G52870.2	14.29	6.31	7.97	9.52
AT1G22300.1	11.00	11.23	6.31	9.52
AT5G51720.1	7.43	7.64	13.44	9.51
AT1G04270.1	10.51	8.80	9.20	9.50
AT5G17710.2	7.94	9.65	10.88	9.49
AT4G16720.1	12.61	6.65	9.18	9.48
AT5G30510.1	10.98	7.18	10.25	9.47
AT5G08410.2	6.53	10.05	11.79	9.46
AT4G24770.1	9.44	9.27	9.64	9.45
AT2G43090.1	7.97	9.65	10.72	9.45
AT4G28660.2	9.85	8.31	10.12	9.43
AT2G45640.1	9.23	9.07	9.97	9.42
AT3G09500.1	10.45	8.02	9.80	9.42
AT3G20390.2	6.12	9.10	12.93	9.38

AT2G33150.1	2.21	5.06	6.77	4.68
AT1G69700.1	9.39	3.30	1.27	4.66
AT3G50000.1	5.29	0.37	8.31	4.66
AT1G01100.1	4.29	2.90	6.75	4.65
AT1G12920.1	4.87	2.25	6.80	4.64
AT4G15930.1	6.81	2.08	5.02	4.63
AT4G12040.1	1.29	2.74	9.84	4.62
AT4G08520.1	1.63	2.11	10.12	4.62
AT1G05190.1	0.12	6.40	7.33	4.62
AT5G43830.1	2.34	-0.78	12.28	4.61
AT1G26670.1	1.73	6.55	5.53	4.60
AT4G40030.2	5.84	5.17	2.81	4.60
AT3G62560.1	6.10	6.94	0.74	4.60
AT2G19760.1	4.86	6.60	2.30	4.59
AT5G43460.1	3.82	4.68	5.23	4.58
AT5G09650.1	2.20	5.07	6.45	4.57
AT1G07770.1	3.93	6.24	3.53	4.57
AT2G33380.1	-5.61	11.05	8.25	4.56
AT5G63670.1	4.39	6.22	3.07	4.56
AT2G47510.1	5.47	4.23	3.94	4.55
AT2G33220.2	4.86	1.99	6.79	4.55
AT2G20360.1	6.93	1.09	5.59	4.54
AT1G47128.1	3.65	7.08	2.87	4.53
AT5G47435.1	3.86	7.88	1.86	4.53
AT4G02230.1	5.85	3.60	4.15	4.53
AT2G47710.1	5.77	3.83	3.98	4.53
AT5G52240.1	6.67	3.27	3.62	4.52
AT1G80500.1	3.98	8.11	1.42	4.51
AT2G44610.1	7.50	8.13	-2.15	4.49
AT2G24020.1	5.00	5.09	3.38	4.49
AT1G77540.1	6.74	3.02	3.71	4.49
AT1G78900.1	5.81	4.60	3.04	4.48
AT5G28050.3	2.94	6.32	4.19	4.48
AT3G09860.1	5.01	5.60	2.81	4.47
AT4G39090.1	3.97	4.56	4.87	4.47
AT2G21170.1	5.56	3.33	4.50	4.47
AT3G12490.2	5.62	3.96	3.80	4.46
AT2G38170.3	7.11	1.85	4.40	4.45
AT2G21330.1	6.78	4.26	2.22	4.42
AT5G58240.1	7.95	2.08	3.22	4.42
AT2G22670.4	4.11	4.98	4.09	4.39
AT3G28220.1	8.72	6.03	-1.61	4.38
AT4G22190.1	6.23	1.52	5.33	4.36
AT3G21865.1	7.41	1.65	4.01	4.35
AT3G11930.3	3.16	5.08	4.82	4.35
AT5G06060.1	6.48	3.35	3.21	4.35
AT3G49910.1	3.81	3.18	6.05	4.35
AT2G15890.1	-1.32	4.12	10.23	4.34
AT4G36250.1	9.73	-2.44	5.74	4.34
AT5G44680.1	2.04	7.25	3.71	4.34
AT5G47110.1	4.75	6.24	2.02	4.33
AT5G05060.1	4.50	3.37	5.13	4.33
AT4G19200.1	4.97	3.83	4.17	4.32
AT5G20500.1	6.47	6.57	-0.07	4.32
AT5G65480.1	1.21	8.05	3.67	4.31
AT2G17390.1	5.44	3.64	3.81	4.29
AT2G27730.1	0.65	7.52	4.71	4.29
AT2G47400.1	0.43	4.46	7.98	4.29
AT5G38660.2	-0.95	2.94	10.88	4.29
AT1G13360.1	0.77	4.61	7.46	4.28
AT3G45030.1	5.04	5.35	2.44	4.28
AT2G45640.1	2.03	4.81	5.96	4.26
AT5G60340.1	3.90	5.95	2.90	4.25
AT1G29910.1	7.46	2.76	2.52	4.25
AT1G69120.1	4.86	4.73	3.12	4.23
AT2G36060.2	4.01	6.35	2.33	4.23
AT1G27450.3	3.34	5.48	3.86	4.22
AT4G17560.1	0.09	4.90	7.66	4.22
AT1G62480.1	4.56	3.97	4.12	4.22
AT2G21660.1	5.03	5.66	1.95	4.21
AT1G21750.1	-1.71	5.30	9.04	4.21
AT1G07590.1	4.49	4.06	4.06	4.20
AT1G10590.3	4.57	2.26	5.70	4.18
AT1G15120.2	5.50	4.66	2.36	4.17
AT3G24160.1	1.88	4.96	5.67	4.17
AT5G53160.2	3.90	1.04	7.56	4.16
AT1G29920.1	9.06	2.82	0.61	4.16
AT4G18030.1	1.41	5.11	5.97	4.16
AT5G54270.1	4.55	4.89	3.03	4.16
AT5G61020.1	7.37	3.07	2.02	4.16
AT4G14270.1	0.41	5.86	6.19	4.15
AT2G22430.1	1.50	4.15	6.80	4.15
AT2G22080.1	2.25	7.65	2.53	4.14
AT4G22000.1	2.48	1.25	8.66	4.13
AT3G02480.1	4.16	5.47	2.72	4.12
AT5G22430.1	4.51	4.14	3.70	4.12
AT3G09820.1	4.12	1.56	6.65	4.11

AT3G44890.1	7.20	9.51	11.42	9.38
AT1G03475.1	7.06	6.11	14.93	9.37
AT1G73885.1	11.72	8.28	8.09	9.36
AT5G42270.1	14.67	5.25	8.13	9.35
AT2G19760.1	8.31	8.78	10.95	9.34
AT4G15802.1	6.59	12.20	9.23	9.34
AT1G70600.1	10.23	8.52	9.25	9.34
AT3G25530.1	13.42	7.40	7.16	9.32
AT4G13500.1	8.56	8.27	11.13	9.32
AT2G39390.1	13.40	5.56	8.99	9.31
AT2G05620.1	8.57	8.59	10.72	9.29
AT5G20160.2	12.47	5.13	10.24	9.28
AT2G19730.1	9.67	9.46	8.69	9.28
AT5G18380.1	10.97	8.49	8.35	9.27
AT2G40880.1	9.77	10.52	7.48	9.26
AT1G71500.1	7.64	7.07	13.05	9.25
AT5G58710.1	5.47	9.32	12.94	9.24
AT5G57290.1	10.89	8.20	8.62	9.24
AT5G47890.1	10.73	7.92	9.05	9.23
AT2G18020.1	9.65	8.19	9.83	9.23
AT2G37600.1	10.81	6.61	10.26	9.22
AT3G59540.1	10.15	9.02	8.49	9.22
AT1G57660.1	11.99	6.59	9.06	9.21
AT3G27050.1	12.68	5.05	9.86	9.20
AT3G44450.1	13.92	4.77	8.88	9.19
AT5G14910.1	8.61	8.12	10.75	9.16
AT1G01620.1	10.94	7.18	9.34	9.15
AT5G51110.1	9.58	10.59	7.23	9.13
AT1G54500.1	11.67	7.58	8.14	9.13
AT2G27840.3	7.43	11.00	8.94	9.12
AT3G25520.1	12.58	6.72	8.01	9.10
AT5G67030.1	8.44	11.30	7.54	9.10
AT1G29920.1	10.39	8.12	8.73	9.08
AT3G53740.2	10.32	7.59	9.31	9.07
AT1G08880.1	10.54	6.66	10.00	9.07
AT5G27850.1	10.81	7.46	8.92	9.06
AT5G38480.1	6.88	11.08	9.21	9.06
AT2G05520.1	7.79	8.75	10.63	9.06
AT1G67700.2	9.39	8.71	8.99	9.03
AT5G02500.1	9.68	9.17	8.24	9.03
AT4G31985.1	9.58	8.66	8.85	9.03
AT3G47370.1	12.58	6.07	8.42	9.02
AT2G30570.1	8.34	9.99	8.73	9.02
AT1G72510.1	8.49	13.25	5.32	9.02
AT1G58290.1	9.45	8.12	9.46	9.01
AT4G37925.1	12.31	6.16	8.55	9.01
AT1G68590.1	7.63	8.04	11.34	9.00
AT1G50732.1	8.31	10.55	8.15	9.00
AT4G15000.1	7.66	8.70	10.61	8.99
AT1G22140.1	9.17	7.98	9.80	8.98
AT1G32050.1	11.63	6.49	8.77	8.97
AT1G07320.1	10.20	8.62	8.08	8.97
AT3G10920.1	9.57	7.95	9.36	8.96
AT2G45820.1	9.25	10.92	6.69	8.96
AT1G78900.1	2.51	7.29	17.03	8.95
AT1G11475.1	12.93	8.67	5.21	8.94
AT3G16640.1	11.23	8.81	6.73	8.92
AT5G48810.1	13.68	6.07	7.02	8.92
AT5G16130.1	8.65	8.97	9.13	8.92
AT4G25050.2	3.87	10.98	11.87	8.91
AT5G47840.1	8.03	9.86	8.81	8.90
AT5G59850.1	9.64	9.74	7.27	8.88
AT4G16520.1	9.61	10.02	6.99	8.88
AT2G36620.1	11.59	6.82	8.21	8.87
AT1G26880.1	10.00	7.85	8.72	8.86
AT1G41880.1	10.97	6.05	9.46	8.83
AT3G52880.2	10.70	7.97	7.79	8.82
AT2G34420.1	5.95	8.37	12.14	8.82
AT3G06145.1	12.11	9.30	5.05	8.82
AT5G17230.3	10.87	7.63	7.95	8.82
AT1G23290.1	8.99	8.24	9.20	8.81
AT5G27770.1	10.34	8.18	7.91	8.81
AT3G01480.1	8.97	10.34	7.08	8.80
AT1G67350.1	8.45	6.58	11.34	8.79
AT1G77940.1	12.07	6.54	7.75	8.79
AT3G13120.1	8.57	9.12	8.63	8.77
AT3G55280.1	8.62	6.63	11.04	8.76
AT1G78380.1	8.57	7.46	10.25	8.76
AT2G46600.1	5.80	9.78	10.69	8.76
AT1G72370.1	9.40	6.55	10.32	8.75
AT5G64770.1	11.02	5.38	9.86	8.75
AT5G42650.1	10.64	8.37	7.24	8.75
AT1G72750.1	8.61	10.71	6.93	8.75
AT2G27530.1	11.29	7.73	7.21	8.74
AT1G08360.1	9.19	6.24	10.77	8.73
AT3G49910.1	9.70	7.27	9.22	8.73
AT1G01100.1	12.99	9.40	3.78	8.72

AT1G73885.1	0.55	4.02	7.73	4.10
AT1G65970.1	1.71	5.08	5.51	4.10
AT5G45670.1	5.58	0.65	6.03	4.09
AT3G47650.1	3.84	6.57	1.83	4.08
AT5G53940.1	0.83	-0.72	12.04	4.05
AT4G01900.1	1.79	4.90	5.45	4.05
AT5G23740.1	4.34	3.41	4.38	4.04
AT3G48140.1	4.98	4.24	2.91	4.04
AT2G35635.1	3.04	3.29	5.74	4.02
AT1G29390.1	4.95	-0.42	7.53	4.02
AT1G69460.1	2.24	2.70	7.09	4.01
AT5G28060.1	3.06	3.17	5.74	3.99
AT5G62360.1	5.78	0.27	5.90	3.98
AT1G61790.1	2.19	3.84	5.91	3.98
AT2G44860.1	4.79	4.94	2.17	3.97
AT2G45960.3	3.84	4.30	3.75	3.97
AT1G59900.1	0.42	0.33	11.14	3.96
AT3G48890.1	3.92	3.37	4.57	3.95
AT2G27960.1	2.04	4.38	5.43	3.95
AT3G45980.1	3.27	4.28	4.28	3.94
AT5G01410.1	4.50	2.55	4.78	3.94
AT4G13520.1	2.64	4.46	4.71	3.93
AT1G77710.1	2.76	4.92	4.12	3.93
AT3G23600.1	2.91	3.88	4.98	3.93
AT1G08830.1	2.88	4.27	4.58	3.91
AT1G65700.3	0.36	6.95	4.42	3.91
AT1G54410.1	2.74	4.52	4.47	3.91
AT1G20430.1	3.00	3.57	5.15	3.91
AT5G05370.1	4.69	3.12	3.89	3.90
AT3G09500.1	3.95	4.73	3.02	3.90
AT3G55770.7	7.17	0.46	4.03	3.89
AT1G67700.2	-0.37	2.89	9.12	3.88
AT3G51880.2	1.10	3.27	7.24	3.87
AT5G50920.1	2.05	3.94	5.62	3.87
AT2G40880.1	5.09	4.50	2.03	3.87
AT1G27530.1	7.03	2.81	1.74	3.86
AT1G73230.1	2.55	5.16	3.86	3.86
AT3G25530.1	3.12	9.28	-0.85	3.85
AT1G31812.1	3.78	4.41	3.36	3.85
AT2G40060.1	7.37	3.57	0.58	3.84
AT5G42790.1	5.35	2.38	3.76	3.83
AT3G20000.1	-1.63	10.26	2.83	3.82
AT4G21105.1	-2.18	6.94	6.68	3.81
AT3G13200.1	3.45	-2.03	10.00	3.81
AT3G02310.1	5.12	-0.90	7.17	3.80
AT3G44310.1	4.08	4.19	3.11	3.80
AT3G19820.1	6.30	2.39	2.67	3.79
AT1G48920.1	8.96	2.08	0.30	3.78
AT1G74050.1	3.08	5.49	2.77	3.78
AT3G14600.1	4.15	4.30	2.88	3.77
AT2G42310.1	5.87	3.75	1.69	3.77
AT3G02080.1	4.29	2.94	4.06	3.76
AT5G39570.2	2.71	3.13	5.41	3.75
AT2G39770.1	1.74	4.02	5.44	3.74
AT1G51650.1	3.61	5.44	2.14	3.73
AT1G66580.1	0.74	6.27	4.12	3.71
AT1G67280.1	1.43	5.70	3.98	3.70
AT3G15900.1	0.85	5.67	4.58	3.70
AT1G49240.1	10.16	1.15	-0.24	3.69
AT5G14410.2	-0.13	4.36	6.84	3.69
AT2G45790.1	1.19	5.91	3.96	3.69
AT5G47890.1	2.97	4.75	3.33	3.68
AT1G53750.1	4.60	5.41	1.04	3.68
AT2G32520.2	3.03	2.24	5.77	3.68
AT2G47170.1	10.09	0.71	0.24	3.68
AT2G29960.1	2.59	5.23	3.22	3.68
AT1G52030.1	-1.46	5.50	7.00	3.68
AT4G34700.1	2.92	3.57	4.51	3.66
AT1G32050.1	2.40	3.64	4.95	3.66
AT2G47690.1	3.07	3.52	4.38	3.66
AT5G65220.1	2.38	3.98	4.60	3.65
AT1G08360.1	3.80	3.43	3.73	3.65
AT1G58290.1	3.17	5.49	2.29	3.65
AT1G74560.3	1.28	4.29	5.29	3.62
AT1G61780.1	1.81	1.02	8.03	3.62
AT2G47610.1	3.47	2.74	4.63	3.62
AT1G01170.1	3.82	2.36	4.65	3.61
AT5G20900.1	4.81	4.74	1.29	3.61
AT2G21190.1	7.62	-1.01	4.16	3.59
AT3G03920.1	1.20	2.49	7.05	3.58
AT1G24020.1	4.12	4.05	2.53	3.56
AT2G16600.1	4.59	2.45	3.61	3.55
AT3G28900.1	3.88	2.88	3.89	3.55
AT5G26000.1	-0.15	6.05	4.74	3.55
AT1G11750.2	1.26	1.15	8.23	3.55
AT1G21930.1	6.23	3.01	1.39	3.54
AT3G26070.1	4.20	1.63	4.79	3.54

AT5G13650.2	6.21	6.96	12.97	8.71
AT4G15910.1	5.11	10.31	10.70	8.71
AT5G52840.1	13.00	8.51	4.59	8.70
AT3G62030.2	12.70	6.91	6.45	8.68
AT1G07770.1	7.20	8.51	10.27	8.66
AT2G23120.1	10.68	7.81	7.40	8.63
AT1G68238.1	7.04	8.76	10.02	8.61
AT3G10860.1	7.20	10.07	8.54	8.60
AT1G03600.1	4.94	10.49	10.38	8.60
AT5G56670.1	11.13	6.74	7.91	8.59
AT3G56290.1	4.95	11.25	9.54	8.58
AT4G38840.1	5.70	12.49	7.54	8.58
AT5G23740.1	11.87	5.37	8.50	8.58
AT5G01350.1	9.58	6.42	9.73	8.58
AT3G11510.1	9.12	7.59	9.00	8.57
AT1G27330.1	9.82	7.88	8.00	8.57
AT2G22670.4	9.30	5.74	10.62	8.56
AT3G02080.1	10.06	6.24	9.27	8.52
AT1G19000.1	12.93	4.69	7.94	8.52
AT2G31610.1	10.36	8.31	6.86	8.51
AT1G27435.1	10.97	10.00	4.55	8.50
AT1G68660.1	11.08	6.06	8.33	8.49
AT3G28940.1	10.66	6.43	8.38	8.49
AT4G34670.1	11.28	4.87	9.29	8.48
AT1G51400.1	9.97	7.11	8.35	8.48
AT3G24830.1	8.91	6.64	9.88	8.48
AT1G26550.1	7.37	5.30	12.68	8.45
AT3G53430.1	11.57	3.59	10.12	8.43
AT2G33040.1	6.51	7.84	10.92	8.42
AT1G56070.1	5.02	8.50	11.72	8.41
AT3G23050.1	8.21	5.23	11.76	8.40
AT5G28840.1	15.04	4.40	5.75	8.39
AT1G29250.1	11.12	6.36	7.70	8.39
AT1G14320.1	9.37	6.66	9.12	8.38
AT5G48580.1	8.17	7.39	9.55	8.37
AT1G72020.1	5.64	13.85	5.62	8.37
AT2G43560.1	9.22	9.69	6.19	8.37
AT4G26840.1	10.55	7.74	6.80	8.36
AT2G31570.1	8.02	7.52	9.55	8.36
AT1G48830.1	10.86	3.21	11.02	8.36
AT1G29930.1	7.47	8.68	8.92	8.36
AT1G32470.1	9.70	7.39	7.97	8.35
AT1G05850.1	4.77	9.83	10.42	8.34
AT4G11010.1	8.13	9.37	7.51	8.34
AT3G46010.2	15.86	4.05	5.04	8.32
AT3G02730.1	6.67	9.30	8.95	8.30
AT4G38680.1	7.65	8.48	8.79	8.30
AT1G18080.1	10.59	8.16	6.15	8.30
AT2G32090.1	8.05	7.59	9.24	8.29
AT1G44575.1	8.46	7.68	8.74	8.29
AT3G22230.1	8.28	9.00	7.58	8.29
AT5G27700.1	10.99	9.53	4.30	8.28
AT4G04640.1	7.21	9.64	7.98	8.28
AT5G17170.1	8.14	7.72	8.95	8.27
AT1G04480.1	11.59	4.90	8.32	8.27
AT3G23400.1	8.64	7.38	8.76	8.26
AT4G29735.2	1.51	14.47	8.79	8.26
AT1G52300.1	13.60	3.05	8.12	8.26
AT1G64370.1	7.60	9.64	7.52	8.26
AT3G04840.1	12.02	6.83	5.91	8.25
AT1G02780.1	10.61	6.97	7.17	8.25
AT5G27760.1	9.86	6.29	8.58	8.24
AT3G21055.2	8.11	7.60	8.98	8.23
AT2G06850.1	12.14	8.10	4.45	8.23
AT2G33370.1	11.06	5.96	7.66	8.23
AT3G45930.1	12.47	5.59	6.58	8.21
AT1G11860.3	7.58	7.61	9.44	8.21
AT3G60770.1	7.79	5.28	11.55	8.21
AT5G24165.1	8.00	8.32	8.24	8.19
AT3G46560.1	11.08	6.90	6.57	8.18
AT2G37470.1	10.15	6.48	7.90	8.18
AT5G40370.2	5.64	8.59	10.24	8.16
AT2G23670.1	10.32	5.96	8.18	8.15
AT1G07890.1	10.17	6.73	7.55	8.15
AT3G16080.1	6.19	8.66	9.59	8.15
AT5G21274.1	4.34	8.51	11.59	8.15
AT3G55750.1	9.38	6.00	9.06	8.14
AT5G61170.1	11.68	4.51	8.23	8.14
AT1G04945.3	5.71	8.00	10.71	8.14
AT3G09860.1	7.15	8.73	8.49	8.12
AT5G64140.1	10.93	6.27	7.12	8.11
AT5G16470.1	5.44	9.54	9.32	8.10
AT5G28750.1	8.03	10.01	6.25	8.10
AT4G12600.2	15.99	2.37	5.94	8.10
AT2G24790.1	10.47	6.32	7.48	8.09
AT5G19760.1	9.09	7.21	7.93	8.08
AT1G64230.4	8.81	6.95	8.44	8.07
AT3G46780.1	4.60	2.40	3.61	3.54
AT1G47970.1	5.82	4.45	0.34	3.53
AT3G30775.1	-1.47	3.69	8.37	3.53
AT2G47470.1	0.84	3.31	6.42	3.52
AT5G02240.1	1.90	5.78	2.87	3.52
AT5G20240.1	3.43	4.17	2.95	3.52
AT5G48810.1	6.77	2.29	1.45	3.50
AT5G19760.1	2.13	4.77	3.60	3.50
AT3G52090.2	3.74	2.32	4.44	3.50
AT3G23390.1	4.86	3.82	1.80	3.49
AT5G01600.1	1.29	2.34	6.84	3.49
AT1G16920.1	-0.25	2.55	8.18	3.49
AT5G16470.1	4.40	0.71	5.36	3.49
AT1G08570.1	-3.84	3.95	10.34	3.48
AT1G47260.1	3.68	4.74	2.01	3.48
AT1G55260.1	3.15	3.47	3.80	3.48
AT5G23940.1	0.50	2.67	7.23	3.47
AT5G19510.1	4.71	4.24	1.42	3.46
AT1G25260.1	5.02	0.97	4.38	3.46
AT1G60010.1	2.59	2.56	5.22	3.46
AT5G01750.2	4.76	-0.79	6.39	3.46
AT5G48760.1	3.83	1.41	5.13	3.45
AT1G78380.1	4.01	3.98	2.37	3.45
AT2G31490.1	3.44	4.27	2.64	3.45
AT2G17360.1	4.94	3.31	2.07	3.44
AT1G09760.1	5.04	3.21	2.06	3.44
AT1G76180.1	1.31	4.83	4.17	3.44
AT1G14450.2	1.56	4.30	4.44	3.43
AT1G20260.1	-0.97	2.16	9.08	3.43
AT3G25220.1	3.89	3.21	3.16	3.42
AT2G28190.1	1.95	3.56	4.72	3.41
AT1G04410.1	5.22	3.25	1.75	3.41
AT1G74270.1	1.89	3.73	4.60	3.41
AT3G54560.1	1.58	4.59	4.02	3.40
AT1G07920.1	3.51	3.74	2.90	3.38
AT2G33370.1	2.42	4.81	2.91	3.38
AT5G09900.3	5.79	4.71	-0.38	3.37
AT1G22450.1	0.37	5.64	4.10	3.37
AT1G78210.1	-0.07	5.09	5.09	3.37
AT3G50820.1	4.31	3.56	2.20	3.36
AT2G15960.1	-1.05	3.74	7.35	3.35
AT2G43810.1	7.40	-1.03	3.65	3.34
AT5G09660.4	5.36	3.79	0.85	3.33
AT1G47278.2	3.32	2.50	4.18	3.33
AT1G34030.1	3.13	3.34	3.49	3.32
AT1G64750.3	1.78	4.31	3.87	3.32
AT1G79010.1	1.49	5.80	2.64	3.31
AT4G14320.2	1.92	4.80	3.19	3.31
AT2G27530.1	2.65	2.51	4.74	3.30
AT4G39330.1	3.86	3.05	2.96	3.29
AT5G43700.1	2.75	-1.43	8.52	3.28
AT5G51940.1	-0.91	2.36	8.36	3.27
AT4G38740.1	3.05	4.94	1.79	3.26
AT2G41840.1	7.10	1.76	0.91	3.26
AT3G15450.1	-7.60	9.17	8.18	3.25
AT4G22310.1	4.76	2.41	2.58	3.25
AT2G37600.1	1.70	6.44	1.61	3.25
AT3G09200.1	5.56	3.47	0.68	3.24
AT4G33110.1	7.49	3.62	-1.40	3.24
AT3G24830.1	4.82	2.19	2.68	3.23
AT5G24314.2	3.51	4.26	1.88	3.22
AT1G17840.1	1.52	4.45	3.68	3.22
AT1G56200.1	1.99	2.93	4.72	3.21
AT1G17200.1	2.59	2.42	4.62	3.21
AT4G05050.1	4.15	3.75	1.73	3.21
AT3G17020.1	3.40	3.21	3.02	3.21
AT5G27700.1	1.86	4.82	2.93	3.20
AT1G71950.1	5.35	0.00	4.26	3.20
AT1G26550.1	2.64	1.53	5.43	3.20
AT4G31990.3	5.43	9.05	-4.91	3.19
AT1G05205.1	3.46	2.86	3.25	3.19
AT3G26740.1	-1.80	4.57	6.80	3.19
AT3G56340.1	5.03	-1.54	6.07	3.19
AT3G15730.1	1.40	2.43	5.71	3.18
AT4G22570.1	-0.64	4.72	5.46	3.18
AT2G01140.1	5.31	1.58	2.64	3.17
AT5G01530.1	4.80	3.08	1.64	3.17
AT2G42210.2	2.22	2.72	4.58	3.17
AT3G18410.1	2.28	3.83	3.38	3.16
AT4G37925.1	-1.52	6.96	4.04	3.16
AT1G16470.1	5.28	1.75	2.43	3.15
AT5G38480.1	5.62	1.06	2.75	3.14
AT3G01390.1	3.73	4.11	1.57	3.14
AT5G20180.1	1.21	3.52	4.67	3.13
AT5G62350.1	4.70	3.91	0.77	3.13
AT3G09980.1	1.43	1.88	6.04	3.12
AT1G69620.1	2.51	2.83	4.01	3.12

AT2G29340.1	8.03	9.83	6.35	8.07	AT2G28430.1	0.66	4.58	4.09	3.11
AT1G18540.1	10.03	5.53	8.62	8.06	AT4G14880.1	0.55	4.82	3.95	3.11
AT2G23600.2	5.64	12.04	6.49	8.06	AT5G64350.1	0.56	4.89	3.87	3.11
AT1G13245.1	6.45	4.12	13.57	8.05	AT2G35120.1	4.05	5.42	-0.16	3.10
AT3G46780.1	5.40	8.90	9.71	8.01	AT5G07960.1	2.28	2.71	4.32	3.10
AT5G02120.1	9.78	6.96	7.24	7.99	AT5G40370.2	0.05	7.18	2.07	3.10
AT1G70410.2	10.22	1.67	12.08	7.99	AT4G15802.1	2.18	1.54	5.56	3.10
AT2G26670.1	8.78	4.14	11.05	7.99	AT4G10340.1	2.79	2.83	3.65	3.09
AT5G43750.1	4.69	8.95	10.28	7.97	AT4G39200.1	3.06	4.63	1.56	3.08
AT2G42220.1	9.79	5.76	8.36	7.97	AT3G61470.1	2.79	2.85	3.58	3.07
AT4G14040.1	7.11	5.76	10.99	7.96	AT5G03660.1	2.25	5.08	1.86	3.07
AT5G51970.1	4.44	7.52	11.91	7.96	AT1G09690.1	2.44	3.99	2.76	3.06
AT2G30410.1	4.89	7.20	11.75	7.94	AT5G22650.1	3.14	3.08	2.96	3.06
AT5G13850.1	7.64	9.17	6.98	7.93	AT1G77080.8	1.68	3.75	3.74	3.06
AT3G05590.1	9.89	5.89	7.99	7.92	AT2G47380.1	1.51	4.35	3.27	3.04
AT5G22440.1	6.60	6.26	10.91	7.92	AT1G79390.1	-0.83	4.56	5.40	3.04
AT5G43850.1	7.90	9.64	6.17	7.90	AT2G24200.1	1.77	8.18	-0.82	3.04
AT4G01050.2	13.12	4.84	5.74	7.90	AT3G47836.1	2.71	4.49	1.91	3.04
AT5G12140.1	8.69	8.58	6.36	7.88	AT5G02380.1	3.02	2.94	3.15	3.03
AT5G65670.1	5.64	7.66	10.30	7.86	AT1G16740.1	6.02	-0.23	3.31	3.03
AT1G79550.1	6.24	6.40	10.93	7.86	AT3G43980.1	0.31	1.40	7.37	3.02
AT5G48490.1	6.97	8.13	8.46	7.85	AT3G55440.1	-0.15	5.35	3.85	3.02
AT1G78040.1	8.00	8.57	6.96	7.85	AT4G33670.1	-0.40	4.81	4.64	3.02
AT1G69620.1	8.92	6.16	8.45	7.84	AT3G15640.1	5.11	1.62	2.31	3.01
AT4G12800.2	7.86	8.75	6.90	7.84	AT5G49720.1	4.16	0.98	3.88	3.01
AT1G23390.1	4.89	11.00	7.60	7.83	AT2G33040.1	2.18	4.36	2.47	3.00
AT1G51060.1	10.41	7.85	5.22	7.83	AT3G15353.1	2.61	2.81	3.59	3.00
AT4G40030.2	8.25	9.74	5.43	7.81	AT1G68660.1	0.50	-0.92	9.40	2.99
AT2G28800.1	12.84	2.97	7.59	7.80	AT5G52470.1	5.71	1.38	1.89	2.99
AT2G32060.1	9.84	5.91	7.63	7.79	AT4G13940.1	4.87	2.92	1.17	2.99
AT2G36170.1	9.88	5.87	7.60	7.79	AT3G57870.1	1.72	4.51	2.73	2.98
AT2G17390.1	7.12	6.55	9.66	7.78	AT5G35530.1	3.70	2.01	3.24	2.98
AT5G02610.2	10.70	4.50	8.12	7.77	AT4G10610.1	4.23	6.23	-1.53	2.98
AT5G63150.1	5.51	9.20	8.60	7.77	AT3G60820.1	5.63	1.21	2.08	2.97
AT1G64090.2	7.96	6.09	9.18	7.74	AT1G30630.1	2.00	4.66	2.25	2.97
AT1G20020.1	10.28	6.02	6.93	7.74	AT1G41880.1	2.96	2.69	3.24	2.97
AT2G37190.1	8.15	7.95	7.10	7.73	AT5G27850.1	2.55	3.15	3.16	2.95
AT1G12440.1	8.26	10.03	4.90	7.73	AT1G04270.1	3.28	3.24	2.32	2.95
AT2G45740.1	6.45	7.72	8.98	7.72	AT1G33990.1	3.84	2.21	2.80	2.95
AT5G48300.1	5.50	8.62	9.02	7.71	AT3G06610.1	4.44	0.80	3.59	2.94
AT1G70830.1	4.75	7.27	11.07	7.70	AT3G26650.1	2.17	2.45	4.18	2.93
AT3G14420.1	12.93	1.92	8.24	7.69	AT4G02080.1	3.05	0.43	5.31	2.93
AT1G74060.1	8.67	5.37	9.03	7.69	AT5G64130.3	1.13	5.14	2.49	2.92
AT4G01897.1	6.87	4.74	11.42	7.68	AT3G02200.2	-1.32	1.17	8.90	2.92
AT3G56800.1	5.36	8.83	8.84	7.68	AT5G65205.1	5.87	1.91	0.95	2.91
AT1G67740.1	4.09	7.42	11.50	7.67	AT5G17770.1	5.36	2.38	0.97	2.90
AT1G52220.1	8.17	7.89	6.90	7.65	AT1G19570.1	3.30	2.66	2.74	2.90
AT3G06700.1	9.25	5.49	8.19	7.65	AT1G77350.1	1.21	4.74	2.74	2.90
AT1G67250.1	5.00	8.42	9.48	7.64	AT1G35310.1	3.04	3.48	2.15	2.89
AT3G46040.1	8.40	7.02	7.45	7.63	AT1G26880.1	2.04	2.78	3.84	2.89
AT4G02080.1	10.33	7.24	5.28	7.62	AT1G12570.1	5.09	2.03	1.53	2.88
AT1G78020.1	7.57	7.90	7.35	7.61	AT4G18730.1	3.35	2.20	3.09	2.88
AT4G09800.1	9.79	3.79	9.24	7.61	AT4G11010.1	2.45	3.11	3.04	2.87
AT3G50820.1	8.25	7.33	7.21	7.60	AT5G48580.1	4.82	2.16	1.61	2.86
AT5G06060.1	6.24	5.52	11.04	7.60	AT5G17870.2	1.41	3.02	4.13	2.85
AT4G34350.1	8.25	2.70	11.82	7.59	AT5G39600.1	2.76	2.97	2.82	2.85
AT2G47450.1	8.09	4.98	9.66	7.58	AT4G27090.1	2.75	1.87	3.92	2.85
AT3G62290.1	5.66	6.86	10.18	7.56	AT3G62400.2	2.35	2.52	3.64	2.84
AT4G33865.1	7.48	7.39	7.81	7.56	AT5G27760.1	0.81	4.65	3.06	2.84
AT4G40040.1	6.76	7.95	7.96	7.56	AT3G44010.1	4.98	2.74	0.79	2.84
AT3G62400.2	10.69	5.88	6.09	7.55	AT2G46230.1	2.28	6.23	0.00	2.84
AT3G44590.1	8.80	5.56	8.30	7.55	AT1G55805.1	2.96	2.82	2.73	2.83
AT3G15353.1	7.09	7.25	8.28	7.54	AT5G10960.1	0.51	6.89	1.09	2.83
AT4G13170.1	8.47	5.38	8.69	7.52	AT1G08380.1	2.75	3.12	2.61	2.83
AT3G45030.1	8.60	4.02	9.87	7.50	AT3G52580.1	4.21	3.44	0.82	2.82
AT5G64130.3	4.16	8.92	9.33	7.47	AT4G35100.1	6.51	1.45	0.50	2.82
AT3G51260.1	9.34	4.68	8.36	7.46	AT2G40510.1	2.02	3.92	2.50	2.81
AT1G07940.1	11.25	3.90	7.21	7.46	AT2G44060.1	4.79	4.73	-1.14	2.79
AT1G54630.1	5.12	7.82	9.41	7.45	AT3G08740.1	-1.22	3.48	6.10	2.79
AT2G21290.1	4.21	10.67	7.39	7.43	AT5G20920.1	0.38	3.95	4.03	2.79
AT5G38660.2	8.72	6.76	6.76	7.41	AT3G08940.2	-1.78	3.74	6.39	2.78
AT5G64040.2	7.06	7.47	7.66	7.40	AT1G32210.1	2.71	1.66	3.94	2.77
AT3G19820.1	8.58	6.50	7.11	7.40	AT3G63540.1	5.94	1.80	0.57	2.77
AT5G48760.1	8.42	5.66	8.10	7.39	AT2G30620.1	2.56	3.11	2.62	2.76
AT5G64850.1	5.87	7.69	8.59	7.38	AT5G47190.1	0.79	5.53	1.96	2.76
AT1G65290.1	9.07	6.79	6.29	7.38	AT1G54690.1	2.03	-0.23	6.44	2.74
AT2G43810.1	3.59	7.57	10.98	7.38	AT1G13440.1	2.17	3.80	2.24	2.74
AT5G44680.1	10.83	4.64	6.66	7.38	AT3G60210.1	-0.44	4.69	3.93	2.73
AT2G44120.2	9.84	5.20	7.05	7.36	AT5G16060.1	0.70	8.12	-0.63	2.73
AT1G67785.1	8.25	5.99	7.85	7.36	AT5G28840.1	0.73	3.17	4.28	2.73
AT2G05070.1	6.77	6.78	8.53	7.36	AT5G54770.1	-0.77	3.02	5.92	2.73
AT5G46430.1	8.08	6.64	7.34	7.35	AT2G44120.2	3.88	3.90	0.37	2.72
AT2G36160.1	8.17	6.19	7.67	7.34	AT5G64040.2	5.42	1.98	0.75	2.72
AT2G29450.1	8.88	6.30	6.83	7.34	AT1G35720.1	2.52	3.92	1.70	2.72
AT2G20260.1	4.95	8.56	8.45	7.32	AT2G21870.1	1.84	3.59	2.71	2.71
AT4G13930.1	9.45	7.63	4.86	7.32	AT2G24790.1	1.95	3.07	3.12	2.71
AT5G11170.1	9.92	6.34	5.53	7.26	AT1G72260.1	1.46	3.32	3.34	2.71

AT5G53560.1	9.11	5.99	6.65	7.25	AT3G09840.1	-1.36	3.83	5.61	2.69
AT4G38100.1	9.96	4.48	7.29	7.24	AT1G75240.1	3.19	0.41	4.46	2.69
AT3G51730.1	10.13	2.21	9.35	7.23	AT1G72970.1	8.20	0.31	-0.44	2.69
AT1G43670.1	8.26	5.28	8.12	7.22	AT4G14420.1	2.11	3.27	2.68	2.69
AT2G44310.1	2.66	6.04	12.93	7.21	AT5G35630.1	2.64	2.91	2.48	2.68
AT3G01120.1	9.87	10.74	0.98	7.20	AT2G27030.3	2.77	2.07	3.17	2.67
AT5G46020.1	8.28	10.34	2.93	7.18	AT1G65290.1	3.27	2.59	2.10	2.65
AT3G55800.1	9.56	4.70	7.26	7.17	AT1G67430.1	1.88	2.31	3.76	2.65
AT2G25210.1	8.38	5.59	7.54	7.17	AT5G18380.1	2.37	1.63	3.96	2.65
AT5G42980.1	10.64	5.89	4.96	7.16	AT5G53560.1	2.62	2.02	3.30	2.65
AT3G04920.1	7.91	4.67	8.91	7.16	AT2G33470.1	3.02	1.98	2.90	2.63
AT3G07230.1	7.11	8.07	6.27	7.15	AT1G75840.1	6.00	0.68	1.19	2.62
AT5G20720.1	5.61	7.14	8.64	7.13	AT2G33800.1	1.98	-0.01	5.87	2.62
AT1G01170.1	8.34	8.01	5.03	7.13	AT1G20020.1	-2.20	5.29	4.72	2.61
AT1G56330.1	7.82	8.17	5.37	7.12	AT3G08610.1	2.16	3.64	2.01	2.60
AT5G04830.1	6.97	8.09	6.26	7.10	AT4G29010.1	-0.42	3.81	4.41	2.60
AT2G24020.1	6.84	8.45	6.01	7.10	AT2G47240.1	-0.73	3.03	5.48	2.59
AT3G60245.1	8.37	6.70	6.22	7.09	AT2G20260.1	2.71	1.35	3.72	2.59
AT4G09650.1	8.67	5.68	6.92	7.09	AT3G61440.1	5.06	2.56	0.15	2.59
AT5G59690.1	7.43	7.13	6.66	7.07	AT4G14385.1	1.10	-3.28	9.92	2.58
AT2G24395.1	4.34	6.21	10.66	7.07	AT1G03475.1	-0.48	2.32	5.89	2.58
AT4G34760.1	8.55	8.17	4.47	7.06	AT4G29735.2	2.67	1.57	3.47	2.57
AT5G35680.3	11.51	3.71	5.95	7.05	AT2G05990.1	2.39	0.21	5.10	2.56
AT1G66580.1	7.43	6.06	7.68	7.05	AT5G04800.1	3.12	3.09	1.47	2.56
AT4G25740.1	10.32	4.57	6.24	7.04	AT5G42890.1	-0.32	3.85	4.14	2.55
AT2G45960.3	7.00	6.72	7.36	7.03	AT3G04400.1	2.36	2.57	2.73	2.55
AT1G79010.1	6.78	5.58	8.72	7.03	AT3G58730.1	5.20	5.17	-2.75	2.54
AT5G23290.1	6.54	6.88	7.65	7.02	AT1G33120.1	3.86	3.00	0.77	2.54
AT3G46030.1	7.89	6.67	6.51	7.02	AT4G21620.1	3.18	3.48	0.96	2.54
AT2G21870.1	5.69	8.05	7.33	7.02	AT5G53650.1	-0.36	2.17	5.80	2.54
AT5G52650.1	8.11	3.61	9.32	7.01	AT5G27770.1	1.49	2.84	3.27	2.53
AT3G44310.1	7.15	6.98	6.91	7.01	AT3G12630.1	-0.03	2.54	5.10	2.53
AT5G40770.1	8.07	6.57	6.38	7.01	AT4G19350.1	-1.37	5.75	3.19	2.52
AT1G34030.1	8.18	6.50	6.25	6.98	AT1G57720.1	4.50	2.26	0.79	2.52
AT5G60670.1	6.47	6.26	8.19	6.97	AT5G37780.3	1.00	2.76	3.77	2.51
AT2G27030.3	6.86	8.03	6.03	6.97	AT5G03300.1	6.51	0.88	0.13	2.51
AT1G29660.1	8.54	2.73	9.63	6.97	AT3G52880.2	2.70	2.70	2.12	2.50
AT4G25890.1	6.58	5.62	8.70	6.97	AT1G09070.1	2.72	3.87	0.90	2.50
AT5G38520.2	5.13	8.66	7.10	6.97	AT5G65430.3	2.07	1.37	4.02	2.49
AT4G27960.2	5.42	7.80	7.65	6.95	AT5G56940.1	3.50	0.22	3.72	2.48
AT5G45775.2	8.29	5.41	7.12	6.94	AT2G47110.1	2.72	2.51	2.19	2.47
AT4G13850.1	10.10	3.56	7.14	6.93	AT1G70490.1	5.71	0.24	1.48	2.47
AT1G70490.1	7.47	8.76	4.47	6.90	AT1G56070.1	2.97	1.88	2.56	2.47
AT2G30870.1	5.50	6.12	9.02	6.88	AT4G30010.1	3.06	1.85	2.50	2.47
AT5G66570.1	5.57	7.08	7.94	6.86	AT3G27360.1	1.65	3.51	2.22	2.46
AT1G31170.4	3.55	6.10	10.88	6.85	AT1G61520.1	2.14	2.35	2.90	2.46
AT1G04250.1	10.42	8.59	1.53	6.84	AT1G55210.1	3.68	1.85	1.82	2.45
AT5G39740.1	10.03	5.16	5.29	6.82	AT3G22845.1	2.70	1.92	2.73	2.45
AT5G28500.1	5.51	4.21	10.75	6.82	AT2G44310.1	0.96	0.20	6.18	2.45
AT2G45070.1	7.83	6.94	5.68	6.82	AT1G02780.1	2.02	2.20	3.11	2.44
AT3G15480.1	7.35	10.50	2.59	6.81	AT2G45860.1	0.12	4.88	2.30	2.43
AT2G28430.1	7.91	3.99	8.53	6.81	AT5G15520.1	2.70	4.74	-0.15	2.43
AT1G77090.1	12.07	3.41	4.92	6.80	AT4G05180.1	5.30	0.73	1.26	2.43
AT5G64460.10	7.32	11.34	1.73	6.80	AT1G11475.1	4.00	2.19	1.09	2.43
AT3G49870.1	10.79	4.65	4.92	6.78	AT5G59970.1	0.77	3.98	2.50	2.42
AT1G48920.1	7.40	4.97	7.97	6.78	AT3G56130.1	3.71	1.26	2.28	2.41
AT5G11480.1	5.68	5.98	8.68	6.78	AT5G67590.1	-0.67	4.14	3.77	2.41
AT4G03280.1	6.90	6.84	6.52	6.75	AT1G20693.1	2.91	2.09	2.24	2.41
AT1G55480.1	5.79	6.84	7.57	6.73	AT4G29040.1	6.87	0.73	-0.42	2.39
AT1G10590.3	6.59	6.31	7.29	6.73	AT3G23830.1	-0.43	4.54	3.06	2.39
AT5G59970.1	7.30	3.61	9.23	6.71	AT5G35360.3	2.04	0.35	4.78	2.39
AT1G11840.6	8.69	3.58	7.86	6.71	AT5G04830.1	3.21	2.65	1.31	2.39
AT1G09590.1	12.75	3.35	3.88	6.66	AT1G13060.2	4.05	-0.71	3.82	2.39
AT2G05100.2	6.92	6.08	6.92	6.64	AT4G11150.1	2.53	1.27	3.36	2.39
AT1G52230.1	8.95	4.61	6.35	6.64	AT5G20290.1	2.59	1.69	2.86	2.38
AT5G50460.1	7.45	3.20	9.20	6.62	AT4G22220.1	2.68	1.96	2.50	2.38
AT2G33470.1	5.83	5.35	8.64	6.61	AT4G27500.1	3.90	2.91	0.32	2.38
AT2G18328.1	5.90	7.28	6.64	6.61	AT3G25520.1	2.88	1.57	2.67	2.37
AT2G27960.1	7.81	6.83	5.16	6.60	AT5G26742.2	2.21	3.44	1.46	2.37
AT2G42540.2	7.08	3.17	9.53	6.60	AT2G36170.1	4.15	1.88	1.05	2.36
AT4G09010.3	2.41	10.03	7.33	6.59	AT2G03440.1	4.09	1.97	1.00	2.35
AT1G07820.1	9.82	5.11	4.82	6.58	AT3G47370.1	3.08	3.53	0.44	2.35
AT5G28060.1	6.42	7.01	6.31	6.58	AT3G12290.1	0.14	3.01	3.90	2.35
AT2G18040.1	9.41	5.63	4.67	6.57	AT2G19730.1	1.47	2.94	2.62	2.34
AT1G60870.1	8.10	8.01	3.61	6.57	AT1G08880.1	1.94	2.41	2.68	2.34
AT5G59910.1	8.82	1.90	8.98	6.57	AT3G16470.1	2.92	2.39	1.69	2.33
AT5G39530.1	11.15	3.94	4.58	6.56	AT2G41650.1	-1.65	3.09	5.56	2.33
AT1G32070.2	5.47	3.16	10.93	6.52	AT1G08200.1	1.02	4.34	1.62	2.33
AT3G53870.1	7.44	4.86	7.25	6.52	AT1G20450.1	2.32	2.17	2.48	2.33
AT5G02160.1	0.49	8.59	10.39	6.49	AT5G59690.1	0.84	2.83	3.29	2.32
AT4G18480.1	7.75	4.93	6.77	6.48	AT3G27380.1	1.40	2.47	3.08	2.32
AT4G14420.1	2.59	8.08	8.78	6.48	AT2G05310.1	2.00	3.94	0.99	2.31
AT4G31700.1	6.37	4.70	8.32	6.47	AT5G55190.1	4.08	-1.40	4.22	2.30
AT5G20290.1	7.41	5.09	6.89	6.46	AT5G54940.1	2.88	0.51	3.51	2.30
AT1G49975.1	7.00	2.91	9.48	6.46	AT4G00810.1	1.85	3.81	1.21	2.29
AT5G62300.1	-0.20	11.31	8.25	6.45	AT1G22780.1	0.50	2.19	4.15	2.28
AT5G07090.1	9.46	2.23	7.64	6.44	AT5G17170.1	0.81	5.40	0.60	2.27

AT3G51600.1	6.07	6.12	7.12	6.43	AT3G53740.2	2.31	2.03	2.48	2.27
AT1G74050.1	7.99	5.32	5.98	6.43	AT1G06760.1	1.68	3.08	2.02	2.26
AT1G14980.1	9.63	4.51	5.12	6.42	AT2G32650.1	2.00	4.76	0.00	2.25
AT1G43170.1	11.42	4.27	3.52	6.40	AT5G53880.1	4.59	3.08	-0.93	2.25
AT4G27380.1	4.11	9.61	5.47	6.40	AT5G43850.1	-4.81	5.16	6.37	2.24
AT3G48930.1	6.86	7.10	5.23	6.40	AT5G44340.1	3.23	1.84	1.65	2.24
AT1G54410.1	9.73	2.99	6.46	6.39	AT1G12080.2	5.19	0.44	1.09	2.24
AT2G39770.1	4.78	4.17	10.22	6.39	AT5G33370.1	4.03	2.19	0.49	2.24
AT1G22780.1	8.42	1.94	8.78	6.38	AT1G23490.1	4.04	-0.34	3.01	2.24
AT5G42790.1	10.20	4.36	4.53	6.37	AT5G59613.1	0.09	3.73	2.86	2.23
AT2G17360.1	9.06	4.51	5.50	6.36	AT5G03345.2	2.36	1.02	3.28	2.22
AT4G21280.2	6.41	6.65	5.99	6.35	AT4G23870.1	0.06	3.21	3.39	2.22
AT2G36060.2	8.59	5.34	5.11	6.35	AT4G32470.1	-4.43	4.19	6.88	2.22
AT2G03440.1	4.62	6.53	7.86	6.34	AT2G46820.1	2.49	2.75	1.40	2.21
AT2G42610.1	5.44	10.84	2.69	6.33	AT1G13930.1	4.78	1.05	0.82	2.21
AT1G12900.5	6.44	5.91	6.56	6.30	AT3G11940.1	0.75	3.07	2.75	2.19
AT3G18740.1	7.73	4.91	6.20	6.28	AT3G13120.1	-1.38	3.46	4.50	2.19
AT3G43980.1	7.61	6.71	4.43	6.25	AT3G44590.1	3.28	0.73	2.53	2.18
AT2G14750.1	2.59	9.32	6.82	6.24	AT4G16500.1	2.22	1.20	3.10	2.17
AT2G09990.1	2.56	7.88	8.19	6.21	AT1G70370.1	7.83	1.56	-2.89	2.17
AT3G62870.1	8.94	4.15	5.54	6.21	AT1G27400.1	1.60	2.91	1.96	2.16
AT1G32210.1	2.26	5.66	10.66	6.19	AT1G73655.1	2.01	0.87	3.60	2.16
AT3G09440.1	9.95	6.43	2.20	6.19	AT3G46010.2	2.36	1.47	2.65	2.16
AT3G56360.1	11.03	3.99	3.54	6.19	AT5G11170.1	0.20	4.46	1.80	2.15
AT1G61780.1	6.83	3.96	7.70	6.16	AT2G21160.1	1.55	0.31	4.59	2.15
AT3G26450.1	7.37	9.32	1.80	6.16	AT1G64090.2	4.48	2.50	-0.54	2.14
AT1G30380.1	5.61	8.21	4.62	6.15	AT3G44890.1	2.16	3.02	1.23	2.14
AT2G45860.1	8.08	4.86	5.46	6.13	AT4G29030.1	4.03	1.94	0.42	2.13
AT5G03345.2	4.79	5.77	7.82	6.13	AT2G40205.1	1.09	2.83	2.46	2.13
AT3G22320.1	2.64	9.98	5.75	6.12	AT4G12600.2	1.14	2.48	2.76	2.13
AT3G54050.1	5.09	5.96	7.30	6.12	AT3G04920.1	2.19	1.51	2.67	2.12
AT4G15930.1	6.37	6.14	5.76	6.09	AT4G38630.1	3.04	-0.17	3.49	2.12
AT3G26710.1	12.13	2.42	3.71	6.09	AT2G19740.1	0.60	2.59	3.17	2.12
AT3G55170.1	5.28	8.19	4.74	6.07	AT1G72020.1	3.10	3.10	0.14	2.11
AT4G19200.1	5.66	6.57	5.97	6.07	AT3G62530.1	0.51	2.46	3.33	2.10
AT2G29960.1	8.83	8.46	0.90	6.06	AT2G43460.1	2.25	2.97	1.09	2.10
AT3G08520.1	7.32	5.34	5.50	6.05	AT2G38540.1	2.29	2.09	1.91	2.10
AT5G42070.1	6.34	5.59	6.19	6.04	AT4G02620.1	1.89	2.20	2.19	2.09
AT1G56200.1	2.54	7.56	8.01	6.04	AT5G54900.1	3.22	4.70	-1.64	2.09
AT2G41840.1	7.67	4.16	6.25	6.03	AT5G22020.1	1.34	2.28	2.64	2.09
AT3G54890.1	6.98	4.85	6.23	6.02	AT1G57860.1	1.94	3.45	0.86	2.08
AT1G20696.2	8.85	7.07	2.06	5.99	AT5G20090.1	0.88	4.00	1.34	2.07
AT2G37270.1	10.46	3.85	3.64	5.98	AT5G47700.1	2.43	2.08	1.70	2.07
AT5G23060.1	6.79	5.24	5.91	5.98	AT1G67250.1	2.26	2.34	1.60	2.06
AT2G18740.1	5.73	8.93	3.26	5.97	AT5G48480.1	-2.04	4.64	3.59	2.06
AT1G29910.1	7.02	5.03	5.86	5.97	AT1G54580.1	2.28	1.52	2.31	2.04
AT5G67510.1	5.64	6.41	5.85	5.97	AT1G67785.1	1.53	3.08	1.49	2.03
AT4G37800.1	8.56	4.16	5.15	5.95	AT4G23820.1	6.21	1.30	-1.43	2.03
AT4G17390.1	9.32	0.99	7.40	5.90	AT1G15400.3	1.40	2.51	2.17	2.02
AT4G09320.1	6.79	3.58	7.24	5.87	AT1G57660.1	2.79	0.75	2.53	2.02
AT4G15630.1	1.87	6.29	9.43	5.86	AT4G15000.1	1.80	1.53	2.73	2.02
AT5G20920.1	2.05	6.03	9.49	5.86	AT1G20696.2	5.71	0.28	0.04	2.01
AT4G29480.1	8.94	5.25	3.33	5.84	AT2G43090.1	1.54	3.75	0.74	2.01
AT4G05050.1	9.19	2.39	5.95	5.84	AT4G01940.1	-0.56	5.72	0.84	2.00
AT1G17200.1	7.75	1.25	8.45	5.82	AT2G46540.1	4.76	0.17	1.07	2.00
AT5G50250.1	7.87	3.55	6.01	5.81	AT4G13615.1	-0.69	4.49	2.20	2.00
AT5G02380.1	5.71	5.62	6.10	5.81	AT5G62700.1	-0.13	5.48	0.65	2.00
AT3G56240.1	6.53	6.74	4.12	5.80	AT1G14320.1	2.30	1.86	1.83	2.00
AT3G12490.2	5.54	4.67	7.17	5.79	AT3G02230.1	-2.42	5.45	2.96	2.00
AT2G25080.1	3.10	9.68	4.59	5.79	AT4G29480.1	1.72	2.63	1.63	1.99
AT3G59940.1	2.60	7.07	7.60	5.76	AT5G25460.1	1.29	5.18	-0.50	1.99
AT3G45980.1	3.52	8.56	5.14	5.74	AT3G29240.1	0.55	-1.49	6.90	1.99
AT4G02725.1	10.05	2.41	4.68	5.71	AT1G27350.1	0.04	4.31	1.61	1.99
AT1G26470.1	6.57	2.31	8.13	5.67	AT5G23290.1	6.57	-1.44	0.83	1.98
AT1G08380.1	7.20	4.32	5.48	5.67	AT2G39730.1	2.81	1.43	1.71	1.98
AT5G22650.1	7.56	2.99	6.42	5.66	AT2G21130.1	1.77	2.88	1.29	1.98
AT2G37170.2	1.47	10.10	5.40	5.66	AT5G67560.1	0.11	3.44	2.36	1.97
AT4G05180.1	6.13	5.21	5.58	5.64	AT1G23290.1	3.46	0.99	1.45	1.97
AT1G74470.1	7.55	4.86	4.47	5.63	AT4G30330.1	5.47	1.94	-1.51	1.97
AT3G01280.1	12.36	2.13	2.27	5.59	AT4G36800.1	4.70	0.35	0.85	1.97
AT4G34870.1	5.50	5.63	5.62	5.58	AT5G58740.1	0.96	-0.67	5.60	1.96
AT5G01530.1	5.38	5.34	5.99	5.57	AT3G48930.1	1.06	2.50	2.32	1.96
AT2G47610.1	7.49	3.71	5.39	5.53	AT1G67090.1	2.43	1.28	2.18	1.96
AT5G10360.1	5.75	4.13	6.71	5.53	AT1G44810.1	2.33	1.34	2.18	1.95
AT3G12390.1	9.39	4.60	2.53	5.51	AT4G25890.1	3.19	1.34	1.33	1.95
AT2G47170.1	7.08	6.24	3.20	5.51	AT5G16130.1	4.04	0.66	1.14	1.94
AT5G47210.1	7.43	1.65	7.43	5.50	AT4G16720.1	1.75	1.02	3.05	1.94
AT1G14400.1	6.22	6.96	3.31	5.49	AT1G74060.1	2.19	1.27	2.35	1.94
AT3G23830.1	5.20	4.51	6.75	5.49	AT3G62030.2	1.01	1.46	3.32	1.93
AT5G02240.1	10.02	0.37	6.01	5.47	AT1G24360.1	1.25	0.56	3.94	1.92
AT3G47470.1	8.09	3.01	5.29	5.46	AT1G53850.1	1.62	2.45	1.67	1.91
AT5G53940.1	6.71	0.00	9.62	5.44	AT4G30996.1	5.04	-1.28	1.94	1.90
AT2G38540.1	5.71	5.15	5.47	5.44	AT4G13930.1	2.48	2.90	0.31	1.90
AT1G52400.1	4.11	3.66	8.56	5.44	AT3G56910.1	3.18	-0.12	2.59	1.88
AT4G21445.1	9.29	2.38	4.58	5.42	AT1G22300.1	1.65	2.27	1.72	1.88
AT1G27400.1	4.94	5.01	6.29	5.41	AT5G06360.1	0.09	3.38	2.17	1.88
AT5G11420.1	5.77	8.46	1.95	5.39	AT3G10860.1	2.60	2.75	0.28	1.88

AT4G23670.1	6.64	5.67	3.86	5.39
AT3G44735.1	7.76	4.62	3.76	5.38
AT5G37770.1	9.80	5.47	0.81	5.36
AT1G20580.1	7.78	3.07	5.19	5.35
AT5G53490.4	5.78	-0.32	10.57	5.35
AT3G10520.1	7.54	6.30	2.06	5.30
AT1G62480.1	7.96	3.37	4.57	5.30
AT1G56045.1	5.78	5.10	4.94	5.27
AT3G11630.1	6.41	6.37	3.05	5.27
AT1G25260.1	6.27	6.01	3.47	5.25
AT5G67370.1	6.66	4.92	4.07	5.22
AT2G21580.1	7.43	1.26	6.91	5.20
AT5G67600.1	0.74	6.08	8.78	5.20
AT5G19940.1	4.95	2.98	7.66	5.20
AT4G19840.1	3.76	5.52	6.30	5.19
AT4G37040.1	5.86	5.69	3.97	5.17
AT5G40810.1	4.25	7.62	3.63	5.16
AT3G56020.1	5.55	5.21	4.71	5.16
AT2G42310.1	0.24	7.22	7.99	5.15
AT1G12250.1	8.12	3.13	4.07	5.11
AT5G22580.1	9.83	3.74	1.71	5.10
AT3G57450.1	0.91	7.16	7.20	5.09
AT4G11175.1	5.97	4.03	5.25	5.08
AT3G56340.1	4.23	6.51	4.32	5.02
AT1G23130.1	6.00	4.33	4.68	5.00
AT3G11400.2	5.67	0.96	8.34	4.99
AT1G72610.1	3.24	5.78	5.83	4.95
AT2G01250.1	6.85	3.01	4.92	4.93
AT3G55250.1	4.64	5.54	4.53	4.90
AT1G24360.1	9.51	0.82	4.37	4.90
AT1G08830.1	1.96	5.03	7.69	4.89
AT3G26070.1	4.32	6.42	3.91	4.88
AT4G30530.1	6.30	2.91	5.36	4.86
AT1G11750.2	8.89	0.19	5.40	4.82
AT3G14600.1	9.07	0.32	5.08	4.82
AT1G45474.1	1.80	6.24	6.37	4.80
AT2G02130.1	2.47	7.95	3.95	4.79
AT2G41310.1	2.50	9.63	2.18	4.77
AT3G08940.2	5.92	3.89	4.36	4.72
AT3G54560.1	6.45	7.33	0.39	4.72
AT1G61520.1	6.70	2.90	4.55	4.72
AT5G16660.1	0.50	7.92	5.61	4.68
AT3G20670.1	3.14	3.02	7.83	4.66
AT1G23490.1	5.66	2.47	5.82	4.65
AT1G06680.1	4.86	3.98	5.09	4.64
AT1G24020.1	4.36	5.58	3.96	4.63
AT4G30760.1	5.96	7.27	0.65	4.63
AT1G73655.1	5.55	3.98	4.29	4.61
AT4G36800.1	8.81	0.82	4.18	4.60
AT2G40490.1	1.47	6.64	5.69	4.60
AT1G07140.1	5.06	-0.09	8.59	4.52
AT3G56940.1	4.23	4.11	5.21	4.52
AT5G65430.3	6.48	2.59	4.46	4.51
AT2G41410.1	3.79	4.13	5.54	4.49
AT3G45160.1	3.99	2.06	7.38	4.48
AT4G34090.3	4.12	4.79	4.41	4.44
AT1G22840.1	3.81	4.59	4.91	4.43
AT4G13770.1	2.62	5.31	5.35	4.43
AT4G20260.4	5.12	2.10	6.00	4.41
AT5G63670.1	7.18	1.96	4.03	4.39
AT5G65730.1	6.40	2.17	4.59	4.39
AT5G20010.1	0.81	4.22	8.05	4.36
AT1G62380.1	6.36	5.13	1.48	4.32
AT3G54600.1	2.06	5.92	4.96	4.31
AT2G43290.1	5.04	2.64	5.24	4.30
AT5G09830.1	6.88	4.73	1.27	4.29
AT1G22700.1	3.38	3.51	5.90	4.27
AT5G46800.1	4.12	3.56	4.98	4.22
AT5G10400.1	2.54	5.22	4.84	4.20
AT1G15820.1	4.99	3.32	4.29	4.20
AT3G61470.1	3.49	4.40	4.66	4.18
AT5G18600.1	2.65	4.97	4.90	4.17
AT1G31330.1	6.63	3.76	2.03	4.14
AT3G11120.1	6.89	5.83	-0.34	4.13
AT4G31990.3	2.53	5.73	4.12	4.12
AT5G54270.1	5.99	1.99	4.35	4.11
AT3G27690.2	6.47	3.16	2.66	4.10
AT5G54940.1	2.83	3.97	5.47	4.09
AT1G55210.1	2.55	5.66	4.03	4.08
AT1G55330.1	3.90	7.09	1.18	4.06
AT5G53880.1	2.47	3.73	5.92	4.04
AT3G57870.1	4.13	3.75	4.23	4.04
AT3G25220.1	6.50	2.36	3.13	4.00
AT3G23805.1	1.35	5.23	5.35	3.98
AT4G15800.1	-1.30	7.89	5.29	3.96
AT3G52580.1	7.67	0.45	3.71	3.95
AT5G05270.1	3.57	4.05	4.11	3.91
AT2G40590.1	2.14	-0.99	4.44	1.86
AT3G02730.1	6.02	-1.50	1.05	1.86
AT3G46040.1	1.70	1.36	2.50	1.85
AT2G14900.1	2.58	3.04	-0.08	1.85
AT5G60400.3	-0.98	2.75	3.75	1.84
AT2G29550.1	3.61	-1.01	2.91	1.84
AT3G56800.1	2.35	2.13	1.02	1.84
AT3G15190.1	2.99	1.92	0.61	1.84
AT1G07890.1	2.84	0.70	1.96	1.84
AT1G21190.1	1.90	4.39	-0.80	1.83
AT1G48830.1	2.97	2.43	0.08	1.83
AT3G16080.1	0.70	2.75	2.02	1.82
AT3G18740.1	2.03	0.99	2.45	1.82
AT4G33865.1	0.35	2.81	2.29	1.82
AT2G35370.1	0.83	2.72	1.91	1.82
AT5G11200.2	7.74	-1.83	-0.47	1.81
AT1G22840.1	0.62	2.32	2.50	1.81
AT2G23120.1	1.75	2.09	1.60	1.81
AT1G33810.1	3.73	3.63	-1.93	1.81
AT1G52300.1	0.24	3.85	1.32	1.80
AT3G12390.1	2.01	-0.04	3.42	1.80
AT2G26500.1	0.31	2.97	2.09	1.79
AT1G12440.1	-1.28	2.04	4.61	1.79
AT1G62380.1	5.96	-0.01	-0.59	1.79
AT5G27670.1	1.51	1.36	2.50	1.79
AT2G02510.1	1.76	3.34	0.26	1.79
AT4G34190.1	0.15	1.14	4.06	1.78
AT4G30660.1	5.49	0.53	-0.68	1.78
AT5G58710.1	-0.22	3.37	2.16	1.77
AT5G42850.1	3.04	2.42	-0.15	1.77
AT2G09990.1	0.98	2.23	2.09	1.77
AT2G18040.1	1.17	2.68	1.42	1.76
AT4G26840.1	1.17	0.95	3.15	1.75
AT3G29350.1	4.68	0.58	0.00	1.75
AT2G30060.1	2.11	1.33	1.80	1.74
AT5G02610.2	4.54	0.92	-0.25	1.74
AT1G08580.1	3.35	0.28	1.57	1.74
AT3G10020.1	-0.05	1.44	3.80	1.73
AT4G18040.1	1.81	4.18	-0.82	1.73
AT4G23680.1	0.38	4.24	0.54	1.72
AT5G12240.2	-0.59	-3.32	9.06	1.72
AT2G42530.1	-2.05	3.04	4.16	1.72
AT1G77940.1	1.27	2.82	1.05	1.72
AT2G46600.1	0.64	2.72	1.78	1.72
AT4G18100.1	2.40	0.71	2.02	1.71
AT5G19940.1	-1.76	1.95	4.91	1.70
AT1G10670.3	-0.33	1.24	4.15	1.69
AT4G24920.2	1.79	2.72	0.51	1.67
AT4G23670.1	3.84	0.77	0.40	1.67
AT3G53610.1	2.93	0.79	1.28	1.67
AT5G16050.1	3.83	-0.90	2.03	1.66
AT1G72370.1	3.74	0.29	0.87	1.63
AT5G08050.1	0.29	2.22	2.37	1.63
AT5G07090.1	2.06	2.64	0.17	1.62
AT5G24165.1	-1.62	3.25	3.21	1.61
AT3G13510.1	2.38	-3.08	5.49	1.60
AT2G37270.1	3.12	-0.37	2.02	1.59
AT2G38670.1	2.35	1.55	0.86	1.59
AT4G38970.1	4.39	-2.08	2.41	1.58
AT5G42980.1	-1.00	1.73	3.99	1.57
AT2G44650.1	1.03	2.29	1.40	1.57
AT5G02500.1	3.14	0.13	1.44	1.57
AT2G03850.1	2.72	1.49	0.49	1.57
AT1G30580.1	-0.25	0.67	4.28	1.57
AT2G18020.1	3.02	1.30	0.38	1.56
AT2G43030.1	-0.89	3.42	2.14	1.56
AT3G16570.1	-0.30	2.91	2.02	1.54
AT1G35680.1	-3.34	3.08	4.89	1.54
AT5G61170.1	5.57	-0.87	-0.08	1.54
AT2G36160.1	0.17	1.78	2.65	1.54
AT2G28740.1	2.47	1.56	0.55	1.53
AT5G44620.1	0.93	2.42	1.23	1.52
AT2G30570.1	1.44	1.55	1.59	1.52
AT5G27470.1	2.22	2.01	0.34	1.52
AT5G58030.1	0.42	1.28	2.86	1.52
AT2G02130.1	2.25	-0.38	2.67	1.52
AT1G20580.1	-0.36	3.13	1.77	1.51
AT3G56070.1	1.95	3.39	-0.81	1.51
AT3G22210.1	-0.37	2.91	1.99	1.51
AT3G51260.1	0.69	1.93	1.89	1.50
AT3G46430.1	1.31	3.27	-0.08	1.50
AT5G45680.1	-0.61	0.75	4.33	1.49
AT2G46390.1	1.91	2.62	-0.07	1.49
AT2G27290.1	-1.50	1.54	4.40	1.48
AT1G52230.1	3.12	1.18	0.12	1.47
AT3G52590.1	0.63	2.53	1.26	1.47
AT2G01250.1	3.14	0.85	0.40	1.47

AT3G22845.1	0.21	4.42	7.02	3.88
AT4G21960.1	5.62	1.97	3.93	3.84
AT1G09310.1	3.20	3.58	4.70	3.83
AT4G36130.1	5.53	5.24	0.68	3.82
AT4G30996.1	6.38	2.78	2.14	3.77
AT1G60000.1	7.47	3.05	0.75	3.76
AT1G13930.1	5.65	1.99	3.57	3.74
AT5G60400.3	1.79	0.98	8.36	3.71
AT4G25080.6	2.92	5.41	2.76	3.70
AT5G19220.1	2.06	2.24	6.79	3.69
AT1G05010.1	3.99	2.10	4.98	3.69
AT4G02890.3	2.88	1.07	6.93	3.63
AT1G22410.1	4.55	0.89	5.40	3.61
AT4G28750.1	3.51	4.97	2.06	3.51
AT5G35620.1	8.17	-2.38	4.69	3.49
AT2G16600.1	4.51	3.05	2.85	3.47
AT1G78630.1	5.47	4.37	0.48	3.44
AT5G52960.1	5.14	2.50	2.57	3.41
AT2G28190.1	1.50	3.77	4.86	3.37
AT3G13520.1	1.93	4.93	3.21	3.36
AT1G06760.1	7.84	-0.48	2.71	3.35
AT1G54780.1	4.07	1.24	4.61	3.31
AT1G72645.1	4.33	0.80	4.74	3.29
AT5G35530.1	3.98	5.81	-0.04	3.25
AT4G39330.1	7.42	1.82	0.45	3.23
AT4G38740.1	5.23	1.40	2.78	3.14
AT5G59870.1	0.08	5.02	4.27	3.13
AT2G04520.1	3.09	5.25	0.89	3.08
AT5G44020.1	4.94	2.78	1.45	3.06
AT2G45790.1	1.66	1.89	5.57	3.04
AT4G14960.2	0.08	4.87	4.11	3.02
AT3G55770.7	2.55	7.22	-0.71	3.02
AT5G58420.1	3.37	0.44	5.21	3.01
AT2G37660.1	3.28	0.97	4.72	2.99
AT1G04750.1	0.40	2.24	6.12	2.92
AT4G36500.1	-3.14	9.55	2.29	2.90
AT1G76180.1	3.66	1.30	3.71	2.89
AT1G55260.1	-1.57	3.69	6.54	2.89
AT4G03210.1	3.41	7.74	-2.49	2.89
AT1G78370.1	3.73	1.36	3.54	2.88
AT3G51510.1	3.49	3.03	2.00	2.84
AT4G30220.2	3.10	-1.54	6.92	2.83
AT2G15050.1	2.46	5.80	0.22	2.82
AT2G22425.1	2.22	4.93	1.20	2.78
AT5G14970.1	4.34	-4.61	8.41	2.71
AT2G41430.1	6.69	-0.35	1.72	2.69
AT5G11740.1	1.29	3.82	2.78	2.63
AT1G78850.1	3.45	-1.43	5.78	2.60
AT3G05730.1	4.89	-0.36	2.91	2.48
AT1G09070.1	-0.53	2.20	5.69	2.45
AT4G14870.1	3.21	2.69	1.44	2.45
AT1G56580.1	0.12	2.88	4.24	2.41
AT5G55190.1	0.71	3.28	3.18	2.39
AT3G09735.1	5.37	1.78	-0.04	2.37
AT5G19140.1	3.45	1.81	1.65	2.30
AT5G06360.1	-2.34	3.13	5.93	2.24
AT2G32650.1	-0.83	1.87	5.65	2.23
AT2G30860.1	4.78	3.56	-2.01	2.11
AT1G23740.1	1.29	1.30	3.71	2.10
AT1G20693.1	-4.21	6.82	3.68	2.10
AT5G07960.1	0.45	-1.80	7.60	2.08
AT5G52240.1	4.53	-0.50	2.20	2.08
AT3G29240.1	1.70	2.45	1.13	1.76
AT4G10340.1	1.99	0.46	2.70	1.72
AT3G16570.1	0.89	3.93	-0.06	1.58
AT4G09890.1	5.22	1.44	-2.36	1.43
AT4G02770.1	2.74	1.55	-0.66	1.21
AT3G11930.3	-0.13	-1.38	4.82	1.11
AT5G26000.1	1.11	2.36	-0.40	1.02
AT3G17390.1	1.69	1.61	-0.33	0.99
AT2G07671.1	0.68	0.63	-0.66	0.22
AT3G05490.1	-2.68	-2.21	-1.02	-1.97
AT1G04800.1	-3.77	-1.90	-2.84	-2.84
AT5G41600.1	6.49	-3.77	1.68	1.47
AT5G13850.1	-0.86	1.76	3.50	1.47
AT3G45930.1	2.20	3.41	-1.22	1.46
AT4G37930.1	2.35	0.84	1.19	1.46
AT3G05590.1	1.32	2.42	0.63	1.46
AT1G06680.1	3.59	0.72	0.04	1.45
AT5G56670.1	1.89	0.68	1.77	1.44
AT5G65670.1	3.09	0.63	0.61	1.44
AT1G42960.1	2.73	-1.91	3.50	1.44
AT5G56710.1	2.13	1.10	1.04	1.42
AT5G66570.1	2.21	1.14	0.91	1.42
AT4G40040.1	2.08	1.30	0.88	1.42
AT1G16000.1	3.09	1.94	-0.78	1.42
AT2G26900.1	4.26	0.54	-0.56	1.41
AT5G56030.2	1.37	3.42	-0.54	1.41
AT3G17160.1	-1.54	1.32	4.46	1.41
AT5G20160.2	1.72	1.03	1.47	1.41
AT1G07140.1	6.14	-1.27	-0.66	1.40
AT5G46030.1	1.49	3.91	-1.19	1.40
AT3G03100.1	1.47	1.12	1.61	1.40
AT2G30410.1	1.80	1.23	1.14	1.39
AT5G12140.1	0.59	2.00	1.56	1.38
AT5G14040.1	2.72	0.19	1.23	1.38
AT1G67350.1	0.35	1.96	1.82	1.38
AT3G12610.1	2.03	-1.54	3.63	1.38
AT5G57290.1	1.05	1.59	1.43	1.36
AT4G25740.1	2.96	1.99	-0.88	1.36
AT4G17390.1	1.17	-0.53	3.43	1.35
AT5G22440.1	1.73	3.50	-1.21	1.34
AT3G43810.2	0.35	2.54	1.11	1.33
AT5G22880.1	1.70	2.26	0.03	1.33
AT1G66430.1	-3.82	5.07	2.73	1.33
AT5G47210.1	1.64	0.65	1.68	1.33
AT5G40770.1	2.19	-0.30	2.06	1.32
AT3G56020.1	1.80	1.00	1.15	1.32
AT1G51060.1	2.76	0.30	0.88	1.32
AT5G57123.1	2.60	2.25	-0.92	1.31
AT4G34870.1	2.22	1.54	0.18	1.31
AT2G37120.1	-0.27	4.55	-0.35	1.31
AT3G28500.1	3.69	-1.32	1.55	1.31
AT2G02100.1	1.53	1.67	0.72	1.31
AT5G16250.1	2.04	0.27	1.60	1.30
AT5G21274.1	-0.56	0.36	4.05	1.28
AT2G29450.1	2.37	0.23	1.25	1.28
AT3G22960.1	1.55	-1.54	3.82	1.28
AT1G01620.1	-0.95	1.83	2.94	1.27
AT4G26230.1	0.96	1.47	1.39	1.27
AT5G59910.1	1.57	-0.82	3.06	1.27
AT2G22425.1	0.04	3.88	-0.13	1.27
AT4G28397.1	0.43	3.03	0.33	1.26
AT1G07660.1	-1.81	2.01	3.58	1.26
AT3G01280.1	1.19	2.66	-0.07	1.26
AT1G09200.1	-0.60	2.67	1.70	1.26
AT2G42540.2	-0.32	1.31	2.78	1.26
AT3G14290.1	0.42	-1.02	4.36	1.26
AT3G53190.1	-5.08	6.96	1.89	1.26
AT5G38410.3	4.13	0.67	-1.04	1.25
AT4G29350.1	3.45	-0.62	0.92	1.25
AT3G62870.1	0.74	1.67	1.33	1.24
AT1G71500.1	-2.69	1.90	4.52	1.24
AT5G52650.1	-0.15	0.37	3.50	1.24
AT4G21280.2	0.73	1.50	1.48	1.24
AT3G53020.1	0.77	1.89	1.02	1.23
AT4G17510.1	5.89	-0.57	-1.65	1.22
AT3G12780.1	2.84	-0.53	1.36	1.22
AT1G66240.1	-1.61	4.37	0.89	1.21
AT3G04120.1	2.54	1.03	0.06	1.21
AT5G28750.1	-0.34	-0.85	4.82	1.21
AT4G21192.1	-5.33	9.50	-0.55	1.21
AT1G24260.2	0.71	3.03	-0.12	1.21
AT1G15690.1	1.03	3.00	-0.42	1.20
AT5G05780.1	0.80	1.00	1.80	1.20
AT3G60770.1	1.80	1.61	0.17	1.19
AT1G02050.1	5.05	-5.36	3.86	1.18
AT1G78370.1	1.96	0.60	0.95	1.17
AT3G54340.1	0.78	3.85	-1.14	1.16
AT5G45010.1	-3.13	5.35	1.24	1.15
AT1G09640.1	4.68	-2.47	1.24	1.15
AT5G54600.1	-0.34	0.17	3.60	1.14
AT3G49100.1	2.70	0.01	0.71	1.14
AT3G09735.1	0.09	2.43	0.87	1.13
AT5G39740.1	2.29	0.58	0.46	1.11
AT3G08520.1	3.43	0.17	-0.27	1.11
AT1G21065.1	2.73	-3.21	3.80	1.11
AT3G54050.1	2.54	2.74	-1.97	1.11
AT2G32060.1	0.42	1.95	0.93	1.10
AT2G27710.1	-2.57	2.50	3.37	1.10
AT2G43530.1	3.26	1.29	-1.25	1.10
AT5G17710.2	-0.30	2.95	0.65	1.10
AT5G30510.1	-1.01	0.93	3.37	1.10

AT3G60750.1	0.27	0.38	2.64	1.10
AT1G43670.1	-1.07	1.17	3.16	1.09
AT5G14320.1	-2.44	5.39	0.30	1.08
AT3G55750.1	0.24	2.05	0.94	1.07
AT1G74840.1	-1.40	4.62	-0.03	1.06
AT3G25920.1	-2.72	4.48	1.42	1.06
AT4G12800.2	0.54	1.69	0.88	1.04
AT3G16240.1	2.61	0.54	-0.05	1.03
AT3G55170.1	1.44	-0.30	1.95	1.03
AT3G05880.1	-4.53	1.45	6.13	1.02
AT4G00430.1	3.14	-0.28	0.19	1.02
AT1G80230.1	-2.11	2.31	2.78	0.99
AT5G02960.1	1.15	2.03	-0.24	0.98
AT4G00585.1	1.41	3.19	-1.67	0.98
AT5G62390.1	5.93	-2.09	-0.93	0.97
AT2G20270.2	1.44	-1.54	3.00	0.97
AT2G21290.1	3.31	1.65	-2.09	0.95
AT3G11120.1	0.60	2.42	-0.18	0.94
AT1G44575.1	-0.14	2.28	0.69	0.94
AT4G03280.1	0.13	-0.01	2.70	0.94
AT2G39390.1	0.57	0.00	2.24	0.94
AT1G67080.1	1.45	-0.19	1.55	0.93
AT3G53870.1	1.71	0.20	0.86	0.92
AT1G16700.1	1.22	-1.30	2.83	0.92
AT1G09310.1	0.18	1.08	1.47	0.91
AT5G05270.1	2.62	1.45	-1.34	0.91
AT5G35680.3	-0.85	3.34	0.22	0.90
AT1G67990.1	1.29	0.73	0.69	0.90
AT1G20010.1	3.22	0.65	-1.18	0.90
AT1G76200.1	1.27	1.18	0.23	0.89
AT1G79550.1	-0.94	3.36	0.26	0.89
AT2G37470.1	-2.10	2.04	2.73	0.89
AT3G53890.1	0.91	-0.56	2.29	0.88
AT5G24890.1	1.46	-2.66	3.73	0.84
AT1G72750.1	1.85	4.06	-3.40	0.84
AT1G12900.5	1.43	0.94	0.11	0.83
AT2G41430.1	-1.29	1.49	2.27	0.82
AT3G47070.1	0.77	1.10	0.58	0.82
AT2G27840.3	4.18	2.52	-4.27	0.81
AT4G34760.1	0.65	4.19	-2.45	0.80
AT1G32470.1	0.23	-1.49	3.62	0.79
AT4G34450.1	-1.95	-0.02	4.33	0.79
AT1G56045.1	-0.01	0.75	1.60	0.78
AT5G57685.1	-0.74	2.74	0.34	0.78
AT3G01500.2	1.07	0.72	0.51	0.77
AT5G45775.2	0.16	1.34	0.80	0.77
AT5G66190.1	1.01	0.34	0.94	0.76
AT3G10920.1	-0.23	-0.08	2.60	0.76
AT3G46560.1	-0.99	1.61	1.67	0.76
AT4G32930.2	-1.54	1.82	1.98	0.75
AT4G25080.6	2.39	-1.97	1.83	0.75
AT4G35450.5	1.91	1.45	-1.13	0.74
AT3G59540.1	0.21	0.97	1.04	0.74
AT2G20450.1	-1.32	2.88	0.65	0.74
AT2G37660.1	-1.77	3.09	0.89	0.74
AT2G39460.1	1.14	0.39	0.65	0.72
AT2G18740.1	2.00	0.06	0.12	0.72
AT1G20330.1	1.91	3.03	-2.78	0.72
AT5G20720.1	0.54	0.04	1.52	0.70
AT4G31985.1	1.22	0.04	0.82	0.70
AT1G48350.1	-0.40	3.21	-0.76	0.68
AT4G35630.1	0.54	1.71	-0.21	0.68
AT1G54630.1	1.05	0.26	0.69	0.67
AT3G22970.1	-1.36	2.16	1.20	0.66
AT1G51400.1	-0.97	2.44	0.52	0.66
AT5G12250.1	-3.88	4.14	1.73	0.66
AT1G70600.1	2.29	-0.36	0.05	0.66
AT3G51510.1	1.67	-1.60	1.89	0.66
AT5G09830.1	4.10	0.73	-2.87	0.65
AT1G43170.1	1.73	0.22	-0.02	0.64
AT5G11450.2	-1.69	-0.92	4.54	0.64
AT4G03210.1	3.85	-0.92	-1.03	0.63
AT5G67510.1	3.29	0.20	-1.63	0.62
AT2G31610.1	3.42	0.78	-2.35	0.62
AT5G56010.1	1.54	0.56	-0.28	0.61
AT1G20340.1	0.52	0.21	1.10	0.61
AT1G04750.1	-1.44	1.09	2.14	0.60
AT3G29370.1	-1.58	0.22	3.14	0.59
AT3G23810.1	-0.40	1.20	0.93	0.58
AT3G63160.1	-0.02	1.11	0.57	0.55
AT5G58420.1	0.56	-1.39	2.43	0.53
AT5G45750.1	2.52	-2.64	1.66	0.51
AT5G09810.1	-0.99	1.02	1.49	0.51
AT3G15360.1	-0.74	3.05	-0.80	0.50
AT4G34850.1	1.23	2.20	-1.94	0.50
AT4G10300.1	-4.89	2.73	3.66	0.50
AT5G35620.1	-1.12	1.05	1.53	0.48
AT2G36620.1	0.93	1.75	-1.24	0.48
AT4G29390.1	-0.94	-0.01	2.38	0.48
AT5G50460.1	-2.98	5.57	-1.16	0.48
AT1G26630.1	-0.78	2.03	0.09	0.45
AT3G27160.2	-2.31	0.99	2.64	0.44
AT2G29180.1	-0.94	-1.04	3.25	0.43
AT5G61790.1	0.57	0.44	0.22	0.41
AT2G31360.1	1.91	0.09	-0.80	0.40
AT4G09320.1	0.10	-0.10	1.21	0.40
AT3G44110.1	-1.61	-1.05	3.83	0.39
AT1G07320.1	-1.54	2.60	0.10	0.39
AT4G04640.1	0.79	-1.92	2.28	0.38
AT4G20260.4	4.90	-2.36	-1.40	0.38
AT2G21580.1	-0.03	1.76	-0.59	0.38
AT1G18730.1	1.22	0.35	-0.46	0.37
AT1G52220.1	-4.19	0.82	4.47	0.37
AT2G30870.1	0.01	-0.79	1.85	0.36
AT1G11860.3	-1.73	2.14	0.66	0.36
AT1G27435.1	-3.17	3.47	0.74	0.35
AT3G60245.1	0.53	0.83	-0.36	0.34

AT1G18540.1	1.49	0.18	-0.67	0.33
AT3G07230.1	0.89	0.38	-0.28	0.33
AT3G08580.1	0.01	2.05	-1.09	0.32
AT4G14800.2	-4.26	5.03	0.20	0.32
AT3G46030.1	0.83	0.95	-0.82	0.32
AT1G68300.1	1.47	-1.53	0.98	0.31
AT4G02530.2	0.73	0.45	-0.27	0.30
AT3G15660.1	-0.50	2.13	-0.76	0.29
AT5G63150.1	0.38	-2.30	2.79	0.29
AT2G25210.1	0.43	-2.43	2.80	0.27
AT2G04700.1	-3.41	-0.87	4.97	0.23
AT3G15480.1	1.17	-2.43	1.92	0.22
AT5G59850.1	1.06	-0.60	0.17	0.21
AT4G36130.1	-0.94	1.30	0.24	0.20
AT2G23670.1	-0.48	1.24	-0.17	0.20
AT3G54820.1	-0.97	3.37	-1.82	0.20
AT1G09590.1	0.78	-1.24	1.02	0.19
AT2G28900.1	0.79	-4.97	4.73	0.18
AT1G55330.1	6.42	-1.64	-4.28	0.17
AT3G11510.1	1.62	1.56	-2.77	0.14
AT5G20740.2	0.13	1.63	-1.35	0.13
AT1G56330.1	1.66	0.48	-1.77	0.12
AT5G10400.1	0.05	0.12	0.16	0.11
AT3G06700.1	1.81	-0.96	-0.71	0.05
AT1G05850.1	-3.09	2.87	0.34	0.04
AT3G51010.1	-0.32	-0.06	0.49	0.04
AT5G19780.1	0.21	0.07	-0.21	0.03
AT3G22320.1	-1.00	-0.79	1.85	0.02
AT3G22230.1	1.01	0.08	-1.04	0.02
AT5G21940.1	-0.08	-3.47	3.57	0.01
AT3G22110.1	-0.37	-1.05	1.42	0.00
AT4G02770.1	0.40	-2.29	1.82	-0.02
AT1G27330.1	-5.63	2.98	2.51	-0.05
AT1G04945.3	-1.64	-0.13	1.53	-0.08
AT5G60670.1	0.72	-0.74	-0.34	-0.12
AT2G07671.1	-1.46	1.69	-0.60	-0.12
AT2G45070.1	-2.29	0.02	1.86	-0.14
AT3G11400.2	-0.01	-2.31	1.79	-0.17
AT1G78170.1	-8.90	2.39	5.99	-0.18
AT5G59870.1	0.71	-1.39	0.14	-0.18
AT2G24090.1	0.05	0.01	-0.67	-0.20
AT4G30220.2	0.36	-1.85	0.88	-0.20
AT4G27960.2	-1.46	0.76	0.07	-0.21
AT1G78020.1	-0.61	-1.15	1.11	-0.21
AT3G11500.1	-5.63	0.76	4.18	-0.23
AT5G42060.1	-2.57	2.69	-0.90	-0.26
AT5G22580.1	0.45	-1.21	-0.06	-0.28
AT4G25050.2	-1.16	0.39	-0.14	-0.31
AT1G72610.1	4.97	-1.92	-3.98	-0.31
AT3G61110.1	-2.21	2.43	-1.17	-0.32
AT1G07820.1	1.85	-0.87	-1.94	-0.32
AT2G37190.1	0.75	-1.25	-0.49	-0.33
AT1G31330.1	-2.80	-0.93	2.71	-0.34
AT5G28540.1	-1.01	-1.26	1.18	-0.36
AT4G29430.1	-1.94	-1.37	2.20	-0.37
AT1G56580.1	1.20	0.82	-3.31	-0.43
AT5G17560.1	0.48	0.49	-2.27	-0.44
AT2G31200.1	-2.66	-2.01	3.27	-0.47
AT1G33140.1	0.21	-2.25	0.32	-0.57
AT3G04840.1	1.16	0.60	-3.51	-0.58
AT4G30760.1	0.33	-1.22	-0.88	-0.59
AT5G67490.1	-5.04	1.33	1.85	-0.62
AT1G66410.2	1.43	0.76	-4.06	-0.62
AT4G35490.1	-2.87	-0.09	1.02	-0.65
AT5G38420.1	3.31	-3.39	-1.93	-0.67
AT4G18480.1	-1.56	0.39	-0.85	-0.67
AT4G24190.1	-1.79	1.38	-1.67	-0.69
AT1G14980.1	-1.27	-0.03	-0.79	-0.70
AT1G07940.1	0.41	0.17	-2.69	-0.70
AT5G55940.1	-2.36	0.66	-0.43	-0.71
AT5G59880.1	-1.48	-0.02	-0.70	-0.74
AT1G57765.2	-6.45	4.95	-0.78	-0.76
AT1G16810.1	-0.48	-1.88	-0.04	-0.80
AT1G10200.1	0.20	-3.60	0.99	-0.80
AT1G76670.1	-0.17	1.23	-3.48	-0.81
AT4G31700.1	-0.29	-2.63	0.37	-0.85
AT5G19770.1	4.56	-5.56	-1.55	-0.85
AT4G14960.2	2.10	-1.14	-3.51	-0.85
AT1G49480.1	-1.66	-1.23	0.33	-0.85
AT1G78630.1	-0.97	0.13	-1.75	-0.86
AT1G42970.1	1.07	-1.67	-2.01	-0.87
AT5G17920.1	3.05	-2.72	-3.01	-0.89
AT2G32720.1	-1.15	1.96	-3.51	-0.90
AT3G20670.1	-0.80	-1.39	-0.55	-0.91
AT5G20010.1	-0.43	-3.04	0.66	-0.94
AT5G47930.1	-2.34	-1.03	0.49	-0.96
AT1G29250.1	4.31	-3.42	-3.80	-0.97
AT1G78040.1	2.11	-2.81	-2.33	-1.01
AT1G68590.1	-2.24	-1.51	0.51	-1.08
AT4G20360.1	-0.60	-0.73	-2.10	-1.14
AT2G37110.1	-0.52	-2.70	-0.30	-1.17
AT2G34160.1	-0.96	1.41	-4.20	-1.25
AT5G15090.1	1.19	-2.80	-2.21	-1.27
AT5G11740.1	2.48	-1.87	-4.47	-1.29
AT3G18780.2	1.07	-1.92	-3.05	-1.30
AT4G09010.3	-1.76	-2.22	-0.25	-1.41
AT5G42300.1	-2.89	0.49	-2.08	-1.49
AT3G62840.1	-0.97	-3.68	0.07	-1.53
AT5G64140.1	-1.66	-1.40	-1.98	-1.68
AT1G04820.1	-0.86	-2.40	-1.90	-1.72
AT4G30650.1	2.09	-4.99	-2.29	-1.73
AT3G13520.1	4.22	-4.73	-4.70	-1.74
AT5G40950.1	-2.20	-2.29	-0.75	-1.75
AT3G53990.1	0.87	-2.69	-3.49	-1.77
AT3G12800.1	-2.33	-2.12	-0.93	-1.79
AT1G76450.1	-1.66	-2.73	-1.07	-1.82
AT4G19640.1	-3.20	-0.05	-2.28	-1.84

AT2G47640.1	1.40	-4.45	-2.74	-1.93
AT3G05060.1	0.43	-4.25	-1.98	-1.93
AT5G26730.1	-2.76	-0.39	-2.82	-1.99
AT1G15820.1	-2.56	-1.71	-1.80	-2.02
AT3G55280.1	0.89	-1.47	-6.04	-2.21
AT1G47980.1	0.49	-3.95	-4.08	-2.51
AT5G20890.1	-0.78	-7.31	-0.12	-2.74
AT1G25275.3	-2.32	-4.68	-1.25	-2.75
AT3G17390.1	3.88	-5.84	-6.91	-2.96
AT1G50010.1	-2.36	-2.50	-4.88	-3.25
AT4G28660.2	-1.56	1.82	-10.15	-3.30
AT2G43560.1	-6.09	-4.49	0.63	-3.32
AT3G05490.1	-0.46	-2.97	-7.51	-3.65
AT3G07450.1	-5.20	-0.41	-5.66	-3.76
AT5G52160.1	-6.06	-4.36	-2.27	-4.23
AT2G06850.1	2.50	-10.47	-6.05	-4.67
AT1G75750.1	-1.86	-6.82	-8.51	-5.73

AGI	Name	PASS position	Notes	References
AT5G07530	GRP17	1/1182	Required for efficient pollen germination. Translated in tapetum and accumulates in the anther locule following tapetum degeneration. Involved in pollen hydration.	Mayfield & Preuss, 2000; Updegraff et al., 2009 ; Suzuki et al., 2013 ; Lu et al., 2020
AT5G07550	GRP19	3/1182	Translated in tapetum and accumulates in the anther locule following tapetum degeneration. Close homolog of GRP17.	Lu et al., 2020
AT1G69940	PPME1	5/1182	Required for efficient pollen germination. Involved in the remodelling of pectins in pollen.	Tian et al., 2006
AT5G07410	PME48	6/1182	Required for efficient pollen germination. Involved in the remodelling of pectins in pollen.	Leroux et al., 2015
AT1G75940	ATA27/BGLU20	14/1182	Homolog of BGL4 in *Brassica napus*, involved in the release of active cytokinins. Knock-down in *B. napus* induces aborted pollen grains.	Dong et al., 2019; Lu et al., 2020
AT2G47040	VGD1/PME5	18/1182	Involved in pollen tube growth. Mutant has fewer seeds because pollen tube cannot reach the farther ovules.	Jiang et al., 2005
AT1G75910	EXL4	17/1182	Involved in pollen hydration.	Updegraff et al., 2009; Lu et al., 2020
AT3G20865	AGP40	19/1182	Important component of the nexine layer. Expressed in pollen and pollen tube. Mutant has reduced fitness. Triple mutant with other AGP has even less fitness.	Ngema-Ona., 2012; Jia et al., 2015
AT3G20865	CP51	21/1182	RNAi line undergo early tapetal PCD, and pollen grain are aborted due to defective exine.	Yang et al., 2014
AT3G01270	AtPLL10	25/1182	Homolog of *Brassica campestris* PLL10. Pollen defects in RNAi line of BcPLL10.	Jiang et al., 2014

Table S4. High PASS mRNAs are involved in essential pollen processes.

Homology	Gene name	AGI	baseMean	log2FoldChange	lfcSE	padj	padj
CAF1 homologs	**CAF1a**	AT3G44260	89.40	0.02	0.16	0.91	0.99
	CAF1b	AT5G22250	57.25	-0.09	0.16	0.55	0.95
	CAF1c	AT1G27820	1.02	0.01	0.05	0.76	NA
	CAF1d	AT1G27890	3.72	0.02	0.08	0.85	NA
	CAF1e	AT1G61470	22.40	-0.13	0.15	0.37	0.90
	CAF1f	AT3G44240	0.42	-0.01	0.03	0.67	NA
	CAF1g	AT1G06450	591.92	-0.08	0.12	0.52	0.94
	CAF1h	AT1G15920	537.30	0.09	0.12	0.47	0.93
	CAF1i	AT5G10960	1224.25	0.14	0.10	0.15	0.73
	CAF1j	AT1G80780	1174.26	0.16	0.10	0.10	0.64
	CAF1k	AT2G32070	583.67	0.21	0.11	0.06	0.54
CCR4 homologs	**CCR4a**	AT3G58560	1082.48	-1.41	0.12	0.00	0.00
	CCR4b	AT3G58560	868.39	-1.01	0.10	0.00	0.00
	CCR4c	AT3G18500	286.84	-0.17	0.13	0.18	0.77
	CCr4d	AT1G31500	303.91	-0.02	0.13	0.88	0.99
	CCR4e	AT1G73875	215.61	0.01	0.14	0.97	1.00
	CCR4f	AT5G11350	495.39	-0.12	0.11	0.30	0.86
	CCr4g	AT1G31530	NA	NA	NA	NA	NA
PARN homologs	**AHG2/PARN**	AT1G55870	361.63	0.09	0.11	0.43	0.92
	RRD1	AT3G25430	287.06	-0.04	0.12	0.74	0.97

Upregulated
Downregulated

Table S5. Differential expression of proteins involved in deadenylation in *ccr4a ccr4b* flower buds.

Table S6. List of enriched proteins in EXA1-GFP IPs.

A threshold of logFC>1 and adjpval < 0.05 was used to select the proteins co-purifying with EXA1-GFP. Proteins are sorted according to the logFC.

LogFC	adjp	TAIR ID	external_gene_name	description
11.41	0.000	AT5G42950	AT5G42950	GYF domain-containing protein [Source:NCBI gene (formerly Entrezgene);Acc:834307]
7.32	0.000	AT2G43460	AT2G43460	Ribosomal L38e protein family [Source:NCBI gene (formerly Entrezgene);Acc:818947]
7.02	0.000	AT5G18110	NCBP	Putative cap-binding protein [Source:NCBI gene (formerly Entrezgene);Acc:831929]
6.62	0.000	AT2G33730	AT2G33730	P-loop containing nucleoside triphosphate hydrolases superfamily protein [Source:NCBI gene (formerly Entrezgene);Acc:817938]
6.56	0.000	AT1G02080	AT1G02080	transcription regulator [Source:NCBI gene (formerly Entrezgene);Acc:839244]
6.53	0.000	AT2G27100	SE	C2H2 zinc-finger protein SERRATE (SE) [Source:NCBI gene (formerly Entrezgene);Acc:817252]
6.46	0.000	AT1G31970	STRS1	DEA(D/H)-box RNA helicase family protein [Source:NCBI gene (formerly Entrezgene);Acc:840087]
6.43	0.000	AT5G40200	DEG9	DegP protease 9 [Source:NCBI gene (formerly Entrezgene);Acc:834018]
6.32	0.000	AT5G22780	AT5G22780	Adaptor protein complex AP-2, alpha subunit [Source:NCBI gene (formerly Entrezgene);Acc:832341]
6.31	0.000	AT1G19880	AT1G19880	Regulator of chromosome condensation (RCC1) family protein [Source:NCBI gene (formerly Entrezgene);Acc:838576]
6.31	0.000	AT3G22310	PMH1	putative mitochondrial RNA helicase 1 [Source:NCBI gene (formerly Entrezgene);Acc:821800]
6.27	0.000	AT5G13530	KEG	protein kinases;ubiquitin-protein ligase [Source:NCBI gene (formerly Entrezgene);Acc:831197]
6.27	0.000	AT1G50030	TOR	target of rapamycin [Source:NCBI gene (formerly Entrezgene);Acc:841427]
6.25	0.000	AT3G13570	SCL30A	SC35-like splicing factor 30A [Source:NCBI gene (formerly Entrezgene);Acc:820559]
6.25	0.000	AT2G24590	RSZ22a	RNA recognition motif and CCHC-type zinc finger domains containing protein [Source:NCBI gene (formerly Entrezgene);Acc:816995]
6.17	0.000	AT2G37080	RIP2	ROP interactive partner 3 [Source:NCBI gene (formerly Entrezgene);Acc:818284]
6.15	0.000	AT5G20920	EIF2 BETA	eukaryotic translation initiation factor 2 beta subunit [Source:NCBI gene (formerly Entrezgene);Acc:832216]
6.13	0.000	AT3G60830	ARP7	actin-related protein 7 [Source:NCBI gene (formerly Entrezgene);Acc:825254]
6.10	0.000	AT5G47010	LBA1	RNA helicase [Source:NCBI gene (formerly Entrezgene);Acc:834747]
6.09	0.000	AT3G54540	ABCF4	ral control non-repressible 4 [Source:NCBI gene (formerly Entrezgene);Acc:824619]
6.09	0.000	AT4G31580	RSZ22	serine/arginine-rich 22 [Source:NCBI gene (formerly Entrezgene);Acc:829285]
6.07	0.000	AT5G09880	AT5G09880	Splicing factor, CC1-like protein [Source:NCBI gene (formerly Entrezgene);Acc:830848]
6.02	0.000	AT4G10840	KLCR1	Tetratricopeptide repeat (TPR)-like superfamily protein [Source:NCBI gene (formerly Entrezgene);Acc:826680]
6.00	0.000	ATCG00500	accD	
5.88	0.000	AT1G62390	Phox2	Octicosapeptide/Phox/Bem1p (PB1) domain-containing protein / tetratricopeptide repeat (TPR)-containing protein [Source:NCBI gene (formerly Entrezgene);Acc:842537]
5.83	0.000	AT3G01780	TPLATE	ARM repeat superfamily protein [Source:NCBI gene (formerly Entrezgene);Acc:821081]
5.83	0.000	AT1G67680	AT1G67680	SRP72 RNA-binding domain-containing protein [Source:NCBI gene (formerly Entrezgene);Acc:843093]
5.83	0.000	AT3G06400	CHR11	chromatin-remodeling protein 11 [Source:NCBI gene (formerly Entrezgene);Acc:819814]
5.83	0.000	AT5G19690	STT3A	staurosporin and temperature sensitive 3-like A [Source:NCBI gene (formerly Entrezgene);Acc:832089]
5.83	0.000	AT2G38580	AT2G38580	Mitochondrial ATP synthase D chain-related protein [Source:NCBI gene (formerly Entrezgene);Acc:818440]
5.78	0.000	AT5G06110	AT5G06110	DnaJ and myb-like DNA-binding domain-containing protein [Source:NCBI gene (formerly Entrezgene);Acc:830498]
5.72	0.000	AT2G46020	BRM	transcription regulatory protein SNF2 [Source:NCBI gene (formerly Entrezgene);Acc:819210]
5.69	0.000	AT2G43970	LARP6b	RNA-binding protein [Source:NCBI gene (formerly Entrezgene);Acc:819002]
5.66	0.000	ATCG00190	rpoB	
5.64	0.000	AT5G18620	CHR17	chromatin remodeling factor17 [Source:NCBI gene (formerly Entrezgene);Acc:831980]
5.61	0.000	AT1G44910	PRP40A	pre-mRNA-processing protein 40A [Source:NCBI gene (formerly Entrezgene);Acc:841057]
5.58	0.000	AT2G37230	AT2G37230	Tetratricopeptide repeat (TPR)-like superfamily protein [Source:NCBI gene (formerly Entrezgene);Acc:818300]
5.48	0.000	AT5G64960	CDKC2	cyclin dependent kinase group C2 [Source:NCBI gene (formerly Entrezgene);Acc:836620]
5.48	0.000	AT3G62240	AT3G62240	RING/U-box superfamily protein [Source:NCBI gene (formerly Entrezgene);Acc:825397]
5.45	0.000	AT2G17870	CSP3	cold shock domain protein 3 [Source:NCBI gene (formerly Entrezgene);Acc:816297]
5.45	0.000	AT1G60780	HAP13	Clathrin adaptor complexes medium subunit family protein [Source:NCBI gene (formerly Entrezgene);Acc:842372]
5.41	0.000	AT1G65440	GTB1	global transcription factor group B1 [Source:NCBI gene (formerly Entrezgene);Acc:842855]
5.41	0.000	AT5G14170	CHC1	SWIB/MDM2 domain superfamily protein [Source:NCBI gene (formerly Entrezgene);Acc:831267]
5.41	0.000	AT2G44530	AT2G44530	Phosphoribosyltransferase family protein [Source:NCBI gene (formerly Entrezgene);Acc:819061]
5.41	0.000	AT1G27430	AT1G27430	GYF domain-containing protein [Source:NCBI gene (formerly Entrezgene);Acc:839633]
5.41	0.000	AT2G22125	CSI1	binding protein [Source:NCBI gene (formerly Entrezgene);Acc:816747]
5.38	0.000	AT1G76810	AT1G76810	eukaryotic translation initiation factor 2 (eIF-2) family protein [Source:NCBI gene (formerly Entrezgene);Acc:844015]
5.38	0.000	AT1G17220	FUG1	Translation initiation factor 2, small GTP-binding protein [Source:NCBI gene (formerly Entrezgene);Acc:838293]
5.38	0.000	AT3G48710	AT3G48710	DEK domain-containing chromatin associated protein [Source:NCBI gene (formerly Entrezgene);Acc:824032]
5.38	0.000	AT4G27060	TOR1	ARM repeat superfamily protein [Source:NCBI gene (formerly Entrezgene);Acc:828814]
5.37	0.000	AT4G39520	AT4G39520	GTP-binding protein-like protein [Source:NCBI gene (formerly Entrezgene);Acc:830106]
5.34	0.000	AT5G13680	ABO1	IKI3 family protein [Source:NCBI gene (formerly Entrezgene);Acc:831213]
5.34	0.000	AT3G15590	AT3G15590	Tetratricopeptide repeat (TPR)-like superfamily protein [Source:NCBI gene (formerly Entrezgene);Acc:820799]
5.31	0.000	AT1G74690	IQD31	IQ-domain 31 [Source:NCBI gene (formerly Entrezgene);Acc:843808]
5.31	0.000	AT2G28540	AT2G28540	RNA binding (RRM/RBD/RNP motifs) family protein [Source:NCBI gene (formerly Entrezgene);Acc:817402]
5.28	0.000	AT1G70710	GH9B1	glycosyl hydrolase 9B1 [Source:NCBI gene (formerly Entrezgene);Acc:843408]
5.27	0.000	AT1G23240	AT1G23240	Caleosin-related family protein [Source:NCBI gene (formerly Entrezgene);Acc:838933]
5.27	0.000	AT3G62310	AT3G62310	RNA helicase family protein [Source:NCBI gene (formerly Entrezgene);Acc:825404]
5.27	0.000	AT2G23070	AT2G23070	Protein kinase superfamily protein [Source:NCBI gene (formerly Entrezgene);Acc:816837]
5.27	0.000	AT2G07360	AT2G07360	SH3 domain-containing protein [Source:NCBI gene (formerly Entrezgene);Acc:815305]
5.27	0.000	AT1G63640	AT1G63640	P-loop nucleoside triphosphate hydrolases superfamily protein with CH (Calponin Homology) domain-containing protein [Source:NCBI gene (formerly Entrezgene);Acc:842668]
5.23	0.000	AT1G52740	HTA9	histone H2A protein 9 [Source:NCBI gene (formerly Entrezgene);Acc:841707]
5.19	0.000	AT4G30720	PDE327	FAD/NAD(P)-binding oxidoreductase family protein [Source:NCBI gene (formerly Entrezgene);Acc:829195]
5.19	0.000	AT3G10380	SEC8	subunit of exocyst complex 8 [Source:NCBI gene (formerly Entrezgene);Acc:820201]
5.19	0.000	AT1G76850	SEC5A	exocyst complex component sec5 [Source:NCBI gene (formerly Entrezgene);Acc:844020]
5.15	0.000	AT5G05470	EIF2 ALPHA	eukaryotic translation initiation factor 2 alpha subunit [Source:NCBI gene (formerly Entrezgene);Acc:830430]
5.15	0.000	AT5G15270	AT5G15270	RNA-binding KH domain-containing protein [Source:NCBI gene (formerly Entrezgene);Acc:831379]
5.15	0.000	AT5G10270	CDKC;1	cyclin-dependent kinase C;1 [Source:NCBI gene (formerly Entrezgene);Acc:830891]
5.15	0.000	AT5G62270	GCD1	ribosomal protein L20 [Source:NCBI gene (formerly Entrezgene);Acc:836348]
5.14	0.000	AT1G26460	AT1G26460	Tetratricopeptide repeat (TPR)-like superfamily protein [Source:NCBI gene (formerly Entrezgene);Acc:839187]
5.11	0.000	AT3G03340	UNE6	LUC7 related protein [Source:NCBI gene (formerly Entrezgene);Acc:821276]
5.11	0.000	AT5G05450	AT5G05450	P-loop containing nucleoside triphosphate hydrolases superfamily protein [Source:NCBI gene (formerly Entrezgene);Acc:830428]
5.11	0.000	AT2G16485	NERD	GW repeat- and PHD finger-containing protein NERD [Source:NCBI gene (formerly Entrezgene);Acc:816147]
5.11	0.000	AT1G09770	CDC5	cell division cycle 5 [Source:NCBI gene (formerly Entrezgene);Acc:837506]
5.11	0.000	AT5G50310	AT5G50310	Galactose oxidase/kelch repeat superfamily protein [Source:NCBI gene (formerly Entrezgene);Acc:835096]
5.11	0.000	AT1G01610	GPAT4	glycerol-3-phosphate acyltransferase 4 [Source:NCBI gene (formerly Entrezgene);Acc:839297]
5.07	0.000	AT3G50590	AT3G50590	Transducin/WD40 repeat-like superfamily protein [Source:NCBI gene (formerly Entrezgene);Acc:824223]

5.07	0.000	AT1G21690	EMB1968	ATPase family associated with various cellular activities (AAA) [Source:NCBI gene (formerly Entrezgene);Acc:838771]
5.07	0.000	AT2G31810	AT2G31810	ACT domain-containing small subunit of acetolactate synthase protein [Source:NCBI gene (formerly Entrezgene);Acc:817738]
5.07	0.000	AT1G08520	ALB1	ALBINA 1 [Source:NCBI gene (formerly Entrezgene);Acc:837374]
5.07	0.000	AT3G04260	PTAC3	plastid transcriptionally active 3 [Source:NCBI gene (formerly Entrezgene);Acc:819581]
5.07	0.000	AT2G29190	PUM2	pumilio 2 [Source:NCBI gene (formerly Entrezgene);Acc:817468]
5.07	0.000	AT1G12920	ERF1-2	eukaryotic release factor 1-2 [Source:NCBI gene (formerly Entrezgene);Acc:837850]
5.02	0.000	AT2G02790	IQD29	IQ-domain 29 [Source:NCBI gene (formerly Entrezgene);Acc:814808]
5.02	0.000	AT2G20280	AT2G20280	Zinc finger C-x8-C-x5-C-x3-H type family protein [Source:NCBI gene (formerly Entrezgene);Acc:816547]
5.02	0.000	AT3G20550	DDL	SMAD/FHA domain-containing protein [Source:NCBI gene (formerly Entrezgene);Acc:821601]
5.02	0.000	AT1G24260	SEP3	K-box region and MADS-box transcription factor family protein [Source:NCBI gene (formerly Entrezgene);Acc:839040]
5.02	0.000	AT5G15680	AT5G15680	ARM repeat superfamily protein [Source:NCBI gene (formerly Entrezgene);Acc:831422]
5.02	0.000	AT1G32380	PRS2	phosphoribosyl pyrophosphate (PRPP) synthase 2 [Source:NCBI gene (formerly Entrezgene);Acc:840131]
5.02	0.000	AT5G63550	AT5G63550	DEK domain-containing chromatin associated protein [Source:NCBI gene (formerly Entrezgene);Acc:836474]
4.97	0.000	AT1G67700	AT1G67700	multidrug resistance protein [Source:NCBI gene (formerly Entrezgene);Acc:843095]
4.97	0.000	AT3G26618	ERF1-3	eukaryotic release factor 1-3 [Source:NCBI gene (formerly Entrezgene);Acc:822273]
4.97	0.000	AT3G15010	AT3G15010	RNA-binding (RRM/RBD/RNP motifs) family protein [Source:NCBI gene (formerly Entrezgene);Acc:820730]
4.97	0.000	AT2G26430	RCY1	arginine-rich cyclin 1 [Source:NCBI gene (formerly Entrezgene);Acc:817183]
4.97	0.000	AT3G48500	PDE312	Nucleic acid-binding, OB-fold-like protein [Source:NCBI gene (formerly Entrezgene);Acc:824009]
4.97	0.000	AT1G50920	AT1G50920	Nucleolar GTP-binding protein [Source:NCBI gene (formerly Entrezgene);Acc:841514]
4.97	0.000	ATCG00170	rpoC2	
4.97	0.000	AT4G35785	AT4G35785	RNA-binding (RRM/RBD/RNP motifs) family protein [Source:NCBI gene (formerly Entrezgene);Acc:829732]
4.97	0.000	AT5G61020	ECT3	evolutionarily conserved C-terminal region 3 [Source:NCBI gene (formerly Entrezgene);Acc:836223]
4.97	0.000	AT3G02830	ZFN1	zinc finger protein 1 [Source:NCBI gene (formerly Entrezgene);Acc:821230]
4.97	0.000	AT2G35390	AT2G35390	Phosphoribosyltransferase family protein [Source:NCBI gene (formerly Entrezgene);Acc:818106]
4.93	0.000	AT2G24420	AT2G24420	DNA repair ATPase-like protein [Source:NCBI gene (formerly Entrezgene);Acc:816978]
4.93	0.000	AT4G32330	AT4G32330	TPX2 (targeting protein for Xklp2) protein family [Source:NCBI gene (formerly Entrezgene);Acc:829367]
4.93	0.000	AT2G38810	HTA8	histone H2A 8 [Source:NCBI gene (formerly Entrezgene);Acc:818463]
4.93	0.000	ATCG00840	rpl23	
4.93	0.000	AT1G79850	RPS17	ribosomal protein S17 [Source:NCBI gene (formerly Entrezgene);Acc:844324]
4.93	0.000	AT5G61140	AT5G61140	U5 small nuclear ribonucleoprotein helicase [Source:NCBI gene (formerly Entrezgene);Acc:836235]
4.89	0.000	AT1G04170	EIF2 GAMMA	eukaryotic translation initiation factor 2 gamma subunit [Source:NCBI gene (formerly Entrezgene);Acc:839238]
4.89	0.000	AT5G53620	AT5G53620	RNA polymerase II degradation factor [Source:NCBI gene (formerly Entrezgene);Acc:835444]
4.88	0.000	AT3G26020	AT3G26020	Protein phosphatase 2A regulatory B subunit family protein [Source:NCBI gene (formerly Entrezgene);Acc:822199]
4.88	0.000	AT2G29200	PUM1	pumilio 1 [Source:NCBI gene (formerly Entrezgene);Acc:817469]
4.88	0.000	AT4G08350	GTA2	global transcription factor group A2 [Source:NCBI gene (formerly Entrezgene);Acc:826391]
4.88	0.000	AT5G19300	AT5G19300	methyltransferase C9orf114 protein [Source:NCBI gene (formerly Entrezgene);Acc:832050]
4.88	0.000	AT1G60070	AT1G60070	Adaptor protein complex AP-1, gamma subunit [Source:NCBI gene (formerly Entrezgene);Acc:842301]
4.88	0.000	AT2G29140	PUM3	pumilio 3 [Source:NCBI gene (formerly Entrezgene);Acc:817463]
4.83	0.000	AT1G23860	RSZ21	RS-containing zinc finger protein 21 [Source:NCBI gene (formerly Entrezgene);Acc:838997]
4.83	0.000	AT1G29320	AT1G29320	Transducin/WD40 repeat-like superfamily protein [Source:NCBI gene (formerly Entrezgene);Acc:839806]
4.83	0.000	AT2G37990	AT2G37990	ribosome biosis regulatory protein (RRS1) family protein [Source:NCBI gene (formerly Entrezgene);Acc:818377]
4.83	0.000	AT2G32000	AT2G32000	DNA topoisomerase, type IA, core [Source:NCBI gene (formerly Entrezgene);Acc:817760]
4.83	0.000	AT5G08180	AT5G08180	Ribosomal protein L7Ae/L30e/S12e/Gadd45 family protein [Source:NCBI gene (formerly Entrezgene);Acc:830714]
4.83	0.000	AT1G14690	MAP65-7	microtubule-associated protein 65-7 [Source:NCBI gene (formerly Entrezgene);Acc:838034]
4.83	0.000	AT2G42570	TBL39	TRICHOME BIREFRINGENCE-LIKE 39 [Source:NCBI gene (formerly Entrezgene);Acc:818857]
4.78	0.000	AT1G14380	IQD28	IQ-domain 28 [Source:NCBI gene (formerly Entrezgene);Acc:838000]
4.78	0.000	AT2G47250	AT2G47250	RNA helicase family protein [Source:NCBI gene (formerly Entrezgene);Acc:819338]
4.78	0.000	AT3G51880	HMGB1	high mobility group B1 [Source:NCBI gene (formerly Entrezgene);Acc:824351]
4.78	0.000	AT2G25670	AT2G25670	
4.78	0.000	AT4G00450	CCT	RNA polymerase II transcription mediator [Source:NCBI gene (formerly Entrezgene);Acc:827954]
4.78	0.000	AT2G35880	AT2G35880	TPX2 (targeting protein for Xklp2) protein family [Source:NCBI gene (formerly Entrezgene);Acc:818161]
4.78	0.000	AT2G25170	PKL	chromatin remodeling factor CHD3 (PICKLE) [Source:NCBI gene (formerly Entrezgene);Acc:817055]
4.78	0.000	AT1G08880	H2AXA	Histone superfamily protein [Source:NCBI gene (formerly Entrezgene);Acc:837409]
4.78	0.000	AT5G60210	RIP5	ROP interactive partner 5 [Source:NCBI gene (formerly Entrezgene);Acc:836143]
4.78	0.000	AT1G52980	AtNug2	GTP-binding family protein [Source:NCBI gene (formerly Entrezgene);Acc:841731]
4.78	0.000	AT4G38600	KAK	HECT ubiquitin protein ligase family protein KAK [Source:NCBI gene (formerly Entrezgene);Acc:830017]
4.78	0.000	AT5G46630	AT5G46630	Clathrin adaptor complexes medium subunit family protein [Source:NCBI gene (formerly Entrezgene);Acc:834706]
4.78	0.000	AT5G35430	AT5G35430	Tetratricopeptide repeat (TPR)-like superfamily protein [Source:NCBI gene (formerly Entrezgene);Acc:833507]
4.78	0.000	AT1G70070	EMB25	DEAD/DEAH box helicase [Source:NCBI gene (formerly Entrezgene);Acc:843343]
4.72	0.000	ATCG00180	rpoC1	
4.72	0.000	AT2G47640	AT2G47640	Small nuclear ribonucleoprotein family protein [Source:NCBI gene (formerly Entrezgene);Acc:819377]
4.72	0.000	AT5G49930	emb1441	zinc knuckle (CCHC-type) family protein [Source:NCBI gene (formerly Entrezgene);Acc:835056]
4.72	0.000	AT1G15940	AT1G15940	Tudor/PWWP/MBT superfamily protein [Source:NCBI gene (formerly Entrezgene);Acc:838164]
4.72	0.000	AT3G50000	CKA2	casein kinase II, alpha chain 2 [Source:NCBI gene (formerly Entrezgene);Acc:824162]
4.72	0.000	AT1G75660	XRN3	5'-3' exoribonuclease 3 [Source:NCBI gene (formerly Entrezgene);Acc:843900]
4.72	0.000	AT4G19410	AT4G19410	Pectinacetylesterase family protein [Source:NCBI gene (formerly Entrezgene);Acc:827682]
4.72	0.000	ATCG00820		
4.72	0.000	AT1G22060	AT1G22060	sporulation-specific protein [Source:NCBI gene (formerly Entrezgene);Acc:838811]
4.72	0.000	AT5G57120	AT5G57120	nucleolar/coiled-body phosphoprotein [Source:NCBI gene (formerly Entrezgene);Acc:835816]
4.72	0.000	AT4G24780	AT4G24780	Pectin lyase-like superfamily protein [Source:NCBI gene (formerly Entrezgene);Acc:828580]
4.72	0.000	AT1G64880	AT1G64880	Ribosomal protein S5 family protein [Source:NCBI gene (formerly Entrezgene);Acc:842796]
4.72	0.000	AT4G31810	AT4G31810	ATP-dependent caseinolytic (Clp) protease/crotonase family protein [Source:NCBI gene (formerly Entrezgene);Acc:829310]
4.72	0.000	AT1G07360	MAC5A	CCCH-type zinc fingerfamily protein with RNA-binding domain-containing protein [Source:NCBI gene (formerly Entrezgene);Acc:837248]
4.72	0.000	AT2G35110	GRL	transcription activator [Source:NCBI gene (formerly Entrezgene);Acc:818077]
4.72	0.000	AT3G08850	RAPTOR1	Regulatory-associated protein of TOR 1 [Source:NCBI gene (formerly Entrezgene);Acc:820032]
4.66	0.000	AT4G32070	Phox4	Octicosapeptide/Phox/Bem1p (PB1) domain-containing protein / tetratricopeptide repeat (TPR)-containing protein [Source:NCBI gene (formerly Entrezgene);Acc:829338]
4.66	0.000	AT5G26710	AT5G26710	Glutamyl/glutaminyl-tRNA synthetase, class Ic [Source:NCBI gene (formerly Entrezgene);Acc:832718]
4.66	0.000	AT3G26560	AT3G26560	ATP-dependent RNA helicase [Source:NCBI gene (formerly Entrezgene);Acc:822264]
4.66	0.000	AT1G29310	AT1G29310	SecY protein transport family protein [Source:NCBI gene (formerly Entrezgene);Acc:839805]
4.66	0.000	AT2G27170	TTN7	Structural maintenance of chromosomes (SMC) family protein [Source:NCBI gene (formerly Entrezgene);Acc:817259]
4.66	0.000	AT5G08610	PDE340	P-loop containing nucleoside triphosphate hydrolases superfamily protein [Source:NCBI gene (formerly Entrezgene);Acc:830762]
4.66	0.000	AT5G43810	AGO10	Stabilizer of iron transporter SufD / Polynucleotidyl transferase [Source:NCBI gene (formerly Entrezgene);Acc:834403]
4.66	0.000	AT2G20190	CLASP	CLIP-associated protein [Source:NCBI gene (formerly Entrezgene);Acc:816539]
4.66	0.000	AT3G61690	AT3G61690	nucleotidyltransferase [Source:NCBI gene (formerly Entrezgene);Acc:825342]
4.66	0.000	AT3G02650	AT3G02650	Tetratricopeptide repeat (TPR)-like superfamily protein [Source:NCBI gene (formerly Entrezgene);Acc:821285]
4.62	0.000	AT4G35850	AT4G35850	Pentatricopeptide repeat (PPR) superfamily protein [Source:NCBI gene (formerly Entrezgene);Acc:829739]
4.62	0.000	AT3G60240	EIF4G	eukaryotic translation initiation factor 4G [Source:NCBI gene (formerly Entrezgene);Acc:825194]

4.61	0.000	AT4G37510	AT4G37510	Ribonuclease III family protein [Source:NCBI gene (formerly Entrezgene);Acc:829906]
4.61	0.000	AT1G36730	AT1G36730	Translation initiation factor IF2/IF5 [Source:NCBI gene (formerly Entrezgene);Acc:840582]
4.61	0.000	AT4G14340	CKI1	casein kinase I [Source:NCBI gene (formerly Entrezgene);Acc:827076]
4.61	0.000	AT3G09735	AT3G09735	S1FA-like DNA-binding protein [Source:NCBI gene (formerly Entrezgene);Acc:820131]
4.61	0.000	AT4G28880	ckl3	casein kinase I-like 3 [Source:NCBI gene (formerly Entrezgene);Acc:829009]
4.61	0.000	AT1G04680	AT1G04680	Pectin lyase-like superfamily protein [Source:NCBI gene (formerly Entrezgene);Acc:839452]
4.54	0.000	AT2G04280	AT2G04280	calcium ion-binding protein [Source:NCBI gene (formerly Entrezgene);Acc:814966]
4.54	0.000	AT1G48610	AT1G48610	AT hook motif-containing protein [Source:NCBI gene (formerly Entrezgene);Acc:841282]
4.54	0.000	AT1G13020	EIF4B2	eukaryotic initiation factor 4B2 [Source:NCBI gene (formerly Entrezgene);Acc:837859]
4.54	0.000	AT1G03930	ADK1	dual specificity kinase 1 [Source:NCBI gene (formerly Entrezgene);Acc:839368]
4.54	0.000	AT4G09730	RH39	RH39 [Source:NCBI gene (formerly Entrezgene);Acc:826559]
4.54	0.000	AT2G28950	EXPA6	expansin A6 [Source:NCBI gene (formerly Entrezgene);Acc:817444]
4.54	0.000	AT1G18250	ATLP-1	Pathosis-related thaumatin superfamily protein [Source:NCBI gene (formerly Entrezgene);Acc:838405]
4.54	0.000	AT3G18600	AT3G18600	P-loop containing nucleoside triphosphate hydrolases superfamily protein [Source:NCBI gene (formerly Entrezgene);Acc:821391]
4.54	0.000	AT2G34160	AT2G34160	Alba DNA/RNA-binding protein [Source:NCBI gene (formerly Entrezgene);Acc:817977]
4.54	0.000	AT1G48090	AT1G48090	calcium-dependent lipid-binding family protein [Source:NCBI gene (formerly Entrezgene);Acc:841226]
4.54	0.000	AT4G03430	EMB2770	pre-mRNA splicing factor-like protein [Source:NCBI gene (formerly Entrezgene);Acc:827925]
4.54	0.000	AT4G29830	VIP3	Transducin/WD40 repeat-like superfamily protein [Source:NCBI gene (formerly Entrezgene);Acc:829105]
4.54	0.000	AT3G59770	SAC9	sacI homology domain-containing protein / WW domain-containing protein [Source:NCBI gene (formerly Entrezgene);Acc:825146]
4.54	0.000	AT4G33200	XI-I	myosin [Source:NCBI gene (formerly Entrezgene);Acc:829456]
4.53	0.000	AT1G47550	SEC3A	exocyst complex component sec3A [Source:NCBI gene (formerly Entrezgene);Acc:841164]
4.49	0.000	AT2G32920	PDIL2-3	PDI-like 2-3 [Source:NCBI gene (formerly Entrezgene);Acc:817854]
4.49	0.000	AT2G16940	AT2G16940	Splicing factor, CC1-like protein [Source:NCBI gene (formerly Entrezgene);Acc:816197]
4.48	0.000	AT2G22400	AT2G22400	S-adenosyl-L-methionine-dependent methyltransferases superfamily protein [Source:NCBI gene (formerly Entrezgene);Acc:816771]
4.48	0.000	AT3G46220	AT3G46220	E3 UFM1-protein ligase-like protein [Source:NCBI gene (formerly Entrezgene);Acc:823767]
4.48	0.000	AT5G64910	AT5G64910	Serine/Threonine-kinase [Source:NCBI gene (formerly Entrezgene);Acc:836615]
4.48	0.000	AT1G78060	AT1G78060	Glycosyl hydrolase family protein [Source:NCBI gene (formerly Entrezgene);Acc:844141]
4.48	0.000	AT2G34680	AIR9	Outer arm dynein light chain 1 protein [Source:NCBI gene (formerly Entrezgene);Acc:818033]
4.48	0.000	AT1G48760	delta-ADR	delta-adaptin [Source:NCBI gene (formerly Entrezgene);Acc:841298]
4.48	0.000	AT1G72710	CKL2	casein kinase 1-like protein 2 [Source:NCBI gene (formerly Entrezgene);Acc:843603]
4.48	0.000	AT2G41500	LIS	WD-40 repeat family protein / small nuclear ribonucleoprotein Prp4p-like protein [Source:NCBI gene (formerly Entrezgene);Acc:818748]
4.48	0.000	AT5G27650	AT5G27650	Tudor/PWWP/MBT superfamily protein [Source:NCBI gene (formerly Entrezgene);Acc:832827]
4.48	0.000	AT1G24300	AT1G24300	GYF domain-containing protein [Source:NCBI gene (formerly Entrezgene);Acc:839046]
4.48	0.000	AT1G64390	GH9C2	glycosyl hydrolase 9C2 [Source:NCBI gene (formerly Entrezgene);Acc:842747]
4.48	0.000	ATCG01120	rps15	
4.48	0.000	AT2G45620	AT2G45620	Nucleotidyltransferase family protein [Source:NCBI gene (formerly Entrezgene);Acc:819170]
4.48	0.000	AT5G51980	AT5G51980	Transducin/WD40 repeat-like superfamily protein [Source:NCBI gene (formerly Entrezgene);Acc:835273]
4.48	0.000	AT5G51280	AT5G51280	DEAD-box protein abstrakt [Source:NCBI gene (formerly Entrezgene);Acc:835202]
4.48	0.000	AT1G73720	SMU1	transducin family protein / WD-40 repeat family protein [Source:NCBI gene (formerly Entrezgene);Acc:843707]
4.48	0.000	AT1G80270	PPR596	PENTATRICOPEPTIDE REPEAT 596 [Source:NCBI gene (formerly Entrezgene);Acc:844367]
4.48	0.000	AT2G18510	emb2444	RNA-binding (RRM/RBD/RNP motifs) family protein [Source:NCBI gene (formerly Entrezgene);Acc:816366]
4.48	0.000	AT3G54890	LHCA1	chlorophyll a-b binding protein 6 [Source:NCBI gene (formerly Entrezgene);Acc:824654]
4.48	0.000	AT3G21140	AT3G21140	Pyridoxamine 5'-phosphate oxidase family protein [Source:NCBI gene (formerly Entrezgene);Acc:821666]
4.48	0.000	AT1G08370	DCP1	decapping 1 [Source:NCBI gene (formerly Entrezgene);Acc:837357]
4.48	0.000	AT2G05170	VPS11	vacuolar protein sorting 11 [Source:NCBI gene (formerly Entrezgene);Acc:815065]
4.46	0.000	AT3G61760	DL1B	DYNAMIN-like 1B [Source:NCBI gene (formerly Entrezgene);Acc:825349]
4.46	0.000	AT5G47690	AT5G47690	binding protein [Source:NCBI gene (formerly Entrezgene);Acc:834820]
4.45	0.000	AT4G26630	AT4G26630	DEK domain-containing chromatin associated protein [Source:NCBI gene (formerly Entrezgene);Acc:828770]
4.41	0.000	AT1G68060	MAP70-1	microtubule-associated proteins 70-1 [Source:NCBI gene (formerly Entrezgene);Acc:843134]
4.41	0.000	AT5G14520	AT5G14520	pescadillo-like protein [Source:NCBI gene (formerly Entrezgene);Acc:831303]
4.41	0.000	AT1G14840	MAP70-4	microtubule-associated proteins 70-4 [Source:NCBI gene (formerly Entrezgene);Acc:838049]
4.41	0.000	AT5G57015	ckl12	casein kinase I-like 12 [Source:NCBI gene (formerly Entrezgene);Acc:835804]
4.41	0.000	AT1G49040	SCD1	stomatal cytokinesis defective / SCD1 protein (SCD1) [Source:NCBI gene (formerly Entrezgene);Acc:841327]
4.41	0.000	AT1G64790	ILA	ILITYHIA [Source:NCBI gene (formerly Entrezgene);Acc:842787]
4.41	0.000	AT1G63160	RFC2	replication factor C 2 [Source:NCBI gene (formerly Entrezgene);Acc:842620]
4.41	0.000	AT1G23170	AT1G23170	transmembrane protein (Protein of unknown function DUF2359, transmembrane) [Source:NCBI gene (formerly Entrezgene);Acc:838925]
4.41	0.000	AT3G19960	ATM1	myosin 1 [Source:NCBI gene (formerly Entrezgene);Acc:821534]
4.41	0.000	AT1G79350	EMB1135	RING/FYVE/PHD zinc finger superfamily protein [Source:NCBI gene (formerly Entrezgene);Acc:844273]
4.41	0.000	AT1G55320	AAE18	acyl-activating enzyme 18 [Source:NCBI gene (formerly Entrezgene);Acc:841977]
4.41	0.000	AT3G19720	ARC5	P-loop containing nucleoside triphosphate hydrolases superfamily protein [Source:NCBI gene (formerly Entrezgene);Acc:821509]
4.41	0.000	AT1G60900	AT1G60900	U2 snRNP auxilliary factor, large subunit, splicing factor [Source:NCBI gene (formerly Entrezgene);Acc:842382]
4.41	0.000	AT1G11650	RBP45B	RNA-binding (RRM/RBD/RNP motifs) family protein [Source:NCBI gene (formerly Entrezgene);Acc:837708]
4.41	0.000	AT1G55325	GCT	RNA polymerase II transcription mediator [Source:NCBI gene (formerly Entrezgene);Acc:841978]
4.41	0.000	AT2G25320	AT2G25320	TRAF-like family protein [Source:NCBI gene (formerly Entrezgene);Acc:817070]
4.41	0.000	AT3G18390	EMB1865	CRS1 / YhbY (CRM) domain-containing protein [Source:NCBI gene (formerly Entrezgene);Acc:821368]
4.41	0.000	AT1G73460	AT1G73460	Protein kinase superfamily protein [Source:NCBI gene (formerly Entrezgene);Acc:843681]
4.35	0.000	AT3G06810	IBR3	acyl-CoA dehydrogenase-like protein [Source:NCBI gene (formerly Entrezgene);Acc:819865]
4.34	0.000	AT1G14900	HMGA	high mobility group A [Source:NCBI gene (formerly Entrezgene);Acc:838055]
4.34	0.000	AT5G12410	AT5G12410	THUMP domain-containing protein [Source:NCBI gene (formerly Entrezgene);Acc:831116]
4.34	0.000	AT3G06610	AT3G06610	DNA-binding enhancer protein-like protein [Source:NCBI gene (formerly Entrezgene);Acc:819840]
4.34	0.000	AT4G26600	AT4G26600	S-adenosyl-L-methionine-dependent methyltransferases superfamily protein [Source:NCBI gene (formerly Entrezgene);Acc:828767]
4.34	0.000	AT1G49480	RTV1	related to vernalization1 1 [Source:NCBI gene (formerly Entrezgene);Acc:841372]
4.34	0.000	AT5G18410	PIR121	transcription activator [Source:NCBI gene (formerly Entrezgene);Acc:831959]
4.34	0.000	AT3G03590	AT3G03590	SWIB/MDM2 domain superfamily protein [Source:NCBI gene (formerly Entrezgene);Acc:821215]
4.34	0.000	AT5G59870	HTA6	histone H2A 6 [Source:NCBI gene (formerly Entrezgene);Acc:836109]
4.34	0.000	AT4G10540	AT4G10540	Subtilase family protein [Source:NCBI gene (formerly Entrezgene);Acc:826646]
4.34	0.000	AT5G40490	AT5G40490	RNA-binding (RRM/RBD/RNP motifs) family protein [Source:NCBI gene (formerly Entrezgene);Acc:834047]
4.34	0.000	AT4G12780	AT4G12780	Chaperone DnaJ-domain superfamily protein [Source:NCBI gene (formerly Entrezgene);Acc:826890]
4.34	0.000	AT5G13300	SFC	ARF GTPase-activating protein [Source:NCBI gene (formerly Entrezgene);Acc:831171]
4.34	0.000	AT1G13320	PP2AA3	protein phosphatase 2A subunit A3 [Source:NCBI gene (formerly Entrezgene);Acc:837892]
4.34	0.000	AT5G16590	AT5G16590	Leucine-rich repeat protein kinase family protein [Source:NCBI gene (formerly Entrezgene);Acc:831521]
4.34	0.000	AT1G10170	NFXL1	NF-X-like 1 [Source:NCBI gene (formerly Entrezgene);Acc:837555]
4.30	0.000	AT5G22060	J2	DNAJ homologue 2 [Source:NCBI gene (formerly Entrezgene);Acc:832267]
4.27	0.000	AT5G02740	AT5G02740	Ribosomal protein S24e family protein [Source:NCBI gene (formerly Entrezgene);Acc:831811]
4.27	0.001	AT3G04470	AT3G04470	Ankyrin repeat family protein [Source:NCBI gene (formerly Entrezgene);Acc:819603]
4.27	0.001	AT2G33450	PRPL28	Ribosomal L28 family [Source:NCBI gene (formerly Entrezgene);Acc:817910]
4.27	0.001	AT4G25340	FKBP53	FK506 BINDING PROTEIN 53 [Source:NCBI gene (formerly Entrezgene);Acc:828637]

4.27	0.001	AT4G39980	DHS1	3-deoxy-D-arabino-heptulosonate 7-phosphate synthase 1 [Source:NCBI gene (formerly Entrezgene);Acc:830159]
4.27	0.001	AT1G17070	STIPL1	GC-rich sequence DNA-binding factor-like protein with Tuftelin interacting domain-containing protein [Source:NCBI gene (formerly Entrezgene);Acc:838277]
4.27	0.001	AT1G14710	AT1G14710	hydroxyproline-rich glycoprotein family protein [Source:NCBI gene (formerly Entrezgene);Acc:838036]
4.27	0.001	AT1G21170	SEC5B	Exocyst complex component SEC5 [Source:NCBI gene (formerly Entrezgene);Acc:838713]
4.27	0.001	AT3G18990	VRN1	AP2/B3-like transcriptional factor family protein [Source:NCBI gene (formerly Entrezgene);Acc:821432]
4.27	0.001	AT2G31900	XIF	myosin-like protein XIF [Source:NCBI gene (formerly Entrezgene);Acc:817748]
4.27	0.001	AT2G15430	NRPB3	DNA-directed RNA polymerase family protein [Source:NCBI gene (formerly Entrezgene);Acc:816035]
4.27	0.001	AT2G02740	WHY3	ssDNA-binding transcriptional regulator [Source:NCBI gene (formerly Entrezgene);Acc:814803]
4.27	0.001	AT2G20760	AT2G20760	Clathrin light chain protein [Source:NCBI gene (formerly Entrezgene);Acc:816605]
4.27	0.001	AT4G20130	PTAC14	plastid transcriptionally active 14 [Source:NCBI gene (formerly Entrezgene);Acc:827759]
4.27	0.001	AT4G32285	AT4G32285	ENTH/ANTH/VHS superfamily protein [Source:NCBI gene (formerly Entrezgene);Acc:829362]
4.22	0.000	AT5G61970	AT5G61970	signal recognition particle-related / SRP-like protein [Source:NCBI gene (formerly Entrezgene);Acc:836318]
4.19	0.000	AT4G36690	ATU2AF65A	U2 snRNP auxilliary factor, large subunit, splicing factor [Source:NCBI gene (formerly Entrezgene);Acc:829822]
4.19	0.001	AT3G50370	AT3G50370	
4.19	0.001	AT5G58710	ROC7	rotamase CYP 7 [Source:NCBI gene (formerly Entrezgene);Acc:835985]
4.19	0.001	AT2G21060	GRP2B	glycine-rich protein 2B [Source:NCBI gene (formerly Entrezgene);Acc:816641]
4.19	0.001	AT3G58660	AT3G58660	Ribosomal protein L1p/L10e family [Source:NCBI gene (formerly Entrezgene);Acc:825035]
4.19	0.001	AT4G13780	AT4G13780	methionine-tRNA ligase, putative / methionyl-tRNA synthetase, putative / MetRS [Source:NCBI gene (formerly Entrezgene);Acc:827012]
4.19	0.001	AT5G51410	AT5G51410	LUC7 N terminus domain-containing protein [Source:NCBI gene (formerly Entrezgene);Acc:835215]
4.19	0.001	AT3G13750	BGAL1	beta galactosidase 1 [Source:NCBI gene (formerly Entrezgene);Acc:820584]
4.19	0.001	AT3G23620	AT3G23620	Ribosomal RNA processing Brix domain protein [Source:NCBI gene (formerly Entrezgene);Acc:821942]
4.19	0.001	AT5G12940	AT5G12940	Leucine-rich repeat (LRR) family protein [Source:NCBI gene (formerly Entrezgene);Acc:831134]
4.19	0.001	AT1G14850	NUP155	nucleoporin 155 [Source:NCBI gene (formerly Entrezgene);Acc:838050]
4.19	0.001	AT4G25730	AT4G25730	FtsJ-like methyltransferase family protein [Source:NCBI gene (formerly Entrezgene);Acc:828678]
4.19	0.001	AT3G03950	ECT1	evolutionarily conserved C-terminal region 1 [Source:NCBI gene (formerly Entrezgene);Acc:819550]
4.19	0.001	AT4G12770	AT4G12770	Chaperone DnaJ-domain superfamily protein [Source:NCBI gene (formerly Entrezgene);Acc:826889]
4.19	0.001	AT3G06980	AT3G06980	DEA(D/H)-box RNA helicase family protein [Source:NCBI gene (formerly Entrezgene);Acc:819883]
4.19	0.001	AT2G15690	AT2G15690	Tetratricopeptide repeat (TPR)-like superfamily protein [Source:NCBI gene (formerly Entrezgene);Acc:816062]
4.15	0.000	AT1G79920	Hsp70-15	Heat shock protein 70 (Hsp 70) family protein [Source:NCBI gene (formerly Entrezgene);Acc:844332]
4.14	0.000	AT5G10010	AT5G10010	myosin-H heavy protein [Source:NCBI gene (formerly Entrezgene);Acc:830863]
4.11	0.000	AT4G16340	SPK1	guanyl-nucleotide exchange factors;GTPase binding;GTP binding protein [Source:NCBI gene (formerly Entrezgene);Acc:827328]
4.11	0.001	AT2G03150	emb1579	ATP/GTP-binding protein family [Source:NCBI gene (formerly Entrezgene);Acc:814844]
4.11	0.001	AT4G24330	AT4G24330	
4.11	0.001	AT1G56580	SVB	plant/protein (Protein of unknown function, DUF538) [Source:NCBI gene (formerly Entrezgene);Acc:842112]
4.11	0.001	AT3G16060	AT3G16060	ATP binding microtubule motor family protein [Source:NCBI gene (formerly Entrezgene);Acc:820851]
4.11	0.001	AT2G41620	AT2G41620	Nucleoporin interacting component (Nup93/Nic96-like) family protein [Source:NCBI gene (formerly Entrezgene);Acc:818760]
4.11	0.001	AT1G42440	AT1G42440	pre-rRNA-processing TSR1-like protein [Source:NCBI gene (formerly Entrezgene);Acc:840848]
4.11	0.001	AT1G49670	NQR	ARP protein (REF) [Source:NCBI gene (formerly Entrezgene);Acc:841391]
4.11	0.001	AT3G28730	HMG	high mobility group [Source:NCBI gene (formerly Entrezgene);Acc:822505]
4.11	0.001	AT5G60170	AT5G60170	RNA binding (RRM/RBD/RNP motifs) family protein [Source:NCBI gene (formerly Entrezgene);Acc:836139]
4.11	0.001	ATCG00330	rps14	
4.11	0.001	AT1G69770	CMT3	chromomethylase 3 [Source:NCBI gene (formerly Entrezgene);Acc:843313]
4.11	0.001	AT1G62330	AT1G62330	O-fucosyltransferase family protein [Source:NCBI gene (formerly Entrezgene);Acc:842531]
4.11	0.001	AT4G27430	CIP7	COP1-interacting protein 7 [Source:NCBI gene (formerly Entrezgene);Acc:828851]
4.11	0.001	AT4G33650	DRP3A	dynamin-related protein 3A [Source:NCBI gene (formerly Entrezgene);Acc:829506]
4.11	0.001	AT3G54090	FLN1	fructokinase-like 1 [Source:NCBI gene (formerly Entrezgene);Acc:824576]
4.11	0.001	AT2G27880	AGO5	Argonaute family protein [Source:NCBI gene (formerly Entrezgene);Acc:817334]
4.11	0.001	AT5G63260	AT5G63260	Zinc finger C-x8-C-x5-C-x3-H type family protein [Source:NCBI gene (formerly Entrezgene);Acc:836446]
4.11	0.001	AT1G29350	AT1G29350	RNA polymerase II degradation factor-like protein (DUF1296) [Source:NCBI gene (formerly Entrezgene);Acc:839809]
4.11	0.001	AT3G17465	RPL3P	ribosomal protein L3 plastid [Source:NCBI gene (formerly Entrezgene);Acc:821011]
4.02	0.002	AT3G22520	AT3G22520	spindle assembly abnormal protein [Source:NCBI gene (formerly Entrezgene);Acc:821823]
4.02	0.002	AT2G43680	IQD14	IQ-domain 14 [Source:NCBI gene (formerly Entrezgene);Acc:818970]
4.02	0.002	AT2G36870	XTH32	xyloglucan endotransglucosylase/hydrolase 32 [Source:NCBI gene (formerly Entrezgene);Acc:818259]
4.02	0.002	AT2G46900	AT2G46900	transcription factor-like protein [Source:NCBI gene (formerly Entrezgene);Acc:819303]
4.02	0.002	AT1G77470	RFC3	replication factor C subunit 3 [Source:NCBI gene (formerly Entrezgene);Acc:844083]
4.02	0.002	AT5G67510	AT5G67510	Translation protein SH3-like family protein [Source:NCBI gene (formerly Entrezgene);Acc:836887]
4.02	0.002	AT5G65810	CGR3	transmembrane protein [Source:NCBI gene (formerly Entrezgene);Acc:836710]
4.02	0.002	AT3G13990	AT3G13990	dentin sialophosphoprotein, putative (DUF1296) [Source:NCBI gene (formerly Entrezgene);Acc:820613]
4.02	0.002	AT1G21700	SWI3C	SWITCH/sucrose nonfermenting 3C [Source:NCBI gene (formerly Entrezgene);Acc:838774]
4.02	0.002	AT2G23940	AT2G23940	transmembrane protein (DUF788) [Source:NCBI gene (formerly Entrezgene);Acc:816926]
4.02	0.002	AT1G10490	AT1G10490	GNAT acetyltransferase (DUF699) [Source:NCBI gene (formerly Entrezgene);Acc:837589]
4.02	0.002	AT2G39260	AT2G39260	regulator of nonsense transcripts UPF2 [Source:NCBI gene (formerly Entrezgene);Acc:818511]
4.02	0.002	AT3G22220	AT3G22220	hAT transposon superfamily [Source:NCBI gene (formerly Entrezgene);Acc:821786]
4.02	0.002	AT2G07696	RPS7	
4.02	0.002	AT4G34910	AT4G34910	P-loop containing nucleoside triphosphate hydrolases superfamily protein [Source:NCBI gene (formerly Entrezgene);Acc:829643]
4.02	0.002	AT1G23900	GAMMA-ADAPTIN 1	gamma-adaptin 1 [Source:NCBI gene (formerly Entrezgene);Acc:839001]
4.02	0.002	AT1G30350	AT1G30350	Pectin lyase-like superfamily protein [Source:NCBI gene (formerly Entrezgene);Acc:839915]
4.02	0.002	AT1G80750	AT1G80750	Ribosomal protein L30/L7 family protein [Source:NCBI gene (formerly Entrezgene);Acc:844414]
4.02	0.002	AT2G26280	CID7	CTC-interacting domain 7 [Source:NCBI gene (formerly Entrezgene);Acc:817168]
4.02	0.002	AT1G54490	XRN4	exoribonuclease 4 [Source:NCBI gene (formerly Entrezgene);Acc:841891]
4.02	0.002	AT3G02880	AT3G02880	Leucine-rich repeat protein kinase family protein [Source:NCBI gene (formerly Entrezgene);Acc:821198]
4.02	0.000	AT3G05560	AT3G05560	Ribosomal L22e protein family [Source:NCBI gene (formerly Entrezgene);Acc:819722]
4.01	0.000	AT5G55660	AT5G55660	DEK domain-containing chromatin associated protein [Source:NCBI gene (formerly Entrezgene);Acc:835660]
3.99	0.000	AT1G79930	HSP91	heat shock protein 91 [Source:NCBI gene (formerly Entrezgene);Acc:844333]
3.98	0.000	AT3G22330	PMH2	putative mitochondrial RNA helicase 2 [Source:NCBI gene (formerly Entrezgene);Acc:821802]
3.96	0.000	AT3G11710	ATKRS-1	lysyl-tRNA synthetase 1 [Source:NCBI gene (formerly Entrezgene);Acc:820343]
3.93	0.002	AT3G18035	HON4	winged-helix DNA-binding transcription factor family protein [Source:NCBI gene (formerly Entrezgene);Acc:821328]
3.93	0.002	AT1G43700	VIP1	VIRE2-interacting protein 1 [Source:NCBI gene (formerly Entrezgene);Acc:840957]
3.93	0.002	AT3G22590	PHP	PLANT HOMOLOGOUS TO PARAFIBROMIN [Source:NCBI gene (formerly Entrezgene);Acc:821831]
3.93	0.002	AT1G79090	AT1G79090	topoisomerase II-associated protein [Source:NCBI gene (formerly Entrezgene);Acc:844250]
3.93	0.002	AT3G07660	AT3G07660	flocculation protein (DUF1296) [Source:NCBI gene (formerly Entrezgene);Acc:819957]
3.93	0.002	AT1G63810	AT1G63810	nucleolar protein [Source:NCBI gene (formerly Entrezgene);Acc:842684]
3.93	0.002	AT3G17340	AT3G17340	ARM repeat superfamily protein [Source:NCBI gene (formerly Entrezgene);Acc:820997]
3.93	0.002	AT1G79280	NUA	nuclear pore anchor [Source:NCBI gene (formerly Entrezgene);Acc:844268]
3.93	0.002	AT1G60170	emb1220	pre-mRNA processing ribonucleoprotein binding region-containing protein [Source:NCBI gene (formerly Entrezgene);Acc:842312]
3.93	0.002	AT1G67730	KCR1	beta-ketoacyl reductase 1 [Source:NCBI gene (formerly Entrezgene);Acc:843098]
3.93	0.002	AT3G42660	AT3G42660	transducin family protein / WD-40 repeat family protein [Source:NCBI gene (formerly Entrezgene);Acc:823286]

3.93	0.002	AT2G40650	AT2G40650	PRP38 family protein [Source:NCBI gene (formerly Entrezgene);Acc:818660]
3.93	0.002	AT5G64330	NPH3	Phototropic-responsive NPH3 family protein [Source:NCBI gene (formerly Entrezgene);Acc:836554]
3.93	0.002	AT1G78580	TPS1	trehalose-6-phosphate synthase [Source:NCBI gene (formerly Entrezgene);Acc:844194]
3.93	0.002	AT5G03040	iqd2	IQ-domain 2 [Source:NCBI gene (formerly Entrezgene);Acc:831696]
3.93	0.002	AT5G38640	AT5G38640	NagB/RpiA/CoA transferase-like superfamily protein [Source:NCBI gene (formerly Entrezgene);Acc:833854]
3.93	0.002	AT1G17470	DRG1	developmentally regulated G-protein 1 [Source:NCBI gene (formerly Entrezgene);Acc:838320]
3.93	0.002	AT5G58430	EXO70B1	exocyst subunit exo70 family protein B1 [Source:NCBI gene (formerly Entrezgene);Acc:835956]
3.93	0.002	AT4G27180	ATK2	kinesin 2 [Source:NCBI gene (formerly Entrezgene);Acc:828826]
3.93	0.002	AT1G61870	PPR336	pentatricopeptide repeat 336 [Source:NCBI gene (formerly Entrezgene);Acc:842484]
3.93	0.002	AT4G18905	AT4G18905	Transducin/WD40 repeat-like superfamily protein [Source:NCBI gene (formerly Entrezgene);Acc:827625]
3.93	0.002	AT2G07734	AT2G07734	Alpha-L RNA-binding motif/Ribosomal protein S4 family protein [Source:NCBI gene (formerly Entrezgene);Acc:815406]
3.93	0.002	AT2G38020	VCL1	vacuoleless1 (VCL1) [Source:NCBI gene (formerly Entrezgene);Acc:818380]
3.93	0.002	AT1G55500	ECT4	evolutionarily conserved C-terminal region 4 [Source:NCBI gene (formerly Entrezgene);Acc:841997]
3.93	0.002	AT2G41100	TCH3	Calcium-binding EF hand family protein [Source:NCBI gene (formerly Entrezgene);Acc:818709]
3.93	0.002	AT1G17745	PGDH	D-3-phosphoglycerate dehydrogenase [Source:NCBI gene (formerly Entrezgene);Acc:838352]
3.93	0.002	AT4G21620	AT4G21620	glycine-rich protein [Source:NCBI gene (formerly Entrezgene);Acc:828249]
3.93	0.002	AT1G04860	UBP2	ubiquitin-specific protease 2 [Source:NCBI gene (formerly Entrezgene);Acc:839397]
3.93	0.002	AT1G79150	AT1G79150	binding protein [Source:NCBI gene (formerly Entrezgene);Acc:844256]
3.93	0.002	AT3G11000	AT3G11000	DCD (Development and Cell Death) domain protein [Source:NCBI gene (formerly Entrezgene);Acc:820271]
3.92	0.000	AT5G20950	AT5G20950	Glycosyl hydrolase family protein [Source:NCBI gene (formerly Entrezgene);Acc:832220]
3.92	0.000	AT5G18420	AT5G18420	CCR4-NOT transcription complex subunit [Source:NCBI gene (formerly Entrezgene);Acc:831960]
3.92	0.000	AT1G48900	AT1G48900	Signal recognition particle, SRP54 subunit protein [Source:NCBI gene (formerly Entrezgene);Acc:841312]
3.86	0.000	AT1G01510	AN	NAD(P)-binding Rossmann-fold superfamily protein [Source:NCBI gene (formerly Entrezgene);Acc:839401]
3.86	0.000	AT1G07320	RPL4	ribosomal protein L4 [Source:NCBI gene (formerly Entrezgene);Acc:837243]
3.83	0.004	AT4G08310	AT4G08310	DNA ligase [Source:NCBI gene (formerly Entrezgene);Acc:826385]
3.83	0.004	AT1G12360	KEU	Sec1/munc18-like (SM) proteins superfamily [Source:NCBI gene (formerly Entrezgene);Acc:837791]
3.83	0.004	AT5G62350	AT5G62350	Plant invertase/pectin methylesterase inhibitor superfamily protein [Source:NCBI gene (formerly Entrezgene);Acc:836356]
3.83	0.004	AT5G17440	AT5G17440	LUC7 related protein [Source:NCBI gene (formerly Entrezgene);Acc:831610]
3.83	0.004	AT3G16630	KINESIN-13A	P-loop containing nucleoside triphosphate hydrolases superfamily protein [Source:NCBI gene (formerly Entrezgene);Acc:820915]
3.83	0.004	AT5G46070	AT5G46070	Guanylate-binding family protein [Source:NCBI gene (formerly Entrezgene);Acc:834648]
3.83	0.004	AT1G69200	FLN2	fructokinase-like protein [Source:NCBI gene (formerly Entrezgene);Acc:843251]
3.83	0.004	ATMG00090	rps3	
3.83	0.004	AT5G03540	EXO70A1	exocyst subunit exo70 family protein A1 [Source:NCBI gene (formerly Entrezgene);Acc:831809]
3.83	0.004	AT3G59990	MAP2B	methionine aminopeptidase 2B [Source:NCBI gene (formerly Entrezgene);Acc:825169]
3.83	0.004	AT2G41475	AT2G41475	Embryo-specific protein 3, (ATS3) [Source:NCBI gene (formerly Entrezgene);Acc:6240499]
3.83	0.004	AT2G34640	PTAC12	plastid transcriptionally active 12 [Source:NCBI gene (formerly Entrezgene);Acc:818029]
3.83	0.004	AT5G65720	NFS1	nitrogen fixation S (NIFS)-like 1 [Source:NCBI gene (formerly Entrezgene);Acc:836701]
3.83	0.004	AT2G36850	GSL8	glucan synthase-like 8 [Source:NCBI gene (formerly Entrezgene);Acc:818258]
3.83	0.004	AT5G10470	KAC1	kinesin like protein for actin based chloroplast movement 1 [Source:NCBI gene (formerly Entrezgene);Acc:830911]
3.83	0.004	AT5G04600	AT5G04600	RNA-binding (RRM/RBD/RNP motifs) family protein [Source:NCBI gene (formerly Entrezgene);Acc:830337]
3.83	0.004	AT1G69120	AP1	K-box region and MADS-box transcription factor family protein [Source:NCBI gene (formerly Entrezgene);Acc:843244]
3.83	0.004	AT4G33510	DHS2	3-deoxy-d-arabino-heptulosonate 7-phosphate synthase [Source:NCBI gene (formerly Entrezgene);Acc:829489]
3.83	0.004	AT3G49240	emb1796	Pentatricopeptide repeat (PPR) superfamily protein [Source:NCBI gene (formerly Entrezgene);Acc:824085]
3.83	0.004	AT5G61840	GUT1	Exostosin family protein [Source:NCBI gene (formerly Entrezgene);Acc:836306]
3.83	0.004	AT3G01790	AT3G01790	Ribosomal protein L13 family protein [Source:NCBI gene (formerly Entrezgene);Acc:821078]
3.83	0.004	AT5G24850	CRY3	cryptochrome 3 [Source:NCBI gene (formerly Entrezgene);Acc:832554]
3.83	0.004	AT5G02310	PRT6	proteolysis 6 [Source:NCBI gene (formerly Entrezgene);Acc:830916]
3.83	0.004	AT5G08420	AT5G08420	RNA-binding KH domain-containing protein [Source:NCBI gene (formerly Entrezgene);Acc:830741]
3.83	0.004	AT1G03230	AT1G03230	Eukaryotic aspartyl protease family protein [Source:NCBI gene (formerly Entrezgene);Acc:838532]
3.83	0.004	AT3G50670	U1-70K	U1 small nuclear ribonucleoprotein-70K [Source:NCBI gene (formerly Entrezgene);Acc:824230]
3.83	0.004	AT2G34970	AT2G34970	Trimeric LpxA-like enzyme [Source:NCBI gene (formerly Entrezgene);Acc:818061]
3.83	0.004	AT2G46780	AT2G46780	RNA-binding (RRM/RBD/RNP motifs) family protein [Source:NCBI gene (formerly Entrezgene);Acc:819291]
3.83	0.004	AT1G13980	GN	sec7 domain-containing protein [Source:NCBI gene (formerly Entrezgene);Acc:837958]
3.83	0.004	AT4G31570	AT4G31570	nucleoporin [Source:NCBI gene (formerly Entrezgene);Acc:829284]
3.83	0.004	AT4G04920	SFR6	sensitive to freezing 6 [Source:NCBI gene (formerly Entrezgene);Acc:825831]
3.83	0.004	AT1G34360	AT1G34360	translation initiation factor 3 (IF-3) family protein [Source:NCBI gene (formerly Entrezgene);Acc:840338]
3.83	0.004	AT5G25060	RRC1	RNA recognition motif (RRM)-containing protein [Source:NCBI gene (formerly Entrezgene);Acc:832577]
3.83	0.004	AT5G54430	PHOS32	Adenine nucleotide alpha hydrolases-like superfamily protein [Source:NCBI gene (formerly Entrezgene);Acc:835531]
3.83	0.004	AT5G13000	GSL12	glucan synthase-like 12 [Source:NCBI gene (formerly Entrezgene);Acc:831140]
3.80	0.000	AT5G20490	XIK	myosin family protein with Dil [Source:NCBI gene (formerly Entrezgene);Acc:832171]
3.77	0.000	AT1G80410	EMB2753	tetratricopeptide repeat (TPR)-containing protein [Source:NCBI gene (formerly Entrezgene);Acc:844381]
3.75	0.000	AT5G08450	AT5G08450	zinc finger CCCH domain protein [Source:NCBI gene (formerly Entrezgene);Acc:830744]
3.73	0.000	AT3G52140	NOXY38	tetratricopeptide repeat (TPR)-containing protein [Source:NCBI gene (formerly Entrezgene);Acc:824378]
3.72	0.005	AT5G47880	ERF1-1	eukaryotic release factor 1-1 [Source:NCBI gene (formerly Entrezgene);Acc:834839]
3.72	0.005	AT5G40950	RPL27	ribosomal protein large subunit 27 [Source:NCBI gene (formerly Entrezgene);Acc:834097]
3.72	0.005	AT3G29075	AT3G29075	glycine-rich protein [Source:NCBI gene (formerly Entrezgene);Acc:822552]
3.72	0.005	AT1G71820	SEC6	SEC6 [Source:NCBI gene (formerly Entrezgene);Acc:843512]
3.72	0.005	AT4G15790	AT4G15790	uveal autoantigen with coiled-coil/ankyrin [Source:NCBI gene (formerly Entrezgene);Acc:827259]
3.72	0.005	AT4G13710	AT4G13710	Pectin lyase-like superfamily protein [Source:NCBI gene (formerly Entrezgene);Acc:827005]
3.72	0.005	AT3G53500	RS2Z32	RNA-binding (RRM/RBD/RNP motifs) family protein with retrovirus zinc finger-like domain-containing protein [Source:NCBI gene (formerly Entrezgene);Acc:824518]
3.72	0.005	AT3G44850	AT3G44850	Protein kinase superfamily protein [Source:NCBI gene (formerly Entrezgene);Acc:823619]
3.72	0.005	AT3G16810	PUM24	pumilio 24 [Source:NCBI gene (formerly Entrezgene);Acc:820934]
3.72	0.005	AT5G64670	AT5G64670	Ribosomal protein L18e/L15 superfamily protein [Source:NCBI gene (formerly Entrezgene);Acc:836588]
3.72	0.005	AT2G18040	PIN1AT	peptidylprolyl cis/trans isomerase, NIMA-interacting 1 [Source:NCBI gene (formerly Entrezgene);Acc:816316]
3.72	0.005	AT3G49080	AT3G49080	Ribosomal protein S5 domain 2-like superfamily protein [Source:NCBI gene (formerly Entrezgene);Acc:824070]
3.72	0.005	AT2G34357	AT2G34357	ARM repeat superfamily protein [Source:NCBI gene (formerly Entrezgene);Acc:2745580]
3.72	0.005	AT3G12590	AT3G12590	
3.72	0.005	AT3G45850	AT3G45850	P-loop containing nucleoside triphosphate hydrolases superfamily protein [Source:NCBI gene (formerly Entrezgene);Acc:823728]
3.72	0.005	AT5G48030	GFA2	gametophytic factor 2 [Source:NCBI gene (formerly Entrezgene);Acc:834854]
3.72	0.005	AT3G07160	GSL10	glucan synthase-like 10 [Source:NCBI gene (formerly Entrezgene);Acc:819903]
3.72	0.005	AT1G04300	AT1G04300	TRAF-like superfamily protein [Source:NCBI gene (formerly Entrezgene);Acc:839551]
3.72	0.005	AT1G28110	SCPL45	serine carboxypeptidase-like 45 [Source:NCBI gene (formerly Entrezgene);Acc:839704]
3.72	0.005	AT3G27180	AT3G27180	S-adenosyl-L-methionine-dependent methyltransferases superfamily protein [Source:NCBI gene (formerly Entrezgene);Acc:822337]
3.72	0.005	AT5G57410	AT5G57410	Afadin/alpha-actinin-binding protein [Source:NCBI gene (formerly Entrezgene);Acc:835847]
3.72	0.005	AT1G29940	NRPA2	nuclear RNA polymerase A2 [Source:NCBI gene (formerly Entrezgene);Acc:839872]
3.72	0.005	AT5G10160	AT5G10160	Thioesterase superfamily protein [Source:NCBI gene (formerly Entrezgene);Acc:830880]
3.72	0.005	AT4G16180	AT4G16180	transmembrane protein [Source:NCBI gene (formerly Entrezgene);Acc:827310]

3.72	0.005	AT5G14460	AT5G14460	Pseudouridine synthase family protein [Source:NCBI gene (formerly Entrezgene);Acc:831297]
3.72	0.005	AT3G61650	TUBG1	gamma-tubulin [Source:NCBI gene (formerly Entrezgene);Acc:825338]
3.72	0.005	AT1G25260	AT1G25260	Ribosomal protein L10 family protein [Source:NCBI gene (formerly Entrezgene);Acc:839109]
3.72	0.005	AT2G18790	PHYB	phytochrome B [Source:NCBI gene (formerly Entrezgene);Acc:816394]
3.72	0.005	AT1G12770	EMB1586	P-loop containing nucleoside triphosphate hydrolases superfamily protein [Source:NCBI gene (formerly Entrezgene);Acc:837833]
3.72	0.005	AT3G18240	AT3G18240	Ribosomal protein S24/S35 [Source:NCBI gene (formerly Entrezgene);Acc:821352]
3.72	0.005	AT1G12470	AT1G12470	zinc ion binding protein [Source:NCBI gene (formerly Entrezgene);Acc:837804]
3.72	0.005	AT3G21100	AT3G21100	RNA-binding (RRM/RBD/RNP motifs) family protein [Source:NCBI gene (formerly Entrezgene);Acc:821662]
3.72	0.005	AT4G36680	AT4G36680	Tetratricopeptide repeat (TPR)-like superfamily protein [Source:NCBI gene (formerly Entrezgene);Acc:829821]
3.72	0.005	AT5G50320	ELO3	radical SAM domain-containing protein / GCN5-related N-acetyltransferase (GNAT) family protein [Source:NCBI gene (formerly Entrezgene);Acc:835098]
3.67	0.000	AT3G26420	ATRZ-1A	RNA-binding (RRM/RBD/RNP motifs) family protein with retrovirus zinc finger-like domain-containing protein [Source:NCBI gene (formerly Entrezgene);Acc:822246]
3.63	0.000	AT1G33430	AT1G33430	Galactosyltransferase family protein [Source:NCBI gene (formerly Entrezgene);Acc:840236]
3.60	0.008	AT3G11450	AT3G11450	DnaJ and Myb-like DNA-binding domain-containing protein [Source:NCBI gene (formerly Entrezgene);Acc:820318]
3.60	0.008	AT1G76300	SmD3	snRNP core protein SMD3 [Source:NCBI gene (formerly Entrezgene);Acc:843963]
3.60	0.008	AT5G10060	AT5G10060	ENTH/VHS family protein [Source:NCBI gene (formerly Entrezgene);Acc:830870]
3.60	0.008	AT4G24270	EMB140	EMBRYO DEFECTIVE 140 [Source:NCBI gene (formerly Entrezgene);Acc:828529]
3.60	0.008	AT4G29730	NFC5	nucleosome/chromatin assembly factor group C5 [Source:NCBI gene (formerly Entrezgene);Acc:829094]
3.60	0.008	AT3G52810	PAP21	purple acid phosphatase 21 [Source:NCBI gene (formerly Entrezgene);Acc:824447]
3.60	0.008	AT4G12600	AT4G12600	Ribosomal protein L7Ae/L30e/S12e/Gadd45 family protein [Source:NCBI gene (formerly Entrezgene);Acc:826873]
3.60	0.008	AT5G18190	AT5G18190	Protein kinase family protein [Source:NCBI gene (formerly Entrezgene);Acc:831937]
3.60	0.008	AT5G07510	GRP14	glycine-rich protein 14 [Source:NCBI gene (formerly Entrezgene);Acc:830644]
3.60	0.008	AT2G38750	ANNAT4	annexin 4 [Source:NCBI gene (formerly Entrezgene);Acc:818457]
3.60	0.008	AT5G53440	AT5G53440	LOW protein: zinc finger CCCH domain protein [Source:NCBI gene (formerly Entrezgene);Acc:835425]
3.60	0.008	AT1G07310	AT1G07310	Calcium-dependent lipid-binding (CaLB domain) family protein [Source:NCBI gene (formerly Entrezgene);Acc:837242]
3.60	0.008	AT5G08440	AT5G08440	transmembrane protein [Source:NCBI gene (formerly Entrezgene);Acc:830743]
3.60	0.008	AT2G14120	DRP3B	dynamin related protein [Source:NCBI gene (formerly Entrezgene);Acc:815898]
3.60	0.008	AT3G13160	AT3G13160	Tetratricopeptide repeat (TPR)-like superfamily protein [Source:NCBI gene (formerly Entrezgene);Acc:820505]
3.60	0.008	AT5G19400	SMG7	Telomerase activating protein Est1 [Source:NCBI gene (formerly Entrezgene);Acc:832060]
3.60	0.008	AT5G66760	SDH1-1	succinate dehydrogenase 1-1 [Source:NCBI gene (formerly Entrezgene);Acc:836809]
3.60	0.008	AT3G19590	BUB3.1	Transducin/WD40 repeat-like superfamily protein [Source:NCBI gene (formerly Entrezgene);Acc:821496]
3.60	0.008	AT1G79200	SCI1	splicing regulatory glutamine/lysine-rich-like protein [Source:NCBI gene (formerly Entrezgene);Acc:844261]
3.60	0.008	AT4G17140	AT4G17140	pleckstrin homology (PH) domain-containing protein [Source:NCBI gene (formerly Entrezgene);Acc:827424]
3.60	0.008	AT2G26570	WEB1	WEAK CHLOROPLAST MOVEMENT UNDER BLUE LIGHT-like protein (DUF827) [Source:NCBI gene (formerly Entrezgene);Acc:817198]
3.60	0.008	AT1G02205	CER1	Fatty acid hydroxylase superfamily [Source:NCBI gene (formerly Entrezgene);Acc:837602]
3.60	0.008	AT5G08620	STRS2	DEA(D/H)-box RNA helicase family protein [Source:NCBI gene (formerly Entrezgene);Acc:830763]
3.60	0.008	AT3G60980	AT3G60980	Tetratricopeptide repeat (TPR)-like superfamily protein [Source:NCBI gene (formerly Entrezgene);Acc:825270]
3.60	0.008	AT5G48900	AT5G48900	Pectin lyase-like superfamily protein [Source:NCBI gene (formerly Entrezgene);Acc:834948]
3.60	0.008	AT1G29790	AT1G29790	S-adenosyl-L-methionine-dependent methyltransferases superfamily protein [Source:NCBI gene (formerly Entrezgene);Acc:839857]
3.60	0.008	AT3G12080	emb2738	GTP-binding family protein [Source:NCBI gene (formerly Entrezgene);Acc:820382]
3.60	0.008	AT5G17510	AT5G17510	mediator of RNA polymerase II transcription subunit-like protein [Source:NCBI gene (formerly Entrezgene);Acc:831617]
3.60	0.008	AT1G49580	AT1G49580	Calcium-dependent protein kinase (CDPK) family protein [Source:NCBI gene (formerly Entrezgene);Acc:841382]
3.60	0.008	AT3G60960	AT3G60960	Tetratricopeptide repeat (TPR)-like superfamily protein [Source:NCBI gene (formerly Entrezgene);Acc:825268]
3.60	0.008	AT4G11050	GH9C3	glycosyl hydrolase 9C3 [Source:NCBI gene (formerly Entrezgene);Acc:826706]
3.60	0.008	AT4G05400	AT4G05400	copper ion binding protein [Source:NCBI gene (formerly Entrezgene);Acc:825888]
3.60	0.008	AT1G75750	GASA1	GAST1 protein homolog 1 [Source:NCBI gene (formerly Entrezgene);Acc:843908]
3.60	0.008	AT5G05970	NEDD1	Transducin/WD40 repeat-like superfamily protein [Source:NCBI gene (formerly Entrezgene);Acc:830483]
3.60	0.008	AT2G20060	AT2G20060	Ribosomal protein L4/L1 family [Source:NCBI gene (formerly Entrezgene);Acc:816525]
3.60	0.008	AT4G15640	AT4G15640	adenylyl cyclase [Source:NCBI gene (formerly Entrezgene);Acc:827241]
3.59	0.000	AT1G32790	CID11	CTC-interacting domain 11 [Source:NCBI gene (formerly Entrezgene);Acc:840173]
3.59	0.000	AT1G10840	TIF3H1	translation initiation factor 3 subunit H1 [Source:NCBI gene (formerly Entrezgene);Acc:837627]
3.58	0.000	AT4G31880	AT4G31880	transcriptional regulator [Source:NCBI gene (formerly Entrezgene);Acc:829318]
3.57	0.000	AT1G28290	AGP31	arabinogalactan protein 31 [Source:NCBI gene (formerly Entrezgene);Acc:839723]
3.55	0.000	AT3G07050	NSN1	GTP-binding family protein [Source:NCBI gene (formerly Entrezgene);Acc:819890]
3.51	0.000	AT5G21160	LARP1a	LA RNA-binding protein [Source:NCBI gene (formerly Entrezgene);Acc:832242]
3.51	0.000	AT1G55210	AT1G55210	Disease resistance-responsive (dirigent-like protein) family protein [Source:NCBI gene (formerly Entrezgene);Acc:841964]
3.48	0.011	AT1G08410	AT1G08410	P-loop containing nucleoside triphosphate hydrolases superfamily protein [Source:NCBI gene (formerly Entrezgene);Acc:837361]
3.48	0.011	AT5G25610	RD22	BURP domain-containing protein [Source:NCBI gene (formerly Entrezgene);Acc:832636]
3.48	0.011	AT4G31985	AT4G31985	Ribosomal protein L39 family protein [Source:NCBI gene (formerly Entrezgene);Acc:829329]
3.48	0.011	AT4G21660	AT4G21660	proline-rich spliceosome-associated (PSP) family protein [Source:NCBI gene (formerly Entrezgene);Acc:828253]
3.48	0.011	AT4G29520	AT4G29520	nucleophosmin [Source:NCBI gene (formerly Entrezgene);Acc:829073]
3.48	0.011	AT5G15230	GASA4	GAST1 protein homolog 4 [Source:NCBI gene (formerly Entrezgene);Acc:831375]
3.48	0.011	AT5G67320	HOS15	WD-40 repeat family protein [Source:NCBI gene (formerly Entrezgene);Acc:836867]
3.48	0.011	AT5G63960	AT5G63960	DNA polymerase delta subunit 1 [Source:NCBI gene (formerly Entrezgene);Acc:836517]
3.48	0.011	AT4G37460	SRFR1	Tetratricopeptide repeat (TPR)-like superfamily protein [Source:NCBI gene (formerly Entrezgene);Acc:829901]
3.48	0.011	AT4G28300	AT4G28300	formin-like protein (DUF1421) [Source:NCBI gene (formerly Entrezgene);Acc:828945]
3.48	0.011	AT4G17950	AT4G17950	AT hook motif DNA-binding family protein [Source:NCBI gene (formerly Entrezgene);Acc:827520]
3.48	0.011	AT3G57180		
3.48	0.011	AT1G18150	ATMPK8	Protein kinase superfamily protein [Source:NCBI gene (formerly Entrezgene);Acc:838394]
3.48	0.011	AT4G02720	AT4G02720	Ras-induced vulval development antagonist protein [Source:NCBI gene (formerly Entrezgene);Acc:828193]
3.48	0.011	AT3G22380	TIC	time for coffee [Source:NCBI gene (formerly Entrezgene);Acc:821807]
3.48	0.011	AT4G11160	AT4G11160	Translation initiation factor 2, small GTP-binding protein [Source:NCBI gene (formerly Entrezgene);Acc:826717]
3.48	0.011	AT3G57940	AT3G57940	GNAT acetyltransferase (DUF699) [Source:NCBI gene (formerly Entrezgene);Acc:824963]
3.48	0.011	AT5G40480	EMB3012	embryo defective 3012 [Source:NCBI gene (formerly Entrezgene);Acc:834046]
3.48	0.011	AT1G01710	AT1G01710	acyl-CoA thioesterase II [Source:NCBI gene (formerly Entrezgene);Acc:839254]
3.48	0.011	AT4G34460	AGB1	GTP binding protein beta 1 [Source:NCBI gene (formerly Entrezgene);Acc:829597]
3.48	0.011	AT1G67580	AT1G67580	Protein kinase superfamily protein [Source:NCBI gene (formerly Entrezgene);Acc:843079]
3.48	0.011	AT1G17760	CSTF77	Tetratricopeptide repeat (TPR)-like superfamily protein [Source:NCBI gene (formerly Entrezgene);Acc:838354]
3.48	0.011	AT2G33610	SWI3B	switch subunit 3 [Source:NCBI gene (formerly Entrezgene);Acc:817927]
3.48	0.011	AT4G03550	GSL05	glucan synthase-like 5 [Source:NCBI gene (formerly Entrezgene);Acc:825650]
3.48	0.011	AT1G05910	AT1G05910	cell division cycle protein 48-related / CDC48-like protein [Source:NCBI gene (formerly Entrezgene);Acc:837101]
3.48	0.011	AT1G52500	MMH-1	MUTM homolog-1 [Source:NCBI gene (formerly Entrezgene);Acc:841681]
3.48	0.011	AT1G53645	AT1G53645	hydroxyproline-rich glycoprotein family protein [Source:NCBI gene (formerly Entrezgene);Acc:841801]
3.48	0.011	AT4G35800	NRPB1	RNA polymerase II large subunit [Source:NCBI gene (formerly Entrezgene);Acc:829734]
3.48	0.011	AT5G44070	CAD1	phytochelatin synthase 1 (PCS1) [Source:NCBI gene (formerly Entrezgene);Acc:834430]
3.48	0.011	AT3G18520	HDA15	histone deacetylase 15 [Source:NCBI gene (formerly Entrezgene);Acc:821382]
3.48	0.011	AT3G48750	CDC2	cell division control 2 [Source:NCBI gene (formerly Entrezgene);Acc:824036]

3.48	0.011	AT1G06190	RHON1	Rho termination factor [Source:NCBI gene (formerly Entrezgene);Acc:837128]
3.48	0.011	AT5G19820	emb2734	ARM repeat superfamily protein [Source:NCBI gene (formerly Entrezgene);Acc:832102]
3.48	0.011	AT2G17380	AP19	associated protein 19 [Source:NCBI gene (formerly Entrezgene);Acc:816245]
3.48	0.011	AT5G49830	EXO84B	exocyst complex component 84B [Source:NCBI gene (formerly Entrezgene);Acc:835046]
3.48	0.011	AT2G40980	AT2G40980	Protein kinase superfamily protein [Source:NCBI gene (formerly Entrezgene);Acc:818698]
3.48	0.011	AT5G64740	CESA6	cellulose synthase 6 [Source:NCBI gene (formerly Entrezgene);Acc:836595]
3.48	0.011	AT3G07630	ADT2	arogenate dehydratase 2 [Source:NCBI gene (formerly Entrezgene);Acc:819954]
3.48	0.011	AT4G23540	AT4G23540	ARM repeat superfamily protein [Source:NCBI gene (formerly Entrezgene);Acc:828454]
3.48	0.011	AT3G04500	AT3G04500	RNA-binding (RRM/RBD/RNP motifs) family protein [Source:NCBI gene (formerly Entrezgene);Acc:819606]
3.48	0.011	AT3G58140	AT3G58140	phenylalanyl-tRNA synthetase class IIc family protein [Source:NCBI gene (formerly Entrezgene);Acc:824983]
3.48	0.011	AT2G35630	MOR1	ARM repeat superfamily protein [Source:NCBI gene (formerly Entrezgene);Acc:818131]
3.48	0.011	AT5G23570	SGS3	XS domain-containing protein / XS zinc finger domain-containing protein-like protein [Source:NCBI gene (formerly Entrezgene);Acc:832422]
3.48	0.011	AT2G44065	AT2G44065	Ribosomal protein L2 family [Source:NCBI gene (formerly Entrezgene);Acc:819012]
3.48	0.011	AT3G54610	HAG1	histone acetyltransferase of the GNAT family 1 [Source:NCBI gene (formerly Entrezgene);Acc:824626]
3.48	0.011	AT3G18110	EMB1270	Pentatricopeptide repeat (PPR) superfamily protein [Source:NCBI gene (formerly Entrezgene);Acc:821336]
3.48	0.011	AT3G13060	ECT5	evolutionarily conserved C-terminal region 5 [Source:NCBI gene (formerly Entrezgene);Acc:820492]
3.48	0.011	AT3G54340	AP3	K-box region and MADS-box transcription factor family protein [Source:NCBI gene (formerly Entrezgene);Acc:824601]
3.48	0.011	AT1G16870	AT1G16870	mitochondrial 28S ribosomal protein S29-like protein [Source:NCBI gene (formerly Entrezgene);Acc:838258]
3.48	0.011	AT1G21630	AT1G21630	Calcium-binding EF hand family protein [Source:NCBI gene (formerly Entrezgene);Acc:838765]
3.48	0.011	AT5G13570	DCP2	decapping 2 [Source:NCBI gene (formerly Entrezgene);Acc:831201]
3.48	0.011	AT5G51550	EXL3	EXORDIUM like 3 [Source:NCBI gene (formerly Entrezgene);Acc:835229]
3.48	0.011	AT1G12430	ARK3	armadillo repeat kinesin 3 [Source:NCBI gene (formerly Entrezgene);Acc:837799]
3.46	0.000	ATCG00740	rpoA	
3.46	0.000	AT4G02840	AT4G02840	Small nuclear ribonucleoprotein family protein [Source:NCBI gene (formerly Entrezgene);Acc:828163]
3.46	0.000	AT1G70770	AT1G70770	transmembrane protein (Protein of unknown function DUF2359, transmembrane) [Source:NCBI gene (formerly Entrezgene);Acc:843414]
3.42	0.000	AT4G28250	EXPB3	expansin B3 [Source:NCBI gene (formerly Entrezgene);Acc:828940]
3.42	0.000	AT5G63420	emb2746	RNA-metabolising metallo-beta-lactamase family protein [Source:NCBI gene (formerly Entrezgene);Acc:836461]
3.41	0.000	AT1G17580	MYA1	myosin 1 [Source:NCBI gene (formerly Entrezgene);Acc:838333]
3.40	0.000	AT5G64270	AT5G64270	splicing factor [Source:NCBI gene (formerly Entrezgene);Acc:836548]
3.37	0.000	AT3G06860	MFP2	multifunctional protein 2 [Source:NCBI gene (formerly Entrezgene);Acc:819870]
3.34	0.000	AT3G01540	DRH1	DEAD box RNA helicase 1 [Source:NCBI gene (formerly Entrezgene);Acc:821116]
3.34	0.016	AT4G31360	AT4G31360	selenium binding protein [Source:NCBI gene (formerly Entrezgene);Acc:829263]
3.34	0.016	AT5G27740	EMB2775	ATPase family associated with various cellular activities (AAA) [Source:NCBI gene (formerly Entrezgene);Acc:832836]
3.34	0.016	AT5G06660	AT5G06660	transmembrane/coiled-coil protein (Protein of unknown function DUF106, transmembrane) [Source:NCBI gene (formerly Entrezgene);Acc:830554]
3.34	0.016	AT5G20510	AL5	alfin-like 5 [Source:NCBI gene (formerly Entrezgene);Acc:832173]
3.34	0.016	AT1G43850	SEU	SEUSS transcriptional co-regulator [Source:NCBI gene (formerly Entrezgene);Acc:840981]
3.34	0.016	AT1G48160	AT1G48160	signal recognition particle 19 kDa protein, putative / SRP19 [Source:NCBI gene (formerly Entrezgene);Acc:841235]
3.34	0.016	AT3G51950	AT3G51950	Zinc finger (CCCH-type) family protein / RNA recognition motif (RRM)-containing protein [Source:NCBI gene (formerly Entrezgene);Acc:824358]
3.34	0.016	AT1G03280	AT1G03280	Transcription factor TFIIE, alpha subunit [Source:NCBI gene (formerly Entrezgene);Acc:838581]
3.34	0.016	AT1G22610	AT1G22610	C2 calcium/lipid-binding plant phosphoribosyltransferase family protein [Source:NCBI gene (formerly Entrezgene);Acc:838867]
3.34	0.016	AT1G19870	iqd32	IQ-domain 32 [Source:NCBI gene (formerly Entrezgene);Acc:838575]
3.34	0.016	AT2G29960	CYP5	cyclophilin 5 [Source:NCBI gene (formerly Entrezgene);Acc:817546]
3.34	0.016	AT5G54260	MRE11	DNA repair and meiosis protein (Mre11) [Source:NCBI gene (formerly Entrezgene);Acc:835514]
3.34	0.016	AT3G07030	AT3G07030	Alba DNA/RNA-binding protein [Source:NCBI gene (formerly Entrezgene);Acc:3768790]
3.34	0.016	AT1G26110	DCP5	decapping 5 [Source:NCBI gene (formerly Entrezgene);Acc:839152]
3.34	0.016	AT1G79730	ELF7	hydroxyproline-rich glycoprotein family protein [Source:NCBI gene (formerly Entrezgene);Acc:844312]
3.34	0.016	AT2G44540	GH9B9	glycosyl hydrolase 9B9 [Source:NCBI gene (formerly Entrezgene);Acc:819062]
3.34	0.016	AT4G36630	EMB2754	Vacuolar sorting protein 39 [Source:NCBI gene (formerly Entrezgene);Acc:829815]
3.34	0.016	AT1G17840	ABCG11	white-brown complex-like protein [Source:NCBI gene (formerly Entrezgene);Acc:838363]
3.34	0.016	AT1G73670	MPK15	MAP kinase 15 [Source:NCBI gene (formerly Entrezgene);Acc:843702]
3.34	0.016	AT4G36730	GBF1	G-box binding factor 1 [Source:NCBI gene (formerly Entrezgene);Acc:829826]
3.34	0.016	AT4G25960	ABCB2	P-glycoprotein 2 [Source:NCBI gene (formerly Entrezgene);Acc:828702]
3.34	0.016	AT3G61310	AT3G61310	AT hook motif DNA-binding family protein [Source:NCBI gene (formerly Entrezgene);Acc:825303]
3.34	0.016	AT2G31890	RAP	RAP [Source:NCBI gene (formerly Entrezgene);Acc:817747]
3.34	0.016	AT3G03560	AT3G03560	
3.34	0.016	AT3G48860	AT3G48860	coiled-coil protein [Source:NCBI gene (formerly Entrezgene);Acc:824047]
3.34	0.016	AT3G54470	AT3G54470	uridine 5'-monophosphate synthase / UMP synthase (PYRE-F) (UMPS) [Source:NCBI gene (formerly Entrezgene);Acc:824612]
3.34	0.016	AT3G47610	AT3G47610	transcription regulator/ zinc ion binding protein [Source:NCBI gene (formerly Entrezgene);Acc:823915]
3.34	0.016	AT2G17930	AT2G17930	Phosphatidylinositol 3- and 4-kinase family protein with FAT domain-containing protein [Source:NCBI gene (formerly Entrezgene);Acc:816303]
3.34	0.016	AT1G04910	AT1G04910	O-fucosyltransferase family protein [Source:NCBI gene (formerly Entrezgene);Acc:839373]
3.34	0.016	AT1G44835	AT1G44835	YbaK/aminoacyl-tRNA synthetase-associated domain-containing protein [Source:NCBI gene (formerly Entrezgene);Acc:841048]
3.34	0.016	AT3G21215	AT3G21215	RNA-binding (RRM/RBD/RNP motifs) family protein [Source:NCBI gene (formerly Entrezgene);Acc:821675]
3.34	0.016	AT3G21220	MKK5	MAP kinase kinase 5 [Source:NCBI gene (formerly Entrezgene);Acc:821676]
3.34	0.016	AT5G10630	AT5G10630	Translation elongation factor EF1A/initiation factor IF2gamma family protein [Source:NCBI gene (formerly Entrezgene);Acc:830928]
3.34	0.016	AT4G30160	VLN4	villin 4 [Source:NCBI gene (formerly Entrezgene);Acc:829139]
3.34	0.016	AT3G23310	AT3G23310	AGC (cAMP-dependent, cGMP-dependent and protein kinase C) kinase family protein [Source:NCBI gene (formerly Entrezgene);Acc:821911]
3.34	0.016	AT1G73620	AT1G73620	Pathosis-related thaumatin superfamily protein [Source:NCBI gene (formerly Entrezgene);Acc:843696]
3.34	0.016	AT5G21150	AGO9	Argonaute family protein [Source:NCBI gene (formerly Entrezgene);Acc:832241]
3.34	0.016	AT3G13670	AT3G13670	Protein kinase family protein [Source:NCBI gene (formerly Entrezgene);Acc:820572]
3.34	0.016	AT2G39330	JAL23	jacalin-related lectin 23 [Source:NCBI gene (formerly Entrezgene);Acc:818518]
3.34	0.016	AT5G49220	AT5G49220	
3.34	0.016	AT1G53720	CYP59	cyclophilin 59 [Source:NCBI gene (formerly Entrezgene);Acc:841810]
3.34	0.016	AT5G67240	SDN3	small RNA degrading nuclease 3 [Source:NCBI gene (formerly Entrezgene);Acc:836859]
3.34	0.016	AT2G19170	SLP3	subtilisin-like serine protease 3 [Source:NCBI gene (formerly Entrezgene);Acc:816434]
3.34	0.016	AT5G17410	AT5G17410	Spc97 / Spc98 family of spindle pole body (SBP) component [Source:NCBI gene (formerly Entrezgene);Acc:831607]
3.34	0.016	AT5G43900	MYA2	myosin 2 [Source:NCBI gene (formerly Entrezgene);Acc:834412]
3.34	0.016	AT2G43610	AT2G43610	Chitinase family protein [Source:NCBI gene (formerly Entrezgene);Acc:818963]
3.34	0.016	AT2G28290	SYD	P-loop containing nucleoside triphosphate hydrolases superfamily protein [Source:NCBI gene (formerly Entrezgene);Acc:817375]
3.34	0.016	AT5G35970	AT5G35970	P-loop containing nucleoside triphosphate hydrolases superfamily protein [Source:NCBI gene (formerly Entrezgene);Acc:833589]
3.34	0.016	AT1G15480	AT1G15480	Tetratricopeptide repeat (TPR)-like superfamily protein [Source:NCBI gene (formerly Entrezgene);Acc:838118]
3.34	0.016	AT1G30440	AT1G30440	Phototropic-responsive NPH3 family protein [Source:NCBI gene (formerly Entrezgene);Acc:839923]
3.34	0.016	AT1G02800	CEL2	cellulase 2 [Source:NCBI gene (formerly Entrezgene);Acc:839385]
3.34	0.016	AT1G51690	B ALPHA	protein phosphatase 2A 55 kDa regulatory subunit B alpha [Source:NCBI gene (formerly Entrezgene);Acc:841594]
3.34	0.016	AT3G03600	RPS2	ribosomal protein S2 [Source:NCBI gene (formerly Entrezgene);Acc:821211]
3.34	0.016	AT4G16390	SVR7	pentatricopeptide (PPR) repeat-containing protein [Source:NCBI gene (formerly Entrezgene);Acc:827333]
3.32	0.000	AT3G55460	SCL30	SC35-like splicing factor 30 [Source:NCBI gene (formerly Entrezgene);Acc:824712]
3.32	0.000	AT4G35020	RAC3	RAC-like 3 [Source:NCBI gene (formerly Entrezgene);Acc:829654]

3.29	0.000	AT2G34810	AT2G34810	FAD-binding Berberine family protein [Source:NCBI gene (formerly Entrezgene);Acc:818046]
3.27	0.000	AT3G12800	SDRB	short-chain dehydrogenase-reductase B [Source:NCBI gene (formerly Entrezgene);Acc:820462]
3.26	0.000	AT3G49470	NACA2	nascent polypeptide-associated complex subunit alpha-like protein 2 [Source:NCBI gene (formerly Entrezgene);Acc:824109]
3.24	0.000	AT4G27500	PPI1	proton pump interactor 1 [Source:NCBI gene (formerly Entrezgene);Acc:828859]
3.22	0.000	AT4G10610	CID12	CTC-interacting domain 12 [Source:NCBI gene (formerly Entrezgene);Acc:826653]
3.19	0.000	AT5G67630	AT5G67630	P-loop containing nucleoside triphosphate hydrolases superfamily protein [Source:NCBI gene (formerly Entrezgene);Acc:836899]
3.19	0.024	AT1G68680	AT1G68680	SH3/FCH domain protein [Source:NCBI gene (formerly Entrezgene);Acc:843198]
3.19	0.024	AT5G57460	AT5G57460	muniscin carboxy-terminal mu-like domain protein [Source:NCBI gene (formerly Entrezgene);Acc:835851]
3.19	0.024	AT2G05940	RIPK	Protein kinase superfamily protein [Source:NCBI gene (formerly Entrezgene);Acc:815147]
3.19	0.024	AT5G21326	CIPK26	Ca2+regulated serine-threonine protein kinase family protein [Source:NCBI gene (formerly Entrezgene);Acc:832246]
3.19	0.024	AT2G31970	RAD50	DNA repair-recombination protein (RAD50) [Source:NCBI gene (formerly Entrezgene);Acc:817756]
3.19	0.024	AT5G06830	AT5G06830	
3.19	0.024	AT2G15270	AT2G15270	PRKR-interacting protein [Source:NCBI gene (formerly Entrezgene);Acc:816016]
3.19	0.024	AT5G60990	AT5G60990	DEA(D/H)-box RNA helicase family protein [Source:NCBI gene (formerly Entrezgene);Acc:836220]
3.19	0.024	AT3G56860	UBA2A	UBP1-associated protein 2A [Source:NCBI gene (formerly Entrezgene);Acc:824853]
3.19	0.024	AT1G15440	PWP2	periodic tryptophan protein 2 [Source:NCBI gene (formerly Entrezgene);Acc:838115]
3.19	0.024	AT4G20330	AT4G20330	Transcription initiation factor TFIIE, beta subunit [Source:NCBI gene (formerly Entrezgene);Acc:827781]
3.19	0.024	AT2G30200	EMB3147	EMBRYO DEFECTIVE 3147 [Source:NCBI gene (formerly Entrezgene);Acc:817570]
3.19	0.024	AT2G17510	EMB2763	ribonuclease II family protein [Source:NCBI gene (formerly Entrezgene);Acc:816257]
3.19	0.024	AT3G22170	FHY3	far-red elongated hypocotyls 3 [Source:NCBI gene (formerly Entrezgene);Acc:821781]
3.19	0.024	AT5G12230	MED19A	mediator of RNA polymerase II transcription subunit 19a-like protein [Source:NCBI gene (formerly Entrezgene);Acc:831097]
3.19	0.024	AT5G67530	PUB49	plant U-box 49 [Source:NCBI gene (formerly Entrezgene);Acc:836889]
3.19	0.024	AT3G52750	FTSZ2-2	Tubulin/FtsZ family protein [Source:NCBI gene (formerly Entrezgene);Acc:824441]
3.19	0.024	AT2G17790	VPS35A	vacuolar protein sorting-associated 35A-like protein [Source:NCBI gene (formerly Entrezgene);Acc:816289]
3.19	0.024	AT5G22320	AT5G22320	Leucine-rich repeat (LRR) family protein [Source:NCBI gene (formerly Entrezgene);Acc:832292]
3.19	0.024	AT5G43070	WPP1	WPP domain protein 1 [Source:NCBI gene (formerly Entrezgene);Acc:834323]
3.19	0.024	AT3G22320	NRPB5	Eukaryotic rpb5 RNA polymerase subunit family protein [Source:NCBI gene (formerly Entrezgene);Acc:821801]
3.19	0.024	AT4G20400	JMJ14	JUMONJI 14 [Source:NCBI gene (formerly Entrezgene);Acc:827788]
3.19	0.024	AT3G54110	PUMP1	plant uncoupling mitochondrial protein 1 [Source:NCBI gene (formerly Entrezgene);Acc:824578]
3.19	0.024	AT3G51550	FER	Malectin/receptor-like protein kinase family protein [Source:NCBI gene (formerly Entrezgene);Acc:824318]
3.19	0.024	AT4G17890	AGD8	ARF-GAP domain 8 [Source:NCBI gene (formerly Entrezgene);Acc:827512]
3.19	0.024	AT3G12400	ELC	Ubiquitin-conjugating enzyme/RWD-like protein [Source:NCBI gene (formerly Entrezgene);Acc:820419]
3.19	0.024	AT2G18876	AT2G18876	Afadin/alpha-actinin-binding protein [Source:NCBI gene (formerly Entrezgene);Acc:816403]
3.19	0.024	AT5G15610	AT5G15610	Proteasome component (PCI) domain protein [Source:NCBI gene (formerly Entrezgene);Acc:831413]
3.19	0.024	AT4G21670	CPL1	C-terminal domain phosphatase-like 1 [Source:NCBI gene (formerly Entrezgene);Acc:828254]
3.19	0.024	AT5G45190	AT5G45190	Cyclin family protein [Source:NCBI gene (formerly Entrezgene);Acc:834555]
3.19	0.024	AT3G20800	AT3G20800	Cell differentiation, Rcd1-like protein [Source:NCBI gene (formerly Entrezgene);Acc:821628]
3.19	0.024	AT2G44730	AT2G44730	Alcohol dehydrogenase transcription factor Myb/SANT-like family protein [Source:NCBI gene (formerly Entrezgene);Acc:819080]
3.19	0.024	AT5G46420	AT5G46420	16S rRNA processing protein RimM family [Source:NCBI gene (formerly Entrezgene);Acc:834685]
3.19	0.024	AT5G26670	AT5G26670	Pectinacetylesterase family protein [Source:NCBI gene (formerly Entrezgene);Acc:832722]
3.19	0.024	AT4G20320	AT4G20320	CTP synthase family protein [Source:NCBI gene (formerly Entrezgene);Acc:827780]
3.19	0.024	AT1G06410	TPS7	trehalose-phosphatase/synthase 7 [Source:NCBI gene (formerly Entrezgene);Acc:837152]
3.19	0.024	AT3G53030	SRPK4	ser/arg-rich protein kinase 4 [Source:NCBI gene (formerly Entrezgene);Acc:824469]
3.19	0.024	AT4G32610	AT4G32610	copper ion binding protein [Source:NCBI gene (formerly Entrezgene);Acc:829396]
3.19	0.024	AT2G35840	AT2G35840	Sucrose-6F-phosphate phosphohydrolase family protein [Source:NCBI gene (formerly Entrezgene);Acc:818157]
3.19	0.024	AT3G09100	AT3G09100	mRNA capping enzyme family protein [Source:NCBI gene (formerly Entrezgene);Acc:820064]
3.19	0.024	AT5G11900	AT5G11900	Translation initiation factor SUI1 family protein [Source:NCBI gene (formerly Entrezgene);Acc:831063]
3.19	0.024	AT3G02760	AT3G02760	Class II aaRS and biotin synthetases superfamily protein [Source:NCBI gene (formerly Entrezgene);Acc:820930]
3.19	0.024	AT5G65460	KAC2	kinesin like protein for actin based chloroplast movement 2 [Source:NCBI gene (formerly Entrezgene);Acc:836671]
3.19	0.024	AT4G35890	LARP1c	winged-helix DNA-binding transcription factor family protein [Source:NCBI gene (formerly Entrezgene);Acc:829743]
3.19	0.024	AT3G18760	AT3G18760	Translation elongation factor EF1B/ribosomal protein S6 family protein [Source:NCBI gene (formerly Entrezgene);Acc:821407]
3.19	0.024	AT3G04740	SWP	RNA polymerase II transcription mediator [Source:NCBI gene (formerly Entrezgene);Acc:819634]
3.19	0.024	AT1G33990	MES14	methyl esterase 14 [Source:NCBI gene (formerly Entrezgene);Acc:840296]
3.19	0.024	AT4G30200	VEL1	vernalization5/VIN3-like protein [Source:NCBI gene (formerly Entrezgene);Acc:829143]
3.19	0.024	AT1G03140	AT1G03140	splicing factor Prp18 family protein [Source:NCBI gene (formerly Entrezgene);Acc:839567]
3.19	0.024	AT3G15680	AT3G15680	Ran BP2/NZF zinc finger-like superfamily protein [Source:NCBI gene (formerly Entrezgene);Acc:820811]
3.19	0.024	AT5G65930	ZWI	kinesin-like calmodulin-binding protein (ZWICHEL) [Source:NCBI gene (formerly Entrezgene);Acc:836723]
3.19	0.024	AT3G53120	VPS37-1	Modifier of rudimentary (Mod(r)) protein [Source:NCBI gene (formerly Entrezgene);Acc:824478]
3.19	0.024	AT5G12900	AT5G12900	DNA double-strand break repair RAD50 ATPase [Source:NCBI gene (formerly Entrezgene);Acc:831130]
3.19	0.024	AT5G12150	AT5G12150	Rho GTPase activation protein (RhoGAP) with PH domain-containing protein [Source:NCBI gene (formerly Entrezgene);Acc:831088]
3.19	0.024	AT4G01700	AT4G01700	Chitinase family protein [Source:NCBI gene (formerly Entrezgene);Acc:828131]
3.19	0.024	AT3G61130	GAUT1	galacturonosyltransferase 1 [Source:NCBI gene (formerly Entrezgene);Acc:825285]
3.19	0.024	AT4G24800	ECIP1	MA3 domain-containing protein [Source:NCBI gene (formerly Entrezgene);Acc:828582]
3.19	0.024	ATCG01020	rpl32	
3.19	0.024	AT1G61040	VIP5	plus-3 domain-containing protein [Source:NCBI gene (formerly Entrezgene);Acc:842395]
3.19	0.024	AT4G05410	YAO	Transducin/WD40 repeat-like superfamily protein [Source:NCBI gene (formerly Entrezgene);Acc:825889]
3.19	0.024	AT5G18580	FASS	tonneau 2 (TON2) [Source:NCBI gene (formerly Entrezgene);Acc:831976]
3.19	0.024	AT5G66470	AT5G66470	GTP-binding protein Era-like protein [Source:NCBI gene (formerly Entrezgene);Acc:836779]
3.16	0.001	AT3G55360	CER10	3-oxo-5-alpha-steroid 4-dehydrogenase family protein [Source:NCBI gene (formerly Entrezgene);Acc:824702]
3.16	0.001	AT1G14510	AL7	alfin-like 7 [Source:NCBI gene (formerly Entrezgene);Acc:838013]
3.16	0.001	AT4G24680	MOS1	modifier of snc1 [Source:NCBI gene (formerly Entrezgene);Acc:828570]
3.12	0.000	AT2G40660	AT2G40660	Nucleic acid-binding, OB-fold-like protein [Source:NCBI gene (formerly Entrezgene);Acc:818661]
3.12	0.000	AT5G14610	AT5G14610	DEAD box RNA helicase family protein [Source:NCBI gene (formerly Entrezgene);Acc:831313]
3.11	0.001	AT1G17370	UBP1B	oligouridylate binding protein 1B [Source:NCBI gene (formerly Entrezgene);Acc:838309]
3.10	0.000	AT2G38040	CAC3	acetyl Co-enzyme a carboxylase carboxyltransferase alpha subunit [Source:NCBI gene (formerly Entrezgene);Acc:818382]
3.09	0.000	AT1G20090	ROP2	RHO-related protein from plants 2 [Source:NCBI gene (formerly Entrezgene);Acc:838598]
3.06	0.000	AT1G14830	DL1C	DYNAMIN-like 1C [Source:NCBI gene (formerly Entrezgene);Acc:838048]
3.05	0.001	AT5G44320	AT5G44320	Eukaryotic translation initiation factor 3 subunit 7 (eIF-3) [Source:NCBI gene (formerly Entrezgene);Acc:834457]
3.03	0.000	AT5G27640	TIF3B1	translation initiation factor 3B1 [Source:NCBI gene (formerly Entrezgene);Acc:832826]
3.02	0.035	AT4G26130	AT4G26130	cotton fiber protein [Source:NCBI gene (formerly Entrezgene);Acc:828719]
3.02	0.035	AT5G22010	RFC1	replication factor C1 [Source:NCBI gene (formerly Entrezgene);Acc:832261]
3.02	0.035	AT2G04940	AT2G04940	scramblase-like protein [Source:NCBI gene (formerly Entrezgene);Acc:815041]
3.02	0.035	AT1G19430	AT1G19430	S-adenosyl-L-methionine-dependent methyltransferases superfamily protein [Source:NCBI gene (formerly Entrezgene);Acc:838527]
3.02	0.035	AT5G03280	EIN2	NRAMP metal ion transporter family protein [Source:NCBI gene (formerly Entrezgene);Acc:831889]
3.02	0.035	AT3G47450	NOA1	P-loop containing nucleoside triphosphate hydrolases superfamily protein [Source:NCBI gene (formerly Entrezgene);Acc:823899]
3.02	0.035	AT2G37550	AGD7	ARF-GAP domain 7 [Source:NCBI gene (formerly Entrezgene);Acc:818331]
3.02	0.035	AT1G10270	GRP23	glutamine-rich protein 23 [Source:NCBI gene (formerly Entrezgene);Acc:837566]

3.02	0.035	AT3G19650	AT3G19650	cyclin-like protein [Source:NCBI gene (formerly Entrezgene);Acc:821502]
3.02	0.035	AT3G11964	AT3G11964	RIBOSOMAL RNA PROCESSING 5 [Source:NCBI gene (formerly Entrezgene);Acc:820370]
3.02	0.035	AT1G21160	AT1G21160	eukaryotic translation initiation factor 2 (eIF-2) family protein [Source:NCBI gene (formerly Entrezgene);Acc:838712]
3.02	0.035	AT5G15980	AT5G15980	Pentatricopeptide repeat (PPR) superfamily protein [Source:NCBI gene (formerly Entrezgene);Acc:831455]
3.02	0.035	AT5G16750	TOZ	Transducin family protein / WD-40 repeat family protein [Source:NCBI gene (formerly Entrezgene);Acc:831538]
3.02	0.035	AT4G24290	AT4G24290	MAC/Perforin domain-containing protein [Source:NCBI gene (formerly Entrezgene);Acc:828532]
3.02	0.035	AT4G16630	AT4G16630	DEA(D/H)-box RNA helicase family protein [Source:NCBI gene (formerly Entrezgene);Acc:827364]
3.02	0.035	AT1G61620	AT1G61620	phosphoinositide binding protein [Source:NCBI gene (formerly Entrezgene);Acc:842458]
3.02	0.035	AT1G04990	AT1G04990	Zinc finger C-x8-C-x5-C-x3-H type family protein [Source:NCBI gene (formerly Entrezgene);Acc:839351]
3.02	0.035	AT2G26910	ABCG32	pleiotropic drug resistance 4 [Source:NCBI gene (formerly Entrezgene);Acc:817232]
3.02	0.035	AT1G54140	TAFII21	TATA binding protein associated factor 21kDa subunit [Source:NCBI gene (formerly Entrezgene);Acc:841854]
3.02	0.035	AT3G55340	PHIP1	phragmoplastin interacting protein 1 [Source:NCBI gene (formerly Entrezgene);Acc:824700]
3.02	0.035	AT3G56460	AT3G56460	GroES-like zinc-binding alcohol dehydrogenase family protein [Source:NCBI gene (formerly Entrezgene);Acc:824813]
3.02	0.035	AT1G67750	AT1G67750	Pectate lyase family protein [Source:NCBI gene (formerly Entrezgene);Acc:843100]
3.02	0.035	AT1G01950	ARK2	armadillo repeat kinesin 2 [Source:NCBI gene (formerly Entrezgene);Acc:839306]
3.02	0.035	AT4G17090	CT-BMY	chloroplast beta-amylase [Source:NCBI gene (formerly Entrezgene);Acc:827419]
3.02	0.035	AT5G15550	AT5G15550	Transducin/WD40 repeat-like superfamily protein [Source:NCBI gene (formerly Entrezgene);Acc:831408]
3.02	0.035	AT5G11490	AT5G11490	adaptin family protein [Source:NCBI gene (formerly Entrezgene);Acc:831021]
3.02	0.035	AT3G12130	AT3G12130	KH domain-containing protein / zinc finger (CCCH type) family protein [Source:NCBI gene (formerly Entrezgene);Acc:820388]
3.02	0.035	AT3G20810	JMJD5	2-oxoglutarate (2OG) and Fe(II)-dependent oxygenase superfamily protein [Source:NCBI gene (formerly Entrezgene);Acc:821629]
3.02	0.035	AT2G23390	AT2G23390	acyl-CoA [Source:NCBI gene (formerly Entrezgene);Acc:816871]
3.02	0.035	AT1G71350	AT1G71350	eukaryotic translation initiation factor SUI1 family protein [Source:NCBI gene (formerly Entrezgene);Acc:843476]
3.02	0.035	AT4G32460	AT4G32460	choice-of-anchor C domain protein, putative (Protein of unknown function, DUF642) [Source:NCBI gene (formerly Entrezgene);Acc:829381]
3.02	0.035	AT3G12250	TGA6	TGACG motif-binding factor 6 [Source:NCBI gene (formerly Entrezgene);Acc:820405]
3.02	0.035	AT1G15200	AT1G15200	protein-protein interaction regulator family protein [Source:NCBI gene (formerly Entrezgene);Acc:838086]
3.02	0.035	AT4G18950	AT4G18950	Integrin-linked protein kinase family [Source:NCBI gene (formerly Entrezgene);Acc:827630]
3.02	0.035	AT4G27690	VPS26B	vacuolar protein sorting 26B [Source:NCBI gene (formerly Entrezgene);Acc:828883]
3.02	0.035	AT4G02350	SEC15B	exocyst complex component sec15B [Source:NCBI gene (formerly Entrezgene);Acc:828060]
3.02	0.035	AT4G23620	AT4G23620	Ribosomal protein L25/Gln-tRNA synthetase, anti-codon-binding domain-containing protein [Source:NCBI gene (formerly Entrezgene);Acc:828462]
3.02	0.035	AT4G02990	BSM	Mitochondrial transcription termination factor family protein [Source:NCBI gene (formerly Entrezgene);Acc:828116]
3.02	0.035	AT3G02110	scpl25	serine carboxypeptidase-like 25 [Source:NCBI gene (formerly Entrezgene);Acc:821207]
3.02	0.035	AT4G18820	AT4G18820	AAA-type ATPase family protein [Source:NCBI gene (formerly Entrezgene);Acc:827616]
3.02	0.035	AT3G18140	LST8-1	Transducin/WD40 repeat-like superfamily protein [Source:NCBI gene (formerly Entrezgene);Acc:821339]
3.02	0.035	AT1G67310	AT1G67310	Calmodulin-binding transcription activator protein with CG-1 and Ankyrin domain [Source:NCBI gene (formerly Entrezgene);Acc:843051]
3.02	0.035	AT3G23325	AT3G23325	Splicing factor 3B subunit 5/RDS3 complex subunit 10 [Source:NCBI gene (formerly Entrezgene);Acc:821913]
3.02	0.035	AT4G02570	CUL1	cullin 1 [Source:NCBI gene (formerly Entrezgene);Acc:825648]
3.02	0.035	AT1G11130	SUB	Leucine-rich repeat protein kinase family protein [Source:NCBI gene (formerly Entrezgene);Acc:837654]
3.02	0.035	AT5G52840	AT5G52840	NADH-ubiquinone oxidoreductase-like protein [Source:NCBI gene (formerly Entrezgene);Acc:835361]
3.02	0.035	AT3G27430	PBB1	N-terminal nucleophile aminohydrolases (Ntn hydrolases) superfamily protein [Source:NCBI gene (formerly Entrezgene);Acc:822364]
3.02	0.035	AT1G51710	UBP6	ubiquitin-specific protease 6 [Source:NCBI gene (formerly Entrezgene);Acc:841596]
3.02	0.035	AT3G62010	AT3G62010	metal ion-binding protein [Source:NCBI gene (formerly Entrezgene);Acc:825374]
3.02	0.035	AT3G48430	REF6	relative of early flowering 6 [Source:NCBI gene (formerly Entrezgene);Acc:824002]
3.02	0.035	AT1G76950	PRAF1	Regulator of chromosome condensation (RCC1) family with FYVE zinc finger domain-containing protein [Source:NCBI gene (formerly Entrezgene);Acc:844030]
3.02	0.035	AT5G64420	AT5G64420	DNA polymerase V family [Source:NCBI gene (formerly Entrezgene);Acc:836563]
3.02	0.035	AT5G10200	AT5G10200	ARM-repeat/Tetratricopeptide repeat (TPR)-like protein [Source:NCBI gene (formerly Entrezgene);Acc:830884]
3.02	0.035	AT3G23750	AT3G23750	Leucine-rich repeat protein kinase family protein [Source:NCBI gene (formerly Entrezgene);Acc:821957]
3.02	0.035	AT5G53070	AT5G53070	Ribosomal protein L9/RNase H1 [Source:NCBI gene (formerly Entrezgene);Acc:835387]
3.02	0.035	AT5G65010	ASN2	asparagine synthetase 2 [Source:NCBI gene (formerly Entrezgene);Acc:836625]
3.02	0.035	AT2G16070	PDV2	plastid division2 [Source:NCBI gene (formerly Entrezgene);Acc:816104]
3.02	0.035	AT3G23780	NRPD2A	nuclear RNA polymerase D2A [Source:NCBI gene (formerly Entrezgene);Acc:821960]
3.02	0.035	AT5G40340	AT5G40340	Tudor/PWWP/MBT superfamily protein [Source:NCBI gene (formerly Entrezgene);Acc:834032]
3.02	0.035	AT4G01040	AT4G01040	Glycosyl hydrolase superfamily protein [Source:NCBI gene (formerly Entrezgene);Acc:827924]
3.02	0.000	AT1G75840	ARAC5	RAC-like GTP binding protein 5 [Source:NCBI gene (formerly Entrezgene);Acc:843917]
3.02	0.000	AT3G46780	PTAC16	plastid transcriptionally active 16 [Source:NCBI gene (formerly Entrezgene);Acc:823831]
3.00	0.000	AT2G45810	AT2G45810	DEA(D/H)-box RNA helicase family protein [Source:NCBI gene (formerly Entrezgene);Acc:819189]
2.99	0.002	AT4G10320	AT4G10320	tRNA synthetase class I (I, L, M and V) family protein [Source:NCBI gene (formerly Entrezgene);Acc:826624]
2.99	0.002	AT3G11400	EIF3G1	eukaryotic translation initiation factor 3G1 [Source:NCBI gene (formerly Entrezgene);Acc:820313]
2.99	0.002	AT1G09620	AT1G09620	ATP binding/leucine-tRNA ligases/aminoacyl-tRNA ligase [Source:NCBI gene (formerly Entrezgene);Acc:837489]
2.99	0.002	AT2G19740	AT2G19740	Ribosomal protein L31e family protein [Source:NCBI gene (formerly Entrezgene);Acc:816493]
2.98	0.000	AT3G13290	VCR	varicose-like protein [Source:NCBI gene (formerly Entrezgene);Acc:820529]
2.97	0.000	AT3G61820	AT3G61820	Eukaryotic aspartyl protease family protein [Source:NCBI gene (formerly Entrezgene);Acc:825355]
2.94	0.000	AT3G25150	AT3G25150	Nuclear transport factor 2 (NTF2) family protein with RNA binding (RRM-RBD-RNP motifs) domain-containing protein [Source:NCBI gene (formerly Entrezgene);Acc:822106]
2.94	0.000	AT4G20980	AT4G20980	Eukaryotic translation initiation factor 3 subunit 7 (eIF-3) [Source:NCBI gene (formerly Entrezgene);Acc:827845]
2.94	0.000	AT3G57290	EIF3E	eukaryotic translation initiation factor 3E [Source:NCBI gene (formerly Entrezgene);Acc:824896]
2.94	0.000	AT1G08730	XIC	Myosin family protein with Dil domain-containing protein [Source:NCBI gene (formerly Entrezgene);Acc:837394]
2.92	0.003	AT5G26210	AL4	alfin-like 4 [Source:NCBI gene (formerly Entrezgene);Acc:832690]
2.92	0.003	AT3G54670	TTN8	Structural maintenance of chromosomes (SMC) family protein [Source:NCBI gene (formerly Entrezgene);Acc:824632]
2.92	0.003	AT1G43190	PTB3	polypyrimidine tract-binding protein 3 [Source:NCBI gene (formerly Entrezgene);Acc:840918]
2.92	0.000	AT5G22330	RIN1	P-loop containing nucleoside triphosphate hydrolases superfamily protein [Source:NCBI gene (formerly Entrezgene);Acc:832293]
2.91	0.000	AT4G00660	RH8	RNAhelicase-like 8 [Source:NCBI gene (formerly Entrezgene);Acc:828042]
2.89	0.000	AT2G04520	AT2G04520	Nucleic acid-binding, OB-fold-like protein [Source:NCBI gene (formerly Entrezgene);Acc:814994]
2.87	0.000	AT1G48830	AT1G48830	Ribosomal protein S7e family protein [Source:NCBI gene (formerly Entrezgene);Acc:841305]
2.86	0.004	AT1G66260	AT1G66260	RNA-binding (RRM/RBD/RNP motifs) family protein [Source:NCBI gene (formerly Entrezgene);Acc:842943]
2.83	0.000	AT1G15290	AT1G15290	Tetratricopeptide repeat (TPR)-like superfamily protein [Source:NCBI gene (formerly Entrezgene);Acc:838097]
2.83	0.000	AT3G61240	AT3G61240	DEA(D/H)-box RNA helicase family protein [Source:NCBI gene (formerly Entrezgene);Acc:825296]
2.82	0.000	AT2G34040	AT2G34040	Apoptosis inhibitory protein 5 (API5) [Source:NCBI gene (formerly Entrezgene);Acc:817965]
2.82	0.000	AT3G15190	PRPS20	chloroplast 30S ribosomal protein S20 [Source:NCBI gene (formerly Entrezgene);Acc:820750]
2.82	0.000	AT5G25780	EIF3B-2	eukaryotic translation initiation factor 3B-2 [Source:NCBI gene (formerly Entrezgene);Acc:832647]
2.81	0.000	AT5G51750	SBT1.3	subtilase 1.3 [Source:NCBI gene (formerly Entrezgene);Acc:835249]
2.80	0.000	AT2G42520	AT2G42520	P-loop containing nucleoside triphosphate hydrolases superfamily protein [Source:NCBI gene (formerly Entrezgene);Acc:818852]
2.79	0.005	AT3G63095	AT3G63095	Tetratricopeptide repeat (TPR)-like superfamily protein [Source:NCBI gene (formerly Entrezgene);Acc:5008106]
2.79	0.005	AT2G47580	U1A	spliceosomal protein U1A [Source:NCBI gene (formerly Entrezgene);Acc:819371]
2.79	0.005	AT3G18190	AT3G18190	TCP-1/cpn60 chaperonin family protein [Source:NCBI gene (formerly Entrezgene);Acc:821346]
2.79	0.005	AT1G63660	AT1G63660	GMP synthase (glutamine-hydrolyzing), putative / glutamine amidotransferase [Source:NCBI gene (formerly Entrezgene);Acc:842670]
2.79	0.005	AT2G07690	MCM5	Minichromosome maintenance (MCM2/3/5) family protein [Source:NCBI gene (formerly Entrezgene);Acc:815415]
2.77	0.000	AT3G15000	RIP1	cobalt ion binding protein [Source:NCBI gene (formerly Entrezgene);Acc:820729]

2.76	0.000	AT1G01300	AT1G01300	Eukaryotic aspartyl protease family protein [Source:NCBI gene (formerly Entrezgene);Acc:839375]
2.73	0.001	AT3G03060	AT3G03060	P-loop containing nucleoside triphosphate hydrolases superfamily protein [Source:NCBI gene (formerly Entrezgene);Acc:821146]
2.73	0.001	AT5G16930	AT5G16930	AAA-type ATPase family protein [Source:NCBI gene (formerly Entrezgene);Acc:831556]
2.73	0.001	AT2G39990	EIF2	eukaryotic translation initiation factor 2 [Source:NCBI gene (formerly Entrezgene);Acc:818587]
2.73	0.001	AT5G16780	DOT2	SART-1 family [Source:NCBI gene (formerly Entrezgene);Acc:831541]
2.73	0.000	AT3G62120	AT3G62120	Class II aaRS and biotin synthetases superfamily protein [Source:NCBI gene (formerly Entrezgene);Acc:825385]
2.71	0.007	AT1G68720	TADA	tRNA arginine adenosine deaminase [Source:NCBI gene (formerly Entrezgene);Acc:843202]
2.71	0.007	AT4G36020	CSDP1	cold shock domain protein 1 [Source:NCBI gene (formerly Entrezgene);Acc:829758]
2.71	0.000	AT3G06480	AT3G06480	DEAD box RNA helicase family protein [Source:NCBI gene (formerly Entrezgene);Acc:819825]
2.71	0.000	AT4G28080	AT4G28080	Tetratricopeptide repeat (TPR)-like superfamily protein [Source:NCBI gene (formerly Entrezgene);Acc:828923]
2.70	0.000	AT4G29010	AIM1	Enoyl-CoA hydratase/isomerase family [Source:NCBI gene (formerly Entrezgene);Acc:829022]
2.69	0.000	AT1G48410	AGO1	Stabilizer of iron transporter SufD / Polynucleotidyl transferase [Source:NCBI gene (formerly Entrezgene);Acc:841262]
2.69	0.001	AT1G75350	emb2184	Ribosomal protein L31 [Source:NCBI gene (formerly Entrezgene);Acc:843871]
2.68	0.000	AT2G06210		
2.64	0.001	AT2G10940	AT2G10940	Bifunctional inhibitor/lipid-transfer protein/seed storage 2S albumin superfamily protein [Source:NCBI gene (formerly Entrezgene);Acc:815558]
2.64	0.001	AT3G14100	AT3G14100	RNA-binding (RRM/RBD/RNP motifs) family protein [Source:NCBI gene (formerly Entrezgene);Acc:820626]
2.63	0.010	AT1G04750	VAMP721	vesicle-associated membrane protein 721 [Source:NCBI gene (formerly Entrezgene);Acc:839419]
2.63	0.010	AT4G18060	AT4G18060	SH3 domain-containing protein [Source:NCBI gene (formerly Entrezgene);Acc:827531]
2.61	0.000	AT5G24710	AT5G24710	Transducin/WD40 repeat-like superfamily protein [Source:NCBI gene (formerly Entrezgene);Acc:832542]
2.59	0.001	AT4G15900	PRL1	pleiotropic regulatory locus 1 [Source:NCBI gene (formerly Entrezgene);Acc:827272]
2.57	0.000	AT5G27770	AT5G27770	Ribosomal L22e protein family [Source:NCBI gene (formerly Entrezgene);Acc:832839]
2.57	0.000	AT1G78630	emb1473	Ribosomal protein L13 family protein [Source:NCBI gene (formerly Entrezgene);Acc:844199]
2.56	0.000	AT4G21710	NRPB2	DNA-directed RNA polymerase family protein [Source:NCBI gene (formerly Entrezgene);Acc:828259]
2.55	0.014	AT3G51050	AT3G51050	FG-GAP repeat-containing protein [Source:NCBI gene (formerly Entrezgene);Acc:824269]
2.55	0.014	AT5G56950	NAP1;3	nucleosome assembly protein 1;3 [Source:NCBI gene (formerly Entrezgene);Acc:835797]
2.55	0.014	AT2G02470	AL6	alfin-like 6 [Source:NCBI gene (formerly Entrezgene);Acc:814776]
2.55	0.014	AT5G41770	AT5G41770	crooked neck protein, putative / cell cycle protein [Source:NCBI gene (formerly Entrezgene);Acc:834182]
2.53	0.000	AT5G35680	AT5G35680	Nucleic acid-binding, OB-fold-like protein [Source:NCBI gene (formerly Entrezgene);Acc:833541]
2.53	0.000	AT2G32080	PUR ALPHA-1	purin-rich alpha 1 [Source:NCBI gene (formerly Entrezgene);Acc:817768]
2.53	0.000	AT5G57370	MSF19.3	
2.53	0.000	AT1G27650	ATU2AF35A	U2 snRNP auxiliary factor small subunit [Source:NCBI gene (formerly Entrezgene);Acc:839657]
2.53	0.000	AT1G48850	EMB1144	chorismate synthase, putative / 5-enolpyruvylshikimate-3-phosphate phospholyase [Source:NCBI gene (formerly Entrezgene);Acc:841307]
2.53	0.000	AT2G46280	TRIP-1	TGF-beta receptor interacting protein 1 [Source:NCBI gene (formerly Entrezgene);Acc:819236]
2.51	0.000	AT2G28790	AT2G28790	Pathosis-related thaumatin superfamily protein [Source:NCBI gene (formerly Entrezgene);Acc:817428]
2.50	0.000	AT2G44590	DL1D	DYNAMIN-like 1D [Source:NCBI gene (formerly Entrezgene);Acc:819067]
2.50	0.000	AT4G34555	AT4G34555	Ribosomal protein S25 family protein [Source:NCBI gene (formerly Entrezgene);Acc:829607]
2.50	0.000	AT4G10710	SPT16	global transcription factor C [Source:NCBI gene (formerly Entrezgene);Acc:826665]
2.50	0.000	AT3G28500	AT3G28500	60S acidic ribosomal protein family [Source:NCBI gene (formerly Entrezgene);Acc:822480]
2.48	0.000	AT1G72970	HTH	Glucose-methanol-choline (GMC) oxidoreductase family protein [Source:NCBI gene (formerly Entrezgene);Acc:843628]
2.46	0.019	AT1G04430	AT1G04430	S-adenosyl-L-methionine-dependent methyltransferases superfamily protein [Source:NCBI gene (formerly Entrezgene);Acc:839522]
2.46	0.019	AT1G19360	RRA3	Nucleotide-diphospho-sugar transferase family protein [Source:NCBI gene (formerly Entrezgene);Acc:838519]
2.46	0.019	AT4G33250	EIF3K	eukaryotic translation initiation factor 3K [Source:NCBI gene (formerly Entrezgene);Acc:829461]
2.46	0.000	AT1G20220	AT1G20220	Alba DNA/RNA-binding protein [Source:NCBI gene (formerly Entrezgene);Acc:838610]
2.46	0.000	AT1G05190	emb2394	Ribosomal protein L6 family [Source:NCBI gene (formerly Entrezgene);Acc:839273]
2.44	0.000	AT5G05010	AT5G05010	clathrin adaptor complexes medium subunit family protein [Source:NCBI gene (formerly Entrezgene);Acc:830383]
2.43	0.000	AT2G40290	AT2G40290	Eukaryotic translation initiation factor 2 subunit 1 [Source:NCBI gene (formerly Entrezgene);Acc:818621]
2.43	0.000	AT4G02290	GH9B13	glycosyl hydrolase 9B13 [Source:NCBI gene (formerly Entrezgene);Acc:828080]
2.43	0.000	AT1G18450	ARP4	actin-related protein 4 [Source:NCBI gene (formerly Entrezgene);Acc:838425]
2.43	0.004	AT1G26550	AT1G26550	FKBP-like peptidyl-prolyl cis-trans isomerase family protein [Source:NCBI gene (formerly Entrezgene);Acc:839195]
2.43	0.004	AT5G63140	PAP29	purple acid phosphatase 29 [Source:NCBI gene (formerly Entrezgene);Acc:836435]
2.43	0.004	AT1G54080	UBP1A	oligouridylate-binding protein 1A [Source:NCBI gene (formerly Entrezgene);Acc:841846]
2.43	0.004	AT3G57660	NRPA1	nuclear RNA polymerase A1 [Source:NCBI gene (formerly Entrezgene);Acc:824935]
2.43	0.000	AT2G38110	GPAT6	glycerol-3-phosphate acyltransferase 6 [Source:NCBI gene (formerly Entrezgene);Acc:818389]
2.42	0.001	AT1G62820	AT1G62820	Calcium-binding EF-hand family protein [Source:NCBI gene (formerly Entrezgene);Acc:842581]
2.42	0.001	AT4G34660	AT4G34660	SH3 domain-containing protein [Source:NCBI gene (formerly Entrezgene);Acc:829618]
2.41	0.000	AT1G01320	AT1G01320	Tetratricopeptide repeat (TPR)-like superfamily protein [Source:NCBI gene (formerly Entrezgene);Acc:839293]
2.38	0.000	AT2G04390	AT2G04390	Ribosomal S17 family protein [Source:NCBI gene (formerly Entrezgene);Acc:814978]
2.38	0.005	AT1G14610	TWN2	valyl-tRNA synthetase / valine-tRNA ligase (VALRS) [Source:NCBI gene (formerly Entrezgene);Acc:838023]
2.37	0.026	AT1G32490	ESP3	RNA helicase family protein [Source:NCBI gene (formerly Entrezgene);Acc:840143]
2.37	0.026	AT5G58230	MSI1	Transducin/WD40 repeat-like superfamily protein [Source:NCBI gene (formerly Entrezgene);Acc:835935]
2.37	0.026	AT3G07810	AT3G07810	RNA-binding (RRM/RBD/RNP motifs) family protein [Source:NCBI gene (formerly Entrezgene);Acc:819972]
2.37	0.026	AT1G60200	AT1G60200	splicing factor PWI domain-containing protein / RNA recognition motif (RRM)-containing protein [Source:NCBI gene (formerly Entrezgene);Acc:842315]
2.37	0.026	AT1G10200	WLIM1	GATA type zinc finger transcription factor family protein [Source:NCBI gene (formerly Entrezgene);Acc:837558]
2.37	0.026	AT1G14410	WHY1	ssDNA-binding transcriptional regulator [Source:NCBI gene (formerly Entrezgene);Acc:838003]
2.37	0.026	AT3G43980	AT3G43980	Ribosomal protein S14p/S29e family protein [Source:NCBI gene (formerly Entrezgene);Acc:823515]
2.37	0.000	AT3G23450	AT3G23450	transmembrane protein [Source:NCBI gene (formerly Entrezgene);Acc:3768908]
2.37	0.000	AT5G27120	AT5G27120	NOP56-like pre RNA processing ribonucleoprotein [Source:NCBI gene (formerly Entrezgene);Acc:832770]
2.36	0.000	AT5G46430	AT5G46430	Ribosomal protein L32e [Source:NCBI gene (formerly Entrezgene);Acc:834686]
2.33	0.000	AT4G39200	AT4G39200	Ribosomal protein S25 family protein [Source:NCBI gene (formerly Entrezgene);Acc:830075]
2.33	0.000	AT4G26870	AT4G26870	Class II aminoacyl-tRNA and biotin synthetases superfamily protein [Source:NCBI gene (formerly Entrezgene);Acc:828794]
2.32	0.000	AT3G60190	DL1E	DYNAMIN-like 1E [Source:NCBI gene (formerly Entrezgene);Acc:825189]
2.29	0.002	AT2G40060	CLC2	Clathrin light chain protein [Source:NCBI gene (formerly Entrezgene);Acc:818594]
2.29	0.002	AT5G09440	EXL4	EXORDIUM like 4 [Source:NCBI gene (formerly Entrezgene);Acc:830803]
2.29	0.000	AT4G25630	FIB2	fibrillarin 2 [Source:NCBI gene (formerly Entrezgene);Acc:828668]
2.29	0.000	AT1G74470	AT1G74470	Pyridine nucleotide-disulfide oxidoreductase family protein [Source:NCBI gene (formerly Entrezgene);Acc:843788]
2.27	0.036	AT5G33370	AT5G33370	GDSL-like Lipase/Acylhydrolase superfamily protein [Source:NCBI gene (formerly Entrezgene);Acc:833315]
2.27	0.036	AT2G29580	MAC5B	CCCH-type zinc fingerfamily protein with RNA-binding domain-containing protein [Source:NCBI gene (formerly Entrezgene);Acc:817507]
2.27	0.036	AT1G02150	AT1G02150	Tetratricopeptide repeat (TPR)-like superfamily protein [Source:NCBI gene (formerly Entrezgene);Acc:839577]
2.27	0.036	AT3G50360	CEN2	centrin2 [Source:NCBI gene (formerly Entrezgene);Acc:824198]
2.27	0.036	AT1G10580	AT1G10580	Transducin/WD40 repeat-like superfamily protein [Source:NCBI gene (formerly Entrezgene);Acc:837599]
2.27	0.036	AT4G24550	AT4G24550	Clathrin adaptor complexes medium subunit family protein [Source:NCBI gene (formerly Entrezgene);Acc:828557]
2.26	0.000	AT3G58510	AT3G58510	DEA(D/H)-box RNA helicase family protein [Source:NCBI gene (formerly Entrezgene);Acc:825020]
2.26	0.009	AT1G67230	LINC1	little nuclei1 [Source:NCBI gene (formerly Entrezgene);Acc:843043]
2.26	0.009	AT3G03920	AT3G03920	H/ACA ribonucleoprotein complex, subunit Gar1/Naf1 protein [Source:NCBI gene (formerly Entrezgene);Acc:821062]
2.25	0.002	AT1G69250	AT1G69250	Nuclear transport factor 2 (NTF2) family protein with RNA binding (RRM-RBD-RNP motifs) domain-containing protein [Source:NCBI gene (formerly Entrezgene);Acc:843256]
2.25	0.002	AT3G06510	SFR2	Glycosyl hydrolase superfamily protein [Source:NCBI gene (formerly Entrezgene);Acc:819829]

2.25	0.002	AT5G27670	HTA7	histone H2A 7 [Source:NCBI gene (formerly Entrezgene);Acc:832829]
2.24	0.000	AT5G25754	AT5G25754	RNA polymerase I-associated factor PAF67 [Source:NCBI gene (formerly Entrezgene);Acc:832643]
2.21	0.001	AT5G03740	HD2C	histone deacetylase 2C [Source:NCBI gene (formerly Entrezgene);Acc:831733]
2.20	0.000	AT5G62190	PRH75	DEAD box RNA helicase (PRH75) [Source:NCBI gene (formerly Entrezgene);Acc:836340]
2.19	0.000	AT1G69620	RPL34	ribosomal protein L34 [Source:NCBI gene (formerly Entrezgene);Acc:843298]
2.19	0.012	AT2G17800	ARAC1	RAC-like 1 [Source:NCBI gene (formerly Entrezgene);Acc:816290]
2.18	0.000	AT5G52040	RS41	RNA-binding (RRM/RBD/RNP motifs) family protein [Source:NCBI gene (formerly Entrezgene);Acc:835279]
2.17	0.000	AT3G54210	AT3G54210	Ribosomal protein L17 family protein [Source:NCBI gene (formerly Entrezgene);Acc:824588]
2.16	0.000	AT2G05920	AT2G05920	Subtilase family protein [Source:NCBI gene (formerly Entrezgene);Acc:815145]
2.16	0.004	AT5G47210	AT5G47210	Hyaluronan / mRNA binding family [Source:NCBI gene (formerly Entrezgene);Acc:834767]
2.14	0.001	AT5G55920	OLI2	S-adenosyl-L-methionine-dependent methyltransferases superfamily protein [Source:NCBI gene (formerly Entrezgene);Acc:835690]
2.13	0.000	AT2G19480	NAP1;2	nucleosome assembly protein 1;2 [Source:NCBI gene (formerly Entrezgene);Acc:816467]
2.12	0.016	AT3G09900	RABE1e	RAB GTPase homolog E1E [Source:NCBI gene (formerly Entrezgene);Acc:820148]
2.11	0.000	AT5G14320	EMB3137	Ribosomal protein S13/S18 family [Source:NCBI gene (formerly Entrezgene);Acc:831282]
2.11	0.000	AT2G27040	AGO4	Argonaute family protein [Source:NCBI gene (formerly Entrezgene);Acc:817246]
2.11	0.005	AT3G14310	PME3	pectin methylesterase 3 [Source:NCBI gene (formerly Entrezgene);Acc:820651]
2.11	0.005	AT1G31850	AT1G31850	S-adenosyl-L-methionine-dependent methyltransferases superfamily protein [Source:NCBI gene (formerly Entrezgene);Acc:840075]
2.11	0.005	AT3G07010	AT3G07010	Pectin lyase-like superfamily protein [Source:NCBI gene (formerly Entrezgene);Acc:819886]
2.10	0.000	AT3G58570	AT3G58570	P-loop containing nucleoside triphosphate hydrolases superfamily protein [Source:NCBI gene (formerly Entrezgene);Acc:825026]
2.10	0.002	AT1G41880	AT1G41880	Ribosomal protein L35Ae family protein [Source:NCBI gene (formerly Entrezgene);Acc:840799]
2.10	0.002	AT3G55750	AT3G55750	Ribosomal protein L35Ae family protein [Source:NCBI gene (formerly Entrezgene);Acc:824741]
2.06	0.000	AT5G26742	emb1138	DEAD box RNA helicase (RH3) [Source:NCBI gene (formerly Entrezgene);Acc:832713]
2.06	0.000	AT1G75930	EXL6	extracellular lipase 6 [Source:NCBI gene (formerly Entrezgene);Acc:843926]
2.06	0.000	AT5G23900	AT5G23900	Ribosomal protein L13e family protein [Source:NCBI gene (formerly Entrezgene);Acc:832455]
2.05	0.021	AT1G80660	HA9	H[+]-ATPase 9 [Source:NCBI gene (formerly Entrezgene);Acc:844405]
2.05	0.021	AT5G05170	CEV1	Cellulose synthase family protein [Source:NCBI gene (formerly Entrezgene);Acc:830399]
2.05	0.021	AT3G53610	RAB8	RAB GTPase homolog 8 [Source:NCBI gene (formerly Entrezgene);Acc:824529]
2.05	0.000	AT1G10290	ADL6	dynamin-like protein 6 [Source:NCBI gene (formerly Entrezgene);Acc:837568]
2.03	0.001	AT5G63120	AT5G63120	P-loop containing nucleoside triphosphate hydrolases superfamily protein [Source:NCBI gene (formerly Entrezgene);Acc:836432]
2.03	0.000	AT5G42080	DL1	dynamin-like protein [Source:NCBI gene (formerly Entrezgene);Acc:834213]
2.02	0.003	AT4G26110	NAP1;1	nucleosome assembly protein1;1 [Source:NCBI gene (formerly Entrezgene);Acc:828717]
2.01	0.000	AT1G04480	AT1G04480	Ribosomal protein L14p/L23e family protein [Source:NCBI gene (formerly Entrezgene);Acc:839511]
2.00	0.000	AT1G26880	AT1G26880	Ribosomal protein L34e superfamily protein [Source:NCBI gene (formerly Entrezgene);Acc:838331]
2.00	0.000	AT5G07030	AT5G07030	Eukaryotic aspartyl protease family protein [Source:NCBI gene (formerly Entrezgene);Acc:830594]
1.98	0.000	AT3G05060	AT3G05060	NOP56-like pre RNA processing ribonucleoprotein [Source:NCBI gene (formerly Entrezgene);Acc:819668]
1.97	0.000	AT4G31340	AT4G31340	myosin heavy chain-like protein [Source:NCBI gene (formerly Entrezgene);Acc:829261]
1.95	0.011	AT5G12370	SEC10	exocyst complex component sec10 [Source:NCBI gene (formerly Entrezgene);Acc:831112]
1.95	0.011	AT4G16130	ARA1	arabinose kinase [Source:NCBI gene (formerly Entrezgene);Acc:827299]
1.94	0.000	AT3G13300	VCS	Transducin/WD40 repeat-like superfamily protein [Source:NCBI gene (formerly Entrezgene);Acc:820530]
1.93	0.005	AT3G02260	BIG	auxin transport protein (BIG) [Source:NCBI gene (formerly Entrezgene);Acc:820398]
1.91	0.000	AT3G57150	NAP57	homologue of NAP57 [Source:NCBI gene (formerly Entrezgene);Acc:824882]
1.91	0.000	AT3G02560	AT3G02560	Ribosomal protein S7e family protein [Source:NCBI gene (formerly Entrezgene);Acc:821308]
1.91	0.000	AT4G11420	EIF3A	eukaryotic translation initiation factor 3A [Source:NCBI gene (formerly Entrezgene);Acc:826746]
1.90	0.037	AT3G55430	AT3G55430	O-Glycosyl hydrolases family 17 protein [Source:NCBI gene (formerly Entrezgene);Acc:824709]
1.90	0.037	AT2G03510	AT2G03510	SPFH/Band 7/PHB domain-containing membrane-associated protein family [Source:NCBI gene (formerly Entrezgene);Acc:814880]
1.90	0.000	AT5G54600	RPL24	Translation protein SH3-like family protein [Source:NCBI gene (formerly Entrezgene);Acc:835549]
1.90	0.000	AT4G02230	AT4G02230	Ribosomal protein L19e family protein [Source:NCBI gene (formerly Entrezgene);Acc:828099]
1.89	0.000	AT1G09590	AT1G09590	Translation protein SH3-like family protein [Source:NCBI gene (formerly Entrezgene);Acc:837486]
1.89	0.000	AT3G44890	RPL9	ribosomal protein L9 [Source:NCBI gene (formerly Entrezgene);Acc:823623]
1.88	0.000	AT4G18100	AT4G18100	Ribosomal protein L32e [Source:NCBI gene (formerly Entrezgene);Acc:827535]
1.85	0.000	AT5G52470	FIB1	fibrillarin 1 [Source:NCBI gene (formerly Entrezgene);Acc:835323]
1.85	0.000	ATCG00800	rps3	
1.84	0.008	AT5G03940	CPSRP54	chloroplast signal recognition particle 54 kDa subunit [Source:NCBI gene (formerly Entrezgene);Acc:830273]
1.84	0.000	AT4G34980	SLP2	subtilisin-like serine protease 2 [Source:NCBI gene (formerly Entrezgene);Acc:829650]
1.83	0.020	AT5G57290	AT5G57290	60S acidic ribosomal protein family [Source:NCBI gene (formerly Entrezgene);Acc:835834]
1.83	0.020	AT5G03520	RAB8C	RAB GTPase homolog 8C [Source:NCBI gene (formerly Entrezgene);Acc:831817]
1.82	0.002	AT2G18330	AT2G18330	AAA-type ATPase family protein [Source:NCBI gene (formerly Entrezgene);Acc:816348]
1.82	0.000	AT3G56150	EIF3C	eukaryotic translation initiation factor 3C [Source:NCBI gene (formerly Entrezgene);Acc:824781]
1.82	0.000	AT2G21580	AT2G21580	Ribosomal protein S25 family protein [Source:NCBI gene (formerly Entrezgene);Acc:816696]
1.81	0.000	AT5G47700	AT5G47700	60S acidic ribosomal protein family [Source:NCBI gene (formerly Entrezgene);Acc:834821]
1.81	0.000	AT2G40590	AT2G40590	Ribosomal protein S26e family protein [Source:NCBI gene (formerly Entrezgene);Acc:818654]
1.81	0.000	AT2G21390	AT2G21390	Coatomer, alpha subunit [Source:NCBI gene (formerly Entrezgene);Acc:816678]
1.80	0.000	AT1G62020	AT1G62020	Coatomer, alpha subunit [Source:NCBI gene (formerly Entrezgene);Acc:842497]
1.79	0.000	AT4G11380	AT4G11380	Adaptin family protein [Source:NCBI gene (formerly Entrezgene);Acc:826741]
1.79	0.000	AT4G23460	AT4G23460	Adaptin family protein [Source:NCBI gene (formerly Entrezgene);Acc:828445]
1.78	0.000	AT4G25740	AT4G25740	RNA binding Plectin/S10 domain-containing protein [Source:NCBI gene (formerly Entrezgene);Acc:828679]
1.78	0.000	AT2G33150	PKT3	peroxisomal 3-ketoacyl-CoA thiolase 3 [Source:NCBI gene (formerly Entrezgene);Acc:817876]
1.77	0.026	AT5G66860	AT5G66860	Ribosomal protein L25/Gln-tRNA synthetase, anti-codon-binding domain-containing protein [Source:NCBI gene (formerly Entrezgene);Acc:836820]
1.77	0.026	AT5G28740	AT5G28740	Tetratricopeptide repeat (TPR)-like superfamily protein [Source:NCBI gene (formerly Entrezgene);Acc:832986]
1.76	0.000	AT3G09500	AT3G09500	Ribosomal L29 family protein [Source:NCBI gene (formerly Entrezgene);Acc:820107]
1.75	0.001	AT3G12860	AT3G12860	NOP56-like pre RNA processing ribonucleoprotein [Source:NCBI gene (formerly Entrezgene);Acc:820468]
1.75	0.014	AT2G37340	RS2Z33	arginine/serine-rich zinc knuckle-containing protein 33 [Source:NCBI gene (formerly Entrezgene);Acc:818311]
1.75	0.014	AT1G22410	AT1G22410	Class-II DAHP synthetase family protein [Source:NCBI gene (formerly Entrezgene);Acc:838847]
1.73	0.007	AT2G21160	AT2G21160	Translocon-associated protein (TRAP), alpha subunit [Source:NCBI gene (formerly Entrezgene);Acc:816651]
1.72	0.000	AT1G59610	DL3	dynamin-like 3 [Source:NCBI gene (formerly Entrezgene);Acc:842251]
1.71	0.002	AT4G16143	IMPA-2	importin alpha [Source:NCBI gene (formerly Entrezgene);Acc:827302]
1.70	0.018	AT5G35180	AT5G35180	ENHANCED DISEASE RESISTANCE protein (DUF1336) [Source:NCBI gene (formerly Entrezgene);Acc:833472]
1.70	0.018	AT1G24510	AT1G24510	TCP-1/cpn60 chaperonin family protein [Source:NCBI gene (formerly Entrezgene);Acc:839066]
1.69	0.009	AT3G28900	AT3G28900	Ribosomal protein L34e superfamily protein [Source:NCBI gene (formerly Entrezgene);Acc:822524]
1.68	0.000	AT3G15730	PLDALPHA1	phospholipase D alpha 1 [Source:NCBI gene (formerly Entrezgene);Acc:820816]
1.68	0.000	AT5G20290	AT5G20290	Ribosomal protein S8e family protein [Source:NCBI gene (formerly Entrezgene);Acc:832151]
1.68	0.000	AT1G78570	RHM1	rhamnose biosynthesis 1 [Source:NCBI gene (formerly Entrezgene);Acc:844193]
1.68	0.000	AT1G36160	ACC1	acetyl-CoA carboxylase 1 [Source:NCBI gene (formerly Entrezgene);Acc:840521]
1.67	0.001	AT4G19210	ABCE2	RNAse l inhibitor protein 2 [Source:NCBI gene (formerly Entrezgene);Acc:827661]
1.67	0.000	AT1G29250	AT1G29250	Alba DNA/RNA-binding protein [Source:NCBI gene (formerly Entrezgene);Acc:839799]
1.65	0.000	AT3G44110	J3	DNAJ homologue 3 [Source:NCBI gene (formerly Entrezgene);Acc:823531]
1.65	0.000	AT2G19520	FVE	Transducin family protein / WD-40 repeat family protein [Source:NCBI gene (formerly Entrezgene);Acc:816471]

1.65	0.003	AT5G13510	EMB3136	Ribosomal protein L10 family protein [Source:NCBI gene (formerly Entrezgene);Acc:831195]
1.64	0.006	AT3G16780	AT3G16780	Ribosomal protein L19e family protein [Source:NCBI gene (formerly Entrezgene);Acc:820931]
1.64	0.006	AT5G46800	BOU	Mitochondrial substrate carrier family protein [Source:NCBI gene (formerly Entrezgene);Acc:834724]
1.64	0.045	AT3G10690	GYRA	DNA GYRASE A [Source:NCBI gene (formerly Entrezgene);Acc:820238]
1.64	0.045	AT5G64260	EXL2	EXORDIUM like 2 [Source:NCBI gene (formerly Entrezgene);Acc:836547]
1.62	0.001	ATCG00160	rps2	
1.62	0.000	AT1G23290	RPL27AB	Ribosomal protein L18e/L15 superfamily protein [Source:NCBI gene (formerly Entrezgene);Acc:838938]
1.61	0.008	AT3G55170	AT3G55170	Ribosomal L29 family protein [Source:NCBI gene (formerly Entrezgene);Acc:824683]
1.60	0.000	AT2G39460	RPL23AA	ribosomal protein L23AA [Source:NCBI gene (formerly Entrezgene);Acc:818531]
1.60	0.000	AT2G37600	AT2G37600	Ribosomal protein L36e family protein [Source:NCBI gene (formerly Entrezgene);Acc:818337]
1.60	0.016	AT4G25550	AT4G25550	Cleavage/polyadenylation specificity factor, 25kDa subunit [Source:NCBI gene (formerly Entrezgene);Acc:828660]
1.58	0.000	AT5G13850	NACA3	nascent polypeptide-associated complex subunit alpha-like protein 3 [Source:NCBI gene (formerly Entrezgene);Acc:831231]
1.57	0.000	AT4G10480	AT4G10480	Nascent polypeptide-associated complex (NAC), alpha subunit family protein [Source:NCBI gene (formerly Entrezgene);Acc:826640]
1.57	0.010	ATCG00065	rps12	
1.57	0.000	AT3G53020	STV1	Ribosomal protein L24e family protein [Source:NCBI gene (formerly Entrezgene);Acc:824468]
1.55	0.020	AT3G17840	RLK902	receptor-like kinase 902 [Source:NCBI gene (formerly Entrezgene);Acc:821053]
1.55	0.020	AT3G07770	Hsp89.1	HEAT SHOCK PROTEIN 89.1 [Source:NCBI gene (formerly Entrezgene);Acc:819968]
1.55	0.000	AT3G12390	AT3G12390	Nascent polypeptide-associated complex (NAC), alpha subunit family protein [Source:NCBI gene (formerly Entrezgene);Acc:820418]
1.55	0.000	AT3G62870	AT3G62870	Ribosomal protein L7Ae/L30e/S12e/Gadd45 family protein [Source:NCBI gene (formerly Entrezgene);Acc:825462]
1.55	0.000	AT1G56110	NOP56	NOP56-like pre RNA processing ribonucleoprotein [Source:NCBI gene (formerly Entrezgene);Acc:842063]
1.54	0.001	AT2G37470	AT2G37470	Histone superfamily protein [Source:NCBI gene (formerly Entrezgene);Acc:818324]
1.53	0.037	AT5G57870	eIFiso4G1	MIF4G domain-containing protein / MA3 domain-containing protein [Source:NCBI gene (formerly Entrezgene);Acc:835897]
1.53	0.013	AT1G76010	AT1G76010	Alba DNA/RNA-binding protein [Source:NCBI gene (formerly Entrezgene);Acc:843932]
1.53	0.002	AT1G48480	RKL1	receptor-like kinase 1 [Source:NCBI gene (formerly Entrezgene);Acc:841269]
1.52	0.000	AT3G13460	ECT2	evolutionarily conserved C-terminal region 2 [Source:NCBI gene (formerly Entrezgene);Acc:820548]
1.51	0.025	AT5G60960	PNM1	Pentatricopeptide repeat (PPR) superfamily protein [Source:NCBI gene (formerly Entrezgene);Acc:836217]
1.49	0.000	AT5G52650	AT5G52650	RNA binding Plectin/S10 domain-containing protein [Source:NCBI gene (formerly Entrezgene);Acc:835342]
1.49	0.016	AT5G37720	ALY4	ALWAYS EARLY 4 [Source:NCBI gene (formerly Entrezgene);Acc:833750]
1.49	0.000	AT1G02780	emb2386	Ribosomal protein L19e family protein [Source:NCBI gene (formerly Entrezgene);Acc:839407]
1.49	0.000	AT2G19730	AT2G19730	Ribosomal L28e protein family [Source:NCBI gene (formerly Entrezgene);Acc:816492]
1.48	0.000	AT3G60770	AT3G60770	Ribosomal protein S13/S15 [Source:NCBI gene (formerly Entrezgene);Acc:825248]
1.48	0.011	AT3G56910	PSRP5	plastid-specific 50S ribosomal protein 5 [Source:NCBI gene (formerly Entrezgene);Acc:824858]
1.48	0.011	AT4G04910	NSF	AAA-type ATPase family protein [Source:NCBI gene (formerly Entrezgene);Acc:825830]
1.46	0.007	AT5G26360	AT5G26360	TCP-1/cpn60 chaperonin family protein [Source:NCBI gene (formerly Entrezgene);Acc:832705]
1.46	0.002	AT1G07920	AT1G07920	GTP binding Elongation factor Tu family protein [Source:NCBI gene (formerly Entrezgene);Acc:837307]
1.46	0.032	AT1G17880	BTF3	basic transcription factor 3 [Source:NCBI gene (formerly Entrezgene);Acc:838367]
1.45	0.021	AT5G09500	AT5G09500	Ribosomal protein S19 family protein [Source:NCBI gene (formerly Entrezgene);Acc:830809]
1.44	0.002	AT1G79990	AT1G79990	coatomer subunit beta-2 [Source:NCBI gene (formerly Entrezgene);Acc:844339]
1.44	0.000	AT3G08530	AT3G08530	Clathrin, heavy chain [Source:NCBI gene (formerly Entrezgene);Acc:820001]
1.44	0.014	AT3G49720	AT3G49720	transmembrane protein [Source:NCBI gene (formerly Entrezgene);Acc:824134]
1.42	0.004	AT5G48880	KAT5	peroxisomal 3-keto-acyl-CoA thiolase 2 [Source:NCBI gene (formerly Entrezgene);Acc:834946]
1.42	0.004	AT1G68530	KCS6	3-ketoacyl-CoA synthase 6 [Source:NCBI gene (formerly Entrezgene);Acc:843182]
1.42	0.000	AT1G80070	SUS2	Pre-mRNA-processing-splicing factor [Source:NCBI gene (formerly Entrezgene);Acc:844347]
1.41	0.040	AT4G38680	GRP2	glycine rich protein 2 [Source:NCBI gene (formerly Entrezgene);Acc:830024]
1.41	0.040	AT3G07100	ERMO2	Sec23/Sec24 protein transport family protein [Source:NCBI gene (formerly Entrezgene);Acc:819896]
1.40	0.000	AT5G07350	Tudor1	TUDOR-SN protein 1 [Source:NCBI gene (formerly Entrezgene);Acc:830626]
1.40	0.017	AT1G53500	MUM4	NAD-dependent epimerase/dehydratase family protein [Source:NCBI gene (formerly Entrezgene);Acc:841785]
1.40	0.000	AT4G31480	AT4G31480	Coatomer, beta subunit [Source:NCBI gene (formerly Entrezgene);Acc:829275]
1.40	0.000	AT4G31490	AT4G31490	Coatomer, beta subunit [Source:NCBI gene (formerly Entrezgene);Acc:829276]
1.39	0.002	AT2G36620	RPL24A	ribosomal protein L24 [Source:NCBI gene (formerly Entrezgene);Acc:818234]
1.39	0.000	AT5G07530	GRP17	glycine rich protein 17 [Source:NCBI gene (formerly Entrezgene);Acc:830646]
1.37	0.000	AT4G00100	RPS13A	ribosomal protein S13A [Source:NCBI gene (formerly Entrezgene);Acc:828167]
1.37	0.000	AT4G34450	AT4G34450	coatomer gamma-2 subunit, putative / gamma-2 coat protein, putative / gamma-2 COP [Source:NCBI gene (formerly Entrezgene);Acc:829596]
1.34	0.011	AT3G51800	ATG2	metallopeptidase M24 family protein [Source:NCBI gene (formerly Entrezgene);Acc:824343]
1.33	0.000	AT2G39800	P5CS1	delta1-pyrroline-5-carboxylate synthase 1 [Source:NCBI gene (formerly Entrezgene);Acc:818566]
1.33	0.000	AT5G60790	ABCF1	ABC transporter family protein [Source:NCBI gene (formerly Entrezgene);Acc:836200]
1.32	0.026	AT1G52730	AT1G52730	Transducin/WD40 repeat-like superfamily protein [Source:NCBI gene (formerly Entrezgene);Acc:841706]
1.31	0.003	AT1G32990	PRPL11	plastid ribosomal protein l11 [Source:NCBI gene (formerly Entrezgene);Acc:840194]
1.30	0.000	AT1G06220	MEE5	Ribosomal protein S5/Elongation factor G/III/V family protein [Source:NCBI gene (formerly Entrezgene);Acc:837131]
1.30	0.001	AT5G19760	AT5G19760	Mitochondrial substrate carrier family protein [Source:NCBI gene (formerly Entrezgene);Acc:832096]
1.28	0.000	AT3G53740	AT3G53740	Ribosomal protein L36e family protein [Source:NCBI gene (formerly Entrezgene);Acc:824541]
1.28	0.000	AT4G21650	AT4G21650	Subtilase family protein [Source:NCBI gene (formerly Entrezgene);Acc:828252]
1.28	0.004	AT2G39390	AT2G39390	Ribosomal L29 family protein [Source:NCBI gene (formerly Entrezgene);Acc:818524]
1.28	0.000	AT2G47610	AT2G47610	Ribosomal protein L7Ae/L30e/S12e/Gadd45 family protein [Source:NCBI gene (formerly Entrezgene);Acc:819374]
1.28	0.000	AT1G70600	AT1G70600	Ribosomal protein L18e/L15 superfamily protein [Source:NCBI gene (formerly Entrezgene);Acc:843397]
1.27	0.000	AT3G11130	AT3G11130	Clathrin, heavy chain [Source:NCBI gene (formerly Entrezgene);Acc:820284]
1.25	0.000	AT3G20820	AT3G20820	Leucine-rich repeat (LRR) family protein [Source:NCBI gene (formerly Entrezgene);Acc:821630]
1.24	0.000	AT3G11510	AT3G11510	Ribosomal protein S11 family protein [Source:NCBI gene (formerly Entrezgene);Acc:820324]
1.24	0.041	ATCG00790	rpl16	
1.24	0.006	AT3G56340	AT3G56340	Ribosomal protein S26e family protein [Source:NCBI gene (formerly Entrezgene);Acc:824801]
1.24	0.003	AT3G04920	AT3G04920	Ribosomal protein S24e family protein [Source:NCBI gene (formerly Entrezgene);Acc:819652]
1.22	0.033	AT5G13780	AT5G13780	Acyl-CoA N-acyltransferases (NAT) superfamily protein [Source:NCBI gene (formerly Entrezgene);Acc:831223]
1.22	0.002	AT5G28060	AT5G28060	Ribosomal protein S24e family protein [Source:NCBI gene (formerly Entrezgene);Acc:832878]
1.21	0.014	AT5G02570	AT5G02570	Histone superfamily protein [Source:NCBI gene (formerly Entrezgene);Acc:831878]
1.20	0.001	AT3G55220	SAP130b	Cleavage and polyadenylation specificity factor (CPSF) A subunit protein [Source:NCBI gene (formerly Entrezgene);Acc:824688]
1.19	0.002	AT1G04270	RPS15	cytosolic ribosomal protein S15 [Source:NCBI gene (formerly Entrezgene);Acc:839564]
1.19	0.000	AT5G61780	Tudor2	TUDOR-SN protein 2 [Source:NCBI gene (formerly Entrezgene);Acc:836300]
1.18	0.040	AT3G46740	TOC75-III	translocon at the outer envelope membrane of chloroplasts 75-III [Source:NCBI gene (formerly Entrezgene);Acc:823827]
1.18	0.001	AT5G09510	AT5G09510	Ribosomal protein S19 family protein [Source:NCBI gene (formerly Entrezgene);Acc:830810]
1.14	0.000	AT2G44120	AT2G44120	Ribosomal protein L30/L7 family protein [Source:NCBI gene (formerly Entrezgene);Acc:819018]
1.13	0.001	AT5G22880	HTB2	histone B2 [Source:NCBI gene (formerly Entrezgene);Acc:832352]
1.12	0.000	AT2G01250	AT2G01250	Ribosomal protein L30/L7 family protein [Source:NCBI gene (formerly Entrezgene);Acc:814652]
1.12	0.000	AT5G23860	TUB8	tubulin beta 8 [Source:NCBI gene (formerly Entrezgene);Acc:832451]
1.12	0.000	AT2G36160	AT2G36160	Ribosomal protein S11 family protein [Source:NCBI gene (formerly Entrezgene);Acc:818188]
1.12	0.003	AT5G25230	AT5G25230	Ribosomal protein S5/Elongation factor G/III/V family protein [Source:NCBI gene (formerly Entrezgene);Acc:832594]
1.10	0.000	AT4G17390	AT4G17390	Ribosomal protein L23/L15e family protein [Source:NCBI gene (formerly Entrezgene);Acc:827451]
1.10	0.000	AT4G16720	AT4G16720	Ribosomal protein L23/L15e family protein [Source:NCBI gene (formerly Entrezgene);Acc:827375]

1.10	0.003	AT1G27400	AT1G27400	Ribosomal protein L22p/L17e family protein [Source:NCBI gene (formerly Entrezgene);Acc:839630]
1.08	0.004	AT1G07790	HTB1	Histone superfamily protein [Source:NCBI gene (formerly Entrezgene);Acc:837293]
1.07	0.000	AT5G61170	AT5G61170	Ribosomal protein S19e family protein [Source:NCBI gene (formerly Entrezgene);Acc:836238]
1.06	0.003	ATCG00380	rps4	
1.06	0.005	AT3G45980	HTB9	Histone superfamily protein [Source:NCBI gene (formerly Entrezgene);Acc:823741]
1.06	0.018	AT5G02610	AT5G02610	Ribosomal L29 family protein [Source:NCBI gene (formerly Entrezgene);Acc:831853]
1.05	0.001	AT5G16130	AT5G16130	Ribosomal protein S7e family protein [Source:NCBI gene (formerly Entrezgene);Acc:831470]
1.04	0.001	AT1G07770	RPS15A	ribosomal protein S15A [Source:NCBI gene (formerly Entrezgene);Acc:837291]
1.03	0.002	AT3G13580	AT3G13580	Ribosomal protein L30/L7 family protein [Source:NCBI gene (formerly Entrezgene);Acc:820560]
1.03	0.027	ATCG00750	rps11	
1.03	0.000	AT1G07660	AT1G07660	Histone superfamily protein [Source:NCBI gene (formerly Entrezgene);Acc:837279]
1.02	0.008	AT4G34110	PAB2	poly(A) binding protein 2 [Source:NCBI gene (formerly Entrezgene);Acc:829557]
1.02	0.000	AT5G27850	AT5G27850	Ribosomal protein L18e/L15 superfamily protein [Source:NCBI gene (formerly Entrezgene);Acc:832848]
1.02	0.004	AT1G48630	RACK1B_AT	receptor for activated C kinase 1B [Source:NCBI gene (formerly Entrezgene);Acc:841284]
1.01	0.033	AT3G60245	AT3G60245	Zinc-binding ribosomal protein family protein [Source:NCBI gene (formerly Entrezgene);Acc:825195]
1.00	0.041	AT1G12310	AT1G12310	Calcium-binding EF-hand family protein [Source:NCBI gene (formerly Entrezgene);Acc:837785]

Table S7. List of enriched and depleted proteins in *ccr4a ccr4b* pollen compared to WT pollen in proteomics

A threshold of adjpval < 0.05 was used to select the proteins significantly enriched or depleted in *ccr4a ccr4b* pollen. Proteins are sorted according to the logFC

TAIR ID	LogFC	Adjp_val	Status	Description
AT5G34930	4.115	0.000	Enriched in ccr4	arogenate dehydrogenase
AT5G44990	3.909	0.000	Enriched in ccr4	Glutathione S-transferase family p...
AT1G58250	3.772	0.000	Enriched in ccr4	Golgi-body localisation protein do...
AT1G64610	3.768	0.000	Enriched in ccr4	Transducin/WD40 repeat-like superf...
AT1G13460	3.398	0.000	Enriched in ccr4	Protein phosphatase 2A regulatory ...
AT1G33230	3.375	0.040	Enriched in ccr4	TMPIT-like protein
AT1G32250	3.363	0.000	Enriched in ccr4	Calcium-binding EF-hand family pro...
AT5G25510	3.341	0.000	Enriched in ccr4	Protein phosphatase 2A regulatory ...
AT3G44600	3.275	0.000	Enriched in ccr4	cyclophilin71, Symbols: CYP71
AT1G03680	3.260	0.003	Enriched in ccr4	thioredoxin M-type 1, Symbols: ATH...
AT4G36490	3.194	0.004	Enriched in ccr4	SEC14-like 12, Symbols: ATSFH12, S...
AT4G17420	3.188	0.000	Enriched in ccr4	Tryptophan RNA-binding attenuator ...
AT3G09880	3.163	0.000	Enriched in ccr4	Protein phosphatase 2A regulatory ...
AT4G04970	3.134	0.001	Enriched in ccr4	glucan synthase-like 1, Symbols: A...
AT5G13210	3.095	0.000	Enriched in ccr4	Uncharacterised conserved protein ...
AT3G09560	3.088	0.000	Enriched in ccr4	Lipin family protein
AT4G22530	3.017	0.000	Enriched in ccr4	S-adenosyl-L-methionine-dependent ...
AT3G55005	2.997	0.000	Enriched in ccr4	tonneau 1b (TON1b), Symbols: TON1B
AT3G10670	2.969	0.000	Enriched in ccr4	non-intrinsic ABC protein 7, Symbo...
AT3G16910	2.860	0.000	Enriched in ccr4	acyl-activating enzyme 7, Symbols:...
AT5G43920	2.850	0.023	Enriched in ccr4	transducin family protein / WD-40 ...
AT3G07020	2.839	0.000	Enriched in ccr4	UDP-Glycosyltransferase superfamil...
AT1G22280	2.795	0.035	Enriched in ccr4	phytochrome-associated protein pho...
AT4G35670	2.775	0.000	Enriched in ccr4	Pectin lyase-like superfamily protein
AT5G52240	2.759	0.029	Enriched in ccr4	membrane steroid binding protein 1...
AT5G19280	2.742	0.001	Enriched in ccr4	kinase associated protein phosphat...
AT2G18180	2.699	0.006	Enriched in ccr4	Sec14p-like phosphatidylinositol t...
AT2G36250	2.680	0.000	Enriched in ccr4	Tubulin/FtsZ family protein, Symbo...
AT4G21670	2.678	0.000	Enriched in ccr4	C-terminal domain phosphatase-like...
AT1G05260	2.669	0.000	Enriched in ccr4	Peroxidase superfamily protein, Sy...
AT3G14950	2.649	0.018	Enriched in ccr4	tetratricopetide-repeat thioredoxi...
AT3G27325	2.612	0.000	Enriched in ccr4	hydrolases, acting on ester bonds
AT5G06560	2.578	0.033	Enriched in ccr4	Protein of unknown function, DUF593
AT4G04610	2.515	0.000	Enriched in ccr4	APS reductase 1, Symbols: APR1, AP...
AT1G73920	2.512	0.000	Enriched in ccr4	alpha/beta-Hydrolases superfamily ...
AT4G12060	2.500	0.000	Enriched in ccr4	Double Clp-N motif protein
AT3G21760	2.488	0.002	Enriched in ccr4	UDP-Glycosyltransferase superfamil...
AT3G52460	2.473	0.001	Enriched in ccr4	hydroxyproline-rich glycoprotein f...
AT2G15490	2.468	0.001	Enriched in ccr4	UDP-glycosyltransferase 73B4, Symb...
AT1G13730	2.461	0.000	Enriched in ccr4	Nuclear transport factor 2 (NTF2) ...
AT4G01220	2.455	0.001	Enriched in ccr4	Nucleotide-diphospho-sugar transfe...
AT4G21860	2.363	0.000	Enriched in ccr4	methionine sulfoxide reductase B 2...
AT4G25920	2.355	0.000	Enriched in ccr4	Protein of unknown function (DUF295)
AT4G21990	2.325	0.000	Enriched in ccr4	APS reductase 3, Symbols: APR3, PR...
AT3G08505	2.320	0.000	Enriched in ccr4	zinc finger (CCCH-type/C3HC4-type ...
AT4G17870	2.295	0.000	Enriched in ccr4	Polyketide cyclase/dehydrase and l...
AT5G51980	2.278	0.003	Enriched in ccr4	Transducin/WD40 repeat-like superf...
AT4G03550	2.267	0.000	Enriched in ccr4	glucan synthase-like 5, Symbols: A...
AT3G26020	2.244	0.000	Enriched in ccr4	Protein phosphatase 2A regulatory ...
AT1G14570	2.237	0.020	Enriched in ccr4	UBX domain-containing protein
AT3G08940	2.214	0.009	Enriched in ccr4	light harvesting complex photosyst...
AT1G62600	2.212	0.000	Enriched in ccr4	Flavin-binding monooxygenase famil...
AT3G48820	2.203	0.008	Enriched in ccr4	Glycosyltransferase family 29 (sia...
AT5G19070	2.191	0.000	Enriched in ccr4	SNARE associated Golgi protein family
AT3G30180	2.116	0.000	Enriched in ccr4	brassinosteroid-6-oxidase 2, Symbo...
AT5G01100	2.096	0.000	Enriched in ccr4	O-fucosyltransferase family protein
AT5G51700	2.093	0.000	Enriched in ccr4	protein binding;zinc ion binding, ...
AT1G20270	2.093	0.001	Enriched in ccr4	2-oxoglutarate (2OG) and Fe(II)-de...
AT1G78980	2.088	0.003	Enriched in ccr4	STRUBBELIG-receptor family 5, Symb...
AT1G74310	2.051	0.000	Enriched in ccr4	heat shock protein 101, Symbols: A...
AT1G51540	2.043	0.000	Enriched in ccr4	Galactose oxidase/kelch repeat sup...
AT3G51810	2.015	0.000	Enriched in ccr4	Stress induced protein, Symbols: A...
AT1G33980	1.940	0.000	Enriched in ccr4	Smg-4/UPF3 family protein, Symbols...
AT5G16570	1.933	0.002	Enriched in ccr4	glutamine synthetase 1;4, Symbols:...
AT1G02305	1.917	0.002	Enriched in ccr4	Cysteine proteinases superfamily p...
AT5G09230	1.890	0.004	Enriched in ccr4	sirtuin 2, Symbols: SRT2
AT5G44240	1.880	0.000	Enriched in ccr4	aminophospholipid ATPase 2, Symbol...
AT3G17970	1.878	0.000	Enriched in ccr4	translocon at the outer membrane o...
AT1G56700	1.875	0.026	Enriched in ccr4	Peptidase C15, pyroglutamyl peptid...
AT1G45050	1.866	0.006	Enriched in ccr4	Ubiquitin-conjugating enzyme famil...
AT5G58070	1.858	0.000	Enriched in ccr4	temperature-induced lipocalin, Sym...
AT5G15860	1.853	0.000	Enriched in ccr4	prenylcysteine methylesterase, Sym...
AT3G58990	1.850	0.000	Enriched in ccr4	isopropylmalate isomerase 1, Symbo...
AT1G08510	1.822	0.000	Enriched in ccr4	fatty acyl-ACP thioesterases B, Sy...
AT3G28480	1.815	0.004	Enriched in ccr4	Oxoglutarate/iron-dependent oxygenase
AT3G54930	1.765	0.000	Enriched in ccr4	Protein phosphatase 2A regulatory ...

AT1G27150	1.746	0.000	Enriched in ccr4	Tetratricopeptide repeat (TPR)-lik...
AT3G18220	1.745	0.002	Enriched in ccr4	Phosphatidic acid phosphatase (PAP...
AT1G75030	1.727	0.000	Enriched in ccr4	thaumatin-like protein 3, Symbols:...
AT5G01700	1.726	0.000	Enriched in ccr4	Protein phosphatase 2C family protein
AT1G74800	1.692	0.021	Enriched in ccr4	Galactosyltransferase family protein
AT5G01760	1.670	0.009	Enriched in ccr4	ENTH/VHS/GAT family protein
AT3G06930	1.664	0.021	Enriched in ccr4	protein arginine methyltransferase...
AT2G20800	1.640	0.000	Enriched in ccr4	NAD(P)H dehydrogenase B4, Symbols:...
AT2G15790	1.632	0.000	Enriched in ccr4	peptidyl-prolyl cis-trans isomeras...
AT1G79910	1.628	0.002	Enriched in ccr4	Regulator of Vps4 activity in the ...
AT1G04830	1.621	0.025	Enriched in ccr4	Ypt/Rab-GAP domain of gyp1p superf...
AT5G11950	1.618	0.003	Enriched in ccr4	Putative lysine decarboxylase fami...
AT4G11800	1.604	0.000	Enriched in ccr4	Calcineurin-like metallo-phosphoes...
AT2G45135	1.603	0.000	Enriched in ccr4	RING/U-box superfamily protein
AT2G28470	1.601	0.000	Enriched in ccr4	beta-galactosidase 8, Symbols: BGAL8
AT2G22570	1.594	0.001	Enriched in ccr4	nicotinamidase 1, Symbols: ATNIC1,...
AT2G31500	1.593	0.025	Enriched in ccr4	calcium-dependent protein kinase 2...
AT1G04970	1.574	0.001	Enriched in ccr4	lipid-binding serum glycoprotein f...
AT2G05920	1.571	0.014	Enriched in ccr4	Subtilase family protein
AT1G52400	1.542	0.000	Enriched in ccr4	beta glucosidase 18, Symbols: BGL1...
AT5G51950	1.534	0.000	Enriched in ccr4	Glucose-methanol-choline (GMC) oxi...
AT3G61710	1.527	0.039	Enriched in ccr4	AUTOPHAGY 6, Symbols: ATATG6, ATG6...
AT2G18080	1.509	0.007	Enriched in ccr4	Serine carboxypeptidase S28 family...
AT1G56440	1.509	0.001	Enriched in ccr4	Tetratricopeptide repeat (TPR)-lik...
AT2G32040	1.502	0.000	Enriched in ccr4	Major facilitator superfamily protein
AT5G08280	1.491	0.000	Enriched in ccr4	hydroxymethylbilane synthase, Symb...
AT1G43860	1.469	0.000	Enriched in ccr4	sequence-specific DNA binding tran...
AT3G23830	1.462	0.000	Enriched in ccr4	glycine-rich RNA-binding protein 4...
AT4G21110	1.462	0.000	Enriched in ccr4	G10 family protein
AT1G33360	1.451	0.001	Enriched in ccr4	ATP-dependent Clp protease
AT1G79820	1.449	0.000	Enriched in ccr4	Major facilitator superfamily prot...
AT4G08790	1.448	0.000	Enriched in ccr4	Nitrilase/cyanide hydratase and ap...
AT5G23395	1.442	0.000	Enriched in ccr4	Cox19-like CHCH family protein, Sy...
AT4G02510	1.423	0.049	Enriched in ccr4	translocon at the outer envelope m...
AT5G53310	1.397	0.001	Enriched in ccr4	myosin heavy chain-related
AT1G06250	1.384	0.001	Enriched in ccr4	alpha/beta-Hydrolases superfamily ...
AT5G52520	1.349	0.014	Enriched in ccr4	Class II aaRS and biotin synthetas...
AT1G21065	1.347	0.000	Enriched in ccr4	unknown protein
AT1G26670	1.346	0.015	Enriched in ccr4	Vesicle transport v-SNARE family p...
AT3G13410	1.341	0.003	Enriched in ccr4	unknown protein
AT3G57530	1.338	0.010	Enriched in ccr4	calcium-dependent protein kinase 3...
AT5G07920	1.322	0.001	Enriched in ccr4	diacylglycerol kinase1, Symbols: D...
AT5G13940	1.320	0.000	Enriched in ccr4	aminopeptidases
AT5G48570	1.318	0.000	Enriched in ccr4	FKBP-type peptidyl-prolyl cis-tran...
AT1G06490	1.314	0.000	Enriched in ccr4	glucan synthase-like 7, Symbols: A...
AT4G26830	1.313	0.001	Enriched in ccr4	O-Glycosyl hydrolases family 17 pr...
AT3G57990	1.311	0.010	Enriched in ccr4	unknown protein
AT2G46505	1.307	0.000	Enriched in ccr4	succinate dehydrogenase subunit 4,...
AT1G61520	1.293	0.018	Enriched in ccr4	photosystem I light harvesting com...
AT5G55960	1.283	0.002	Enriched in ccr4	unknown protein
AT1G08040	1.279	0.001	Enriched in ccr4	Protein of unknown function (DUF707)
AT3G01040	1.274	0.015	Enriched in ccr4	galacturonosyltransferase 13, Symb...
AT3G19390	1.268	0.000	Enriched in ccr4	Granulin repeat cysteine protease ...
AT5G13300	1.262	0.001	Enriched in ccr4	ARF GTPase-activating protein, Sym...
AT5G62390	1.260	0.000	Enriched in ccr4	BCL-2-associated athanogene 7, Sym...
AT5G54550	1.259	0.012	Enriched in ccr4	Protein of unknown function (DUF295)
AT2G37220	1.257	0.000	Enriched in ccr4	RNA-binding (RRM/RBD/RNP motifs) f...
AT4G14790	1.256	0.001	Enriched in ccr4	ATP-dependent RNA helicase, mitoch...
AT3G54690	1.255	0.000	Enriched in ccr4	Sugar isomerase (SIS) family protein
AT3G09830	1.251	0.031	Enriched in ccr4	Protein kinase superfamily protein
AT5G62980	1.248	0.000	Enriched in ccr4	Dihydroneopterin aldolase, Symbols...
AT3G52390	1.246	0.002	Enriched in ccr4	TatD related DNase
AT3G11780	1.238	0.035	Enriched in ccr4	MD-2-related lipid recognition dom...
AT5G44860	1.232	0.004	Enriched in ccr4	unknown protein
AT3G02875	1.225	0.000	Enriched in ccr4	Peptidase M20/M25/M40 family prote...
AT2G33380	1.224	0.030	Enriched in ccr4	Caleosin-related family protein, S...
AT3G59140	1.213	0.032	Enriched in ccr4	multidrug resistance-associated pr...
AT5G47620	1.211	0.001	Enriched in ccr4	RNA-binding (RRM/RBD/RNP motifs) f...
AT1G68100	1.209	0.000	Enriched in ccr4	ZIP metal ion transporter family, ...
AT4G26260	1.186	0.001	Enriched in ccr4	myo-inositol oxygenase 4, Symbols:...
AT3G18070	1.185	0.000	Enriched in ccr4	beta glucosidase 43, Symbols: BGLU43
AT1G04510	1.183	0.005	Enriched in ccr4	MOS4-associated complex 3A, Symbo...
AT1G29890	1.176	0.031	Enriched in ccr4	O-acetyltransferase family protein
AT3G15690	1.175	0.010	Enriched in ccr4	Single hybrid motif superfamily pr...
AT2G27490	1.167	0.005	Enriched in ccr4	dephospho-CoA kinase family, Symbo...
AT1G13170	1.166	0.000	Enriched in ccr4	OSBP(oxysterol binding protein)-re...
AT3G57340	1.156	0.024	Enriched in ccr4	Heat shock protein DnaJ, N-termina...
AT4G23920	1.154	0.013	Enriched in ccr4	UDP-D-glucose/UDP-D-ga...
AT4G38710	1.145	0.007	Enriched in ccr4	glycine-rich protein
AT2G29620	1.141	0.033	Enriched in ccr4	unknown protein
AT3G09890	1.140	0.000	Enriched in ccr4	Ankyrin repeat family protein
AT3G23380	1.136	0.019	Enriched in ccr4	ROP-interactive CRIB motif-contain...
AT5G63870	1.136	0.000	Enriched in ccr4	serine/threonine phosphatase 7, Sy...
AT4G28680	1.135	0.001	Enriched in ccr4	L-tyrosine decarboxylase, Symbols:...
AT3G18750	1.133	0.004	Enriched in ccr4	with no lysine (K) kinase 6, Symbo...
AT1G71840	1.133	0.009	Enriched in ccr4	transducin family protein / WD-40 ...
AT3G52950	1.132	0.001	Enriched in ccr4	CBS / octicosapeptide/Phox/Bemp1 (...

AT1G16570	1.130	0.037	Enriched in ccr4	UDP-Glycosyltransferase superfamil...
AT1G61250	1.127	0.000	Enriched in ccr4	secretory carrier 3, Symbols: SC3
AT4G13850	1.122	0.026	Enriched in ccr4	glycine-rich RNA-binding protein 2...
AT4G34380	1.108	0.005	Enriched in ccr4	Transducin/WD40 repeat-like superf...
AT4G01690	1.104	0.005	Enriched in ccr4	Flavin containing amine oxidoreduc...
AT1G62960	1.098	0.000	Enriched in ccr4	ACC synthase 10, Symbols: ACS10
AT1G75040	1.094	0.001	Enriched in ccr4	pathogenesis-related gene 5, Symbo...
AT1G47750	1.092	0.000	Enriched in ccr4	peroxin 11A, Symbols: PEX11A
AT4G17010	1.087	0.035	Enriched in ccr4	unknown protein
AT1G67540	1.083	0.000	Enriched in ccr4	unknown protein
AT5G11420	1.074	0.047	Enriched in ccr4	Protein of unknown function, DUF642
AT3G58310	1.070	0.003	Enriched in ccr4	Domain of unknown function (DUF26)
AT1G12570	1.067	0.008	Enriched in ccr4	Glucose-methanol-choline (GMC) oxi...
AT1G05360	1.057	0.001	Enriched in ccr4	unknown protein
AT5G14220	1.053	0.001	Enriched in ccr4	Flavin containing amine oxidoreduc...
AT2G45000	1.029	0.001	Enriched in ccr4	structural constituent of nuclear ...
AT5G46850	1.028	0.001	Enriched in ccr4	unknown protein
AT2G31710	1.025	0.050	Enriched in ccr4	Vacuolar ATPase assembly integral ...
AT3G07820	1.015	0.023	Enriched in ccr4	Pectin lyase-like superfamily protein
AT5G11700	1.014	0.017	Enriched in ccr4	unknown protein
AT4G08630	1.012	0.007	Enriched in ccr4	unknown protein
AT2G29700	1.009	0.036	Enriched in ccr4	pleckstrin homologue 1, Symbols: A...
AT3G13530	1.009	0.000	Enriched in ccr4	mitogen-activated protein kinase k...
AT3G06540	1.006	0.000	Enriched in ccr4	Rab escort protein, Symbols: REP, ...
AT3G10860	1.005	0.005	Enriched in ccr4	Cytochrome b-c1 complex, subunit 8...
AT3G18940	0.988	0.000	Enriched in ccr4	clast3-related
AT5G44250	0.986	0.041	Enriched in ccr4	Protein of unknown function DUF829...
AT1G76405	0.977	0.004	Enriched in ccr4	unknown protein
AT5G59140	0.971	0.027	Enriched in ccr4	BTB/POZ domain-containing protein
AT4G33530	0.970	0.021	Enriched in ccr4	K+ uptake permease 5, Symbols: KUP5
AT1G62730	0.968	0.000	Enriched in ccr4	Terpenoid synthases superfamily pr...
AT1G55900	0.965	0.002	Enriched in ccr4	Haloacid dehalogenase-like hydrola...
AT3G45770	0.962	0.000	Enriched in ccr4	Polyketide synthase, enoylreductas...
AT3G56090	0.961	0.001	Enriched in ccr4	ferritin 3, Symbols: ATFER3, FER3
AT2G31432	0.955	0.001	Enriched in ccr4	Plant invertase/pectin methylester...
AT2G32410	0.953	0.005	Enriched in ccr4	AXR1-like, Symbols: AXL
AT5G42660	0.951	0.007	Enriched in ccr4	Protein of unknown function (DUF616)
AT5G51200	0.950	0.024	Enriched in ccr4	Protein of unknown function (DUF3414)
AT5G54010	0.950	0.000	Enriched in ccr4	UDP-Glycosyltransferase superfamil...
AT3G13490	0.948	0.032	Enriched in ccr4	Lysyl-tRNA synthetase, class II, S...
AT4G15410	0.948	0.016	Enriched in ccr4	serine/threonine protein phosphata...
AT3G23540	0.939	0.005	Enriched in ccr4	alpha/beta-Hydrolases superfamily ...
AT1G05430	0.938	0.005	Enriched in ccr4	unknown protein
AT2G32900	0.936	0.036	Enriched in ccr4	centromere/kinetochore protein, pu...
AT2G31800	0.931	0.016	Enriched in ccr4	Integrin-linked protein kinase family
AT5G37600	0.923	0.014	Enriched in ccr4	glutamine synthase clone R1, Symbo...
AT5G11100	0.922	0.000	Enriched in ccr4	Calcium-dependent lipid-binding (C...
AT4G32720	0.919	0.014	Enriched in ccr4	La protein 1, Symbols: AtLa1, La1
AT2G35040	0.919	0.002	Enriched in ccr4	AICARFT/IMPCHase bienzyme family p...
AT4G23000	0.914	0.007	Enriched in ccr4	Calcineurin-like metallo-phosphoes...
AT4G04180	0.908	0.000	Enriched in ccr4	P-loop containing nucleoside triph...
AT1G28510	0.905	0.024	Enriched in ccr4	Optic atrophy 3 protein (OPA3)
AT3G22980	0.902	0.011	Enriched in ccr4	Ribosomal protein S5/Elongation fa...
AT5G45900	0.895	0.001	Enriched in ccr4	ThiF family protein, Symbols: APG7...
AT2G18790	0.895	0.031	Enriched in ccr4	phytochrome B, Symbols: PHYB, HY3,...
AT1G30000	0.893	0.000	Enriched in ccr4	alpha-mannosidase 3, Symbols: MNS3
AT1G25380	0.892	0.003	Enriched in ccr4	NAD+ transporter 2, Symbols: ATNDT...
AT4G00290	0.888	0.000	Enriched in ccr4	Mechanosensitive ion channel protein
AT4G17650	0.886	0.002	Enriched in ccr4	Polyketide cyclase / dehydrase and...
AT5G41390	0.883	0.006	Enriched in ccr4	PLAC8 family protein
AT2G36660	0.882	0.046	Enriched in ccr4	poly(A) binding protein 7, Symbols...
AT1G06970	0.881	0.013	Enriched in ccr4	cation/hydrogen exchanger 14, Symb...
AT3G01020	0.876	0.008	Enriched in ccr4	ISCU-like 2, Symbols: ISU2, ATISU2
AT2G44525	0.874	0.000	Enriched in ccr4	Protein of unknown function (DUF49...
AT4G00090	0.869	0.001	Enriched in ccr4	Transducin/WD40 repeat-like superf...
AT4G30260	0.868	0.031	Enriched in ccr4	Integral membrane Yip1 family protein
AT1G70540	0.864	0.000	Enriched in ccr4	Plant invertase/pectin methylester...
AT1G10740	0.859	0.050	Enriched in ccr4	alpha/beta-Hydrolases superfamily ...
AT4G17720	0.852	0.001	Enriched in ccr4	RNA-binding (RRM/RBD/RNP motifs) f...
AT5G38820	0.842	0.009	Enriched in ccr4	Transmembrane amino acid transport...
AT4G22540	0.839	0.001	Enriched in ccr4	OSBP(oxysterol binding protein)-re...
AT1G09830	0.833	0.001	Enriched in ccr4	Glycinamide ribonucleotide (GAR) s...
AT3G29160	0.830	0.003	Enriched in ccr4	SNF1 kinase homolog 11, Symbols: A...
AT4G11740	0.828	0.007	Enriched in ccr4	Ubiquitin-like superfamily protein...
AT3G01311	0.825	0.012	Enriched in ccr4	Protein of unknown function (DUF569)
AT4G38220	0.822	0.000	Enriched in ccr4	Peptidase M20/M25/M40 family protein
AT3G18860	0.815	0.007	Enriched in ccr4	transducin family protein / WD-40 ...
AT5G06970	0.809	0.049	Enriched in ccr4	Protein of unknown function (DUF810)
AT2G44530	0.806	0.000	Enriched in ccr4	Phosphoribosyltransferase family p...
AT5G19360	0.804	0.000	Enriched in ccr4	calcium-dependent protein kinase 3...
AT3G21865	0.804	0.006	Enriched in ccr4	peroxin 22, Symbols: PEX22
AT5G50840	0.797	0.003	Enriched in ccr4	unknown protein
AT5G12180	0.797	0.000	Enriched in ccr4	calcium-dependent protein kinase 1...
AT5G53120	0.797	0.005	Enriched in ccr4	spermidine synthase 3, Symbols: SPDS3
AT1G31860	0.796	0.004	Enriched in ccr4	histidine biosynthesis bifunctiona...
AT5G66150	0.793	0.004	Enriched in ccr4	Glycosyl hydrolase family 38 protein
AT2G46320	0.790	0.021	Enriched in ccr4	Mitochondrial substrate carrier fa...

AT1G80680	0.786	0.028	Enriched in ccr4	SUPPRESSOR OF AUXIN RESISTANCE 3, ...
AT1G73930	0.786	0.000	Enriched in ccr4	unknown protein
AT3G56320	0.784	0.016	Enriched in ccr4	PAP/OAS1 substrate-binding domain ...
AT2G17010	0.781	0.002	Enriched in ccr4	Mechanosensitive ion channel famil...
AT3G21160	0.779	0.008	Enriched in ccr4	alpha-mannosidase 2, Symbols: MNS2...
AT2G27900	0.778	0.001	Enriched in ccr4	unknown protein
AT3G07690	0.774	0.008	Enriched in ccr4	6-phosphogluconate dehydrogenase f...
AT2G14110	0.773	0.043	Enriched in ccr4	Haloacid dehalogenase-like hydrola...
AT2G36630	0.772	0.005	Enriched in ccr4	Sulfite exporter TauE/SafE family ...
AT4G17260	0.771	0.000	Enriched in ccr4	Lactate/malate dehydrogenase famil...
AT5G63030	0.766	0.004	Enriched in ccr4	Thioredoxin superfamily protein
AT4G24680	0.761	0.044	Enriched in ccr4	modifier of snc1, Symbols: MOS1
AT1G04850	0.758	0.000	Enriched in ccr4	ubiquitin-associated (UBA)/TS-N do...
AT3G08780	0.758	0.001	Enriched in ccr4	unknown protein
AT2G38010	0.756	0.001	Enriched in ccr4	Neutral/alkaline non-lysosomal cer...
AT3G03980	0.753	0.025	Enriched in ccr4	NAD(P)-binding Rossmann-fold super...
AT4G34180	0.753	0.029	Enriched in ccr4	Cyclase family protein
AT3G54360	0.752	0.027	Enriched in ccr4	zinc ion binding
AT4G11790	0.746	0.001	Enriched in ccr4	Pleckstrin homology (PH) domain su...
AT3G62940	0.742	0.003	Enriched in ccr4	Cysteine proteinases superfamily p...
AT2G33670	0.740	0.012	Enriched in ccr4	Seven transmembrane MLO family pro...
AT4G38350	0.734	0.024	Enriched in ccr4	Patched family protein
AT3G18490	0.733	0.013	Enriched in ccr4	Eukaryotic aspartyl protease famil...
AT1G05730	0.726	0.023	Enriched in ccr4	Eukaryotic protein of unknown func...
AT2G39080	0.722	0.013	Enriched in ccr4	NAD(P)-binding Rossmann-fold super...
AT3G11740	0.719	0.000	Enriched in ccr4	Protein of unknown function (DUF567)
AT1G55560	0.708	0.042	Enriched in ccr4	SKU5 similar 14, Symbols: sks14
AT1G80500	0.706	0.029	Enriched in ccr4	SNARE-like superfamily protein
AT5G42340	0.704	0.000	Enriched in ccr4	Plant U-Box 15, Symbols: PUB15
AT4G36690	0.703	0.006	Enriched in ccr4	U2 snRNP auxilliary factor, large ...
AT3G21800	0.697	0.002	Enriched in ccr4	UDP-glucosyl transferase 71B8, Sym...
AT1G21480	0.696	0.001	Enriched in ccr4	Exostosin family protein
AT3G07120	0.692	0.004	Enriched in ccr4	RING/U-box superfamily protein
AT3G66654	0.690	0.002	Enriched in ccr4	Cyclophilin-like peptidyl-prolyl c...
AT1G48320	0.686	0.018	Enriched in ccr4	Thioesterase superfamily protein
AT2G47390	0.683	0.003	Enriched in ccr4	Prolyl oligopeptidase family protein
AT1G79470	0.682	0.003	Enriched in ccr4	Aldolase-type TIM barrel family pr...
AT2G38910	0.679	0.008	Enriched in ccr4	calcium-dependent protein kinase 2...
AT2G43945	0.673	0.018	Enriched in ccr4	unknown protein
AT2G38960	0.669	0.003	Enriched in ccr4	endoplasmic reticulum oxidoreducti...
AT2G40316	0.668	0.039	Enriched in ccr4	unknown protein
AT2G04750	0.661	0.035	Enriched in ccr4	Actin binding Calponin homology (C...
AT5G04710	0.660	0.048	Enriched in ccr4	Zn-dependent exopeptidases superfa...
AT5G50100	0.659	0.000	Enriched in ccr4	Putative thiol-disulphide oxidored...
AT5G02770	0.651	0.027	Enriched in ccr4	unknown protein
AT1G12070	0.651	0.006	Enriched in ccr4	Immunoglobulin E-set superfamily p...
AT3G18270	0.648	0.033	Enriched in ccr4	cytochrome P450, family 77, subfam...
AT4G04360	0.645	0.003	Enriched in ccr4	Protein of unknown function (DUF1068)
AT4G34860	0.643	0.002	Enriched in ccr4	Plant neutral invertase family pro...
AT4G03620	0.643	0.002	Enriched in ccr4	myosin heavy chain-related
AT5G58700	0.643	0.001	Enriched in ccr4	phosphatidylinositol-speciwc phosp...
AT1G03330	0.642	0.006	Enriched in ccr4	Small nuclear ribonucleoprotein fa...
AT4G01070	0.640	0.001	Enriched in ccr4	UDP-Glycosyltransferase superfamil...
AT3G22650	0.640	0.003	Enriched in ccr4	F-box and associated interaction d...
AT2G03820	0.630	0.000	Enriched in ccr4	nonsense-mediated mRNA decay NMD3 ...
AT1G05820	0.630	0.028	Enriched in ccr4	SIGNAL PEPTIDE PEPTIDASE-LIKE 5, S...
AT3G27350	0.629	0.017	Enriched in ccr4	unknown protein
AT2G31060	0.625	0.033	Enriched in ccr4	elongation factor family protein
AT1G07040	0.624	0.011	Enriched in ccr4	unknown protein
AT5G60600	0.623	0.027	Enriched in ccr4	4-hydroxy-3-methylbut-2-enyl dipho...
AT1G10620	0.619	0.006	Enriched in ccr4	Protein kinase superfamily protein
AT3G02600	0.619	0.005	Enriched in ccr4	lipid phosphate phosphatase 3, Sym...
AT2G20470	0.618	0.002	Enriched in ccr4	AGC (cAMP-dependent, cGMP-dependen...
AT2G33240	0.618	0.001	Enriched in ccr4	myosin XI D, Symbols: XID, ATXID
AT1G07850	0.617	0.007	Enriched in ccr4	Protein of unknown function (DUF604)
AT5G08200	0.617	0.008	Enriched in ccr4	peptidoglycan-binding LysM domain-...
AT5G20350	0.617	0.000	Enriched in ccr4	Ankyrin repeat family protein with...
AT1G51160	0.617	0.001	Enriched in ccr4	SNARE-like superfamily protein
AT4G28700	0.615	0.001	Enriched in ccr4	ammonium transporter 1;4, Symbols:...
AT4G27780	0.614	0.001	Enriched in ccr4	acyl-CoA binding protein 2, Symbol...
AT4G19860	0.612	0.001	Enriched in ccr4	alpha/beta-Hydrolases superfamily ...
AT1G19450	0.611	0.003	Enriched in ccr4	Major facilitator superfamily protein
AT5G18480	0.610	0.050	Enriched in ccr4	plant glycogenin-like starch initi...
AT5G41780	0.610	0.001	Enriched in ccr4	myosin heavy chain-related
AT2G37020	0.609	0.001	Enriched in ccr4	Translin family protein
AT3G52810	0.606	0.007	Enriched in ccr4	purple acid phosphatase 21, Symbol...
AT1G22170	0.602	0.018	Enriched in ccr4	Phosphoglycerate mutase family pro...
AT3G07320	0.600	0.008	Enriched in ccr4	O-Glycosyl hydrolases family 17 pr...
AT1G47640	0.598	0.003	Enriched in ccr4	unknown protein
AT3G28490	0.596	0.005	Enriched in ccr4	Oxoglutarate/iron-dependent oxygenase
AT4G28090	0.596	0.041	Enriched in ccr4	SKU5 similar 10, Symbols: sks10
AT1G80510	0.595	0.003	Enriched in ccr4	Transmembrane amino acid transport...
AT5G18340	0.593	0.027	Enriched in ccr4	ARM repeat superfamily protein
AT1G75660	0.592	0.042	Enriched in ccr4	5'-3' exoribonuclease 3, Symbols: ...
AT4G08870	0.590	0.003	Enriched in ccr4	Arginase/deacetylase superfamily p...
AT3G45810	0.589	0.001	Enriched in ccr4	ferric reductase-like transmembran...
AT1G76060	0.581	0.027	Enriched in ccr4	LYR family of Fe/S cluster biogene...

AT1G22510	0.575	0.048	Enriched in ccr4	RING/U-box protein with domain of ...
AT1G78460	0.570	0.004	Enriched in ccr4	SOUL heme-binding family protein
AT4G20410	0.564	0.004	Enriched in ccr4	gamma-soluble NSF attachment prote...
AT1G17190	0.562	0.004	Enriched in ccr4	glutathione S-transferase tau 26, ...
AT2G20990	0.561	0.041	Enriched in ccr4	synaptotagmin A, Symbols: SYTA
AT4G05160	0.558	0.000	Enriched in ccr4	AMP-dependent synthetase and ligas...
AT1G01920	0.557	0.031	Enriched in ccr4	SET domain-containing protein
AT2G05170	0.556	0.001	Enriched in ccr4	vacuolar protein sorting 11, Symbo...
AT1G30270	0.555	0.034	Enriched in ccr4	CBL-interacting protein kinase 23,...
AT1G23240	0.555	0.013	Enriched in ccr4	Caleosin-related family protein
AT5G55060	0.555	0.047	Enriched in ccr4	unknown protein
AT3G10460	0.552	0.001	Enriched in ccr4	Plant self-incompatibility protein...
AT5G58160	0.551	0.016	Enriched in ccr4	actin binding
AT2G26830	0.551	0.014	Enriched in ccr4	Protein kinase superfamily protein...
AT4G11850	0.551	0.046	Enriched in ccr4	phospholipase D gamma 1, Symbols: ...
AT2G25050	0.550	0.002	Enriched in ccr4	Actin-binding FH2 (Formin Homology...
AT1G61860	0.548	0.041	Enriched in ccr4	Protein kinase superfamily protein
AT2G22450	0.546	0.013	Enriched in ccr4	riboflavin biosynthesis protein, p...
AT1G27500	0.545	0.043	Enriched in ccr4	Tetratricopeptide repeat (TPR)-lik...
AT1G79260	0.541	0.009	Enriched in ccr4	unknown protein
AT4G30060	0.539	0.014	Enriched in ccr4	Core-2/I-branching beta-1,6-N-acet...
AT3G04080	0.538	0.005	Enriched in ccr4	apyrase 1, Symbols: ATAPY1, APY1
AT3G48010	0.538	0.003	Enriched in ccr4	cyclic nucleotide-gated channel 16...
AT1G60740	0.534	0.015	Enriched in ccr4	Thioredoxin superfamily protein
AT5G13120	0.534	0.001	Enriched in ccr4	cyclophilin 20-2, Symbols: ATCYP20...
AT1G56560	0.533	0.001	Enriched in ccr4	Plant neutral invertase family pro...
AT5G57810	0.532	0.003	Enriched in ccr4	tetraspanin15, Symbols: TET15
AT5G65090	0.529	0.006	Enriched in ccr4	DNAse I-like superfamily protein, ...
AT4G34940	0.523	0.012	Enriched in ccr4	armadillo repeat only 1, Symbols: ...
AT5G66530	0.523	0.004	Enriched in ccr4	Galactose mutarotase-like superfam...
AT4G15093	0.521	0.002	Enriched in ccr4	catalytic LigB subunit of aromatic...
AT5G46930	0.521	0.013	Enriched in ccr4	Plant invertase/pectin methylester...
AT5G25980	0.521	0.015	Enriched in ccr4	glucoside glucohydrolase 2, Symbol...
AT1G04810	0.520	0.001	Enriched in ccr4	26S proteasome regulatory complex,...
AT1G32170	0.519	0.001	Enriched in ccr4	xyloglucan endotransglucosylase/hy...
AT4G02120	0.519	0.034	Enriched in ccr4	CTP synthase family protein
AT3G27000	0.519	0.013	Enriched in ccr4	actin related protein 2, Symbols: ...
AT5G23050	0.518	0.002	Enriched in ccr4	acyl-activating enzyme 17, Symbols...
AT3G61560	0.517	0.008	Enriched in ccr4	Reticulon family protein
AT5G51100	0.516	0.029	Enriched in ccr4	Fe superoxide dismutase 2, Symbols...
AT2G16430	0.513	0.002	Enriched in ccr4	purple acid phosphatase 10, Symbol...
AT5G08470	0.513	0.004	Enriched in ccr4	peroxisome 1, Symbols: PEX1
AT2G01690	0.509	0.028	Enriched in ccr4	ARM repeat superfamily protein
AT1G74380	0.509	0.013	Enriched in ccr4	xyloglucan xylosyltransferase 5, S...
AT4G10710	0.508	0.035	Enriched in ccr4	global transcription factor C, Sym...
AT5G60660	0.504	0.006	Enriched in ccr4	plasma membrane intrinsic protein ...
AT3G51390	0.504	0.014	Enriched in ccr4	DHHC-type zinc finger family protein
AT3G56070	0.501	0.001	Enriched in ccr4	rotamase cyclophilin 2, Symbols: ROC2
AT4G02370	0.501	0.012	Enriched in ccr4	Protein of unknown function, DUF538
AT1G12470	0.497	0.004	Enriched in ccr4	zinc ion binding
AT1G04450	0.496	0.007	Enriched in ccr4	ROP-interactive CRIB motif-contain...
AT3G24160	0.496	0.003	Enriched in ccr4	putative type 1 membrane protein, ...
AT3G07960	0.495	0.002	Enriched in ccr4	Phosphatidylinositol-4-phosphate 5...
AT5G62250	0.495	0.040	Enriched in ccr4	microtubule-associated protein 65-...
AT5G24810	0.493	0.017	Enriched in ccr4	ABC1 family protein
AT5G61970	0.491	0.001	Enriched in ccr4	signal recognition particle-relate...
AT1G19940	0.488	0.004	Enriched in ccr4	glycosyl hydrolase 9B5, Symbols: A...
AT2G04700	0.487	0.018	Enriched in ccr4	ferredoxin thioredoxin reductase c...
AT1G09850	0.486	0.004	Enriched in ccr4	xylem bark cysteine peptidase 3, S...
AT4G18990	0.486	0.021	Enriched in ccr4	xyloglucan endotransglucosylase/hy...
AT3G10360	0.486	0.003	Enriched in ccr4	pumilio 4, Symbols: APUM4, PUM4
AT3G24715	0.483	0.038	Enriched in ccr4	Protein kinase superfamily protein...
AT5G27660	0.482	0.014	Enriched in ccr4	Trypsin family protein with PDZ do...
AT5G35620	0.482	0.005	Enriched in ccr4	Eukaryotic initiation factor 4E pr...
AT5G55630	0.481	0.003	Enriched in ccr4	Outward rectifying potassium chann...
AT5G13980	0.480	0.046	Enriched in ccr4	Glycosyl hydrolase family 38 protein
AT1G50610	0.478	0.005	Enriched in ccr4	Leucine-rich repeat protein kinase...
AT3G55400	0.477	0.002	Enriched in ccr4	methionyl-tRNA synthetase / methio...
AT4G25840	0.477	0.046	Enriched in ccr4	glycerol-3-phosphatase 1, Symbols:...
AT5G16500	0.476	0.006	Enriched in ccr4	Protein kinase superfamily protein
AT3G58170	0.472	0.006	Enriched in ccr4	BET1P/SFT1P-like protein 14A, Symb...
AT1G53345	0.470	0.012	Enriched in ccr4	unknown protein
AT3G07980	0.469	0.002	Enriched in ccr4	mitogen-activated protein kinase k...
AT4G40100	0.467	0.014	Enriched in ccr4	GRAM domain family protein
AT4G31770	0.467	0.016	Enriched in ccr4	debranching enzyme 1, Symbols: ATD...
AT3G59820	0.465	0.021	Enriched in ccr4	LETM1-like protein
AT4G36020	0.464	0.005	Enriched in ccr4	cold shock domain protein 1, Symbo...
AT3G10540	0.462	0.006	Enriched in ccr4	3-phosphoinositide-dependent prote...
AT5G55470	0.460	0.021	Enriched in ccr4	Na+/H+ (sodium hydrogen) exchanger...
AT1G06780	0.457	0.028	Enriched in ccr4	galacturonosyltransferase 6, Symbo...
AT2G45440	0.453	0.023	Enriched in ccr4	dihydrodipicolinate synthase, Symb...
AT5G62850	0.453	0.006	Enriched in ccr4	Nodulin MtN3 family protein, Symbo...
AT3G25050	0.450	0.005	Enriched in ccr4	xyloglucan endotransglucosylase/hy...
AT2G17340	0.450	0.006	Enriched in ccr4	Uncharacterised conserved protein ...
AT1G04200	0.450	0.013	Enriched in ccr4	unknown protein
AT4G15980	0.447	0.006	Enriched in ccr4	Plant invertase/pectin methylester...
AT5G17190	0.447	0.002	Enriched in ccr4	unknown protein

AT5G23670	0.444	0.016	Enriched in ccr4	long chain base2, Symbols: LCB2
AT5G43680	0.444	0.022	Enriched in ccr4	unknown protein
AT4G34660	0.443	0.036	Enriched in ccr4	SH3 domain-containing protein
AT3G05820	0.439	0.002	Enriched in ccr4	invertase H, Symbols: INVH, At-A/N...
AT2G02500	0.438	0.018	Enriched in ccr4	Nucleotide-diphospho-sugar transfe...
AT4G35700	0.433	0.011	Enriched in ccr4	zinc finger (C2H2 type) family pro...
AT4G19640	0.432	0.002	Enriched in ccr4	Ras-related small GTP-binding fami...
AT5G56360	0.430	0.033	Enriched in ccr4	calmodulin-binding protein, Symbol...
AT2G38020	0.430	0.022	Enriched in ccr4	vacuoleless1 (VCL1), Symbols: VCL1...
AT5G08170	0.426	0.010	Enriched in ccr4	porphyromonas-type peptidyl-argini...
AT5G39050	0.426	0.032	Enriched in ccr4	HXXXD-type acyl-transferase family...
AT5G50950	0.422	0.008	Enriched in ccr4	FUMARASE 2, Symbols: FUM2
AT2G46300	0.421	0.018	Enriched in ccr4	Late embryogenesis abundant (LEA) ...
AT1G57600	0.416	0.012	Enriched in ccr4	MBOAT (membrane bound O-acyl trans...
AT4G29530	0.416	0.036	Enriched in ccr4	Pyridoxal phosphate phosphatase-re...
AT2G16130	0.413	0.044	Enriched in ccr4	polyol/monosaccharide transporter ...
AT5G47010	0.413	0.039	Enriched in ccr4	RNA helicase, putative, Symbols: U...
AT2G10970	0.412	0.007	Enriched in ccr4	Plant invertase/pectin methylester...
AT4G11220	0.412	0.035	Enriched in ccr4	VIRB2-interacting protein 2, Symbo...
AT3G08710	0.411	0.018	Enriched in ccr4	thioredoxin H-type 9, Symbols: ATH...
AT3G49490	0.409	0.008	Enriched in ccr4	unknown protein
AT3G52570	0.409	0.032	Enriched in ccr4	alpha/beta-Hydrolases superfamily ...
AT3G42880	0.408	0.030	Enriched in ccr4	Leucine-rich repeat protein kinase...
AT5G14105	0.407	0.010	Enriched in ccr4	unknown protein
AT3G60880	0.407	0.009	Enriched in ccr4	dihydrodipicolinate synthase 1, Sy...
AT2G41970	0.407	0.003	Enriched in ccr4	Protein kinase superfamily protein
AT5G61980	0.406	0.003	Enriched in ccr4	ARF-GAP domain 1, Symbols: AGD1
AT5G45130	0.402	0.048	Enriched in ccr4	RAB homolog 1, Symbols: ATRAB5A, A...
AT3G10650	0.401	0.042	Enriched in ccr4	unknown protein
AT5G39310	0.400	0.007	Enriched in ccr4	expansin A24, Symbols: ATEXPA24, E...
AT1G50140	0.399	0.043	Enriched in ccr4	P-loop containing nucleoside triph...
AT3G62110	0.398	0.010	Enriched in ccr4	Pectin lyase-like superfamily protein
AT5G53140	0.396	0.018	Enriched in ccr4	Protein phosphatase 2C family protein
AT3G25290	0.396	0.038	Enriched in ccr4	Auxin-responsive family protein
AT5G40480	0.393	0.019	Enriched in ccr4	embryo defective 3012, Symbols: EM...
AT3G62530	0.392	0.034	Enriched in ccr4	ARM repeat superfamily protein
AT4G23460	0.391	0.016	Enriched in ccr4	Adaptin family protein
AT1G56050	0.391	0.004	Enriched in ccr4	GTP-binding protein-related
AT2G15570	0.390	0.047	Enriched in ccr4	Thioredoxin superfamily protein, S...
AT4G37880	0.390	0.046	Enriched in ccr4	LisH/CRA/RING-U-box domains-contai...
AT1G21380	0.388	0.023	Enriched in ccr4	Target of Myb protein 1
AT2G05260	0.384	0.018	Enriched in ccr4	alpha/beta-Hydrolases superfamily ...
AT3G10410	0.383	0.008	Enriched in ccr4	SERINE CARBOXYPEPTIDASE-LIKE 49, S...
AT5G18320	0.382	0.019	Enriched in ccr4	ARM repeat superfamily protein
AT1G64430	0.375	0.023	Enriched in ccr4	Pentatricopeptide repeat (PPR) sup...
AT5G49900	0.373	0.003	Enriched in ccr4	Beta-glucosidase, GBA2 type family...
AT3G26370	0.372	0.033	Enriched in ccr4	O-fucosyltransferase family protein
AT5G64270	0.370	0.008	Enriched in ccr4	splicing factor, putative
AT5G45420	0.369	0.036	Enriched in ccr4	Duplicated homeodomain-like superf...
AT3G49470	0.368	0.030	Enriched in ccr4	nascent polypeptide-associated com...
AT3G51300	0.367	0.016	Enriched in ccr4	RHO-related protein from plants 1,...
AT4G17690	0.367	0.008	Enriched in ccr4	Peroxidase superfamily protein
AT2G19080	0.366	0.011	Enriched in ccr4	metaxin-related
AT2G45710	0.364	0.009	Enriched in ccr4	Zinc-binding ribosomal protein fam...
AT1G64110	0.361	0.035	Enriched in ccr4	P-loop containing nucleoside triph...
AT5G65720	0.361	0.028	Enriched in ccr4	nitrogen fixation S (NIFS)-like 1,...
AT2G41500	0.361	0.028	Enriched in ccr4	WD-40 repeat family protein / smal...
AT1G02090	0.361	0.021	Enriched in ccr4	Proteasome component (PCI) domain ...
AT2G30290	0.360	0.007	Enriched in ccr4	VACUOLAR SORTING RECEPTOR 2, Symbo...
AT2G23370	0.360	0.009	Enriched in ccr4	unknown protein
AT2G35490	0.360	0.040	Enriched in ccr4	Plastid-lipid associated protein P...
AT2G29690	0.360	0.035	Enriched in ccr4	anthranilate synthase 2, Symbols: ...
AT4G29260	0.358	0.021	Enriched in ccr4	HAD superfamily, subfamily IIIB ac...
AT4G23420	0.357	0.005	Enriched in ccr4	NAD(P)-binding Rossmann-fold super...
AT1G76400	0.353	0.030	Enriched in ccr4	Ribophorin I
AT5G11670	0.352	0.020	Enriched in ccr4	NADP-malic enzyme 2, Symbols: ATNA...
AT3G61230	0.350	0.016	Enriched in ccr4	GATA type zinc finger transcriptio...
AT2G17290	0.347	0.015	Enriched in ccr4	Calcium-dependent protein kinase f...
AT2G17720	0.346	0.026	Enriched in ccr4	2-oxoglutarate (2OG) and Fe(II)-de...
AT5G20690	0.346	0.033	Enriched in ccr4	Leucine-rich repeat protein kinase...
AT5G56380	0.344	0.044	Enriched in ccr4	F-box/RNI-like/FBD-like domains-co...
AT4G26410	0.343	0.012	Enriched in ccr4	Uncharacterised conserved protein ...
AT4G33200	0.343	0.005	Enriched in ccr4	myosin, putative, Symbols: XI-I, A...
AT5G21080	0.343	0.010	Enriched in ccr4	Uncharacterized protein
AT5G54900	0.342	0.021	Enriched in ccr4	RNA-binding protein 45A, Symbols: ...
AT5G46200	0.340	0.014	Enriched in ccr4	Protein of Unknown Function (DUF239)
AT4G12590	0.339	0.032	Enriched in ccr4	Protein of unknown function DUF106...
AT1G56200	0.338	0.042	Enriched in ccr4	embryo defective 1303, Symbols: em...
AT5G52882	0.338	0.024	Enriched in ccr4	P-loop containing nucleoside triph...
AT5G53470	0.337	0.008	Enriched in ccr4	acyl-CoA binding protein 1, Symbol...
AT2G43090	0.336	0.005	Enriched in ccr4	Aconitase/3-isopropylmalate dehydr...
AT3G14067	0.334	0.033	Enriched in ccr4	Subtilase family protein
AT1G23700	0.333	0.005	Enriched in ccr4	Protein kinase superfamily protein
AT1G61290	0.330	0.018	Enriched in ccr4	syntaxin of plants 124, Symbols: S...
AT4G33390	0.327	0.017	Enriched in ccr4	Plant protein of unknown function ...
AT3G16110	0.323	0.006	Enriched in ccr4	PDI-like 1-6, Symbols: ATPDIL1-6, ...
AT2G22370	0.318	0.036	Enriched in ccr4	unknown protein

AT2G32730	0.317	0.023	Enriched in ccr4	26S proteasome regulatory complex,...
AT2G04400	0.316	0.038	Enriched in ccr4	Aldolase-type TIM barrel family pr...
AT5G25550	0.315	0.025	Enriched in ccr4	Leucine-rich repeat (LRR) family p...
AT2G24050	0.311	0.009	Enriched in ccr4	MIF4G domain-containing protein / ...
AT3G54700	0.309	0.048	Enriched in ccr4	phosphate transporter 1;7, Symbols...
AT1G71880	0.301	0.009	Enriched in ccr4	sucrose-proton symporter 1, Symbol...
AT2G33870	0.301	0.007	Enriched in ccr4	RAB GTPase homolog A1H, Symbols: A...
AT1G36280	0.299	0.018	Enriched in ccr4	L-Aspartase-like family protein
AT4G32610	0.298	0.012	Enriched in ccr4	copper ion binding
AT1G11910	0.297	0.019	Enriched in ccr4	aspartic proteinase A1, Symbols: A...
AT3G16630	0.297	0.022	Enriched in ccr4	P-loop containing nucleoside triph...
AT3G55180	0.296	0.034	Enriched in ccr4	alpha/beta-Hydrolases superfamily ...
AT1G04880	0.291	0.015	Enriched in ccr4	HMG (high mobility group) box prot...
AT3G24530	0.287	0.018	Enriched in ccr4	AAA-type ATPase family protein / a...
AT3G13930	0.284	0.021	Enriched in ccr4	Dihydrolipoamide acetyltransferase...
AT5G47490	0.282	0.011	Enriched in ccr4	RGPR-related
AT3G12690	0.277	0.015	Enriched in ccr4	AGC kinase 1.5, Symbols: AGC1.5
AT1G34220	0.276	0.047	Enriched in ccr4	Regulator of Vps4 activity in the ...
AT5G51030	0.274	0.031	Enriched in ccr4	NAD(P)-binding Rossmann-fold super...
AT4G34490	0.271	0.016	Enriched in ccr4	cyclase associated protein 1, Symb...
AT5G57490	0.270	0.037	Enriched in ccr4	voltage dependent anion channel 4,...
AT3G04790	0.270	0.050	Enriched in ccr4	Ribose 5-phosphate isomerase, type...
AT4G33230	0.268	0.023	Enriched in ccr4	Plant invertase/pectin methylester...
AT1G73670	0.263	0.032	Enriched in ccr4	MAP kinase 15, Symbols: ATMPK15, M...
AT1G28550	0.263	0.020	Enriched in ccr4	RAB GTPase homolog A1I, Symbols: A...
AT1G70310	0.262	0.040	Enriched in ccr4	spermidine synthase 2, Symbols: SPDS2
AT5G60860	0.261	0.016	Enriched in ccr4	RAB GTPase homolog A1F, Symbols: A...
AT1G09760	0.260	0.031	Enriched in ccr4	U2 small nuclear ribonucleoprotein...
AT5G03905	0.258	0.048	Enriched in ccr4	Iron-sulphur cluster biosynthesis ...
AT1G18150	0.258	0.024	Enriched in ccr4	Protein kinase superfamily protein...
AT2G41790	0.256	0.029	Enriched in ccr4	Insulinase (Peptidase family M16) ...
AT4G01470	0.255	0.021	Enriched in ccr4	tonoplast intrinsic protein 1;3, S...
AT3G06830	0.255	0.023	Enriched in ccr4	Plant invertase/pectin methylester...
AT4G16710	0.255	0.044	Enriched in ccr4	glycosyltransferase family protein 28
AT3G18190	0.254	0.037	Enriched in ccr4	TCP-1/cpn60 chaperonin family protein
AT5G37475	0.251	0.027	Enriched in ccr4	Translation initiation factor eIF3...
AT3G01340	0.250	0.042	Enriched in ccr4	Transducin/WD40 repeat-like superf...
AT1G79250	0.250	0.030	Enriched in ccr4	AGC kinase 1.7, Symbols: AGC1.7
AT2G30720	0.247	0.042	Enriched in ccr4	Thioesterase/thiol ester dehydrase...
AT3G19760	0.246	0.038	Enriched in ccr4	eukaryotic initiation factor 4A-II...
AT5G05920	0.242	0.027	Enriched in ccr4	deoxyhypusine synthase, Symbols: D...
AT2G25290	0.240	0.043	Enriched in ccr4	Octicosapeptide/Phox/Bem1p (PB1) d...
AT1G09920	0.239	0.015	Enriched in ccr4	TRAF-type zinc finger-related
AT1G11250	0.235	0.046	Enriched in ccr4	syntaxin of plants 125, Symbols: S...
AT1G48850	0.231	0.030	Enriched in ccr4	chorismate synthase, putative / 5-...
AT2G35210	0.228	0.048	Enriched in ccr4	root and pollen arfgap, Symbols: R...
AT3G07830	0.228	0.044	Enriched in ccr4	Pectin lyase-like superfamily protein
AT1G73630	0.225	0.023	Enriched in ccr4	EF hand calcium-binding protein fa...
AT1G70770	0.225	0.031	Enriched in ccr4	Protein of unknown function DUF235...
AT5G53460	0.221	0.022	Enriched in ccr4	NADH-dependent glutamate synthase ...
AT2G47510	0.219	0.039	Enriched in ccr4	fumarase 1, Symbols: FUM1
AT1G52240	0.218	0.041	Enriched in ccr4	RHO guanyl-nucleotide exchange fac...
AT1G16290	0.218	0.030	Enriched in ccr4	unknown protein
AT4G18360	0.218	0.026	Enriched in ccr4	Aldolase-type TIM barrel family pr...
AT4G23630	0.218	0.038	Enriched in ccr4	VIRB2-interacting protein 1, Symbo...
AT2G04030	0.213	0.036	Enriched in ccr4	Chaperone protein htpG family prot...
AT3G15060	0.212	0.033	Enriched in ccr4	RAB GTPase homolog A1G, Symbols: A...
AT4G20670	0.209	0.048	Enriched in ccr4	Domain of unknown function (DUF26)
AT3G04690	0.206	0.028	Enriched in ccr4	Malectin/receptor-like protein kin...
AT2G47050	0.203	0.047	Enriched in ccr4	Plant invertase/pectin methylester...
AT4G01660	0.201	0.032	Enriched in ccr4	ABC transporter 1, Symbols: ATABC1...
AT1G63000	0.196	0.038	Enriched in ccr4	nucleotide-rhamnose synthase/epime...
AT1G70410	0.195	0.043	Enriched in ccr4	beta carbonic anhydrase 4, Symbols...
AT1G73250	0.194	0.047	Enriched in ccr4	GDP-4-keto-6-deoxymannose-3,5-epim...
AT5G61790	0.191	0.042	Enriched in ccr4	calnexin 1, Symbols: CNX1, ATCNX1
AT5G13780	0.187	0.047	Enriched in ccr4	Acyl-CoA N-acyltransferases (NAT) ...
AT4G17190	-0.180	0.049	Depleted in ccr4	farnesyl diphosphate synthase 2, S...
AT5G13850	-0.191	0.049	Depleted in ccr4	nascent polypeptide-associated com...
AT3G52880	-0.191	0.043	Depleted in ccr4	monodehydroascorbate reductase 1, ...
AT5G34850	-0.191	0.042	Depleted in ccr4	purple acid phosphatase 26, Symbol...
AT3G48680	-0.195	0.047	Depleted in ccr4	gamma carbonic anhydrase-like 2, S...
AT1G24180	-0.198	0.046	Depleted in ccr4	Thiamin diphosphate-binding fold (...
AT4G02620	-0.200	0.046	Depleted in ccr4	vacuolar ATPase subunit F family p...
AT1G79230	-0.200	0.046	Depleted in ccr4	mercaptopyruvate sulfurtransferase...
AT1G79690	-0.201	0.036	Depleted in ccr4	nudix hydrolase homolog 3, Symbols...
AT3G10380	-0.201	0.046	Depleted in ccr4	subunit of exocyst complex 8, Symb...
AT5G23390	-0.203	0.037	Depleted in ccr4	Plant protein of unknown function ...
AT5G58290	-0.207	0.027	Depleted in ccr4	regulatory particle triple-A ATPas...
AT5G27540	-0.209	0.044	Depleted in ccr4	MIRO-related GTP-ase 1, Symbols: M...
AT5G60980	-0.209	0.048	Depleted in ccr4	Nuclear transport factor 2 (NTF2) ...
AT2G40800	-0.210	0.048	Depleted in ccr4	unknown protein
AT1G51980	-0.211	0.026	Depleted in ccr4	Insulinase (Peptidase family M16) ...
AT2G21130	-0.212	0.030	Depleted in ccr4	Cyclophilin-like peptidyl-prolyl c...
AT2G21390	-0.213	0.030	Depleted in ccr4	Coatomer, alpha subunit
AT1G67280	-0.214	0.046	Depleted in ccr4	Glyoxalase/Bleomycin resistance pr...
AT4G20850	-0.215	0.047	Depleted in ccr4	tripeptidyl peptidase ii, Symbols:...
AT2G21870	-0.216	0.032	Depleted in ccr4	copper ion binding;cobalt ion bind...

AT2G27020	-0.219	0.030	Depleted in ccr4	20S proteasome alpha subunit G1, S...
AT2G31980	-0.221	0.039	Depleted in ccr4	PHYTOCYSTATIN 2, Symbols: AtCYS2, ...
AT5G48810	-0.221	0.046	Depleted in ccr4	cytochrome B5 isoform D, Symbols: ...
AT3G57890	-0.222	0.031	Depleted in ccr4	Tubulin binding cofactor C domain-...
AT5G03160	-0.225	0.021	Depleted in ccr4	homolog of mamallian P58IPK, Symbo...
AT2G32885	-0.225	0.027	Depleted in ccr4	Rapid alkalinization factor (RALF)...
AT5G58240	-0.229	0.025	Depleted in ccr4	FRAGILE HISTIDINE TRIAD, Symbols: ...
AT5G15070	-0.229	0.047	Depleted in ccr4	Phosphoglycerate mutase-like famil...
AT2G42010	-0.232	0.037	Depleted in ccr4	phospholipase D beta 1, Symbols: P...
AT3G12260	-0.232	0.036	Depleted in ccr4	LYR family of Fe/S cluster biogene...
AT1G08110	-0.233	0.034	Depleted in ccr4	lactoylglutathione lyase family pr...
AT4G16450	-0.233	0.035	Depleted in ccr4	unknown protein
AT2G40770	-0.233	0.045	Depleted in ccr4	zinc ion binding;DNA binding;helic...
AT5G08530	-0.233	0.046	Depleted in ccr4	51 kDa subunit of complex I, Symbo...
AT5G19600	-0.233	0.025	Depleted in ccr4	sulfate transporter 3;5, Symbols: ...
AT4G02450	-0.234	0.034	Depleted in ccr4	HSP20-like chaperones superfamily ...
AT4G29040	-0.234	0.036	Depleted in ccr4	regulatory particle AAA-ATPase 2A,...
AT2G30110	-0.234	0.037	Depleted in ccr4	ubiquitin-activating enzyme 1, Sym...
AT3G22370	-0.235	0.048	Depleted in ccr4	alternative oxidase 1A, Symbols: A...
AT5G48140	-0.235	0.037	Depleted in ccr4	Pectin lyase-like superfamily protein
AT1G19920	-0.236	0.017	Depleted in ccr4	Pseudouridine synthase/archaeosine...
AT5G04180	-0.237	0.041	Depleted in ccr4	alpha carbonic anhydrase 3, Symbol...
AT2G17420	-0.238	0.038	Depleted in ccr4	NADPH-dependent thioredoxin reduct...
AT5G43070	-0.240	0.039	Depleted in ccr4	WPP domain protein 1, Symbols: WPP1
AT3G19930	-0.242	0.032	Depleted in ccr4	sugar transporter 4, Symbols: STP4...
AT1G48600	-0.246	0.044	Depleted in ccr4	S-adenosyl-L-methionine-dependent ...
AT1G12310	-0.248	0.039	Depleted in ccr4	Calcium-binding EF-hand family pro...
AT4G21490	-0.248	0.035	Depleted in ccr4	NAD(P)H dehydrogenase B3, Symbols:...
AT3G03080	-0.250	0.019	Depleted in ccr4	Zinc-binding dehydrogenase family ...
AT5G43850	-0.251	0.024	Depleted in ccr4	RmlC-like cupins superfamily prote...
AT2G44060	-0.252	0.021	Depleted in ccr4	Late embryogenesis abundant protei...
AT2G27460	-0.252	0.016	Depleted in ccr4	sec23/sec24 transport family protein
AT5G63510	-0.253	0.017	Depleted in ccr4	gamma carbonic anhydrase like 1, S...
AT4G35890	-0.253	0.046	Depleted in ccr4	winged-helix DNA-binding transcrip...
AT1G79010	-0.255	0.020	Depleted in ccr4	Alpha-helical ferredoxin
AT3G56640	-0.255	0.036	Depleted in ccr4	exocyst complex component sec15A, ...
AT1G31500	-0.255	0.040	Depleted in ccr4	DNAse I-like superfamily protein
AT2G35120	-0.256	0.039	Depleted in ccr4	Single hybrid motif superfamily pr...
AT3G17940	-0.256	0.014	Depleted in ccr4	Galactose mutarotase-like superfam...
AT1G73600	-0.257	0.041	Depleted in ccr4	S-adenosyl-L-methionine-dependent ...
AT4G10440	-0.257	0.048	Depleted in ccr4	S-adenosyl-L-methionine-dependent ...
AT3G54110	-0.258	0.043	Depleted in ccr4	plant uncoupling mitochondrial pro...
AT1G51690	-0.258	0.045	Depleted in ccr4	protein phosphatase 2A 55 kDa regu...
AT5G40760	-0.259	0.022	Depleted in ccr4	glucose-6-phosphate dehydrogenase ...
AT2G30870	-0.260	0.031	Depleted in ccr4	glutathione S-transferase PHI 10, ...
AT1G48940	-0.260	0.040	Depleted in ccr4	early nodulin-like protein 6, Symb...
AT4G11600	-0.261	0.022	Depleted in ccr4	glutathione peroxidase 6, Symbols:...
AT2G19940	-0.261	0.038	Depleted in ccr4	oxidoreductases, acting on the ald...
AT1G30400	-0.263	0.047	Depleted in ccr4	multidrug resistance-associated pr...
AT1G04070	-0.265	0.046	Depleted in ccr4	translocase of outer membrane 22-I...
AT5G58440	-0.265	0.037	Depleted in ccr4	sorting nexin 2A, Symbols: SNX2a
AT4G27090	-0.265	0.023	Depleted in ccr4	Ribosomal protein L14
AT3G13290	-0.266	0.018	Depleted in ccr4	varicose-related, Symbols: VCR
AT1G17470	-0.268	0.014	Depleted in ccr4	developmentally regulated G-protei...
AT2G37550	-0.269	0.009	Depleted in ccr4	ARF-GAP domain 7, Symbols: ASP1, AGD7
AT1G10385	-0.270	0.050	Depleted in ccr4	Vps51/Vps67 family (components of ...
AT5G54890	-0.270	0.022	Depleted in ccr4	RNA-binding CRS1 / YhbY (CRM) doma...
AT1G35720	-0.270	0.024	Depleted in ccr4	annexin 1, Symbols: ANNAT1, OXY5, ...
AT4G38740	-0.272	0.009	Depleted in ccr4	rotamase CYP 1, Symbols: ROC1
AT4G18050	-0.273	0.045	Depleted in ccr4	P-glycoprotein 9, Symbols: PGP9
AT3G28500	-0.273	0.024	Depleted in ccr4	60S acidic ribosomal protein family
AT5G48300	-0.274	0.025	Depleted in ccr4	ADP glucose pyrophosphorylase 1, ...
AT4G13560	-0.275	0.038	Depleted in ccr4	Late embryogenesis abundant protei...
AT1G62820	-0.275	0.025	Depleted in ccr4	Calcium-binding EF-hand family pro...
AT5G45560	-0.275	0.027	Depleted in ccr4	Pleckstrin homology (PH) domain-co...
AT5G63680	-0.276	0.012	Depleted in ccr4	Pyruvate kinase family protein
AT1G04920	-0.277	0.009	Depleted in ccr4	sucrose phosphate synthase 3F, Sym...
AT1G48860	-0.279	0.034	Depleted in ccr4	RNA 3'-terminal phosphate cyclase/...
AT3G52730	-0.280	0.031	Depleted in ccr4	ubiquinol-cytochrome C reductase U...
AT5G65950	-0.280	0.037	Depleted in ccr4	unknown protein
AT1G69460	-0.280	0.047	Depleted in ccr4	emp24/gp25L/p24 family/GOLD family...
AT1G02000	-0.280	0.029	Depleted in ccr4	UDP-D-glucuronate 4-epimerase 2, S...
AT2G03510	-0.281	0.015	Depleted in ccr4	SPFH/Band 7/PHB domain-containing ...
AT5G21274	-0.281	0.026	Depleted in ccr4	calmodulin 6, Symbols: CAM6, ACAM-6
AT4G23885	-0.283	0.011	Depleted in ccr4	unknown protein
AT3G20000	-0.283	0.016	Depleted in ccr4	translocase of the outer mitochond...
AT3G13860	-0.284	0.010	Depleted in ccr4	heat shock protein 60-3A, Symbols:...
AT2G24450	-0.286	0.016	Depleted in ccr4	FASCICLIN-like arabinogalactan pro...
AT5G49650	-0.287	0.044	Depleted in ccr4	xylulose kinase-2, Symbols: XK-2, XK2
AT5G49810	-0.287	0.007	Depleted in ccr4	methionine S-methyltransferase, Sy...
AT1G22840	-0.288	0.010	Depleted in ccr4	CYTOCHROME C-1, Symbols: CYTC-1, A...
AT3G63460	-0.289	0.009	Depleted in ccr4	transducin family protein / WD-40 ...
AT4G01100	-0.291	0.009	Depleted in ccr4	adenine nucleotide transporter 1, ...
AT1G54100	-0.292	0.018	Depleted in ccr4	aldehyde dehydrogenase 7B4, Symbol...
AT4G27270	-0.293	0.019	Depleted in ccr4	Quinone reductase family protein
AT4G30810	-0.295	0.038	Depleted in ccr4	serine carboxypeptidase-like 29, S...
AT3G07330	-0.295	0.036	Depleted in ccr4	Cellulose-synthase-like C6, Symbol...

AT2G16600	-0.297	0.016	Depleted in ccr4	rotamase CYP 3, Symbols: ROC3
AT3G21220	-0.299	0.043	Depleted in ccr4	MAP kinase kinase 5, Symbols: ATMK...
AT1G29900	-0.301	0.039	Depleted in ccr4	carbamoyl phosphate synthetase B, ...
AT4G14160	-0.302	0.016	Depleted in ccr4	Sec23/Sec24 protein transport fami...
AT1G71220	-0.304	0.011	Depleted in ccr4	UDP-glucose:glycoprotein glucosylt...
AT5G08570	-0.304	0.007	Depleted in ccr4	Pyruvate kinase family protein
AT5G61240	-0.304	0.050	Depleted in ccr4	Leucine-rich repeat (LRR) family p...
AT2G38650	-0.305	0.042	Depleted in ccr4	galacturonosyltransferase 7, Symbo...
AT4G18596	-0.309	0.032	Depleted in ccr4	Pollen Ole e 1 allergen and extens...
AT3G18590	-0.309	0.045	Depleted in ccr4	early nodulin-like protein 5, Symb...
AT5G35680	-0.310	0.013	Depleted in ccr4	Nucleic acid-binding, OB-fold-like...
AT1G05270	-0.310	0.027	Depleted in ccr4	TraB family protein
AT1G50480	-0.311	0.007	Depleted in ccr4	10-formyltetrahydrofolate syntheta...
AT4G16830	-0.311	0.014	Depleted in ccr4	Hyaluronan / mRNA binding family
AT4G29840	-0.312	0.036	Depleted in ccr4	Pyridoxal-5'-phosphate-dependent e...
AT5G49910	-0.312	0.018	Depleted in ccr4	chloroplast heat shock protein 70-...
AT4G36195	-0.312	0.035	Depleted in ccr4	Serine carboxypeptidase S28 family...
AT5G43830	-0.313	0.020	Depleted in ccr4	Aluminium induced protein with YGL...
AT5G13280	-0.314	0.009	Depleted in ccr4	aspartate kinase 1, Symbols: AK-LY...
AT4G14880	-0.316	0.005	Depleted in ccr4	O-acetylserine (thiol) lyase (OAS-...
AT2G24765	-0.317	0.046	Depleted in ccr4	ADP-ribosylation factor 3, Symbols...
AT2G20760	-0.318	0.013	Depleted in ccr4	Clathrin light chain protein
AT5G41310	-0.319	0.021	Depleted in ccr4	P-loop nucleoside triphosphate hyd...
AT5G49680	-0.321	0.008	Depleted in ccr4	Golgi-body localisation protein do...
AT1G47200	-0.321	0.011	Depleted in ccr4	WPP domain protein 2, Symbols: WPP2
AT3G03070	-0.323	0.036	Depleted in ccr4	NADH-ubiquinone oxidoreductase-rel...
AT1G23140	-0.323	0.037	Depleted in ccr4	Calcium-dependent lipid-binding (C...
AT2G30690	-0.323	0.012	Depleted in ccr4	Protein of unknown function, DUF593
AT4G10140	-0.323	0.018	Depleted in ccr4	unknown protein
AT4G21105	-0.325	0.017	Depleted in ccr4	cytochrome-c oxidases;electron car...
AT5G63980	-0.326	0.011	Depleted in ccr4	Inositol monophosphatase family pr...
AT5G63220	-0.326	0.022	Depleted in ccr4	unknown protein
AT1G59900	-0.327	0.018	Depleted in ccr4	pyruvate dehydrogenase complex E1 ...
AT3G20630	-0.328	0.014	Depleted in ccr4	ubiquitin-specific protease 14, Sy...
AT5G20070	-0.329	0.013	Depleted in ccr4	nudix hydrolase homolog 19, Symbol...
AT1G30890	-0.330	0.037	Depleted in ccr4	Integral membrane HRF1 family protein
AT3G52720	-0.331	0.011	Depleted in ccr4	alpha carbonic anhydrase 1, Symbol...
AT5G15770	-0.331	0.033	Depleted in ccr4	glucose-6-phosphate acetyltransfer...
AT2G29960	-0.332	0.024	Depleted in ccr4	cyclophilin 5, Symbols: CYP5, ATCY...
AT2G29260	-0.332	0.009	Depleted in ccr4	NAD(P)-binding Rossmann-fold super...
AT5G02240	-0.335	0.018	Depleted in ccr4	NAD(P)-binding Rossmann-fold super...
AT1G74920	-0.335	0.032	Depleted in ccr4	aldehyde dehydrogenase 10A8, Symbo...
AT4G21210	-0.336	0.026	Depleted in ccr4	PPDK regulatory protein, Symbols: ...
AT2G04520	-0.336	0.012	Depleted in ccr4	Nucleic acid-binding, OB-fold-like...
AT1G12150	-0.337	0.018	Depleted in ccr4	Plant protein of unknown function ...
AT2G25310	-0.339	0.006	Depleted in ccr4	Protein of unknown function (DUF2012)
AT4G35000	-0.339	0.010	Depleted in ccr4	ascorbate peroxidase 3, Symbols: APX3
AT4G14240	-0.341	0.008	Depleted in ccr4	CBS domain-containing protein with...
AT4G32470	-0.343	0.004	Depleted in ccr4	Cytochrome bd ubiquinol oxidase, 1...
AT4G11120	-0.343	0.019	Depleted in ccr4	translation elongation factor Ts (...
AT3G28720	-0.343	0.049	Depleted in ccr4	unknown protein
AT3G51840	-0.343	0.015	Depleted in ccr4	acyl-CoA oxidase 4, Symbols: ACX4,...
AT1G66410	-0.344	0.029	Depleted in ccr4	calmodulin 4, Symbols: CAM4
AT5G16300	-0.344	0.007	Depleted in ccr4	Vps51/Vps67 family (components of ...
AT4G17170	-0.346	0.008	Depleted in ccr4	RAB GTPase homolog B1C, Symbols: A...
AT5G25070	-0.346	0.027	Depleted in ccr4	unknown protein
AT4G24620	-0.346	0.018	Depleted in ccr4	phosphoglucose isomerase 1, Symbol...
AT3G12050	-0.347	0.029	Depleted in ccr4	Aha1 domain-containing protein
AT4G02580	-0.347	0.007	Depleted in ccr4	NADH-ubiquinone oxidoreductase 24 ...
AT3G52640	-0.348	0.049	Depleted in ccr4	Zn-dependent exopeptidases superfa...
AT3G55480	-0.349	0.016	Depleted in ccr4	protein affected traficking...
AT1G69510	-0.350	0.006	Depleted in ccr4	cAMP-regulated phosphoprotein 19-r...
AT5G47880	-0.350	0.030	Depleted in ccr4	eukaryotic release factor 1-1, Sym...
AT1G20580	-0.351	0.029	Depleted in ccr4	Small nuclear ribonucleoprotein fa...
AT1G71440	-0.353	0.030	Depleted in ccr4	tubulin folding cofactor E / Pfiff...
AT3G51460	-0.353	0.005	Depleted in ccr4	Phosphoinositide phosphatase famil...
AT1G34575	-0.353	0.022	Depleted in ccr4	FAD-binding Berberine family protein
AT2G33220	-0.354	0.037	Depleted in ccr4	GRIM-19 protein
AT5G12140	-0.354	0.022	Depleted in ccr4	cystatin-1, Symbols: ATCYS1, CYS1
AT3G01200	-0.354	0.012	Depleted in ccr4	PPDK regulatory protein 2, Symbols...
AT1G45145	-0.355	0.003	Depleted in ccr4	thioredoxin H-type 5, Symbols: ATT...
AT5G54870	-0.355	0.024	Depleted in ccr4	unknown protein
AT2G07707	-0.356	0.036	Depleted in ccr4	Plant mitochondrial AT...
AT3G10610	-0.356	0.027	Depleted in ccr4	Ribosomal S17 family protein
AT2G45790	-0.356	0.006	Depleted in ccr4	phosphomannomutase, Symbols: ATPMM...
AT1G55160	-0.357	0.010	Depleted in ccr4	unknown protein
AT1G20480	-0.360	0.005	Depleted in ccr4	AMP-dependent synthetase and ligas...
AT3G02780	-0.360	0.007	Depleted in ccr4	isopentenyl pyrophosphate:dimethyl...
AT3G58500	-0.361	0.049	Depleted in ccr4	protein phosphatase 2A-4, Symbols:...
AT5G51740	-0.361	0.015	Depleted in ccr4	Peptidase family M48 family protein
AT4G29340	-0.361	0.042	Depleted in ccr4	profilin 4, Symbols: PRF4
AT5G60620	-0.361	0.040	Depleted in ccr4	glycerol-3-phosphate acyltransfera...
AT3G05600	-0.362	0.021	Depleted in ccr4	alpha/beta-Hydrolases superfamily ...
AT3G12130	-0.363	0.047	Depleted in ccr4	KH domain-containing protein / zin...
AT2G31680	-0.364	0.007	Depleted in ccr4	RAB GTPase homolog A5D, Symbols: A...
AT5G45880	-0.365	0.036	Depleted in ccr4	Pollen Ole e 1 allergen and extens...
AT5G35430	-0.367	0.029	Depleted in ccr4	Tetratricopeptide repeat (TPR)-lik...

AT1G23310	-0.370	0.003	Depleted in ccr4	glutamate:glyoxylate aminotransfer...
AT2G04842	-0.371	0.022	Depleted in ccr4	threonyl-tRNA synthetase, putative...
AT3G05190	-0.371	0.004	Depleted in ccr4	D-aminoacid aminotransferase-like ...
AT1G10590	-0.373	0.016	Depleted in ccr4	Nucleic acid-binding, OB-fold-like...
AT2G42500	-0.375	0.038	Depleted in ccr4	protein phosphatase 2A-3, Symbols:...
AT5G24420	-0.376	0.010	Depleted in ccr4	6-phosphogluconolactonase 5, Symbo...
AT3G16760	-0.382	0.020	Depleted in ccr4	Tetratricopeptide repeat (TPR)-lik...
AT5G58110	-0.384	0.008	Depleted in ccr4	chaperone binding;ATPase activators
AT3G08790	-0.386	0.018	Depleted in ccr4	ENTH/VHS/GAT family protein
AT4G24280	-0.388	0.003	Depleted in ccr4	chloroplast heat shock protein 70-...
AT4G37020	-0.389	0.037	Depleted in ccr4	unknown protein
AT3G02870	-0.389	0.006	Depleted in ccr4	Inositol monophosphatase family pr...
AT3G07680	-0.389	0.042	Depleted in ccr4	emp24/gp25L/p24 family/GOLD family...
AT1G29150	-0.390	0.013	Depleted in ccr4	non-ATPase subunit 9, Symbols: ATS...
AT1G13860	-0.390	0.014	Depleted in ccr4	QUASIMODO2 LIKE 1, Symbols: QUL1
AT2G32520	-0.391	0.010	Depleted in ccr4	alpha/beta-Hydrolases superfamily ...
AT3G47630	-0.392	0.024	Depleted in ccr4	unknown protein
AT5G16440	-0.393	0.032	Depleted in ccr4	isopentenyl diphosphate isomerase ...
AT1G30710	-0.396	0.004	Depleted in ccr4	FAD-binding Berberine family protein
AT1G75220	-0.396	0.008	Depleted in ccr4	Major facilitator superfamily protein
AT5G43960	-0.396	0.017	Depleted in ccr4	Nuclear transport factor 2 (NTF2) ...
AT1G08470	-0.399	0.032	Depleted in ccr4	strictosidine synthase-like 3, Sym...
AT5G46800	-0.399	0.026	Depleted in ccr4	Mitochondrial substrate carrier fa...
AT2G29040	-0.399	0.009	Depleted in ccr4	Exostosin family protein
AT1G08770	-0.402	0.039	Depleted in ccr4	prenylated RAB acceptor 1.E, Symbo...
AT5G40670	-0.406	0.004	Depleted in ccr4	PQ-loop repeat family protein / tr...
AT5G52840	-0.407	0.018	Depleted in ccr4	NADH-ubiquinone oxidoreductase-rel...
AT1G49540	-0.408	0.042	Depleted in ccr4	elongator protein 2, Symbols: ELP2...
AT1G16860	-0.410	0.016	Depleted in ccr4	Ubiquitin-specific protease family...
AT4G00720	-0.412	0.046	Depleted in ccr4	shaggy-like protein kinase 32, Sym...
AT1G25350	-0.412	0.003	Depleted in ccr4	glutamine-tRNA ligase, putative / ...
AT5G38760	-0.413	0.018	Depleted in ccr4	Late embryogenesis abundant protei...
AT5G52340	-0.414	0.047	Depleted in ccr4	exocyst subunit exo70 family prote...
AT5G47570	-0.414	0.014	Depleted in ccr4	unknown protein
AT1G15750	-0.417	0.011	Depleted in ccr4	Transducin family protein / WD-40 ...
AT1G71770	-0.417	0.003	Depleted in ccr4	poly(A)-binding protein 5, Symbols...
AT1G12640	-0.420	0.003	Depleted in ccr4	MBOAT (membrane bound O-acyl trans...
AT2G19770	-0.420	0.020	Depleted in ccr4	profilin 5, Symbols: PRF5
AT1G07220	-0.421	0.014	Depleted in ccr4	Arabidopsis thaliana protein of un...
AT5G04510	-0.421	0.008	Depleted in ccr4	3'-phosphoinositide-dependent prot...
AT5G41950	-0.423	0.006	Depleted in ccr4	Tetratricopeptide repeat (TPR)-lik...
AT1G02140	-0.424	0.004	Depleted in ccr4	mago nashi family protein, Symbols...
AT5G64350	-0.425	0.044	Depleted in ccr4	FK506-binding protein 12, Symbols:...
AT2G17700	-0.425	0.033	Depleted in ccr4	ACT-like protein tyrosine kinase f...
AT1G12930	-0.426	0.035	Depleted in ccr4	ARM repeat superfamily protein
AT2G23350	-0.427	0.002	Depleted in ccr4	poly(A) binding protein 4, Symbols...
AT3G53110	-0.432	0.008	Depleted in ccr4	P-loop containing nucleoside triph...
AT3G49680	-0.432	0.011	Depleted in ccr4	branched-chain aminotransferase 3,...
AT2G44640	-0.432	0.008	Depleted in ccr4	unknown protein
AT4G31340	-0.434	0.048	Depleted in ccr4	myosin heavy chain-related
AT1G66680	-0.435	0.030	Depleted in ccr4	S-adenosyl-L-methionine-dependent ...
AT1G55860	-0.436	0.009	Depleted in ccr4	ubiquitin-protein ligase 1, Symbol...
AT1G34130	-0.436	0.005	Depleted in ccr4	staurosporin and temperature sensi...
AT3G06610	-0.437	0.003	Depleted in ccr4	DNA-binding enhancer protein-related
AT1G06950	-0.437	0.049	Depleted in ccr4	translocon at the inner envelope m...
AT5G18550	-0.443	0.008	Depleted in ccr4	Zinc finger C-x8-C-x5-C-x3-H type ...
AT5G27410	-0.443	0.007	Depleted in ccr4	D-aminoacid aminotransferase-like ...
AT3G45400	-0.443	0.039	Depleted in ccr4	exostosin family protein
AT5G20080	-0.444	0.002	Depleted in ccr4	FAD/NAD(P)-binding oxidoreductase
AT3G03100	-0.445	0.007	Depleted in ccr4	NADH:ubiquinone oxidoreductase, 17...
AT2G28020	-0.445	0.014	Depleted in ccr4	unknown protein
AT1G06890	-0.446	0.007	Depleted in ccr4	nodulin MtN21 /EamA-like transport...
AT5G52650	-0.450	0.003	Depleted in ccr4	RNA binding Plectin/S10 domain-con...
AT5G45550	-0.450	0.020	Depleted in ccr4	Mob1/phocein family protein
AT2G43420	-0.451	0.015	Depleted in ccr4	3-beta hydroxysteroid dehydrogenas...
AT5G65010	-0.455	0.001	Depleted in ccr4	asparagine synthetase 2, Symbols: ...
AT1G05810	-0.457	0.032	Depleted in ccr4	RAB GTPase homolog A5E, Symbols: A...
AT3G54680	-0.459	0.026	Depleted in ccr4	proteophosphoglycan-related
AT4G17770	-0.460	0.006	Depleted in ccr4	trehalose phosphatase/synthase 5, ...
AT4G38190	-0.461	0.013	Depleted in ccr4	cellulose synthase like D4, Symbol...
AT4G18930	-0.461	0.004	Depleted in ccr4	RNA ligase/cyclic nucleotide phosp...
AT1G64550	-0.462	0.005	Depleted in ccr4	general control non-repressible 3,...
AT1G06220	-0.463	0.024	Depleted in ccr4	Ribosomal protein S5/Elongation fa...
AT5G62310	-0.464	0.050	Depleted in ccr4	AGC (cAMP-dependent, cGMP-dependen...
AT5G27970	-0.464	0.032	Depleted in ccr4	ARM repeat superfamily protein
AT4G01320	-0.464	0.022	Depleted in ccr4	Peptidase family M48 family protei...
AT3G13224	-0.465	0.016	Depleted in ccr4	RNA-binding (RRM/RBD/RNP motifs) f...
AT4G30580	-0.466	0.030	Depleted in ccr4	Phospholipid/glycerol acyltransfer...
AT2G35010	-0.466	0.003	Depleted in ccr4	thioredoxin O1, Symbols: ATO1, TO1
AT1G01620	-0.466	0.026	Depleted in ccr4	plasma membrane intrinsic protein ...
AT5G08060	-0.467	0.001	Depleted in ccr4	unknown protein
AT5G04740	-0.468	0.010	Depleted in ccr4	ACT domain-containing protein
AT5G48940	-0.469	0.005	Depleted in ccr4	Leucine-rich repeat transmembrane ...
AT5G25230	-0.469	0.039	Depleted in ccr4	Ribosomal protein S5/Elongation fa...
AT2G31010	-0.470	0.025	Depleted in ccr4	Protein kinase superfamily protein
AT4G26570	-0.470	0.003	Depleted in ccr4	calcineurin B-like 3, Symbols: ATC...
AT2G15900	-0.474	0.003	Depleted in ccr4	Phox-associated domain;Phox-like;S...

AT5G04990	-0.474	0.013	Depleted in ccr4	SAD1/UNC-84 domain protein 1, Symb...
AT1G26550	-0.476	0.004	Depleted in ccr4	FKBP-like peptidyl-prolyl cis-tran...
AT1G15415	-0.478	0.026	Depleted in ccr4	The protein encoded by this gene w...
AT4G16510	-0.480	0.037	Depleted in ccr4	YbaK/aminoacyl-tRNA synthetase-ass...
AT2G42810	-0.480	0.005	Depleted in ccr4	protein phosphatase 5.2, Symbols: ...
AT2G18340	-0.480	0.009	Depleted in ccr4	late embryogenesis abundant domain...
AT1G07110	-0.481	0.050	Depleted in ccr4	fructose-2,6-bisphosphatase, Symbo...
AT1G08820	-0.483	0.029	Depleted in ccr4	vamp/synaptobrevin-associated prot...
AT3G26720	-0.483	0.011	Depleted in ccr4	Glycosyl hydrolase family 38 protein
AT5G67265	-0.484	0.012	Depleted in ccr4	unknown protein
AT1G29850	-0.484	0.022	Depleted in ccr4	double-stranded DNA-binding family...
AT3G16230	-0.485	0.009	Depleted in ccr4	Predicted eukaryotic LigT
AT5G23140	-0.486	0.002	Depleted in ccr4	nuclear-encoded CLP protease P7, S...
AT3G55120	-0.488	0.011	Depleted in ccr4	Chalcone-flavanone isomerase famil...
AT5G55610	-0.489	0.015	Depleted in ccr4	unknown protein
AT1G26110	-0.491	0.007	Depleted in ccr4	decapping 5, Symbols: DCP5
AT3G10740	-0.491	0.012	Depleted in ccr4	alpha-L-arabinofuranosidase 1, Sym...
AT3G26690	-0.492	0.015	Depleted in ccr4	nudix hydrolase homolog 13, Symbol...
AT5G14260	-0.492	0.017	Depleted in ccr4	Rubisco methyltransferase family p...
AT1G30070	-0.493	0.033	Depleted in ccr4	SGS domain-containing protein
AT2G40850	-0.494	0.003	Depleted in ccr4	phosphoinositide 4-kinase gamma 1,...
AT5G02050	-0.494	0.016	Depleted in ccr4	Mitochondrial glycoprotein family ...
AT3G08850	-0.495	0.036	Depleted in ccr4	HEAT repeat ;WD domain, G-beta rep...
AT5G41970	-0.496	0.011	Depleted in ccr4	Metal-dependent protein hydrolase
AT1G79870	-0.496	0.016	Depleted in ccr4	D-isomer specific 2-hydroxyacid de...
AT3G62310	-0.497	0.014	Depleted in ccr4	RNA helicase family protein
AT1G79660	-0.497	0.002	Depleted in ccr4	unknown protein
AT2G42680	-0.498	0.003	Depleted in ccr4	multiprotein bridging factor 1A, S...
AT3G03810	-0.498	0.010	Depleted in ccr4	O-fucosyltransferase family protei...
AT3G52610	-0.500	0.004	Depleted in ccr4	unknown protein
AT5G11770	-0.500	0.003	Depleted in ccr4	NADH-ubiquinone oxidoreductase 20 ...
AT1G02410	-0.505	0.018	Depleted in ccr4	cytochrome c oxidase assembly prot...
AT1G30810	-0.509	0.001	Depleted in ccr4	Transcription factor jumonji (jmj)...
AT4G23490	-0.510	0.029	Depleted in ccr4	Protein of unknown function (DUF604)
AT5G63620	-0.512	0.004	Depleted in ccr4	GroES-like zinc-binding alcohol de...
AT3G47800	-0.512	0.002	Depleted in ccr4	Galactose mutarotase-like superfam...
AT1G61690	-0.514	0.042	Depleted in ccr4	phosphoinositide binding
AT3G45090	-0.515	0.006	Depleted in ccr4	P-loop containing nucleoside triph...
AT2G02050	-0.516	0.004	Depleted in ccr4	NADH-ubiquinone oxidoreductase B18...
AT2G28000	-0.519	0.012	Depleted in ccr4	chaperonin-60alpha, Symbols: CPN60...
AT1G30050	-0.520	0.005	Depleted in ccr4	unknown protein
AT1G30660	-0.524	0.013	Depleted in ccr4	nucleic acid binding;nucleic acid ...
AT1G34430	-0.524	0.001	Depleted in ccr4	2-oxoacid dehydrogenases acyltrans...
AT3G55920	-0.526	0.001	Depleted in ccr4	Cyclophilin-like peptidyl-prolyl c...
AT4G11760	-0.527	0.016	Depleted in ccr4	low-molecular-weight cysteine-rich...
AT5G62810	-0.530	0.001	Depleted in ccr4	peroxin 14, Symbols: PEX14, ATPEX1...
AT4G33250	-0.530	0.001	Depleted in ccr4	eukaryotic translation initiation ...
AT1G09200	-0.532	0.038	Depleted in ccr4	0
AT5G65350	-0.532	0.038	Depleted in ccr4	histone 3 11, Symbols: HTR11
AT1G66850	-0.535	0.026	Depleted in ccr4	Bifunctional inhibitor/lipid-trans...
AT3G12640	-0.536	0.029	Depleted in ccr4	RNA binding (RRM/RBD/RNP motifs) f...
AT1G21370	-0.537	0.001	Depleted in ccr4	unknown protein
AT3G03380	-0.538	0.001	Depleted in ccr4	DegP protease 7, Symbols: DegP7
AT3G07640	-0.538	0.003	Depleted in ccr4	unknown protein
AT5G44390	-0.538	0.032	Depleted in ccr4	FAD-binding Berberine family protein
AT5G36210	-0.539	0.007	Depleted in ccr4	alpha/beta-Hydrolases superfamily ...
AT5G37830	-0.540	0.002	Depleted in ccr4	oxoprolinase 1, Symbols: OXP1
AT2G34660	-0.540	0.008	Depleted in ccr4	multidrug resistance-associated pr...
AT4G26550	-0.543	0.033	Depleted in ccr4	Got1/Sft2-like vescicle transport ...
AT1G22410	-0.545	0.001	Depleted in ccr4	Class-II DAHP synthetase family pr...
AT5G10240	-0.545	0.000	Depleted in ccr4	asparagine synthetase 3, Symbols: ...
AT5G47630	-0.546	0.030	Depleted in ccr4	mitochondrial acyl carrier protein...
AT4G39420	-0.548	0.020	Depleted in ccr4	unknown protein
AT1G08420	-0.549	0.022	Depleted in ccr4	BRI1 suppressor 1 (BSU1)-like 2, S...
AT1G62390	-0.550	0.001	Depleted in ccr4	Octicosapeptide/Phox/Bem1p (PB1) d...
AT5G14540	-0.553	0.002	Depleted in ccr4	Protein of unknown function (DUF1421)
AT1G48430	-0.553	0.001	Depleted in ccr4	Dihydroxyacetone kinase
AT5G02790	-0.554	0.011	Depleted in ccr4	Glutathione S-transferase family p...
AT5G18110	-0.556	0.011	Depleted in ccr4	novel cap-binding protein, Symbols...
AT3G49800	-0.559	0.001	Depleted in ccr4	BSD domain-containing protein
AT1G58080	-0.559	0.000	Depleted in ccr4	ATP phosphoribosyl transferase 1, ...
AT3G16980	-0.562	0.032	Depleted in ccr4	RNA polymerases M/15 Kd subunit, S...
AT1G12360	-0.563	0.006	Depleted in ccr4	Sec1/munc18-like (SM) proteins sup...
AT1G20925	-0.563	0.022	Depleted in ccr4	Auxin efflux carrier family protein
AT1G05720	-0.568	0.007	Depleted in ccr4	selenoprotein family protein
AT5G24010	-0.568	0.003	Depleted in ccr4	Protein kinase superfamily protein
AT5G04590	-0.569	0.006	Depleted in ccr4	sulfite reductase, Symbols: SIR
AT5G16660	-0.570	0.048	Depleted in ccr4	unknown protein
AT3G51830	-0.572	0.003	Depleted in ccr4	SAC domain-containing protein 8, S...
AT2G32930	-0.574	0.013	Depleted in ccr4	zinc finger nuclease 2, Symbols: ZFN2
AT5G47760	-0.575	0.005	Depleted in ccr4	2-phosphoglycolate phosphatase 2, ...
AT5G50020	-0.577	0.029	Depleted in ccr4	DHHC-type zinc finger family protein
AT4G00231	-0.579	0.009	Depleted in ccr4	ARM repeat superfamily protein, Sy...
AT4G31580	-0.581	0.002	Depleted in ccr4	serine/arginine-rich 22, Symbols: ...
AT1G15500	-0.585	0.020	Depleted in ccr4	TLC ATP/ADP transporter, Symbols: ...
AT2G18040	-0.589	0.006	Depleted in ccr4	peptidylprolyl cis/trans isomerase...
AT5G25450	-0.590	0.001	Depleted in ccr4	Cytochrome bd ubiquinol oxidase, 1...

AT5G53000	-0.593	0.035	Depleted in ccr4	2A phosphatase associated protein ...
AT1G12410	-0.594	0.040	Depleted in ccr4	CLP protease proteolytic subunit 2...
AT4G20440	-0.594	0.006	Depleted in ccr4	small nuclear ribonucleoprotein as...
AT5G42980	-0.594	0.000	Depleted in ccr4	thioredoxin 3, Symbols: ATTRX3, AT...
AT1G59830	-0.600	0.020	Depleted in ccr4	protein phosphatase 2A-2, Symbols:...
AT4G30600	-0.603	0.004	Depleted in ccr4	signal recognition particle recept...
AT1G10940	-0.604	0.017	Depleted in ccr4	Protein kinase superfamily protein
AT3G51310	-0.605	0.005	Depleted in ccr4	VPS35 homolog C, Symbols: VPS35C
AT3G03210	-0.607	0.001	Depleted in ccr4	unknown protein
AT4G10750	-0.610	0.003	Depleted in ccr4	Phosphoenolpyruvate carboxylase fa...
AT2G37720	-0.611	0.003	Depleted in ccr4	TRICHOME BIREFRINGENCE-LIKE 15, Sy...
AT1G48090	-0.611	0.005	Depleted in ccr4	calcium-dependent lipid-binding fa...
AT2G42270	-0.613	0.025	Depleted in ccr4	U5 small nuclear ribonucleoprotein...
AT1G61010	-0.614	0.022	Depleted in ccr4	cleavage and polyadenylation speci...
AT3G02830	-0.617	0.001	Depleted in ccr4	zinc finger protein 1, Symbols: ZFN1
AT2G33730	-0.618	0.001	Depleted in ccr4	P-loop containing nucleoside triph...
AT1G19360	-0.620	0.022	Depleted in ccr4	Nucleotide-diphospho-sugar transfe...
AT4G20760	-0.621	0.018	Depleted in ccr4	NAD(P)-binding Rossmann-fold super...
AT5G64510	-0.623	0.044	Depleted in ccr4	unknown protein
AT3G07950	-0.624	0.011	Depleted in ccr4	rhomboid protein-related
AT4G16580	-0.625	0.007	Depleted in ccr4	Protein phosphatase 2C family protein
AT1G04870	-0.626	0.047	Depleted in ccr4	protein arginine methyltransferase...
AT1G70320	-0.626	0.001	Depleted in ccr4	ubiquitin-protein ligase 2, Symbol...
AT5G05970	-0.630	0.036	Depleted in ccr4	Transducin/WD40 repeat-like superf...
AT4G15955	-0.630	0.041	Depleted in ccr4	alpha/beta-Hydrolases superfamily ...
AT1G29310	-0.630	0.000	Depleted in ccr4	SecY protein transport family protein
AT3G56130	-0.631	0.022	Depleted in ccr4	biotin/lipoyl attachment domain-co...
AT3G42170	-0.633	0.001	Depleted in ccr4	BED zinc finger ;hAT family dimeri...
AT4G16360	-0.634	0.003	Depleted in ccr4	5'-AMP-activated protein kinase be...
AT2G39260	-0.634	0.029	Depleted in ccr4	binding;RNA binding
AT1G10430	-0.634	0.017	Depleted in ccr4	protein phosphatase 2A-2, Symbols:...
AT1G03030	-0.634	0.012	Depleted in ccr4	P-loop containing nucleoside triph...
AT5G44265	-0.635	0.010	Depleted in ccr4	Bifunctional inhibitor/lipid-trans...
AT4G26110	-0.639	0.009	Depleted in ccr4	nucleosome assembly protein1;1, Sy...
AT5G01500	-0.648	0.019	Depleted in ccr4	thylakoid ATP/ADP carrier, Symbols...
AT4G01810	-0.650	0.044	Depleted in ccr4	Sec23/Sec24 protein transport fami...
AT4G18040	-0.651	0.001	Depleted in ccr4	eukaryotic translation initiation ...
AT1G69960	-0.653	0.018	Depleted in ccr4	serine/threonine protein phosphata...
AT5G59710	-0.654	0.025	Depleted in ccr4	VIRE2 interacting protein 2, Symbo...
AT5G40260	-0.658	0.003	Depleted in ccr4	Nodulin MtN3 family protein, Symbo...
AT1G04190	-0.661	0.019	Depleted in ccr4	Tetratricopeptide repeat (TPR)-lik...
AT2G38770	-0.665	0.017	Depleted in ccr4	P-loop containing nucleoside triph...
AT4G20720	-0.667	0.017	Depleted in ccr4	dentin sialophosphoprotein-related
AT1G68710	-0.668	0.000	Depleted in ccr4	ATPase E1-E2 type family protein /...
AT4G36440	-0.672	0.012	Depleted in ccr4	unknown protein
AT1G04910	-0.673	0.008	Depleted in ccr4	O-fucosyltransferase family protein
AT1G56360	-0.675	0.002	Depleted in ccr4	purple acid phosphatase 6, Symbols...
AT1G27540	-0.675	0.016	Depleted in ccr4	Protein of unknown function (DUF295)
AT3G59455	-0.682	0.000	Depleted in ccr4	Bifunctional inhibitor/lipid-trans...
AT3G13330	-0.683	0.040	Depleted in ccr4	proteasome activating protein 200,...
AT1G10130	-0.684	0.002	Depleted in ccr4	endoplasmic reticulum-type calcium...
AT3G19870	-0.686	0.008	Depleted in ccr4	unknown protein
AT5G19860	-0.686	0.022	Depleted in ccr4	Protein of unknown function, DUF538
AT1G03150	-0.686	0.038	Depleted in ccr4	Acyl-CoA N-acyltransferases (NAT) ...
AT3G52230	-0.690	0.000	Depleted in ccr4	unknown protein
AT3G03890	-0.690	0.001	Depleted in ccr4	FMN binding
AT1G76150	-0.691	0.008	Depleted in ccr4	enoyl-CoA hydratase 2, Symbols: EC...
AT4G39220	-0.692	0.000	Depleted in ccr4	Rer1 family protein, Symbols: ATRER1A
AT1G26160	-0.693	0.005	Depleted in ccr4	Metal-dependent phosphohydrolase
AT5G16130	-0.693	0.001	Depleted in ccr4	Ribosomal protein S7e family protein
AT4G23850	-0.694	0.000	Depleted in ccr4	AMP-dependent synthetase and ligas...
AT2G44310	-0.694	0.001	Depleted in ccr4	Calcium-binding EF-hand family pro...
AT4G33640	-0.694	0.004	Depleted in ccr4	unknown protein
AT5G57900	-0.696	0.019	Depleted in ccr4	SKP1 interacting partner 1, Symbol...
AT4G26780	-0.696	0.007	Depleted in ccr4	Co-chaperone GrpE family protein, ...
AT5G24350	-0.696	0.002	Depleted in ccr4	unknown protein
AT1G80110	-0.697	0.004	Depleted in ccr4	phloem protein 2-B11, Symbols: ATP...
AT5G22650	-0.706	0.006	Depleted in ccr4	histone deacetylase 2B, Symbols: H...
AT2G19480	-0.707	0.004	Depleted in ccr4	nucleosome assembly protein 1;2, S...
AT5G13500	-0.712	0.049	Depleted in ccr4	unknown protein
AT4G23710	-0.713	0.001	Depleted in ccr4	vacuolar ATP synthase subunit G2, ...
AT5G60930	-0.716	0.012	Depleted in ccr4	P-loop containing nucleoside triph...
AT1G27450	-0.716	0.001	Depleted in ccr4	adenine phosphoribosyl transferase...
AT2G35900	-0.719	0.013	Depleted in ccr4	unknown protein
AT3G50360	-0.722	0.003	Depleted in ccr4	centrin2, Symbols: ATCEN2, CEN1, CEN2
AT4G25360	-0.724	0.002	Depleted in ccr4	TRICHOME BIREFRINGENCE-LIKE 18, Sy...
AT1G45150	-0.724	0.007	Depleted in ccr4	unknown protein
AT4G08550	-0.730	0.006	Depleted in ccr4	electron carriers;protein disulfid...
AT1G64760	-0.730	0.001	Depleted in ccr4	O-Glycosyl hydrolases family 17 pr...
AT3G20970	-0.730	0.010	Depleted in ccr4	NFU domain protein 4, Symbols: NFU...
AT1G06900	-0.731	0.026	Depleted in ccr4	Insulinase (Peptidase family M16) ...
AT1G76690	-0.733	0.002	Depleted in ccr4	12-oxophytodienoate reductase 2, S...
ATCG00270	-0.741	0.043	Depleted in ccr4	photosystem II reaction center pro...
AT1G48110	-0.742	0.009	Depleted in ccr4	evolutionarily conserved C-termina...
AT2G24940	-0.743	0.008	Depleted in ccr4	membrane-associated progesterone b...
AT1G78870	-0.745	0.006	Depleted in ccr4	ubiquitin-conjugating enzyme 35, S...
AT5G20710	-0.753	0.000	Depleted in ccr4	beta-galactosidase 7, Symbols: BGAL7

AT3G24360	-0.754	0.006	Depleted in ccr4	ATP-dependent caseinolytic (Clp) p...
AT5G58100	-0.755	0.004	Depleted in ccr4	unknown protein
AT3G02020	-0.761	0.003	Depleted in ccr4	aspartate kinase 3, Symbols: AK3
AT1G43710	-0.761	0.001	Depleted in ccr4	Pyridoxal phosphate (PLP)-dependen...
AT5G54170	-0.762	0.002	Depleted in ccr4	Polyketide cyclase/dehydrase and l...
AT1G17745	-0.763	0.000	Depleted in ccr4	D-3-phosphoglycerate dehydrogenase...
AT4G00585	-0.765	0.003	Depleted in ccr4	unknown protein
AT5G03370	-0.768	0.019	Depleted in ccr4	acylphosphatase family
AT4G03200	-0.768	0.041	Depleted in ccr4	catalytics
AT4G13450	-0.771	0.035	Depleted in ccr4	Adenine nucleotide alpha hydrolase...
AT5G15340	-0.771	0.000	Depleted in ccr4	Pentatricopeptide repeat (PPR) sup...
AT4G21120	-0.771	0.001	Depleted in ccr4	amino acid transporter 1, Symbols:...
AT3G14010	-0.778	0.000	Depleted in ccr4	CTC-interacting domain 4, Symbols:...
AT1G76300	-0.778	0.002	Depleted in ccr4	snRNP core protein SMD3, Symbols: ...
AT5G58490	-0.778	0.000	Depleted in ccr4	NAD(P)-binding Rossmann-fold super...
AT5G21050	-0.781	0.001	Depleted in ccr4	unknown protein
AT5G25530	-0.783	0.000	Depleted in ccr4	DNAJ heat shock family protein
AT1G60940	-0.784	0.030	Depleted in ccr4	SNF1-related protein kinase 2.10, ...
AT5G40370	-0.789	0.010	Depleted in ccr4	Glutaredoxin family protein
AT5G18800	-0.790	0.000	Depleted in ccr4	Cox19-like CHCH family protein
AT5G22790	-0.790	0.005	Depleted in ccr4	reticulata-related 1, Symbols: RER1
AT5G62750	-0.792	0.001	Depleted in ccr4	unknown protein
AT1G16890	-0.793	0.006	Depleted in ccr4	ubiquitin-conjugating enzyme 36, S...
AT1G35220	-0.795	0.000	Depleted in ccr4	unknown protein
AT3G05520	-0.798	0.001	Depleted in ccr4	Subunits of heterodimeric actin fi...
AT4G15020	-0.799	0.028	Depleted in ccr4	hAT transposon superfamily
AT2G18740	-0.801	0.010	Depleted in ccr4	Small nuclear ribonucleoprotein fa...
AT5G26570	-0.801	0.044	Depleted in ccr4	catalytics;carbohydrate kinases;ph...
AT2G19760	-0.802	0.002	Depleted in ccr4	profilin 1, Symbols: PFN1, PRF1
AT5G14240	-0.803	0.037	Depleted in ccr4	Thioredoxin superfamily protein
AT3G11070	-0.804	0.016	Depleted in ccr4	Outer membrane OMP85 family protein
AT5G20890	-0.807	0.000	Depleted in ccr4	TCP-1/cpn60 chaperonin family protein
AT4G15240	-0.808	0.000	Depleted in ccr4	Protein of unknown function (DUF604)
AT5G19130	-0.809	0.002	Depleted in ccr4	GPI transamidase component family ...
AT5G06410	-0.810	0.001	Depleted in ccr4	DNAJ heat shock N-terminal domain-...
AT1G76270	-0.810	0.027	Depleted in ccr4	O-fucosyltransferase family protein
AT1G09770	-0.813	0.028	Depleted in ccr4	cell division cycle 5, Symbols: AT...
AT1G72175	-0.815	0.011	Depleted in ccr4	RING/U-box protein with domain of ...
AT5G46210	-0.816	0.000	Depleted in ccr4	cullin4, Symbols: CUL4, ATCUL4
AT5G59810	-0.817	0.022	Depleted in ccr4	Subtilase family protein, Symbols:...
AT2G38680	-0.822	0.040	Depleted in ccr4	5'-nucleotidases;magnesium ion bin...
AT1G27650	-0.823	0.044	Depleted in ccr4	U2 snRNP auxiliary factor small su...
AT3G44620	-0.824	0.016	Depleted in ccr4	protein tyrosine phosphatases;prot...
AT2G46580	-0.832	0.015	Depleted in ccr4	Pyridoxamine 5'-phosphate oxidase ...
AT2G16405	-0.832	0.034	Depleted in ccr4	Transducin/WD40 repeat-like superf...
AT1G66240	-0.836	0.001	Depleted in ccr4	homolog of anti-oxidant 1, Symbols...
AT3G49590	-0.836	0.025	Depleted in ccr4	Autophagy-related protein 13
AT3G22850	-0.843	0.000	Depleted in ccr4	Aluminium induced protein with YGL...
AT1G43620	-0.844	0.044	Depleted in ccr4	UDP-Glycosyltransferase superfamil...
AT3G17210	-0.847	0.019	Depleted in ccr4	heat stable protein 1, Symbols: AT...
AT4G39860	-0.859	0.011	Depleted in ccr4	unknown protein
AT4G30550	-0.866	0.006	Depleted in ccr4	Class I glutamine amidotransferase...
AT4G15802	-0.866	0.004	Depleted in ccr4	heat shock factor binding protein,...
AT2G07040	-0.867	0.011	Depleted in ccr4	Leucine-rich repeat protein kinase...
AT5G37590	-0.870	0.021	Depleted in ccr4	Tetratricopeptide repeat (TPR)-lik...
AT4G04770	-0.872	0.003	Depleted in ccr4	ATP binding cassette protein 1, Sy...
AT5G15680	-0.873	0.016	Depleted in ccr4	ARM repeat superfamily protein
AT2G27200	-0.877	0.007	Depleted in ccr4	P-loop containing nucleoside triph...
AT1G53040	-0.884	0.023	Depleted in ccr4	Protein of unknown function (DUF616)
AT3G60740	-0.887	0.000	Depleted in ccr4	ARM repeat superfamily protein, Sy...
AT5G13610	-0.887	0.031	Depleted in ccr4	Protein of unknown function (DUF155)
AT5G42370	-0.891	0.000	Depleted in ccr4	Calcineurin-like metallo-phosphoes...
AT4G35450	-0.892	0.000	Depleted in ccr4	ankyrin repeat-containing protein ...
AT2G02140	-0.893	0.001	Depleted in ccr4	low-molecular-weight cysteine-rich...
AT5G39730	-0.895	0.005	Depleted in ccr4	AIG2-like (avirulence induced gene...
AT3G63150	-0.898	0.000	Depleted in ccr4	MIRO-related GTP-ase 2, Symbols: M...
AT5G19660	-0.898	0.008	Depleted in ccr4	SITE-1 protease, Symbols: ATSBT6.1...
AT4G14110	-0.901	0.021	Depleted in ccr4	COP9 signalosome, subunit CSN8, Sy...
AT4G32960	-0.909	0.007	Depleted in ccr4	unknown protein
AT3G14270	-0.916	0.021	Depleted in ccr4	phosphatidylinositol-4-phosphate 5...
AT1G77470	-0.925	0.024	Depleted in ccr4	replication factor C subunit 3, Sy...
AT1G15200	-0.929	0.037	Depleted in ccr4	protein-protein interaction regula...
AT1G68690	-0.936	0.018	Depleted in ccr4	Protein kinase superfamily protein
AT4G28088	-0.940	0.002	Depleted in ccr4	Low temperature and salt responsiv...
AT1G08630	-0.943	0.017	Depleted in ccr4	threonine aldolase 1, Symbols: THA1
AT2G18600	-0.944	0.029	Depleted in ccr4	Ubiquitin-conjugating enzyme famil...
AT5G16150	-0.945	0.000	Depleted in ccr4	plastidic GLC translocator, Symbol...
AT5G19400	-0.948	0.005	Depleted in ccr4	Telomerase activating protein Est1...
AT3G58680	-0.951	0.001	Depleted in ccr4	multiprotein bridging factor 1B, S...
AT5G10270	-0.952	0.037	Depleted in ccr4	cyclin-dependent kinase C;1, Symbo...
AT2G35820	-0.954	0.001	Depleted in ccr4	ureidoglycolate hydrolases
AT1G26640	-0.962	0.010	Depleted in ccr4	Amino acid kinase family protein
AT4G12430	-0.965	0.008	Depleted in ccr4	Haloacid dehalogenase-like hydrola...
AT3G16830	-0.969	0.011	Depleted in ccr4	TOPLESS-related 2, Symbols: TPR2
AT4G27480	-0.969	0.001	Depleted in ccr4	Core-2/I-branching beta-1,6-N-acet...
AT5G17990	-0.970	0.030	Depleted in ccr4	tryptophan biosynthesis 1, Symbols...
AT5G05480	-0.970	0.002	Depleted in ccr4	Peptide-N4-(N-acetyl-beta-glucosam...

AT5G10050	-0.975	0.001	Depleted in ccr4	NAD(P)-binding Rossmann-fold super...
AT4G08900	-0.975	0.000	Depleted in ccr4	arginase
AT1G65320	-0.976	0.035	Depleted in ccr4	Cystathionine beta-synthase (CBS) ...
AT1G23900	-0.978	0.011	Depleted in ccr4	gamma-adaptin 1, Symbols: GAMMA-AD...
AT5G19150	-0.979	0.035	Depleted in ccr4	pfkB-like carbohydrate kinase fami...
AT1G65520	-0.984	0.007	Depleted in ccr4	delta(3), delta(2)-enoyl CoA isome...
AT5G64130	-0.987	0.000	Depleted in ccr4	cAMP-regulated phosphoprotein 19-r...
AT4G24570	-0.990	0.007	Depleted in ccr4	dicarboxylate carrier 2, Symbols: ...
AT4G24770	-0.996	0.001	Depleted in ccr4	31-kDa RNA binding protein, Symbol...
AT4G03420	-1.001	0.027	Depleted in ccr4	Protein of unknown function (DUF789)
AT5G65260	-1.004	0.001	Depleted in ccr4	RNA-binding (RRM/RBD/RNP motifs) f...
AT3G52190	-1.012	0.033	Depleted in ccr4	phosphate transporter traffic faci...
AT2G37790	-1.015	0.009	Depleted in ccr4	NAD(P)-linked oxidoreductase super...
AT1G70170	-1.015	0.010	Depleted in ccr4	matrix metalloproteinase, Symbols:...
AT2G29530	-1.015	0.000	Depleted in ccr4	Tim10/DDP family zinc finger prote...
AT1G04120	-1.021	0.001	Depleted in ccr4	multidrug resistance-associated pr...
AT4G27420	-1.026	0.030	Depleted in ccr4	ABC-2 type transporter family protein
AT1G79090	-1.030	0.035	Depleted in ccr4	unknown protein
AT2G25840	-1.032	0.009	Depleted in ccr4	Nucleotidylyl transferase superfam...
AT1G18700	-1.032	0.017	Depleted in ccr4	DNAJ heat shock N-terminal domain-...
AT2G39970	-1.033	0.001	Depleted in ccr4	Mitochondrial substrate carrier fa...
AT1G04890	-1.042	0.000	Depleted in ccr4	Protein of unknown function, DUF593
AT1G77610	-1.042	0.024	Depleted in ccr4	EamA-like transporter family protein
AT2G25110	-1.043	0.030	Depleted in ccr4	stromal cell-derived factor 2-like...
AT5G60615	-1.044	0.001	Depleted in ccr4	Defensin-like (DEFL) family protein
AT2G01650	-1.048	0.006	Depleted in ccr4	plant UBX domain-containing protei...
AT5G47840	-1.062	0.021	Depleted in ccr4	adenosine monophosphate kinase, Sy...
AT2G24590	-1.063	0.000	Depleted in ccr4	RNA recognition motif and CCHC-typ...
AT3G43120	-1.063	0.020	Depleted in ccr4	SAUR-like auxin-responsive protein...
AT1G04440	-1.070	0.003	Depleted in ccr4	casein kinase like 13, Symbols: CKL13
AT3G47410	-1.074	0.000	Depleted in ccr4	unknown protein
AT4G12790	-1.074	0.047	Depleted in ccr4	P-loop containing nucleoside triph...
AT3G25150	-1.075	0.007	Depleted in ccr4	Nuclear transport factor 2 (NTF2) ...
AT2G17200	-1.077	0.002	Depleted in ccr4	ubiquitin family protein, Symbols:...
AT2G01490	-1.078	0.005	Depleted in ccr4	phytanoyl-CoA dioxygenase (PhyH) f...
AT1G20200	-1.078	0.000	Depleted in ccr4	PAM domain (PCI/PINT associated mo...
AT3G62710	-1.081	0.011	Depleted in ccr4	Glycosyl hydrolase family protein
AT3G05000	-1.083	0.001	Depleted in ccr4	Transport protein particle (TRAPP)...
AT1G49740	-1.088	0.045	Depleted in ccr4	PLC-like phosphodiesterases superf...
AT5G56950	-1.088	0.003	Depleted in ccr4	nucleosome assembly protein 1;3, S...
AT5G40490	-1.094	0.005	Depleted in ccr4	RNA-binding (RRM/RBD/RNP motifs) f...
AT5G08560	-1.100	0.005	Depleted in ccr4	transducin family protein / WD-40 ...
AT3G02320	-1.102	0.001	Depleted in ccr4	N2,N2-dimethylguanosine tRNA methy...
AT3G46510	-1.107	0.006	Depleted in ccr4	plant U-box 13, Symbols: PUB13, AT...
AT1G80780	-1.110	0.001	Depleted in ccr4	Polynucleotidyl transferase, ribon...
AT2G24490	-1.111	0.000	Depleted in ccr4	replicon protein A2, Symbols: RPA2...
AT3G50050	-1.113	0.000	Depleted in ccr4	Eukaryotic aspartyl protease famil...
AT5G50640	-1.119	0.000	Depleted in ccr4	CBS / octicosapeptide/...
AT1G47280	-1.126	0.000	Depleted in ccr4	unknown protein
AT2G20930	-1.133	0.019	Depleted in ccr4	SNARE-like superfamily protein
AT2G32810	-1.136	0.002	Depleted in ccr4	beta galactosidase 9, Symbols: BGAL9
AT1G04530	-1.139	0.000	Depleted in ccr4	Tetratricopeptide repeat (TPR)-lik...
AT3G09350	-1.142	0.014	Depleted in ccr4	Fes1A, Symbols: Fes1A
AT2G34585	-1.142	0.037	Depleted in ccr4	unknown protein
AT1G20110	-1.146	0.002	Depleted in ccr4	RING/FYVE/PHD zinc finger superfam...
AT2G06530	-1.153	0.002	Depleted in ccr4	SNF7 family protein, Symbols: VPS2.1
AT2G33340	-1.155	0.003	Depleted in ccr4	MOS4-associated complex 3B, Symbo...
AT3G03340	-1.162	0.001	Depleted in ccr4	LUC7 related protein, Symbols: UNE6
AT1G31812	-1.167	0.000	Depleted in ccr4	acyl-CoA-binding protein 6, Symbol...
AT1G76550	-1.168	0.001	Depleted in ccr4	Phosphofructokinase family protein
AT5G06680	-1.168	0.000	Depleted in ccr4	spindle pole body component 98, Sy...
AT1G10280	-1.170	0.006	Depleted in ccr4	Core-2/I-branching beta-1,6-N-acet...
AT4G08960	-1.171	0.010	Depleted in ccr4	phosphotyrosyl phosphatase activat...
AT2G48020	-1.178	0.000	Depleted in ccr4	Major facilitator superfamily protein
AT4G25150	-1.183	0.001	Depleted in ccr4	HAD superfamily, subfamily IIIB ac...
AT1G09010	-1.186	0.001	Depleted in ccr4	glycoside hydrolase family 2 protein
AT5G63310	-1.189	0.000	Depleted in ccr4	nucleoside diphosphate kinase 2, S...
AT1G08780	-1.197	0.003	Depleted in ccr4	ABI3-interacting protein 3, Symbol...
AT5G55160	-1.202	0.000	Depleted in ccr4	small ubiquitin-like modifier 2, S...
AT4G25890	-1.210	0.049	Depleted in ccr4	60S acidic ribosomal protein family
AT5G58330	-1.210	0.001	Depleted in ccr4	lactate/malate dehydrogenase famil...
AT5G49540	-1.211	0.020	Depleted in ccr4	Rab5-interacting family protein
AT4G36350	-1.213	0.001	Depleted in ccr4	purple acid phosphatase 25, Symbol...
AT2G43240	-1.221	0.002	Depleted in ccr4	Nucleotide-sugar transporter famil...
AT1G20950	-1.223	0.008	Depleted in ccr4	Phosphofructokinase family protein
AT1G77060	-1.225	0.001	Depleted in ccr4	Phosphoenolpyruvate carboxylase fa...
AT1G70570	-1.226	0.034	Depleted in ccr4	anthranilate phosphoribosyltransfe...
AT4G39090	-1.229	0.006	Depleted in ccr4	Papain family cysteine protease, S...
AT3G16310	-1.239	0.008	Depleted in ccr4	mitotic phosphoprotein N' end (MPP...
AT5G51880	-1.240	0.000	Depleted in ccr4	2-oxoglutarate (2OG) and Fe(II)-de...
AT5G45840	-1.243	0.000	Depleted in ccr4	Leucine-rich repeat protein kinase...
AT4G24730	-1.246	0.011	Depleted in ccr4	Calcineurin-like metallo-phosphoes...
AT2G17190	-1.250	0.001	Depleted in ccr4	ubiquitin family protein
AT1G16010	-1.259	0.001	Depleted in ccr4	magnesium transporter 2, Symbols: ...
AT3G51520	-1.271	0.015	Depleted in ccr4	diacylglycerol acyltransferase family
AT1G25420	-1.277	0.000	Depleted in ccr4	Regulator of Vps4 activity in the ...
AT4G34890	-1.280	0.000	Depleted in ccr4	xanthine dehydrogenase 1, Symbols:...

AT4G35335	-1.282	0.002	Depleted in ccr4	Nucleotide-sugar transporter famil...
AT1G58230	-1.289	0.014	Depleted in ccr4	binding
AT5G56730	-1.291	0.000	Depleted in ccr4	Insulinase (Peptidase family M16) ...
AT1G54860	-1.293	0.000	Depleted in ccr4	Glycoprotein membrane precursor GP...
AT5G61350	-1.308	0.002	Depleted in ccr4	Protein kinase superfamily protein
AT1G64040	-1.316	0.000	Depleted in ccr4	type one serine/threonine protein ...
AT4G01290	-1.321	0.000	Depleted in ccr4	unknown protein
AT5G59950	-1.322	0.000	Depleted in ccr4	RNA-binding (RRM/RBD/RNP motifs) f...
AT1G22150	-1.331	0.000	Depleted in ccr4	sulfate transporter 1;3, Symbols: ...
AT4G31310	-1.336	0.006	Depleted in ccr4	AIG2-like (avirulence induced gene...
AT4G33410	-1.344	0.030	Depleted in ccr4	SIGNAL PEPTIDE PEPTIDASE-LIKE 1, S...
AT5G09680	-1.347	0.001	Depleted in ccr4	reduced lateral root formation, Sy...
AT3G54240	-1.354	0.004	Depleted in ccr4	alpha/beta-Hydrolases superfamily ...
AT5G57000	-1.355	0.000	Depleted in ccr4	unknown protein
AT3G62030	-1.363	0.001	Depleted in ccr4	rotamase CYP 4, Symbols: ROC4
AT2G28520	-1.376	0.001	Depleted in ccr4	vacuolar proton ATPase A1, Symbols...
AT4G27750	-1.377	0.008	Depleted in ccr4	binding, Symbols: ISI1
AT4G05090	-1.378	0.001	Depleted in ccr4	Inositol monophosphatase family pr...
AT1G78920	-1.382	0.008	Depleted in ccr4	vacuolar H+-pyrophosphatase 2, Sym...
AT3G46960	-1.386	0.043	Depleted in ccr4	RNA helicase, ATP-dependent, SK12/...
AT5G56150	-1.387	0.000	Depleted in ccr4	ubiquitin-conjugating enzyme 30, S...
AT2G36070	-1.391	0.011	Depleted in ccr4	translocase inner membrane subunit...
AT1G06540	-1.392	0.004	Depleted in ccr4	unknown protein
AT3G08890	-1.399	0.001	Depleted in ccr4	Protein of unknown function, DUF538
AT5G43340	-1.404	0.017	Depleted in ccr4	phosphate transporter 1;6, Symbols...
AT3G51550	-1.406	0.000	Depleted in ccr4	Malectin/receptor-like protein kin...
AT4G09150	-1.406	0.000	Depleted in ccr4	T-complex protein 11
AT3G47833	-1.413	0.000	Depleted in ccr4	unknown protein
AT5G03650	-1.416	0.000	Depleted in ccr4	starch branching enzyme 2.2, Symbo...
AT5G17550	-1.421	0.005	Depleted in ccr4	peroxin 19-2, Symbols: PEX19-2, At...
AT4G28860	-1.430	0.027	Depleted in ccr4	casein kinase I-like 4, Symbols: ckl4
AT4G19880	-1.431	0.000	Depleted in ccr4	Glutathione S-transferase family p...
AT1G71695	-1.439	0.002	Depleted in ccr4	Peroxidase superfamily protein
AT1G57620	-1.444	0.013	Depleted in ccr4	emp24/gp25L/p24 family/GOLD family...
AT5G42770	-1.450	0.000	Depleted in ccr4	Maf-like protein
AT5G16120	-1.455	0.004	Depleted in ccr4	alpha/beta-Hydrolases superfamily ...
AT3G53180	-1.465	0.000	Depleted in ccr4	glutamate-ammonia ligases;catalyti...
AT1G52670	-1.471	0.003	Depleted in ccr4	Single hybrid motif superfamily pr...
AT2G47320	-1.491	0.002	Depleted in ccr4	Cyclophilin-like peptidyl-prolyl c...
AT3G15880	-1.506	0.000	Depleted in ccr4	WUS-interacting protein 2, Symbols...
AT3G19770	-1.523	0.008	Depleted in ccr4	Vacuolar sorting protein 9 (VPS9) ...
AT4G34310	-1.530	0.007	Depleted in ccr4	alpha/beta-Hydrolases superfamily ...
AT1G24020	-1.535	0.001	Depleted in ccr4	MLP-like protein 423, Symbols: MLP423
AT2G23310	-1.541	0.001	Depleted in ccr4	Rer1 family protein, Symbols: ATRE...
AT4G14600	-1.544	0.000	Depleted in ccr4	Target SNARE coiled-coil domain pr...
AT4G33360	-1.547	0.009	Depleted in ccr4	NAD(P)-binding Rossmann-fold super...
AT5G64640	-1.547	0.000	Depleted in ccr4	Plant invertase/pectin methylester...
AT1G76860	-1.571	0.001	Depleted in ccr4	Small nuclear ribonucleoprotein fa...
AT2G47250	-1.577	0.004	Depleted in ccr4	RNA helicase family protein
AT1G53290	-1.580	0.001	Depleted in ccr4	Galactosyltransferase family protein
AT5G65890	-1.586	0.002	Depleted in ccr4	ACT domain repeat 1, Symbols: ACR1
AT3G51780	-1.600	0.000	Depleted in ccr4	BCL-2-associated athanogene 4, Sym...
AT5G08100	-1.602	0.000	Depleted in ccr4	N-terminal nucleophile aminohydrol...
AT5G23890	-1.612	0.000	Depleted in ccr4	unknown protein
AT5G55950	-1.618	0.002	Depleted in ccr4	Nucleotide/sugar transporter famil...
AT3G15350	-1.628	0.000	Depleted in ccr4	Core-2/I-branching beta-1,6-N-acet...
AT4G38800	-1.634	0.023	Depleted in ccr4	methylthioadenosine nucleosidase 1...
AT1G18800	-1.637	0.000	Depleted in ccr4	NAP1-related protein 2, Symbols: NRP2
AT4G11980	-1.640	0.002	Depleted in ccr4	nudix hydrolase homolog 14, Symbol...
AT3G56600	-1.641	0.001	Depleted in ccr4	Protein kinase superfamily protein
AT5G51820	-1.661	0.011	Depleted in ccr4	phosphoglucomutase, Symbols: PGM, ...
AT5G09880	-1.669	0.000	Depleted in ccr4	Splicing factor, CC1-like
AT3G28700	-1.722	0.000	Depleted in ccr4	Protein of unknown function (DUF185)
AT2G39820	-1.734	0.007	Depleted in ccr4	Translation initiation factor IF6
AT5G17500	-1.754	0.000	Depleted in ccr4	Glycosyl hydrolase superfamily pro...
AT2G33690	-1.756	0.008	Depleted in ccr4	Late embryogenesis abundant protei...
AT5G53510	-1.768	0.000	Depleted in ccr4	oligopeptide transporter 9, Symbol...
AT1G51730	-1.807	0.035	Depleted in ccr4	Ubiquitin-conjugating enzyme famil...
AT1G03140	-1.810	0.033	Depleted in ccr4	splicing factor Prp18 family protein
AT3G29100	-1.856	0.000	Depleted in ccr4	vesicle transport V-snare 13, Symb...
AT2G06990	-1.862	0.023	Depleted in ccr4	RNA helicase, ATP-dependent, SK12/...
AT1G18450	-1.884	0.000	Depleted in ccr4	actin-related protein 4, Symbols: ...
AT3G13080	-1.916	0.000	Depleted in ccr4	multidrug resistance-associated pr...
AT3G52760	-1.936	0.000	Depleted in ccr4	Integral membrane Yip1 family protein
AT5G12410	-1.964	0.000	Depleted in ccr4	THUMP domain-containing protein
AT3G11825	-1.978	0.000	Depleted in ccr4	Bifunctional inhibitor/lipid-trans...
AT3G49430	-1.983	0.000	Depleted in ccr4	SER/ARG-rich protein 34A, Symbols:...
AT3G03800	-2.001	0.010	Depleted in ccr4	syntaxin of plants 131, Symbols: S...
AT4G33380	-2.037	0.003	Depleted in ccr4	unknown protein
AT3G47780	-2.049	0.000	Depleted in ccr4	ABC2 homolog 6, Symbols: ATATH6, ATH6
AT3G02900	-2.071	0.000	Depleted in ccr4	unknown protein
AT4G37760	-2.075	0.000	Depleted in ccr4	squalene epoxidase 3, Symbols: SQE3
AT3G10620	-2.088	0.000	Depleted in ccr4	nudix hydrolase homolog 26, Symbol...
AT2G02740	-2.089	0.001	Depleted in ccr4	ssDNA-binding transcriptional regu...
AT5G18910	-2.094	0.002	Depleted in ccr4	Protein kinase superfamily protein
AT4G01897	-2.111	0.000	Depleted in ccr4	unknown protein
AT4G25230	-2.128	0.000	Depleted in ccr4	RPM1 interacting protein 2, Symbol...

AT3G05610	-2.155	0.000	Depleted in ccr4	Plant invertase/pectin methylester...
AT2G01320	-2.166	0.000	Depleted in ccr4	ABC-2 type transporter family protein
AT4G21540	-2.179	0.000	Depleted in ccr4	sphingosine kinase 1, Symbols: SPHK1
AT5G65160	-2.194	0.000	Depleted in ccr4	tetratricopeptide repeat (TPR)-con...
AT3G19640	-2.196	0.000	Depleted in ccr4	magnesium transporter 4, Symbols: ...
AT3G51150	-2.199	0.020	Depleted in ccr4	ATP binding microtubule motor fami...
AT3G05060	-2.222	0.003	Depleted in ccr4	NOP56-like pre RNA processing ribo...
AT1G03930	-2.266	0.000	Depleted in ccr4	dual specificity kinase 1, Symbols...
AT3G58560	-2.312	0.000	Depleted in ccr4	DNAse I-like superfamily protein
AT5G23110	-2.326	0.000	Depleted in ccr4	Zinc finger, C3HC4 type (RING fing...
AT1G51770	-2.341	0.000	Depleted in ccr4	Core-2/I-branching beta-1,6-N-acet...
AT3G18790	-2.346	0.000	Depleted in ccr4	unknown protein
AT5G57700	-2.411	0.001	Depleted in ccr4	BNR/Asp-box repeat family protein
AT5G48270	-2.420	0.002	Depleted in ccr4	Plant protein of unknown function ...
AT3G23020	-2.456	0.000	Depleted in ccr4	Tetratricopeptide repeat (TPR)-lik...
AT5G41730	-2.483	0.020	Depleted in ccr4	Protein kinase family protein
AT5G28740	-2.487	0.001	Depleted in ccr4	Tetratricopeptide repeat (TPR)-lik...
AT3G24040	-2.489	0.046	Depleted in ccr4	Core-2/I-branching beta-1,6-N-acet...
AT3G06260	-2.515	0.000	Depleted in ccr4	galacturonosyltransferase-like 4, ...
AT5G42000	-2.580	0.001	Depleted in ccr4	ORMDL family protein
AT1G79590	-2.584	0.046	Depleted in ccr4	syntaxin of plants 52, Symbols: SY...
AT5G57035	-2.645	0.000	Depleted in ccr4	U-box domain-containing protein ki...
AT5G24130	-2.691	0.000	Depleted in ccr4	unknown protein
AT3G13060	-2.771	0.000	Depleted in ccr4	evolutionarily conserved C-termina...
AT1G44790	-2.775	0.000	Depleted in ccr4	ChaC-like family protein
AT1G74560	-2.792	0.000	Depleted in ccr4	NAP1-related protein 1, Symbols: NRP1
AT4G29510	-2.793	0.017	Depleted in ccr4	arginine methyltransferase 11, Sym...
AT1G28335	-2.804	0.000	Depleted in ccr4	low-molecular-weight cysteine-rich...
AT1G54410	-2.824	0.000	Depleted in ccr4	dehydrin family protein
AT5G20950	-2.881	0.003	Depleted in ccr4	Glycosyl hydrolase family protein
AT5G27030	-2.896	0.000	Depleted in ccr4	TOPLESS-related 3, Symbols: TPR3
AT5G03540	-2.956	0.000	Depleted in ccr4	exocyst subunit exo70 family prote...
AT1G50510	-3.004	0.002	Depleted in ccr4	indigoidine synthase A family protein
AT5G48440	-3.135	0.000	Depleted in ccr4	FAD-dependent oxidoreductase famil...
AT1G02840	-3.148	0.000	Depleted in ccr4	RNA-binding (RRM/RBD/RNP motifs) f...
AT4G04040	-3.195	0.000	Depleted in ccr4	Phosphofructokinase family protein...
AT5G64200	-3.264	0.000	Depleted in ccr4	ortholog of human splicing factor ...
AT3G62010	-3.286	0.000	Depleted in ccr4	unknown protein
AT5G07120	-3.465	0.000	Depleted in ccr4	sorting nexin 2B, Symbols: SNX2b
AT2G22400	-3.607	0.000	Depleted in ccr4	S-adenosyl-L-methionine-dependent ...
AT4G32120	-3.945	0.000	Depleted in ccr4	Galactosyltransferase family protein
AT2G47490	-4.199	0.010	Depleted in ccr4	NAD+ transporter 1, Symbols: ATNDT...
AT5G40010	-4.283	0.000	Depleted in ccr4	AAA-ATPase 1, Symbols: AATP1
AT3G58580	-4.516	0.000	Depleted in ccr4	DNAse I-like superfamily protein
AT4G16745	-4.732	0.000	Depleted in ccr4	Exostosin family protein

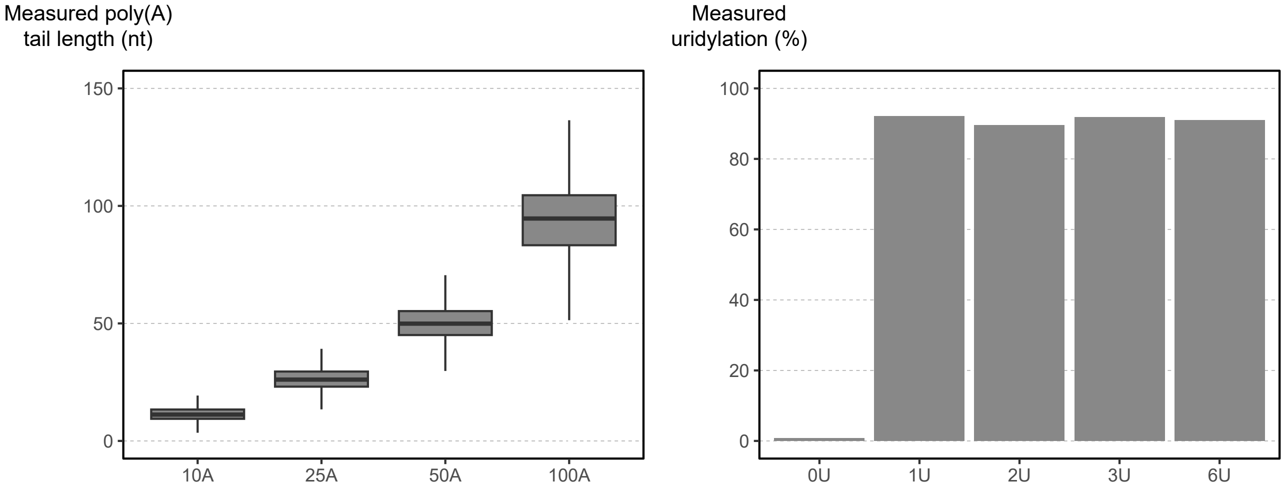

Figure S1. FLEP-seq2 efficiently measures the poly(A) tail and uridylation levels of custom spike-ins

A) FLEP-seq2 is accurately at measuring the length of poly(A) tails of up to 100 As (tested spike-in). Variability increases as the poly(A) tail gets longer, but the technique is much more accurate than Illumina-based techniques. The horizontal line in each box represents the median and lower and upper hinges indicate first and third quartiles, respectively. **B)** Uridylation levels of polyadenylated spike-ins with various size of uridine extensions, with no background measured using non-uridylated poly(A) spike-in. Spike-ins and sequencing experiments were conducted by Jeanne Roignant, former engineer of the team.

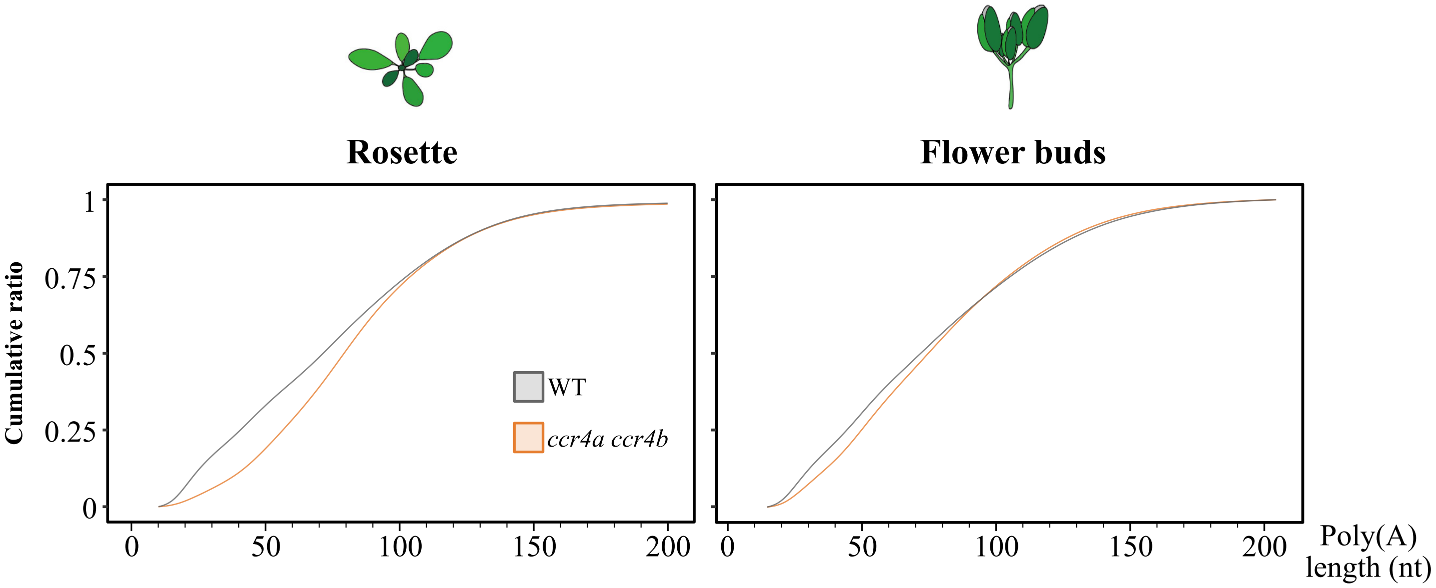

Figure S2. Cumulative curve for PASS calculation.

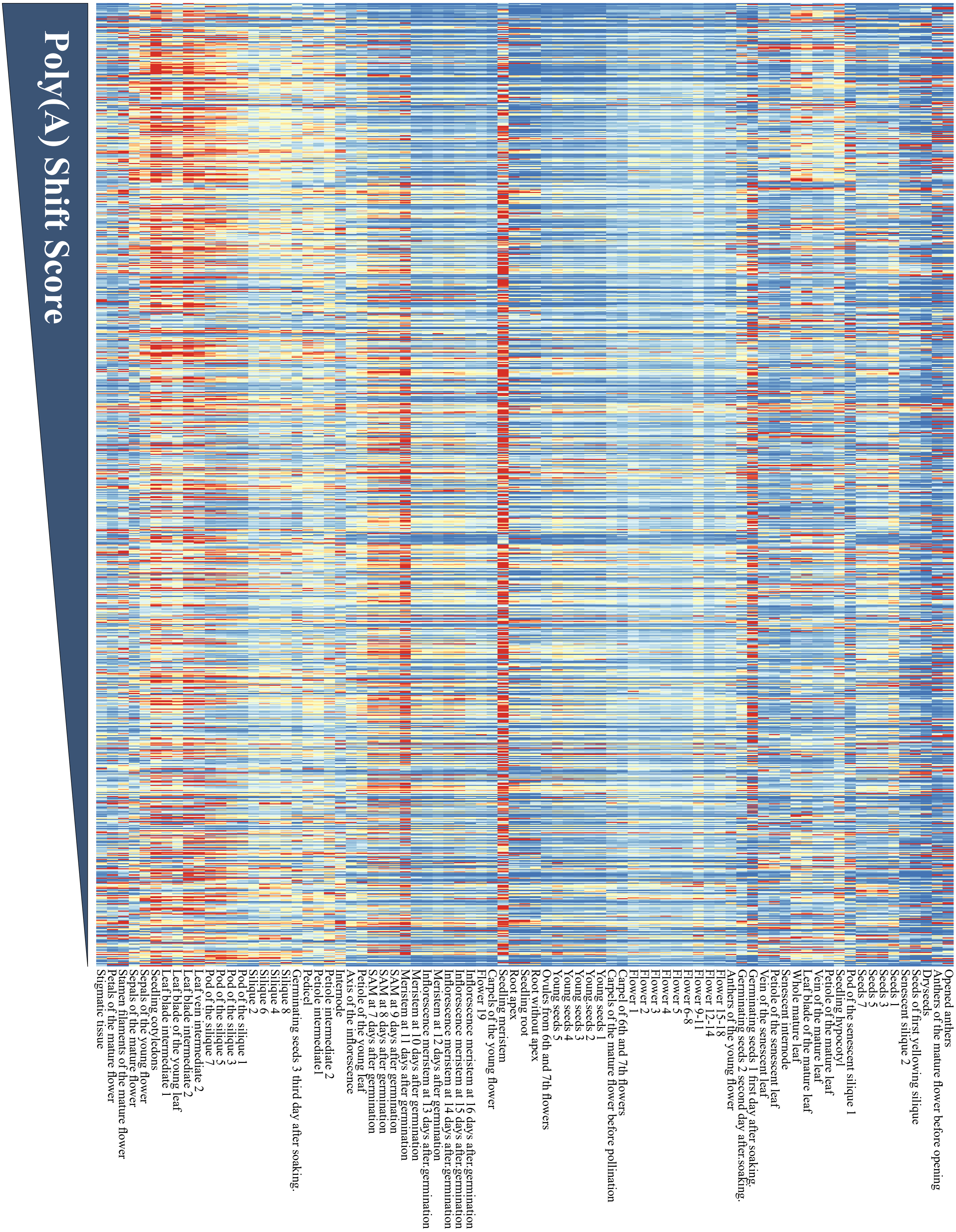

Figure S3. Full size gene expression atlas for rosette mRNAs.
Gene expression atlas for all 934 mRNAs identified in rosette with more than 200 reads per sample. Full size heatmap related to figure 24. 79 tissues/developmental stages were used to plot the heatmap.

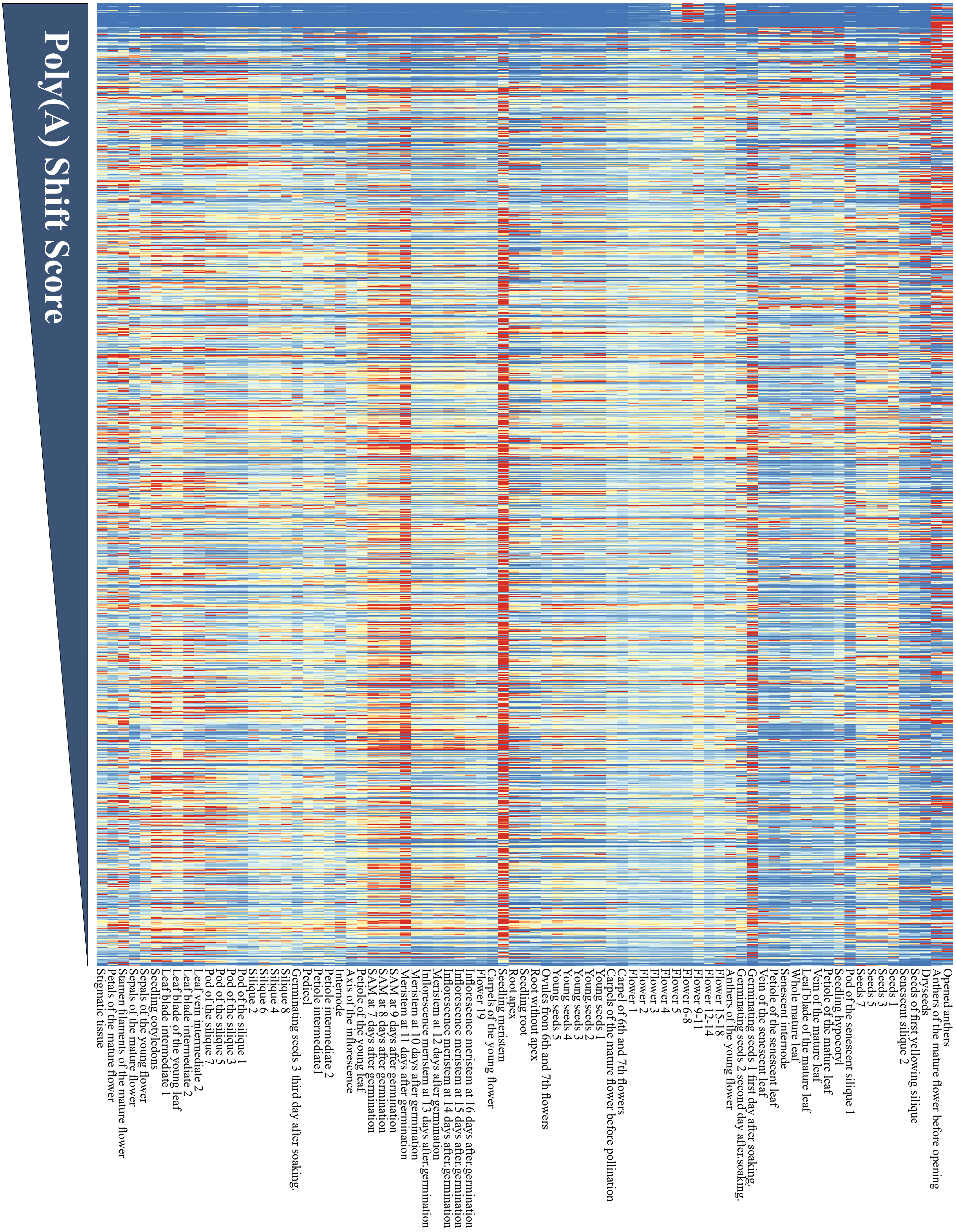

Figure S4. Full size gene expression atlas for flower buds mRNA.
Gene expression atlas for all 1182 mRNAs identified in flowers with more than 200 reads per sample. Full size heatmap related to figure 24. 79 tissues/developmental stages were used to plot the heatmap.

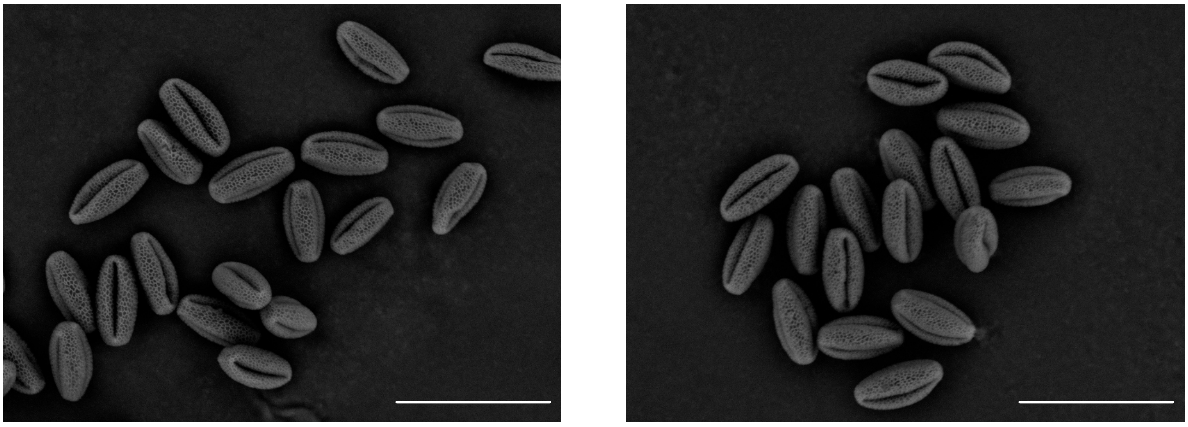

Wild-type ***ccr4a ccr4b***

Figure S5. No visible impact of *ccr4a ccr4b* mutation on pollen grain shape and aspect. Representative images of pollen grains from wild-type (left panel) and *ccr4a ccr4b* (right panel) observed by SEM. Scale bar: 50µm.

Université de Strasbourg

Quentin Simonnot

École Doctorale des Sciences de la Vie et de la Santé
STRASBOURG

Deciphering the roles of CCR4a and CCR4b deadenylases in the modulation of mRNA deadenylation and its interplay with uridylation in *Arabidopsis thaliana*

Résumé

L'interaction entre les différents facteurs de dégradation des ARN messagers (ARNm) joue un rôle crucial dans la régulation de l'expression génique. La déadénylation, le raccourcissement de la queue poly(A) des ARNm, constitue une étape préliminaire, tandis que l'uridylation, l'ajout d'uridines en 3' des ARNm, cible préférentiellement les ARNm déadénylés et favorise leur dégradation. De plus, chez *Arabidopsis*, l'uridylation prévient une déadénylation excessive des ARNm. Ce lien étroit entre uridylation et déadénylation souligne une coordination mécanistique importante des étapes du métabolisme des ARNm. **Mes travaux de thèse ont eu pour but de préciser les relations moléculaires qui régissent la déadénylation des ARNm par le complexe CCR4-NOT et leur subséquente uridylation par la TUTase URT1.** L'analyse par séquençage nanopore des ARNm d'une lignée mutante *ccr4a ccr4b* a démontré le rôle crucial des déadénylases majeures du complexe CCR4-NOT dans le façonnage particulier des queues poly(A), vraisemblablement impliqué lors de la réponse immunitaire et la germination du tube pollinique. De plus, l'activité de CCR4-NOT participe activement à la définition précise du profil d'uridylation des ARNm par URT1, puisque la diminution de la déadénylation provoque un allongement conséquent des queues poly(A) uridylées. Inversement, le niveau d'uridylation par URT1 influence directement l'ampleur de la déadénylation par CCR4-NOT. Enfin, j'ai identifié l'interaction d'URT1 avec EXA1, une protéine partenaire de CCR4-NOT. Ces résultats précisent les liens entre ces acteurs de la dégradation des ARNm, soulignant leur rôle conjoint dans la définition précise de l'extrémité 3' des ARNm.

Mots clés : déadénylation, uridylation, dégradation des ARNm, séquençage nanopore, Arabidopsis

Abstract

The interplay among different factors involved in messenger RNA (mRNA) degradation plays a crucial role in gene expression regulation. Deadenylation, the shortening of the poly(A) tail of mRNAs, serves as a preliminary step, while uridylation, the addition of uridines at the 3' end of mRNAs, selectively targets deadenylated mRNAs and favours their decay. Additionally, in *Arabidopsis*, uridylation prevents excessive mRNA deadenylation. This close connection between uridylation and deadenylation underscores a precise mechanistic coordination of mRNA metabolism processes. **My doctoral research aimed to elucidate the molecular relationship governing mRNA deadenylation by the CCR4-NOT complex and subsequent uridylation by the TUTase URT1.** RNA sequencing by nanopore of a *ccr4a ccr4b* double mutant demonstrated the crucial role of the major deadenylases of the CCR4-NOT complex in the precise shaping of poly(A) tails, likely essential for immune response and pollen tube germination. Furthermore, the CCR4-NOT complex actively contributes to the specific definition of uridylation profiles by URT1, as reduced deadenylation leads to a significant elongation of uridylated poly(A) tails. Conversely, the level of uridylation by URT1 directly influences the extent of deadenylation by CCR4-NOT. Finally, I identified the interaction between URT1 and EXA1, an interactant of CCR4-NOT. These findings shed light on the connections among mRNA degradation factors, emphasising their interplay in the precise definition of the 3' end of mRNAs.

Keywords: deadenylation, uridylation, mRNA degradation, nanopore sequencing, Arabidopsis

Résumé de la thèse

La dégradation des ARN est un processus essentiel dans le monde du vivant, devant être finement régulée pour garantir un développement optimal et une bonne adaptation aux conditions environnementales. La majorité des voies de dégradation des ARNm décrites jusqu'à présent chez les eucaryotes sont initiées par une étape de déadénylation, consistant au raccourcissement de la queue poly(A) des ARNm. La déadénylation, souvent considérée comme le facteur limitant de la dégradation, est catalysée par les déadénylases. Parmi les quelques protéines ayant une activité de déadénylation, la littérature s'accorde sur le rôle prépondérant du complexe CCR4-NOT dans le raccourcissement de la queue poly(A) des ARNm. Ce complexe est composé de 6 ou 7 protéines NOT selon les organismes, et des deux déadénylases CAF1 et CCR4. Si les deux déadénylases ont des fonctions distinctes mais également complémentaires, CCR4 joue un rôle crucial au cours de la déadénylation. Contrairement à CAF1, CCR4 est en effet capable de retirer la PABP recouvrant et protégeant la queue poly(A) des ARNm, et d'ainsi catalyser leur déadénylation.

L'activité des déadénylases est finement régulé, et à l'interface avec de nombreux autres mécanismes de dégradation des ARNm. Parmi eux, l'uridylation entretient des liens étroits avec la déadénylation. L'uridylation consiste en l'ajout d'uridines à l'extrémité 3' des ARN, et est catalysée par les Terminal Uridylyl Transférases (TUTases). L'uridylation des ARNm est précédée par une première étape de déadénylation. En effet, les populations d'ARNm les plus uridylées sont celles ayant des queues poly(A) courtes, et étant activement déadénylées. Également, l'uridylation des ARNm freine l'action des déadénylases, confirmant un lien mécanistique fort et complexe entre uridylation et déadénylation.

Chez Arabidopsis, des données publiées par l'équipe indiquent que ce lien pourrait également être physique. En effet, de nombreuses protéines appartenant au complexe CCR4-NOT, ou associées au complexe, co-purifient avec URT1, la TUTase majeure des ARNm chez Arabidopsis. Il est ainsi probable que certaines protéines interagissant aussi bien avec URT1 qu'avec le complexe CCR4-NOT, jouent le rôle de pont moléculaire permettant de lier uridylation et déadénylation.

Mon travail de thèse s'est articulé autour de deux axes principaux. Tout d'abord, j'ai étudié les fonctions moléculaires et physiologiques de la déadénylation effectuée par les déadénylases CCR4a et CCR4b, deux sous-unités catalytiques du complexe CCR4-NOT. Dans un second temps, j'ai également étudié les liens physiques et mécanistiques qui lient l'uridylation par URT1 et la déadénylation par le complexe CCR4-NOT.

Partie I – Déadénylation des ARNm par les protéines CCR4a et CCR4b

La principale partie de mon travail a porté sur l'étude du processus de déadénylation par le complexe CCR4-NOT, et plus particulièrement sur l'importance des paralogues CCR4a et CCR4b dans la dégradation de la queue poly(A) des ARNm, et les rôles biologiques qu'ils occupent lors du développement d'Arabidopsis.

Les gènes *CCR4a* et *CCR4b* étant en close proximité sur le génome, l'équipe a dû utiliser une stratégie de mutagénèse dirigée par CRISPR-Cas9 afin d'éteindre l'expression des deux gènes. Durant ma thèse, j'ai sélectionné ces mutants CRISPR jusqu'à l'obtention de deux allèles indépendants, homozygotes pour des insertions/délétions qui décalent le cadre de lecture de chacun des deux gènes, et ce faisant, introduisent des codons STOP prématurés. L'analyse phénotypique des mutants suggérait que le mutant *ccr4a ccr4b* subissait une réponse auto-immune constitutive, caractérisée par un nanisme, ainsi que des feuilles en état de sénescence précoce et recroquevillées. Cette constatation a été corroborée par une analyse de RNA-seq, révélant une surexpression des gènes liés à l'immunité et une répression des gènes jouant un rôle majeur dans la photosynthèse.

Pour déterminer l'impact de la mutation des gènes *CCR4a* et *CCR4b* sur la taille des queues poly(A) des ARNm, nous avons décidé d'utiliser une approche de séquençage utilisant la technologie de séquençage par nanopore développée par Oxford Nanopore Technologies. Ainsi, j'ai participé à la mise en place dans le laboratoire et à l'optimisation du FLEP-seq2, technique récemment publiée par Jia et collègues. Cette technique se base sur la ligation d'un adaptateur en 3' sur des ARN purifiés par ribodéplétion. Les ARNm sont rétrotranscrits et au cours de cette réaction, une séquence adaptatrice est ajoutée en 3' des ADNc en utilisant un processus de *template switching* de la transcriptase inverse. Les ADNc sont ensuite amplifiés par PCR. Enfin, les adaptateurs contenant la protéine motrice nécessaire au séquençage nanopore sont liés à la banque d'ADNc. Le FLEP-seq2 permet non seulement d'établir un profil précis et reproductible des queues poly(A), mais permet également de détecter les nucléotides ajoutés en 3' des ARNm, nécessaire à l'étude de la dynamique entre uridylation et déadénylation.

L'analyse des mutants *ccr4a ccr4b* par FLEP-seq2 confirme bien le rôle de CCR4a et CCR4b en tant que déadénylases. En effet, nous avons pu observer dans les ARNm de rosette un allongement global des queues poly(A), attestant d'une fonction générale de déadénylation par les protéines CCR4a et CCR4b. En effet, nous observons que la population majeure des ARNm possède des queues poly(A) courtes de 20-22 adénosines, et c'est précisément cette population dont l'accumulation est la plus diminuée. De manière intéressante, les ARNm surexprimés dans les rosettes de mutants *ccr4a ccr4b* subissent un allongement plus prononcé. De plus, ce sont également des ARNm caractérisés par une demi-vie relativement courte. Ainsi, il est possible que dans des conditions physiologiques, cette population d'ARNm est activement déadénylée par CCR4a et CCR4b, induisant leur rapide dégradation. Lorsque la déadénylation est entravée, ces ARNm sont potentiellement stabilisés, expliquant leur surexpression.

Afin d'avoir une idée générale des fonctions de la déadénylation par CCR4a et CCR4b au cours du développement d'Arabidopsis, nous avons également analysé les profils de poly(A) d'ARNm extraits à partir de boutons floraux. De manière intéressante, les ARNm exprimés aussi bien dans les feuilles que dans les boutons floraux présentent des profils de queues poly(A) différents dans les plantes sauvages, et sont également affectés de manière distincte par la mutation des déadénylases. Cette observation illustre parfaitement la complexité des mécanismes qui régulent la taille de la queue poly(A) des ARNm, et indique également qu'il existe des processus spécifiques à certains tissus qui permettent de moduler la déadénylation par CCR4a et CCR4b.

De manière intéressante, l'augmentation de la taille des queues poly(A) dans le mutant *ccr4a ccr4b* est homogène dans les ARNm de rosette. En revanche, dans le cas des boutons floraux, on observe une petite population d'ARNm dont les queues poly(A) sont nettement allongées, tandis que le reste des ARNm est également touché, mais de manière moins prononcée. Il semblerait donc que

CCR4a et CCR4b soient des facteurs généraux de déadénylation capables de déadényler virtuellement tous les transcrits, tout en ayant des cibles préférentielles.

Curieusement, cette population est exprimée uniquement et spécifiquement dans les anthères matures et en cours de maturation. La majorité de ces ARNm sont connus dans la littérature comme ayant un rôle plus ou moins essentiel dans la structure et la fonction du pollen, notamment en régulant la germination du tube pollinique. De manière intéressante, la germination *in vitro* du pollen *ccr4a ccr4b* est fortement diminuée. Il semblerait donc qu'en régulant la taille de la queue poly(A) de ces ARNm, CCR4a et CCR4b s'imposent comme des acteurs majeurs de la maturation et la fonction du pollen d'Arabidopsis.

En vue d'évaluer les répercussions de l'allongement de la queue poly(A) de cette population sur leur métabolisme (accumulation et traduction), une collaboration a été entreprise avec Rémy Merret du LGDP de Perpignan. J'ai été accueilli au LGDP afin de procéder à la préparation de polysomes à partir de boutons floraux. Le séquençage des ARNm purifiés de ces fractions polysomales nous indique que la mutation des gènes *CCR4a* et *CCR4b* n'influe pas la traduction des ARNm, tant au niveau global que sur les ARNm dont les queues poly(A) sont les plus allongées. Curieusement, nous n'observons pas de lien entre allongement de la taille de la queue poly(A) et différence d'expression, à la différence de ce que nous avons observé dans les ARNm de rosette. Ceci peut s'expliquer par une régulation très différente de la déadénylation en fonction des tissus, déjà indiquée précédemment par une disparité des profils de poly(A) entre fleurs et rosettes pour des ARNm exprimés dans les deux tissus.

Dans le même temps, nous avons caractérisé par spectrométrie de masse le protéome total de grains de pollen *ccr4a ccr4b*. Nous n'avons pas observé de différence d'accumulation de protéines impliquées dans la germination du tube pollinique et dont les ARNm subissent un changement important de profils de poly(A). Nos résultats démontrent que l'allongement des queues poly(A) de ces ARNm n'est donc pas responsable d'un défaut de production des protéines correspondantes, du moins pour celles détectées par spectrométrie de masse. La suite immédiate de ce projet serait de déterminer si l'activité catalytique de CCR4a et CCR4b est requise pour la germination du pollen, ou si ces deux déadénylases jouent également un rôle structural essentiel à la régulation du métabolisme des ARNm ou d'autres types d'ARN à ce stade particulier du développement.

Partie II – Etude des liens entre uridylation et déadénylation

La seconde partie de ma thèse a consisté à étudier les liens fonctionnels qu'il existe entre uridylation et déadénylation. Ainsi, j'ai utilisé les données d'uridylation fournies par le FLEP-seq2 pour déterminer l'impact de la mutation *ccr4a ccr4b* sur les profils d'uridylation du transcriptome d'Arabidopsis. En condition WT, l'uridylation est précédée par une première étape de déadénylation. Ainsi, l'on peut s'attendre à une diminution des niveaux d'uridylation dans le mutant *ccr4a ccr4b* puisque la déadénylation est altérée. Cependant, nous n'observons pas de réduction significative des taux d'uridylation dans les plantes *ccr4a ccr4b*. Néanmoins, un allongement général des queues poly(A) uridylées est observé. Ceci suggère que la déadénylation par CCR4a et CCR4b ne constitue pas une condition préalable à l'uridylation par URT1. Bien que la population < 22As ne soit plus la population majoritaire des ARNm dans *ccr4a ccr4b*, il s'agit toujours bien de la population la plus uridylée. Ainsi, cet allongement pourrait être causé par une meilleure accessibilité d'URT1 aux queues poly(A) en raison de l'absence de compétition avec CCR4. Alternativement, il est possible qu'URT1 ait une affinité accrue pour les queues poly(A) courtes, mais est néanmoins capable d'uridyler des queues longues lorsque celles-ci s'accumulent.

En outre, nous avons voulu caractériser les modalités d'interaction entre URT1 et le complexe CCR4-NOT. Nous avons déterminé l'interactome d'EXA1, une protéine co-précipitant avec URT1, comme un potentiel candidat permettant de lier URT1 et le complexe CCR4-NOT. En effet, les orthologues d'EXA1 chez l'humain et la drosophile interagissent directement avec NOT1, la protéine de structure du complexe CCR4-NOT. De plus, EXA1 lie spécifiquement des motifs PPGF (Proline-Proline-Glycine-Phénylalanine), et URT1 possède un tel motif, largement conservé chez les plantes terrestres, dans sa région N-terminale. Nous avions donc émis l'hypothèse qu'EXA1 permettait de lier URT1 et le complexe CCR4-NOT par l'interaction directe entre ces partenaires. La résolution de l'interactome d'EXA1 a permis de caractériser NOT1 comme un interactant majeur d'EXA1, confirmant la conservation de cette interaction chez Arabidopsis.

Pour démontrer l'interaction entre URT1 et EXA1, j'ai généré des lignées de plantes exprimant URT1-GFP comportant une mutation sur le motif PPGF, en remplaçant la glycine et la phénylalanine par deux acides glutamiques. En réalisant l'interactome différentiel URT1^{WT} / URT1^{PPEE}, EXA1 est la seule protéine significativement déplétée, confirmant que l'interface PPGF-GYF est essentiel à la co-précipitation d'EXA1. Cependant, nous n'observons pas de déplétion de partenaires d'EXA1 dans les IP d'URT1^{PPEE}. Potentiellement, la redondance des interactions qui lient les différents partenaires des complexes impliquant URT1 et EXA1 pourrait permettre de connecter URT1 aux partenaires d'EXA1 en l'absence de la protéine à domaine GYF.

L'analyse des profils poly(A) et des niveaux d'uridylation par FLEP-seq2 dans un mutant *exa1* n'a pas montré de chute de niveau d'uridylation ou d'allongement de la queue poly(A), ce à quoi nous aurions pu nous attendre si EXA1 était requis pour recruter URT1 au niveau des ARNm. De la même manière, nous n'avons observé aucune différence d'uridylation ou de taille de queue poly(A) dans les plantes exprimant URT1^{PPEE}. Nous pensons donc que le recrutement d'URT1 vers les ARNm et le CCR4-NOT *via* EXA1, si existant, n'est qu'un des mécanismes potentiels permettant la reconnaissance des ARNm déadénylés par URT1. Nos données expérimentales indiquent que la mutation du motif PPGF n'induit pas la perte d'interaction entre URT1 et le complexe CCR4-NOT, bien qu'elle abroge l'interaction avec EXA1. Il est ainsi possible que la perte d'interaction avec EXA1 soit compensée par d'autres réseaux d'interactions qui permettent à terme de lier le CCR4-NOT et de recruter la TUTase sur des ARNm en cours de déadénylation.

En conclusion, mes travaux de thèse ont contribué à déterminer la fonction biologique et moléculaire du complexe CCR4-NOT chez Arabidopsis. Mes travaux ont également rapporté la première interaction entre une TUTase et une protéine à domaine GYF, qui agissent comme des véritables plateformes de recrutement permettant de lier de nombreuses voies métaboliques.